Vol. 285, No. 1–2, January 20, 1994 ISSN 0003-2670

ANALYTICA CHIMICA ACTA

An international journal devoted to all branches of analytical chemistry

ELSEVIER

ANALYTICA CHIMICA ACTA

Scope. *Analytica Chimica Acta* publishes original papers, rapid publication letters and reviews dealing with every aspect of modern analytical chemistry. Reviews are normally written by invitation of the editors, who welcome suggestions for subjects. Letters can be published within **four months** of submission. For information on the Letters section, see inside back cover.

Submission of Papers

Americas

Prof. Harry L. Pardue
Department of Chemistry
1393 BRWN Bldg, Purdue University
West Lafayette, IN 47907–1393
USA

Tel:(+1-317) 494 5320
Fax:(+1-317) 496 1200

Computer Techniques

Prof. J.T. Clerc
Universität Bern
Pharmazeutisches Institut
Baltzerstrasse 5, CH-3012 Bern
Switzerland

Tel:(+41-31) 6314191
Fax:(+41-31) 6314198

Prof. Sarah C. Rutan
Department of Chemistry
Virginia Commonwealth University
P.O. Box 2006
Richmond, VA 23284-2006
USA
Tel:(+1-804) 367 1298
Fax:(+1-804) 367 7517

Other Papers

Prof. Alan Townshend
Department of Chemistry
The University
Hull HU6 7RX
Great Britain

Tel:(+44-482) 465027
Fax:(+44-482) 466410

Prof. Willem E. van der Linden
Laboratory for Chemical Analysis
Department of Chemical Technology
Twente University of Technology
P.O. Box 217, 7500 AE Enschede
The Netherlands
Tel:(+31-53) 892629
Fax:(+31-53) 356024

Prof. Paul Worsfold
Dept. of Environmental Sciences
University of Plymouth
Plymouth PL4 8AA
Great Britain

Tel:(+44-752) 233006
Fax:(+44-752) 233009

Submission of an article is understood to imply that the article is original and unpublished and is not being considered for publication elsewhere. *Anal. Chim. Acta* accepts papers in English only. There are no page charges. Manuscripts should conform in layout and style to the papers published in this issue. See inside back cover for "Information for Authors".

Publication. *Analytica Chimica Acta* appears in 16 volumes in 1994 (Vols. 281–296). *Vibrational Spectroscopy* appears in 2 volumes in 1994 (Vols. 6 and 7). Subscriptions are accepted on a prepaid basis only, unless different terms have been previously agreed upon. It is possible to order a combined subscription (*Anal. Chim. Acta* **and** *Vib. Spectrosc.*).
Our p.p.h. (postage, packing and handling) charge includes surface delivery of all issues, except to subscribers in the U.S.A., Canada, Australia, New Zealand, China, India, Israel, South Africa, Malaysia, Thailand, Singapore, South Korea, Taiwan, Pakistan, Hong Kong, Brazil, Argentina and Mexico, who receive all issues by air delivery (S.A.L.–Surface Air Lifted) at no extra cost. For Japan, air delivery requires 25% additional charge of the normal postage and handling charge; for all other countries airmail and S.A.L. charges are available upon request.

Subscription orders. Subscription prices are available upon request from the publisher. Subscription orders can be entered only by calendar year and should be sent to: Elsevier Science B.V., Journals Department, P.O. Box 211, 1000 AE Amsterdam, The Netherlands. Tel: (+31-20) 5803 642, Telex: 18582, Telefax: (+31-20) 5803598, to which requests for sample copies can also be sent. Claims for issues not received should be made within six months of publication of the issues. If not they cannot be honoured free of charge. Readers in the U.S.A. and Canada can contact the following address: Elsevier Science Inc., Journal Information Center, 655 Avenue of the Americas, New York, NY 10010, U.S.A. Tel: (+1-212) 6333750, Telefax: (+1-212) 6333990, for further information, or a free sample copy of this or any other Elsevier Science journal.
Advertisements. Advertisement rates are available from the publisher on request.

US mailing notice – Analytica Chimica Acta (ISSN 0003-2670) is published 3 times a month (total 42 issues) by Elsevier Science B.V. (Molenwerf 1, Postbus 211, 1000 AE Amsterdam). Annual subscription price in the USA US$ 3035.75 (valid in North, Central and South America), including air speed delivery. Second class postage paid at Jamaica, NY 11431. *USA Postmasters*: Send address changes to Anal. Chim. Acta, Publications Expediting, Inc., 200 Meacham Av., Elmont, NY 11003. Airfreight and mailing in the USA by Publication Expediting.

ANALYTICA CHIMICA ACTA
VOL. 285 (1994)

ANALYTICA CHIMICA ACTA

An international journal devoted to all branches of analytical chemistry
Revue internationale consacrée à tous les domaines de la chimie analytique
Internationale Zeitschrift für alle Gebiete der analytischen Chemie

Anal. Chim. Acta, Vol. 285 (1994)

ELSEVIER, Amsterdam–London–New York–Tokyo

0003-2670/94/$07.00

ANALYTICA CHIMICA ACTA

An international journal devoted to all branches of analytical chemistry

(Full texts are incorporated in CJELSEVIER, a file in the Chemical Journals Online database available on STN International; Abstracted, indexed in: Aluminum Abstracts; Anal. Abstr.; Biol. Abstr.; BIOSIS; Chem. Abstr.; Curr. Contents Phys. Chem. Earth Sci.; Engineered Materials Abstracts; Excerpta Medica; Index Med.; Life Sci.; Mass Spectrom. Bull.; Material Business Alerts; Metals Abstracts; Sci. Citation Index)

VOL. 285 NO. 1–2 JANUARY 20, 1994

CONTENTS

(Continued overleaf)

Analytica Chimica Acta, 285 (1994) 1–8
Elsevier Science B.V., Amsterdam

Monitoring of reducing sugars by flow-injection analysis using *p*-hydroxybenzoic acid hydrazide

Peter Hartmann

Institut für Analytische Chemie, Technische Universität Wien, Getreidemarkt 9, A-1060 Wien (Austria)

Stephen J. Haswell [1]

School of Chemistry, The University of Hull, Hull HU6 7RX (UK)

Manfred Grasserbauer

Institut für Analytische Chemie, Technische Universität Wien, Getreidemarkt 9, A-1060 Wien (Austria)

(Received 24th June 1993; revised manuscript received 26th August 1993)

Abstract

In this work, *p*-hydroxybenzoic acid hydrazide has been used as a reagent to determine reducing sugars using flow-injection analysis with photometric detection (410 nm). Parameters such as the temperature, alkalinity, reactor length, injection volume, flows and reagent concentration were examined for their optimum conditions. Systems catalysed by bismuth for low analyte concentrations and non-catalysed for higher levels, containing only a single sugar (sampling frequency 60–80 h^{-1}) and a system with a longer residence time (sampling frequency 30 h^{-1}) in which the different responses of various sugars can be minimised, are described. Samples (fruits and beverages) measured with the latter system in the calibration range 0.08–0.6 g/l gave a typical R.S.D. of 2%.

Keywords: Flow injection; Beer; Fruit juice; PAHBAH; Reducing sugars; Sugars; Wine

The determination of reducing sugars is often required for the monitoring of food products as they may effect both taste and texture of a product. Simple and robust analytical methods are therefore required to determine reducing sugars in food and drink products.

A relatively simple colorimetric reaction first reported by Pinkus [1] was further developed as a batch method for the analysis of reducing sugars by several workers [2–10]. In hot alkaline solutions, reducing sugars are degraded and react with benzoic acid hydrazides allowing the formation of anionic forms of bisbenzoyl hydrazones of glyoxal and mono- or dimethylglyoxal. These products show an intense yellow colour which can be monitored photometrically at wavelengths around 400 nm. One of the most popular reagents of this type has been *p*-hydroxybenzoic acid hydrazide (PAHBAH) [2] which displays an absorption maximum around 410 nm.

One potential problem with this reagent is that product can act as a chelating agent resulting in a shift in its absorption maximum with the presence of ions, such as calcium and cadmium [3,5]. However careful selection of the reaction conditions can significantly reduce this effect. Bismuth, for

Correspondence to: S.J. Haswell, School of Chemistry, The University of Hull, Hull HU6 7RX (UK).

SSDI 0003-2670(93)E0509-6

example has been reported to have a catalytic effect on the reaction of PAHBAH with reducing sugars [8] such that bismuth will not form a complex with the reaction products in an alkaline medium and therefore the absorption maximum remains unchanged. Lever and co-workers [3–5,8,10] reported the development of a batch method for the determination of glucose in blood and other clinical samples. The method was also used to monitor the total reducing sugars in tobacco products [11] using an AutoAnalyzer system.

The PAHBAH method was adapted for FIA by Trent and Christiansen [12] and used for the determination of total monosaccharides after the hydrolysis of all higher saccharides in forage tissue such as wheat, Johnsongrass and Caucasian Bluestem. A detailed description of the system used and the operating conditions are not given in the paper, but the method did appear to require an extremely long analysis time (190 s), and a catalyst was not used nor was any indication given that a catalyst had been considered.

The indication from the literature is that the PAHBAH reaction offers good sensitivity and selectivity in the batch and AutoAnalyzer version. In addition tolerance of non-sugar interferences appears to be greater than for other reactions based only on reducing property since the specific steric form of sugars is required for reaction with PAHBAH. Like most of the photometric sugar detection methods the reaction needs to be carried out at elevated temperatures (> 70°C) and in a moderate to strong alkaline solution. Therefore sucrose and other non-reducing carbohydrates can undergo hydrolysis and form glucose or other reducing monosaccharides. The PAHBAH reagent is relatively unstable when stored in alkaline solution and is therefore prepared in hydrochloric acid and mixed with excess of sodium hydroxide on line. This can cause problems if the pH value does not increase immediately since the reagent precipitates in neutral solution. When the method is adapted to FIA, small differences in the reaction rates between the different sugars may become important as steady state is not achieved. Therefore either only one sugar can be monitored or very long residence times are necessary to minimise the differences in response of different sugars.

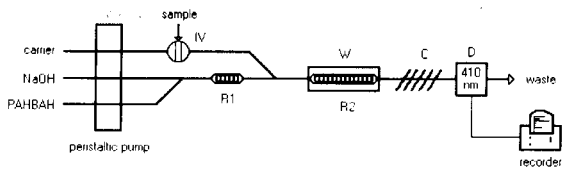

Fig. 1. Schematic diagram of the flow-injection manifold. R1, mixing coil, 1.5 m; R2, reactor; W, water bath; C, cooling bath, ice; D, photometric detector; IV, injection valve.

This work has been divided into two parts. The first describes a flow injection analysis (FIA) system for the determination of glucose only, whereas the second part focuses on a FIA system that will determine combined response for both glucose and fructose.

EXPERIMENTAL

Instrumentation

The spectrophotometers were a Cecil Instruments, linear UV spectrophotometer series 2, CE 272, used in the FIA manifold; PYE UNICAM, UV/VIS spectrophotometer PU 8800 used for spectra and enzymatic assay. The recorder was from Kipp and Zonen (EML). The FIA manifold (Fig. 1) consisted of a Peristaltic pump (Gilson, Minipuls 2, 4 channels, variable speed), a water bath (Grant instruments, thermostatic bath JB1) and a cooling bath (aluminium bowl). All the tubing in the manifold was 0.5 mm i.d. PTFE (Whatman) except the coil in the cooling bath which consists of 0.3 mm i.d. tubing; this was used to suppress the formation of gas bubbles. The fittings were from Omnifit (Flangeless). The injection valve was a standard PTFE 4-way valve, with sample loops of 0.8 or 0.5 mm internal diameter.

Reagents

All reagents are analytical grade unless stated otherwise. *para*-Hydroxy benzoic acid hydrazide: 98% m.p. 264–266°C, supplied by Aldrich (Gillingham), bright, white crystals; and Aldrich-

Chemie (Steinheim), slightly yellow powder. Sodium hydroxide: pellets, Prolabo (Manchester). Hydrochloric acid: 35–38% w/w, BDH (Merck, Lutterworth). Bismuth nitrate: BDH. Citric acid: M and B (Prolabo, Manchester). D-Glucose: FSA. D(−)-Fructose: < 0.05% glucose, Sigma (Poole). Sucrose: < 0.01% red. sugars, BDH. Maltose: general purpose reagent, 4.5–5.5% H_2O, BDH. Lactose: 4.8–5.4% H_2O, BDH. Purified water: purified by Elgastat Prima reverse osmosis. Charcoal: decolorizing powder, BDH. Filter paper: Whatman, No. 1, No. 42. D-Glucose/D-Fructose enzymatic UV-testkit for food analysis: Boehringer Mannheim, Cat. No. 139 106. $ZnSO_4 \times H_2O \times 7H_2O$: BDH. $K_4[Fe(CN)_6] \times 3H_2O$: Hopkin and William (Merck, Lutterworth). $CuSO_4 \times 5H_2O$: BDH. Potassium sodium tartrate: BDH. Methylene blue: Timstar Laboratory Suppliers. Universal buffer: laboratory reagent, BDH universal buffer mixture.

Reagents preparation

PAHBAH reagent: 1% m/v (0.0655 mol/l). 2.5 g ± 1 mg PAHBAH and 5.25 g citric acid were dissolved in 250 ml 0.5 M HCl. Other concentrations were prepared in the same way. Also reagents without citric acid were used.

0.5 M HCl. 10.6 ml conc. HCl were diluted to 250 ml.

Bismuth stock solution: 0.83 mol/l Bi^{3+}. 12.6128 g NaOH pellets were weighed accurately into a 400-ml beaker and dissolved with ca. 100 ml water. 21.067 g potassium sodium tartrate and 39.6154 g $Bi(NO_3)_3$ were added and the mixture were stirred under heating for 2 h. The volume was adjusted to 120 ml.

Sodium hydroxide. 32.000 g ± 1 mg or any other amount according to concentrations mentioned, of NaOH pellets were weighed into a 1-l volumetric flask and filled up to volume with water. If bismuth was required, 4 ml of bismuth stock solution was added before dilution.

0.1 M $CaCl_2$ solution. 5.4787 g $CaCl_2 \times 6H_2O$ were dissolved in 250 ml H_2O

Carrez solution 1. 3.6 g $K_4[Fe(CN)_6] \times 3H_2O$ were dissolved in 100 ml H_2O.

Carrez solution 2. 7.2 g $ZnSO_4 \times H_2O \times 7H_2O$ were dissolved in 100 ml H_2O.

Soxhlet solution 1. 34.639 g $CuSO_4 \times 5H_2O$ were dissolved in water, diluted to 500 ml and filtered.

Soxhlet solution 2. 173 g potassium sodium tartrate $\times 4H_2O$ and 50 g NaOH pellets were dissolved in water and diluted to 500 ml. The solution was filtered two days later.

Standards preparation

Main standards of every sugar were prepared daily by dissolving 1.000 g ± 1 mg of one sugar or 0.5 g of two sugars in 500 ml H_2O. Subsequent standards of all desired concentrations were prepared by diluting the main standards.

Sample pretreatment

Mixed glucose/fructose standards were added to samples for the recovery experiments.

The samples were diluted in order to accommodate the response of the samples into the linear range (from 1:5 to 1:200) and decoloration of red wines by charcoal (0.15 g to 100 ml diluted sample, filtration) was carried out.

Beers were diluted 1:20 or 1:25 and dark beers clarified with Carrez solutions (5 ml of each solution, 10 ml 0.1 M NaOH and 5 ml sample made up to volume (100 ml) with water, shaken and filtered).

Lucozade was diluted 1:500 and filtered, the juice diluted 1:100 and measured with and without decoloration by charcoal. Cola drinks were also diluted 1:100 and measured without decolorization. 10 ml of pH 6.88 universal buffer were added prior to dilution to compensate for the acidity.

Banana, apple and kiwi fruit were homogenised and 5–10 g weighed into a 100-ml volumetric flask. The dispersions were treated in an ultrasonic bath for 20 min and filtered. The obtained filtrates were diluted 1:20.

Measuring procedure

Initially injection was carried out using a 2-ml plastic syringe but later an extra sample pumping line was added to the system. Injection was always made immediately after the heating indicator light of the bath switched off (about every 2 min). This was done to minimise variation due to

thermal instabilities in the system used. To avoid blockage of the tubing when switching off the apparatus, it was necessary to substitute first the PAHBAH reagent for water and after 5 min rinsing time, substitute the NaOH for water. Purified water was used as the sample carrier.

To compare the results obtained from the FIA system, two independent methods were chosen. Firstly the D-glucose/D-fructose enzymatic UV-test kit from Boehringer Mannheim and secondly the Lane-Eynon general volumetric method for invert sugar (described in Official Methods of Analysis 1990 [13]). The enzymatic method is based on the enzymes hexokinase/phosphogluco isomerase/glucose-6-phosphate dehydrogenase and UV detection of NADPH. The batch determination was strictly performed according to the manual. The volumetric method uses the reduction of $CuSO_4$ in boiling alkaline medium.

RESULTS AND DISCUSSION

Optimisation of flow-injection variables

Optimisation was not simply performed in order to obtain the greatest absorption value or peak height, but peak shape, calibration range and analytes concentration were all taken into consideration. The parameters investigated were temperature of the water bath, reactor length, flow-rates and the concentrations of the reagents used. Univariant scanning of the parameters was carried out based on experience, chemical knowledge and technical limitations.

Three different systems were evaluated

(A) Non-catalysed for glucose at high concentration (0.025–1.5 g/l)

(B) Catalysed for glucose at low concentration (0.004–0.040 g/l)

(C) Non-catalysed for glucose and fructose (0.08–0.6 g/l)

Temperature

For catalysed and non-catalysed of any configuration a minimum temperature of 70°C was found to be necessary to reach a detectable response within a reasonable time. Since acceptable absorbances were achieved at 90°C, and in order to keep clear of boiling, no attempt was made to raise temperature for systems A and B further. The increase of temperature from 70 to 90°C gave a response peak increase of about 40 times. However, in later work the temperature was increased to 95°C (method C) since at this level the signal variations for the different reducing sugars was minimised.

NaOH concentration

Attempts to optimise the alkalinity for system A resulted in a gradual but continuous increase in signal with no apparent maximum at concentrations up to 7 M NaOH (about 1.9 M in the reaction mixture). In order to keep alkalinity low and so avoid hydrolysis of sucrose and to minimise the corrosive nature of the reagent, it was decided to fix the concentration at 1.1 M (0.25 M in reaction mixture) for system A.

In the catalysed system the signal response increased with rising alkalinity, but the effect of the Bi^{3+} ion concentration was found to be of much greater significance than the sodium hydroxide concentration. A 1 M NaOH solution was chosen, containing 3.34 mmol/l Bi^{3+}, and this solution proved to be stable for several days.

The influence of alkalinity on the longer reaction system C was found to give a response that increased with lower concentration of NaOH whilst the interference by sucrose increased at higher NaOH concentrations as expected. Therefore a NaOH concentration of 0.8 mol/l (about 0.14 mol/l in the mixture) was chosen for the system C.

Flow-rates and reagent concentrations

The flows and concentrations used for the optimisation of systems A and B were initially derived from those used for the AutoAnalyzer procedure described by Davis [11]. After some modifications (removal of Ca-line, addition of cooling, longer reactor), the optimum flow-rates were found to be 0.82 ml/min (NaOH), 0.4 ml/min (reagent) and 1.4 ml/min (carrier). For the PAHBAH reagent, the response was found to be satisfactory with a 0.06 M or later 1% solution for the flow-rate given.

For system C a carrier flow-rate of 0.82 ml/min was found to provide an acceptable compromise between a too long reactor coil and broadening peaks. Increasing the reagent concentration resulted in a decrease of the response, probably caused by a higher blank absorbance resulting in a low analyte/blank ratio. The flow-rates for the reagent (0.4 ml/min) and the NaOH (0.56 ml/min) solutions were not allowed to get too small compared to the carrier.

Injection volume

The injection volume was optimized for the non-catalysed system A and an optimum for the peak height/width function was found to be 300 μl using a reactor coil of 300 cm. Larger sample volumes resulted in a broadening of the peak and little gain in peak height was achieved. This injection volume was used in both system A and the catalysed system B for which the reactor coil was longer. Using the long residence time system C (with a dispersion coefficient of 19), the injection volume was reduced to as small as possible so as to obtain a better sampling frequency. A 20-μl injection volume was therefore used in system C.

Reactor length

The length of the reaction coil was investigated for systems A and B in the range 2 and 17 m monitoring a signal for 20 ppm glucose standard. The peak height/width function indicated a suitable reaction coil length would be 10 m and this value was taken for both system A and B.

With due consideration for the differences in reaction time between the various sugars expected in system C it became necessary to increase the reaction coil length to 30 m in order to provide a sufficient residence time (about 3 min) when using a moderate carrier flow (0.82 ml/min).

Addition of bismuth catalyst

It was difficult to obtain analytical signals for low range (ppm) or a fast determination for high range (g/l) without the presence of a catalyst. Bismuth was used to increase the performance, however, the major disadvantage of using bismuth was the fact that there were no noticeable differences in the maximum colour yield between glucose and fructose although the reaction rates are reported to be equivalent [8]. These variations in colour yield were found to be relatively small compared to the differences between glucose and fructose in the non-catalysed system A, with a short residence time, where also the reaction rates were different. However the difference between glucose and fructose signals were still found to be 12% which although not completely satisfactory was better than expected, considering the reported differences [8] in the maximum colour yield (fructose only 70% of glucose) for the batch method. The increase in performance using bismuth was about 4 times over the catalysed system.

Calcium, interferences

Calcium is reported to be the most serious interferent with the PAHBAH reaction [3,5] since other highly interfering cations such as cadmium and vanadium are not likely to occur in samples such as food at the levels effecting the determination.

Experiments with system A using a 20 ppm glucose standard did not reveal an interference from calcium up to a concentration of 10 mmol Ca^{2+}/l at which point the catalysed system showed a decrease in absorbance of 11%. With the longer reaction times system C, the effect of calcium was found to increase sharply after 2 mmol/l to a deviation in absorbance of 6–7% at 5 mmol/l.

Comparison of analyte signals for different sugars with the three systems studied

Analysis of fructose on the non-catalysed system (A) revealed a much larger response than

TABLE 1

Comparison of sugars, system A

Concentration (g/l)	Absorbance		Ratio to glucose
	Glucose	Fructose	
0.05	0.0134	0.0825	6.2
0.25	0.0652	0.3975	6.1
1.00	0.2600	1.4550	6.0

TABLE 2

Comparison of sugars, system B

Concentration	Absorbance		Ratio to glucose
	Glucose	Fructose	
1	0.0610	0.0535	0.88
8	0.4917	0.4125	0.84
30	1.7867	1.4733	0.82

that for glucose (Table 1) whilst the catalysed System (B) gave a slightly higher absorbance signal for glucose (Table 2). With system C (Table 3) fructose, gave a similar response to that observed for glucose, however, maltose and lactose gave a somewhat reduced response. The effect of sucrose on the system was found to be minimal.

Calibration

Using the optimized conditions summarised in Table 4, the calibration for the three systems with various sugars was carried out. The standards were repeated 5 times for system A and 4 times for systems B and C. The calibration data and the practical sampling frequencies (h^{-1}, obtained by measuring the peak width.) are summarised in Table 5. System C was calibrated with various

TABLE 3

Comparison of sugars, system C

Sugar	Absorbance	Relative response compared to glucose	Relative response, literature value [2]
Glucose	0.1775	1.00	1.00
Fructose	0.1881	1.06	1.04
Maltose	0.0938	0.52	0.56
Lactose	0.0663	0.37	0.39
Sucrose, 1 g/l	0.0098	0.005	0.03
Sucrose, 10 g/l	0.0725	0.004	–

sugars and with a mixed standard of glucose–fructose of 1 : 1. In the regression the absorbance = concentration $\times a + b$. The limit of detection (LOD) was calculated from $3 \times s_{y/x} + b$.

Analysis of samples

For all the samples where an analysis for total reducing sugars (mainly glucose, fructose and maltose) was required, system C was used and results obtained were compared with those for the enzymatic and the volumetric methods (Table 6). The results were calculated as glucose–fruc-

TABLE 4

Optimised flow-injection parameters

System	Conc. NaOH (mol/l)	Flow NaOH (ml/min)	Conc. PAHBAH (mol/l)	Flow PAHBAH (ml/min)	Flow carrier (ml/min)	Injection (μl)	Temp. (°C)	Bi^{3+} (mmol/l NaOH)
A	1.1	0.82	0.06	0 40	1.40	300	90	–
B	1.0	0.82	0 06	0.40	1.40	300	90	3.34
C	0.8	0.56	0.06	0.40	0.82	20	95	–

TABLE 5

Calibration data

System	Sugar	Sample freq. (h^{-1})	a	b	r	Range (g/l)	$s_{y/x}$	LOD (g/l)
A	glucose	50	0.2593	0.0004	0.9998	0.025–1.5	0.0020	0.025
B	glucose	40	0.0334	−0.0162	0.9998	0.004–0.040	0.0080	0.0007
C	glucose	30	1.8208	0.0010	0.9999	0.002–0.6	0.0027	0.005
C	fructose	30	1.8992	0.0018	0.9999	0.002–0.6	0.0051	0.008
C	maltose	30	0.9671	0.0040	0.9998	0.02 –0.8	0.0028	0.009
C	lactose	30	0.6956	0.0022	0.9999	0.02 –0.8	0.0013	0.006
C	gluc/fruc	30	1.8003	0.0048	0.9999	0.08 –0.6	0.0020	0.003

TABLE 6

Comparison of results obtained by different methods (g/l) for a range of beverages and fruits

Sample	Sample type	Replicas (days)	FIA	Enzymatic	Titration
Liebfraunlilch	white wine(German), medium	6	25.17 ± 0.6	24.14 ± 0.3	23.60
Eisberg	white wine(German), alcohol free	6	37.70 ± 1.1	35.97 ± 0.6	–
Caves de France	white wine (French), medium	4	19.60 ± 0.2	17.25 ± 0.5	–
Chianti	red wine (Italian)	3	1.61 ± 0.03	0.32 ± 0.19	1.66
Rinnender Zapfen	red wine (Austrian), dry	3	1.53 ± 0.03	1.01 ± 0.03	1.65
Blaufränkisch	red wine (Austrian), dry	3	1.68 ± 0.01	0.91 ± 0.03	2.04
Hirter Privat Pils	beer (Austrian), pils type	3	12.36 ± 0.1	–	12.08
Carlsberg lager	beer (UK), lager type	2	4.84 ± 0.05	–	5.02
Haagen	beer (UK), lagertype	2	4.31 ± 0.06	–	4.15
Newcastle brown	beer (UK), Ale	1	9.35	–	10.35
Guinness	beer (UK), Stout	1	7.07	–	7.70
Lucozade	energy drink (UK)	4	135.9 ± 2.3	116.4 ± 2.1	138.1
Coca Cola	Cola drink, classic style	1	10.25	10.57	–
Pepsi Cola	Cola drink, non-diet version	1	19.98	19.58	–
Juice drink	apple and black current	4	9.64 ± 0 26	8.55 ± 0.06	–
Banana	1. extraction, 10.04 g/100 ml	–	6.34	6.69	–
	2. extraction, 5.891 g/100 ml	–	7.11	7.24	–
Apple	1. extraction, 10.23 g/100 ml	–	7.31	6.16	–
	2. extraction, 5.337 g/100 ml	–	7.76	7.62	–
Kiwi fruit	1. extraction, 10.23 g/100 ml	–	10.23	10.76	–
	2. extraction, 6.060 g/100 ml	–	9.01	8.95	–

tose = 1 : 1 except for the beers, where the sugars were calculated as maltose. The enzymatic determination was performed in duplicate whilst the volumetric titrations were performed three times. It should be noted that the data given for the replicate flow injection analysis ($n = 3–6$) was obtained however on different days. The results indicate that, the between sample variation, for the FIA method was no worse than, the within sample variation, for the enzymatic and titration method.

For white wines, FIA yielded higher values than the enzymatic method. The methods were statistically tested for significant difference at a 95% level, revealing a significant difference for Caves de France. The dry red wines revealed limitations for all methods and whilst the reproducibility of the values obtained by the FIA were quite good, they were far from the expected residual sugar contents as specified by the official analysis (Rinnender Zapfen: 1.0 g/l, Blaufrankisch: 1.2 g/l, no data for Chianti). The titration gave results closer to, if a little higher than, those obtained by FIA. In the case of red wines the titrimetric endpoints were sometimes difficult to define, and red wines were subsequently decolorized with charcoal. The enzymatic assay corresponded well to the official value for Rinnender Zapfen, on the other hand, results for the second Austrian wine and Chianti showed a very poor performance. Both enzymatic determinations carried out on the Chianti yielded results too low to be plausible with the reaction not coming to an end within twenty minutes. The value obtained with the enzymatic assay for Lucozade was as expected, considering its specificity for glucose and fructose. Coca Cola and Pepsi Cola give similar results for both the enzymatic and FIA methods.

Conclusions

The determination of reducing sugars by the flow-injection analysis method developed offers a reasonably rapid sampling frequency, low sample and reagent consumption and requires inexpen-

sive instrumentation. The calibration of all systems yielded an adequate calibration range with good reproducibility and adequate sensitivity. The analysis of samples demonstrated the uses of this method in food analysis, the results however were sometimes different to independent methods and make further investigations into sample preparation and standard solutions necessary. In general, the method can be easily adapted to various applications by changing the sample carrier and the sensitivity can be adjusted by altering the injection volume.

This work was carried out within the ERASMUS exchange programme between the analytical groups of The University of Hull and TU-Wien.

REFERENCES

1 G. Pinkus, Ber. Deutsch. Chem. Ges., 31 (1898) 31.
2 M. Lever, Anal. Biochem., 47 (1972) 273.
3 M. Lever, Anal. Chim. Acta, 65 (1973) 311.
4 M. Lever, J.C. Powell, M. Killip and C.W. Small, J. Lab. Clin. Med., 82 (4) (1973) 649.
5 M. Lever, Biochem. Med., 7 (1973) 274.
6 B. Fingerhut, Clin. Chem., 19/9 (1976) 1022.
7 J.J. Ferraro, Clin. Chem., 22 (1976) 263.
8 M. Lever, Anal. Biochem., 81 (1977) 21.
9 M.J. Koziol, Anal. Chim. Acta, 128 (1981) 195.
10 M. Lever, T.A. Walmsley, R.S. Visser and S.J. Ryde, Anal. Biochem., 139 (1983) 205.
11 R.E. Davis, Tob. Sci., XX (1976) 146
12 J.D. Trent and S. Christiansen, J. Agric. Food Chem., 34 (1986) 1033.
13 K. Helrich (Ed.), Official Methods of Analysis, Vol. 2, AOAC, Arlington, 15th edn., 1990, 712, 741, 1013, 1016, 1017, 1018, 1285.

Analytica Chimica Acta, 285 (1994) 9–12
Elsevier Science B.V., Amsterdam

Flow-injection spectrophotometric determination of tetracycline antibiotics

R. Karlíček and P. Solich

Department of Analytical Chemistry, Faculty of Pharmacy, Charles University, 501 65 Hradec Králové (Czech Republic)

(Received 1st March 1993; revised manuscript received 11th August 1993)

Abstract

The determination of the tetracycline antibiotics doxycycline, oxytetracycline, rolitetracycline and tetracycline using a flow-injection method with spectrophotometric detection based on their reaction with 4-aminophenazone and hexacyanoferrate(III) is described. The flow-injection system was optimized using a modified simplex method and the results were compared with those from a univariate procedure of optimization. Under the optimized conditions, the determination of the tetracyclines in the ranges 1–20 and 20–250 mg l^{-1} with a relative standard deviation of $\leqslant 1\%$ for 10 and 100 mg l^{-1}, respectively ($n = 10$), and a sample throughput of 60–70 h^{-1} was achieved. The method was applied to the determination of tetracyclines in pharmaceutical preparations.

Keywords: Flow injection; UV–Visible spectrophotometry; Antibiotics; Tetracyclines

Tetracyclines and especially their semi-synthetic derivatives are antibiotics widely used in human and veterinary therapy. Biological assays, as described in many Pharmacopoeias [1–3], although giving an exact picture of the efficiency of individual tetracyclines, are tedious and time consuming. Therefore, various alternative instrumental methods for the determination of tetracyclines, e.g., using spectrophotometric [4,5], amperometric [6] and chemiluminescence [7] detection, most of them based on the flow-injection (FI) principle, have been reported. A liquid chromatographic method for the determination of traces of tetracyclines in mixtures has also been described [8].

In this paper, a sensitive FI method is described for the determination of four tetracyclines (doxycycline, oxytetracycline, rolitetracycline and tetracycline) based on the spectrophotometric detection of the coloured products formed by their reaction with 4-aminophenazone and hexacyanoferrate(III). The quinoneimine dye produced is measured at the absorbance maximum at 520 nm.

Correspondence to: R. Karlíček, Department of Analytical Chemistry, Faculty of Pharmacy, Charles University, 501 65 Hradec Králové (Czech Republic).

EXPERIMENTAL

Reagents

Pure standards of the tetracyclines doxycycline hydrochloride (DC), oxytetracycline hydrochloride (OC), rolitetracycline nitrate (RC) and tetracycline hydrochloride (TC) were kindly donated by the Research Institute of Antibiotics and Biotransformation, (Prague). Stock standard solutions were prepared by dissolving the tetracyclines in water to give concentrations of 200–500 mg l^{-1}. Working standard solutions were prepared by appropriate dilution of the stock stan-

SSDI 0003-2670(93)E0514-8

dard solutions to give final concentrations of 1–200 mg l^{-1}.

A buffer (pH 10.0) was prepared by mixing equal volumes of Na_2EDTA (0.2 mol l^{-1}) and sodium hydroxide (0.2 mol l^{-1}) solutions and adjusting the pH to 10.0 with sodium hydroxide solution (5 mol l^{-1}).

Reagent I was prepared by dissolving 4.1 g of 4-aminophenazone (Merck, Darmstadt) in 400 ml of water and mixing it with 500 ml of the buffer (pH 10.0) and 100 ml of a 1% solution of the non-ionogenic surfactant Brij 35. This reagent was stable for several weeks. Reagent II was prepared by dissolving 17.5 g of potassium hexacyanoferrate(III) in water, transferring it into a 1000-ml volumetric flask and diluting it to the mark. When stored in dark glassware at laboratory temperature, the solution was stable.

All other chemicals were of analytical-reagent grade (Lachema, Brno). Distilled, deionized water was used throughout for the preparation of solutions and as a carrier stream. All solutions were filtered through a 0.85-μm filter (Synpor, Prague) and degassed under reduced pressure.

Apparatus

The FI manifold is shown in Fig. 1. It consists of a commercial FIA-20 Analyser (ZD Pouchov, Hradec Králové, Czech Republic) which is linked to a Spekol 10 single wavelength photometer (Zeiss, Jena, Germany) equipped with a EKMi

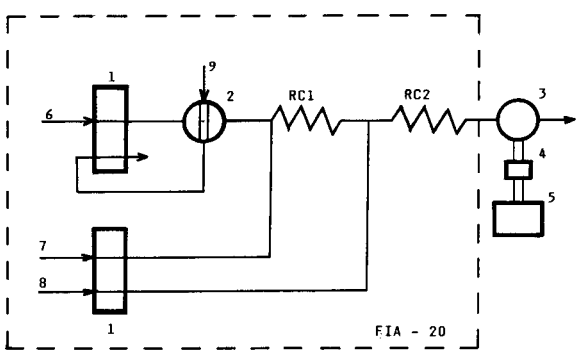

Fig. 1. Flow-injection manifold for determination of tetracyclines. 1 = Peristaltic pump; 2 = injection valve; 3 = flow cell; 4 = logarithmic converter; 5 = chart recorder; 6 = carrier; 7 = reagent I; 8 = reagent II; 9 = standards and samples; RC1, RC2 = reaction coils.

TABLE 1

Range of optimized variables studied

Variable	Range studied	
	Min.	Max.
Coil length I (cm)	30	400
Coil length II (cm)	30	400
Concentration of reagent I (mg per 10 ml)	2	50
Concentration of reagent II (mg per 10 ml)	2	200

accessory consisting of a flow-through cell of path length 10 mm (volume 18 μl) or 30 mm (volume 54 μl), a logarithmic converter (laboratory made) and a TZ 4600 chart recorder (Laboratorní Přístroje, Prague). All connections and reaction coils were made using 0.5 mm i.d. PTFE tubing.

Optimization procedure

For the simultaneous optimization of several mutually affected variables, the modified simplex method was used [9]. The calculation of individual variables was performed by a computer using a laboratory-produced program. On the basis of preliminary experiments, four variables of the flow system (length of coils I and II and concentration of the reagents I and II) were optimized simultaneously and the range studied was defined (Table 1). Five experiments were designed according to the procedure described previously [10] as the initial simplex. The peak height expressed in absorbance was chosen as the corresponding response function of the optimization. For these experiments, the temperature (laboratory), the sample volume (200 μl), flow-through cell path length (30 mm) and flow-rates of the carrier (0.67 ml min^{-1}) and of the reagents (0.54 ml min^{-1}) were kept constant. After adjusting the baseline absorbance to zero, a sample of doxytetracycline at a concentration of 10 mg l^{-1} was injected into the flowing stream and the absorbance of the quinoneimine dye formed was recorded at the wavelength of maximum absorbance of 520 nm. Each absorbance value was calculated as an average of seven peaks. When the limit values were exceeded, a zero value was selected for the absorbance.

RESULTS AND DISCUSSION

Optimization of flow-injection and chemical variables

The reaction between tetracyclines and 4-aminophenazone in the presence of hexacyanoferrate(III) as an oxidant is relatively slow. For the measurement in the flow system it is important to ensure that the necessary reaction time can be achieved by using a satisfactorily long reaction coil. Lengthening the reaction coil, however, increases the dispersion of the sample zone and therefore decreases the sensitivity of the method. The optimum values are thus a compromise.

The values of the four variables in the initial simplex were chosen so that they would be situated inside the range studied and they covered an area of 10–40% of the whole range of the variable optimized. In the initial simplex the maximum value of the response function (absorbance) was 0.2044. After 19 optimization experiments the maximum of the response function was established (experiment No. 14).

The optimized conditions for the determination of tetracyclines are shown in Table 2. With the optimum values of the variables the dispersion coefficient of the system was $D = 6.1$. This system was utilized for the determination of tetracyclines in the concentration range 1–20 mg l^{-1}. For the determination of tetracyclines at > 20 mg l^{-1}, a similar optimization procedure was performed using a sample volume of 50 μl, 250 mg l^{-1} doxytetracycline and a flow-through cell of path length 10 mm. The dispersion coefficient of this system was $D = 7.7$.

TABLE 2

Optimum values of variables for the determination of doxycycline (flow-rates: carrier 0.67 ml min^{-1}, reagents 0.54 ml min^{-1})

Variable	Determination of doxycycline [a]		
	Below 20 mg l^{-1};	Above 20 mg l^{-1}	
	S	S	U
Injected volume (μl)	200	50	50
Flow cell (mm)	30	10	10
Coil length I (cm)	293	134	50
Coil length II (cm)	270	190	100
Concentration of reagent I (g l^{-1})	4.2	1.8	1
Concentration of reagent II (g l^{-1})	17.6	5.2	4
Relative sensitivity	11	1	0.7

[a] S = simplex method; U = univariate method.

TABLE 3

Linear regression calibration parameters [a] of tetracyclines (c = 1–20 mg l^{-1})

Drug	a	b	r	R.S.D. (%) [b]
Doxycycline	0.03109	−0.0034	0.9998	0.52
Oxytetracycline	0.00796	−0.0079	0.9995	0.28
Rolitetracycline	0.00652	−0.0092	0.9996	0.89
Tetracycline	0.01044	−0.0090	0.9999	0.70

[a] $A = ac + b$, where A = absorbance, c = concentration (mg l^{-1}), a = slope and b = intercept, r = correlation coefficient and number of calibration points $n = 6$. [b] RSD = relative standard deviation for ten solutions, $c = 10$ mg l^{-1}.

Because of the mutual effects of chemical and flow-injection variables, it was not possible to achieve satisfactory results using only univariate method of optimization. This is clearly demonstrated in Table 2, where a univariate method was compared with the modified simplex method. Also twice as many experiments were carried out in the univariate method as for the modified simplex method. Therefore, the optimum conditions used for the determination of tetracyclines are those obtained by the modified simplex method.

Analytical application to doxycycline

The calibration equation was calculated from the peak-height absorbance (A) and was linear for doxycycline concentration (c) in the range 20–250 mg l^{-1}. The linear regression calibration equation was $A = 0.00282\ c + 0.0166$ with a correlation coefficient $r = 0.99988$. The results for the samples of 100 mg l^{-1} of doxycycline ($n = 10$) had a relative standard deviation (R.S.D.) of 0.59%. The sample throughput was 60–70 h^{-1}.

Determination of various tetracyclines

The calibration graph obtained under the optimized conditions for seven solutions of doxycy-

cline in the range 1–20 mg l^{-1} was also linear. Linear regression calibration parameters are given in Table 3. The same optimized conditions were used for the determination of oxytetracycline, rolitetracycline and tetracycline; their linear regression calibration parameters are also given in Table 3. From the different values of the slope it is clear that the difference in weight sensitivity for various tetracyclines depends not only on their molecular weights but also on their different reactivities arising from their different chemical structures. The limit of detection expressed as three–times the standard deviation of the blank is lowest for doxycycline (0.2 mg l^{-1}) and highest for rolitetracycline (0.5 mg l^{-1}).

In comparison with the method described previously [5], in which the determination of oxytetracycline was based on complexation with iron(III), the 4-aminophenazone method is at least 25 times more sensitive and four times faster. For the determination of tetracycline, the 4-aminophenazone method is about 20 times more sensitive than the chemiluminescence method [7] and attains approximately the same sensitivity as the amperometric method [6].

TABLE 4

Flow-injection determination of doxycycline in Deoxymykoin tablets (Spofa) using the standard addition method and an official UV spectrophotometric method [3]

Determination No.	Standard addition (mg)	Found [a]	
		mg	% [b]
1	–	98.2 ± 0.41	98.2
2	–	99.2 ± 0.25	99.2 [c]
3	10	109.4 ± 0.58	99.4
4	20	118.0 ± 0.54	98.3
5	30	128.4 ± 0.61	98.8

[a] Claimed content = 100 mg. [b] Mean ± S.D. for three samples, each injected in triplicate. [c] Determined by the official UV spectrophotometric method [3].

Determination of doxycycline in tablets

Each tablet was weighed and dissolved by stirring in 500 ml of water at the laboratory temperature. After the sedimentation of insoluble particles, the solution obtained by passing the sample solution through small membrane filter inserted at the end of the sample tubing of the injection valve was directly injected into the carrier. The results obtained by the FI method and compared with an official standard method [3] based on UV spectrophotometry are given in Table 4. The effect of compounds such as lactose, starch, glucose and gelatin, which can be found in typical pharmaceutical preparations containing tetracyclines, was investigated by using solutions similar to those used for reproducibility studies and the addition of various concentrations of interfering compounds. It was found that none of the excipients influenced the proposed determination.

REFERENCES

1 British Pharmacopoeia 1988, HM Stationery Office, London, 1988.
2 United States Pharmacopeia, 22nd Revision, US Pharmacopeial Convention, Rockville, MD 1990.
3 Pharmacopoeia Bohemoslovaca, 4th edn., Avicenum, Prague, 1987.
4 M. Ayad, M. El-Sadek and S. Mostaffa, Anal. Lett., 19 (1986) 2169.
5 A.A. Alwarthan, S.A. Al-Tamrah and S.M. Sultan, Analyst, 116 (1991) 183.
6 H. Ji and E. Wang, Analyst, 113 (1988) 1541.
7 A.A. Alwarthan and A. Townshend, Anal. Chim. Acta, 205 (1988) 261.
8 E.J. Mulders and D. Van de Lagemaat, J. Pharm. Biomed. Anal., 7 (1989) 1829.
9 S.L. Morgan and S.N. Deming, Anal. Chem., 46 (1974) 1170.
10 S.M. Sultan, F.O. Suliman, S.O. Duffuaa and I.I. Abu-Abdoun, Analyst, 117 (1992) 1179.

Analytica Chimica Acta, 285 (1994) 13–22
Elsevier Science B.V., Amsterdam

Time-resolved immunofluorometric assays for urinary luteinizing hormone and follicle stimulating hormone

James S. Kesner, Edwin A. Knecht and Edward F. Krieg, Jr.

Experimental Toxicology Branch and Statistics Activity, Division of Biomedical and Behavioral Science, National Institute for Occupational Safety and Health, 4676 Columbia Parkway, Mail Stop C-23, Cincinnati, OH 45226-1998 (USA)

(Received 18th August 1993; revised manuscript received 28th September 1993)

Abstract

The goal of this effort was to develop and validate non-radioisotopic immunoassays for measuring luteinizing hormone and follicle stimulating hormone in unextracted urine. Towards this goal, commercial time-resolved immunofluorometric assays (IFMAs) were modified. Validation demonstrated that the resultant assays were specific, sensitive, accurate, and precise. Urine matrix was shown not to interfere with the assay. Gonadotropin profiles generated using these assays conformed to those measured in urine and serum by other established immunoassays. These IFMAs afford the collective advantages of non-radioisotopic procedures and urine sample collection (convenience, noninvasiveness, integration of pulsatile secretion), plus the superior sensitivity and specificity of IFMAs. Applications include epidemiology and medicine.

Keywords: Fluorimetry; Epidemiology; Gonadotropins; Menstrual cycle; Two-site immunofluorimetric assay

Estimating endocrine secretion rates historically was performed by measuring biological activity in urine. This approach was virtually abandoned with the advent of radioimmunoassays (RIAs), which permitted the measurement of the low hormone concentrations that circulate in the blood [1]. Recently, however, measuring urinary analytes has been rediscovered as a convenient, non-invasive means to monitor endocrine status daily for epidemiological and clinical evaluations. Furthermore, urinary measurements provide an integral of the pulsatile secretion patterns characteristic of most hormones [2–6].

Time-resolved immunofluorometric assays (IFMAs) yield superior sensitivity and specificity relative to RIA and obviate the drawbacks inherent to radioisotopes [4,7–10]. The present report describes specific IFMAs for measuring urinary luteinizing hormone (LH) and follicle stimulating hormone (FSH).

Correspondence to: J.S. Kesner, Experimental Toxicology Branch, Division of Biomedical and Behavioral Science, National Institute for Occupational Safety and Health, 4676 Columbia Parkway, Mail Stop C-23, Cincinnati, OH 45226-1998 (USA).

SSDI 0003-2670(93)E0581-Q

MATERIALS AND METHODS

Subjects and samples

Urine samples were collected from healthy men and non-pregnant women for use in validation studies. First morning urine was collected daily by 10 women for a total of 19 menstrual cycles [2,3] for evaluation of urinary endocrine profiles. All aspects of the study protocol were reviewed and approved by the National Institute for Occupational Safety and Health Human Subject Review Board. All donating subjects provided signed consent.

Reagents

Two-site IFMAs (DELFIA®; Wallac Oy, Turku) described for measuring LH [1] (Cat. No. 1244-031) and FSH (Cat. No. 1244-017) in serum [7–9] were adapted and validated for measuring LH and FSH in urine. The capture antibody in both assays was coated onto the wells of polystyrene microtiter plates (Labsystems, Cat. No. 9502-107; Middlesex). The detection antibody was labeled with europium. Both LH monoclonal antibodies were directed against distinct epitopes on the specificity imparting β subunit. The FSH capture antibody binds to the β subunit and the detection antibody recognizes the α subunit. Cross-reactivity of these antibody combinations has been described previously [7,8].

Double demineralized water was used for all aspects of the assays. The wash solution and enhancement solution [2] have been described previously [7] and were supplied with the kits; we prepared the assay buffer as previously described [11] excluding Aramanth cherry red [3].

The FSH IFMA was calibrated against the World Health Organization Second International Reference Preparation of Human Pituitary FSH and LH for Bioassay (WHO FSH/LH IRP 78/549). The LH IFMA was calibrated against the WHO Second International Standard for LH, Pituitary (WHO LH IS 80/552). The WHO First International Standard for urinary human FSH and urinary human LH (WHO FSH/LH 1st IS 71/223) was donated by the National Institute for Biological Standards Control (UK) for validations.

[1] Note that the LH IFMA used herein does not cross-react significantly with human chorionic gonadotropin (hCG), in contrast to the DELFIA LH IFMA Cat No. 1244-006 that freely cross-reacts with hCG [9].

[2] The enhancement solution dissociates the europium atom from the antibody molecule, thereby enabling the europium to fluoresce with greater efficiency.

[3] One lot of assay buffer provided by the manufacturer yielded FSH levels that were 51.8% lower than historic values for the quality control urine pools; serum pool values were normal (2.8% lower). Assay buffer prepared in the laboratory yielded results equivalent to the "good" lots of the commercial assay buffer and was successfully used thereafter.

Assay procedure development

The assay procedure as previously described [12] exhibited intra-plate shift. To minimize this shift, studies were conducted to test variables including: sample pipetting time; pipetting order of sample and assay buffer; plate temperature (ambient or ice bath) while pipetting samples; and time of incubation of sample with capture antibody before adding detection antibody.

Briefly, the assay procedure, as modified based on these studies, was as follows: (1) plates were washed once; (2) 200 μl assay buffer, then 25 μl sample were pipetted into assay plates coated with capture antibody; (3) plates were incubated on a shaker (3 h for FSH; 60 min for LH); (4) plates were washed (thrice for FSH; once for LH); (5) 200 μl labeled antibody was added; (6) plates were again incubated on a shaker (30 min for FSH; 15 min for LH); (7) plates were washed (six times for FSH; four times for LH); (8) 200 μl enhancement solution was added; (9) plates were incubated for 5 min on a shaker, then 10 min off shaker; and (10) plates were counted. All procedures were conducted at 20–25°C. Plates were washed with wash buffer.

Assay validations

WHO FSH/LH 1st IS 71/223 was used to compare urinary FSH and LH standards with the kit pituitary standards. Relative potencies of the pituitary and urinary standards in these IFMAs were calculated by dividing each urinary concentration by the pituitary concentration which produced an equal number of counts. The ratios calculated for the five levels used in the standard curves were then averaged to provide mean relative potencies for FSH and LH respectively.

Analytical recovery was studied by adding WHO FSH/LH 1st IS 71/223 spikes to assay buffer or urine samples ($n = 4$ for FSH, $n = 3$ for LH) containing low or undetectable amounts of endogenous gonadotropin. Spikes were 2.63, 10.4, 42.0, and 176 mIU FSH/ml and 1.70, 7.08, 28.4, and 108 mIU LH/ml. Spikes were prepared in assay buffer and then added as 10% of the assay sample volume. Recovery was calculated as a percentage of the spiked assay buffer samples.

Curves generated from serially-diluted urine

samples were tested for parallelism against pituitary FSH and LH standard curves. Original gonadotropin concentrations in the urine samples used for these studies ranged from 26.3 to 134 mIU FSH/ml ($n = 3$) and 10.6 to 82.9 mIU LH/ml ($n = 4$). Samples were diluted 1 + 1 progressively with assay buffer.

The effects of urinary pH and osmolality on gonadotropin measures were determined. For the pH experiments, more urine samples were studied for FSH ($n = 11$) than for LH ($n = 3$) since initial studies suggested a non-significant trend for low pH to alter FSH estimates. Urine samples were adjusted to pH 3–4.5 using 12 M HCl and to pH 8–10 using 10 M NaOH. Urinary osmolality was augmented 500 and 1000 mOsm/kg using granular NaCl ($n = 5$). Unadjusted urine samples served as the baseline. Original pH for unadjusted samples ranged from 5.4–7.4 and osmolality ranged from 524–1023 mOsm/kg.

Precision was determined using five urine pools that span the range of the FSH and LH standard curves. Pools were measured in duplicate at the front and back of each of 2–7 micro-titer plates in 3–5 assays. Limits of detection were calculated as the smallest concentration of analyte for which there was 95% confidence of detection by the method [13], based on 11–14 assays.

LH and FSH were measured in urine samples containing 0.52 M glycerol [14] collected daily during 19 menstrual cycles. Values were divided by creatinine concentration [15]. LH, 1,3,5(10)-estratrien-3-ol-17-one glucosiduronate (estrone 3-glucuronide, $E_1$3G), and 5β-pregnane-3α,20α-diol 3-glucosiduronate (pregnanediol 3-glucuronide, Pd3G) had previously been measured in these samples by RIA [2]. Presence or absence of ovulation during these cycles was evaluated by transvaginal ultrasonography [2]. Correlation was calculated between LH values determined by IFMA and RIA [2].

Instrumentation

Instrumentation used to perform the IFMAs included a robotic sample processor (Tecan US Inc; Hillsborough, NC; Model RSP-8051-ID), a time-resolved fluorometer (Model 1232), plate washer (Cat. No. 1296-024), reagent dispenser and dispensing unit (Cat. Nos. 1296-041, 1296-043), and plate shaker (Cat. No. 1296-002) (Wallac Oy; Turku). The time-resolved fluorometer excites, then after a 400 μs delay, counts fluorescent activity in each microtiter plate well 1000 times for one second.

Statistical analyses

LH and FSH concentrations were calculated using a smoothed spline [16]. Analysis of variance (ANOVA) was used to analyze the time-course of intra-plate shift. ANOVA for repeated measures was used to analyze effects of pH and osmolality, recovery of mass, and assay modifications. Contrasts were performed in the case of significant main effects or interactions. Linear regression analysis was used to compare values obtained by IFMA vs. RIA and to test parallelism between curves generated from hormone preparations and samples [17]. Variance components were estimated using a mixed model ANOVA. Coefficients of variation were calculated using the estimated variance components and the urine pool means. Precision about the mean is expressed in the text as ± standard errors.

RESULTS

Assay procedure development

Using the IFMA kit manufacturer's procedures yielded a downward shift in urinary LH

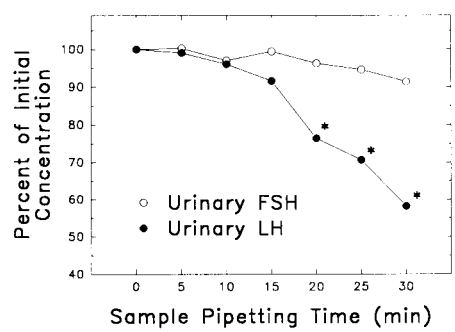

Fig. 1. Time-course of intra-plate drift for urinary gonadotropin concentrations. A urine pool was pipetted in duplicate at 5-min intervals. * Indicates LH values that are less than initial concentration ($P < 0.0003$). FSH levels did not decrease over the 30-min period ($P = 0.33$).

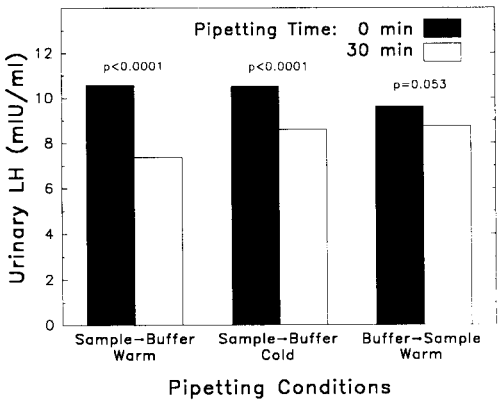

Fig. 2. Effect of pipetting conditions on intra-plate drift for urinary LH levels. Samples were pipetted into the micro-titer plates before (Sample → Buffer) or after (Buffer → Sample) the assay buffer. During pipetting, plates sat on the counter top at ambient temperature (Warm) or on ice (Cold). Statistical interaction of shift by pipetting conditions; $P = 0.029$. P Values for contrasts are depicted. Means represent three incubation times (45, 90 and 360 min) for 3 urine pools pipetted in duplicate at 0 and 30 min. Urine pools spanned the standard curve range.

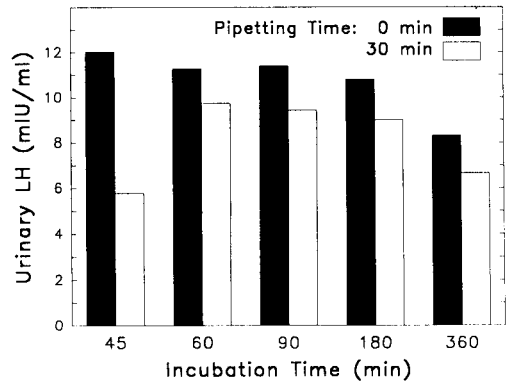

Fig. 3. Effect of incubation time (samples with capture antibody) on intra-plate drift for urinary LH levels. Samples were pipetted into the micro-titer plates immediately before the assay buffer at room temperature. Shift-by-incubation time interaction; $P = 0.34$. 60 min incubation was selected based on the smallest shift. Values represent means for 3 quality control urine pools pipetted in duplicate at 0 and 30 min. Urine pools spanned the range of the standard curve.

TABLE 1

Precision of IFMAs for FSH and LH [a]

	Mean mIU/ml	C.V. (%) [b]			
		Between assay	Within assay		
			Plate	Repl.	Total
Urine pools, FSH					
Normal	8.82	4.2	1.4	4.5	4.9
Postmenopausal	39.9	7.2	3.1	3.4	4.6
Low-spike [c]	2.48	4.1	3.5	4.2	5.5
Medium-spike	15.8	6.3	2.4	3.1	4.0
High-spike	127.0	4.0	2.6	3.2	4.8
Mean		5.2	2.6	3.7	4.8
Urine Pools, LH					
Normal	7.69	4.5	2.1	3.9	4.5
Postmenopausal	39.3	8.8	4.9	3.1	5.8
Low-spike	1.61	8.4	5.4	7.7	9.7
Medium-spike	12.1	7.1	0.4	4.7	4.9
High-spike	110.0	4.7	0.0	5.0	6.4
Mean		6.7	2.6	4.9	6.3

[a] IFMA = Immunofluorometric assay; FSH = follicle stimulating hormone; LH = luteinizing hormone. [b] Coefficients of variation (C.V.s) represent variation among assays, plates, and replicates (Repl.). Within-assay C.V. is the sum of variation due to plates, replicates and the interactions of assay and plate with front-to-back within-plate variation. Note that C.V.s are not additive. Values represent duplicate determinations for pools positioned at the front and back of each of 2–7 microtiter plates in 3–5 assays. [c] Urine pools spiked with World Health Organization First International Standard for urinary human FSH and urinary human LH, 71/223.

concentrations across the micro-titer plate as a function of sample pipetting time ($P = 0.0001$); this drift was significant by 20 min ($P = 0.0003$; Fig. 1). Drift was not observed over a 30-min interval for FSH ($P = 0.33$). LH drift was substantial ($P < 0.0001$) when sample was pipetted before assay buffer, but marginal ($P = 0.053$) when buffer was pipetted before sample (Fig. 2). Although there was not a significant statistical interaction between shift and the incubation time for sample with capture antibody ($P = 0.34$; Fig. 3), the 60-min incubation was selected based on the smallest shift.

Based on these results, the LH IFMA procedure was modified to: (1) minimize the time required to pipette samples into a single plate by using a robotic sample processor; (2) add assay buffer before the sample; and (3) increase the incubation time to 60 min. Modifications 1 and 2 were also incorporated into the FSH IFMA procedure.

Assay validations

IFMA standard curves, plotted as log counts vs. log standard concentrations, were linear from 0.25 to 256 mIU FSH/ml and 0.6 to 250 mIU

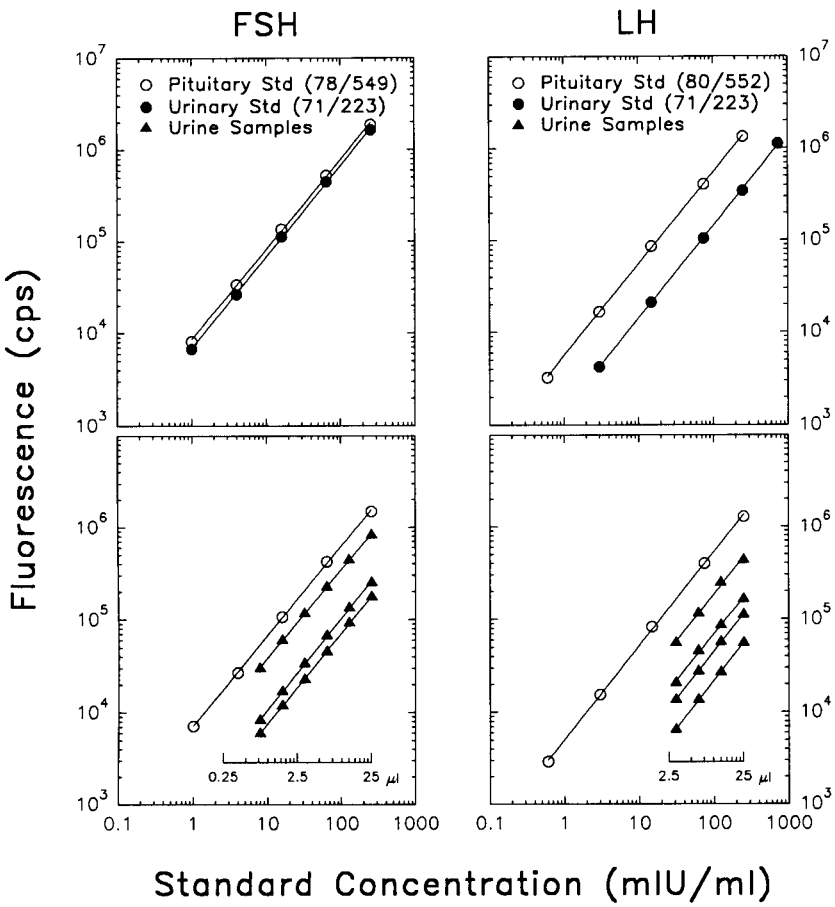

Fig. 4. Parallelism between standard curves derived from pituitary and urinary references (top panels) and between pituitary standard curves and serially-diluted urine samples (bottom panels) for the FSH and LH IFMAs. Pituitary FSH and LH references were from the DELFIA kits and calibrated by the manufacturer against WHO FSH/LH IRP 78/549 and WHO LH IS 80/552, respectively. Urinary reference was WHO FSH/LH 1st IS 71/223. Standard concentrations were based on bioactivities of the reference preparations as reported by WHO. Standards and urine samples were diluted with assay buffer.

LH/ml. Slopes of standard curves generated from pituitary and urinary references (Fig. 4) were not different from each other for FSH (0.98 ± 0.01 vs. 1.00 ± 0.01; $P = 0.43$) or LH (1.00 ± 0.01 vs. 1.01 ± 0.01; $P = 0.48$). Pituitary FSH and LH references, respectively, were 1.2 and 3.9 times more potent than the urinary references.

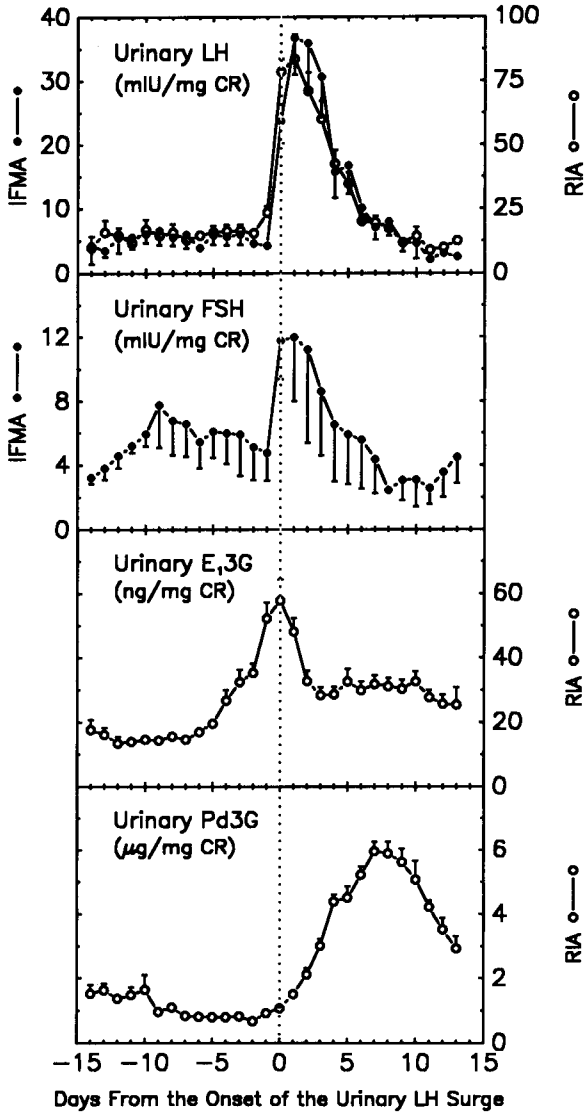

Fig. 5. Urinary endocrine profiles during normal ovulatory menstrual cycles. Values are means ± S.E. for 13 cycles from seven women. FSH values for one cycle were omitted because early follicular phase levels exceeded 40 mIU/mg CR; this cycle did exhibit an FSH surge coincident with the LH surge. FSH and LH were measured by IFMA (•); LH, $E_1$3G, and Pd3G were measured by RIA (○). The ordinate scales for LH IFMA and RIA are different.

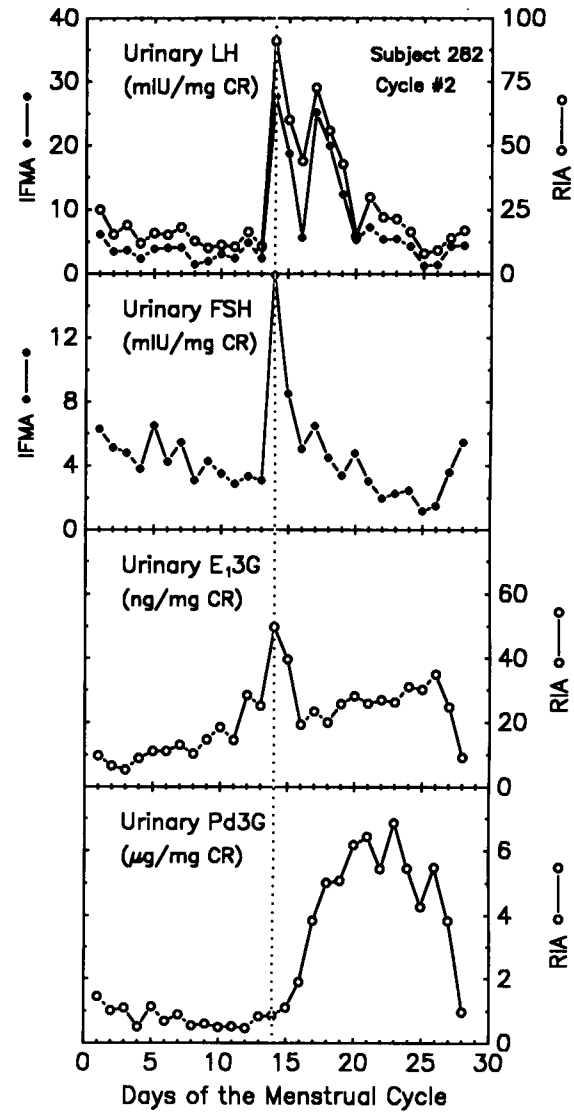

Fig. 6. Urinary endocrine profiles during a single ovulatory cycle. FSH and LH were measured by IFMA (•); LH, $E_1$3G, and Pd3G were measured by RIA (○). Note the correlation between LH values measured by IFMA and RIA, and the concomitance between the FSH and LH surges. A bimodal LH surge was occasionally detected. The ordinate scales for LH IFMA and RIA are different.

Mean recoveries of added urinary gonadotropin were 96.4 ± 1.5% for FSH and 98.1 ±

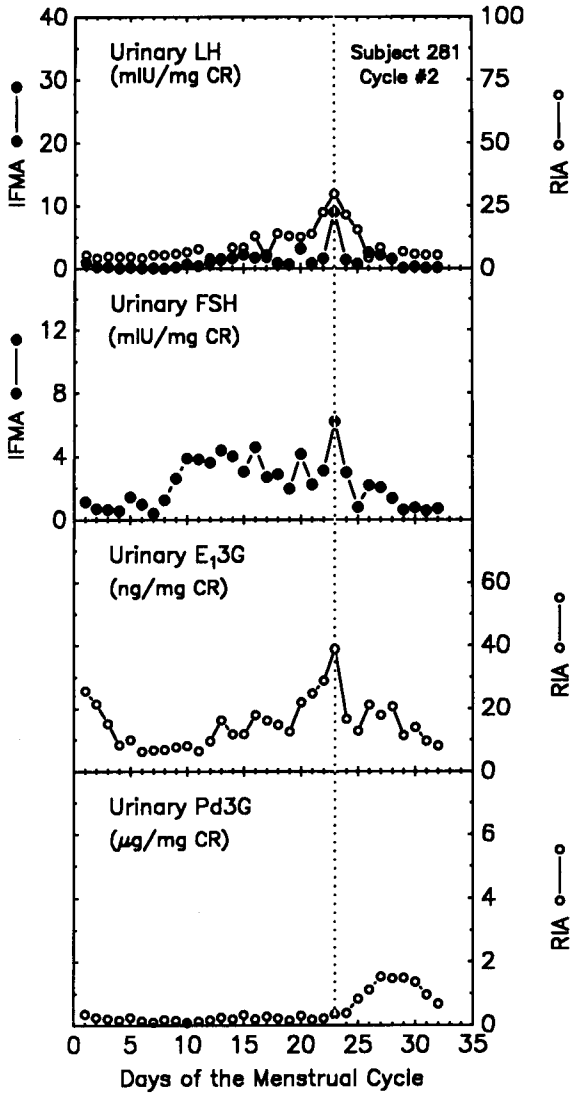

Fig. 7. Urinary endocrine profiles during a single cycle. The short luteal phase and low progestin levels are consistent with luteal phase deficiency. FSH and LH were measured by IFMA (•); LH, $E_1$3G, and Pd3G were measured by RIA (○). The ordinate scales for LH IFMA and RIA are different.

1.3% for LH and were not different from 100% ($P = 0.098$, $P = 0.29$, respectively). Recovery did not vary between levels of spikes ($P \geqslant 0.22$).

Serial-dilution curves for standards and urine samples were parallel for FSH (slope = 0.97 ± 0.01 vs. 0.96 ± 0.01; $P = 0.74$) and LH (slope = 1.01 ± 0.01 vs. 1.00 ± 0.03; $P = 0.80$) (Fig. 4).

Adjusting pH to, or beyond, the limits of the normal physiological range did not alter urinary FSH ($P = 0.18$) or LH ($P = 0.16$) values. Original pH levels ranged from 5.4 to 7.4. Similarly, urinary FSH and LH concentrations were not affected by increasing osmolality 500 and 1000 mOsm/kg (FSH $P = 0.19$; LH $P = 0.66$). Origi-

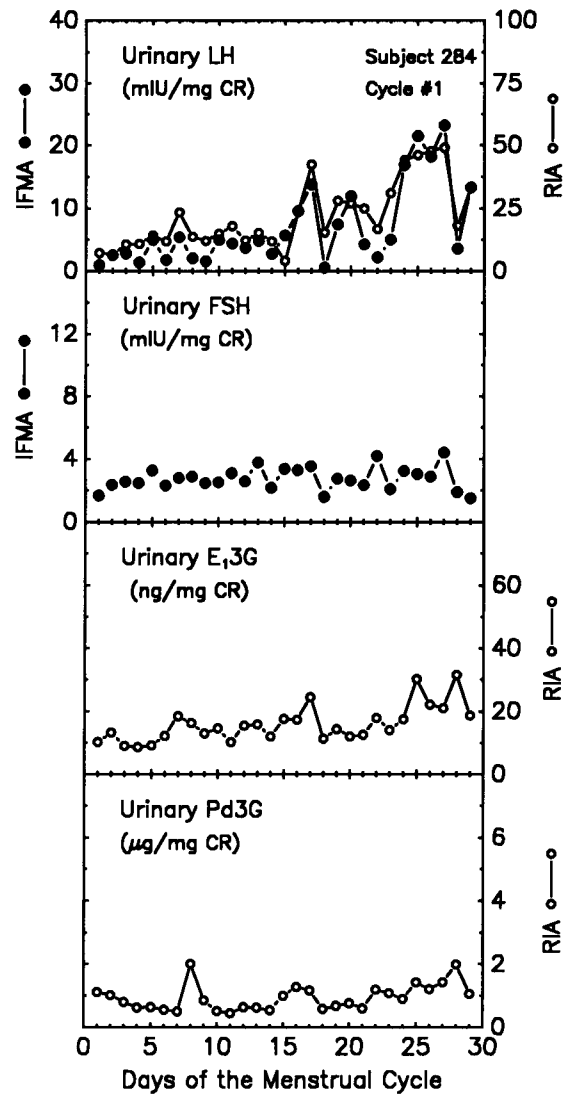

Fig. 8. Urinary endocrine profiles during a single cycle. The absence of LH and FSH surges and $E_1$3G and Pd3G elevations indicates that this cycle was anovulatory. FSH and LH were measured by IFMA (•); LH, $E_1$3G, and Pd3G were measured by RIA (○). The ordinate scales for LH IFMA and RIA are different.

nal osmolality levels ranged from 524 to 1023 mOsm/kg.

Measures of precision are presented in Table 1. After modifying the IFMA procedures, intra-plate drift was absent for the five quality control urine pools for both LH ($P \geqslant 0.14$) and FSH ($P \geqslant 0.88$). The limits of detection for the urinary FSH and LH IFMAs were 0.11 and 0.19 mIU/ml, respectively.

Of the 19 menstrual cycles characterized, 13 were normal ovulatory cycles and 6 were atypical. Figure 5 depicts the mean profiles of urinary LH and FSH measured by IFMA during the normal cycles plus urinary LH, $E_1$3G and Pd3G measured by RIA. Basal LH levels surged abruptly coincident with the peak of the $E_1$3G peak and initiation of the increase of Pd3G. FSH levels were elevated at the beginning of the follicular phase and decreased until the emergence of the preovulatory surge. (Graphic depiction of rising FSH levels during the first 6 days of the cycle is an artifact caused by relatively high FSH values from cycles with short follicular phases.)

Urinary endocrine data for individual cycles are consistent with normal ovulation (Fig. 6; bimodal LH surges were occasionally detected), luteal phase deficiency (Fig. 7), and anovulation (Fig. 8). LH concentrations measured by IFMA were regressed on those measured by RIA using data from 13 normal and 6 atypical menstrual cycles (partial $r = 0.87$; slope = 0.45; $P < 0.0001$).

DISCUSSION

There is a growing need for convenient, noninvasive methods to evaluate menstrual function. One application is epidemiological evaluation of female populations exposed, for instance, to toxicants or other hazards in the environment or workplace [2–5,18]. Another is monitoring daily progress of the menstrual cycle in clinical settings, for instance to support in vitro fertilization and gamete intra-fallopian transfer [19].

The present report describes IFMAs that were modified and validated for measuring urinary FSH and LH. These assays are precise, accurate, sensitive, specific, and are not biased by urine matrix or extreme pH or osmolality. Modifications incorporated to eliminate drift across assay plates included using a robotic sample processor, which reduces pipetting time for a single plate from 15–30 min by hand to 3–6 min by robot.

An issue paramount to measuring urinary gonadotropins is validating the reference preparation to be used for standardization [20–22]. The IFMA assays described herein employ standards of pituitary origin; our goal, however, is to measure urinary gonadotropins. We demonstrated parallelism between the linear curves derived from pituitary and urinary preparations, for both FSH and LH. So while the urinary preparations were less potent than those from pituitaries, the difference in calibration was constant across the standard curve. WHO urinary and pituitary preparations calibrated on the basis of bioactivity were used in this study [23–25].

The preovulatory LH surges described here and elsewhere [2,4], measured by IFMA and RIA, are of greater duration than those measured in the circulation [26]. The DELFIA LH kit insert depicts this same phenomenon – brief LH surges in serum and prolonged LH surges in urine – indicating that this dichotomy is demonstrable within the same assay.

Some assays fail to detect LH surges in all ovulatory cycles [27]. An assay, such as the IFMA described in this report, which measures a prolonged preovulatory LH surge has clear advantage in detecting this event essential to reproduction.

Explanations for this dichotomy of surge duration are rather elusive. One possibility is that gonadotropins filtrate through the glomerulus, reabsorb into the proximal tubule [28], accumulate in the proximal convoluted tubules, and may then be secreted back into the urine during subsequent days [29]. Conceivably, through this circuitous renal pathway, gonadotropins could be slowly released into the urine for days after having been cleared from the circulation.

LH concentrations measured by the IFMA were lower than those measured by the RIA. This difference does not appear to be due to calibration, since both assays appear accurately calibrated to the WHO LH IS 80/552 [data

herein, 20]. Rather, this difference most likely reflects the greater specificity imparted by the two-site monoclonal immunometric assay compared to the competitive polyclonal immunoassay [30–32].

The many epitopes on FSH and LH and the range of sites recognized by different antibodies or antisera make it difficult or impossible to attribute accuracy, in a classical sense, to immunoassays that measure these types of complex antigens, even after conducting conventional validation tests [16,17]. This is exemplified by proficiency program surveys [4] which index analyte values according to the specific assays. Indeed values across assays may vary by 20-fold.

Thus, assays should be validated against a standard preparation that matches the sample as closely as possible. For our studies, we determined that a urinary gonadotropin preparation (WHO FSH/LH 1st IS 71/223) was recognized in a manner parallel to the pituitary reference *and* with approximately proportional potency relative to those determined by bioassay [23–25].

Despite differences in absolute values, the correlation between the profiles generated by the two LH assays is remarkable (Figs. 5–8). Others [31,32] have demonstrated that serum LH bioactivity correlates better with values measured by two-site immunometric assays than with RIA, especially during physiological and clinical conditions during which LH levels are low. Whether this relationship is also true for LH measured in urine remains to be determined. The superior sensitivity of these IFMAs, relative to other immunoassays, enhances the ability to measure low gonadotropin levels in dilute urine samples.

The urinary FSH profiles conform to those previously described in serum. Levels were high at the early stages of the follicular phase and decreased as the phase progressed [26]. A preovulatory FSH surge was generally, but not always, discernable and attendant to the LH surge.

In summary, time-resolved immunofluorometric assays were validated for measuring urinary FSH and LH. These non-radioisotopic assays afford advantages for epidemiological or clinical application inherent to urine sample collection (convenience, noninvasiveness, integration of pulsatile secretion) and the superior sensitivity and specificity of IFMAs.

[4] The Interlaboratory Comparison Program, College of American Pathologists, Northfield, IL; and The Bio-Rad Quality Control Program, Bio-Rad Labs., Anaheim, CA.

The authors acknowledge Ms. Catherine M. Miller for her technical assistance, Mr. Dennis W. Lynch for his critical review of the manuscript, and Dr. Patrick Storring, National Institute for Biological Standards and Control, Hertfordshire, England, for his generous donation of WHO gonadotropin references. Mention of a tradename, proprietary product, or specific equipment in this article does not constitute an endorsement, guarantee, or warranty by the National Institute for Occupational Safety and Health.

REFERENCES

1 J.A. Loraine and E.T. Bell, Hormone Assays and their Clinical Application, Churchill Livingstone, Edinburgh, 4th edn., 1976.
2 J.S. Kesner, D.M. Wright, S.M. Schrader, N.W. Chin and E.F. Krieg Jr., Reprod. Toxicol., 6 (1992) 385.
3 D.M. Wright, J.S. Kesner, S.M. Schrader, N.W. Chin, V.E. Wells and E.F. Krieg Jr., Reprod. Toxicol., 6 (1992) 401.
4 J.S. Kesner, E.F. Krieg Jr, E.A. Knecht and D.M. Wright, Scand. J. Work Environ. Health, 18(Suppl 2) (1992) 33.
5 D.D. Baird, C.R. Weinberg, A.J. Wilcox, D.R. McConnaughey, P.I. Musey and D.C. Collins, J. Clin. Endocrinol. Metab., 72 (1991) 793.
6 H. Landy, A.L. Schneyer, R.W. Whitcomb and W.F. Crowley Jr., Clin. Chem., 36 (1990) 340.
7 K.S.I. Pettersson and J.R.-M. Söderholm, Clin. Chem., 36 (1990) 1928.
8 T. Jaakkola, Y.-Q. Ding, P. Kellokumpu-Lehtinen, R. Valavaara, H. Martikainen, J. Tapanainen, L. Rönnberg and I. Huhtaniemi, J. Clin. Endocrinol. Metab., 70 (1990) 1496.
9 F.C.W. Wu, G.E. Butler, C.J.H. Kelnar, H.F. Stirling and I. Huhtaniemi, J. Clin. Endocrinol. Metab., 72 (1991) 1229.
10 J.S. Kesner, E.A. Knecht, E.F. Krieg, Jr, G. Barnard, H.J. Mikola, F. Kohen, M.M. Gani and J. Coley, Steroids, 58 (1994) in press.
11 T. Lövgren, I. Hemmilä, K. Pettersson, J.U. Eskola and E. Bertoft, Talanta, 31 (1984) 909.
12 A.-M. Haavisto, L. Dunkel, K. Pettersson and I. Huhtaniemi, Pediatr. Res., 27 (1990) 211.
13 R. Caulcutt and R. Boddy, Satistics for Analytical Chemists, Chapman and Hall, New York, 1983, pp. 201–205.

14 J.H. Livesey, H.K. Roud, M.G. Metcalf and R.A. Donald, J. Endocrinol., 98 (1983) 381.
15 H.H. Taussky, J. Biol. Chem., 208 (1954) 853.
16 A. DeLean, P.J. Munson and D. Rodbard, Am. J. Physiol., 235 (1978) E97.
17 D. Rodbard, P.J. Munson and A. DeLean, Improved curve-fitting, parallelism testing, characterization of sensitivity and specificity, validation, and optimization for radioligand assays, in Radioimmunoassay and Related Procedures in Medicine (International Atomic Energy Agency, Vienna), Vol. 1, UNipub, New York, 1978, pp. 469–504.
18 C.L. Hughes Jr., Reprod. Toxicol., 2 (1988) 163.
19 C.L. Hughes Jr., W.C. Dodson, D.K. Walmer and S.B. Dixon, J. Reprod. Med., 35 (1990) 211.
20 I. Vermes, H.A. Bonte, G. van der Sluijs-Veer and J. Schoemaker, Clin. Chem., 37 (1991) 415.
21 S. Chappel, J. Clin. Endocrinol. Metab., 70 (1990) 1494.
22 R.L. Rosenfield and J. Helke, J. Androl., 13 (1992) 1.
23 P.L. Storring, H. Dixon and D.R. Bangham, Acta Endocrinol., 83 (1976) 700.
24 P.L. Storring and R.E. Gaines Das, J. Endocrinol., 123 (1989) 275.
25 P.L. Storring, Scand. J. Clin. Lab. Invest., 49 (Suppl 193) (1989) 34.
26 E.A. Lenton, R. Sulaiman, O. Sobowale and I.D. Cooke, J. Reprod. Fertil., 65 (1982) 131.
27 A.J. Wilcox, D.D. Baird, C.R. Wienberg, E.G. Armstrong, P.I. Musey, R.E. Wehmann and R.E. Canfield, Environ. Health Perspect., 75 (1987) 29.
28 I.Z. Beitins, A. Shah, K. O'Loughlin, L. Johnson, T.R. Ostrea, J. Van Wart and J.W. McArthur, J. Clin. Endocrinol. Metab., 51 (1980) 26.
29 B.C. Nisula, D.L. Blithe, A. Akar, G. Lefort and R.E. Wehmann, J. Steroid Biochem., 33 (1989) 733.
30 K.S.I. Pettersson and J.R.-M. Söderholm, Clin. Chem., 37 (1991) 333.
31 I. Huhtaniemi, Y.-Q. Ding, R. Tähtelä and M. Välimäki, J. Clin. Endocrinol. Metab., 75 (1992) 1442.
32 E.C. Ditkoff, J.H. Levin, W.L. Paul and R.A. Lobo, Fertil. Steril., 59 (1993) 305.

Analytica Chimica Acta, 285 (1994) 23–31
Elsevier Science B.V., Amsterdam

Simplex optimization of the plasma parameters and ion optics of an inductively coupled mass spectrometer with pure argon and doped argon plasmas, using a multi-element figure of merit

Michael J. Ford, Les Ebdon, Robert C. Hutton [a] and Steve J. Hill

Plymouth Analytical Chemistry Research Unit, Department of Environmental Sciences, University of Plymouth, Drake Circus, Plymouth, Devon PL4 8AA (UK)

(Received 11th May 1993; revised manuscript received 15th September 1993)

Abstract

A simplex procedure has been successfully applied to the optimization of both the plasma parameters and the ion optics of a commercial inductively coupled plasma mass spectrometry (ICP-MS) instrument for the maximization of SBRs for pneumatic nebulization. The objective function for the simplex was based on the signal to background ratios (SBRs) of 10 elements across the mass range with varying ionization efficiencies, to account for the various influences on ion transmission. This procedure has been applied to pure argon and molecular gas-doped-argon plasmas, to investigate the possible use of molecular gases as sensitivity enhancers. The simplex procedure successfully identified optimal operating conditions for maximum SBRs across the mass range, for the all argon and mixed gas plasmas. It was found, that simple manual tuning on the gross signal of a mid mass element did not result in a significant drop in SBRs and detection limits, compared to the simplex optimized conditions. Rigorous optimization of ICP-MS using pneumatic nebulization and the addition of molecular gases to the ICP, did not result in any significant improvements in SBRs and detection limits, when compared to the all argon system.

Keywords: Inductively coupled plasma MS; Ion optics; Simplex optimization; Multi-element figure of merit; Plasmas

Inductively coupled plasma mass spectrometry (ICP-MS) is now widely accepted as the leading analytical method available for trace- and ultra-trace elemental determinations. The use of a quadrupole mass spectrometer allows for the quasi-simultaneous determination of elements across the mass range, and it is this multi-element capability that makes ICP-MS attractive over techniques with comparable sensitivity, such as graphite furnace atomic absorption spectrometry.

Correspondence to: S.J. Hill at the above address.
[a] Present address: Fisons Instruments Elemental, Ion Path, Road Three, Winsford, Cheshire (UK).

Absolute sensitivity in ICP-MS is controlled by the generation of ions in the plasma and the sampling and transmission of these ions through the interface region, ion optics into the mass analyzer and finally to the detector. This generation of ions is linked for example to the plasma power, nebulizer gas flow and the extraction and transmission of the ions is linked to the ion optic settings, all of which have to be optimized to achieve the maximum signal to background ratios (SBRs).

The optimization of these various conditions is typically performed using a single element, often indium, and this single element optimization has

SSDI 0003-2670(93)E0551-H

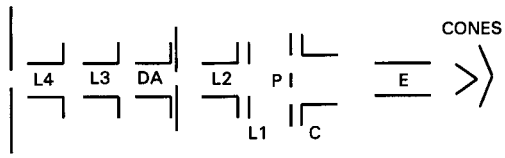

Fig. 1. Schematic diagram of the ion optics system in the VG plasmaquad, where: E = extraction lens; P = photon stop; C = collector lens; L1–L4 = lenses; DA = differential apperture.

often been considered to be disadvantageous to the application of ICP-MS in the multi element mode of operation, being detrimental to the response of elements at the extremes of the mass range. In addition to this, optimization is usually performed as a series of cyclical univariate optimizations and this relies on a skilled operator to achieve maximum signal.

The key plasma operating parameters, with regard to sensitivity, are the nebulizer (carrier) gas flow and the forward power applied to the plasma. The nebulizer gas has been shown to define very sharp optima for all analyte elements, e.g. [1,2] and this reflects the role of the nebulizer gas in altering the region of maximum ion population, the normal analytical zone (NAZ) of the plasma. The rate of the nebulizer gas flow also effects the size of the random background under the analyte peaks. The forward power effects the position of the NAZ as well as the ionization temperature of the plasma, both of which influence analyte and background responses. Once generated the ions are sampled through a two stage interface before entering the ion optics, which are essentially a series of electrostatic lenses. On the spectrometer used in this laboratory (VG Plasmaquad), there are six lenses as well as a photon stop (to prevent excessive continuum background from high energy photons) and a differential aperture. This is illustrated in Fig. 1. The optimization of the ion beam is again a complex process involving all of the lens settings acting in an interrelated manner, in addition to the interaction of the plasma settings prior to extraction. To further complicate the issue of sensitivity in ICP-MS recent reports have shown that the addition of a molecular gas to the plasma can be used to bring about an increase in SBRs [3–6]. [a] These reports add a further element to the already complex optimization procedure that has to be employed. None of the reports on molecular gases which show such enhancements used a rigorous optimization routine such as simplex optimization.

There is obviously a need for the optimization of these variables to be performed using a method that accounts for their inter-dependence. simplex optimization is an obvious choice for this and has been employed already in ICP-AES to improve detection limits and reduce interferences [11,12], in ICP-MS to reduce interferences [13–15], and aid organics analysis [16]. All of these studies optimized the plasma operating conditions, with, where appropriate, manual tuning of the lens settings after each iteration. To date few reports have used simplex, or comparable multivariate methods, to optimize the ion optics. Schmit and Chauvette [17] successfully optimized the ion optics of their instrument (Sciex Elan) to improve ion transmission across the mass range, and Evans and Caruso [18] have used the same approach to reduce the effects of a 10 000 μg cm^{-3} U matrix solution.

In this paper we aim to demonstrate the use of the simplex approach to the optimization of both the plasma operating parameters and the ion optics to achieve maximum analyte SBRs. This has been done to optimize fully the whole interactive process of ion formation, extraction and transmission. In addition to these experiments on the all argon system work has been undertaken to look at mixed gas plasmas and their use as sensitivity enhancers, using this rigorous optimization procedure to discover whether enhancements exist and are reproducible.

EXPERIMENTAL

Instrumentation

The instrument used was an inductively coupled plasma mass spectrometer (PQ2, V.G. Elemental, Winsford). The sample introduction sys-

[a] Other papers [7–10] report suppression with mixed gas plasmas.

TABLE 1

Boundary and start conditions and step size used for the simplex optimizations

Parameter	Lower boundary	Upper boundary	Step size	Start conditions
Nebulizer gas (dm^3 min^{-1})	0.5	1.5	0.3	1.0
Power (W)	1200	1800	150	1500
Nitrogen (percentage (v/v))	0.0	8.0	2.0	0.0
Hydrogen (percentage (v/v))	0.0	8.0	2.0	0.0
Methane (percentage (v/v))	0.0	1.0	0.3	0.0
Extraction [a]	0.00	5.00	1.5	1.0
Collector [a]	0.00	10.0	1.5	7.7
Lens 1 [a]	0.00	10.0	1.5	7.7
Lens 3 [a]	0.00	10.0	1.5	5.0

[a] These values refer to lens digipot settings, which are directly related to the voltage of each lens element. See text for details.

tem included a modified high solids nebulizer (Ebdon type, PS Analytical, Sevenoaks) which allowed higher nebulizer gas flows than the standard high solids nebulizer. Gas addition to the nebulizer gas was achieved using a gas blender (Series 850, Signal, Standards House, Camberley). Sampler and skimmer cones were the standard nickel cones supplied by VG Elemental, having orifice diameters of 1.0 and 0.7 mm respectively. Sample uptake rate was 1.0 cm^3 min^{-1} and spray chamber temperature was approximately 18–20°C. With the VG instrument the settings of the six lenses as well as the pole bias, which controls the quadrupole, are controlled by a series of digipots, which read incremantally from 0.00–10.0. These settings relate to voltage applied to the lenses, which fall within the following ranges: extraction −100 V to −1000 V; collector and L1–L4 −150 V to + 150 V and pole bias −30 V to + 30 V.

Materials and chemicals

Standard solutions were prepared from 1000 μg cm^{-3} stock solutions of Au, Bi, Li and Te (Merck, Poole), Be, Co, and In (Aldrich, Milwaukee, WI) and Rb, Tb and U (prepared from RbCl, Tb_2O_3, $UO_2(NO_3)_2 \cdot 6H_2O$ respectively obtained form Merck) diluted to a final concentration of 100 ng cm^{-3}. Blank solutions were prepared to match the standard solutions, being 2% nitric acid solutions (Aristar grade, Merck) made with de-ionized, distilled water. Blank solutions also contained 100 ng cm^{-3} Ce as a marker to ensure the blank solution was being analyzed and was stable.

Simplex optimization

A variable step size simplex optimization procedure was applied to the optimization of the nebulizer gas flow rate, forward power, added gas (if used), extraction, collector, L1 and L3 lenses, for maximum SBR using a multi-element figure of merit discussed below. The other operating and ion optic parameters have little influence on the SBR so were excluded from the simplex optimization to save time. The boundary conditions, step size and start conditions of the simplex variables are given in Table 1, and the settings of the other variables are given in Table 2. Boundary conditions, particularly for the lens elements, were set wide to allow a large factor space to be investigated. The extraction lens was assigned an upper boundary below its working maximum, as it is known that at high extraction lens settings, secondary discharges can occur in the interface.

TABLE 2

Settings for operating parameters not included in simplex optimization

Parameter	Setting
Coolant gas (dm^3 min^{-1})	15.0
Auxiliary gas (dm^3 min^{-1})	1.0
Lens 2 [a]	3.8
Lens 4 [a]	1.5
Pole bias [a]	8.0

[a] Digipot settings.

TABLE 3

Elements used in simplex optimization

Element	Mass	First ionization potential (eV)
Li	7	5.39
Be	9	9.32
Co	59	7.86
Rb	85	4.18
In	115	5.79
Te	130	9.01
Tb	159	5.98
Au	197	9.22
Bi	209	7.42
U	238	6.08

Start conditions for the lenses were set according to defaults given by the manufacturer. The optimization was deemed to have run to completeness when $n + 1$ (i.e., 7 or 8) vertices agreed to within 5%. On completion of the procedure the defined optimum conditions were tested by the use of univariate searches, in which each of the optimized variables were varied in turn whilst the others were held at the defined optimum.

TABLE 4

Example of sensitivity of simplex figure of merit to changes in analyte SBR

Element [a]	Decrease SBR		Original FoM	Increase SBR	
	10×	2×		2×	10×
Be	18.15	29.39	33.17	36.09	39.72
Au	20.45	30.24	33.17	35.27	37.86
Bi	23.67	31.25	33.17	34.45	35.96
U	28.35	32.31	33.17	33.70	34.31

[a] in order of increasing response.

The figure of merit (FoM), that was used in this experiment was based on the SBRs of ten elements across the mass range, which had a range of first ionization potentials, shown in Table

TABLE 5

Simplex optimal conditions for maximum signal to background ratios for a range of elements using all argon and nebulizer gas addition mixed gas plasmas. Also shown are conditions obtained by tuning on ^{140}Ce

Parameter	All argon [a] plasma (1)	All argon plasma (2)	nitrogen/argon plasma	Hydrogen/argon plasma	Methane/argon plasma
Nebulizer gas (l min^{-1})	1.09	1.01	1.00	1.18	1.075
Power (W)	1518	1500	1495	1475	1569
Percentage added gas (v/v)	–	–	0.52	1.32	0.03
Extraction (V)	−210	−240	−205	−220	−210
Collector (V)	70	85	75	90	85
L1 (V)	65	65	80	70	90
L3/V	30	30	30	15	15

[a] All argon (1) is simplex optimized, all argon (2) is manually tuned on ^{140}Ce. Lens votages given to nearest 5 V.

Fig. 2. (a) Univariate search of nebulizer gas flow at simplex optimized conditions for the maximization of the multi-element figure of merit with the other operating parameters held constant. Solid arrow is the optimal setting, dashed arrows show the range of values at the stop condition. (b) Univariate search of forward power at simplex optimized conditions for the maximization of the multi-element figure of merit with the other operating parameters held constant. Solid arrow is the optimal setting, dashed arrows show the range of values at the stop condition. (c) Univariate search of extraction lens voltage at simplex optimized conditions for the maximization of the multi-element figure of merit with the other operating parameters held constant. Solid arrow is the optimal setting, dashed arrows show the range of values at the stop condition. (d) Univariate search of collector lens voltage at simplex optimized conditions for the maximization of the multi-element figure of merit with the other operating parameters held constant. Solid arrow is the optimal setting, dashed arrows show the range of values at the stop condition. (e) Univariate search of L1 lens voltage at simplex optimized conditions for the maximization of the multi-element figure of merit with the other operating parameters held constant. Solid arrow is the optimal setting, dashed arrows show the range of values at the stop condition. (f) Univariate search of L3 lens voltage at simplex optimized conditions for the maximization of the multi-element figure of merit with the other operating parameters held constant. Solid arrow is the optimal setting, dashed arrows show the range of values at the stop condition.

3, and more essentially free from polyatomic ion overlap interference. A concentration of 100 ng cm^{-3} was used for all of these elements. It was necessary to use a suite of elements as the optimization was attempting to enhance the SBRs across the whole of the mass range, in addition SBR was chosen as it is easy to increase analyte sensitivity, i.e. by increasing the forward power,

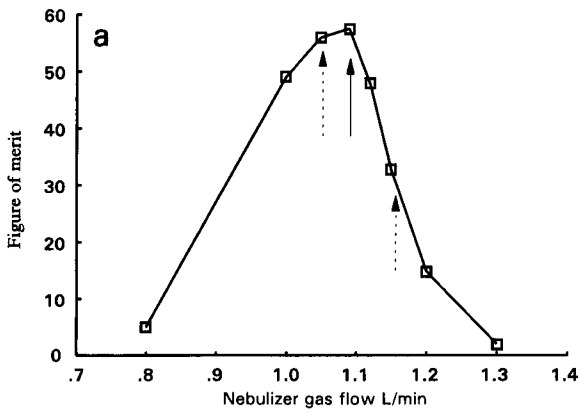

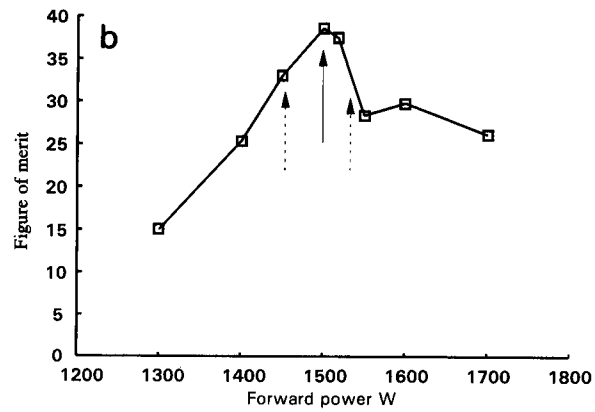

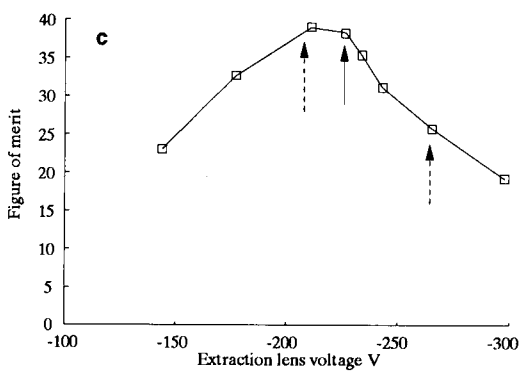

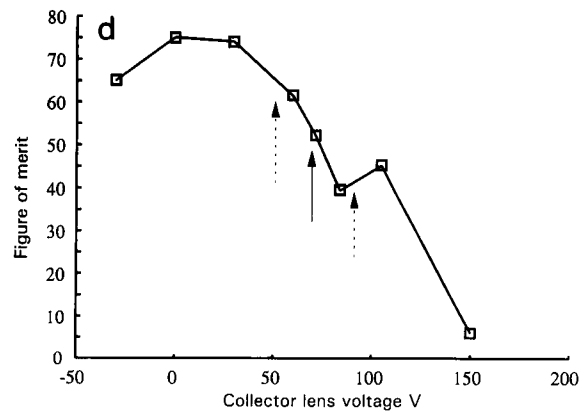

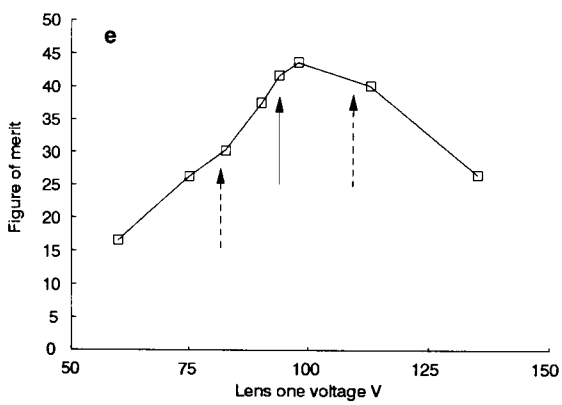

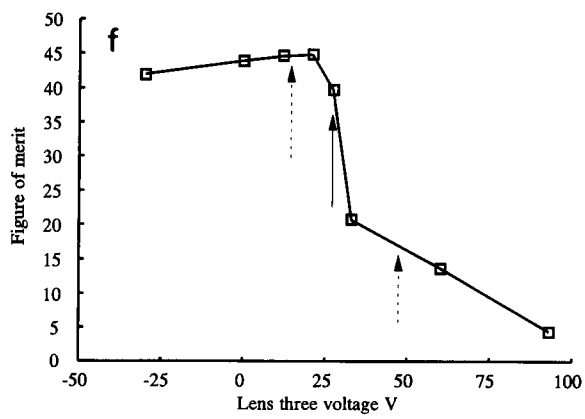

but this will also increase the random background at the analyte mass and hence reduce SBR. It was necessary however, to take the FoM one step further. It was considered that merely summing the SBRs was going to be to use as an FoM, and it was feared that bias towards high response elements might occur, for example at increased nebulizer gas flows (i.e. 1.2 dm^3 min^{-1}) Li signal can be in the order of 10 000 000 area counts per second (ACPS) compared to an indium value of 500 000 ACPS. This problem had previously been considered by Ebdon and Carpenter [11] for an ICP-AES optimization of trace and minor species and to overcome the problem a FoM was defined that removed the bias explained above. The FoM was defined as:

$$n/\Sigma\ (\mathrm{SBR})^{-0.7}$$

Where n is the number of elements used in the optimization. The effectiveness of this FoM is demonstrated in Table 4 where the effect on the overall SBR of increasing and decreasing the SBR of four elements (Be, Bi, Au and U) is shown. This is based on data from one of the simplex optimizations. A further advantage of the SBR based FoM was that the use of ratios minimized problems from instrumental drift.

RESULTS AND DISCUSSION

Optimization of unmodified argon plasma system

The optimization was complete in 34 steps, which took approximately five hours. The optimal conditions are given in column one of Table 5. This is obviously an extensive period of time but this reflects the complex interaction of all of the variables, and as Evans and Carusso [18] correctly stated when considering this point, the use of univariate searches would also be time consuming with no guarantee of the true optimum being defined. After the completion of the optimization the defined parameters were tested by the use of univariate searches, which are demonstrated in Fig. 2a–f. Firstly it can be seen from these graphs that all of the univariates have well defined optima, and generally speaking significant variation from these optima leads to a rapid fall in the FoM. Secondly it is apparent that the optima defined in the univariate searches do not always agree exactly with those defined by the simplex optimization. This, however, is not significant as in most cases the difference is both small and is within the bounds of the values of the stopping conditions. The large value for the FoM for the collector lens was not found to be repeatable, so was not considered a problem. The defined conditions lie fairly close to the starting conditions and this is reflected in the fact that the FoM increased by just 50% through the course of the optimization.

The objective test of these conditions is to measure the detection limits of the elements that contributed to the FoM, and to compare these to detection limits obtainable using the manual univariate optimization approach. This manual optimization was performed using the gross response of the ^{140}Ce isotope, which lies close to the mid-mass point, and is an element which is relatively easily ionized. The optimal conditions defined by this approach are given in column two of Table 4, and can be seen to be similar to those defined by the simplex optimization. Detection limits for these two sets of conditions are given in Table 6. It can be seen that the two sets of data are very similar and this once again reflects the similarity in the two sets of operating conditions. The simplex tuned conditions do give an improvement at the lowest masses, (i.e., Li and Co), and this is no doubt a function of the higher nebulizer gas flow used in these conditions, which improves low mass transmission in our instrument. Another reason for the slight improvement at the bottom end is the lower extraction voltage used in the simplex conditions, as increasing the extraction voltage will lead to increased random (continuum) background. The agreement between the two sets of conditions is in contrast to that found by Schmit and Chauvette [17], who reported improvements in ion transmission ranging from 33–380% when comparing simplex optimized with manually tuned conditions. Comparisons between the two reports can not be made to any extent due to a number of differences between the two. In their work, Schmit and Chauvette used a dif-

TABLE 6

Detection limits (3σ, ng cm^{-3}) for a range of elements using simplex optimal conditions for all argon and nebulizer gas addition mixed gas plasmas

Element	All argon plasma 'simplex' tuning	All argon plasma 'manual' tuning	Nitrogen–argon plasma	Hydrogen–argon plasma	Methane–argon plasma
Li	0.23	0.51	0.040	0.86	0.18
Be	0.036	0.035	0.043	1.1	0.20
Co	0.015	0.024	0.026	0.011	0.011
Rb	0.11	0.11	0.060	0.55	0.040
In	0.021	0.017	0.020	0.025	0.041
Te	0.19	0.21	0.41	0.19	0.18
Tb	0.011	0.003	0.010	0.024	0.011
Au	0.62	0.38	1.4	0.95	0.21
Bi	0.022	0.013	0.027	0.057	0.14
U	0.010	0.008	0.004	0.019	0.009

ferent instrument, which has different ion optics and transmission characteristics, (i.e., the very low transmission at the top end is opposite to the situation with our instrument) and also the authors did not include the plasma operating parameters in their optimization. What is significant about the similarity in the two sets of conditions is that the commonly held belief that manual tuning of the ICP-MS is detrimental to the signal at the extremes of the mass range has not been seen to be true. The implication is that careful optimization of the ICP-MS on a mid-mass element can define conditions which are applicable to the whole mass range.

Optimization of mixed gas–argon plasma systems

Mixed gas plasmas were generated by the addition of nitrogen, methane and hydrogen to both the nebulizer and coolant (outer) gas flows of the ICP. Simplex optimizations were performed in the same manner as described above, but owing to the extra variable took slightly longer to run to completion. With the exception of nitrogen, experiments with the addition of gases to the coolant flow proved to be unsuccessful, with the simplex optimization failing to define optimal conditions even after in excess of 30 vertices. This is interesting as some of the reports [3,6] of analyte enhancement have been with the addition of gases to the coolant flow. In these experiments it was found that enhancements in *gross* signal did occur, but this was matched by a rise in the random background at the same mass, and hence the SBR was reduced. The addition of nitrogen to the coolant did result in a set of optimized conditions, but it was found through the univariate searches that the nitrogen concentration in the coolant gas had no effect on the overall figure of merit, and hence was not a significant parameter. The addition of nitrogen, and indeed other gases to the coolant was not investigated further.

The addition of nitrogen, hydrogen and methane to the nebulizer gas was, however, more successful, and the optimal conditions for these gases are given in columns 3–5 of Table 5. Univariate searches were performed as described above, and showed clearly defined peaks which corresponded closely to the optimal values described by the simplex procedure. Once again all of the optimized parameters proved to be significant in defining the optimal conditions, but in the case of nitrogen addition the extraction and collector lenses were found to be far less sensitive than normal, relatively flat plots were produced. This difference may relate to the physical change in the plasma with the addition of nitrogen, that is the widening of the central channel, or may relate to changes in ion energies within the ion optics.

Detection limits were once again calculated using these conditions and these are given in Table 6. Generally it was found that when compared to the all argon system, the detection limits

for these three sets of conditions showed little or no improvement, indeed the four sets are not significantly different from each other. This rather broad statement does however mask some of the underlying information obtained. The addition of nitrogen was seen to degrade the detection limits of the poorly ionized elements, for example Au 1.45 ng cm^{-3} with nitrogen addition and 0.62 ng cm^{-3} without, though nitrogen has little effect on Be, and to improve or not affect the detection limits of the more easily ionized elements. Nitrogen is known to reduce the ionization temperature of the plasma [19] and probably reduced its ionization efficiency which has the most dramatic effect on the more poorly ionized elements. This is *somewhat* supported by the data for the other two mixed gas plasmas where hydrogen, which increases the ionization temperature [20,21] of the plasma by increasing thermal conductivity, is present. The Au and Te detection limits are seen to be *generally*, unaffected or improved by the addition of hydrogen and methane, though the detection limit for gold for example is worse with the addition of hydrogen. The addition of hydrogen and methane does indeed increase the gross response of most elements, this is however matched by a rise in random background and this is demonstrated in the degraded detection limits of the light mass elements where the continuum background is most intense. Again this is supported by the nitrogen data, where the less ionizing plasma resulted in a lowered continuum background at the low mass, especially for Li.

As stated there is a difference in opinion as to whether adding gases to the ICP can increase sensitivity. In the conflicting reports nitrogen, xenon, hydrogen, and methane have been added to the nebulizer and coolant gas flows of different ICP-MS instruments. This conflict of opinion has been to a certain extent reflected in the experience in our laboratories, where we have seen both enhancements and suppressions with all of the gases they have used (nitrogen, methane, ethene and hydrogen). These enhancements and suppressions were, however, only observed during the course of univariate searches. It has been suggested that added gases may be effective by increasing the ionization capabilities of the plasma, or by reducing the formation of MO^+ species or by charge transfer processes involving species such as CO^+ and NO^+. Whilst the above processes do occur they have not been conclusively shown to be the source of enhancements that have been found. Of those authors who have found additions of gas to the ICP to be beneficial only Louie and Yoke Peng Soo [5] quoted improvements in terms of SBR, the other authors reported improvements in signal with no reference to the response of the background at the same mass. It has been shown already that, in this study, increases in gross signal were seen, but these were matched by an increase in background. The data reported by Louie and Yoke Peng Soo [5] with the addition of nitrogen and hydrogen to the argon gas inlet, yielding only modest improvements in SBR, with some SBRs being degraded, is similar to the results of this study. In contrast to these data, Craig and Beauchemin [10] who measured the effect of nitrogen addition to the coolant, found that SBRs were degraded for all elements, except those which suffered polyatomic interferences.

The real potential for mixed gas plasmas as sensitivity enhancers may be when used in conjunction with desolvated 'dry' plasmas. In a standard 'wet' plasma the dominant ions, after the Ar^+, are H^+ and O^+ from the solvent, and the concentration of these is far in excess of those derived from the added gas. In a desolvated plasma where the H^+ and O^+ concentrations are far smaller, the effects on various plasma parameters, such as ionization temperature, will be far more apparent. This is an area which we are now investigating.

Conclusions

It has been shown that it is possible to use simplex optimization to define plasma operating parameters and ion optics settings of a commercial ICP-MS instrument, which offer maximum SBRs for elements across the mass range. It has been further shown that, on our instrument, simple manual tuning of the instrument does not result in a significant drop in SBRs, when compared to the simplex optimized conditions. This is somewhat contrary to previous opinion on the use

of a single element tuning procedure for this multi-element technique. Finally it has been shown that if a rigorous optimization procedure is employed, the addition of molecular gases to the ICP, does not result in any significant improvements in SBRs and detection limits, when compared to the all argon system.

The authors gratefully acknowledge the financial support through the CASE scheme of the Science and Engineering Research Council and VG Elemental to one of us (MF) that has made this work possible. The helpful comments of Dr. Phill Goodall at the outset of this work are gratefully acknowledged.

REFERENCES

1 G. Horlick, S.H. Tan, M.A. Vaughan and C.A. Rose, Spectrochim. Acta, 40B (1986) 1555.
2 A.L. Gray and J.G. Williams, J. Anal. At. Spectrom., 2 (1987) 599.
3 J.W.H. Lam and G. Horlick, Spectrochim. Acta, 45B (1990) 1313.
4 P. Allain, L. Jaunault, Y. Mauras, J.M. Mermet and T. Delaporte, Anal. Chem. 63 (1991) 1497.
5 H. Louie and S. Yoke Peng Soo, J. Anal. At. Spectrom., 7 (1992) 557.
6 J. Wang, E.H. Evans and J.A. Caruso, J. Anal. At. Spectrom., 7 (1992) 929.
7 E.H. Evans and L. Ebdon, J. Anal. At. Spectrom., 5 (1990) 425.
8 D. Beauchemin and J.M. Craig, Spectrochim. Acta, 46B (1991) 603.
9 F.G. Smith, D.R. Weiderin and R.S. Houk, Anal. Chem., 63 (1991) 1458.
10 J.M. Craig and D. Beauchemin, J. Anal. At. Spectrom., 7 (1992) 937.
11 L. Ebdon and R.C. Carpenter, Anal. Chim. Acta., 200 (1987) 551.
12 L. Ebdon and R.C. Carpenter, Anal. Chim. Acta., 209 (1988) 135.
13 S.J. Hill, M.J. Ford and L. Ebdon, J. Anal. At. Spectrom., 7 (1992) 719.
14 L. Ebdon, M.J. Ford, P.S. Goodall and S.J. Hill, Microchem. J., in press.
15 S.J. Hill, M.J. Ford and L. Ebdon, J. Anal. At. Spectrom., 7 (1992) 1157.
16 S.J. Hill, J.H.D. Hartley and L. Ebdon, J. Anal. At. Spectrom., 7 (1992) 895.
17 J.P. Schmit and A. Chauvette, J. Anal. At. Spectrom., 4 (1989) 755.
18 E.H. Evans and J.A. Caruso, Spectrochim. Acta, 47B (1992) 1001.
19 R.S. Houk, A. Montaser and V.A. Fassel, Appl. Spectrosc., 37 (1983) 425.
20 N. Shibata, N. Fudagawa and M Kubota., Spectrochim. Acta, 47B (1992) 505.
21 J.H.D. Hartley, S.J. Hill and L. Ebdon, Spectrochim. Acta, submitted for publication.

Analytica Chimica Acta, 285 (1994) 33–43
Elsevier Science B.V., Amsterdam

Determination of cadmium, copper and lead in environmental samples. An evaluation of flow injection on-line sorbent extraction for flame atomic absorption spectrometry

Renli Ma, Willy Van Mol and Freddy Adams

Department of Chemistry, University of Antwerp (UIA), B-2610 Wilrijk (Belgium)

(Received 4th June 1993; revised manuscript received 23rd August 1993)

Abstract

A flow injection on-line sorbent extraction system was studied in conjunction with flame atomic absorption spectrometry to determine cadmium, copper and lead in digest solutions of solid environmental samples using octadecyl functional groups (C_{18}) bonded silica gel as sorbent with diethylammonium-*N*,*N*-diethyldithiocarbamate (DDDC) or ammonium diethyldithiophosphate (DDPA) as complexing agent and methanol as eluent. Using DDDC as complexing agent, citric acid was used as masking agent for iron and manganese. The complexing agent DDPA selectively extracts cadmium, copper and lead at pH values 1 to 3. Using DDPA as complexing agent with citric acid at pH 1.0, the results of the analysis of five environmental standard reference materials, including coal fly ash (CRM 038), calcareous loam soil (CRM 141), lake sediment (CRM 280), river sediment (CRM 320) and estuarine sediment (CRM 277) after digestion were in good agreement with the certified values except cadmium in the river sediment with a very high iron content. With a 20-s sample loading at 8.7 ml min^{-1}, detection limits (3σ) were 0.8, 1.4 and 10.0 $\mu g\ l^{-1}$ respectively for cadmium, copper and lead.

Keywords: Atomic absorption spectrometry; Flow injection; Cadmium; Copper; Environmental samples; Flame atomic absorption spectrometry; Lead; Sorbent extraction

As one of the most extensively used detection techniques, flame atomic absorption spectrometry (FAAS) is very precise and accurate, but, generally, it can not be used to determine trace heavy metals in environmental samples because of insufficient sensitivity and/or matrix interference. The analyte preconcentration and matrix separation in manual batch approaches is time and reagent consuming with a risk of contamination or losses [1]. Flow-injection (FI) on-line analyte preconcentration and matrix separation is a powerful on-line automated sample handling procedure to enhance the sensitivity and selectivity of FAAS [2–4]. In digest solutions from solid environmental samples, the concentrations of some trace heavy metals are too low to be measured directly with the flame and too high with the graphite furnace AAS. The concentration of coexisting metals, such as iron and manganese, is many times higher than those of the trace heavy metals of interest. FAAS combined with FI on-line preconcentration can readily cover the concentration levels between conventional flame and graphite furnace AAS and remove the interferents.

Following FI on-line continuous liquid–liquid extraction [5,6] and micro-column ion-exchange

Correspondence to: F. Adams, Department of Chemistry, University of Antwerp (UIA), B-2610 Wilrijk (Belgium).

SSDI 0003-2670(93)E0490-X

or chelating adsorption [7,8], the sorbent extraction on the column containing reversed-phase bonded silica with organic hydrophobic groups was proposed combining the advantages of both above mentioned procedures [9]. This system was further improved by using a conical microcolumn eluted in the direction opposite to the sample loading to minimize the dispersion of the eluted complexes [10] or by introducing air segments before and after elution to prevent the mixing of eluent with sample solution [11]. The development was reviewed recently [12]. So far no determination of trace heavy metals in digest solutions from solid environmental samples has been reported with a sorbent extraction system.

Diethyldithiocarbamate (DDC) was used as one of the chelating agents in all so far published works on FI on-line sorbent extraction for AAS [9–16]. The elements of the first and second main periodic groups, normally present in high concentrations, can be separated from the trace heavy metal analytes which are selectively extracted by the sorbent as DDC complexes. The interference, for example, of magnesium on cadmium with a controlled-pore glass–8-quinolinol (CPG-8Q) column for chelating adsorption [8] can be eliminated [10]. Nevertheless, the complexation of DDC with a large number of metals limits its application to the separation of various heavy metals. Interferences may occur in the extraction stage from coexisting extractable metallic elements present in high concentrations [10,11]. When a certain element at relatively lower concentration is determined, a high total metal amount is collected on the column from other existing metals and the adsorptive capacity of the column becomes the limiting factor [12]. Using diethylammonium-*N*,*N*-diethyldithiocarbamate (DDDC) as complexing agent, Fang et al. [10] demonstrated the determination of trace heavy metals in water for flame and graphite furnace AAS [13–15] and in digested biological samples for FAAS [11]. For FAAS they found that high concentrations of copper, lead and iron depressed significantly the cadmium signal [10–12]. For iron this effect was reduced by increasing the sample acidity [11,12]. The cause for the interference might be that coexisting extractable metals compete with the analyte for the complexing agent and the binding sites on the column packing materials [10,12]. It can be eliminated by controlling the appropriate pH for extraction, using a masking agent or a highly selective complexing agent.

The critical condition for the sorbent extraction is the end pH of the mixture of the sample solution with the complexing agent. Different optimum pH ranges are necessary for different heavy metals. The influence of sample acidity on the cadmium recovery from standard solutions and synthetic seawater samples with DDDC reagent has already been reported [10]. The extraction in acidic medium can prevent hydrolysis of heavy metals and provide high selectivity, but DDC itself can also be retained on the column to compete sorption for sites with tested metals [9]. In liquid–liquid extraction DDDC is present in the organic phase at a pH < 4 while at pH > 8 it is present in the aqueous phase [17]. In addition, this reagent is very unstable in acidic aqueous solution although the extraction can be performed in very acidic medium. According to the half-lives of diethyldithiocarbamic acid in water at room temperature, its concentration remains at more than half of its original over an eight-hour period when the pH is higher than 7 [17]. Normally, DDDC is dissolved at pH 9 to keep it stable. Because of this, the end pH has to be controlled by the sample acidity. Xu et al. [11] measured copper and cadmium in biological samples with 0.5 M HNO_3 acidity for a high tolerance of iron.

Iron and manganese are considered to be the most important interfering elements in trace heavy metal determination in environmental samples. The stability of their DDC complexes is lower than that of the determined elements, cadmium, copper and lead [17], which provides the possibility to use a masking agent. Citric acid can be used for this purpose based on the high stability of its iron or manganese complex [18].

Some of the coexisting heavy metals can also be separated using an element-specific chelating agent. Compared with DDC, ammonium diethyldithiophosphate (DDPA) is more selective and stable, and can be used directly at very low pH.

In liquid–liquid extraction it can not react with cobalt, iron(II) and zinc while its nickel complex is soluble in both water and organic solvents. Its cadmium, copper and lead complexes can be extracted completely from acidic, neutral or slightly alkaline media. The iron(III) complex can be extracted at pH 2–3, but iron(III) is reduced to iron(II) at lower pH [17,19]. This reagent has been successfully used to separate cadmium, copper and lead selectively on activated carbon from different matrices, including high-purity iron, chromium and manganese [20,21].

The elution flow-rate of the extraction column and the nebulizer uptake rate of FAAS which both influence the sensitivity and reproducibility, are essential for the analytical performance and the coupling between FI system and flame AAS. Fang et al. [10] used a low elution (2.5 ml min^{-1}) with a high nebulizer uptake rate (7.2 ml min^{-1}) to increase the nebulization efficiency. The elution stage is simultaneous with the sample introduction process into the flame detector, so these two rates should be optimized at the same time.

In the present study, analytical parameters were optimized for the sorbent extraction system combined with FAAS. These include sample loading flow-rate, concentration of the complexing agent, elution flow-rate, nebulizer uptake rate and length of the capillary tube connecting FI system with AA spectrometer. The influence of extractable metals on the extraction column was also studied. The control of medium pH value and the use of a masking agent or a selective complexing agent were investigated to improve the selectivity. Cadmium, copper and lead in five solid environmental standard reference materials from the Community Bureau of Reference (BCR), coal fly ash (CRM 038), calcareous loam soil (CRM 141), lake sediment (CRM 280), estuarine sediment (CRM 277) and river sediment (CRM 320), were determined after digestion under the improved extraction conditions with DDPA as complexing agent.

EXPERIMENTAL

Apparatus

A Perkin-Elmer FIAS-200 flow-injection system was combined with a Perkin-Elmer Model 3030 atomic absorption spectrophotometer. The setup shown in Fig. 1 is the same as that described by the manufacture [16] but without the 3-D reactor. The working programme of the FI sorbent extraction system is listed in Table 1. Tygon pump tubes were used for the complexing agent (0.76 mm i.d.) and the sample (1.52 mm i.d.). A solvent resistant silicone rubber pump tube (Isoversinic) was used for the organic eluent (1.00 mm i.d.). All other tubing was made of PTFE with 0.35 mm i.d. The commercially available conic extraction column (PE B050-4047) was

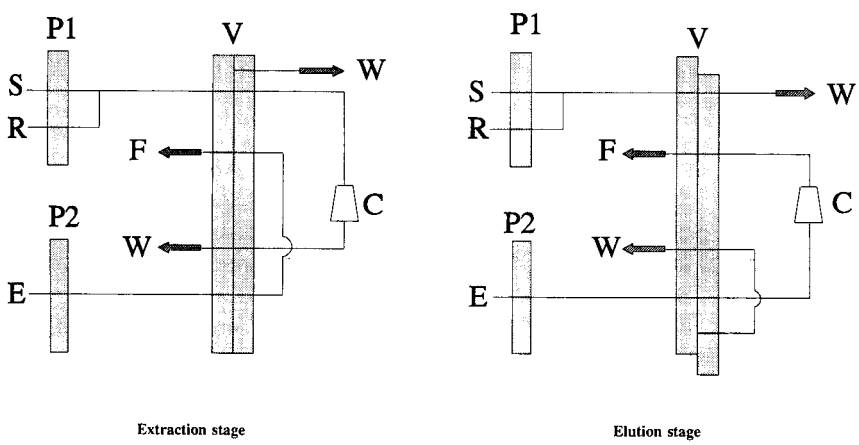

Fig. 1. Schematic diagram of FI on-line sorbent extraction system for FAAS. P1 = Sample pump; P2 = eluent pump; S = sample; R = complexing reagent; E = eluent; V = valve; C = column; W = waste; F = FAAS.

TABLE 1

FIAS-200 programme [a]

Step No.	Time (s)	Pump 1 (rpm)[b]	Pump 2 (rpm) [b]	Valve	Read (s)
1	10–50 [c]	100		Inject	
2	10	100	120 [d]	Inject	
3	2	100	120 [d]	Fill	−3
4	8		120 [d]	Fill	

[a] A prefill step, as step 3, of 20 s was performed for a new sample solution. [b] rpm = Revolutions per minute. [c] Sample loading time dependent on the preconcentration factor required. [d] 120 rpm set for DDPA reagent and 80 rpm set for DDDC reagent.

packed with about 20 mg of octadecyl functional groups (C_{18}) bonded silica gel whose particle size was 40–63 μm. The PTFE tube between the conjunction point of the sample with the reagent and the valve was made as short as possible (5 cm) to avoid adsorption of the complexes on the tube wall [14]. The nebulizer capillary, connecting the FIAS valve with the nebulizer, was also as short as possible (25 cm × 0.35 mm i.d., PTFE) to minimize the dispersion of the eluted complex. Hollow cathode lamps were used as light sources at the most sensitive resonance lines except for lead, for which the second resonance line, 283.3 nm, was used because of the better signal-to-noise ratio. Deuterium arc background correction was used for all tested metals except copper. The ratio of acetylene to air had an influence on the sensitivity, precision and background. The acetylene flow was set at 0.7 l min^{-1} with the flow spoiler in the spray chamber and the air flow was set from 11.5 to 18.5 l min^{-1} for different elements to provide normal background correction and high sensitivity.

Reagents

All chemical reagents were of analytical grade except that supra pure concentrated nitric acid (Merck 441), hydrochloric acid (Merck 318), perchloric acid (Merck 517) and hydrofluoric acid (Merck 335) were used for the sample digestion. Methanol (Merck 6009) was used as the eluent. Ethanol (Merck 983) and methyl isobutyl ketone (MIBK, Aldrich, M 6710-9) were also used as eluents for comparison purpose. 0.1% (w/v) DDDC (Merck 3408) in 0.1 M acetic acid (Merck 62) with or without 0.05 M citric acid (Merck 244) adjusted to pH 9.0 with ammonia (Merck 5432), was prepared every day as chelating agent. 0.2% (w/v) DDPA (95%, Aldrich, 17,779-2) in 0.1 M citric acid adjusted with nitric acid (Merck 456) to pH 1.0, was used as selective chelating agent. Deionized water from Milli-Q water system (Milli-pore) was used throughout all experiments. Standard solutions of all tested metals were made by dilution from 1000 mg l^{-1} stock solutions (Merck).

Sample digestion

4.0 ml of conc. HF and 5.0 ml of conc. HNO_3 were added to 1.0 g of lake sediment (CRM 280), river sediment (CRM 320) or calcareous loam soil (CRM 181), or 2.0 ml of HF and 2.5 ml of HNO_3 were added to 0.5 g coal fly ash (CRM 038) or estuarine sediment (CRM 277) in the PTFE beaker of a digestion bomb. The open bomb, covered by a cap with a small hole to prevent contamination, was heated gently on a hot plate till fuming. After the solution was cooled down, 4.0 ml $HClO_4$ per gram of samples was added. Then the bomb was sealed and heated in the oven at 150°C for 8 h. The contents of the open bomb was evaporated till completely dry on a hot plate. Remaining silicates were removed by repetitively adding a mixture of HF and HNO_3 and heating till dryness. The residue was dissolved in 0.5 ml HNO_3 and 0.25 ml HCl with 5 ml H_2O and diluted till 50 ml.

RESULTS AND DISCUSSION

Optimization of analytical parameters

Sample loading rate. The sample loading rate did not influence the extraction efficiency of 200 μg l^{-1} copper with DDDC when different sample loading times were set at different sample loading rates so as to pump the same sample volume through the column. A pump 1 speed of 100 rpm was selected, 8.7 ml min^{-1} for the sample solution and 2.2 ml min^{-1} for the complexing agent solution. The atomic absorption signal of 100 μg l^{-1} copper with DDDC increased linearly within

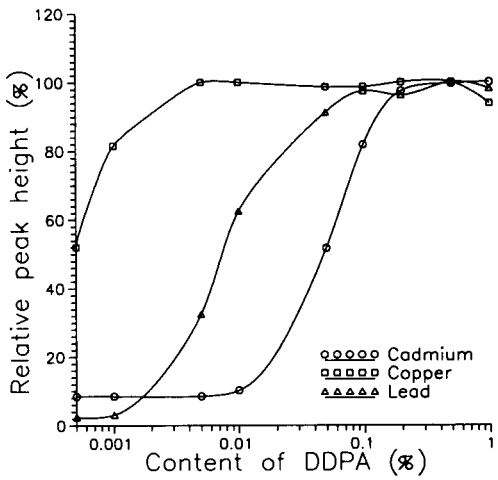

Fig. 2. Influence of DDPA concentration on the extraction efficiency.

the sample loading time of four minutes in peak area or within one minute in peak height.

Concentration of complexing agent. Minimum concentrations of DDPA were found for the quantitative extraction of 50 $\mu g\ l^{-1}$ cadmium, 100 $\mu g\ l^{-1}$ copper and 600 $\mu g\ l^{-1}$ lead (Fig. 2). The reason for the differences could be the different stability and extractability of the three complexes (Cu > Pb > Cd) [17,19]. 0.2% DDPA was used for all metals throughout this work. 0.1% DDDC was used according to the recommendation of the manufacture [16].

Eluent. MIBK is considered suitable for liquid–liquid extraction combined with FAAS [1] while alcohol is popular for hydrophobic sorbent elution [9]. Methanol, ethanol and MIBK containing different concentrations of nitric acid were compared as the eluent for copper extraction with DDDC. They all effectively eluted the complex. There was no significant difference in sensitivity and precision between methanol and ethanol. Increasing the content of nitric acid in methanol, peak widths and peak areas decreased; but peak heights and the precision remained nearly similar. MIBK provided doubled peak height signals because the elution peak was much sharper, even with a long tailing. The reproducibility became worse, 6.6% instead of 1.5% with methanol for peak height measurement. The addition of 1.0% nitric acid into MIBK increased the peak height only by 15%, but the precision ameliorated with peak height measurement (1.8%) and tailing was less pronounced. The disadvantage of MIBK was that it damaged the pump tube after a few hours of use. Therefore pure methanol was used in further work.

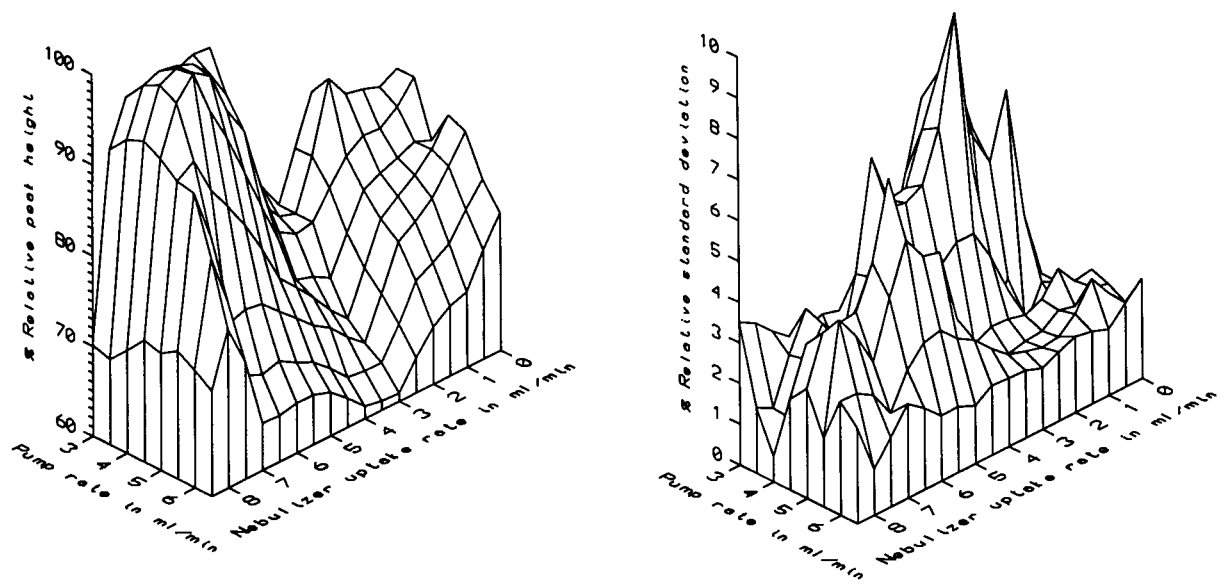

Fig. 3. Influence of the elution pump rate and the nebulizer uptake rate on the sensitivity and precision.

Column elution rate and nebulizer uptake rate. The elution rate and the nebulizer uptake rate were optimized together using DDPA as complexing agent with methanol or ethanol as eluent. Because the peak area signal was dependent on the peak width and its precision could not reflect the situation of the peak shape, the optimization was carried out according to the sensitivity and reproducibility of peak height measurement of copper within the whole ranges of the two rates. Low elution rates produced a high elution and nebulization efficiency. However, with decreasing elution rate, peak areas became larger and the elution peak became broader necessitating a longer elution time. When the nebulizer uptake rate exceeded the elution rate, vacuum segments or/and gas bubbles formed in the capillary tube connecting the FIAS valve with the nebulizer and the peaks started to become abnormally shaped with high sensitivity and poor precision for peak height measurement. When the elution rate was higher than the uptake rate, the system performed precisely. The situation with methanol is shown in Fig. 3. The optimum ranges of these two rates with good precision and relatively high sensitivity were 0–2 ml min^{-1} of the uptake rate together with 5–6.5 ml min^{-1} of the elution rate with methanol or 6 ml min^{-1} of the uptake rate together with 5–6.5 ml min^{-1} of the elution rate with ethanol. At the optimum rates, ethanol produced the same sensitivity and precision as methanol but its optimum uptake rate was much higher. A reasonable explanation for this is that ethanol has a lower nebulization efficiency. At the maximum elution rate of 6.5 ml min^{-1} (120 rpm), the precision was always better than 2% R.S.D. for both eluents. Finally, a high elution rate, 6.5 ml min^{-1} (120 rpm), and a low nebulizer uptake rate, 2.0 ml min^{-1} for methanol, were selected for the other work with DDPA in this paper. The nebulizer uptake rate used was much lower than the optimum uptake rate in conventional FAAS of 7.6 ml min^{-1} for 2.0 mg Cu l^{-1} in methanol.

Using DDDC and methanol, the elution rate of 4.0 ml min^{-1} (80 rpm) was selected for optimum precision in agreement with the value recommended by the manufacture [16]. The reason for the higher optimum elution rate for the DDPA complex was that the tailing of its elution peak was longer than that of the DDDC complex. A good precision was achieved at the uptake rates between 0 and 4 ml min^{-1}. A uptake rate of 2.0 ml min^{-1} was also selected.

Capillary connecting FIAS with FAAS. The FIAS valve was connected with the FAAS by the nebulizer capillary, the length of which affects the dispersion of the eluted complex. The peak height signal decreased greatly with capillary length while the peak area signal remained nearly stable. The highest sensitivity and best precision were achieved with the shortest nebulizer capillary.

Reproducibility

A 3-D reactor between the FI system and the spectrometer, and a degassing procedure for the eluent are suggested to prevent the formation of gas bubbles, which degrades the precision when the nebulizer uptake rate is higher than the elution rate [10,16]. Under the optimum condition in the present work, the 3-D reactor negatively affected the sensitivity and precision. Also the precision was similar with and without degassing of the eluent and standard solutions. Hence a 3-D reactor and a degassing procedure were not used.

The precision of 150 successive copper measurements (100 $\mu g\ l^{-1}$ with DDDC, 20 s sample loading during 2 h) was 1.5% for peak height and 2.7% for peak area. The mean precision of 30 series for each five measurements was 1.6% for peak height or 0.8% for peak area. These data suggest that the peak area measurements are more precise than the peak height for every series; but the peak height signals are more stable in time than the peak area. The sensitivity decreased from series 1 to 30 when measurements were based on both peak height (5%) and peak area (7%).

Influence of the extractable heavy metals on the column

Figure 4 shows the typical influence of extractable metals on the sample-loaded volume and the copper peak height signal. Standard solutions acidified with 0.1% HNO_3 containing 20 μg

l^{-1} Cu^{2+} and different concentrations of Cd^{2+}, Co^{2+}, Fe^{3+}, Mn^{2+}, Ni^{2+}, Pb^{2+} or Zn^{2+} as coexisting metal ions were loaded with DDDC for 2 min in order to measure the sample volume accurately. The theoretical total amounts of extracted metals on the column were calculated on the basis on the real sample-loaded volumes. No interference occurred till 2 μg of the theoretical total amount of extracted metals on the column, which corresponds with 100 $\mu g\ l^{-1}$ of coexisting metals. With the theoretical total amount of extracted metals around 17 μg and coexisting metals of 1000 $\mu g\ l^{-1}$, the peak height signal was depressed by 20–50% with all coexisting metal ions except Mn^{2+}; and the sample loaded volume was reduced by 20–40% with Ni^{2+} or Fe^{3+} (Fig. 4a), but no influence occurred on the sample volume with Cd^{2+}, Co^{2+}, Mn^{2+}, Pb^{2+} or Zn^{2+} (Fig. 4b). With 1000 $\mu g\ l^{-1}$ of Cd^{2+}, Pb^{2+} or Zn^{2+} the peak width became significantly larger, which implied the elution rate was already decreased. With a higher extracted metal amount corresponding to 10 000 $\mu g\ l^{-1}$ all coexisting metals, both sample volume and peak height signal were decreased significantly. The peak area signals were depressed also for concentrations exceeding 1000 $\mu g\ l^{-1}$ of Fe^{3+} or Ni^{2+} and 10 000 $\mu g\ l^{-1}$ of Cd^{2+}, Co^{2+}, Mn^{2+}, Pb^{2+} or Zn^{2+}. Sometimes the normal integration time was not long enough for such peak signals with long tailing. From these experiments it was evident that the column could be clogged by a large quantity of extracted metals, between 2 and 17 μg. This clogging decreased the sensitivity of the peak height measurements because the sample loaded volume was less and/or the elution rate was lower resulting in broadening of the elution peak. It was still possible, however, to obtain normal peak area signals in these circumstances. In practice, checking the sample loaded volume only or loading a fixed sample volume is not enough to ascertain that the system preforms well. A series of measurements whose peak height decreases gradually or whose peak shape broadens demonstrates clearly the clogging effect.

Improvement of the selectivity

pH effect. Cd^{2+}, Cu^{2+} and Pb^{2+} could be extracted quantitatively with DDDC from a pure Milli-Q water medium to 10% HNO_3 which produced a final pH of the mixture of the sample solution with the reagent solution < 0. Co^{2+},

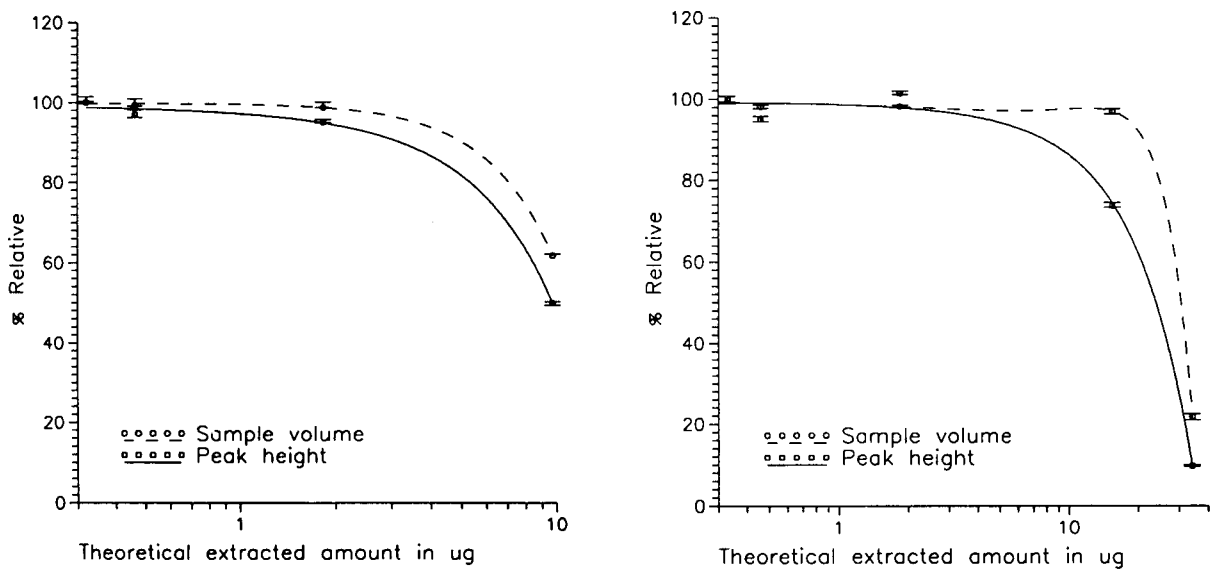

Fig. 4. Influence of the extracted metal amount on the sample-loaded volume and peak height signal.

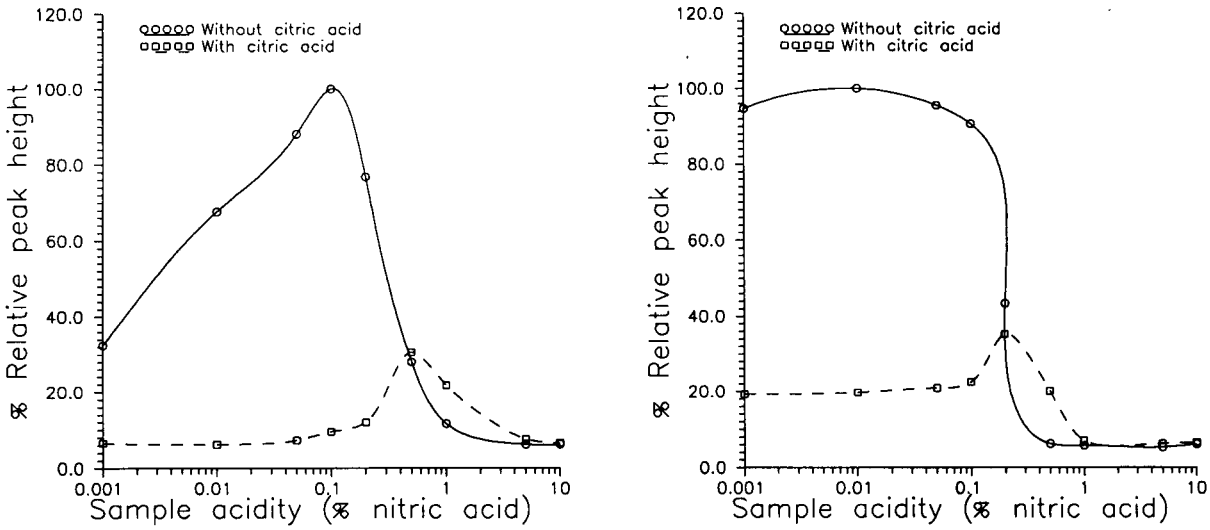

Fig. 5. Effect of sample acidity on the extraction efficiency with DDDC.

Ni^{2+} and Zn^{2+} could be extracted quantitatively up to a sample acidity of 0.2% HNO_3 (final pH 3). Fe^{3+} produced a maximum absorption signal with very poor precision only at 0.1% HNO_3 (final pH 6) (Fig. 5a). Mn^{2+} could be extracted up to 0.1% HNO_3 (Fig. 5b). A sample acidity > 1.0% HNO_3 (final pH 1) provided a nearly selective extraction for Cd^{2+}, Cu^{2+} and Pb^{2+}.

Masking effect. Using 0.05 M citric acid with DDDC, no interference was observed for determination of Cd^{2+}, Co^{2+}, Cu^{2+}, Pb^{2+} and Zn^{2+}. However, there was a significant masking effect for Fe^{3+} and Mn^{2+} (Fig. 5), which could decrease the total amount of metal extracted on the column. Fe^{3+} and Mn^{2+} masked with citric acid passed through the column during the extraction stage. Compared with the system without masking agent, the tolerance for Fe^{3+} or Mn^{2+} was five to ten times higher.

Selective complexing agent. The extraction efficiency using DDPA as complexing agent with 0.1 M citric acid was tested between pH 0 and 9 for eight metal ions. The optimum pH ranges were from 1.0 to 3.0 for Cd^{2+}, 0 to 4.0 for Cu^{2+} and 0 to 3.0 for Pb^{2+} (Fig. 6). DDPA provided a similar sensitivity for Cd^{2+}, Cu^{2+} and Pb^{2+} as DDDC. Co^{2+}, Fe^{3+}, Mn^{2+}, Ni^{2+} and Zn^{2+} were not extracted, and all these gave similar signals to the blank. Without citric acid the iron signal was significantly higher at a level of 400 $\mu g\ l^{-1}$ at pH 2.0. A pH of 1.0 was used for DDPA reagent with 0.1 M citric acid to minimize the influence of iron.

Using DDPA and citric acid at pH 1.0 for a 120-s sample loading of 10 $\mu g\ l^{-1}$ Cd^{2+}, 100 μg

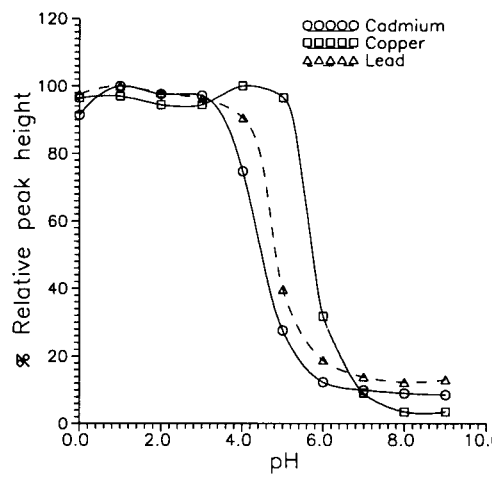

Fig. 6. Effect of pH on the extraction efficiency with DDPA.

TABLE 2

Determination of copper with DDDC and citric acid [a]

Reference material	Certified concentration ($\mu g\ g^{-1}$)	Measured concentration ($\mu g\ g^{-1}$)	
		Peak height	Peak area
Coal fly ash	176 ± 9	178.9 ± 1.0	170.7 ± 1.1
Calcareous loam soil	32.6 ± 1.4	29.6 ± 0.3	31.0 ± 0.4
Lake sediment	70.5 ± 1.5	64.0 ± 0.8	68.9 ± 0.8

[a] The digest solutions were diluted 40 times for fly ash, 25 times for lake sediment and 12.5 times for soil. The sample loading time was 20 s.

l^{-1} of Cu^{2+} or Pb^{2+} as a coexisting metal ion had no influence on the sample loading and the cadmium signal. 1000 $\mu g\ l^{-1}$ Cu^{2+} decreased the sample loaded volume and peak height or area by ca. 10%. 1000–10 000 $\mu g\ l^{-1}$ Pb^{2+} depressed the peak height by 5–10% with an almost stable sample loaded volume and peak area. A serious effect was produced by 50 000 $\mu g\ l^{-1}$ Pb^{2+} which gave a 15% lower sample loaded volume and peak area and a 25% lower peak height. 100 mg l^{-1} Mn^{2+} (the maximum concentration tested) had no influence. The sample loaded volume was normal up to 1000 mg l^{-1} Fe^{3+} (the maximum concentration tested), but peak area and height signals were depressed by 4–6% with 500–1000 mg l^{-1} Fe^{3+}. The tolerance of iron was at least 1000 times better than the system using DDDC as complexing agent without masking agent.

Determination of cadmium, copper and lead in digested environmental samples

The iron concentration was much higher than the other heavy metals in the analyzed environmental samples, which could interfere the measurement of cadmium, copper and lead. A determination using DDDC without masking agent and medium pH control was therefore impossible. After each sample measurement, the system sensitivity became lower and could not be increased subsequently. The sample tubing between the pump and the valve even broke by too high a back pressure caused by the clogging of the column. Sometimes the column was damaged permanently.

Copper was determined in three samples using DDDC with 0.05 M citric acid as masking agent (Table 2). In this table and in succeeding tables, measured concentrations are the average results and standard deviation of the determinations of three independent digestions. In the analyzed solutions the total amount of extracted metals except iron and manganese is < 2 μg (0.92 μg in coal fly ash, 1.24 μg in lake sediment and 0.85 μg in soil). The result for fly ash is very accurate. The measured values for calcareous loam soil and lake sediment are in agreement with the certified values for data based on peak area measurement, but the measured concentrations are too low when

TABLE 3

Determination of cadmium with DDPA and citric acid [a]

Reference material	Certified concentration ($\mu g\ g^{-1}$)	Measured concentration ($\mu g\ g^{-1}$)		Metal amount	
		Peak height	Peak area	Cd + Cu + Pb (μg)	Fe (mg)
Coal fly ash	4.6 ± 0.3	4.36 ± 0.07	4.36 ± 0.01	7.70	0.6
Calcareous loam soil	0.36 ± 0.10	0.30 ± 0.01	0.35 ± 0.03	4.34	1.6
Lake sediment	1.6 ± 0.1	1.44 ± 0.02	1.51 ± 0.02	6.63	1.8
Estuarine sediment	11.9 ± 0.4	11.4 ± 0.1	12.0 ± 0.2	1.13	0.2
River sediment	0.533 ± 0.026	0.403 ± 0.020	0.398 ± 0.015	6.05	3.1

[a] The digest solutions were diluted 20 times for estuarine sediment, 5 times for fly ash, 4 times for lake sediment and 2.5 times for soil and river sediment. The sample loading time was 60 s.

TABLE 4

Determination of copper with DDPA and citric acid [a]

Reference material	Certified concentration ($\mu g\ g^{-1}$)	Measured concentration ($\mu g\ g^{-1}$)	
		Peak height	Peak area
Coal fly ash	176 ± 9	176.0 ± 3.9	172.3 ± 0.4
Calcareous loam soil	32.6 ± 1.4	33.0 ± 0.6	32.1 ± 0.3
Lake sediment	70.5 ± 1.5	71.7 ± 0.1	70.5 ± 0.4
Estuarine sediment	101.7 ± 1.6	105.0 ± 1.7	102.2 ± 0.9
River sediment	44.1 ± 1.0	45.0 ± 0.7	44.3 ± 0.3

[a] The digest solutions were diluted 40 times for fly ash, 25 times for lake sediment, 20 times for estuarine and river sediments and 12.5 times for soil. The sample loading time was 20 s.

results are based on peak height measurements. These low results could be explained by the depression of the peak height signal by unmasked iron. The amount of iron in the loaded sample for the determination was 24.50 μg in the ash, 98.37 μg in the lake sediment or 109.50 μg in the soil. When citric acid was used as masking agent, the unmasked iron content can be estimated at 5–10% of the original amount (Fig. 5), which is still very high for the soil and lake sediment.

The determination of cadmium and lead was much worse using DDDC with citric acid because their measurements acquired the collection of more complexes on the column and the influence of unmasked iron was more critical.

The analytical results obtained by using DDPA with 0.1 M citric acid at pH 1.0 are listed in Tables 3–5. All measured concentrations were in good agreement with the certified values except for cadmium in river sediment. The sample loading rate decreased during the measurements as the column was clogged gradually. The total extracted amount of cadmium, copper and lead for river sediment was comparable with that for fly ash and lake sediment (Table 3). The iron concentration in the diluted solution of river sediment is 360 mg l^{-1}, much higher than that for the other samples. In the standard solution with contents of copper, lead, manganese and iron similar to the diluted solution of the river sediment, the cadmium peak height signal was depressed 8%, but the sampling rate and peak area signal were not influenced. A very high iron absorption signal was still obtained after the extraction of this solution with 1.0 M citric acid. This means that a relatively high portion of the iron remains on the column. The low result might hence be explained by the joint interference of the matrix and the less sample volume. But it is not clear why the column became clogged in these circumstances.

With flow spoiler for peak height measurement after 20-s sample loading with DDPA, the

TABLE 5

Determination of lead with DDPA and citric acid [a]

Reference material	Certified concentration ($\mu g\ g^{-1}$)	Measured concentration ($\mu g\ g^{-1}$)	
		Peak height	Peak area
Coal fly ash	262 ± 11	261.9 ± 4.8	257.0 ± 2.9
Calcareous loam soil	29.4 ± 2.6	31.2 ± 0.6	30.1 ± 1.2
Lake sediment	80.2 ± 2.3	82.9 ± 2.6	80.5 ± 2.4
Estuarine sediment	146 ± 3	145.3 ± 1.1	139.7 ± 0.9
River sediment	42.3 ± 1.6	41.4 ± 1.2	40.7 ± 1.6

[a] The digest solutions were diluted 10 times for fly ash, 6.25 times for lake and estuarine sediments, 5 times for soil and river sediment. The sample loading time was 20 s.

enhancement factors compared with conventional flame AAS were 35 for cadmium and copper and 26 for lead, which were similar to the values, 19–25, in the literature [10]; the detection limits (3σ) of 0.8, 1.4 and 10.0 $\mu g\ l^{-1}$ were comparable with the reported values, 0.3, 0.2 and 3 $\mu g\ l^{-1}$ for cadmium, copper and lead, respectively [10]; the linear calibration ranges were $\leqslant 50\ \mu g\ l^{-1}$ cadmium, $\leqslant 300\ \mu g\ l^{-1}$ copper and $\leqslant 1000\ \mu g\ l^{-1}$ lead.

Conclusion

In combination with flame AAS, the FI sorbent extraction system using DDDC reagent could be applied to the samples with a simple matrix, such as water samples. For the samples containing a high content of extractable coexisting metals, however, the main problem is the influence of the extracted complexes on the extraction column. Interference could occur on the sample loading rate and the elution rate caused by clogging of the column with excessive extracted complexes. The tolerance for coexisting metallic elements is greatly improved by using a selective chelating agent DDPA with a masking agent at low pH. Cadmium, copper and lead could be measured if the iron concentration is not too high. Otherwise instead of flame AAS, a more sensitive detector, e.g., graphite furnace AAS should be used, in which the sample solution can be further diluted and the amount of extracted metals can be reduced by two to three orders of magnitude.

REFERENCES

1 Yu.A. Zolotov and N.M. Kuz'min, Preconcentration of Trace Elements, Elsevier, Amsterdam, 1990.
2 M. Valcárcel and M. Gallego, in J.L. Burguera (Ed.), Flow Injection Atomic Spectroscopy, Marcel Dekker, New York, 1989, p. 157.
3 J.F. Tyson, Anal. Chim. Acta, 234 (1990) 3.
4 V. Carbonell, A. Salvador and M. de la Guardia, Fresenius' J. Anal. Chem., 342 (1992) 529.
5 L. Nord and B. Karlberg, Anal. Chim. Acta, 125 (1981) 199.
6 B. Karlberg, Anal. Chim. Acta, 214 (1988) 29.
7 S. Olsen, L.C.R. Pessenda, J. Ruzicka and E.H. Hansen, Analyst, 108 (1983) 905.
8 Z. Fang and B. Welz, J. Anal. At. Spectrom., 4 (1989) 543.
9 J. Ruzicka and A. Arndal, Anal. Chim. Acta, 216 (1989) 243.
10 Z. Fang, T. Guo and B. Welz, Talanta, 38 (1991) 613.
11 S. Xu, M. Sperling and B. Welz, Fresenius' J. Anal. Chem., 344 (1992) 535.
12 B. Welz, Microchem. J., 45 (1992) 163.
13 Z. Fang, M. Sperling and B. Welz, J. Anal. At. Spectrom., 5 (1990) 639.
14 M. Sperling, X. Yin and B. Welz, J. Anal. At. Spectrom., 6 (1991) 295.
15 M. Sperling, X. Yin and B. Welz, J. Anal. At. Spectrom., 6 (1991) 615.
16 F. Portala and T. Guo, Perkin Elmer Report Nr 4.8E, 1991.
17 J. Starý, The Solvent Extraction of Metal Chelates, Pergamon, Oxford, 1964, p. 155.
18 A. Hulanicki, Talanta, 14 (1967) 1371.
19 A.K. De, S.M. Khopkar and R.A. Chalmers, Solvent Extraction of Metals, Van Nostrand Reinhold, London, 1970, p. 169.
20 H. Berndt and J. Messerschmidt, Fresenius' Z. Anal. Chem., 308 (1981) 104.
21 H. Berndt, J. Messerschmidt and E. Reiter, Fresenius' Z. Anal. Chem., 310 (1982) 230.

Analytica Chimica Acta, 285 (1994) 45–51
Elsevier Science B.V., Amsterdam

Determination of rhodium in organic solutions by flame atomic absorption spectrometry, with methyl isobutyl ketone and ethanol as solvents

Matti Kauppinen [a] and Kimmo Smolander

Department of Chemistry, University of Joensuu, P.O. Box 111, SF-80101 Joensuu (Finland)

(Received 12th May 1993; revised manuscript received 31st August 1993)

Abstract

A flame atomic absorption spectrometric method for the determination of rhodium in organic solutions containing toluene, 1-hexene, 1-heptanol and 1-heptanal is described. Methyl isobutyl ketone (MIBK) and ethanol were used as solvents and 1-heptanal as buffering agent. In addition to burner position, the composition of the organic solution significantly affected the absorbance. The recovery of 5 μg/ml rhodium was only 60% in a solution containing 75% MIBK, 20% toluene and 5% hexene, but improved as the ratio of alcohol or aldehyde to hexene increased. When the amount of hexene was reduced to zero and 5% heptanol, 5% heptanal or 2.5% heptanol + 2.5% heptanal was used instead, recoveries were 97%, 92% and 95%, respectively. The recoveries of 10 μg/ml rhodium in solutions containing 75% ethanol, 20% toluene and 2.5% hexene + 2.5% heptanol, heptanal or their mixtures were 97%, 104% and 103%, respectively. Ethanol has several advantages over MIBK as a solvent: it is cheaper, the smell is less unpleasant, the burner and chamber assembly keep cleaner and sensitivity is slightly better.

Keywords: Atomic absorption spectrometry; Ethanol; MIBK; Rhodium; Methyl isobutyl ketone

Atomic absorption spectrometry has been used for the determination of rhodium since 1959 [1]. In most of the studies undertaken, the matrix has been a synthetic aqueous solvent [2–12] or geological material [13–17]. In these matrices the interference of some cations can be eliminated by buffering [6–11]. Atwell and Hebert [5] found that unlike the air–acetylene flame, there was virtually no interference from cations and acids with the nitrous oxide–acetylene flame, and Kabil and Mostafa [12] eliminated the interferences of some organic compounds by adding *n*-butylamine.

Only a few of the methods reported in the literature describe the determination of rhodium in organic solvents. Deily [18] reported no interferences when determining rhodium with air–acetylene in benzene–ethanol and cyclohexane–ethanol solutions, where in each case ethylene glycol monomethyl ether was the solvent. In an analysis of ethylene glycol monomethyl ether–benzene solutions and acidified aqueous solutions, Garska [19] found that, under optimum conditions, the air–acetylene flame provides a sensitivity four times that of the nitrous oxide–acetylene flame. Hebisch et al. [20] studied the determination of rhodium in organic matrices (acetic acid and methanol) using an air–acetylene flame and achieved a detection limit of 0.2 μg/ml in acetic acid matrix.

In the work described here, we investigated the determination of rhodium in simple organic solutions (methyl isobutyl ketone and ethanol)

Correspondence to: M. Kauppinen, Department of Chemistry, University of Joensuu, P.O. Box 111, SF-80101 (Finland).

SSDI 0003-2670(93)E0513-7

and in organic solutions containing toluene, 1-hexene, 1-heptanol and 1-heptanal. Mixtures like these are found in hydroformulation reactions where rhodium cluster compounds are used as catalysts.

EXPERIMENTAL

Apparatus

A Varian SpectrAA-400 atomic absorption spectrometer equipped with a Varian Mark 5 A burner and the new spray chamber assembly 99 100611 00 for aqueous and organic solvents was used for all measurements. Instrumental parameters are given in Table 1.

Reagents

All chemicals were of analytical-reagent grade. 1-Hexene, 1-heptanol and 1-heptanal were from Sigma (St. Louis, MO), methyl isobutyl ketone (MIBK) was from Baker (Deventer), toluene from Riedel de Häen (Seelze) and ethanol (EtOH) from Alko (Rajamäki).

Standards for the determination of rhodium in organic solvents were prepared using sublimated rhodium carbonyl acetylacetonate [$Rh(CO)_2(O_2C_5H_7)$] synthesised by Neste (Porvoo).

Glassware and polypropylene tubes were acid washed with a solution containing 2 mol/l HNO_3 and 1.6 mol/l HCl and rinsed with deionized water (17.5 $M\Omega\ cm^{-1}$).

100 μg/ml Rh standard stock solutions were prepared daily by dissolving 23.13 mg of $Rh(CO)_2(O_2C_5H_7)$ in 100 ml of MIBK, toluene or ethanol.

Samples

Standard series containing sublimated rhodium carbonyl acetylacetonate in MIBK or in ethanol were prepared, and samples containing 80% toluene and 20% 1-hexene, 1-heptanol, 1-heptanal or their mixtures and 4–40 μg/ml of rhodium. Solvents were pure MIBK, MIBK with different amounts of ethanol, and absolute ethanol. The ratio of solvent to sample was 3:1, so that concentrations in final solutions were 1–10 μg/ml of rhodium, 75% solvent, 20% toluene and 5% 1-hexene, 1-heptanol, 1-heptanal or their mixtures.

TABLE 1

Instrumental parameters

Wavelength	343.5 nm
Lamp current	5 mA
Slit width	0.2 nm
Air flow	15 l/min
Acetylene flow	1.5 l/min
Delay time	1 s
Time constant	0.05 s
Measurement time	3 s
Replicates	3
Burner height	2.5
Sample uptake	8.9 ml/min

Many studies were done on 5 μg/ml Rh solutions containing 75% solvent (MIBK, ethanol or their mixtures), 20% toluene, 5–0% hexene, and 0–5% 1-heptanol, 1-heptanal or their mixtures.

RESULTS AND DISCUSSION

The new spray chamber, which is made of fluorinated high density polyethylene (FHDPE), withstood organic solvents well, unlike the earlier aluminium model 99 100379 00, which was quickly corroded.

Effect of burner height

We used as lean a gas mixture as possible in the burner since the organic solvents serve as a fuel. The burner height is critical, as can be seen in Figs. 1 and 2. Figure 1 shows how in each of three solutions the absorbances of 5 μg/ml Rh solutions in MIBK decreased when the burner was raised. At burner heights from 0 to 6 the absorbances of blanks containing MIBK, toluene, 1-hexene, and 1-heptanol or 1-heptanal were considerably stronger than the absorbance of pure MIBK and fairly constant, but when the burner was raised from position 6 to position 12 the absorbances of the mixture began to decrease, while the absorbance of MIBK slightly increased.

As shown in Fig. 2, the effect of burner height was the same in solvents containing 50% ethanol as in MIBK. In each case the absorbances of 5

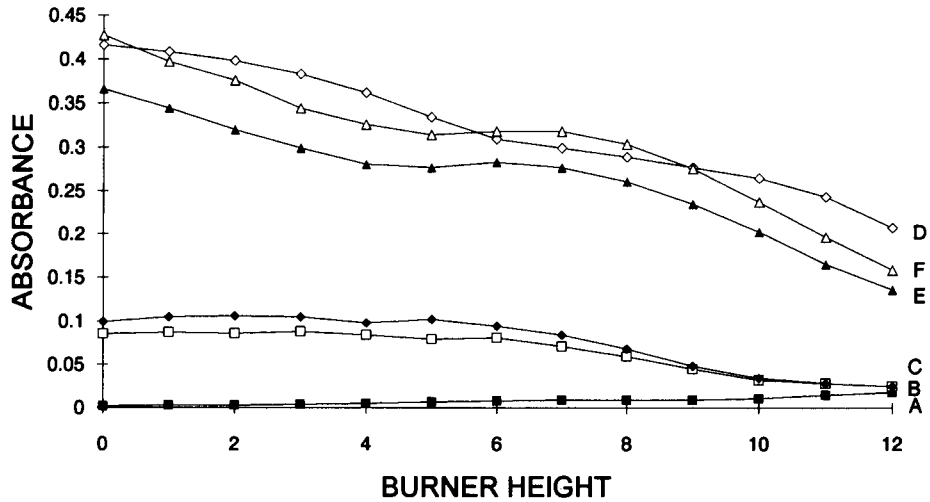

Fig. 1. Effect of burner height on absorbances of blanks (A, B, C) and of 5 μg/ml Rh solutions (D, E, F). Matrix compositions: A and D MIBK, B and E 75% MIBK + 20% toluene + 2.5% hexene + 2.5% heptanol, C and F 75% MIBK + 20% toluene + 2.5% hexene + 2.5% heptanal.

μg/ml Rh solutions decreased when the burner was raised. Note however, that the absorbances of blanks containing ethanol (Fig. 2, curves A and B), MIBK, toluene, 1-hexene, and 1-heptanol or 1-heptanal were about 50% less than those of blanks not containing ethanol (Fig. 1, curves B and C). The absorbance of a blank containing 50% ethanol and 50% MIBK (Fig. 2, curve C) was similar to the absorbance of pure MIBK (Fig. 1, curve A). The absorbances of rhodium solutions depended on both the composition of the organic solvent and the position of the burner.

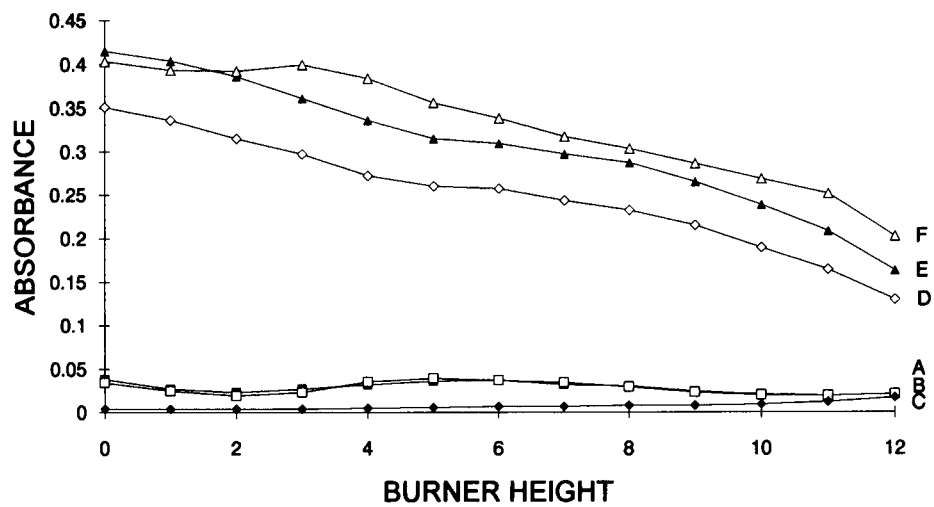

Fig. 2. Effect of burner height on absorbances of blanks (A, B, C) and of 5 μg/ml Rh solutions (D, E, F). Matrix compositions: C and F 50% ethanol + 50% MIBK, A and D 50% ethanol + 25% MIBK + 20% toluene + 2.5% hexene + 2.5% heptanol, B and E 50% ethanol + 25% MIBK + 20% toluene + 2.5% hexene + 2.5% heptanal.

The absorbances of 5 μg/ml rhodium solutions varied with the matrix and it was not possible to equalize the signal by adjusting the burner height.

MIBK as solvent

The calibration graph for rhodium in MIBK was nearly linear between 0 and 10 μg/ml (Fig. 3, curve A), but standards prepared in pure MIBK are not suitable for the analysis of solutions containing toluene, 1-hexene, 1-heptanol and 1-heptanal or only some of these compounds. One reason is that, at lower burner height, toluene increased the absorbances of blanks by as much as 0.09 (Fig. 1, curves A, B, C). The effect of toluene is also clearly seen if one compares blanks and solutions containing 1 μg/ml of rhodium (Fig. 3, curves B, C, D). For example, the absorbances of blanks containing 20% toluene with 5% of other organic solutions are equivalent to the absorbance of an analyte concentration of more than 1 μg/ml in pure MIBK, which especially in diluted solutions would give unacceptably high results (Table 4).

1-Hexene, 1-heptanol and 1-heptanal, like toluene, also affect the absorbances of solutions containing rhodium, which is a second reason why pure MIBK standards are not suitable for other solutions. 1-Hexene decreases the intensity of the absorption signal of rhodium dramatically: comparison of the calibration curves B and A in Fig. 3 shows that the absorbances of solutions containing 5% hexene and 20% toluene and 5–10 μg/ml of rhodium are only 50–60% of the absorbances of rhodium solutions in pure MIBK. The curves C and D show the effects of 2.5% of 1-heptanol and 1-heptanal together with 2.5% of hexene and 20% of toluene. Absorbances are greater than in curve B, but still less than in pure MIBK.

In addition to providing calibration graphs of rhodium in different matrices solutions were studied where the concentration of rhodium was constant and the ratio of 1-hexene, 1-heptanol and 1-heptanal varied. The results, presented in Table 2, show that the recovery of rhodium was only 60% in a solution containing 75% MIBK, 20% toluene, 5% hexene and 5 μg/ml of rhodium. However, when the ratio of alcohol or aldehyde to hexene increased, the recoveries increased as well. In the absence of hexene, and with 5% heptanol, 5% heptanal or 2.5% heptanol + 2.5% heptanal present instead, recoveries were, 97%, 92% and 95%, respectively (Table 2).

Buffering agents in MIBK

One way to determine rhodium in organic solutions directly is to prepare blanks and standards identical with the samples. Another way is to

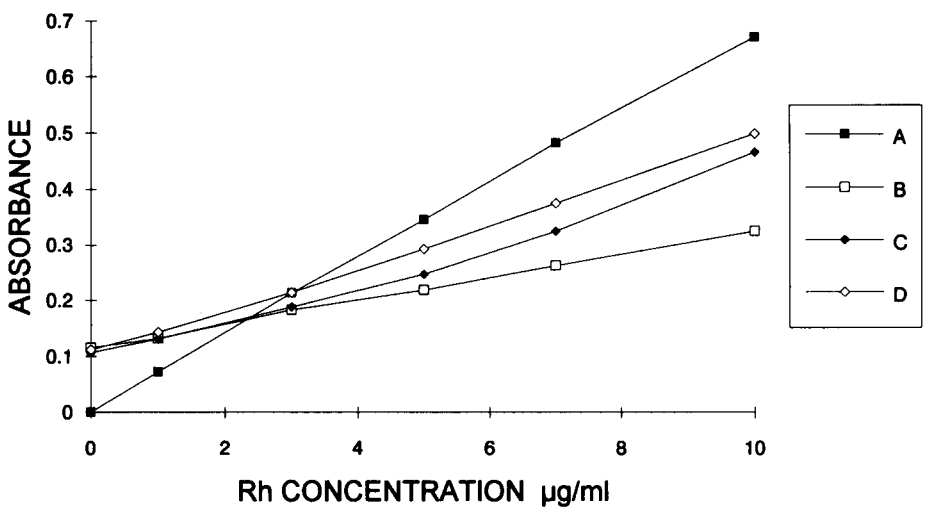

Fig. 3. Calibration curves of rhodium in organic solutions. A: 100% MIBK. B: 75% MIBK + 20% toluene + 5% hexene. C: 75% MIBK + 20% toluene + 2.5% hexene + 2.6% heptanol. D: 75% MIBK + 20% toluene + 2.5% hexene + 2.5% heptanal.

TABLE 2

Recovery of 5 μg/ml Rh in a solution containing 75% MIBK, 20% toluene, 5–0% 1-hexene and 0–5% 1-heptanol, 1-heptanal or 1-heptanol + 1-heptanal

Volume ratio of 1-hexene to alcohol, aldehyde or mixture	Recovery (%)		
	Heptanol	Heptanal	Heptanol + heptanal
5:0	60	60	60
4:1	66	75	74
3:2	70	78	76
2:3	78	87	83
1:4	82	89	88
0:5	97	92	95

use a buffering agent, if a suitable one exists. We tested uranyl nitrate ($UO_2(NO_3) \cdot 6H_2O$) in concentrations 1% and 0.1% in final MIBK solution, and *n*-butylamine ($C_6H_9NH_2$) in concentrations 0.1 M and 0.05 M in final MIBK solution, but the absorbances of the various solution mixtures remained different.

Ethanol as solvent

MIBK is not a good solvent for determining rhodium in organic solutions. It has a strong unpleasant smell and after every run the chamber assembly and burner must be cleaned with alcohol. This prompted us to test ethanol as solvent, first mixed with MIBK and finally alone. Original samples contained 20 μg/ml of rhodium in 80% toluene and 20% 1-hexene, 1-heptanol, 1-heptanal or their mixtures. After dilution the rhodium concentration was 5 μg/ml and final solutions contained 75% solvent, 20% toluene, 5–0% 1-hexene, 0–5% 1-heptanol, 1-heptanal or their mixtures.

In a first set of experiments, concentrations of ethanol in final solutions were 10% and 25% (Table 3). The absorbances were slightly stronger in solvents containing ethanol than where pure MIBK provided the solvent, but the differences between the absorbances of the various solution mixtures remained.

Next we tested solutions containing 5 μg/ml and 10 μg/ml of rhodium in 50% ethanol, 25% MIBK and 20% toluene, 2.5% 1-hexene and 2.5% 1-heptanol, 1-heptanal or their mixtures. The absorbances of blanks were now considerably decreased relative to pure MIBK solvent, while the absorbances of solution mixtures containing rhodium were closely similar (Figs. 1 and 2). Equivalent analyte concentrations were nearly identical in blanks of 2.5% heptanol and 2.5% heptanal (Table 4), but the differences in the absorbances of the various solution mixtures containing rhodium persisted (Table 5).

In a final set of experiments were ethanol alone provided the solvent, the absorbances of blanks were still further decreased (Table 4) and

TABLE 3

Recovery of 5 μg/ml of Rh in a solution containing 10% or 25% ethanol, 65% or 50% MIBK, 20% toluene, 5–0% 1-hexene and 0–5% 1-heptanol, 1-heptanal or 1-heptanol + 1-heptanal

Vol. % of ethanol in final solution	Volume ratio of hexene to heptanol, heptanal	Recovery (%)		
		Heptanol	Heptanal	Heptanol + heptanal
10	5:0	62	61	62
	4:1	70	82	76
	3:2	72	85	79
	2:3	88	88	84
	1:4	91	91	93
	0:5	108	96	105
25	5:0	63	62	63
	4:1	71	82	75
	3:2	72	87	81
	2:3	82	89	84
	1:4	93	92	93
	0:5	109	100	107

TABLE 4

Equivalent analyte concentrations of blanks in different matrices. Measured after calibration with standards in pure MIBK with burner at position 3

Vol.% of solvent in final solution	Matrix in final solution: 20% toluene, 2.5% hexene and	
	2.5% heptanol	2.5% heptanal
75% MIBK	1.10 μg/ml	1.32 μg/ml
50% ethanol + 25% MIBK	0.32 μg/ml	0.27 μg/ml
75% ethanol	0.17 μg/ml	0.15 μg/ml
75% ethanol[a]	< 0.01 μg/ml	< 0.01 μg/ml

[a] Calibration made with standards in 80% ethanol–20% toluene.

TABLE 5

Recoveries of 5 μg/ml and 10 μg/ml Rh in different matrices as percentage of recoveries from pure MIBK and from a solvent mixture containing 80% ethanol and 20% toluene

Matrix: 75% ethanol, 20% toluene, 2.5% hexene,	Recovery % relative to pure MIBK		Recovery % relative to 80% ethanol–20% toluene	
and 2.5%	5 μg/ml	10 μg/ml	5 μg/ml	10 μg/ml
Heptanol	97	102	90	97
Heptanal	111	109	103	104
Heptanol + heptanal	109	109	101	103

the absorbances of solvent mixtures containing rhodium increased relative to solutions where pure MIBK was as solvent. The recoveries of 5 μg/ml and 10 μg/ml of Rh in the different matrixes exceeded 100% relative to pure MIBK solutions, but the differences between the various solution mixtures remained (Table 5).

Heptanal as buffering agent in ethanol

As noted already, in the presence of 1-hexene, the absorption signal of rhodium was increased more by 1-heptanal than by 1-heptanol. The samples of 2.5 ml heptanol or heptanal in toluene that we studied contained 10% of 1-hexene, and the 1-hexene decreased the absorbances. However, when 0.5 ml of 1-heptanol and 7 ml of ethanol were added to the samples, the differences between the absorbances in the three matrices tended to disappear (Table 5). In this case, in final solutions, 1-heptanal was the main component increasing the absorbances. In experiments (Table 6) where the composition of final solutions was 70% ethanol, 20% toluene, 2.5% 1-hexene, 0–2.5% 1-heptanol and 5–7.5% 1-heptanal, the signal-decreasing effect of 1-hexene was still seen at rhodium concentrations of 5 μg/ml, and thus standards in MIBK or in ethanol–toluene cannot be recommended.

TABLE 6

Recoveries of 5 and 10 μg/ml of Rh in different matrixes as percentage of recoveries from pure MIBK and from a solvent mixture containing 80% ethanol and 20% toluene with 5% of heptanal as buffering agent

Matrix: 70% ethanol, 5% heptanal, 20% toluene, 2.5% hexene,	Recovery % relative to solutions in pure MIBK		Recovery % relative to solutions in 80% ethanol/ 20% toluene	
and 2.5%	5 μg/ml	10 μg/ml	5 μg/ml	10μg/ml
Heptanol	93	102	91	96
Heptanal	94	104	92	99
Heptanol + heptanal	94	103	92	98

Conclusions

No problems occur in the determination of rhodium in pure organic solutions such as MIBK or ethanol, but considerable problems arise when solutions contain toluene or other organic substances. Standards prepared in pure MIBK are not suitable for the analysis of solutions containing toluene, 1-hexene, 1-heptanol or 1-heptanal or even some of these compounds. Toluene increases the absorbances of blanks and decreases the absorbances of solutions containing rhodium, and 1-hexene, 1-heptanol and 1-heptanal affect the absorbances of solutions containing rhodium.

The use of ethanol instead of MIBK as solvent decreases the absorbances of blanks, but the various effects of other organic substances on the absorbances remain, so that standards prepared in pure ethanol or ethanol–toluene are not suitable for the analysis of solutions containing other organic substances.

When toluene solutions contain not more than 10% 1-hexene plus 10% 1-heptanol, 1-heptanal or their mixtures, one can compensate for the effects of these organic substances by adding 20% 1-heptanal as buffering agent and 70% ethanol as solvent.

However, when there are not many samples to analyse the best approach is to use ethanol as solvent and employ blanks and standards identical with the samples.

REFERENCES

1 R. Lockyer and G.E. Hames, Analyst, 84 (1959) 385.
2 A. Strasheim and G.J. Wessels, Appl. Spectrosc., 17 (1963) 65.
3 P. Heneage, At. Absorp. Newslett., 5 (1966) 64.

4 P.B. Zeeman and J.A. Brink, Analyst, 93 (1968) 388.
5 M.G. Atwell and J.Y. Hebert, Appl. Spectrosc., 23 (1969) 480.
6 M.M. Schnepfe and F.S. Grimaldi, Talanta, 16 (1969) 1461.
7 A. Janssen and F.Z. Umland, Anal. Chem., 251 (1970) 101.
8 G. Pannetier and P. Toffoli, Bull. Soc. Chem. Fr., 10 (1971) 3775.
9 S. Kallman and E.W. Hobart, Anal. Chim. Acta, 51 (1970) 120.
10 W.Z. Heinemann, Anal. Chem., 281 (1976) 291.
11 M.A. Mostafa and M.A. Kabil, Ind. J. Chem., 24A (1985) 260.
12 M.A. Kabil and M.A. Mostafa, Rev. Roum. Chim., 30 (1985) 631.
13 G.P. Sighinolfi, C. Gorgoni and A.H. Mohamed, Geostand. Newslett., 8 (1984) 25.
14 K. Slonawska and B.J. Krystyna, Anal. At. Spectrom., 4 (1989) 653.
15 M. Bergeron, M. Beaumier and A. Hebert, Analyst, 116 (1991) 1019.
16 J.G. Sen Gupta, Talanta, 36 (1989) 651.
17 H. Niskavaara and E. Kontas, Anal. Chim. Acta., 231 (1990) 273.
18 J.R. Deily, At. Absorp. Newslett., 6 (1967) 65.
19 K.J. Garska, At. Absorp. Newslett., 15 (1976) 38.
20 R. Hebisch, G. Emrich and H. Dilcher, Z. Chem., 29 (1989) 217.

Analytica Chimica Acta, 285 (1994) 53–56
Elsevier Science B.V., Amsterdam

Determination of zinc in aluminium metal by sequential metal vapour elution analysis

Kiyohisa Ohta, Syn-ya Inui, Masayoshi Yokoyama and Takayuki Mizuno

Department of Chemistry for Materials, Faculty of Engineering, Mie University, Tsu, Mie 514 (Japan)

(Received 8th April 1993; revised manuscript received 3rd August 1993)

Abstract

The determination of zinc in aluminium metal by sequential metal vapour elution analysis (column temperature > 1650 K) with argon as carrier gas and with atomic absorption spectrometric detection is described. The column was made of a molybdenum capillary tube (250 mm × 1.22 mm i.d.). The zinc vapour was separated from Al, Cu, Fe, Mg, Si and Ti metal vapour at the column temperature of 1650 K. The absolute detection limit was 12 pg (12 ng g^{-1}). The relative standard deviation for the determination of zinc in aluminium metals was 4.9–13%. The results were in good agreement with those obtained by a spectrometric method and a certified value.

Keywords: Atomic absorption spectrometry; Aluminium; Sequential metal vapour elution; Zinc

Aluminium metal contains some trace impurity metals, including zinc, which can affect its quality, and numerous papers concerning the determination of zinc in aluminium metal by atomic absorption spectrometry (AAS) or inductively coupled plasma atomic emission spectrometry (ICP-AES) have been reported [1–5]. In these methods, however, there are some problems such as poor sensitivity and optical and chemical interferences. In order to eliminate the interferences from the aluminium matrix, liquid–liquid extraction, coprecipitation or an ion-exchange method to separate zinc from the matrix has been used [2,3,5].

Investigating separation systems for high temperature metal vapours, Sokolov et al. [6] developed a separation system for metal alloys (Hg–Cd–Zn, etc.) using a stainless-steel column (970–1270 K) packed with graphite, silica gel or Chromosorb, over 20 years ago. More recently, Yanagisawa et al. [7,8] have demonstrated a separation system with a separative column atomizer (1070–1630 K) packed with molecular sieve, activated charcoal, graphite or metal-coated graphite. In these methods, however, the separation is effective only for volatile elements such as Hg, Cd and Pb. The special merit of sequential metal vapour elution analysis (SMVEA), developed recently [9–14], is a direct separation–detection system for the metal vapour with a relatively high melting point, without prior chemical treatment such as liquid–liquid extraction, coprecipitation, ion exchange, bubble separation, chemical modification and standard addition methods. Despite the advantages, few SMVEA studies for different elements have been reported.

In this study, the separation of zinc from aluminium, copper, iron, magnesium, silicon and titanium by SMVEA using a high-temperature column (> 1650° K) with argon as carrier gas and

Correspondence to: K. Ohta, Department of Chemistry for Materials, Faculty of Engineering, Mie University, Tsu, Mie 514 (Japan).

SSDI 0003-2670(93)E0508-5

with AAS detection was evaluated. The SMVEA–AAS system was applied to the determination of zinc in aluminium metal.

EXPERIMENTAL

Apparatus

The SMVEA set-up was reported in detail in a previous paper [9]. It contains a high-temperature column combined with three electrodes in a Pyrex glass dome. An open-tubular column is used, made of molybdenum capillary tubing (250 mm × 1.22 mm i.d.), 99.95% purity (Goodfellow). A 0.5-mm diameter hole is drilled at the mid-point of the atomization portion in the column for injection of sample solution. The detection portion has a 0.8-mm hole, perpendicular to the hole in the atomization portion, for atomic absorption measurement. A monochromator (Nippon Jarrell-Ash 0.5-m Ebert type), a lock-in amplifier (NF LI-575), a storage oscilloscope (Kikusui 5516 ST) and a microcomputer (EPSON, PC-286VG) are used for AA signal detection. Hollow-cathode lamps (Hamamatsu Photonics) are used as light sources. The analytical lines are 309.27, 324.75, 248.33, 285.21, 251.61, 364.27 and 213.86 nm for aluminium, copper, iron, magnesium, silicon, titanium and zinc, respectively. The absorption signal from the amplifier is fed into the microcomputer. The temperature of column is measured with an optical pyrometer (Chino Works). Two pinhole apertures are placed in front of and behind the detection hole portion to provide a narrow beam of light and to remove background emission from the column surface.

Reagents

Stock standard solutions (1 mg ml^{-1}) of Zn, Al, Cu, Fe and Mg were prepared from the high-purity metals as chlorides in 0.1–1 M hydrochloric acid. Si and Ti standard solutions (spectroscopic purity) were obtained from Nacalai Tesque (Kyoto). Working standard solutions for measurements were prepared by dilution of the stock standard solutions with distilled, deionized water just before use. All chemicals were of analytical-reagent grade.

Procedure

The flow-rates of purge gas in the column chamber were 3.0 l min^{-1} for argon and 200 ml min^{-1} for hydrogen. The slight hydrogen flow in the chamber was needed to protect the metal column from oxidization by residual oxygen in the argon. The flow-rate of argon carrier gas was 0.6 ml min^{-1}. The column temperature was in the range 1650–2040 K. The atomization temperature was 2120 K.

Aluminium metal samples of ca. 1–10 mg in a Teflon beaker were dissolved in 2 ml of 6 M hydrochloric acid. After the decomposition, the solution was evaporated by heating on a polyethylene glycol bath, the residue was dissolved in 10 ml of 1 M hydrochloric acid and the solution was diluted so as to obtain zinc in the optimum concentration range.

After stopping the flow of carrier gas, 1 μl of sample solution was pipetted into the atomization portion. The sample was dried at 400 K for 10 s and pyrolysed 760 K for 10 s. After starting the flow of the carrier gas, the column was heated at 1650 and 2040 K and then the residue in the atomization portion was atomized at 2120 K for > 1 min.

RESULTS AND DISCUSSION

Interference of aluminium on the zinc AA signal in conventional AAS has been reported [2,3]. In AAS using a metal tube atomizer, severe interference was also observed, as shown in Fig. 1. Less than 50 ng of aluminium did not interfere with 50 pg of zinc, but > 10000-fold aluminium

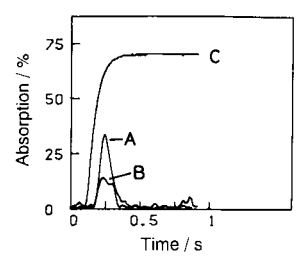

Fig. 1. Interference of aluminium on zinc AA signal in AAS using a metal tube atomizer. (A) Zn (50 pg) alone, (B) Zn (50 pg) + Al (500 ng); (C) temperature increasing.

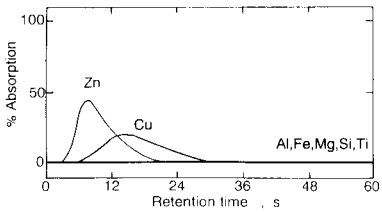

Fig. 2. SMVEA profiles at a column temperature of 1650 K. Atomization temperature, 2120 K; carrier gas, Ar at 0.6 ml min^{-1}; purge gas, Ar at 3000 and H_2 at 200 ml min^{-1}.

interfered considerably with the zinc signal. Therefore, the separation of zinc from aluminium, copper, iron, magnesium, silicon and titanium by SMVEA–AAS with argon as carrier gas was evaluated. The amounts of Al, Cu, Fe, Mg, Si, Ti and Zn introduced into the column were 1 μg and 20, 50, 10, 10, 10 and 5 ng, respectively.

The column temperature influences the retention time and separation power. Therefore, the performance characteristics of the metal column in SMVEA–AAS were evaluated at column temperatures of 1650–2040 K and an atomization temperature of 2120 K. Figures 2 and 3 show the SMVEA graphs at column temperatures of 1650 and 2040 K, respectively, and Tables 1 and 2 give the retention times (t_r) and their relative standard deviations (R.S.D.).

Zinc and copper metal vapours at 2040 K eluted away from Mg, Al, Fe, Si and Ti, but the separation of both elements was incomplete. The difference between the retention times of Zn and Cu is too small (only 0.9 s) for the R.S.D. of the t_r, as given in Table 2. However, zinc vapour at 1650 K was completely separated from Al, Cu, Fe, Mg, Si and Ti. Although the R.S.D. at the

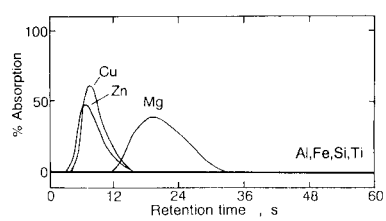

Fig. 3. SMVEA profiles at a column temperature of 2040 K. Conditions as in Fig. 2.

TABLE 1

Retention times obtained by sequential metal vapour elution analysis at a column temperature of 1650 K

Element	Retention time, t_r (s)	R.S.D. of t_r [a] (%)
Al	–	–
Cu	15	7.6
Fe	–	–
Mg	–	–
Si	–	–
Ti	–	–
Zn	7.9	8.1

[a] $n = 4–6$.

column temperature is poor (7–13%), it did not influence the separation power. From Figs. 2 and 3, it was found that the separation of zinc at a relatively low column temperature is preferable to a high column temperature. The boiling points of Zn, Al, Cu, Fe, Mg, Si and Ti metal are 1180, 2740, 2840, 3023, 1380, 2628 and 3560 K, respectively [15]. An element having a relatively low boiling point tends to elute more rapidly. The shorter retention time of copper signal is due to the greater facility of atomization on the molybdenum metal surface [16] and the lower adsorptivity on molybdenum metal. If there is no appreciable interaction between the metal vapours and the surface of the column, as the void volume of the column is 0.175 ml, the signals of Zn, Cu and Mg must appear at about 3.0 s under the experimental conditions. The retention times for the elements, even considering the atomization rate (< 1 s up to 2120 K), are much longer. Therefore,

TABLE 2

Retention times obtained by sequential metal vapour elution analysis at a column temperature of 2040 K

Element	Retention time, t_r (s)	R.S.D. of t_r [a] (%)
Al	–	–
Cu	8.1	13
Fe	–	–
Mg	19	8.2
Si	–	–
Ti	–	–
Zn	7.2	6.8

[a] $n = 4–6$.

TABLE 3

Determination of zinc in aluminium metal

Sample	Zn (μg g^{-1})		
	This method [a]	Spectrometric method [b]	Certified value
Al metal No. 1	40.7 ± 5.1	40.0	
Al metal No. 2	100.4 ± 4.9	100.0	
Si–Al alloy, SRM 87a [c]	1520 ± 150		1600

[a] Mean ± standard deviation (n = 3–4). [b] Ref. 17. [c] NIST standard.

the separation mechanism of these metal vapours may be due to the differential vapour pressure between each metal and the adsorptivity.

The absolute detection limit was 12 pg (corresponding to 12 ng g^{-1}). The relative standard deviation for peak area calculated for ten repeated measurements of 5 ng of zinc was 3.8%.

Zinc in aluminium metal was determined under the optimum experimental conditions. At a column temperature of 1650 K, residues of Al, Fe, Mg, Si and Ti might remain in the column after the determination of zinc. On subsequent heating of the column, however, no memory effect for these elements was observed. A calibration graph was prepared from zinc standard solutions and the absorbance peak areas. The calibration graph was linear up to 2 μg ml^{-1}. As shown in Table 3, the relative standard deviation for the determination of zinc in aluminium metal by the proposed method was in the range 4.9–12.6%. A reason of the relatively poor R.S.D. may be uneven distribution (localization) of zinc in the sample. However, the analytical results were in good agreement with those obtained by a spectrometric method [17] and the certified value for a NIST standard.

As described above, zinc vapour was separated from Al, Fe, Mg, Si and Ti metal vapours at a column temperature of 2040 K and even from Cu vapour at 1650 K.

The merits of the method are direct separation of metal vapours, rapid analysis, simplicity, elimination of the spectral and chemical interferences that occur in conventional AAS and ICP-AES and the possibility of using tandem mass spectrometric detection. Further, the excellent performance of SMVEA with the metal column may allow the accurate determination of various elements in metals after only acid dissolution of the metal samples without prior chemical treatment.

This work was supported financially by the Ministry of Education, Science and Culture of Japan. The authors thank Hajime Kawai for technical assistance.

REFERENCES

1 X. Xiao, Guangpuxue Yu Guangpu Fexi, 9 (1989) 55.
2 C.L. Sethi, B.K. Puri and M. Satake, Bunseki Kagaku, 33 (1984) E17.
3 R.C. Calkins, Appl. Spectrosc., 20 (1966) 146.
4 A. Quentmeier, K. Laqua and W.-D. Hagenah, Spectrochim. Acta, Part B, 35 (1980) 139.
5 J. Dumont, M. Cote and J. Hubert, Appl. Spectrosc., 43 (1989) 1132.
6 D.N. Sokolov, M.A. Baidarovtseva and N.A. Vakin, Izv. Akad. Nauk SSSR, Ser. Khim., 1968 (1968) 1396; D.N. Sokolov, J. Chromatogr., 47 (1970) 320.
7 M. Yanagisawa, K. Kitagawa and S. Tsuge, Spectrochim. Acta, 37 (1982) 493.
8 M. Yanagisawa, K. Katoh and K. Kitagawa, Anal. Sci., 6 (1990) 471.
9 K. Ohta, B.W. Smith, M. Suzuki and J.D. Winefordner, Spectrochim. Acta, Part B, 37 (1982) 343.
10 K. Ohta, B.W. Smith and J.D. Winefordner, Anal. Chem., 54 (1982) 320.
11 K. Ohta, B.W. Smith and J.D. Winefordner, Microchem. J., 32 (1985) 50.
12 K. Ohta, N. Nakajima, S. Inui, J.D. Winferordner and T. Mizuno, Talanta, 39 (1992) 1643.
13 K. Ohta, T. Sugiyama, S. Inui, T. Suzuki and T. Mizuno, J. Anal. At. Spectrom., 8 (1993) 595.
14 K. Ohta, N. Yamanaka, S. Inui, J.D. Winferordner and T. Mizuno, Analyst, 118 (1993) 1031.
15 D.R. Lide (Ed.), Handbook of Chemistry and Physics, CRC Press, Boston, 72nd edn., 1991, pp. 4–36, -56, -64, -71, -94, -108, and -111.
16 M. Suzuki and K. Ohta, Prog. Anal. At. Spectrosc., 6 (1983) 49.
17 H. Pohl, Aluminium, 38 (1962) 162.

Analytica Chimica Acta, 285 (1994) 57–61
Elsevier Science B.V., Amsterdam

Inductively coupled plasma atomic emission spectrometric determination of trace amounts of metals in palladium compounds

S.K. Atanasov and G.G. Stoyanova

University of Mining and Geology, Central Research Laboratory, 1156 Sofia (Bulgaria)

S.P. Bratinova and S.P. Popova

Technological University, Central Research Laboratory, 1156 Sofia (Bulgaria)

(Received 10th August 1993)

Abstract

A method for the determination of traces of Cu, Ni, Zn, Fe, Pb, Ag, Au and Pt in pure palladium salts using inductively coupled plasma atomic emission spectrometry was established. The most suitable spectral lines for the analysis were selected by considering two essential criteria: sensitivity and spectral interferences. Pb and Pt were determined using dynamic off-peak correction because of the complicated background close to their lines.

Keywords: Atomic emission spectrometry; Inductively coupled plasma spectrometry; Palladium compounds; Trace metals

Palladium salts such as diaminodichloropalladium $[Pd(NH_3)_2Cl_2]$ and diaminodinitropalladium $[Pd(NH_3)_2(NO_2)_2]$ are used as raw materials in the production of microelectronic systems; hence they have to conform to a high degree of purity. The contents of Cu, Ni, Zn, Pb, Fe, Au, Ag and Pt should not exceed 0.001–0.0001%. This necessitates the development of an accurate method of analysis with high sensitivity and selectivity.

There are few data in the literature on impurity determinations in palladium compounds. Spectral and neutron activation methods have gained widespread use for multi-element analysis [1]. Different versions of arc and spark atomic emission spectrometry [2–5] allow the simultaneous determination of many impurities in the range 10^{-1}–10^{-3}%. More sensitive are methods based on fractional evaporation [6], where 10^{-4}–10^{-5}% of some elements can be determined. The main problem, however, is related to the preparation of standards whose composition and properties are identical with those of the samples.

Neutron activation analysis (NAA) [7,8] and spark-source mass spectrometry (SSMS) [9] are highly sensitive and with possibilities for the determination of many elements. However, their great expense, the long duration of analysis (for NAA) and the need for specially prepared standards (for SSMS) make them unsuitable for laboratory analytical control.

Inductively coupled plasma mass spectrometry (ICP-MS) is one of the best techniques for trace analysis but is still very expensive. It has been

Correspondence to: S.P. Bratinova, Technological University, Central Research Laboratory, 1156 Sofia (Bulgaria).

SSDI 0003-2670(93)E0487-R

used in the analysis of palladium salts [10], but no details were given about the conditions under which the determinations were made.

Atomic emission spectrometry (AES) with an ICP is the most appropriate and widespread method for simultaneous multi-element control. The aim of this work was to develop an accurate and reproducible method for the determination of traces of Cu, Ni, Zn, Pb, Fe, Ag, Au and Pt in palladium compounds by ICP-AES.

EXPERIMENTAL

Apparatus

A Spectroflame inductively coupled plasma atomic emission spectrometer (Spectroanalytical Instruments, Germany) was used. It has three air and one vacuum polychromators and one monochromator in air. The reciprocal dispersion is 0.37 nm mm^{-1} (first order), which means 0.016 nm at the 250-nm B doublet. The wavelength range is 170–850 nm. The spectrometer has 32 channels, 8 of which are in vacuum. The operating parameters are presented in Table 1.

TABLE 1

ICP-AES instrumental parameters

Generator	Lynn r.f. generator, power and frequency electronically stabilized, maximum power output 2.5 kW, working power output 1.2 kW, frequency 27.12 MHz.
Nebulizer	TR-30-k3 (Meinhard); nebulizer spray chamber, Scott double-pass; peristaltic pump, 1.6 ml min^{-1} sample uptake.
Torch	Fassel, quartz, undemountable torch: coolant gas flow, 12.00 l min^{-1}; auxiliary gas flow, 0.75 l min^{-1}; carrier gas flow, 1.00 l min^{-1}; observation height, 13 mm above the coil
Optical system	1 monochromator in air, grating 2400 grooves mm^{-1}; 3 air polychromators, 2 gratings 3600 grooves mm^{-1}, 1 grating 1800 grooves mm^{-1}; 1 vacuum polychromator, grating 3600 grooves mm^{-1}
Integrator	dynamic type; integration time 5 s
Computer	IBM PS/2.

Reagents

All reagents were of analytical-reagent grade and doubly distilled, deionized water was used throughout.

Stock standard solutions of 1 g l^{-1} of each of Cu, Ni, Zn, Fe, Pb, Ag, Au, Pt and Pd (BDH) were prepared. Working standard solutions were prepared daily by appropriate dilution of the stock standard solutions.

Sample preparation

A 1.000-g amount of $Pd(NH_3)_2Cl_2$ or $Pd(NH_3)_2(NO_2)_2$, dried at 105°C, was dissolved in 25 ml of 2 M HNO_3 with heating at about 90°C for 1 h. After cooling to room temperature, the solution was diluted to 50 ml with water.

RESULTS AND DISCUSSION

Spectral interferences could occur owing to the presence of the high palladium concentration, exceeding 10 000-fold the contents of the impurities under examination. The remainder of the elements were present in commensurable amounts and could not cause inter-element influences. Hence not only the sensitivity but also the spectral purity of the chosen line were very important. Some of the most frequently used analytical lines in ICP-AES for Cu, Ni, Zn, Pb, Fe, Ag, Au and Pt are given in Table 2 together with nearby palladium lines. Only the 328.068-nm Ag line, the 259.940-nm Fe line and the 213.836-nm Zn line are free from spectral influences of palladium.

The most sensitive Cu line, 324.754 nm, has two palladium lines nearby, at 324.270 and 325.160 nm. The distance between them, however, exceeded several times the resolution of the spectrometer. Spectral scans around the 324.754-nm Cu line were made with two solutions, containing separately 100 μg Cu l^{-1} and 10 g Pd l^{-1}, and with a corresponding blank. The results showed that Pd caused only a slight increase in the blank under the peak of the Cu line, and its intensity was not sufficient to interfere (Fig. 1).

TABLE 2

Spectral lines for AES determination of Cu, Ni, Zn, Pb, Fe, Au, Ag and Pt, Pd lines, lying nearby and limits of detection (LOD)

Element	Line (nm)	LOD [a] ($\mu g\ l^{-1}$)	Pd line (nm)	$\Delta\lambda$ (nm)
Cu I	324.754	1.5	325.164	0.211
			324.270	0.480
Ni II	221.647	5.0	221.404	0.243
Ni II	231.603	5.0		
Ni II	232.000	6.8		
Zn I	213.856	2.0		
Fe II	259.940	2.0		
Ag I	328.068	2.7		
Au I	242.795	6.0	242.687	0.103
			243.093	0.170
Au II	267.595	9.3		
Pb II	220.353	20.0	220.236	0.117
Pb I	283.306	27.4		
Pt I	265.945	29.6	265.872	0.073
			266.114	0.163
Pt II	214.423	19.7		

[a] LOD is two standard deviations of the background in water.

Detection limit differences between the first and second resonance lines for Au and Ni are negligible. The choice fell on the latter, the 231.604-nm Ni line and the 267.595-nm Au line, which are fixed in the polychromator because they are spectrally clearer than the former not only with respect to palladium. The spectral scans done around them with solutions containing 10 g Pd l^{-1} and 1.0 mg Ni or Au l^{-1} show the same behaviour as for the 324.751-nm Cu line.

The situation with Pt and Pb was more complicated. The 220.353-nm Pb line and the 265.945-nm

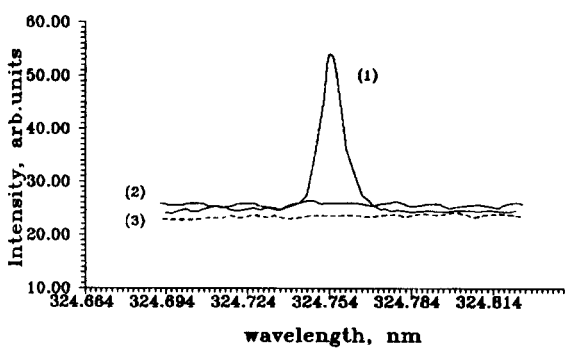

Fig. 1. Spectral scans around the 324.754-nm Cu line with (1) 100 μg Cu l^{-1}, (2) 10 g Pd l^{-1} and (3) blank.

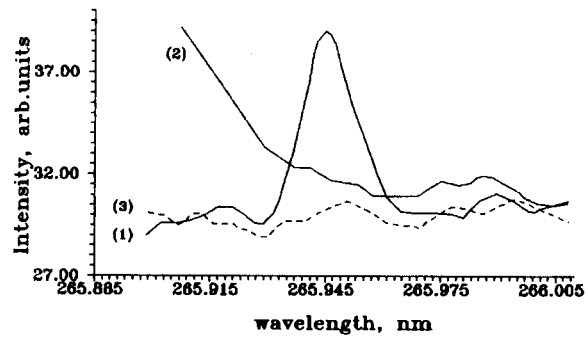

Fig. 2. Spectral scans around the 265.945-nm Pt line with (1) 1 mg Pt l^{-1}, (2) 10 g Pd l^{-1} and (3) blank. Spectral scans around the 220.236-nm Pb line are the same.

Pt line fixed in the polychromator have Pd lines nearby, at 220.236 and 265.872 nm. The scans done in a window of 20 nm around them with a 10 g Pd l^{-1} solution show an increase in intensity of the blank due to the wing spectral interference (Fig. 2). The 214.423-nm Pt line is free from palladium interference, but is not suitable owing to the decrease in signal caused by the quartz fibres in the monochromator. The 283.306-nm Pb line is also free from Pd interference and is more sensitive, but owing to the higher background the detection limit is poorer then for the 220.253-nm line. Both lines for both elements were used, for comparison, but correction for spectral interferences is required. They were taken into account by previously determining the correction coefficients for each element (Table 3) and applying an on-peak correction where necessary (for Pb and Pt).

The most suitable analytical lines for ICP-AES determination of Cu, Ni, Zn, Pb, Fe, Ag, Au and Pt in palladium salts were chosen as a result of these investigations.

Determination of Cu, Ni, Zn, Fe, Ag and Au

The procedure for the determination of Cu, Ni, Zn, Fe, Ag, Au, Pb and Pt was based on five calibration solutions. The concentrations of the calibration standards were in accordance with the expected amounts of these elements, i.e., 0.10, 0.25, 0.50 and 1.00 mg l^{-1} in 1 M HNO_3. A blank was also prepared, containing the same amount of HNO_3. A preliminary evaluation was made of

TABLE 3

Correction coefficients for spectral influence of Pd

Element	Wavelength (nm)	Correction coefficient K [a]
Zn	213.856	4.25×10^{-6}
Ag	328.068	5.00×10^{-6}
Fe	259.940	7.20×10^{-6}
Cu	324.754	1.43×10^{-5}
Ni	231.603	1.95×10^{-5}
Au	242.795	1.68×10^{-5}
Pb	220.351	6.92×10^{-4}
Pt	265.945	3.16×10^{-4}
Pb	283.306	5.81×10^{-5}
Pt	214.432	4.86×10^{-5}

[a] K is the slope of the function $C_{ed} = f(C_{ing})$, where C_{ed} is the concentration of the disturbed element (mg l^{-1}) and C_{ing} is the concentration of disturbing element (mg l^{-1}).

the chemical compatibility of the elements in the solution. Some of them were introduced into the multi-element standard solution as solutions in HCl. Hence conditions for AgCl precipitation may occur, in spite of the HNO_3 medium. Therefore, separation of Ag from other standards was necessary. Pd standards of 100, 1000 and 10000 mg l^{-1} were used for calculation of the correction coefficient and calibration of the Pd line. Calibration of the spectrometer was done with the chosen conditions and calibration standards. The results are presented in Table 4.

TABLE 4

Calibration data [a] for ICP-AES determination of Cu, Ni, Zn, Pb, Fe, Ag, Au and Pt and limit of detection (LOD)

Element	Wavelength (nm)	A_1	A_0	LOD (mg l^{-1})
Cu	324.754	+0.28005	−0.2556	0.00511
Ni	231.603	+3.75372	−0.3988	0.00798
Zn	213.856	+0.61192	−0.0796	0.00159
Fe	259.940	+0.85280	−0.1819	0.00364
Au	267.595	+0.77039	−0.3565	0.00713
Ag	328.068	+0.78493	−0.1843	0.00369
Pb	220.351	+24.45271	−1.0401	0.02080
Pt	265.945	+3.17058	−1.3919	0.02784
Pd	363.470	+2.51035	−7.3271	0.14654
Pt1	214.423	+80.00000	−5.1200	0.10240
Pb1	283.306	+3.78823	−2.8808	0.05762

[a] $C = A_1 I + A_0$, where C = concentration (mg l^{-1}), I = intensity, A_1 = slope (mg l^{-1}/digits) and A_0 = intercept (mg l^{-1}).

TABLE 5

ICP-AES and AAS determination of Cu, Ni, Zn, Fe, Pb, Ag, Au and Pt in $Pd(NH_3)_2Cl_2$

Element	ICP-AES determination in HNO_3		AAS determination	
	Content (%)	R.S.D. (%) [a]	Content (%)	R.S.D. (%) [a]
Cu	2.45×10^{-4}	5.51	2.62×10^{-4}	5.60
Ni	7.63×10^{-4}	4.60	7.21×10^{-4}	3.50
Zn	2.17×10^{-4}	5.50	2.37×10^{-4}	6.80
Au	2.46×10^{-4}	5.40	2.38×10^{-4}	6.30
Ag	3.16×10^{-4}	4.06	3.20×10^{-4}	2.86
Fe	8.15×10^{-4}	4.95	8.53×10^{-4}	3.80
Pb	6.55×10^{-3}	7.68	1.17×10^{-3}	5.90
Pb1	2.18×10^{-3}	11.32		
Pt	5.01×10^{-3}	8.20	9.00×10^{-4}	6.70
Pt1	2.65×10^{-3}	15.30		

[a] $n = 9$.

Results obtained with the proposed ICP-AES method are given in Table 5. The contents of Cu, Ni, Zn, Fe, Pb, Ag, Au and Pt were determined by flame atomic absorption spectrometry (AAS) after extraction of its complexes in an ammonium pyrolidinedithio-carbamate–tetrahexylammonium iodide/methyl isobutyl ketone system or by graphite furnace AAS (for Pt) for comparison by a statistical method. The contents of Cu, Ni, Zn, Ag and Au determined by ICP-AES coincided perfectly not only between themselves but also with those obtained by AAS [$t_{calc} < t_{crit}(8, 0.05) = 2.306$].

Determination of Pb and Pt

ICP-AES determination of Pb and Pt gave results that are several times higher than those obtained by AAS (Table 5). This is probably due to the large influence of Pd, worsening the effective detection limits. It could not be completely overcome even after introducing on-peak correction coefficients for the Pt and Pb lines. The use of dynamic off-peak correction was expedient because of the non-identical structure of the blank in the spectral range near the Pt and Pb lines. Scans with both elements at both wavelengths were carried out with a 20-step window (0.45 nm) and a 3 s per step integration time. First it was necessary to check whether the element content

TABLE 6

ICP-AES and AAS determination of Pb and Pt in $Pd(NH_3)_2Cl_2$ with dynamic off-peak correction

Element	Wavelength	ICP-AES determination		AAS determination	
		Content (%)	R.S.D. (%) [a]	Content (%)	R.S.D. (%) [a]
Pb	220.351	1.28×10^{-3}	7.1	1.17×10^{-3}	5.9
	283.306	1.06×10^{-3}	6.8		
Pt	265.940	8.52×10^{-4}	7.4	9.00×10^{-4}	6.7
	214.423	8.35×10^{-4}	13.0		

[a] $n = 9$.

was higher than its detection limit under the given conditions. Scans were done of analyte solutions and blank, and $\bar{I}_{blank}$ (mean value), $S.D._{blank}$ (standard deviation) and $\Delta I_{sample} = I_{s,max} - \bar{I}_{blank}$ were calculated. $\Delta I_{sample} > 2S.D._{blank}$ was found for both elements at both wavelengths. The Pb and Pt contents in the solutions were determined after a scan of the respective standard (1 mg l^{-1}) by the equation

$$C = C_{st} \times \Delta I_{sample} / \Delta I_{st}$$

As can be seen from the data in Table 6, the results obtained at both wavelengths agreed well with those given by AAS. Statistical analysis (Student's t) showed that the three mean values for element concentrations belonged to the same general population $[t_{calc} < t_{crit}(8, 0.05) = 2.306]$, and the differences between them are due only to random errors.

In conclusion, an accurate and sensitive method for the ICP-AES determination of Cu, Ni, Zn, Pb, Fe, Ag, Au and Pt has been developed. It can be applied not only for the analysis of palladium salts, but also of pure palladium.

REFERENCES

1 S.I. Ginsburg, Analytical Chemistry of the Elements. Analytical Chemistry of Platinum Metals, Nauka, Moscow, 1972, p. 531.
2 J. Hawley, W. Wark, C. Lewis and W. Ott, Trans. Can. Inst. Min. Metall., 54 (1951) 669.
3 C. Lewis and W. Ott, Trans. Can. Inst. Min. Metall., 56 (1953) 17.
4 F.E. Beamish, The Analytical Chemistry of the Noble Metals, Pergamon Press, Oxford, 1966.
5 A.D. Gutko, Analytical methods for Platinum Metals, Gold and Silver, Metalurgizdat, Moscow, 1960, pp. 191 and 202.
6 A.D. Gutko and E.I. Schurova, Improvements in Methods for Spectral Analysis of Noble Metals, MIR, Moscow, 1967, p. 39.
7 S. Sterlinski, H. Maleszewska, Z. Szopa and R. Dybczynski, J. Radioanal. Chem., 59 (1980) 141.
8 A.G. Ganiev, D.U. Karimkulov and H.R. Rahimov, Methods for Activation Analysis of the Noble and Rare Earth Metals, FAN, Tashkent, 1977, p. 85.
9 J.A. Karpov, U.Ch. Udelevich, E.N. Gilbert, E.A. Startseva, D.B. Kormilitsin and O.V. Schuvaeva, Zh. Anal. Khim., 40 (1985) 373.
10 G.R. Fuchs-Pohl and K. Solinska, GIT Fachz. Lab., 9 (1990) 1115.

Analytica Chimica Acta, 285 (1994) 63–71
Elsevier Science B.V., Amsterdam

Voltammetric determination of *tert*-butylhydroxyanisole in micellar and emulsified media

A. González, M.A. Ruiz, P. Yáñez-Sedeño and J.M. Pingarrón

Department of Analytical Chemistry, Faculty of Chemistry, University Complutense of Madrid, 28040 Madrid (Spain)

(Received 23rd July 1993; revised manuscript received 10th September 1993)

Abstract

A voltammetric study of the oxidation process of the antioxidant *tert*-butylhydroxyanisole (BHA) in micellar and emulsified media is described. The non-ionic surfactant Pluronic F-68, in Britton-Robinson buffer at pH 2.0, was found to be the most suitable surfactant for the determination of BHA in micellar solutions. The characteristics of the oxidation process were established. An emulsified medium formed with ethyl acetate as organic solvent and Pluronic F-68 as emulsifying agent was also used. Linear calibration graphs for BHA were obtained by differential pulse voltammetry within the ranges 1.0×10^{-6}–1.0×10^{-5} mol l^{-1} and 1.0×10^{-5}–5.0×10^{-5} mol l^{-1}. The limits of determination were found to be 1.3×10^{-6} mol l^{-1} and 8.5×10^{-7} mol l^{-1} BHA in micellar and emulsified media, respectively. Interferences from BHT (*tert*-butylhydroxytoluene), TBHQ (*tert*-butylhydroquinone), citric acid, propyl gallate and propylene glycol were tested. The method was applied to the determination of BHA in chewing gum samples by direct emulsification of an aliquot of the antioxidant extract from the sample in ethyl acetate.

Keywords: Voltammetry; Antioxidants; *tert*-Butylhydroxyanisole; Emulsions; Foods

Phenolic antioxidants are extensively used in the food industry as additives to oils or fats in order to prevent oxidative rancidity. One of the most common of these substances is BHA (*tert*-butylhydroxyanisole), which is also employed as preservative in chewing gum preparations.

Methods for the determination of these antioxidants have been reviewed [1]. Most of them have been applied to lipid-containing foods using gas chromatography (GC) [2–5] or liquid chromatography (LC) [6–9]. Few electrochemical methods have been described in the literature. Differential-pulse voltammetry has been used to determine phenolic antioxidants [10,11] and preconcentration of BHA at a carbon paste electrode has been studied [12]. Finally, amperometric detection has been used in LC [13–15] and flow-injection analysis (FIA) [16] to determine BHA and other antioxidants in food samples.

In this paper, micellar and oil–water emulsified media are used, preventing solubility problems and thus allowing to carry out voltammetric studies of the BHA oxidation process in predominantly aqueous media where special reference electrodes and solvent purification are not needed [17,18]. On the other hand, the direct emulsification from the extract of the samples allows the determination of BHA without a preceding solvent evaporation step, which means a significant improvement in the simplicity and rapidity of the method with respect to conventional electroanalytical methods and other non-electrochemical methods. Moreover, possible analyte losses occurring during the organic solvent evaporation step are avoided.

Correspondence to: J.M. Pingarron, Department of Analytical Chemistry, Faculty of Chemistry, University Complutense of Madrid, 28040 Madrid (Spain).

SSDI 0003-2670(93)E0504-Z

EXPERIMENTAL

Apparatus

The measurements were performed on an EG &G PAR 273 potentiostat using the 270 Electrochemical Analysis Software. A Metrohm E 510 pH meter, a P-Selecta Ultrasons ultrasonic bath and a Griffin flask shaker were also used.

Electrodes and electrochemical cell

A Metrohm 6.0804.010 glassy carbon electrode, a Metrohm 6.0702.100 saturated calomel electrode, a counter-electrode consisting of a platinum wire immersed in the solution and a double-walled Metrohm EA 867-20 cell were used for voltammetric studies. Controlled-potential coulometric studies were performed using a Pt mesh macroelectrode.

Reagents and solutions

Micellar stock solutions of BHA (5.0×10^{-4} mol l^{-1}) were prepared by weighing the product (Sigma) and dissolving it in a 1% (w/v) Pluronic F-68 (Fluka) aqueous solution by stirring for 5 min in the ultrasonic bath. More dilute standards were prepared by suitable dilution with water and stirring for 2 min in the ultrasonic bath.

Stock solutions of BHA (1.0×10^{-3} mol l^{-1}) in ethyl acetate were also used.

Aqueous 1% (w/v) stock solutions of the following surfactants: Triton X-405, Pluronic F-68, Hyamine 1622, cetyltrimethylammonium bromide, sodium laurylsulphate and pentanesulphonic acid, were prepared by weighing and dilution with water.

A Britton-Robinson buffer solution containing each component acid at 0.2 mol l^{-1} was used as supporting electrolyte. All other chemicals were of analytical-reagent grade. The water used was obtained from a Millipore Milli-Q purification system.

The analysed samples were commercial chewing gum sticks containing an unknown quantity of BHA (E-320) and the following ingredients: sorbitol, gum base, xylitol, hydrogenated glucose, syrup, mannitol, glycerol, natural flavourings, lecithine and aspartame.

Procedures

Pretreatment of the glassy carbon electrode. A scan from +0.9 V up to −0.9 V by applying an square-wave waveform (amplitude, 50 mV; step height, 10 mV; frequency, 50 Hz) was applied to the GCE [19], immersed in a solution of the supporting electrolyte, before each measurement in order to clean the electrode surface. In addition to this, polishing with alumina powder (0.3 μm) was performed daily.

When BHA was determined in chewing gum samples, the electrode was pretreated first by polishing with alumina and then by applying the square wave scan before each measurement.

Voltammetry in micellar solutions. A suitable volume of the micellar stock solution of BHA was transferred to a 50-ml flask and varying volumes of a 1% (w/v) Pluronic F-68 stock solution were added depending on the required final concentration. Then, 25.0 ml of 0.2 mol l^{-1} Britton-Robinson buffer solution at the required pH were added and the solution was diluted to the mark with water. The flask was placed in the ultrasonic bath for 2 min and finally, the micellar solution was transferred into the electrochemical cell and voltammograms were recorded at 20 ± 1°C.

Voltammetry in oil–water emulsions. A suitable volume of the BHA stock solution in ethyl acetate was transferred into a 50-ml flask, and varying volumes of a 1% (w/v) Pluronic F-68 solution and of ethyl acetate (up to 4.0 ml) were added. Then, 25.0 ml of 0.2 mol l^{-1} Britton-Robinson buffer solution at the required pH were added and the solution was diluted to the mark with water. After shaking for a few seconds, the flask was placed in the ultrasonic bath for 5 min and shaken by hand each minute. The emulsion obtained was transferred to the electrochemical cell and voltammograms were obtained.

Determination of BHA in chewing gum samples. About 5 g of sample, cut in small portions, was accurately weighed and introduced into a 100-ml Erlenmeyer flask. 50 ml of ethyl acetate were added and the capped flask was shaken on a flask shaker for 12 h. The mixture was placed into a freezer for 2 h in order to precipitate the gum base polymer components. Then, a 2-ml aliquot of the supernatant solution was emulsified by

following the procedure specified above. The determination of BHA was carried out by applying the standard additions method, which involved the addition of 27 to 135 μg of BHA from a 3.0×10^{-3} mol l^{-1} BHA stock solution in ethyl acetate.

RESULTS AND DISCUSSION

Micellar solutions

In order to choose the most suitable surfactant for the voltammetric study of BHA, various cationic (Hyamine 1622 and cetyltrimethylammo-

TABLE 1
DPV in micellar solutions
(1.0×10^{-4} mol l^{-1} BHA; 0.1% surfactant; 0.1 mol l^{-1} Britton-Robinson buffer)

Surfactant	pH	i_p, μA	E_p, V	Observations
Hyamine 1622	4.0	0.538	0.538	One peak. The descending part overlaps
		0.064	0.622	with a second worse-defined peak. A small
				background peak at 0.7 V.
	7.0	0.300	0.400	One peak and a shoulder at more positive
			0.685	potential. A small background peak at 0.6 V.
	10.0	0.750	0.165	Two well-resolved peaks.the first of them
		0.136	0.700	better defined. A small background peak at 0.3 V.
CTAB	4.0	0.542	0.513	Two overlapped peaks.
			0.621	
	7.0	0.312	0.352	Two bad defined peaks.
			0.588	
	10.0	0.705	0.152	Two well-resolved peaks, the first of the
		0.092	0.600	better defined.
Laurylsulphate (Na salt)	4.0	1.100	0.480	Two close peaks, the first of them very well-defined
	7.0	0.500	0.376	Low reproducibility.
			0.506	
	10.0	0.510	0.172	Low reproducibility.
			0.490	
Pentanosulphonic acid (Na salt)	4.0	1.020	0.493	One very broad peak appears. Low reproducibility.
	7.0	0.720	0.358	One peak and a shoulder at a more
				positive potential.
	10.0	0.857	0.148	Two well resolved peaks. Low reproducibility.
		0.115	0.579	
Triton X-405	4.0	0.850	0.515	Two very close peaks. A small background
				peak at 0.8 V.
	7.0	0.641	0.368	Two close peaks.
		0.074	0.544	
	10.0	0.680	0.150	Two very well-resolved peaks. A small
		0.128	0.570	background at 0.40 V.
Pluronic F-68	4.0	1.100	0.495	One well-defined peak.
	7.0	0.700	0.360	Two close peaks.
		0.072	0.572	
	10.0	0.800	0.154	Two well-resolved peaks.
		0.163	0.580	

nium bromide), anionic (sodium laurylsulphate and pentanesulphonic acid) and non-ionic (Triton X-405 and Pluronic F-68) surfactants, all of them quite soluble in water, were tested at three pH values, 4.0, 7.0 and 10.0 in a 0.1 mol l^{-1} Britton-Robinson buffer. The results obtained by differential pulse voltammetry (DPV) are summarized in Table 1. As can be observed, in all the studied media, BHA shows either a broad peak or two very close peaks at pH 4.0, and two peaks at pH 7.0 and 10.0, these peaks being better resolved in basic media. Taking into account the analytical characteristics of the responses (sensitivity, background signal and reproducibility) of the BHA oxidation signals in these media, Pluronic F-68 was chosen as the most suitable surfactant. The peak current for BHA does not depend on the Pluronic F-68 concentration between 0.02 and 0.2%. A Pluronic percentage of 0.06% was chosen for further studies. This low surfactant concentration minimizes its possible adsorption on the electrode surface.

Linear sweep voltammetry at a rotating disk electrode. At a concentration of 2.0×10^{-5} mol l^{-1} and 2000 rev. min^{-1}, BHA shows one well-defined wave at pH 1.5 and 2.0. This wave is gradually split as pH increases and, from pH 5.0, two well-defined waves can be observed being more separated at higher pH values (Fig. 1). Moreover, and also from pH 5.0, a third wave, which becomes better defined as pH increases, was observed, the half-wave potential being roughly 1.0 V. Figure 2 shows the effect of pH on

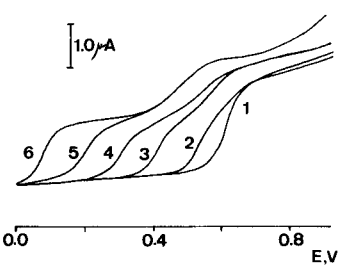

Fig. 1. Linear sweep voltammograms in micellar solution at a glassy carbon rotating disk electrode: 2.0×10^{-5} mol l^{-1} BHA, 0.06% Pluronic F-68, 0.1 mol l^{-1} Britton-Robinson buffer, 2000 rev. min^{-1}; 1, pH 1.5; 2, pH 3.0; 3, pH 5.0; 4, pH 7.0; 5, pH 9.0; 6, pH 11.0.

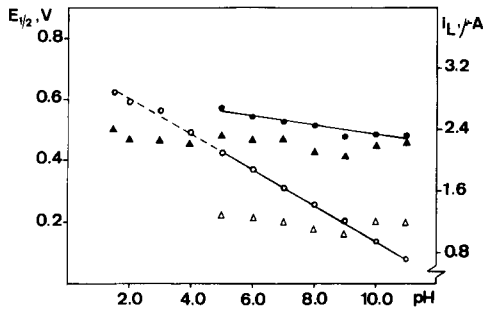

Fig. 2. Effect of pH on $E_{1/2}$ and i_L in LSV at a glassy carbon rotating disk electrode: ○ and △, $E_{1/2}$ and i_L of the first wave; ● and ▲, $E_{1/2}$ of the second wave and overall current, respectively. 2.0×10^{-5} mol l^{-1} BHA; 0.06% Pluronic F-68; 0.1 mol l^{-1} Britton-Robinson buffer.

$E_{1/2}$ and i_L values for the first and the second waves. As can be observed, $E_{1/2}$ values of the wave appearing at pH values lower than 5.0 fit remarkably with $E_{1/2}$ values of the wave appearing at less positive potentials when these two waves are considered (pH > 5). The decrease of $E_{1/2}$ as pH increases shows a linear relationship ($r = 0.9997$) with a slope of -0.057 V. This behaviour indicates that protons are involved in the electrodic process, the electrochemical oxidation being easier in basic media. The $E_{1/2}$ values of the wave appearing at more positive potentials in the pH range 5.0–11.0 decrease only slightly with increasing pH.

On the other hand, limiting current of the first wave remains practically constant over the 5.0–11.0 pH range. The values of the overall i_L for the two waves considered at pH > 5.0 are also similar to those of the single wave observed in more acidic media, and approximately two-fold of the other wave, indicating that the number of electrons involved in the overall oxidation of BHA is the same in the whole pH range.

In order to have the best sensitivity and simplicity, pH 2.0 was chosen as working pH for subsequent voltammetric studies.

Levich's law was obeyed within the range of rotation rates studied, 500–3000 rev. min^{-1} and over the concentration range 1.0×10^{-5}–6.0×10^{-5} mol l^{-1}, the correlation coefficient values ranging between 0.999 an 0.992. This indicates

that the limiting current is probably diffusion controlled in this concentration range.

The i_L vs. concentration plots were also linear in the same concentration range for different rotation rates, 500–3000 rev. min^{-1} ($r = 0.999$–0.998), thus confirming that the BHA oxidation wave is diffusion controlled at these concentration levels. The slope of the linear portion of the E vs. $\log(i/i_L - i)$ plot for 2.0×10^{-5} mol l^{-1} BHA at pH 2.0 was 0.058 V. The number of electrons involved in the oxidation process was two, as determined by controlled-potential coulometry at this pH value using a Pt mesh as macroelectrode. Therefore, the non-reversibility of the electrode process can be stated. An $(1-\alpha)n_a$ value of 0.98 was obtained, which is consistent again with a double electron exchange in the BHA oxidation process, as observed for substituted phenols [16]. The $(1-\alpha)n_a$ value is in good agreement with that obtained from the Tafel plot, 0.99.

Linear sweep voltammetry at a stationary electrode. Voltammograms obtained for 4.0×10^{-5} mol l^{-1} BHA showed a single well-developed oxidation peak at pH 1.5 and 2.0. A second worse-defined peak and a little shoulder appeared at more positive potentials for higher pH values. The potential of the first oxidation peak decreases linearly ($r = 0.9994$ and slope of -0.058 V) as the pH increases.

The dependence of the peak current and peak potential on the scan rate was examined for 6.0×10^{-5} mol l^{-1} BHA at pH 2.0. The plot of i_p vs. the square root of the scan rate was linear within the range 5–200 mV s^{-1} ($r = 0.999$), but deviates from linearity at higher scan rates. Peak currents higher than those expected for a linear i_p vs. $v^{1/2}$ plot were obtained in the range of scan rates 350–2000 mV s^{-1}. In this range, the function i_p/v remains practically constant indicating adsorption of BHA on the electrode surface. Moreover, E_p becomes more positive with increasing v in the same range.

Cyclic voltammetry. Cyclic voltammograms for 6.0×10^{-5} mol l^{-1} BHA at pH 2.0 and $v = 50$ mV s^{-1} are shown in Fig. 3a. As it can be observed, one oxidation peak (peak A) and two reduction peaks (peaks B and B′) appear in the

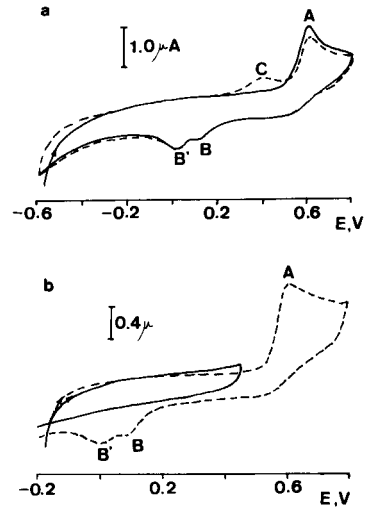

Fig. 3. Cyclic voltammograms in micellar solution for 6.0×10^{-5} mol l−1 BHA: (a) ——— first scan; — — — second scan; (b) — — — first scan up to +0.80 V; ——— first scan up to +0.30 V; 0.06% Pluronic F-68; 0.1 mol l^{-1} Britton-Robinson buffer of pH 2.0; $v = 50$ mV s^{-1}.

first scan, whereas a new oxidation peak (peak C) was obtained in the course of the second scan. Peaks B and B′ can be attributed to the reduction of some oxidation product of BHA because they do not appear when the scan is reversed at a potential value before the apparition of peak A (Fig. 3b). On the other hand, peak C must correspond to the oxidation of the product formed in the former reduction and this product must be different than BHA. All these results suggest a chemical reaction following the BHA initial anodic reaction, and the next oxidation mechanism can be proposed:

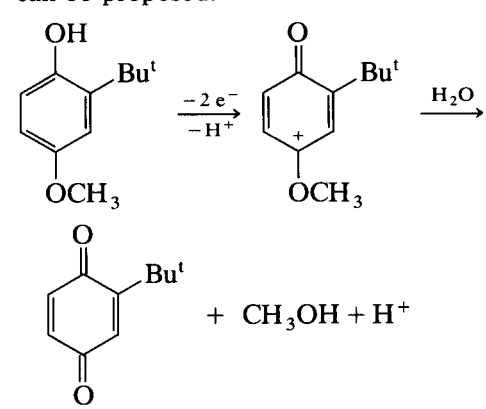

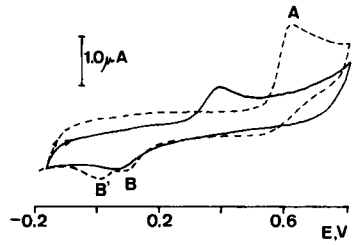

Fig. 4. Cyclic voltammograms in micellar solution: ——— 6.0×10^{-5} mol l^{-1} BHA; ——— 6.0×10^{-5} TBHQ; 0.06% Pluronic F-68; 0.1 mol l^{-1} Britton-Robinson buffer of pH 2.0; $v = 50$ mV s^{-1}.

The formation of *o*- or *p*-benzoquinones or products derived from the quinones has been reported for the anodic oxidation of phenols bearing methoxy groups in the 2- or 4-positions in the presence of water [20].

The proposed final product of the reaction, *tert*-butylquinone (TBQ), is also the oxidation product of the antioxidant *tert*-butylhydroquinone (TBHQ). A polarographic study of the oxidation process of TBHQ in micellar and emulsified media has been recently reported [18]. Thus, in order to verify the proposed mechanism, a cyclic voltammogram of TBHQ was recorded at the same experimental conditions used for BHA and compared with those shown in Fig. 3a. This comparison is illustrated in Fig. 4. As it can be observed, the oxidation peak for TBHQ coincides with the peak C observed in the second scan for BHA, which confirms the proposed reaction sequence. Moreover, the reduction peak obtained in the cyclic voltammogram of TBHQ also coincides with the reduction peaks (B and B') appearing in the cyclic voltammogram of BHA, which suggests that at least one of these peaks should correspond to the reduction of TBQ formed as an oxidation product of BHA.

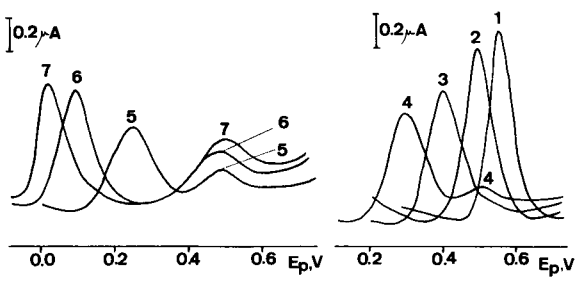

Fig. 5. Differential pulse voltammograms in micellar solution for 4.0×10^{-5} mol l^{-1} BHA; 0.06% Pluronic F 68; 0.1 mol l^{-1} Britton-Robinson buffer; $\Delta E = 50$ mV; 1, pH 1.5; 2, pH 3.0; 3, pH 5.0; 4, pH 7.0; 5, pH 8.0; 6, pH 10.0; 7, pH 11.0.

Differential pulse voltammetry at a stationary electrode. Differential pulse voltammograms, scanned in the potential range of analytical interest using $\Delta E = 50$ mV, at different pH values are shown in Fig. 5. As expected, only one peak was observed between pH 1.5 and 5.0; however, two peaks appeared for higher pH values in the potential range scanned. At pH 2.0, where the best signal-to-background ratio was observed, the plots of peak current against concentration of BHA were linear within the ranges 1.0×10^{-5}–5.0×10^{-5} mol l^{-1} ($r = 0.999$) and 1.0×10^{-6}–1.0×10^{-5} mol l^{-1} ($r = 0.999$). The slopes and intercepts of these plots were $(2.9\pm0.3)\times10^{4}$ μA l mol^{-1} and 0.09 ± 0.09 μA and $(3.7\pm0.1)\times10^{4}$ μA l mol^{-1} and 0.009 ± 0.008 μA for the upper and lower range of linearity, respectively. For concentrations higher than 5.0×10^{-5} mol l^{-1} the linearity was lost, indicating adsorption of BHA at high concentrations of the antioxidant.

The analytical characteristics of the method based on the lower calibration graph mentioned above are: relative standard deviation of 5.3% for a concentration level of 5.0×10^{-6} mol l^{-1} ($n = 10$); limit of determination, according to the 10 × standard deviation criterion [21], 1.3×10^{-6} mol l^{-1}; and limit of detection, defined as $3s_b/m$ [22], 3.9×10^{-7} mol l^{-1}, where m is the slope of the calibration graph and s_b is the standard deviation ($n = 10$) of the signals from 1.0×10^{-6} mol l^{-1} BHA.

Emulsified medium

The determination of BHA in different samples, particularly food, involves its extraction into an organic solvent. For this purpose ethyl acetate can be used and, moreover, it has been successfully used to form oil-in-water emulsions [17]. Consequently, ethyl acetate was chosen as organic solvent to form emulsions in this work, as well as Pluronic F-68 as emulsifying agent. For the optimization of the chemical parameters in emulsified medium (surfactant percentage, vol-

ume of the organic phase and emulsification time), differential pulse voltammetry of 1.0×10^{-5} mol l^{-1} BHA solutions at pH 2.0 was used. The surfactant percentage did not have a significant influence on the oxidation peak in the range 0.02–0.20%, and thus, the same Pluronic F-68 percentage employed in micellar solutions, i.e., 0.06% was chosen for subsequent studies. The volume of ethyl acetate, neither had an influence on BHA peak current nor on peak potential in the range 0.5–4.0 ml when an emulsification time of 5 min was used. However, for higher organic phase volumes, an emulsification time higher than 5 min was required to form emulsions, its stability being considerably decreased. Consequently, a volume of 2.0 ml was used in further studies, as well as an emulsification time of 5 min.

The effect of pH on the BHA oxidation signal was studied by linear sweep and differential pulse voltammetry. A similar behaviour than that reported for micellar solutions was observed in both cases. For example, the E_p for the first oxidation peak observed in LSV decreases linearly ($r = 0.998$) as the pH increases with the same slope value, -0.058 V, than that obtained in micellar solutions. Likewise, the highest signal-to-background ratio for differential pulse voltammograms was observed at pH 2.0.

Cyclic voltammograms of 4.0×10^{-5} mol l^{-1} BHA at pH 2.0 were also similar to that shown in Fig. 3a, showing one oxidation peak at 0.610 V and two reduction peaks at 0.145 V and 0.064 V in the first scan.

On the other hand, $(1-\alpha)n_a$ values of 1.09 and 0.99 were calculated at pH 2.0 from the slope of the linear portion of the E vs. $\log(i/i_L - i)$ plot and from the Tafel plot, respectively, both plots having been obtained from the voltammogram at a rotating disc electrode of 2.0×10^{-5} mol l^{-1} BHA. These results suggest that, regarding the BHA oxidative voltammetric behaviour, similar conclusions than those commented for micellar solutions can be achieved in the oil-in water emulsions used.

Using differential pulse voltammetry with a pulse amplitude of 50 mV, the plots of i_p vs. BHA concentration were linear within the following concentration ranges: 1.0×10^{-5}–5.0×10^{-5} mol l^{-1} ($r = 0.998$, slope $(3.9 \pm 0.4) \times 10^4$ μA l mol^{-1}, and intercept -0.009 ± 0.1 μA) and 1.0×10^{-6}–1.0×10^{-5} mol l^{-1} ($r = 0.999$, slope $(3.7 \pm 0.1) \times 10^4$ μA l mol^{-1}, and intercept -0.008 ± 0.007 μA). The analytical characteristics of the proposed method, obtained from the calibration graph for the lowest of these concentration ranges are: relative standard deviation of 4.5%, calculated for a concentration level of 5.0×10^{-6} mol l^{-1} ($n = 10$), and limits of determination and detection of 8.5×10^{-7} mol l^{-1} and 2.5×10^{-7} mol l^{-1} respectively, calculated from the standard deviation ($n = 10$) of the signals from 1.0×10^{-6} mol l^{-1} BHA.

Interferences. Different substances commonly present in commercial antioxidant mixtures: BHT (*tert*-butylhydroxytoluene), TBHQ, citric acid, ascorbic acid, PG (propyl gallate) and propylene glycol were tested by DPV in order to check for interferences with respect to the BHA peak. Various interferent-to-analyte ratios were studied for a BHA concentration of 5.0×10^{-6} mol l^{-1}. Voltammograms from solutions containing citric acid or propylene glycol alone, under the experimental conditions used for the BHA determination in the emulsified medium, showed no oxidation peak in the potential range scanned (0.00–1.00 V), and these substances did not interfere even at a BHA-to-interferent ratio of 1:200. However, BHT, TBHQ, ascorbic acid and PG exhibited well-defined oxidation peaks at 0.46, 0.33, 0.49 and 0.43 V. The closeness among the peak potentials for BHT and ascorbic acid compared to that of BHA (0.53 V) yielded only one overall oxidation peak when voltammograms of 1:1 mixtures of BHT and BHA and of ascorbic acid and BHA were recorded. On the contrary, two peaks were obtained for mixtures of BHA with PG or TBHQ. The presence of TBHQ affects the BHA signal for a TBHQ-to-BHA ratio of 10:1 or higher; for example a relative error of 9.7% was obtained for a 20:1 TBHQ-to-BHA ratio. This is because high TBHQ concentrations give rise to a high oxidation peak whose descending part overlaps the BHA peak. PG showed an intense oxidation peak in this emulsified medium and, consequently, the same effect commented above for TBHQ was now perceived at lower

PG-to-BHA ratios. Thus, PG affects the BHA signal for PG-to-BHA ratios higher than 3:1. On the other hand, BHT causes a high fouling of the glassy carbon electrode surface, which give rise to interference (relative errors higher than 5%) even for a BHT-to-BHA ratio of 0.1:1. Finally, an ascorbic acid-to-BHA ratio of 5:1 yielded a relative error of 10%.

Determination of BHA in chewing gum samples. The procedure described in the Experimental section for DPV in emulsified medium was used to determine BHA in commercial chewing gum samples containing an unknown amount of this antioxidant. No interferences were observed from other substances present in the samples, thus direct analysis of various aliquots of the extract in ethyl acetate was performed, by applying the standard additions method in order to minimize the matrix effects.

The results obtained from five BHA determinations are summarized in Table 2, the confidence interval being calculated for a significance level of 0.05. The mean value was 0.20 ± 0.02 mg g^{-1} BHA, which agrees well with the expected concentration levels for this antioxidant in this kind of samples [23]. In order to evaluate the accuracy of the proposed method, recovery studies were carried out after adding a known quantity of BHA to the sample, by following the procedure described in the Experimental section. As Table 3 shows, good results were obtained, the mean recovery being 99%. The relative standard deviation was 2.6% and the confidence interval was $\pm 3\%$ for a significance level of 0.05.

TABLE 2

Determination of BHA in commercial chewing gum samples by DPV in emulsified medium
(0.1 mol l^{-1} Britton-Robinson buffer, pH 2.0; 0.06% Pluronic F-68; $\Delta E = 50$ mV; $t_{95\%} = 2.776$)

Sample	BHA, mg g^{-1} of sample	$\bar{x}$, mg g^{-1}	s_{n-1}	$\bar{x} \pm t\frac{s_{n-1}}{n^{1/2}}$
1	0.19			
2	0.22			
3	0.18	0.20	±0.02	0.20±0.02
4	0.22			
5	0.20			

TABLE 3

Recovery studies on chewing gum samples by DPV in emulsified medium
(Britton-Robinson buffer, pH 2.0, Pluronic F-68, 0.06%, $\Delta E = 50$ mV)

Sample	BHA, mg g^{-1} [a]			Recovery, %
	Added	Total		
		Theoretical	Experimental	
1	0.135	0.335	0.342	102
2	0.135	0.335	0.340	99
3	0.135	0.335	0.340	101
4	0.135	0.335	0.324	97
5	0.135	0.335	0.322	96

[a] Concentration in the chewing gum sample.

In conclusion, the voltammetric determination of BHA in an emulsified medium formed with ethyl acetate and Pluronic F-68 may be suitable as a quick control test for this antioxidant in food samples, taking into account that the direct emulsification of the analyte extract from the sample allows the determination to be carried out without an organic solvent evaporation step. This implies an improvement of the simplicity and rapidity of the method as well as of the obtained recoveries.

Financial support from the Spanish CICYT (project ALI 92-0049) and the Comunidad de Madrid (project C009/91) is gratefully acknowledged.

REFERENCES

1 K. Robards and S. Dilli, Analyst, 112 (1987) 933.
2 L.Z.Yu, M.Inoko and T. Matsuno, J. Agric. Food Chem., 32 (1984) 681.
3 O. Suzuki, S. Yoneyama, K. Iimura, K. Kumozaki, A. Tanaka, A. Takeshita, I. Tajima, S. Tanabe and A. Nagao, Yukagaku, 39 (1990) 685.
4 Official Methods of Analysis of the Association of Official Analytical Chemists, AOAC, Arlington, VA, 14th edn., 1984 Procedure 20012 p. 373.
5 A. Baillet, S. Rakotomanga, D. Ferrier and F. Pellerin, J. Chromatogr., 519 (1990) 337.
6 B.D. Page, J. Assoc. Off. Anal. Chem., 66 (1983) 727.
7 A. Dieffenbacher, M.J. Trisconi and B. Durieux, Mitt. Geb. Lebensmittel-Unters. Hyg., 80 (1989) 204; Anal. Abstr., 52 (1990) 2F13.

8 G. Montedoro, M. Servili, M. Baldioli and E. Miniati, J. Agric. Food Chem., 40 (1992) 1571.
9 J.M. Irache, F.A. Vega and I. Ezpeleta, Pharm. Acta Helv., 67 (1992) 152.
10 C.H. Brieskorn and K. Mahlmeister, Z. Lebensm.-Unters. Forsch., 171 (1980) 348.
11 S.C. Rifkin and D.M. Evans, Anal. Chem., 48 (1976) 2174.
12 J. Wang and B.H. Freiha, Anal. Chim. Acta, 154 (1983) 87.
13 W.P. King, K.T. Joseph and P.T. Kissinger, J. Assoc. Off. Anal. Chem., 63 (1980) 137.
14 Y. Kitada, Y. Ueda, M. Yamamoto, K. Shinomiya and H. Nakazawa, J. Liq. Chromatogr., 8 (1985) 47.
15 C. Grosset, D. Cantin, A. Villet and J. Alary, Talanta, 37 (1990) 301.
16 P. Yáñez-Sedeño, J.M. Pingarrón and L.M. Polo Díez, Anal. Chim. Acta, 252 (1991) 153.
17 A.J. Reviejo, A. Samprón, J.M. Pingarrón and L.M. Polo, Electroanalysis, 4 (1992) 111.
18 A. González Cortés, A.J. Reviejo García, P. Yáñez-Sedeño and J.M. Pingarrón, Anal. Chim. Acta, 273 (1993) 545.
19 J. Wang and M.S. Lin, Anal. Chem., 60 (1988) 499.
20 O. Hammerich and B. Svensmark, in H. Lund and M.M. Baizer (Eds.), Organic Electrochemistry, an Introduction and a Guide, Marcel Dekker, New York, 3rd edn., 1991, pp. 615–650.
21 ACS Commitee on Environmental Improvement, Principles of Environmental Analysis, Anal. Chem., 55 (1983) 2210.
22 K. Hasebe and J. Osteryoung, Anal. Chem., 47 (1975) 2412.
23 F. Pellerin, P. Delaveau, D. Dumitrescu and F. Safta, Ann. Pharm. Françaises, 40 (1982) 221.

Analytica Chimica Acta, 285 (1994) 73–80
Elsevier Science B.V., Amsterdam

Correction of the induced charging current in staircase voltammetry

Chuang-Yung Chang, Ching-Fang Ju and Hsuan-Jung Huang

Department of Chemistry, National Sun Yat-Sen University, Kaohsiung, 80424 (Taiwan)

(Received 2nd July 1993; revised manuscript received 10th September 1993)

Abstract

Based on an electrolysis model and the analysis of the equivalent circuit, equations and procedures applicable to the correction of induced charging current for staircase voltammetry were derived. A system containing solutions of 0.25 mM ferrocene and 0.1 M tetraethylammonium tetrafluoroborate in acetonitrile was studied. The feasibility of the proposed procedures was confirmed by a linear plot of corrected peak currents obtained with different sampling periods (from 100 μs to 10 ms) versus the reciprocal of the square root of sampling time.

Keywords: Voltammetry; Ferrocene; Induced charging current

The effect of double-layer charging resulting from a change in applied potential can be considered as the major background current in voltammetric measurements. It limits the possibility of using higher scan rates and shorter sampling times [1–4]. To some extent the interference of the double-layer charging current may be corrected for by subtracting the charging current obtained from blank solutions. In addition to this charging effect, the flow of faradaic current in an electrolytic cell will induce another type of charging current owing to the existence of uncompensated resistance in solution [5–9]. It is very difficult to correct for this type of charging current experimentally unless the potential drop due to the flow of current through the uncompensated resistance in solution can be compensated for completely. Although the positive feedback approach assuming 100% compensation and appropriate electronics to provide "instantaneous" charging of the double layer, is the best way to solve the problems arising from uncompensated resistance, it has not yet been used in practice. Another strategy for correcting the induced charging current is to adopt a theoretical model that takes into account the effect of the ohmic drop and double-layer charging. By means of flash photolysis studies, Perone and co-workers [5,6] developed a theoretical model for the correction of the induced charging current in potentiostatic and potential step chronoamperometry. The complexity of the mathematical treatment involved may be the reason why no further developments for other voltammetric methods have been reported. It is of interest to explore the possibility of extending its applicability to other voltammetric methods.

In this experiment, based on the same model as used by Perone and co-workers, equations and procedures applicable to the correction of induced charging current for staircase voltammetry were derived. To demonstrate the feasibility of the derived procedures, a system with solutions of 0.25 mM ferrocene and 0.1 M tetraethylammonium tetrafluoroborate (TEATFB) in acetonitrile

Correspondence to: H.-J. Huang, Department of Chemistry, National Sun Yat-Sen University, Kaohsiung, 80424 (Taiwan).

SSDI 0003-2670(93)E0505-2

was studied. Currents of staircase voltammetry were sampled at periods ranging from 100 μs to 10 ms and corrected with the derived procedures in order to obtain pure faradaic currents. From a series of corrected voltammograms, a linear plot of the peak current versus the reciprocal of the square root of sampling time could be obtained, confirming the applicability of the derived equations and procedures.

DERIVATION OF EQUATIONS

From the analysis of the equivalent circuit for an electrochemical cell, it can be seen that changes in the electrolysis current (i_F) will cause variation in the potential drop across the uncompensated resistance (R_u) and double layer in solution. The variation thus induces a change of charging current (i_C) in the electrolysis system. The measured total current, i_T, can be related to the pure electrolysis current and charging current by the following equation [5]:

$$i_T = i_F + R_u C(\mathrm{d}i_T/\mathrm{d}t) \quad (1)$$

where the last term represents the induced charging current. From this relationship, the induced charging current can be calculated if the theoretical total current and the faradaic current are known. The theoretical total current can be derived from the analysis of the corresponding equivalent circuit. With the standard procedures of electric circuit analysis, components in the equivalent circuit can be transformed into their equivalent frequency domain terms by taking the Laplace transformation. After analysis of the circuit in the Laplace domain, the inverse transform can be processed to give the explicit relationship between circuit components [10].

The relationship between faradaic and charging current in the Laplace domain is

$$i_T(\mathrm{S}) = i_C(\mathrm{S}) + i_F(\mathrm{S}) \quad (2)$$

For the electrolysis of a reversible reaction, O + $ne \rightleftharpoons$ R, in semi-infinite linear diffusion conditions the current flows after application of the step potential in staircase voltammetry is given by

$$i = nFAC_0 D_0^{1/2} \Psi_s(j, \Delta E, t) \quad (3)$$

where Ψ_s is the current function and the other symbols have their usual meanings; j is the number of the potential step applied, ΔE is the amplitude of the step potential and t is the time elapsed. The explicit form of the current function has been given by Christie and Lingane as [11]

$$\Psi_{s.c.} = \frac{1}{\sqrt{\pi}}\left[\frac{\epsilon_0}{1+\epsilon_0}\cdot\frac{1}{\sqrt{t}} + \left(\frac{1}{1+\epsilon_0} - \frac{1}{1+\epsilon_1}\right)\frac{1}{\sqrt{t-\omega}} + \ldots + \left(\frac{1}{1+\epsilon_{j-1}} - \frac{1}{1+\epsilon_j}\right)\frac{1}{\sqrt{t-(j)\omega}}\right] \quad (4)$$

where ω is the duration of the potential step, $j\omega < t < (j+1)\omega$ and $\epsilon_j = \exp[-(nF/RT)(E_i + j\Delta E - E_{1/2})]$. For convenience, Eqn. 4 was rewritten as

$$\Psi_{s.c.}(j, \Delta E, t) = \frac{1}{\sqrt{\pi}}\left[\frac{\epsilon_0}{1+\epsilon_0}\cdot\frac{1}{\sqrt{t+j\omega}} + \left(\frac{1}{1+\epsilon_0} - \frac{1}{1+\epsilon_1}\right)\frac{1}{\sqrt{t+(j-1)\omega}} + \ldots + \left(\frac{1}{1+\epsilon_{j-1}} - \frac{1}{1+\epsilon_j}\right)\frac{1}{\sqrt{t}}\right] \quad (5)$$

In Eqn. 5, t was redefined as the time elapsed from the beginning of each step. From Eqns. 3 and 5, the faradaic current flows after the application of potential step in staircase voltammetry can be expressed as

$$i_F(j, \Delta E, t) = \frac{K}{\sqrt{\pi}}\left[\frac{\epsilon_0}{1+\epsilon_0}\cdot\frac{1}{\sqrt{t+j\omega}} + \sum_{m=1}^{m=j}\left(\frac{1}{1+\epsilon_{m-1}} - \frac{1}{1+\epsilon_m}\right)\times\frac{1}{\sqrt{t+(j-m)\omega}}\right] \quad (6)$$

where $K = nFAC_0 D_0^{1/2}$.

After following the standard transformation procedures [12], the faradaic current represented

by Eqn. 6 was transferred into the Laplace domain and shown to be

$$I_F(s) = \frac{K}{\sqrt{s}}\left\{\frac{\epsilon_0}{1+\epsilon_0}\cdot e^{j\omega s}\,\mathrm{erfc}\sqrt{j\omega s} + \sum_{m=1}^{m=j}\left[\left(\frac{1}{1+\epsilon_{m-1}}-\frac{1}{1+\epsilon_m}\right)e^{(j-m)\omega s} \times \mathrm{erfc}\sqrt{(j-m)\omega s}\right]\right\} \quad (7)$$

With the substitution of Eqn. 7 into Eqn. 2, the time-dependent total current could be obtained by taking the appropriate inverse transformation and was derived as

$$i_T(j, \Delta E, t) = \frac{(E_f - E_i)\,e^{-\tau}}{R} + \frac{K\,e^{\tau}}{\sqrt{\pi RC}}\left[\frac{\epsilon_0}{1+\epsilon_0}\int_0^t \frac{e^{\frac{\mu}{RC}}}{\sqrt{\mu + j\omega}} + \sum_{m=1}^{m=j-1}\left(\frac{1}{1+\epsilon_{n-1}}-\frac{1}{1+\epsilon_m}\right) \times \int_0^t \frac{e^{\frac{\mu}{RC}}\,d\mu}{\sqrt{\mu+(j-m)\omega}} + 2\sqrt{RC}\left(\frac{1}{1+\epsilon_{j-1}}-\frac{1}{1+\epsilon_j}\right)\int_0^t e^{\lambda^2}\,d\lambda\right] \quad (8)$$

where $\tau = t/RC$, by letting

$$F(j-m) = \int_0^t \frac{e^{\frac{\mu}{RC}}\,d\mu}{\sqrt{\mu+(j-m)\omega}} \quad (9)$$

$$F(t) = \int_0^t e^{\lambda^2}\,d\lambda \quad (10)$$

Equation 8 can be rewritten as

$$i_T(j, \Delta E, t) = \frac{(E_f - E_i)\,e^{-\tau}}{R} + \frac{K\,e^{\tau}}{\sqrt{\pi RC}}\left[\frac{\epsilon_0}{1+\epsilon_0}F(j) + \sum_{m=1}^{m=j-1}\left(\frac{1}{1+\epsilon_{m-1}}-\frac{1}{1+\epsilon_m}\right)F(j-m) + 2\sqrt{RC}\left(\frac{1}{1+\epsilon_{j-1}}-\frac{1}{1+\epsilon_j}\right)F(\tau)\right] \quad (11)$$

As $i_C = i_T - i_F$, the induced charging current i_C can be calculated from the difference between i_T (Eqn. 11) and i_F (Eqn. 6). From Eqns. 6 and 11, the theoretical ratio i_F/i_T at different potential steps can be calculated, and the pure faradaic current i_F can thus be corrected from the measured total current i_T at any specified step.

EXPERIMENTAL

Reagents

All chemicals were of analytical-reagent grade or better. Acetonitrile (Baker, analyzed reagent) and tetraethylammonium tetrafluoroborate (Aldrich, 99%) were purified prior to use [13,14]. Ferrocene was used as received.

Apparatus

The electrodes and cell used consisted of the BAS C-1 A/B cell assembly, which includes an MF-2012 glassy carbon working electrode, an Ag/AgCl reference electrode and a Pt wire counter electrode. The content of the reference electrode was changed by replacing the aqueous NaCl solution with trimethylammonium chloride saturated acetonitrile solution. All the potentials applied at the working electrode were referred to the Ag/AgCl electrode. An IBM PC-AT compatible microcomputer was interfaced to an EG&G PARC Model 264A potentiostat/galvanostat. The main part of the interface is a PC ADDA-12 card (available from Flytech Technology, Taipei, Taiwan). It consists of 12-bit DAC and ADC. The output voltage range of the DAC is from −5 to +5 V, with a current settling time of 500 ns. The input voltage range of the ADC is from 0 to 9 V (unipolar), with a conversion time of 40 μs. Components 8255A (programmable peripheral inter-

face), 8253 (programmable interval timer) and LF398 (sample and hold) were also included in the interface circuitry to process the required function of the interface. Assembly language was used for the programming when fast execution was required during experiments and BASIC was used for work such as data processing where timing is not so critical.

Procedures for the correction of induced charging current

From the equations derived for i_T and i_F, it was found that the contribution of the induced charging current to the measured total current varied from step to step. It is therefore necessary to correct the current measured at each step with its corresponding i_F/i_T ratio. The values of the integral given in Eqns. 9 and 10 were evaluated by the numerical method of integration based on Simpson's rule.

The charging current arising from the step potential can be calculated theoretically. It is equal to $(\Delta E/R_u)e^{-\tau}$ for a step potential with an amplitude ΔE. The first term on the right-hand side of Eqns. 8 and 11 represented this effect. Its contribution to the measured total current can be calculated if the values of the time constant of the cell, R_uC, are known. In the system studied, as the values of R_uC varied with changes in the potential applied (Table 1), it became difficult to correct the charging current arising from the step potential by this calculation method. Alternatively the background correction procedure was adopted. With this procedure the charging current from the step potential and the possible residual current from the electrolysis are assumed to be eliminated [1]. With adoption of the background correction procedures, the first term on the right-hand side of Eqns. 8 and 11 was then deleted. The total current should thus be modified to

$$i_T(i, \Delta E, t) = \frac{K\, e^{\tau}}{\sqrt{\pi RC}}\left[\frac{\epsilon_0}{1+\epsilon_0}F(j) + \sum_{m=1}^{m=j-1}\left(\frac{1}{1+\epsilon_{m-1}} - \frac{1}{1+\epsilon_m}\right)F(j-m) + 2\sqrt{RC}\left(\frac{1}{1+\epsilon_{j-1}} - \frac{1}{1+\epsilon_j}\right)F(\tau)\right] \quad (12)$$

The ratio i_F/i_T was then calculated from Eqns. 6 and 12 for further corrections.

TABLE 1

Uncompensated resistance R_u and cell time constant R_uC determined from a solution of 0.1 M TEATFB in acetonitrile at various potentials

Potential (mV)	R_u (Ω)	R_uC (μs)
300	189	143
400	189	143
500	189	143
600	187	154
700	187	173
800	187	186
900	186	203
1000	186	203

RESULTS AND DISCUSSION

As the uncompensated resistance R_u and the cell time constant R_uC are important parameters in Eqn. 12, they have to be evaluated prior to the calculation of the i_F/i_T ratio. Values of R_u and R_uC of the studied system at various potential were measured from the blank solution with the BAS-100A electrochemical analyser, and the results are given in Table 1. From Table 1, values of R_u are essentially constant whereas values of R_uC increase with increase in applied potential. For simplicity, a value of 150 μs was used as the time constant of the cell for the system studied.

The staircase voltammetric scan was run with an initial potential of 300 mV (vs. AgCl/AgCl) and stopped at 1000 mV. The amplitude of the potential step was 10 mV, the duration of the potential step was 12 ms and the sampling time varied from 100 μs to 10 ms. Figure 1a shows the voltammograms obtained from a solution of 0.25 mM ferrocene and 0.1 M TEATFB with different sampling times, and Fig. 1b shows the voltammograms obtained from a blank solution. The data shown are averages of three runs.

To process the induced charging current correction, the background currents shown in Fig. 1b were subtracted from their corresponded voltammograms in Fig. 1a. Figure 2a shows the background-corrected voltammograms. As the background currents shown in Fig. 1b came mainly from the charging effect of the step potential, the curves in Fig. 2a thus represent voltammograms corrected for the charging current of the step potential. With the substitution of appropriate parameters into Eqns. 6 and 12, values of $i_F(j)$, $i_T(j)$ and therefore $i_C(j)$ and $i_F(j)/I_T(j)$ for the jth step could be calculated. From the $i_F(j)/i_T(j)$ ratio calculated and total current $i_T(j)$ measured, a pure faradaic current $i_F(j)$ could be obtained. Figure 2b shows the induced charging current corrected voltammograms obtained. In Fig. 2b, the irregularity of the current magnitude with sampling time in Fig. 2a disappeared. According to the literature, the peak potential will shift cathodically if the sampling time decreases [15,16]. The peak potential in Fig. 2b shows this effect except for those obtained at very short sampling times. The deviation found is believed to be due to imperfections in the step potential (as will be discussed below).

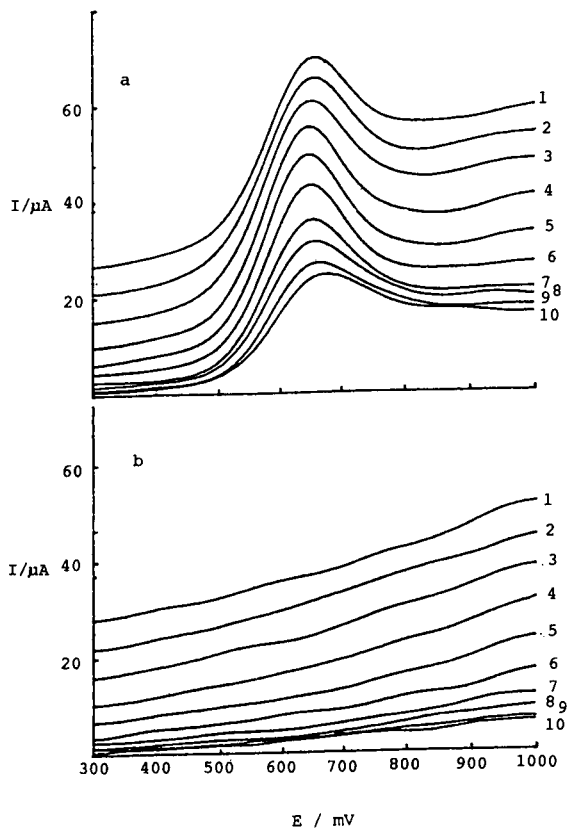

Fig. 1. Staircase voltammograms obtained from solutions of (a) 0.25 mM ferrocene and 0.1 M TEATFB in acetonitrile and (b) 0.1 mM TEATFB in acetonitrile (blank). Sampling times of (1) 100, (2) 120, (3) 150, (4) 200, (5) 300, (6) 500, (7) 1000, (8) 2000, (9) 5000 and (10) 10000 μs were used.

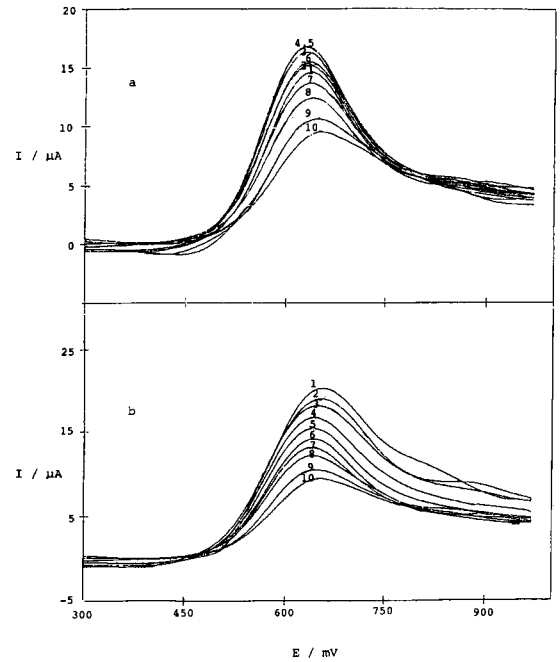

Fig. 2. (a) Background-corrected staircase voltammograms and (b) induced charging current-corrected staircase voltammograms. The numbers on the curves indicate the sampling times as given in Fig. 1.

The validity of these correction procedures was tested by plotting the peak currents of the voltammogram in Fig. 2a and b against the reciprocal of the square root of the sampling time (Fig. 3). The straight line (with $r = 0.9993$) obtained from the plot of the peak current in Fig. 2b shows the characteristic of diffusion control of the studied system. For comparison, theoretical voltammograms were constructed by substituting the appropriate experimental parameters into Eqn. 6. Figure 4 shows the plot of $\pi^{1/2}\Psi_s$ versus $E - E_{1/2}$. Values of the current function $\pi^{1/2}\Psi_s$ at

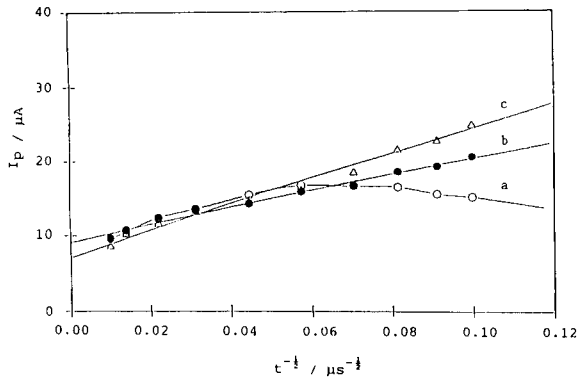

Fig. 3. Plots of peak current versus reciprocal square root of sampling time. (a) Peak currents obtained before correction of the induced charging current; (b) and (c) peak currents corrected for induced charging current with time constants of the cell of 150 and 200 μs, respectively.

peak potential E_p were plotted versus the reciprocal of the square root of the sampling time. A straight line was obtained, providing support for the validity of the induced charging current correction procedures. Although the cell time constant was determined to be ca. 150 μs, a larger value of 200 μs was also used in the related calculation for comparison. Line c in Fig. 3 shows the plot.

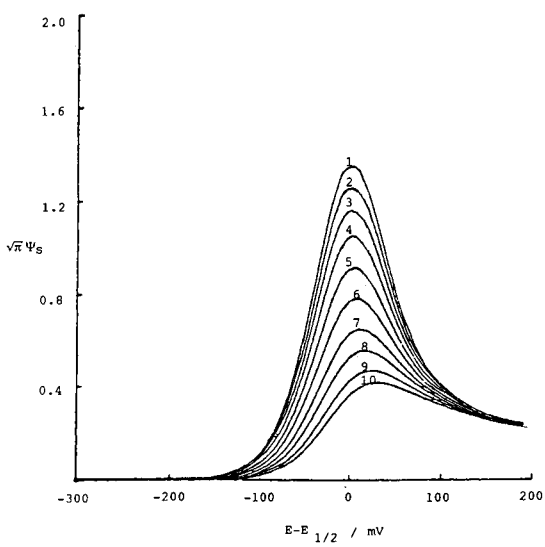

Fig. 4. Theoretical plots of $\pi^{1/2}\Psi_s$ versus $E - E_{1/2}$. The numbers on the curves indicate the sampling times shown in Fig. 1.

Problems were encountered in this study. As the cell time constant is ca. 150 μs, it took at least 500 μs for the potential of the rising step to become stable. This effect made the expectation that an instantaneous potential step could be applied unattainable. When however, the step potential was generated continuously during the experiment, the charging effect could be restricted to the latest applied 10-mV step. According to the experimental conditions, with an elapsed time of 100 μs, the step potential may have arisen by only ca. 5 mV instead of 10 mV. The current resulting in this experiment was therefore different from that with an instantaneous increment of a 10-mV step. With increase in elapsed time, the error due to this imperfection should become smaller and smaller. It seems reasonable to assume that a less than 5 mV difference may result in only a small or negligible error. The plot with very good linearity shown in Fig. 3 supports this argument.

The imperfection in the step potential may cause another problem in this experiment. As Eqn. 3 was derived by assuming that the potential step was applied instantaneously, the imperfection in the instantaneous potential rise made the applicability of Eqn. 3 questionable. However, as can be understood from the characteristics of staircase voltammetry, the imperfection of the potential step affects only the current arising in the latest 10-mV step. From Eqn. 3, the current function Ψ_s at the jth step is the current function accumulated from the first to the jth step. As the duration of the potential step in the studied system is long enough for the applied potential to become stable at the end of the step, the current arising at the $(j-1)$th or an earlier step should be free from the problem of instantaneous setting of the step potential. The effect of the imperfection of the potential step on the faradaic current can be estimated from previous equations. At the jth step, the potential applied at the electrode should be equal to $E_i + \Delta E(j - e^{-\tau})$ instead of $E_i + j\Delta E$. The deviation of the current resulting from this difference in potential may become pronounced when the sampling time is very short

(i.e., with a very small value of τ) and as $E_i + j\Delta E$ is close to $E_{1/2}$ of the studied system. The anodic shift of the peak potential found for curves 1–3 in Fig. 2b should be attributed to this effect.

For a Cottrell plot, a straight line passing through the origin should be obtained for a pure diffusion-controlled faradic process. The positive intercept shown in Fig. 3 indicates that a certain amount of residual current was contained in the measured current. This residual current may possible be attributed to the incomplete correction of the background current, as the double-layer capacitance of an electrode in a blank solution may be different from that in a solution containing electroactive species. From lines a–c in Fig. 3, it can be seen that currents sampled at later times ($t > 500$ μs) showed essentially the same characteristics (of both linearity and slope). Currents sampled at later times (see line a) should approximate Eqn. 3 very well in theory, as the charging current due to the rising step and the change in the faradaic current are assumed to decrease to negligible values at later times. Extrapolation of these later sampled data should therefore pass through the origin of the plot. The positive intercept obtained for line a indicates that the background current was not eliminated completely. A certain amount of residual current was still present in the faradaic measurements. In the studied system, the adsorption of ferrocene on the working electrode may be the cause of these residual currents. If the eliminated current can be corrected completely, lines b and c in Fig. 3 would pass through the origin.

Apart from the practical application of Eqns. 6 and 11 to the correction of faradaic-induced charging current, it is also interesting to explore the relationships between the faradaic current i_F, the measured total current i_T and the induced charging current i_C and also the variation of these currents with time. Currents corresponding to the step of peak potential (at 0.64 V) in the studied ferrocene system were calculated to show these relationships. Figure 5 shows the variation of i_F, i_T and i_C with time from the beginning of the application of the potential step to 10 ms. From these curves, the contribution of the induced charging current to the measured total

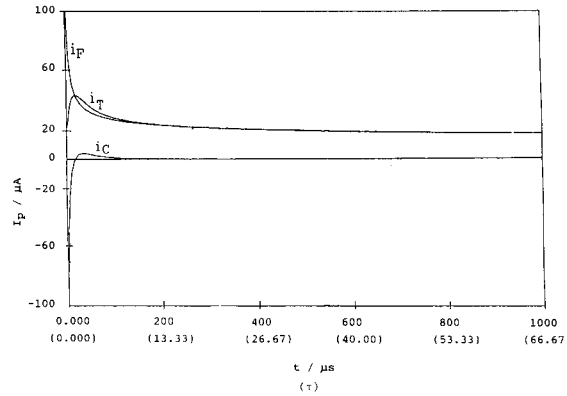

Fig. 5. Variation of i_F, i_T were i_C with time and τ. Values of i_F, i_T and i_C were calculated according to Eqns. 5 and 10 for the step of peak potential (at 0.64 V). Cell time constant, 150 μs.

current at different times can be observed. At $\tau = 4$, 10% of the total current can be attributed to the induced charging current. The induced charging current decreases to less than 2% of the total current at $\tau = 13$. It is therefore concluded that in staircase voltammetry, the pure faradaic current could be obtained with an elapsed time longer than 13 τ (with 2% error). The strategy used by previous workers to minimize the charging current contribution in potential-step chronoamperometry by measuring the current at $\tau > 4$ is not applicable in staircase voltammetry.

With an appropriate correction of the background and following the proposed procedures, pure faradaic current in staircase voltammetry could be recovered quantitatively from current measured at an earlier time in the potential step. It may therefore provide valuable data for the kinetic studies of very fast electrochemical processes. The analytical application of these correction procedures was demonstrated by the construction of calibration graphs (peak current vs. concentration) from solutions of various ferrocene concentrations (from 5 to 25 mM). Linear calibration graphs were obtained for those sampled at different times (e.g., at 100, 200 and 10000 μs). The fact that the slopes of these calibration graphs increase with decrease in the sampling time suggests that the proposed correction procedures are applicable to improving the

sensitivity of staircase voltammetry by sampling the electrolysis current at an earlier time.

The authors express their gratitude to the National Science Council of the Republic of China for their financial support of this work.

REFERENCES

1 D.O. Wipf, E.W. Kristensen, M.R. Deakin and R.M. Wightman, Anal. Chem., 60 (1988) 306.
2 A. Fitch and D.H. Evans, J. Electroanal. Chem., 202 (1986) 83.
3 J.O. Howell and R.M. Wightman, Anal. Chem., 56 (1984) 524.
4 C.A. Amatore and A. Jutland, J. Electroanal. Chem., 218 (1987) 361.
5 S.S. Fratoni, Jr., and S.P. Perone, Anal. Chem., 48 (1976) 287.
6 K.F. Dahnke, S.S. Fratoni, Jr., and S.P. Perone, Anal. Chem., 48 (1976) 256.
7 A.A. Pila, in J.S. Mattson, H.B. Mark and H.C. MacDonald (Eds.), Electrochemistry Calculations, Simulations, and Instrumentation, Dekker, New York, 1972 pp. 139–181.
8 K. Holub, G. Tessari and P. Delahay, J. Phys. Chem., 71 (1967) 2612.
9 P. Delahay, J. Phys. Chem., 70 (1966) 3150.
10 H. Huelsman and P. Lawrence, Basic Circuit Theory, Prentice-Hall, Englewood Cliffs, NJ, 1984.
11 J.H. Christie and P.J. Lingane, J. Electroanal. Chem., 10 (1965) 176.
12 M.R. Spiegel, Theory and Problems of Laplace Transforms, Schaum, New York, 1965.
13 M. Walter and L. Ramalay, Anal. Chem., 45 (1973) 165.
14 O.H. House, E. Feng and N.P. Peet, J. Org. Chem., 36 (1971) 2371.
15 J.J. Zipper and S.P. Perone, Anal. Chem. 45 (1973) 452.
16 A.J. Bard and L.R. Faulker, Electrochemical Methods, Wiley, New York, 1980.

Analytica Chimica Acta, 285 (1994) 81–88
Elsevier Science B.V., Amsterdam

Primary amine drug-sensitive poly(vinyl chloride) membrane electrodes based on synthetic macrocyclic polyether derivatives of *o*-phenanthroline

Zeng-Rong Zhang and Ru-Qin Yu

Department of Chemistry and Chemical Engineering, Hunan University, Changsha (China)

(Received 28th January 1993; revised manuscript received 9th June 1993)

Abstract

Eight macrocyclic polyether derivatives of *o*-phenanthroline were synthesized and used as neutral carriers for preparing poly(vinyl chloride) (PVC) membrane electrodes that sense primary amine species. The potentiometric response characteristics of the electrodes were investigated. The effect of experimental parameters on the electrode performance was studied. The optimum pH range for the benzylamine-sensitive electrode was found to be 6.6–9.0. The membrane composition was optimized by using orthogonal polynomial regression, and the following optimum membrane composition was found: 5.8 mg of PHEN19C7, 180 mg of diisooctyl sebacate, 84 mg of PVC and 1.0 mg of potassium tetraphenylborate in a membrane of ca. 5.3 cm^2. The electrode sensitive to benzylamine as a model analyte showed a linear response range of 8.0×10^{-6}–0.1 mol/l with a detection limit of 8.9×10^{-7} mol/l and a slope of 56.5 mV per decade at 25°C. The linear potentiometric response of the mexiletine-sensitive electrode was 4.7×10^{-6}–0.1 mol/l and the detection limit was 5.0×10^{-7} mol/l with a slope of 59.0 mV per decade at 25°C. These potentiometric response characteristics of the electrodes compared favourably with those of electrodes based on dinaphthyl macrocyclic polyethers. The PHEN19C7-based electrode was used to determine the mexiletine content in pharmaceutical preparations with satisfactory results.

Keywords: Potentiometry; Amine-sensitive electrodes; Membrane electrodes; Pharmaceuticals; Phenanthroline macrocyclic polyether derivatives

In a search for electrochemical carriers for primary amine species, several macrocyclic polyethers with 2,2′-dinaphthyl subunits capable of forming host–guest complexes with amine species have been synthesized. These compounds have been used as neutral carriers for the preparation of poly(vinyl chloride) (PVC) membrane electrodes which are able to sense primary amine drugs [1]. It has been found that macrocyclic

Correspondence to: R.-Q. Yu, Department of Chemistry and Chemical Engineering, Hunan University, Changsha (China).

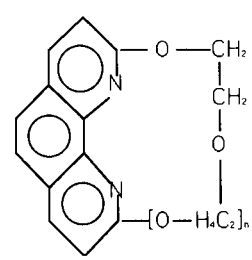

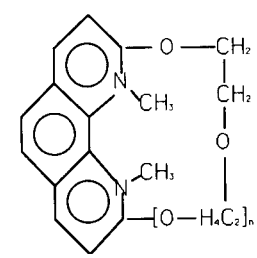

(I) n=1, PHEN13C5
(II) n=2, PHEN16C6
(III) n=3, PHEN19C7
(IV) n=4, PHEN22C8

(V) n=1, MPHEN13C5
(VI) n=2, MPHEN16C6
(VII) n=3, MPHEN19C7
(VIII) n=4, MPHEN22C8

Fig. 1. Structures of carriers.

SSDI 0003-2670(93)E0494-R

polyether derivatives of *o*-phenanthroline are promising carrier compounds for this class of amines. In this work, eight such macrocyclic polyether derivatives (**I–VIII**, Fig. 1) were synthesized as neutral carriers for the preparation of benzylamine- and mexiletine-sensitive PVC membrane electrodes. Benzylamine was taken as a model primary amine and mexiletine [1-(2,6-dimethylphenoxy)isopropylamine chloride] is an effective retardant widely used for arrhythmia. The potentiometric response characteristics of the electrodes were investigated. One electrode was applied to the assay of mexiletine in pharmaceutical preparations with satisfactory results.

EXPERIMENTAL

Synthesis of macrocyclic polyether derivatives of o-phenanthroline (I–VIII)

Synthesis of 2,9-dihydroxy-1,10-phenanthroline (IX). 2.9-Dichloro-1,10-phenanthroline (**X**), was prepared by a six-step reaction route according to the method described by Lewis and O'Donoghue [2]. Compound **X** was refluxed with lithium methoxide in tetrahydrofuran (THF) for 12 h to give 2,9-dimethoxy-1,10-phenanthroline (**XI**). Compound **XI** was dissolved in dioxane and refluxed for 16 h after addition of anhydrous lithium iodide to give **IX** as a yellow product.

Synthesis of 2,9-dihydroxy-1,10-dimethyl-1,10-phenanthroline (XII). The intermediate product, 1-methyl-2-*o*-phenanthrolone (**XIII**), was prepared from 1,10-phenanthroline according to the method described by Lewis and O'Donoghue [2]. Compound **XIII** was dissolved in dimethyl sulphate and heated at 150°C for 4 h. The reaction mixture was cooled and poured into dried diethyl ether to obtain the salt **XIV** (Fig. 2). The separated salt **XIV** was dissolved in water for use in the next reaction step.

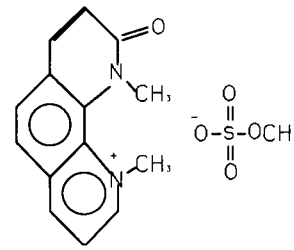

Fig. 2. Structure of the intermediate salt **XIV**.

Solutions of potassium hexacyanoferrate(III) and sodium hydroxide were prepared. These two aqueous solutions were added dropwise alternatively to a stirred aqueous solution of **XIV** and the mixture was stirred for a further 3 h. The precipitated, 1,10-dimethyl-2,9-dio-phenanthrolone (**XV**) was filtered and extracted with chloroform and washed with water. After drying and evaporation of solvent, the yellow solid **XV** was obtained. The product **XV** was reacted with metallic lithium in THF for 4 h. After evaporation of THF, the reaction product was extracted with chloroform and washed with water. The

TABLE 1

Analytical data of carrier compounds

Polyether	Calculated (%)			Found (%)			IR (cm^{-1})	*m/z* (M^+)
	C	H	N	C	H	N		
I	68.14	4.93	9.86	68.10	4.95	9.89	2940, 1671, 1605, 1471, 1131, 853	282
II	66.26	5.52	8.59	66.20	5.48	8.67	2937, 1661, 1599, 1465, 1130, 843	326
III	64.86	5.96	7.57	64.81	5.94	7.60	2942, 1600, 1606, 1469, 1131, 850	370
IV	63.77	6.28	6.77	63.71	6.19	6.88	2947, 1661, 1604, 1466, 1131, 848	414
V	69.23	6.41	8.97	69.31	6.50	8.92	2941, 2818, 1669, 1605, 1470, 1131, 851	312
VI	67.42	6.74	7.87	67.35	6.82	7.86	2939, 2820, 1663, 1600, 1465, 1130, 837	356
VII	66.00	7.00	7.00	66.12	7.11	6.89	2940, 2813, 1665, 1603, 1469, 1131, 850	400
VIII	64.86	7.21	6.31	64.97	7.25	6.26	2932, 2810, 1670, 1600, 1470, 1131, 834	444

yellow solid product of **XII** was obtained by drying the extract and evaporating the solvent.

Synthesis of macrocyclic polyether derivatives of o-phenanthroline. The syntheses were carried out in analogy with the method described by Cram and co-workers [3,4]. Compound **IX** or **XII** was dissolved in THF dried with sodium. To this solution potassium *tert*-butoxide and polyethylene glycol ditosylate were added under nitrogen and the mixture was stirred and refluxed for 5 h. The solvent was evaporated under reduced pressure and the residue was extracted with chloroform. The chloroform phase was washed sequentially with saturated sodium carbonate solution and water, then dried with anhydrous magnesium sulphate. The solvent was removed by evaporation, followed by separation of the residue by chromatography on silica gel. The product was eluted from the silica gel column with diethyl ether as solvent.

The synthetic reactions and the products obtained (**IX–XV**) were monitored by using a GC–MS system consisting of GCMS-QP1000 and a GCMS-QP1000A (Japan). Eight macrocyclic polyether derivatives of *o*-phenanthroline (**I–VIII**) were synthesized and their structures were identified (Table 1).

Preparation of electrodes

The general procedure for the preparation of the PVC membrane [5] is as follows. A THF solution containing the carrier compound (5.8 mg), PVC (84 mg), diisooctyl sebacate (180 mg) and $KBPh_4$ (1.0 mg) was poured on to a flat glass plate (ca. 5.3 cm^2). The THF was evaporated at room temperature to obtain a transparent, flexible membrane. A disc of 7 mm diameter was cut from the PVC membrane by using a cork borer and cemented on to the flat end of a PVC tube with an adhesive consisting of a 5% THF solution of PVC. An internal solution of 0.1 mol l^{-1} KCl and an Ag/AgCl internal reference electrode were used. The prepared PVC membrane electrode was conditioned by soaking in 0.01 mol l^{-1} test solution overnight. The external reference electrode was a saturated calomel electrode. The electrochemical cell used was Ag/AgCl|0.1 mol l^{-1} KCl|PVC membrane|sample solution|SCE.

Electromotive force (e.m.f.) measurements

The e.m.f.s were measured at 25°C using a Model PHS-3 pH meter (Shanghai Analytical Instruments) or a Model 901 Microprocessor Ionanalyzer (Orion Research). The sample solutions were stirred with a magnetic stirrer in a double-walled glass container with thermostated water circulating in a water-jacket.

A.c. impedance experiments

The a.c. impedance of the electrode membranes was recorded with a PAR M368-2 system (EG&G Princeton Applied Research) in 0.05 mol l^{-1} Tris–HCl buffer solution (pH 8.5). The frequency region used was from 10^5 to 10^{-2} Hz (at 25°C).

RESULTS AND DISCUSSION

Effect of structures of carriers on electrode performance

Eight ion-selective electrodes were prepared using membranes containing the different carriers and their potentiometric response performances were compared (Fig. 3). On comparing the linear response range, the slope and the detec-

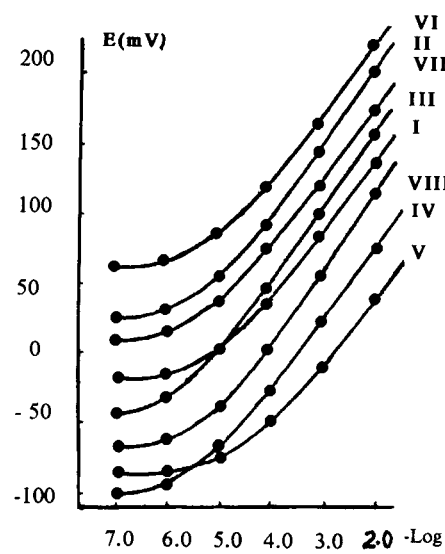

Fig. 3. Response performances of electrodes with different carriers.

tion limit of the electrodes prepared, it is seen that the electrode based on carrier **III** possesses the best potentiometric response performance, the sequence being **III** > **IV** > **VIII** > **II** > **VII** > **VI** > **I** > **V**. The structure of macrocyclic polyether derivatives substantially affects the response performances of benzylamine-sensitive electrodes. The cavity size provided by the carriers **I–IV** increases in the order **I** < **II** < **III** < **IV**. Compounds with small (**I** and **II**) and large (**IV**) cavity sizes showed inferior performance characteristics compared with the carrier with a medium size cavity (**III**). These results seem to indicate that the size of the cavity provided by the carriers is important and one would expect better electrode performance for a carrier with a cavity size that sterically matches the analyte species to be sensed. The a.c. impedance measurements supported this argument to some extent (see below). The electrode based on carrier **VII** is inferior to that based on carrier **III** in their potentiometric response characteristics. It seems that the presence of methyl groups attached to the nitrogen atoms in the phenanthroline moiety of the carrier **VII** molecules prevents the interaction of protonated benzylamine species with the carrier molecules, with a negative effect on the electrode performance. The electrode with carrier **III** showed the largest slope, the widest range of linear response and the lowest detection limit among the eight polyethers. This carrier, PHEN19C7, 1,15-(1′,10′-diazaphenanthro[2′,9′])-2,5,8,11,14-pentaoxacyclononadecane (**III**), was taken for the preparation of a PVC membrane electrode to sense primary drugs in subsequent experiments.

A.c. impedance of PVC membrane

Figure 4 shows the a.c. impedance of membranes with or without the carrier compound present in the membrane phase in contact with electrolyte solutions containing 0.1 mol l^{-1} benzylamine. A membrane containing only the solvent mediator diisooctyl sebacate showed a relatively high bulk resistance. The lowering of the bulk resistance in the presence of the carrier is clearly due to the facilitated transfer of analyte species through the membrane phase. The a.c. impedance of membranes containing different carrier compounds in contact with electrolyte solutions containing 0.1 mol l^{-1} benzylamine was recorded and compared. The following a.c. impedance (in MΩ) sequence was found: **III** (0.28) < **IV** (0.30) < **VIII** (0.32) < **II** (0.35) < **VII** (0.47) < **VI** (0.70) < **I** (0.93) < **V** (1.12). The membrane containing carrier compound **III** showed the lowest bulk resistance. This agrees well with the best response characteristics of the electrode based on this carrier. On the other hand, membranes containing carrier compound **I** or **V** showed the highest bulk resistance, which was in agree-

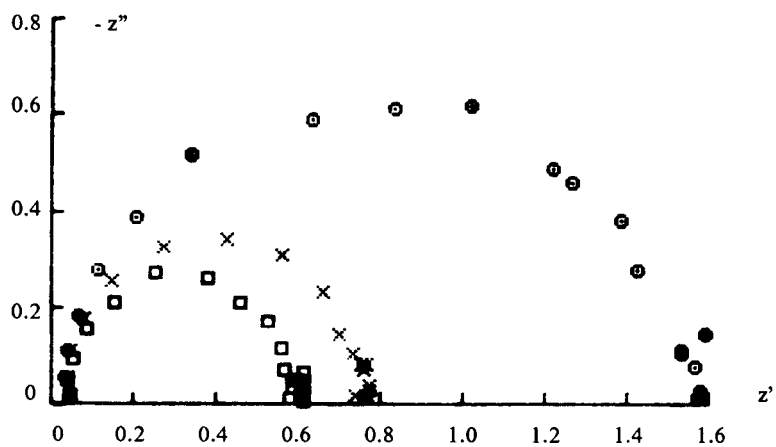

Fig. 4. Impedance plot of membranes containing (⊙) diisooctyl sebacate, (×) PHEN19C7 and diisooctyl sebacate and (□) PHEN-19C7, potassium tetraphenylborate and diisooctyl sebacate. z' and $-z''$ in MΩ.

TABLE 2

Response performance of membranes for benzylamine

Membrane [a]	Slope (mV per decade)	Lower limit of linear response (mol l^{-1})	Detection limit (mol l^{-1})
1	45.03±0.73	1.0×10^{-5}	2.5×10^{-6}
2	56.04±0.68	1.0×10^{-5}	1.0×10^{-6}
3	56.50±0.50	8.0×10^{-6}	8.9×10^{-7}

[a] Membranes containing (1) diisooctyl sebacate, (2) carrier **III** and diisooctyl sebacate and (3) carrier **III**, potassium tetraphenylborate and diisooctyl sebacate.

ment with the steric hindrance as assumed in the previous section.

Potentiometric response characteristics of electrodes based on macrocyclic polyether derivatives of o-phenanthroline

The macrocyclic polyether derivative was an essential component in the construction of an efficient membrane to sense the primary amine species. Without this component, a membrane containing a solvent mediator, say diisooctyl sebacate, also showed some potentiometric response to benzylamine, but the slope was far below the theoretical value (Table 2). The addition of potassium tetraphenylborate affected the performance characteristics only slightly, but decreased the a.c. impedance of the membrane (Fig. 4). In addition to decreasing the impedance of the membrane, the addition of potassium tetraphenylborate also decreases the interference of anion species. This aspect was discussed by Armstrong et al. [6,7] and Morf and Simon [8].

Optimization of membrane composition

The membrane composition was optimized. The contents of PVC and potassium tetraphenylborate were fixed and the contents of carrier **III** and solvent mediator (diisooctyl sebacate) were chosen as the factors to be optimized. Three levels for each factor were selected and nine electrodes were prepared according to the orthogonal design table $L_9(3^4)$ [9], as shown in Table 3. By using an orthogonal polynomial regression approach for treatment of the experimental data [10], the following optimum membrane composition was found: 5.8 mg of PHEN19C7 (**III**), 180 mg of diisooctyl sebacate, 84 mg of PVC and 1.0 mg of potassium tetraphenylborate for preparing a membrane of ca. 5.3 cm^2 as described under Experimental.

TABLE 3

Orthogonal design table

Membrane No.	Factor to be optimized (mg) [a]	
	A	B
1	3.00	170.0
2	3.00	210.0
3	3.00	250.0
4	5.00	170.0
5	5.00	210.0
6	5.00	250.0
7	7.00	170.0
8	7.00	210.0
9	7.00	250.0

[a] A = carrier **III**; B = diisooctyl sebacate.

Effect of pH on electrode performance

The optimum pH range for the benzylamine-sensitive electrode was found to be 6.6–9.0. The useful pH range narrows when the analyte concentration decreases from 1.0×10^{-3} to 2.0×10^{-5} mol l^{-1} (Fig. 5). Macrocyclic polyether com-

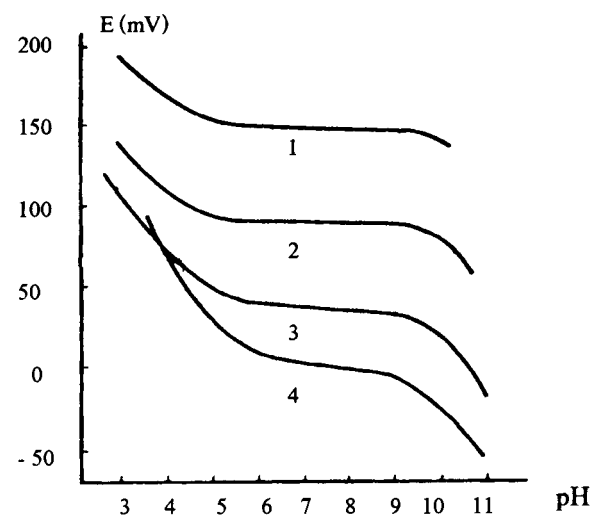

Fig. 5. Effect of pH on response performance of electrode. Concentration of benzylamine: (1) 1.0×10^{-2}; (2) 1.0×10^{-3}; (3) 1.0×10^{-4}; (4) 2.0×10^{-5} mol l^{-1}.

TABLE 4

Time-dependent potential drift of the electrode (carrier **III**)

Time (min)	10	20	30	40	50	60	70	80	90	100	110	120
E (mV)	164.1	164.2	164.3	164.4	164.4	164.5	164.5	164.6	164.5	164.7	164.8	164.8

pounds can complex hydrogen ions. At lower pH values (e.g., pH < 6.0), a large amount of hydrogen ions might permeate into the membrane phase from aqueous phase and react with the carrier molecule through the oxygen and nitrogen atoms, decreasing the content of neutral polyether carrier molecules and affecting the electrode response. On the other hand, there is a protonation equilibrium of amine species:

$$RNH_2 + H^+ \rightleftharpoons RNH_3^+ \quad (pK_a = 4.63)$$

and a change of PH shifts the protonation equilibrium of amine species. At higher pH values (e.g., pH > 9.0), the protonated benzylamine species (RNH_3^+) is transformed into the neutral amine (RNH_2) which is not sensed by the electrode and the response performance of electrode is poor. The determinations should be carried out under careful pH control. A buffer system of 0.05 mol l^{-1} Tris adjusted with hydrochloric acid to about pH 8.5 was chosen as an appropriate background electrolyte solution.

Electrode performance

The benzylamine-sensitive electrode based on PHEN19C7 prepared according to the optimum membrane composition showed a linear potentiometric response to benzylamine over the concentration range 8.0×10^{-6}–0.1 mol l^{-1} with a detection limit of 8.9×10^{-7} mol l^{-1} and a slope of 56.50 mV per decade (correlation coefficient 0.9998, $n = 6$, standard deviation $s = 0.21$ mV/pC, slope = 56.50 ± 0.50 mV/pC) at 25°C. The electrode has a short potentiometric response time and the equilibrium potential was obtained within 10 s. The potential fluctuation was less than 1 mV during continuous monitoring of a 1.0×10^{-2} mol l^{-1} test solution for 2 h (Table 4) and the potential values were well reproduced in repeated measurements, the relative standard deviation of five measurements of 1.0×10^{-2} mol l^{-1} test solution being 1.85%. The lifetime of the electrode was 6 months, after which there is degradation of the sensitivity.

The potentiometric selectivity coefficients were determined by the fixed interference method [11] for the benzylamine-sensitive electrode, in which the concentrations of interfering ions were fixed at 0.01 mol l^{-1} (Table 5). The results show two outstanding features of the electrode. First, it has high potentiometric selectivity coefficients for the primary amine species against alkali and alkaline earth metal ions. This important feature might be explained by the complexing efficiency of the primary amine with the aza–oxa macrocyclic polyether [12]. Ordinary macrocyclic polyethers such as 18-crown-6 are able to complex both metal cations and primary ammonium cation [13,14]; moreover, these polyethers bind the alkali metal cations K^+ and Rb^+ appreciably more strongly than the protonated primary ammonium groups [15], hence these macrocyclic polyethers are not feasible for use as selective carriers for amine or ammonium ion-selective electrodes. As hydrogen bonding of the type $^+N–H\cdots N$ is stronger than the $^+N–H\cdots O$ type [16], the presence of nitrogen atoms in the phenanthroline moiety of the carrier molecule might increase the stability of the complex formed by the protonated primary amine ($R–NH_3^+$) and the carrier com-

TABLE 5

Potentiometric selectivity coefficients of the benzylamine-sensitive electrode (carrier **III**)

Interferent (j)	$K_{i,j}^{pot}$	Interferent (j)	$K_{i,j}^{pot}$
Ca^{2+}	3.98×10^{-5}	Phenylamine	3.24×10^{-4}
Mg^{2+}	3.23×10^{-5}	Tetramethylammonium bromide	1.03×10^{-2}
Na^+	6.59×10^{-4}	Diethylamine	8.28×10^{-3}
K^+	7.02×10^{-3}	Triethylamine	9.96×10^{-3}
NH_4^+	2.17×10^{-3}		

pound. The second outstanding feature is that the electrodes were fairly selective to primary amines over secondary and tertiary amines and quaternary ammonium ions. For an ordinary ion-associate type of electrode that senses drugs, the selectivity sequence for drugs containing an amino nitrogen has been found to be [17] $RNH_3^+ < R_2NH_2^+ < R_3NH^+ < R_4N^+$, drugs containing quaternary ammonium groups being preferentially detected. This sequence is drastically changed on using macrocyclic polyether derivatives as carriers: $RNH_3^+ > R_4N^+ > R_3NH^+ > R_2NH_2^+$, the primary amine drugs becoming the most favourably sensed species.

APPLICATION

An electrode sensitive to mexiletine was prepared under similar conditions to those for the benzylamine-sensitive electrode. The electrode based on PHEN19C7 showed a linear potentiometric response for 4.7×10^{-6}–0.1 mol l^{-1} mexiletine, with a detection limit of 5.0×10^{-7} mol l^{-1} and a slope of 59.00 mV per decade (correlation coefficient $r = 0.9995$, $n = 6$, standard deviation $s = 0.28$ mV/pC, slope = 59.00 ± 0.70 mV/pC) at 25°C. The potentiometric selectivity coefficients were determined by the fixed interference method for the mexiletine electrode with concentrations of interfering ions fixed at 0.01 mol l^{-1} (Table 6).

The sample solution of mexiletine was prepared according to a pharmacopoeial method [18] followed by potentiometric analysis after appropriate dilutions. Direct potentiometry by a calibration graph method gave an average content of 61.9% of mexiletine, with a relative standard deviation of 1.1%. This result was in fair agreement with that obtained by the standard pharmacopoeial method based on non-aqueous titrations [18] (61.3%).

TABLE 6

Potentiometric selectivity coefficients of the mexiletine-sensitive electrode (carrier **III**)

Interferent (j)	$K_{i,j}^{pot}$	Interferent (j)	$K_{i,j}^{pot}$
Mg^{2+}	6.02×10^{-6}	Phenylamine	5.30×10^{-5}
Ca^{2+}	5.57×10^{-6}	Tranexamic acid	3.68×10^{-5}
K^+	1.01×10^{-3}	Aminomethyl-benzoic acid	3.53×10^{-5}
Na^+	1.04×10^{-4}	Ephedrine	1.24×10^{-2}
NH_4^+	5.39×10^{-4}	Diphenhydramine	2.02×10^{-1}

Conclusion

Eight macrocyclic polyethers of *o*-phenanthroline were synthesized and used as neutral carriers for preparing the PVC membrane electrodes sensing primary amine species. The benzylamine- and mexiletine-sensitive electrodes prepared compared favourably with those based on dinaphthyl macrocyclic polyethers in their potentiometric response performance (Table 7). The PHEN19C7-based electrode was used to determine the mexiletine content in pharmaceutical preparations with satisfactory results.

The work described in this paper was supported by the National Natural Science Foundation of China and partly by the Electroanalytical Laboratory of Changchun Institute of Applied Chemistry, Academia Sinica.

TABLE 7

Comparison of the potentiometric response performances of electrodes

Analyte	Carrier	Slope (mV per decade)	Linear response range (mol l^{-1})	Detection limit (mol l^{-1})
Benzylamine	Carrier **III**	56.50 ± 0.50	8.0×10^{-6}–0.1	8.9×10^{-7}
	Dinaphthyl 20c6 [1]	51.30 ± 0.70	4.2×10^{-5}–0.1	4.6×10^{-6}
Mexiletine	Carrier **III**	59.00 ± 0.70	4.7×10^{-6}–0.1	5.0×10^{-7}
	Dinaphthyl 20c6 [1]	52.10 ± 0.64	2.0×10^{-5}–0.1	5.0×10^{-6}

REFERENCES

1 K.Y. Liu, Z.R. Zhang and R.Q. Yu, Mikrochim Acta, I (1989) 281.
2 J. Lewis and T.D. O'Donoghue, J. Chem. Soc., Dalton, Trans. (1980) 736.
3 D.J. Cram, US Pat., 4001279 (1977).
4 E.P. Kyba, G.W. Gokel, F.D. Jong, K. Koga, L.R. Sousa, M.G. Siegel, L. Kaplan, G. Dotsevi, Y. Sogah and D.J. Cram, J. Org. Chem., 42 (1977) 4173.
5 G.J. Moody, R.B. Oke and J.D.R. Thomas, Analyst, 95 (1970) 910.
6 R.D. Armstrong, A.K. Covington and G.P. Evans, Anal. Chim. Acta, 166 (1984) 103.
7 R.D. Armstrong, Electrochim. Acta, 32 (1987) 1549.
8 W.E. Morf and W. Simon, Anal. Lett., 7 (1974) 9.
9 G.D. Hu and Y.C. Zhang, Multivariate Data Analysis Methods, Nankai University Press, Beijng, 1990, p. 410.
10 Z.R. Zhang, Y.P. Lin and R.Q. Yu, Fenxi Huaxue, 19 (1991) 129.
11 D.B. Huong, Z.T. Sheng and G.L. Wu, Principles and Applications of Ion Selective Electrodes, New Time Press, Beijing, 1982, p. 51.
12 J.M. Lehn and P. Vierling, Tetrahedron Lett., 21 (1980) 1323.
13 C.J. Pedersen and H.K. Frensdorff, Angew. Chem., 84 (1972) 16.
14 D.J. Cram and J.M. Cram, Acc. Chem. Rev., 11 (1978) 8.
15 R.M. Izatt, R.E. Terry, B.L. Haymone, L.D. Hansen, N.K. Dalley, A.G. Avondet and J.J. Christensen, J. Am. Chem. Soc., 98 (1976) 7620.
16 S.N. Vinogradov and R.H. Linnell, Hydrogen Bonding, Van Nostrand Reinhold, New York, 1971, Chap. 5.
17 Z.R. Zhang and V.V. Cosofret, Sel. Electrode Rev., 12 (1990) 35.
18 Pharmacopoeia of the People's Republic of China, Chemical Industry Press, People's Health Press, Beijing, 1985, p. 339.

Analytica Chimica Acta, 285 (1994) 89–94
Elsevier Science B.V., Amsterdam

Self-driven coulometry without an external electric source

Shunichi Uchiyama, Seiji Maeda, Yasushi Hasebe and Shuichi Suzuki

Department of Environmental Engineering, Saitama Institute of Technology, 1690 Fusaiji, Okabe, Saitama 369-02 (Japan)

(Received 18th May 1993; revised manuscript received 2nd September 1993)

Abstract

During the usual electrolysis, an electric power supply is needed to transfer electrons between the electroactive species and an electrode. If the substance in the sample solution is to be oxidized (reduced) without an external electric power supply, the potential of the half-cell containing the sample solution must be sufficiently lower (higher) than that of the half-cell in which the counter electrode is placed. If on short-circuiting both half-cells electrolysis in the sample-containing half-cell occurs spontaneously, i.e., without external power supply, the cell is so-called self-driven. This concept has been used in a coulometric cell with a carbon felt electrode impregnated with electrolyte not containing an electroactive species and a carbon felt counter electrode impregnated with hexacyanoferrate(III) solution. Determinations of L-ascorbic acid and NADH were carried out with nearly 100% discharging efficiencies and it was demonstrated that self-driven coulometry exhibited the same properties as conventional electrolytic coulometry using an external electric power supply.

Keywords: Coulometry; Ascorbic acid; Self-driven coulometry; NADH

When a sufficiently large electrode potential difference is maintained between the working and the counter electrodes using an external electric power supply, an electrolytic current may flow owing to the conversion of a chemical substance. This type of electrolysis has been extensively used as an important analytical procedure in various fields. However, an external electric source is not necessary to realize the electrode reaction if the required electromotive force can be created by chemical species. In fact, batteries discharge without an external electric source.

Coulometry is based on the integration of the electrolytic current consumed by the electrolysis of a sample or the electrochemical generation of a titrant, and the absolute value can be obtained by applying Faraday's law. Conventional coulometry has been restricted to electrolysis of two different types: controlled-potential coulometry [1] and controlled-current coulometry [2]. In both techniques, an electric power supply is essential to maintain the constant potential or current during electrolysis. The controlled-potential or amperometric method is subdivided into polarographic and galvanic types. For the galvanic method, an analyte is electrolysed by the electromotive force generated between the working and counter electrodes, and no external electric source is needed. If a large potential difference between the working and counter electrodes is needed to carry out the complete discharge of analyte, concentration-step coulometry [3,4] without an external electric source should be realized. A self-driven amperometric or potentiometric method for gas samples has been realized by using different kinds of electrodes (i.e., Pb and Pt) [5,6], but coulometry for non-volatile compounds in solution based on a self-driven method has not been

Correspondence to: S. Uchiyama, Department of Environmental Engineering, Saitama Institute of Technology, 1690 Fusaiji, Okabe Saitama 369-02 (Japan).

SSDI 0003-2670(93)E0500-7

reported. In this paper, a novel coulometric method is proposed for chemical substances in solution based on a self-driven method using the same kind of electrode material for the working and counter electrodes.

The same structural cell using carbon felt electrodes impregnated with electrolyte and a counter solution was used to demonstrate self-driven coulometry in which the electromotive force was varied by changing the content of electroactive species in the counter solution. The direct discharge of L-ascorbic acid and the indirect discharge of the reduced form of nicotinamide adenine dinucleotide (NADH) using mediators were carried out to demonstrate the applicability of the method.

The determination of NADH allows the monitoring of biochemical substrates that produce NADH from NAD^+ in their dehydrogenase reactions. The electrooxidation of NADH has also been carried out at metal and chemically modified electrodes [7,8] to perform rapid and interference-free electrochemical measurements. However, the stability of the electrode is poor and the absolute determination of NADH has not been reported.

PRINCIPLE

The principle of self-driven coulometry for the determination of a reducing agent is shown schematically in Fig. 1. During conventional electrolysis of a reducing agent (sample), the oxidation potential of the sample (E_O) is generally higher than the reduction potential of the counter species (E_R), and the electric potential difference (ΔE) has to be applied to carry out electrolysis; i_O and i_R represent the oxidation current of the sample and the reduction current of the counter species during electrolysis, respectively.

On the other hand, in the self-driven method, if the oxidation potential of the sample is lower than E_R, the sample discharges spontaneously, being driven by ΔE_G, and the sample oxidation current (i_S) is abruptly generated by adding the sample to an electrolyte not containing an electroactive substance; i_C represents the counter electrode current induced by the sample addition. Therefore, if ΔE_G is sufficiently large, the sample discharges completely, accompanied by a decrease in the potential difference between the electrodes. The reason why the potential difference decreases is that the concentration of the electroactive substance in the counter cell is gradually decreased by discharging. This consideration leads to the conclusion that coulometry can be performed by integrating the current generated on sample addition. Moreover, even if the samples are not electroactive substances, it can be expected that many of them can also be indirectly discharged by using mediators whose oxidation potential is lower than the reduction potential of the counter species.

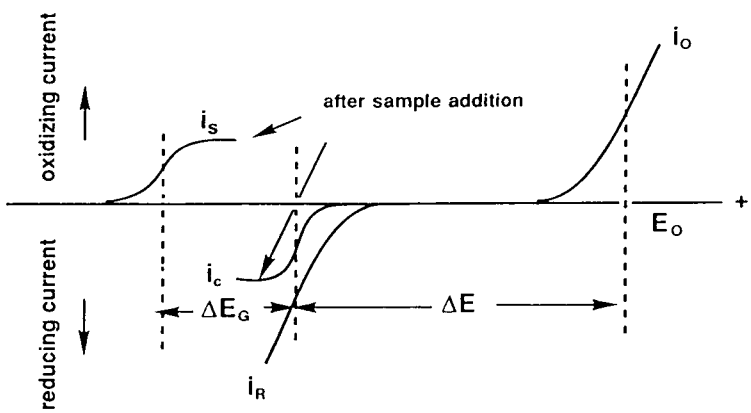

Fig. 1. Principle of self-driven coulometry for the determination of a reducing agent.

EXPERIMENTAL

A device similar to an electrolytic cell described previously [9,10] was used as a self-driven cell and was connected to a coulometer (Nikko Keisoku NDCM-1). Phosphate buffer solution (pH 7.0) and the same solution with dissolved analytical-reagent grade potassium hexacyanoferrate(III) were used as the electrolyte and counter solution, respectively, when L-ascorbic acid was measured. Phenazine methosulphate (PMS^+) is well known as a selective oxidation agent for NADH, which stoichiometrically produces NAD^+ [11,12], so this reagent was used as the mediator for the determination of NADH. The whole coulometric cell was covered with a box with a small hole for sample addition throughout the measurement of NADH in order to protect the cell against room light when PMS^+ is used, because PMS^+ is a photosensitive species. Standard sample solutions of L-ascorbic acid and NADH were prepared by dissolving the analytical-reagent grade chemicals in distilled water. These solutions were standardized by iodimetric titration.

The experimental procedure is as follows. First, two round carbon felt electrodes, one containing the electrolyte and the other the counter solution, were separated by an ion-exchange membrane and were connected to a coulometer. After the background current had reached a constant value (about 0.05 mA), the sample solution was added to the carbon felt working electrode using a micropipette. The total charge that flowed on addition of the sample was measured and the discharge current vs. time curve during the experiment was recorded on an x–t recorder.

RESULTS AND DISCUSSION

When 0.1 M hexacyanoferrate(II) solution was used as the counter solution, a very small oxidation current was generated on adding 0.01 ml of 10^{-3} M L-ascorbic acid to the working electrode impregnated with pH 7.0 buffer solution and about 0.05 mC was measured. However, a characteristic current peak was not observed. This indicates that L-ascorbic acid cannot be oxidized because a suitable reducible species is not contained in the counter solution and the small current that is observed is considered to be due to the presence of an electroactive impurity in the counter solution. Apparently it is not possible to perform the coulometric measurement of L-ascorbic acid using a cell containing hexacyanoferrate(II) as the counter solution.

On the other hand, direct oxidation of L-ascorbic acid took place when hexacyanoferrate(III) ion was used as the counter solution. If the counter solution contains both hexacyanoferrate(III) and hexacyanoferrate(II) ions, the current response rate and discharging efficiency of L-ascorbic acid are highly dependent on the hexacyanoferrate(III) content in the counter solution because the potential of the counter electrode is changed by variations in the ratio of the concentrations of the oxidized and reduced forms (ox/red) according to the Nernst equation. This potential can also be varied by adding other oxidizing agents such as cerium(IV) or permanganate to the hexacyanoferrate(III) counter solution, because the standard electrode potentials of these ions are higher than that of the hexacyanoferrate(III) ion. The current response curves of L-ascorbic acid obtained for three hexacyanoferrate(III)-to-hexacyanoferrate-(II) ratios are shown in Fig. 2. These results indicate that a rapid discharge does not take place when a solution with a low ox/red ratio is used as the counter solution, but the complete discharge of L-ascorbic acid can be carried out within 1 min when the ox/red ratio is high, such as when 0.1 M hexacyanoferrate(III) counter solution is used.

The electromotive force of the self-driven cell was measured for different hexacyanoferrate(III)-to-hexacyanoferrate(II) ratios as shown in Fig. 3. The results show that the relationship between the logarithm of the ox/red ratio and the electromotive force between the working and counter electrodes is linear according to the Nernst equation, and the electromotive force obtained when an electrolyte containing 0.1 M PMS^+ is used is about 40 mV lower than that obtained with electrolyte without PMS^+. This means that PMS^+ is

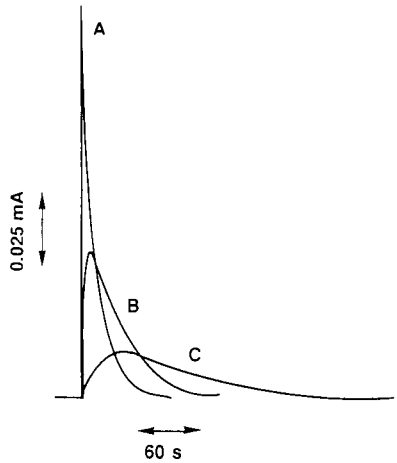

Fig. 2. Shape of the discharge current response curves obtained on addition of 1×10^{-3} M L-ascorbic acid (0.01 ml). Electrolyte: phosphate buffer solution (pH 7.0). Counter solution: (A) 0.1 M hexacyanoferrate(III) ion; (B) 0.05 M hexacyanoferrate(II) ion + 0.05 M hexacyanoferrate(III) ion; (C) 0.099 M hexacyanoferrate(II) ion + 0.001 M hexacyanoferrate(III) ion.

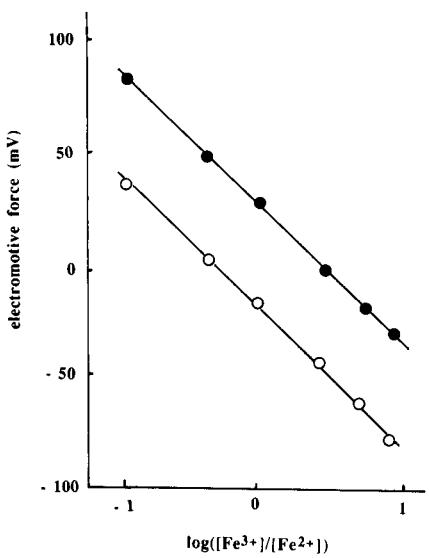

Fig. 3. Effect of hexacyanoferrate(III)-to-hexacyanoferrate(II) ratio in the counter solution on the electromotive force between working and counter electrodes. Fe^{3+} = hexacyanoferrate(III) ion; Fe^{2+} = hexacyanoferrate(II) ion; $[Fe^{2+}]+[Fe^{3+}]=0.1$ M. Electrolyte: ● = pH 7.5 buffer solution without mediator; ○ = pH 7.5 buffer solution with 0.1 M phenazine methosulphate.

adequate to discharge the sample with a high oxidation potential.

NADH reduces hexacyanoferrate(III) directly [13] and self-driven coulometry of NADH should be possible by using hexacyanoferrate(III) as the counter solution. However, in contrast to L-ascorbic acid no NADH current response was obtained when the electrolyte was mediator free because the oxidation of NADH at the carbon felt electrode is irreversible. Therefore, the oxidation of NADH had to be carried out using an appropriate mediator. Figure 4 shows the current response curves of NADH obtained by using the PMS^+ mediator. From these results, it can be concluded that the direct oxidation of NADH without mediators does not take place smoothly when hexacyanoferrate(III) solution is used as the counter solution but that in the presence of PMS^+ NADH gives a rapid current response. This indicates that a mediator is required to accelerate the electron transfer of NADH in a self-driven method using a hexacyanoferrate(III) counter solution.

The results for L-ascorbic acid and NADH obtained by self-driven coulometry are summarized in Table 1. These results show that the determination of NADH can be performed using PMS^+ and hexacyanoferrate(III) ion as mediator and counter species, respectively. The relative standard deviations were below 3%. However, the potential difference between the two electrodes in self-driven coulometry gradually decreases with the sucessive addition of the sample because the cell active species in the counter solution is decreased. Owing to the electrode potential changes, the selectivity of the method decreases. However, a large amount of cell active species can be dissolved in the counter solution and in that case the successive addition of a small amount of sample does not substantially change the potential difference. The sucessive determination of NADH was very easy and twenty samples (0.01 ml) could be analysed with 100% current efficiency using the same electrolyte.

In self-driven coulometry, the electromotive force is dependent on the kind and concentration of the counter species and discharging potential of the sample or mediator. If a strong reducing

TABLE 1

Results of self-driven coulometric analysis [a]

Sample	Concentration (M)	Mediator	Counter solution	Charge (mC)	R.S.D. (%)	DE (%)	DT (s)
L-Ascorbic acid	1×10^{-3}	None	0.099 M Fe^{2+} + 0.001 M Fe^{3+}	1.863	3.0	96.5	300
	1×10^{-3}	None	0.05 M Fe^{2+} + 0.05 M Fe^{3+}	1.920	1.1	99.5	60
	1×10^{-3}	None	0.1 M Fe^{3+}	1.930	0.5	100.0	50
NADH	4.59×10^{-4}	0.1 M PMS^{+}	0.1 M Fe^{3+}	0.879	2.8	99.3	15
	9.25×10^{-4}	0.1 M PMS^{+}	0.1 M Fe^{3+}	1.744	1.7	99.3	25

[a] Mean values of 15 experimental data. pH values of electrolyte and counter solution are 7.0 DE = discharging efficiency of the added sample; DT = discharge time of the added sample. Fe^{2+} = hexaycanoferrate(II) ion; Fe^{3+} = hexacyanoferrate(III) ion.

agent is used as the counter species, the sample should be reduced and then coulometry of the oxidizing agent would be possible. An advantage of the technique would be that side-reactions are avoided in a self-driven cell, because the driving reaction and the reaction to be analysed are the same. In contrast, reactions other than the reaction to be measured might occur in controlled-potential or -current coulometry. In fact, no charging current of self-driven cell flows when a working electrode is electrically connected or disconnected with a counter electrode after the background current has become constant. The determination of the sample can be carried out immediately after electrical contact between the two electrodes has been made; however, in conventional controlled-potential coulometry a waiting period is needed until the background current (including charging current) has become constant. This rapid experimental set-up of self-driven coulometry is a major advantage compared with conventional coulometry.

In conclusion, a novel electroanalytical method without an external electric power supply has been developed that can be applied to the determination of various electroactive and electroinactive species.

This research was supported by the Nakano Foundation. The authors express their appreciation to Mr. S. Kodaira and Mr. M. Ubukata for experimental assistance.

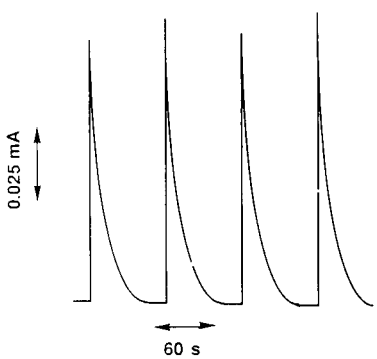

Fig. 4. Discharge current vs. time curves obtained by successive addition of NADH. Electrolyte: 0.1 M phenazine methosulphate buffer solution. Counter solution: 0.1 M hexaycyanoferrate(III) solution (pH 7.0).

REFERENCES

1 J.E. Harrar, in A.J. Bard (Ed.), Electroanalytical Chemistry, Vol. 8, Dekker, New York, 1975, pp. 1–167.
2 J. Janata, in A.J. Bard (Ed.), Electroanalytical Chemistry, Vol. 3, Dekker, New York, 1969, pp. 1–55.
3 S. Uchiyama, K. Nozaki and G. Muto, J. Electroanal. Chem., 91 (1978) 301.
4 S. Uchiyama and G. Muto, Anal. Chem., 56 (1984) 2408.
5 L.C. Clark, Jr., R. Wolf, D. Granger and Z. Tayler, J. Appl. Physiol., 6 (1953) 189.
6 I. Karube, T. Matsunaga and S. Suzuki, J. Solid-Phase Biochem., 2 (1978) 19.
7 T. Yao and Y. Musha, Anal. Chim. Acta, 110 (1979) 203.
8 A. Malinauskas and J.J. Kulys, Anal. Chim. Acta, 98 (1978) 31.

9 S. Uchiyama, M. Ono, S. Suzuki and O. Hamamoto, Anal. Chem., 60 (1988) 1835.
10 S. Uchiyama, Y. Kobayashi, S. Suzuki and O. Hamamoto, Anal. Chem., 63 (1991) 2059.
11 V.S.F. Chew and R. Bolton, J. Phys. Chem., 84 (1980) 1903.
12 V.S.F. Chew, J.R. Bolton, R.G. Brown and G. Porter, J. Phys. Chem., 84 (1980) 1909.
13 S. Uchiyama, T. Mizunuma, Y. Hasebe and S. Suzuki, Bunseki Kagaku, 42 (1993) 333.

Analytica Chimica Acta, 285 (1994) 95–102
Elsevier Science B.V., Amsterdam

Deconvolution of non-resolved voltammetric signals

Ivanka Pižeta

Centre for Marine Research Zagreb, Rudjer Bošković Institute, P.O. Box 1016, HR-41001 Zagreb (Croatia)

(Received 17th November 1992; revised manuscript received 22nd July 1993)

Abstract

A summary of the necessary details on the deconvolution of voltammetric signals for the recognition or better separation of signals of two energetically similar processes is given, in order to facilitate program writing for such signal processing. Once the program has been written, the user has to take two decisions for processing the set of experimental curves according to the proposed method.

Keywords: Signal processing method; Voltammetry; Deconvolution

Deconvolution is on the one hand a complicated signal processing method, involving Fourier transformation and spectra of the signals. On the other hand, it is attractive because the ideal result of its application to the voltammetric peaks is their transformation into Dirac δ functions, which permit the separation of the signals of two energetically similar processes.

Useful information on the basic concepts and applications of deconvolution is available [1–5]. Engblom and Ivaska [6,7] have carried out comprehensive theoretical work, transforming analytical terms of voltammetric waves and deriving expressions for deconvolution functions such that the peak height or the area under the peak after deconvolution would be preserved. Results on some systematic calculations with close differential-pulse polarographic peaks of reversible processes have also been published and limitations of the resolution enhancement due to the application of the deconvolution method have been given [8], in addition to some applications in the detection of adsorption peaks [9,10]. However, in order to use this procedure, there are some details that may be time consuming if one starts from the beginning, i.e., from the existing literature descriptions. It would be useful for future users of this method to have a summary of it in such detail that would shorten the time needed to write the necessary programs. It is also considered that this method deserves more users and this paper is intended to contribute to its wider use. This is possible because electrochemical instrumentation has recently become more compatible with computers and data processing has become easier according to individual needs. The memory and speed of personal computers now allow complicated operations to be performed in a reasonable time. In addition to deconvolution, the ability to have an insight into the spectra of the voltammetric signals obtained by Fourier transformation could bring some other benefits, as recently shown by Engblom [11].

Correspondence to: I. Pižeta, Centre for Marine Research Zagreb, Rudjer Bošković Institute, P.O. Box 1016, HR-41001 Zagreb (Croatia).

DECONVOLUTION METHOD

To be able to deconvolute a measured voltammetric curve, it is presumed that it consists of

SSDI 0003-2670(93)E0530-K

equidistant discrete points. As the half-width of the voltammetric peaks is a few tens of mV, a sampling rate of about 2 mV, which is usual with the existing instrumentation where discrete current values are taken, is acceptable for fulfilling the Nyquist criterion, i.e., that the sampling rate must be at least twice the largest frequency component of the signal. For fast Fourier transformation (FFT) algorithm that will be used [12,13], it is recommended that the number of points is 2^{integer}, so if possible the measurement should be performed under that condition, and if not then extra zero points will be added afterwards in the procedure. The voltammetric curve obtained should be stored in a file. The procedure is given in the flow chart in Scheme 1.

For illustration, the reduction signal of 1×10^{-4} M thallium and 8×10^{-5} M cadmium in 7.8×10^{-2} M NaCl–4 M $NaClO_4$ (pH 2) will be given. The method used is differential-pulse polarography (DPP), with a step increment of 2 mV and a pulse height of 24 mV. The curve has 256 points and is shown in Fig. 1a.

The first decision is taken by choosing the deconvolution function and its width. Previous investigations and experience [8] indicated the following function as the simplest and fundamental deconvolution function:

$$I(E) = \exp(\varphi)/[1 + \exp(\varphi)]^2 \qquad \text{(I)}$$

where $\varphi = nF/RT(E - E_0)$ and the other symbols have their usual meanings, n is not necessarily an integer but can be a decimal number, for the possibility of finer regulation of the width of the deconvolution function. Of course, any other expression for the voltammetric peak may be used for the deconvolution function, including a measured curve of a single peak previously stored in the file.

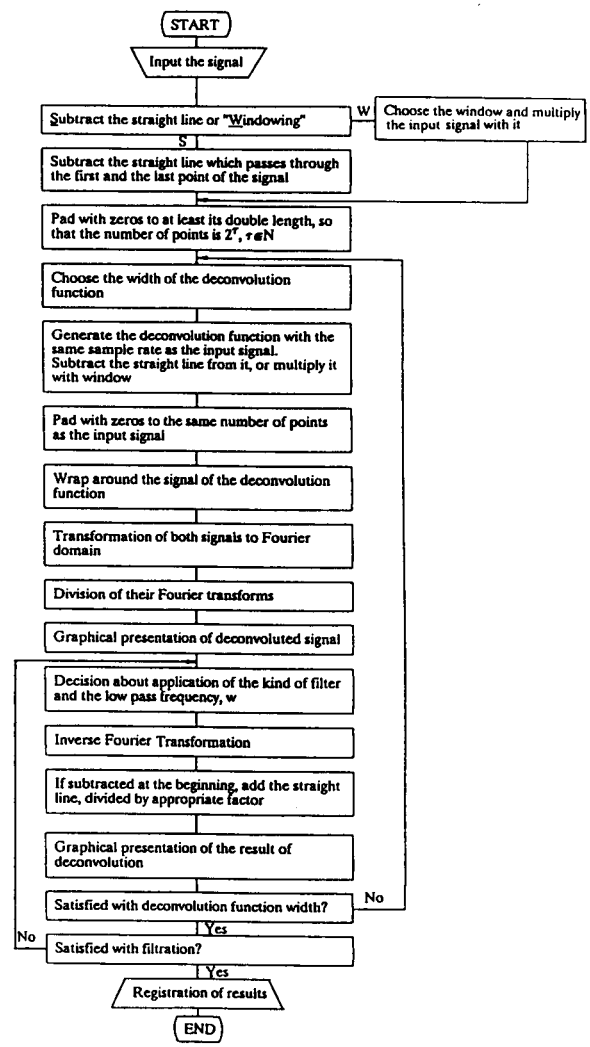

Scheme 1. Flow chart of the program for deconvolution using Fourier transformation.

Next n, which regulates the width of the deconvolution function, is chosen. As seen from the flow chart in Scheme 1, this can be done itera-

Fig. 1. (a) (1) Signal of reduction of 1×10^{-4} M Tl^+ and 8×10^{-5} M Cd^{2+} in 7.8×10^{-2} M NaCl–4 M $NaClO_4$ (pH 2), sample rate 2 mV, curve with 256 points; (2) straight line passing through the first and the last point of curve 1; (b) deconvolution function (I), $n = 2$, same sampling rate and number of points as in (a); (c) signal from (a) where 1 − 2 is performed; (d) signal from (b) where straight line passing through the first and the last point is subtracted; (e) signal from (c) padded with zero points to double its length (512 points); (f) signal from (d) padded with zero points to double its length (512 points) and wrapped around; (g) amplitudes of the positive frequencies of Fourier transform of the signal from (e), $T_0 = 1.024$ V, 1 = linear scale, 2 = logarithmic scale; (h) amplitudes of the positive frequencies of Fourier transform of the signal from (f), $T_0 = 1.024$ V, 1 = linear scale, 2 = logarithmic scale.

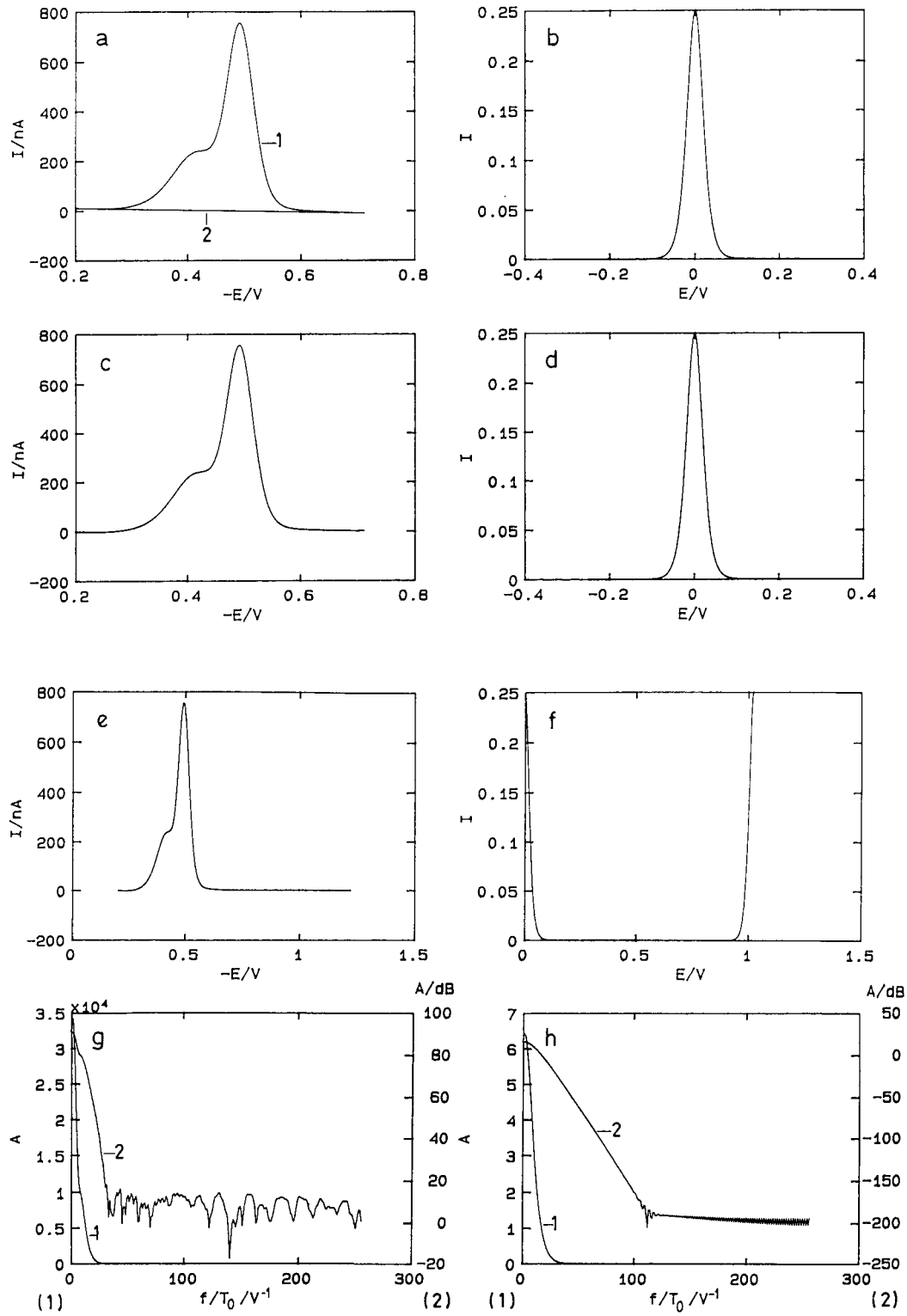
a
b
c
d
e
f
g
h
I/nA
I
-E/V
E/V
A/dB
A
x10⁴
f/T₀ /V⁻¹
(1)
(2)
1
2

tively. If one is not satisfied with the result of deconvolution, it can be repeated with another n. The rule governing the decision regarding n is that the deconvolution function must be of the same width as or narrower than the narrowest peak in the signal being deconvoluted. Too narrow a function would not affect the signal at all, whereas too wide a function would produce meaningless oscillations. At this point it should be explicitly said that an "expert eye" is included in the data processing. It is assumed that the person who is processing the data understands the shape of the voltammetric signals and the background currents. Criteria for the decision regarding n, when processing a signal from a real sample, cannot be given exactly. They should be made by the analyst who should know the limits governed by the main rules, and make a decision based on several tries. A decision should be made between side oscillations of the whole signal (waves on the feet of the deconvoluted curves) and the degree of separation of the overlapped signals. One should also not be misled by those side oscillations and declare them as peaks. For the signal in Fig. 1a, it was decided to use deconvolution function (I) with $n = 2$ (Fig. 1b). It is calculated in discrete points with a 2-mV spacing, the same as for the measured curve in Fig. 1a, and it also has 256 points.

When performing discrete Fourier transformation of the signal, it is assumed that the signal is one period of a periodic function [14]. As it was not wanted to have discontinuities between periods, the signal was modified so that it started and ended with the same value, zero. This can be achieved in two ways, by straight-line subtraction or by multiplication with the appropriate window. The advantages and drawbacks of these two approaches will be elaborated upon elsewhere [15]. Here straight-line subtraction was used. From curve 1 in Fig. 1a a straight line (2) should be subtracted. The resulting curve is shown in Fig. 1c. The straight line is also subtracted from the deconvolution curve but, as it is a theoretical curve, the result is hardly seen (Fig. 1d).

The algorithm for deconvolution assumes circular deconvolution, and it must be performed as if it were linear. For that reason, the measured curve should be at least doubled by zero padding (if the starting number of points was 2^{integer}, doubling is sufficient; if not, even more zero points should be added so that both criteria, doubling of the points and 2^{integer}, are satisfied). Both the measured and deconvolution curves are expanded to the same number of points (in this case to 512 points). The length of curve so obtained is called T_0, and it is the length of one period (in this case $T_0 = 1.024$ V). Further, the deconvolution curve is wrapped around as the algorithm in [12] demands. The conditioned measured and deconvolution curves obtained are shown in Fig. 1e and f, respectively.

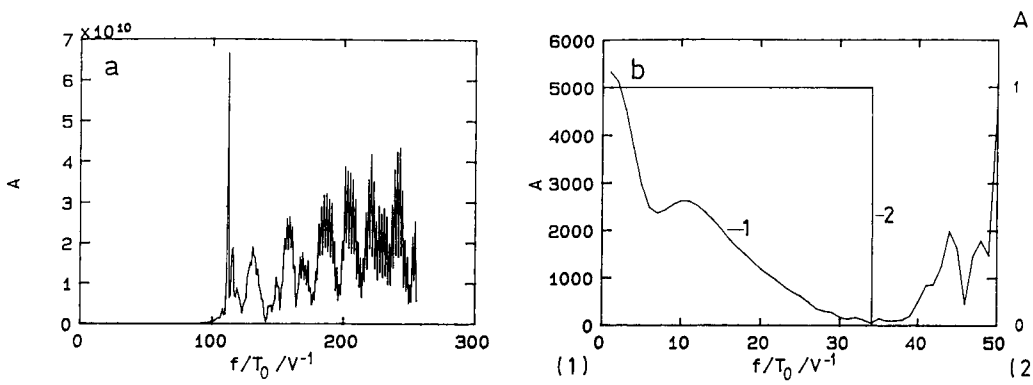

Fig. 2. Amplitudes of positive frequencies of deconvoluted signal from Fig. 1g with signal from Fig. 1h, i.e. the result of division of these two signals in the Fourier domain. (a) Amplitudes of all 256 positive frequencies; (b) (1) amplitudes of first 50 frequencies, (2) boxcar filter with cut-off frequency $w = 34/T_0$, $T_0 = 1.024$ V.

Now FFT of both signals can occur. The amplitudes of positive frequencies of the transformed measured and deconvolution curves in linear and logarithmic scales are shown in Fig. 1g and h, respectively. Dividing their Fourier transformations leads to deconvolution. The results of dividing, i.e., the amplitudes of the positive frequencies of the deconvoluted signal in the linear scale, are shown in Fig. 2. Figure 2a shows all amplitudes and Fig. 2b only the first 50. The measured signal is described with only the first few frequencies, which can be seen and checked by looking at the Fourier transform of the measured curve itself (Fig. 1g), so high amplitudes on higher frequencies represent noise due to deconvolution, which is in fact result of division by small numbers (compare the signals in Fig. 1g and h on the dB scale), and they should be filtered out.

At this point a second decision must be taken. One has to decide about the cut-off frequency of the low-pass filter and about its shape. Here again there are some frame rules and experience that help in making the decision. In this case the frequency $34/T_0$ and the boxcar filter were adopted. The cut-off frequency was chosen at the frequency which has minimum amplitude, before the steep rise in amplitude caused by deconvolution. This decision can also be made iteratively, as seen from the flow chart in Scheme 1, because it can significantly influence the shape of the final

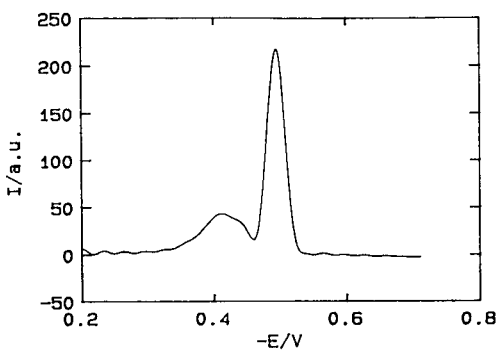

Fig. 3. Result of deconvolution after filtration and inverse Fourier transformation of the signal from Fig. 1. Deconvolution function, (I) with $n = 2$; filter, boxcar with $w = 34/T_0$, $T_0 = 1.024$ V.

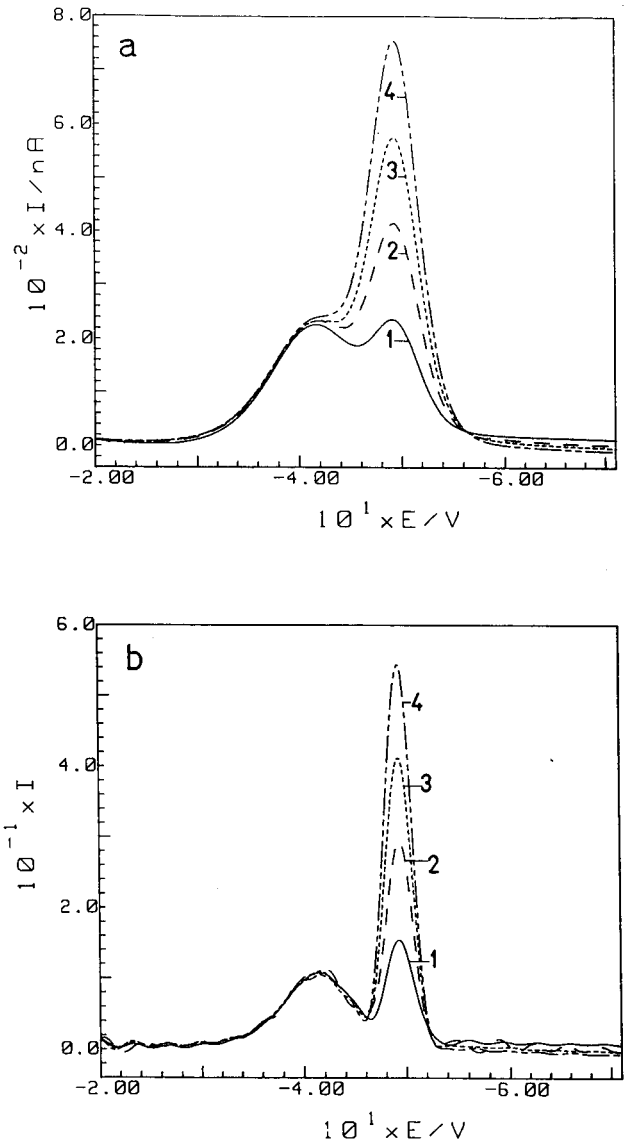

Fig. 4. (a) Overlapping reduction waves in DPP excitation mode with constant 1×10^{-4} M Tl^+ concentration and increasing Cd^{2+} concentration of (1) 2×10^{-5}; (2) 4×10^{-5}; (3) 6×10^{-5}; (4) 8×10^{-5} M in the supporting electrolyte of 4 M $NaClO_4$–0.078 M NaCl (pH 2). Instrumental set-up of EG&G Model 384B polarograph: voltage pulse, 24 mV; clock time, 1.0 s; scan rate, 2 mV s^{-1}; potential range, −0.20 to −0.71 V vs. reference electrode. Electrode system, PAR 303A, medium drop size. (b) FFT deconvolution method applied to the experimental signals presented in (a) for Cd^{2+} determination by standard additions method in the presence of a constant height but overlapping reduction wave of Tl^+. Deconvolution function, (I), $n = 2$; filter, boxcar, $w = 33/T_0$, $T_0 = 1.024$ V.

curve. When choosing filters, if one writes a program, for instance, in MATLAB [13,16], there is no problem in using filters such as the Chebyshev, Kaiser or a similar filter, because they are part of MATLAB's instructions, but if one uses basic languages, such as Quick Basic or similar, one must take account of the algorithms for the filters. As far as it was tested, the boxcar filter in most cases is not much worse and it is much easier to program. If there is not a pronounced minimum between the first part of the spectrum containing the signal and the noise, in a simpler version, a Gauss filter was used [17]. Using MATLAB, it is not a problem to construct a filter with a defined transition width, passband ripple and stopband attenuation.

The final stage is the inverse FFT and the addition of the subtracted straight line which is divided by a transformation factor Max, where $Max = Max_1/Max_2$, Max_1 is the maximum of the original signal after the subtraction of the straight line and Max_2 is the amplitude of the deconvo-

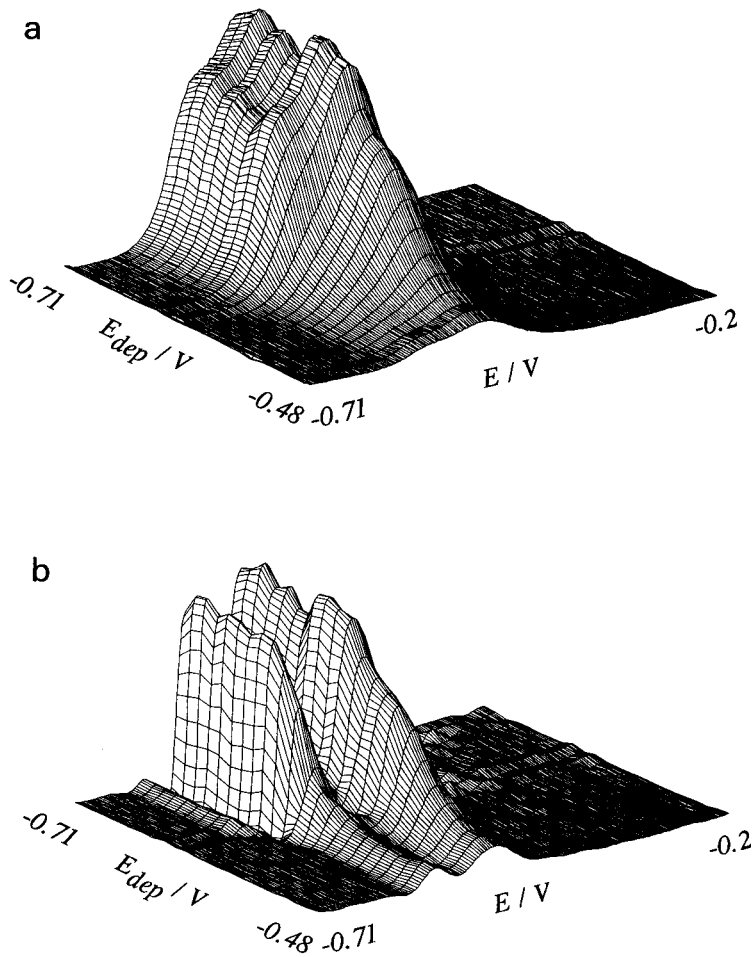

Fig. 5. (a) A series of 24 voltammograms of 5×10^{-5} M Cd^{2+} and 5×10^{-5} M Tl^{+} in 1 M $Mg(ClO_4)_2$ (pH 2) measured to obtain their pseudo-polarogram. Instrumental set-up of Autolab (Eco Chemie): SWV technique; $f = 100$ Hz; amplitude, 0.010 V; step increment, 0.00244 V; potential range, −0.71 to −0.2 V vs. reference electrode; deposition potential, from −0.48 to −0.71 V in steps of 0.01 V. Electrode system, PAR 303A, medium drop size. (b) FFT deconvolution method applied to the experimental signals presented in (a). Deconvolution function, (I), $n = 1.5$; filter, boxcar, $w = 24/T_0$, $T_0 = 1.25$ V.

luted signal before the straight line is added at the place of Max_1. If a set of curves belonging to one experiment is to be processed, it is sufficient to determine the transformation factor Max once, and to use it for the whole set of curves.

The deconvoluted curve is shown in Fig. 3. The two peaks are narrower and better separated with a pronounced minimum between them, so each peak height and peak potential can be more accurately read out. Deconvolution has more influence on the narrower peak, which is a property of deconvolution procedure. The height of the peaks is not preserved, nor is their ratio, if their width is not equal, but this is not an obstacle if the standard additions method is used. The application of the standard additions method to the voltammetric signals of Cd^{2+} and Tl^{+} resolved by FFT deconvolution is illustrated in Fig. 4.

Figure 4a shows four voltammograms representing the reduction waves for a sample (curve 1) and three standard additions (curves 2–4) of Cd^{2+} in presence of a constant concentration of Tl^{+}. The same voltammograms after deconvolution are shown in Fig. 4b. The determination of the concentration of the sample is obviously more accurate and unambiguous in the latter instance. Briefly, the accuracy of concentration determination depends on the distance between the overlapped peaks, on the ratio of their amplitudes and on the ratio of their half-widths [8]. Because of the noise resulting from deconvolution (waves on the feet of the deconvoluted curves), the amplitude ratio in any case should not be greater than 20, which is the limitation of the method as obtained by simulated signals within 5% accuracy [8].

An example is given in Fig. 5 to show the effect of deconvolution on a series of voltammetric curves. In order to obtain a pseudo-polarographic curve for Cd^{2+} and Tl^{+} in 1 M $Mg(ClO_4)_2$, a set of 24 curves was measured by changing the deposition potential from -0.48 to -0.71 V. The technique applied was square-wave voltammetry (SWV). The original data are shown in Fig. 5a and the same data after deconvolution in Fig. 5b. Only after deconvolution could two separate pseudo-polarograms be obtained.

Further uses of the deconvolution procedure in analytical applications in combination with the standard additions method are elaborated upon elsewhere [18].

Conclusion

Although the deconvolution procedure involves Fourier transformation of the signal, where complex numbers appear, it is an elementary signal-processing method, each step of which is easily visualized. It is also easy to write a program giving satisfactory results when the described steps are followed. In each curve processing there are basically two decisions to be taken, with regard to n, the width of deconvolution function, and w, the cut-off frequency, assuming that the shapes of the deconvolution function and the low-pass filter are determined generally and that an "expert eye" with a knowledge of the shape of voltammetric signals is included. Even for the whole set of curves obtained by standard additions, these decisions should just be repeated.

The proposed method is suitable for analytical purposes and it is recommended as a future automatic procedure built into electrochemical instruments.

This work was supported by the Ministry of Science, Technology and Informatics of the Republic of Croatia in the framework of the EUREKA-ELANI 37/12 (EUROMAR) project. The Department of Electronic Measurements and Systems of the Faculty of Electronic Engineering, Zagreb, is gratefully acknowledged for the use of MATLAB.

REFERENCES

1 D.E. Smith, Anal. Chem., 48 (1976) 221A.
2 D.E. Smith, Anal. Chem., 48 (1976) 517A.
3 B.S. Grabarić, R.J. O'Halloran and D.E. Smith, Anal. Chim. Acta, 133 (1981) 349.
4 P.R. Griffiths, Transform Techniques in Chemistry, Plenum, New York, 1978.
5 A.G. Marshall, Fourier, Hadamard, and Hilbert Transforms in Chemistry, Plenum, New York, 1982.
6 S.O. Engblom and A.U. Ivaska, in M.R. Smyth and J.G. Vos (Eds.), Electrochemistry, Sensors and Analysis (Analytical Chemistry Symposia Series, Vol. 25), Elsevier, Amsterdam, 1986, p. 49.

7 S.O. Engblom, J. Electroanal. Chem., 296 (1990) 371.
8 I. Pižeta, M. Lovrić and M. Branica, J. Electroanal. Chem., 296 (1990) 395.
9 I. Pižeta, M. Lovrić, M. Zelić and M. Branica, J. Electroanal. Chem., 318 (1991) 25.
10 M. Zelić, I. Pižeta and M. Branica, Anal. Chim. Acta, 281 (1993) 63.
11 S.O. Engblom, J. Electroanal. Chem., 332 (1992) 73.
12 W.H. Press, B.P. Flannery, S.A. Teukolsky and W.T. Vetterling, Numerical Recipes, Cambridge University Press, Cambridge, 1987.
13 MATLAB for 80386-based MS-DOS Personal Computers, MathWorks, Natic, MA, 1990.
14 E.O. Brigham, The Fast Fourier Transform, Prentice-Hall, Englewood Cliffs, NJ, 1974.
15 I. Pižeta and B. Jeren, in preparation.
16 J. Little and L. Shure, Signal Processing Toolbox for Use with MATLAB, User's Guide, MathWorks, Natick, MA, 1989.
17 J.K. Kauppinen, D.J. Moffatt, D.G. Cameron and H.H. Mantsch, Appl. Opt., 20 (1981) 1866.
18 B. Raspor, I. Pižeta and M. Branica, Anal. Chim. Acta, 285 (1994) 103.

Analytica Chimica Acta, 285 (1994) 103–111
Elsevier Science B.V., Amsterdam

Comparative quantitative analysis of overlapping voltammetric signals

Biserka Raspor, Ivanka Pižeta and Marko Branica

Centre for Marine Research Zagreb, Rudjer Bošković Institute, P.O. Box 1016, HR-41001 Zagreb (Croatia)

(Received 17th November 1992; revised manuscript received 22nd July 1993)

Abstract

Catalytic hydrogen evolution according to the Brdička reaction was applied for the rapid detection and determination of metallothionein isolated from rabbit liver. The heights of two catalytic hydrogen waves, of different widths, Cat_1 (overlapped with the reduction wave of Co^{2+}) and Cat_2 (overlapped with Cat_1) were evaluated as non-resolved peaks by polarography or by manual tangent fitting and after signal deconvolution applying windowing or straight-line subtraction, as the difference between the current at the peak potential and the baseline at the same potential. Calibration straight lines were statistically verified and compared. Additive interference of the overlapping peaks is the cause of the systematic error of the calibration straight lines. After deconvolution the interference was diminished but not completely eliminated. A significant improvement was achieved for the Cat_1 signal, applying deconvolution with straight-line subtraction. In this manner concentrations of metallothionein as low as 19 $\mu g\ l^{-1}$ could be determined. The sensitivity of the calibration straight line of the Cat_1 peak is nine times higher than that of the Cat_2 peak. The error of the calibration straight line intercept for the Cat_2 peak is similar irrespective of whether it is evaluated as the unprocessed signal by manual tangent fitting or after deconvolution with straight-line subtraction.

Keywords: Signal processing methods; Voltammetry; Deconvolution; Metallothionein

In electroanalysis, the interference which often arises is due to the overlap of the signal of the determinand with the signal of another species of similar reduction energy. The degree of overlap can be such that the existence of two parallel processes cannot be visually distinguished. Therefore, in quantitative analysis erroneous results and misinterpretation might occur.

Much work has been done on the systematization of errors due to the degree of overlap of two close signals of various peak-height ratios [1,2]. The problem might be resolved by chemical, instrumental or mathematical approaches. Applying a suitable physico-chemical method [3], two reactants with close responses could be separated, but it can be time consuming and can cause contamination of the sample. By choosing an appropriate electrolyte or by addition of a complexing agent the peaks can be separated [4]. The peak separation depends on the composition of the sample, the stability of the complexes and the concentration of the complexing agent. It presumes a good knowledge on the existing species distribution and can help in only a limited number of cases. The mathematical approach is based on the subtraction of one peak from the whole signal [5]. In that case, there is no need for a mathematical description of the wave shape; only the signal of one component needs to be measured separately and subtracted from the

Correspondence to: B. Raspor, Centre for Marine Research Zagreb, Rudjer Bošković Institute, P.O. Box 1016, HR-41001 Zagreb (Croatia).

SSDI 0003-2670(93)E0529-G

overall signal. Reproducibility, especially of the baseline current, is demanded. Separation of the peaks by fitting the signals to a mathematical expression that describes the applied excitation mode has been applied, but this approach is technique specific [6,7]. In this study, the deconvolution method was applied for the separation of the overlapping catalytic signals, which are not defined in terms of electrochemical reversibility. For the application of this deconvolution procedure, which was discussed in detail by Pižeta [8], it is not necessary to define the mathematical function which describes the applied excitation mode. Considering polarographic and voltammetric signals as bell-shaped, for the deconvolution function a bell-shaped representation was selected. For the successful application of the procedure the following conditions should be fulfilled:

The half-width of the deconvolution function should be equal to or less than the half-width of the narrowest peak of the overall signal. As too narrow a function would not affect the signal at all, between these two limits the half-width has to be determined in several attempts taking into account the judgement of the analyst.

The number of points of the measured voltammetric curve has to be 2^{τ}, where $\tau \in N$.

The curve that is to be deconvoluted should start and end with zero, by subtracting the straight line from it or by windowing.

The measured curve and the curve of the deconvolution function should be padded with zeros to their double length.

The curve of the deconvolution function should be wrapped around.

After the deconvolution, the straight line should be added back if it has previously been subtracted. When the baseline current is low the effect of re-addition of the straight line is not evident. It becomes evident when the baseline current is high and/or steep on one end, as is the case in this study, or when it is steep at both ends. In such a case, without the re-addition of the straight line the signal is not complete. The subject was discussed by Pižeta and Jeren [9];

After deconvolution, filtering in the Fourier domain is applied, inspecting the amplitudes of the signal with interactive graphics. In the example discussed in this paper, the amplitudes at the lower frequencies, which contain the information about the signal, are not well separated from the amplitudes at higher frequencies, which represent noise due to the deconvolution procedure, and therefore a Gaussian filter was applied. The cut-off frequency is decided by several tries, its lower limit being determined by the spectra of the signal and the upper limit by the unresolved noise and relying on the experience of the analyst.

The aim of this work was to compare the error of calibration straight line determination of overlapped voltammetric signals before and after peak separation by deconvolution. In order to define the interferences of the overlapping signals, the response of the measurement system was related to samples of accurately known composition. During the entire calibration the working conditions were kept constant and at the optimum values with respect to the technique applied. The accuracy of the calibration straight lines will be discussed on the example of metallothionein determination according to the Brdička reaction [10], which represents a real experimental problem, contrary to the unrealistic simulated data that are often used to illustrate the possibilities of deconvolution.

EXPERIMENTAL

The Brdička reaction was performed in 1 M ammonia–ammonium chloride buffer (pH 9.5). In the polarographic cell, the concentration of 6×10^{-4} M $Co(NH_3)_6Cl_3$ has been present [11]. The Brdička reaction was applied for the determination of mammalian-type metallothionein isolated from rabbit liver (Sigma). All solutions were prepared from analytical-reagent grade chemicals and doubly destilled water.

The overlapping, close reduction signals were measured by differential-pulse polarography (DPP) using an EG&G Model 384B polarograph. The polarograph was controlled by a Hewlett-Packard 9816S technical computer system, as described previously [12].

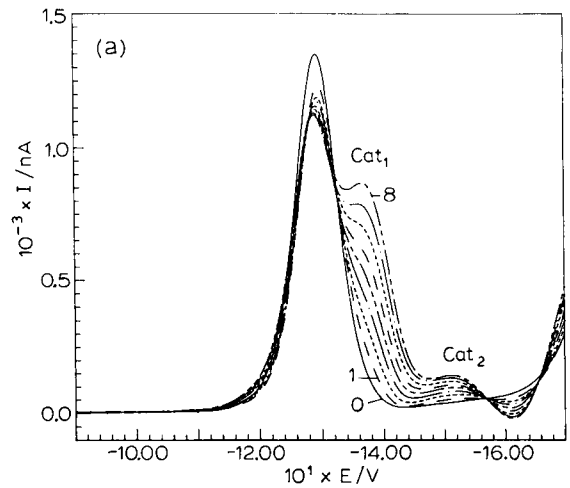

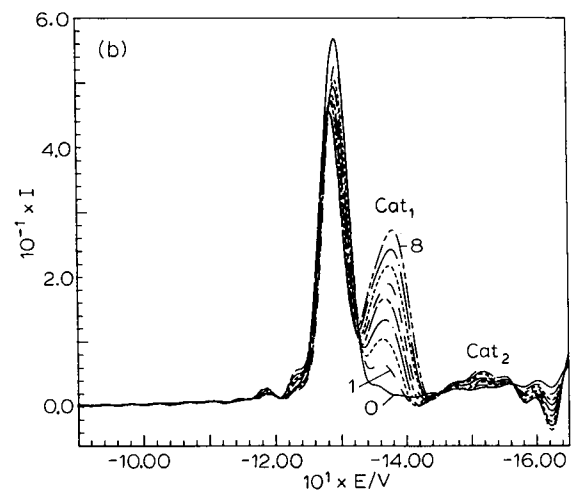

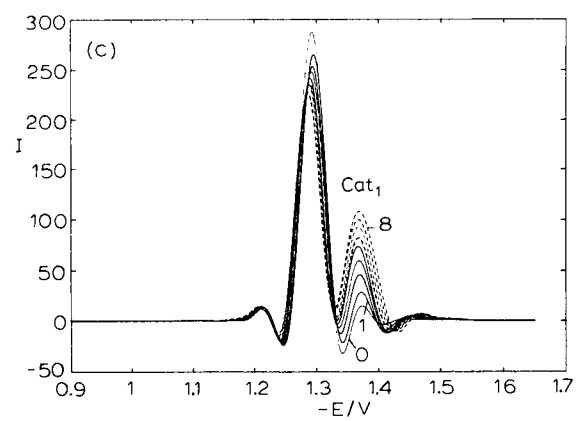

Protein content according to the Brdička reaction was determined in a 10-ml thermostated Metrohm-type cell at 7°C [13,14]. The measurements were performed in the DPP mode with a cathodic potential scan from −0.90 to −1.70 V vs. an Ag/AgCl/saturated KCl reference electrode. Measurements were performed under potentiostatic control with a three-electrode system, consisting of a Metrohm 290 E hanging mercury drop electrode (HMDE) as the working electrode, a platinum wire as the counter electrode and Ag/AgCl/saturated KCl as the reference electrode, which was connected to the cell via a salt bridge filled with 1 M ammonia–ammonium chloride buffer (pH 9.5). The HMDE surface area was 2.20 ± 0.05 mm^2, with a drop diameter of 0.84 mm.

In the DPP excitation mode the polarographic conditions were voltage pulse 24 mV, clock time 0.5 s and scan rate 2 mV s^{-1}.

The pH was measured with an Orion Model EA 920 pH meter and a combined Ross Type 8102SC glass electrode.

RESULTS AND DISCUSSION

Amino acids, polypeptides and proteins containing mercapto groups, dissolved in a cobalt-

Fig. 1. (a) Non-resolved catalytic waves of hydrogen evolution, Cat_1 and Cat_2, recorded in the DPP excitation mode in the presence of analytical concentrations of metallothionein isolated from rabbit liver: (1) 19; (2) 38; (3) 57; (4) 76; (5) 95; (6) 114; (7) 133; (8) 152 μg l^{-1}. In the absence of metallothionein the reduction signal of Co^{2+} to Co^0 is described by curve 0, which represents the blank. Supporting electrolyte: 1 M ammonia–ammonium chloride buffer (pH 9.5). Polarographic conditions: voltage pulse, 24 mV; clock time, 0.5 s; scan rate, 2 mV s^{-1}; potential range, −0.90 to −1.70 V vs. reference electrode; HMDE surface area, 2.20 ± 0.05 mm^2. (b), (c) Fast Fourier transformation (FFT) deconvolution method applied to the first 376 points of a total of 401 points of the experimental signals presented in (a) for catalytic waves Cat_1 and Cat_2 which are a measure of the metallothionein content. (b) Straight-line subtraction. Deconvolution function [I] from [8]; $n = 1.2$; filter, Gauss $w_g = 50/T_0$; $T_0 = 2.048$ V. (c) Windowing by Blackman window. Deconvolution function [I] from [8]; $n = 1.2$; filter, Chebyshev of 151st order; 240 dB ripple suppression; $w_g = 30/T_0$; $T_0 = 2.048$ V.

containing buffer of suitable pH, produce a catalytic reaction at a mercury electrode, which is called the Brdička reaction [10,11]. This reaction is applied for the rapid detection and determination of proteins containing mercapto groups [15]. The Brdička reaction has been applied to the determination of a specific type of protein rich in mercapto groups, the so-called metallothionein of mammalian [11] and invertebrate [13,14,16] origin.

The series of electrochemical signals in Fig. 1a, recorded in the DPP mode in the potential range from −0.90 to −1.70 V, represent the Brdička reaction applied to the determination of mammalian-type metallothionein, isolated from rabbit liver. A characteristic feature of these signals is the reduction peak of Co^{2+}, with a peak potential at −1.28 V (curve 0 was obtained in the absence of metallothionein), representing the blank of the analytical system. If metallothionein is present in the solution, the reduction peak of Co^{2+} is followed by two catalytic hydrogen waves, Cat_1 and Cat_2 (Fig. 1a, curves 1–8). The amplitude of these signals is related to the amount of metallothionein present in the solution. These catalytic hydrogen waves appear in the potential range from −1.35 to −1.55 V vs. the reference electrode (Fig. 1a).

The assumption is that the relationship between the instrumental response and the metallothionein concentration is linear. The reduction peak of Co^{2+} overlaps with Cat_1, while Cat_1 overlaps Cat_2. The signal of Cat_2 is broader than that of Cat_1. And applying the deconvolution procedure to signals of different broadness is problematic.

The accuracy of the slope and the intercept of the calibration straight line depends on the unbiased reading of the peak height of the determinand, if all other components of the measuring system are under statistical control. The reliability of the calibration straight line depends on the contribution of the background value and on interferences [17]. For this analytical system, on which different data processing procedures are compared, the systematic error of the response cannot be ascribed to the background value, because it is almost zero (Fig. 1a, curve 0), but to the effect of the additive interference due to the non-resolved peaks of Cat_1 and Cat_2. In order to define the interferences of the overlapping signals, the response of the measurement system was related to samples of accurately known concentration of metallothionein. Otherwise, the analysis of samples containing an unknown amount of metallothionein [13–16] is performed with the method of standard additions. In the absence of systematic error, the calibration straight line should pass through the origin. A deviation of the intercept of the straight line along the abscissa reflects the bias of the calibration straight line. This deviation reflects the erroneous peak-height determination of the non-resolved catalytic signals. For different data processing procedures the slope of the calibration lines is not discussed, because the units on the ordinate are different (see Table 1): the reading of the signal height by the polarograph is in the

TABLE 1

Comparative evaluation of the height of the catalytic waves Cat_1 and Cat_2 as a measure of analytical concentration of metallothionein [a]

Concentration of metallothionein ($\mu g\,l^{-1}$)	Peak height							
	Unprocessed signals				Deconvoluted signals			
	Polarograph (nA)		Manual (mm)		Windowing (arbitrary units)		Straight line subtraction (arbitrary units)	
	Cat_1	Cat_2	Cat_1	Cat_2	Cat_1	Cat_2	Cat_1	Cat_2
19	ND [b]	13.7	20.5	1.0	13.98	ND [c]	3.74	0.39
38	ND	29.5	26.0	2.0	32.47	ND	7.64	0.85
57	ND	37.1	32.0	3.0	47.56	ND	10.9	1.12
76	ND	44.1	38.0	4.0	61.67	ND	14.2	1.47
95	ND	46.6	42.5	4.5	69.91	ND	16.9	1.84
114	ND	50.7	48.5	5.5	80.74	ND	19.7	2.15
133	ND	52.4	53.5	6.5	87.93	ND	22.4	2.46
152	212	57.9	59.5	7.0	96.23	ND	25.4	2.82

[a] Blank solution consists of 1 M ammonia–ammonium chloride buffer (pH 9.5) and 6×10^{-4} M $Co(NH_3)_6Cl_3$. Overlapping catalytic reduction waves were recorded on HMDE in the DPP excitation mode. [b] ND in this column = not determined because the polarograph cannot perform a tangent fit on a non-peak-shaped signal. [c] ND in this column = not determined owing to a suppressed signal because of its position close to the edge of the strongly converging windowing function (Fig. 1c).

TABLE 2

Calibration straight line expressed as the dependence of voltammetric peak heights of Cat_1 and Cat_2 on metallothionein concentration [a]

Unprocessed signals			
Polarograph		Manual	
Cat_1	Cat_2	Cat_1	Cat_2
ND	$Y = 16.47 + 0.293X$ $X_0 = -56\ \mu g\ l^{-1}$ $s_a = 3.790$; $t_a = 4.343$ $s_b = 0.040$ $F = 23.7$	$Y = 15.18 + 0.291X$ $X_0 = -52\ \mu g\ l^{-1}$ $s_a = 0.307$; $t_a = 49.44$ $s_b = 0.003$ $F = 0.2$	$Y = 0.303 + 0.045X$ $X_0 = -7\ \mu g\ l^{-1}$ $s_a = 0.136$; $t_a = 2.240$ $s_b = 0.001$ $F = 0.03$

[a] Estimated parameters of the straight line calculated by the least-squares method based on the pairs of calibration data from Table 1, for 95% confidence limits. In the absence of the systematic error the calibration straight line should pass through the origin. Symbols: ND = not determined; Y = voltammetric peak height in appropriate units (see Table 1); X = analytical concentration of metallothionein; s_a = standard deviation of the intercept on the ordinate; s_b = standard deviation of the slope; X_0 = intercept on the abscissa; t_a = Student's t-value of the estimated intercept on the ordinate, for $\alpha = 0.05$ (6) degrees of freedom; $F_{0.95}(6,1)$ degrees of freedom.

units of current (nA), whereas for the manual and computer-based evaluation procedure after deconvolution the signal is in units of length (mm) or arbitrary units, respectively. It is important that after deconvolution the proportionality between the peak heights is preserved.

In this study the height of the Cat_1 and Cat_2 signals was evaluated for unprocessed signals by the polarograph and by manual tangent fitting and for signals processed by FFT deconvolution and stored in the file by reading from zero (windowing) and as the difference between current at the peak potential and the baseline at the same potential.

Manual evaluation of the peak height was performed because in spite of possible instrumental and/or computer-based analysis, electrochemical results often depend on the visual judgement of the analyst.

The data sets were fitted to a straight line by the linear least-squares method. For each data processing procedure, the estimated parameters of the straight line with the respective standard errors [17] are presented in Tables 2 and 3. The standard deviation s_a refers to the intercept on the ordinate and concerns different units of measure. The calculated Student's t-value for s_a, i.e., t_a values, are dimensionless and were compared with the expected t value. The evaluation refers to the 95% confidence limits and six degrees of freedom. The intercept on the abscissa is also indicated. The intercepts X_0 along the abscissa

TABLE 3

Calibration straight line expressed as the dependence of voltammetric peak heights of Cat_1 and Cat_2 on metallothionein concentration [a]

Deconvoluted signals			
Windowing		Straight-line subtraction	
Cat_1	Cat_2	Cat_1	Cat_2
$Y = 9.838 + 0.602X$ $X_0 = -16\ \mu g\ l^{-1}$ $s_a = 3.835$; $t_a = 2.565$ $s_b = 0.040$ $F = 24.2$	ND	$Y = 1.468 + 0.160X$ $X_0 = -9\ \mu g\ l^{-1}$ $s_a = 0.365$; $t_a = 4.027$ $s_b = 0.0038$ $F = 0.2$	$Y = 0.110 + 0.018X$ $X_0 = -6\ \mu g\ l^{-1}$ $s_a = 0.030$; $t_a = 3.605$ $s_b = 0.0003$ $F = 0.002$

[a] Symbols as in Table 2.

are not compared statistically, because this method of calibration assumes that one variable, i.e., the signal height, is affected by the measurement error, due to the overlapping interference, while the deviation of the metallothionein concentration from the true value is negligible. Such an approach is justified by the fact that the parameters of the calibration straight lines, presented in Tables 2 and 3, were calculated based on one measurement step, differing only in the signal processing procedures. A high degree of correlation (0.949–0.999) exists between the response and the analytical concentration of metallothionein.

The signals after FFT deconvolution with straight-line subtraction and windowing [9] are presented in Figs. 1b and c, respectively. The side lobe of the Co^{2+} peak at -1.2 V (Fig. 1c) is the result of windowing and filtering and represents an artefact of the method. The amplitudes of the spectra of the deconvoluted signals had minima which do not attain zero in the region of cut-off frequencies. Therefore, for the range of possible widths of the deconvolution function, Gauss and Chebyshev, rather than boxcar, filters were used. The decision about the value of the cut-off frequency was taken after several attempts, in combination with n, the parameter determining the width of the deconvolution function. A three-dimensional representation of the overall reduction signals from Fig. 1a is presented in Fig. 2a, and the same representation of deconvoluted signals with straight-line subtraction is given in Fig. 2b. The considerable separation of the analyte peaks and the effect of deconvolution on signals of different broadness are well observed in Fig. 2b.

Catalytic wave Cat_1

In previous studies [14,16], the determination of the metallothionein was based exclusively on the peak-height determination of the catalytic wave Cat_2 (Fig. 1a). In the same range of metallothionein concentration the signal of Cat_1 cannot be resolved from the reduction peak of Co^{2+} without applying the deconvolution method. Therefore, until now the signal of Cat_1 was not

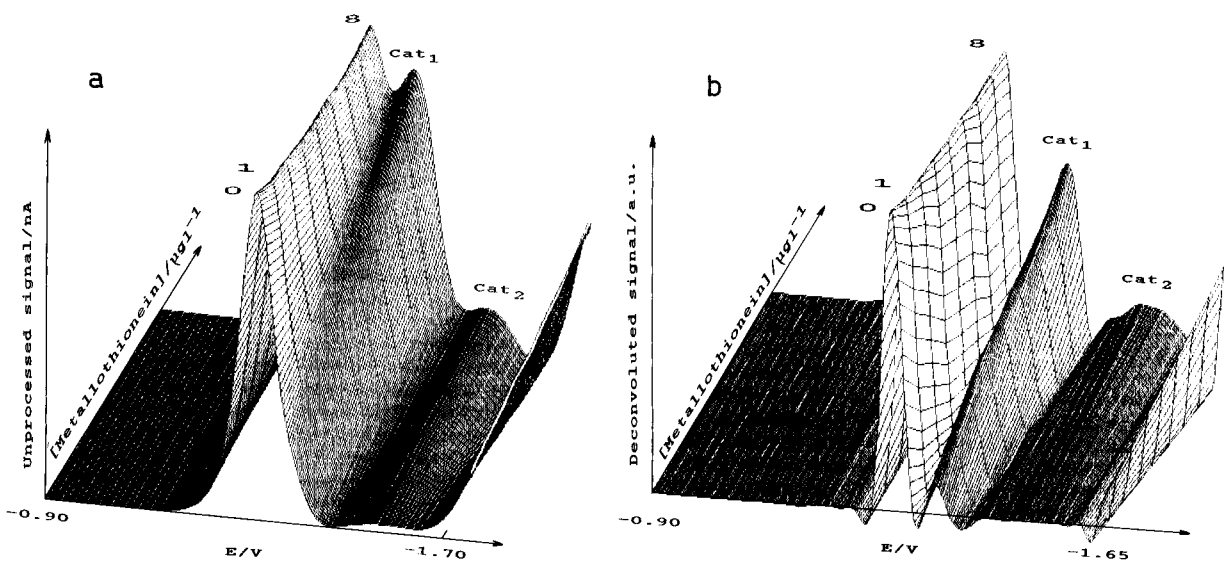

Fig. 2. (a) Three-dimensional representation of the overall signals from Fig. 1a related to the equal analytical concentrations of metallothionein on z-axis. The capture of curves 0–8 on the z-axis is the same as in Fig. 1a. In the potential range -0.90 to -1.70 V there are 401 points. (b) Three-dimensional representation of the FFT deconvolution method applied to the first 376 points of a total of 401 points of the experimental signal presented in (a). Curves 0–8 on the z-axis correspond to equal analytical concentrations of metallothionein as described in Fig. 1a. Parameters of deconvolution: $n = 1.2$; Chebyshev filter of 151st order; $w_g = 31/T_0$; $T_0 = 1.024$ V.

used for the evaluation of the concentration of metallothionein. The advantage of following Cat_1 instead of Cat_2 is that in the presence of the same concentration of metallothionein the slope of the calibration straight line and therefore the sensitivity of the analytical system for Cat_1 are nine times higher than for Cat_2 (compare the estimated slopes between the last two columns in Table 3).

Comparing the results of the different data processing methods in Table 1, it can be seen that the Cat_1 signal is not resolved by the polarograph until the amount of metallothionein is $\geqslant 152$ $\mu g\ l^{-1}$, because the polarograph cannot perform a tangent fit on a signal that does not have the form of the peak. The height of Cat_1 can be evaluated manually. The intercept on the abscissa of the calibration straight line deviates from zero and amounts to -52 $\mu g\ l^{-1}$. If the calibration is performed only up to 114 $\mu g\ l^{-1}$ metallothionein, i.e., in the concentration range where Cat_1 does not yet have the shape of the peak, the error can be even higher because the analyst cannot decide at which potential the signal height of Cat_1 should be read off. The peak potential of Cat_1 is well defined if the metallothionein concentration is > 114 $\mu g\ l^{-1}$ (curves 6–8, Fig. 1a).

After deconvolution with straight-line subtraction, the Cat_1 signal is well resolved (Fig. 1b). The lowest concentration of metallothionein, i.e., 19 $\mu g\ l^{-1}$, is identified as a separate peak of Cat_1 (compare curves 1 in Fig. 1a and b). The peak height of the separated Cat_1 signal is determined as the difference between the current at the peak potential, i.e., at -1.37 V, in the presence of metallothionein (Fig. 1b, curves 1–8) and the baseline at the same potential (Fig. 1b, curve 0). The intercept of the straight line with the abscissa amounts to -9 $\mu g\ l^{-1}$ (Table 3). Evaluation of the Cat_1 signal after deconvolution by windowing results in an intercept on the abscissa of -16 $\mu g\ l^{-1}$ (Table 3). The intercept of the calibration straight line with the abscissa is the smallest (-9 $\mu g\ l^{-1}$) if the signal height of Cat_1 is determined after FFT deconvolution with straight-line subtraction as the difference between the current at the peak potential and the baseline at the same potential. Comparing the different data processing procedures, it is obvious that after applying deconvolution with straight-line subtraction the systematic error of Cat_1 calibration line has been reduced but not completely removed. Establishing the significance of the estimated a in comparison with the expected value $a_0 = 0$, i.e., comparing t_a values for the Cat_1 response (Tables 2 and 3) with the expected $t_{0.05}(6)$ degrees of freedom = 2.447 [17,18], the hypothesis of a significant difference in the estimated intercept from the expected value cannot be rejected. For three different procedures for the determination of the calibration straight line, based on Cat_1 evaluation, the plot of the residuals for certain data sets indicated some trend in the dispersion of the data points. Therefore, we verified whether the linear regression is justified, i.e., whether the mean Y value for given X value lies on a straight line [19]. The F-values presented in Tables 2 and 3 for Cat_1 peak evaluation are lower than $F_{0.95}(6,1)$ degrees of freedom = 234 [19]. Therefore, the hypothesis of linearity is not disproved for the three different procedures of Cat_1 peak evaluation.

Catalytic wave Cat_2

From Table 1, it follows that the Cat_2 signal is determined by the polarograph applying the built-in procedure which cannot be tuned. The tangent drawn by the polarograph connects two closest minima. In the DPP mode, at a potential of ca. -1.60 V, with increasing metallothionein concentration the minimum becomes more pronounced (Fig. 1a). Consequently, the slope of the tangent changes. We assume that this is the reason for what seems to be a non-linear behaviour of the Cat_2 response, which also seems to indicate the plot of the residuals and the trend of dispersion of the points.

As shown in Table 1, the height of Cat_2 was evaluated by manual tangent fitting. The intercept with the abscissa of the calibration straight line deviates from zero and amounts to -7 $\mu g\ l^{-1}$ (Table 2). After deconvolution with straight-line subtraction, the Cat_2 signal (Fig. 1b) is determined as the difference between the current at the peak potential, i.e., at -1.52 V, in the presence of metallothionein (Fig. 1b, curves 1–8) and

the baseline at the same potential (Fig. 1b, curve 0). The intercept of the straight line with the abscissa amounts to $-6\ \mu g\ l^{-1}$ (Table 3). Evaluation of the Cat_2 peak height after deconvolution with windowing is not possible owing to signal suppression, while its position is closer to the edge of the strongly converging windowing function. Evaluation of the Cat_2 signal after deconvolution is not possible when windowing because the peak is diminished because it is smaller than the Cat_1 or Co^{2+} signals and it is located close to the range of the noise and out of the centre of the measuring curve. The intercept of the calibration straight line with the abscissa is very similar for an unprocessed signal (by manual tangent fitting) and a processed signal after deconvolution with straight-line subtraction (i.e., -7 and $-6\ \mu g\ l^{-1}$, respectively). The systematic error was significantly reduced only if the polarographic reading of the peak height of Cat_2 was replaced with the reading of the unprocessed signal by manual tangent fitting. Establishing the significance of the estimated a in comparison with the expected value $a_0 = 0$, i.e., comparing t_a values for the Cat_2 response (Tables 2 and 3) with the expected $t_{0.05}(6)$ degrees of freedom = 2.447 [17,18], only for manual tangent fitting of the Cat_2 peak height can the hypothesis of a significant difference be rejected. In order to prove the assumption of linearity, the F-values for Cat_2 calibration line from Tables 2 and 3 were compared with $F_{0.95}(6,1)$ degrees of freedom = 234 [19]. The hypothesis of linearity is not disproved for the three different procedures of Cat_2 peak-height evaluation.

Conclusions

The results for the comparative quantitative analysis of non-resolved and differently broad catalytic waves (Cat_1 and Cat_2) suggest particular improvements. In order to increase the accuracy of reading off the peak heights of Cat_1 and Cat_2, the signals were processed by FFT deconvolution. The deconvolution procedure enables one to establish the calibration straight line for the Cat_1 signal which is overlapped by the Co^{2+} reduction wave. The deconvolution function has to be equal to or less than the half-width of the narrowest signal. Therefore, the deconvolution procedure improves significantly the accuracy of reading off the height and the position of the Cat_1 signal, which is the narrower one. A particular advantage of the deconvolution procedure is the quantitative analysis of the completely overlapped signals and those to which tangent fitting by the polarograph is inappropriate.

According to the results, the recommended procedure for metallothionein determination should be based on processing the Cat_1 signal by FFT deconvolution with straight-line subtraction and not by windowing. For Cat_2 signal evaluation the recommended procedure is the manual tangent fitting of the unprocessed signal and not FFT deconvolution by straight-line subtraction and specifically not by windowing.

The deconvolution procedure can be easily accomplished owing to computer data storage and processing. It is recommended as a complementary software application to computer-based polarographic instrumentation.

The authors gratefully acknowledge financial support from the Ministry of Science of the Republic of Croatia and cooperation via Project JF 927 with the National Institute of Standards and Technology (USA). The Ministry of Science is acknowledged for the use of MATLAB software.

REFERENCES

1 A. Bobrowski, Chem. Anal. (Warsaw), 28 (1983) 557.
2 A. Bobrowski and I. Roterman, Chem. Anal. (Warsaw), 31 (1986) 167.
3 J. Wang, D.B. Luo and B. Freiha, Talanta, 33 (1986) 397.
4 A. Bobrowski and M. Walczak, Chem. Anal. (Warsaw), 29 (1984) 663.
5 A.M. Bond and B.S. Grabarić, Anal. Chem., 48 (1976) 1624.
6 W.F. Gutknecht and S.P. Perone, Anal. Chem., 42 (1970) 906.
7 P.A. Boudreau and S.P. Perone, Anal. Chem., 51 (1979) 811.
8 I. Pižeta, Anal. Chim. Acta, 285 (1994) 95.
9 I. Pižeta and B. Jeren, in preparation.
10 R. Brdička, Collect. Czech. Chem. Commun., 5 (1933) 112.
11 P.F. Kehr, PhD Thesis, Purdue University, West Lafayette, IN, 1973.

12 I. Pižeta and M. Branica, J. Electroanal. Chem., 250 (1988) 293.
13 R.W. Olafson and R.G. Sim, Anal. Biochem., 100 (1979) 343.
14 B. Raspor, J. Pavičić and M. Branica, Fresenius, Z. Anal. Chem., 326 (1987) 719.
15 O.H. Müller, in D. Glick (Ed.), Methods in Biochemical Analysis, Interscience, New York, Vol. 11, 1975, p. 329.
16 B. Raspor and J. Pavičić, Chem. Spec. Bioavail., 3 (1991) 39.
17 C. Litenau and I. Rîcă, Statistical Theory and Methodology of Trace Analysis, Horwood, Chichester, 1980.
18 J.K. Taylor, Quality Assurance of Chemical Measurements, Lewis, Chelsea, MI, 1987, pp. 95–106.
19 M.G. Natrella, Experimental Statistics, National Bureau of Standards Handbook 91, US Government Printing Office, Washington, DC, 1966, pp. 5–23.

Analytica Chimica Acta, 285 (1994) 113–123
Elsevier Science B.V., Amsterdam

Tuning colourimetric and fluorimetric gas sensors for carbon dioxide

Andrew Mills and Qing Chang

Department of Chemistry, University College of Swansea, Singleton Park, Swansea SA2 8PP (UK)

(Received 17th May 1993; revised manuscript received 23rd August 1993)

Abstract

The basic theory behind conventional colourimetric and fluorimetric optical sensors for CO_2 is examined and special attention is given to the effect on sensor response of the key parameters of initial base concentration and dye acid dissociation constant, K_D. Experimental results obtained in aqueous solution using a variety of different dyes and initial base concentrations are consistent with the predictions made by the theoretical model. A series of model-generated pK_D versus $\%CO_2$ curves for different initial base concentrations allow those interested in constructing an optical CO_2 sensor to readily identify the optimum dye/initial base combination for their sensor; the response of the sensor can be subsequently fine-tuned through a minor variation in the initial base concentration. The model and all its predictions appear also to apply to the new generation of plastic film CO_2 sensors which have just been developed.

Keywords: Colourimetry; Fluorimetry; Sensors; Carbon dioxide

There is a growing body of interest in colourimetric and fluorimetric sensors of analytes of physiological significance, such as pH, CO_2 and O_2. Such sensors are attractive in that they are usually cheap to make and, via fibre optics, open to exploitation as remote sensors. These two features offer the possibility of the development of a new and flexible range of disposable sensors, capable of multiple analyses for in vivo and in vitro clinical analysis work [1].

Almost all the colourimetric and fluorimetric CO_2 gas sensors developed todate [1–12] rely upon the pH changes induced in an aqueous solution upon its exposure to different levels of CO_2 and utilise a pH-sensitive dye, D^-, to provide a qualitative and/or quantitative measure of the extent of the change in pH and, therefore, the change in $\%CO_2$; the major reactions involved are summarised in Table 1 along with their associated equilibrium constants at infinite dilution [13]. Not only must a pH sensitive dye be present in the CO_2 sensing element of the sensor, but also the pH of the aqueous solution must be adjusted with a base, such as NaOH or $NaHCO_3$, so that some, if not all, of the dye is initially in its deprotonated form, D^-.

Although most colourimetric and fluorimetric sensors for CO_2 have been developed on the above principles, it appears that often an empirical approach is adopted for selecting key parameters, such as: type of dye and initial base concentration, in the formulation of a CO_2 optical sensor with the optimum required response [1–12]. Although this approach has proved effective in the past it is probably not the most efficient, given that the theory behind the working of such sensors is reasonably well-established [14], and values of the relevant constants are known [13].

Correspondence to: A. Mills, Department of Chemistry, University College of Swansea, Singleton Park, Swansea SA2 8PP (UK).

SSDI 0003-2670(93)E0506-3

TABLE 1

Key reactions for most colourimetric CO_2 gas sensors [a]

Reaction	Equilibrium constant
(I) $CO_2(g) \overset{K_H}{\rightleftharpoons} CO_2(aq)$	$K_H = [CO_2(aq)]/P_{CO_2} = 3.4 \times 10^{-2}$ mol dm^{-3} atm^{-1}
(II) $CO_2(aq) + H_2O \overset{K_{a1}}{\rightleftharpoons} H^+ + HCO_3^-$	$K_{a1} = [HCO_3^-][H^+]/[CO_2(aq)] = 4.47 \times 10^{-7}$ mol dm^{-3}
(III) $HCO_3^- \overset{K_{a2}}{\rightleftharpoons} H^+ + CO_3^{2-}$	$K_{a2} = [CO_3^{2-}][H^+]/[HCO_3^-] = 4.68 \times 10^{-11}$ mol dm^{-3}
(IV) $D^- + H^+ \overset{K^*}{\rightleftharpoons} DH$ (colour A) (colour B)	$(K^*)^{-1} = K_D = [D^-][H^+]/[DH]$

[a] K_D is the acid dissociation constant of the pH indicating dye.

Thus, it should be possible to predict theoretically the best formulation for a conventional colourimetric or fluorimetric optical sensor of CO_2 with an optimal response around the $\%CO_2$ value of interest.

In this paper we investigate the basic theory behind colourimetric and fluorimetric optical sensors for CO_2 and identify and quantify the crucial factors of initial base concentration and dye acid dissociation constant, pK_D which define the sensitivity of a colourimetric or fluorimetric CO_2 sensor. This theory is then tested using dyes in aqueous solution and in thin plastic films.

EXPERIMENTAL

Materials

Unless stated otherwise all materials were obtained from Aldrich in the highest purity available. A list of the dyes used, their abbreviations, values of λ(max) and molar absorptivity of their deprotonated and protonated forms and measured acid dissociation contants (K_D) is given in Table 2 [15–19]. The water used to make up solutions was doubly distilled and deionised. The air, N_2 and CO_2 used were of a high purity (> 99%) and obtained from BOC. N_2/CO_2 gas

TABLE 2

Characterisation details of the dyes used

Dye	Abbreviation	D^- λ_{max}/nm [$\epsilon(\lambda_{max})$ /dm^3 mol^{-1} cm^{-1}]	DH λ_{max}/nm [$\epsilon(\lambda_{max})$ /dm^3 mol^{-1} cm^{-1}]	pK_D [a]
Phenolphthalein	PP	544 (2.9×10^4)	colourless	9.46 (9.6) [15]
o-Cresolphthalein	OCP	562 (3.7×10^4)	colourless	9.32 (9.4) [16]
Thymol blue	TB	590 (5.3×10^4)	432 (2.9×10^4)	8.86 (9.0) [17]
Cresol red	CR	563 (5.0×10^4)	426 (2.4×10^4)	7.95 (8.3) [16]
m-Cresol purple	MCP	571 (4.0×10^4)	428 (2.0×10^4)	8.28 (8.3) [18]
8-Hydroxy-1,3-pyrene-tris-sulphonic acid	HPTS	455	403	– (8.1) [19] [b]
Phenol red	PR	540 (3.9×10^4)	422 (2.7×10^4)	7.52 (7.9) [16]
Rosilic acid	RA	520 (5.4×10^4)	468 (3.7×10^3)	7.40 (–)

[a] Measured in this work by monitoring the change in the absorbance of D^- at its λ(max) as a function of pH. The pK_D data in parenthesis are literature values. [b] In distilled H_2O; $pK_D^* = 7.3$ at usual buffer concentrations.

mixtures of different specified compositions, spanning the range 0–10% CO_2, were generated using a gas blender (Signal Instruments, Model 852V1-B).

Methods

UV–visible spectra and single wavelength absorbance measurements were carried out using either a double-beam scanning spectrophotometer (Perkin Elmer, Model Lambda 3) or a single-beam scanning spectrophotometer (Phillips, Model PU8620). The aqueous solution colourimetric CO_2 sensors typically comprised 5×10^{-5} mol dm^{-3} dye under test, added in its protonated form, and 10^{-2} mol dm^{-3} NaOH.

The thin plastic film colourimetric sensors for CO_2 used in this work had the general composition: indicator dye/tetraoctyl ammonium hydroxide (a phase transfer agent used to solubilise the dye in the plastic film)/ ethylcellulose (a polymer)/ tributylphosphate (a plasticiser)/ glass slide. Component solution (I) was typically prepared by adding 0.012 g of the dye under test to 1 cm^3 of a 0.5 mol dm^{-3} tetraoctylammonium hydroxide methanolic solution and a further 2.5 cm^3 of methanol was then added to provide a final dye concentration which was appropriate for making absorbance measurements. The second component solution, i.e. solution (II), was prepared by dissolving 10 g of ethyl cellulose into a solution comprising 20 cm^3 of ethanol and 80 cm^3 of toluene. The final solution used to produce the plasticised *m*-cresol purple film was made up of 1 cm^3 of solution (I), 10 g of solution (II), 1 cm^3 of tributyl phosphate and 1 cm^3 of the 0.5 mol dm^{-3} tetraoctylammonium hydroxide methanolic solution.

The dry, thin plastic film colourimetric sensor for CO_2 containing the dye under test was generated using the final film solution and casting it through a 100 μm thick brass sheet with a rectangular hole (0.5×1 cm) onto a glass microscope slide; the thickness of the dried film was typically 20 μm.

The plastic film sensors had the general formulation: dye/tetraoctyl ammonium hydroxide/ ethyl cellulose/ tributyl phosphate and were supported on individual small glass microscope slides; the method of preparation of these films has been described elsewhere [7].

The variation in absorbance due to the deprotonated form of the dye as a function of $\%CO_2$ in the gas phase was tested for each aqueous solution and plastic film colourimetric CO_2 sensor. In this work, 4 cm^3 of the aqueous solution colourimetric sensor under test were placed in a quartz cuvette. The solution was then saturated with gases of different CO_2 composition, delivered from the gas blender to the solution via a hypodermic needle dipped into the solution; a similar system of gas delivery was used for the plastic film colourimetric CO_2 sensors. The latter sensors were fixed in an otherwise empty plastic cuvette so that the spectrophotometer's beam passed directly through the film. Unless stated otherwise all single wavelength absorbance measurements were made at λ(max) of the deprotonated form of the dye under test.

THEORY

The classic work of Severinghaus and Bradley [14] which provided one of the first characterisation studies of the CO_2 electrode, also enunciated the theoretical relationship between the pH of an aqueous solution and the partial pressure of CO_2, $\%CO_2$, in the saturating gas in the absence and presence of an initial concentration of base, usually $NaHCO_3$. The key working equation obtained by these workers was as follows:

$$\%CO_2 = \frac{100\{[H^+]^3 + [H^+]^2[Na^+] - K_w[H^+]\}}{K_{a1}K_H\{[H^+] + 2K_{a2}\}} \quad (1)$$

The CO_2 electrode comprises a pH electrode in contact with a thin layer of aqueous solution containing sodium bicarbonate with the whole system encapsulated by a thin, gas-permeable membrane, such as silastic. Most colourimetric or fluorimetric CO_2 gas sensors have some similar design features with respect to the CO_2 electrode, although with the former, (i) a pH-sensitive dye is encapsulated, either in the thin aqueous solution or, fixed on an inert support (such as

polyacrylamide or activated alumina), and (ii) the pH electrode is usually replaced with a fibre optic system for deliverying and returning the essential light component of the sensor.

The above devices are popularly referred to as CO_2 optodes and dominate the present literature on CO_2 optical sensors. However, there are other, much less sophisticated, optical sensors for CO_2, including the Einstein CO_2 detector [20], which is a device used to ensure the correct placement of an endotracheal tube and which relies on the change in colour in an aqueous solution containing phenolphthalein and cresol red when expired air (typical CO_2 content: 4–6%) is passed through it. A list of most of the CO_2 sensors reported in the literature is given in Table 3.

If the initial concentration of the protonated dye in the aqueous solution is $[HD]_0$, it can be shown that the relationship between $\%CO_2$ and solution pH is given by the following expression:

$$\%CO_2 = \left(100\{[H^+]^3 + [H^+]^2[Na^+] - K_w[H^+] - [H^+]^2 K_D[HD]_0/([H^+] + K_D)\}\right) \times \left(K_{a1}K_H\{[H^+] + 2K_{a2}\}\right)^{-1} \quad (2)$$

where K_D is the acid dissociation contant for the dye.

In most colourimetric and fluorimetric CO_2 gas sensors the dye concentration/content is usually low, i.e., typically $< 10^{-4}$ mol dm^{-3}. For colourimetric sensors, the molar absorptivity of the deprotonated form of the dye, is usually sufficiently large (i.e., $> 10^4$ dm^3 mol^{-1} cm^{-1}) so as to ensure that the absorbance changes due to changes in the relative concentrations of HD and

TABLE 3

Established colourimetric and fluorimetric CO_2 sensors

Dye [a]	Sensor type [b]	Dye support	Medium [c]	Gas-permeable membrane	Ref.
PR	Col	none	water	silicone rubber	2
PR + PP	Col	none	water	none	3
PR, TB	Col	none	water	silicone rubber	4
TB	Col	activated alumina	water	none	5
PR, CR or TB	Col	polyacrylamide or polyethyleneoxide	water	silicone rubber of PTFE	6
MCP or CR	Col	–	ethyl cellulose	ethyl cellulose	7
HPTS	Fl	cellulose granules	water	silicone rubber	8
Fluorescein	Fl	copolymerised with acrylamide or hydroxyethyl methacrylate	water	DMS–BPAC block copolymer	9
HPTS	Fl	acrylamide	water	DMS–BPAC block copolymer	9
Fluorescein	Fl	none	polyethylene glycol	polyethylene glycol	10
Ru(II) complex	Fl	carboxymethyl Sephadex	water	silicone rubber	11
HPTS	Fl	none	ethyl cellulose	ethyl cellulose	12

[a] Abbreviations as in Table 1. [b] Type of sensor: colourimetric (Col) or fluorimetric (Fl). [c] Usually containing bicarbonate (10–20 μmol dm^{-3}).

D^-, due in turn to changes in $\%CO_2$, are measurable.

Using Eqn. 2 and the constants in Table 1 it can be shown that for any dye with a pK_D value which lies in the range 7.5–10, if $[HD]_0 < 5 \times 10^{-5}$ mol dm^{-3}, then the extra term in Eqn. 2 compared with Eqn. 1, i.e., $[H^+]^2K_D[HD]_0/([H^+] + K_D)$, is negligible (< 10%) compared with the other terms, i.e. $100\{[H^+]^3 + [H^+]^2[Na^+] - K_w[H^+]$, over the $\%CO_2$ range 0.1% to 100% CO_2. As a consequence, under most conditions under which CO_2 optodes are operated, especially in the monitoring of physiological significant levels of CO_2 (i.e., 0.1–10% CO_2), the variation in solution pH with $\%CO_2$ is adequately described by Eqn. 1, as is often assumed.

Using Eqn. 1, we have calculated the variations in pH with $\log(\%CO_2)$ for a variety of different initial base concentrations. spanning the range 0–1 mol dm^{-3}, and the results of this work are illustrated in Fig. 1a and will apply even when a pH-indicating dye is present, provided its concentration is $< 10^{-4}$ mol dm^{-3} and its pK_D lies in the range 7.5–10. In these calculations. the variations of the constants: K_{a1}, K_{a2}, K_H and K_w as a function of ionic strength have been taken into account by using known values [13] for these constants at different ionic strengths. The gradient, m, of each one of these pH versus $\log(\%CO_2)$ plots was determined over the full $\%CO_2$ range: 10^{-3}–100% CO_2 and the narrower, physiologically more significant, $\%CO_2$ range 0.1–10% CO_2 and the plots of m versus $\%CO_2$ are illustrated in Fig. 1b. From the results of this work it can be seen that at initial base concentrations $\ll 10^{-6}$ mol dm^{-3}, $m = 0.5$ and, therefore, $\%CO_2$ is proportional to $[H^+]^2$. This relationship arises because under the conditions of little or no base Eqn. 1 approximates to:

$$\%CO_2 = \frac{100[H^+]^2}{K_{a1}K_H} \quad (3)$$

From the data illustrated in Fig. 1b it can also be seen that at base concentrations $> 10^{-4}$ mol dm^{-3}, $m \simeq 1$, i.e., $\%CO_2$ is proportional to $[H^+]$, especially over the narrower $\%CO_2$ range 0.1–10% CO_2. This relationship arises because under the conditions of a moderate to high concentration of base Eqn. 2 approximates to:

$$\%CO_2 = \frac{100[H^+][Na^+]}{K_{a1}K_H} \quad (4)$$

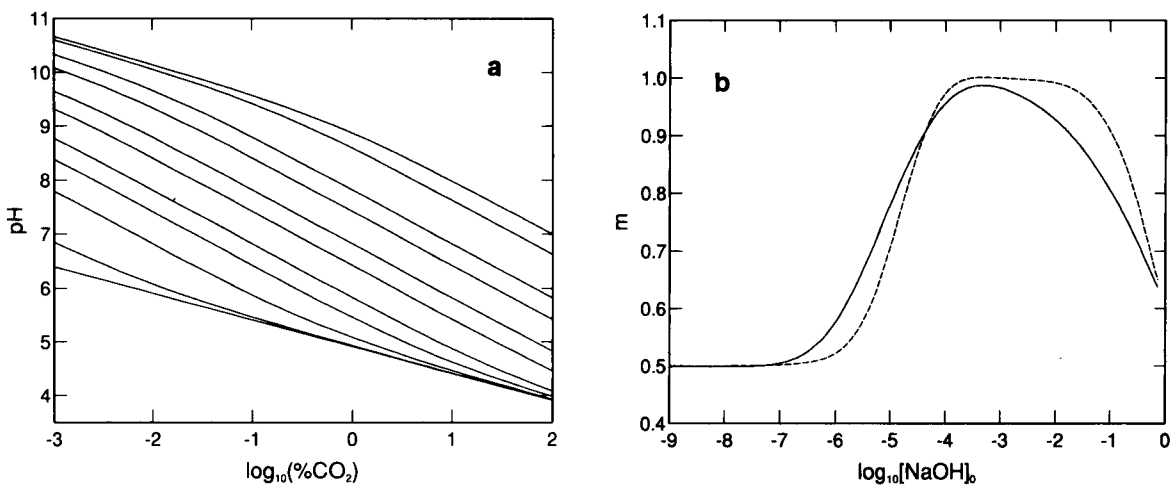

Fig. 1. (a) Variations in pH in aqueous solution, calculated using Eqn. 1 of the model and literature values for the different constants, versus $\log(\%CO_2)$ of the saturating gas (total gas pressure always 1 atm) for solutions with the following initial base (NaOH) concentrations (from top to bottom): 0.3, 0.1, 1×10^{-2}, 4×10^{-3}, 10^{-3}, 4×10^{-4}, 10^{-4}, 4×10^{-5}, 10^{-5}, 10^{-6} and 10^{-9} mol dm^{-3}. (b) Plot of the gradient, m, of each of the lines illustrated in (a) as a function of $\log(\%CO_2)$. The solid and broken lines correspond to evaluation of m using data over the $\log(\%CO_2)$ ranges: (−3 to 2) and (−1 to 1), respectively.

Under the conditions in which Eqn. 4 applies it follows that for a colourimetric CO_2 sensor the measured absorbance (due to the deprotonated form of the dye), $Abs(D^-)$, is related to $\%CO_2$ via the expression:

$$\%CO_2 = \frac{100K_D\{Abs(D^-)_0 - Abs(D^-)\}[Na^+]}{Abs(D^-)K_{a1}K_H} \quad (5)$$

where $Abs(D^-)_0$ is the absorbance of the dye in the sensor in the absence of CO_2. In addition, under the conditions in which Eqn. 4 applies it follows that for a fluorimetric CO_2 sensor the measured intensity of fluorescence (due to the deprotonated form of the dye), $I_f(D^-)$, is related to $\%CO_2$ via the expression:

$$\%CO_2 = \frac{100K_D\{I_f(D^-)_0 - I_f(D^-)\}[Na^+]}{I_f(D^-)K_{a1}K_H} \quad (6)$$

where $I_f(D^-)_0$ is the fluorescence intensity of the dye in the sensor in the absence of CO_2. Most of the CO_2 optodes reported todate have established and utilise the model-predicted simple relationship between $\%CO_2$ and $Abs(D^-)$, or $I_f(D^-)$, described by Eqn. 5, or Eqn. 6 [2–12]. From the above theory, it can be seen that in such cases the initial base concentration must necessarily have been moderate to high, i.e., 10^{-4}–1 mol dm^{-3}.

USING THE MODEL

From the above theory, under conditions of low dye concentration and moderate to high base concentration, a quantitative measure of any level of $\%CO_2$, falling in the range 10^{-3} to 100% CO_2, can be readily obtained using any a colourimetric or fluorimetric CO_2 sensor. In practice, however, a particular dye will only be effective as a CO_2 sensor over a specific, narrow range of $\%CO_2$, the value of which is determined by the acid dissociation constant of the dye, vide infra. The major limitation on the effective response range of these type of sensors arises from the combination of their hyperbolic-type response and the inevitable %error associated with making any absorbance of fluorescence intensity measurements.

We can obtain some idea of the effective working range of a conventional CO_2 optode by considering Eqns. 5 and 6, both of which are of the form:

$$\%CO_2 \propto (1-S)/S \quad (7)$$

where S = the normalised optical signal, i.e., $Abs(D^-)/Abs(D^-)_0$, or $I_f(D^-)/I_f(D^-)_0$. With optodes it is customary practice to illustrate the effective response range of the sensor as a function of $\%CO_2$ by plotting: $Abs(D^-)/Abs(D^-)_0$, or $I_f(D^-)/I_f(D^-)_0$, versus $\%CO_2$, i.e., S versus $\%CO_2$. As we have seen from theory, i.e., Eqns. 5 or 6, ideally, such plots will have a hyperbolic form, starting at a value of $S = 1$ (at $\%CO_2 = 0$) and decreasing with increasing $\%CO_2$, with S tending to 0 as the $\%CO_2$ tends to ∞. If we now assume that for each measurement of S there is a small constant error, i.e., $S \pm f$, it can be shown that the corresponding average fractional error in $\%CO_2$, i.e., $\Delta\%CO_2/\%CO_2$, that this systematic error produces is given by the expression:

$$\frac{\Delta\%CO_2}{\%CO_2} = \frac{f}{(S+f)(S-f)} \cdot \frac{S}{(1-S)} \quad (8)$$

A plot of $\Delta\%CO_2/\%CO_2$ versus S for values of f of 0.01, 0.005 and 0.001, is illustrated in Fig. 2 and shows that even for a quite small constant error in the measurement of S, i.e., $f = 0.001$, the corresponding error in $\%CO_2$ rapidly becomes significant with decreasing S values below 0.05 and increasing S values above 0.95. From the results illustrated in Fig. 2 it can be seen that for many CO_2 optodes the effective operating range of the sensor would usually be considered to span the range $0.95 \geqslant S \geqslant 0.05$. A useful and quick measure of the $\%CO_2$ level at which the optode's response is optimal is provided by the value of the $\%CO_2$, which we will call $\%CO_2(S = 1/2)$, at which the normalised optical signal, S, is equal to 1/2, i.e., the point at which the concentrations of the protonated and deprotonated forms of the dye are the same.

Figure 3a illustrates the variation in log $\{\%CO_2(S = 1/2)\}$ as a function of the pK_D of the dye (solid line), predicted by Eqn. 2 of the

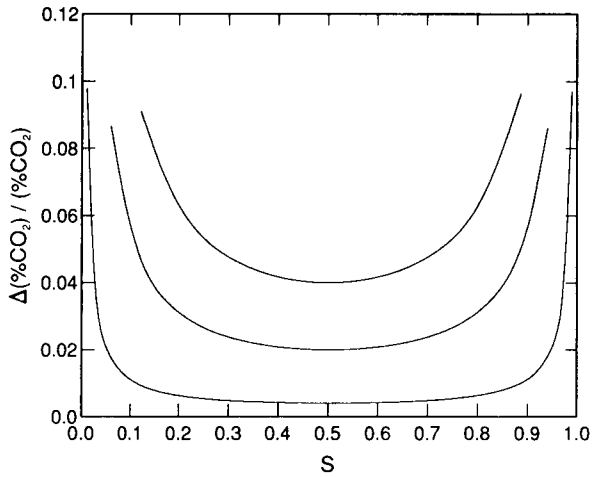

Fig. 2. Plot of the relative fractional error in $\%CO_2$, i.e., $\Delta\%CO_2/\%CO_2$, versus normalised optical sensor signal, S, calculated using Eqn. 8, for the following different constant values of error in S, i.e., values of f (from top to bottom): 0.01, 0.005 and 0.001.

model for a sensor in which $[HD]_0 \leqslant 1 \times 10^{-4}$ mol dm^{-3} and $[NaOH]_0 = 10^{-2}$ mol dm^{-3}. In addition, in Fig. 3a are illustrated data points which show the experimentally determined values of $\log\{\%CO_2(S = 1/2)\}$ and associated pK_D values for the series of dyes listed in Table 2. From the results of this work there appears to be a reasonable agreement between the theoretical and experimental determined data.

Figure 3b illustrates the model predicted variations in $\log\{\%CO_2(S = 1/2)\}$ as a function of the pK_D for initial base concentrations which span the range 10^{-4} to 1 mol dm^{-3}. As can be seen in Fig. 3a, knowledge of these curves will allow workers who wish to construct a colourimetric or fluorimetric CO_2 sensor with a required optimal response at some defined $\%CO_2(S = 1/2)$ value, to select the correct combination of dye, with its particular pK_D, and initial base concentration so that the sensor is sensitive in the required $\%CO_2$ range and gives a response which readily quantified over the operating range $0.95 \geqslant S \geqslant 0.05$, using Eqn. 5 or 6, respectively.

For example, from the data in Fig. 3a and b it would appear from the theoretical curves that an aqueous solution containing the combination of a colourimetric dye *m*-cresol purple (MCP) and 10^{-2} mol dm^{-3} NaOH is well suited to provide a-measure of $\%CO_2$ levels about a $\%CO_2(S = 1/2)$ level of 0.3%, and would be reasonably effective as a CO_2 sensor over the signal range

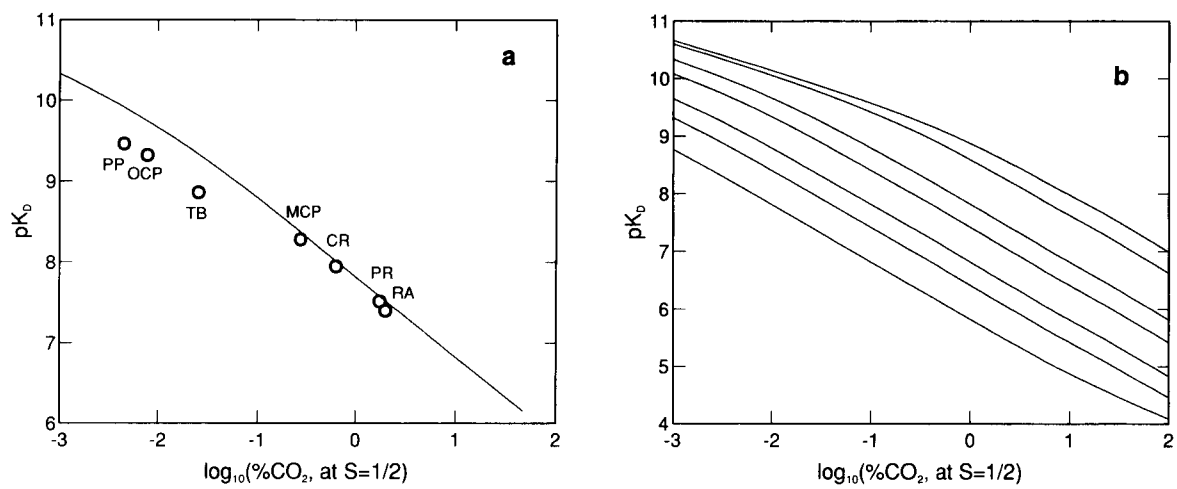

Fig. 3. (a) Plot of pK_D versus $\log\{\%CO_2(S = 1/2)\}$ for an aqueous solution containing $< 10^{-4}$ mol dm^{-3} of dye and an initial base concentration = 0.01 mol dm^{-3}; the data used to construct the solid line were calculated using Eqn. 2 of the model; the data points refer to the results determined in actual experiments (abbreviations used to identify the different dyes are as in Table 2). (b) Plot of pK_D versus $\log\{\%CO_2(S = 1/2)\}$ for an aqueous solution containing $< 10^{-4}$ mol dm^{-3} of dye and the following initial base concentrations (from top to bottom): 0.3, 0.1, 1×10^{-2}, 4×10^{-3}, 10^{-3}, 4×10^{-4} and 10^{-4} mol dm^{-3}.

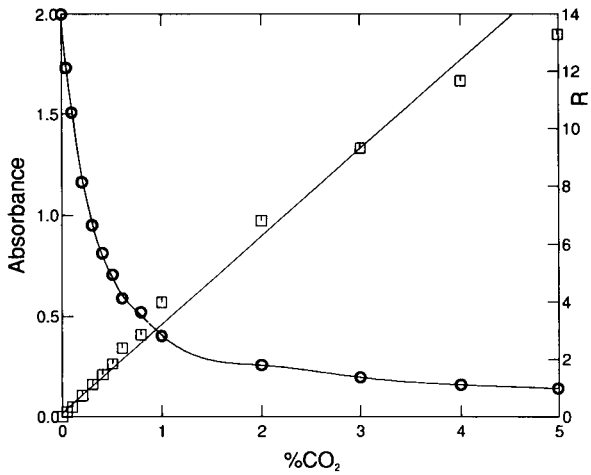

Fig. 4. Plot of the measured absorbance due to the deprotonated form of the dye at its λ(max), i.e., Abs(D^-), and plot of calculated values for R [= {Abs(D^-)$_0$ − Abs(D^-)}/Abs(D^-)], versus %CO_2 for an aqueous solution containing 5×10^{-5} mol dm^{-3} MCP and 0.01 mol dm^{-3} NaOH.

$0.95 \geqslant S \geqslant 0.05$, which corresponds to a %CO_2 range of $0.053 \times$ %$CO_2(S = 1/2) \leqslant$ %$CO_2 \leqslant 19 \times$ %$CO_2(S = 1/2)$, i.e., in this case $0.015\% \leqslant$ %$CO_2 \leqslant 5.7\%$, since S is related to %CO_2 via Eqn. 7, with %$CO_2(S = 1/2)$ as the proportionality constant.

In order to test the above prediction a series of experiments were carried out in which an aqueous solution containing MCP and 10^{-2} mol dm^{-3} NaOH were purged with N_2–CO_2 gas mixtures of different composition and the variation in Abs(D^-) as a function of %CO_2 recorded. The results of this work are illustrated in Fig. 4 along with the plot of the data in the form of $R = \{= (1 - S)/S\}$ versus %CO_2, which gives a good straight line as predicted by Eqn. 5 of the theoretical model. The results of this work confirm the model prediction that this system would be ideally suited as a CO_2 sensor of %CO_2 levels about a value of 0.3% CO_2, although the actual effective response range of the sensor, ca. $0.03\% \leqslant$ %$CO_2 \leqslant 3\%$ is less than expected, indicating that the systematic error, f, in the measurement of S may be slightly larger than the value of 0.001, assumed.

From the data points in Fig. 3a, it appears that of all the dyes tested in 0.01 mol dm^{-3} NaOH, phenol red and rosilic acid would be most suitable to use in a CO_2 optode designed for monitoring CO_2 levels of physiological significance; it is no surprise, therefore, that at least one of these dyes, phenol red, is a common feature of the CO_2 optodes listed in Table 3.

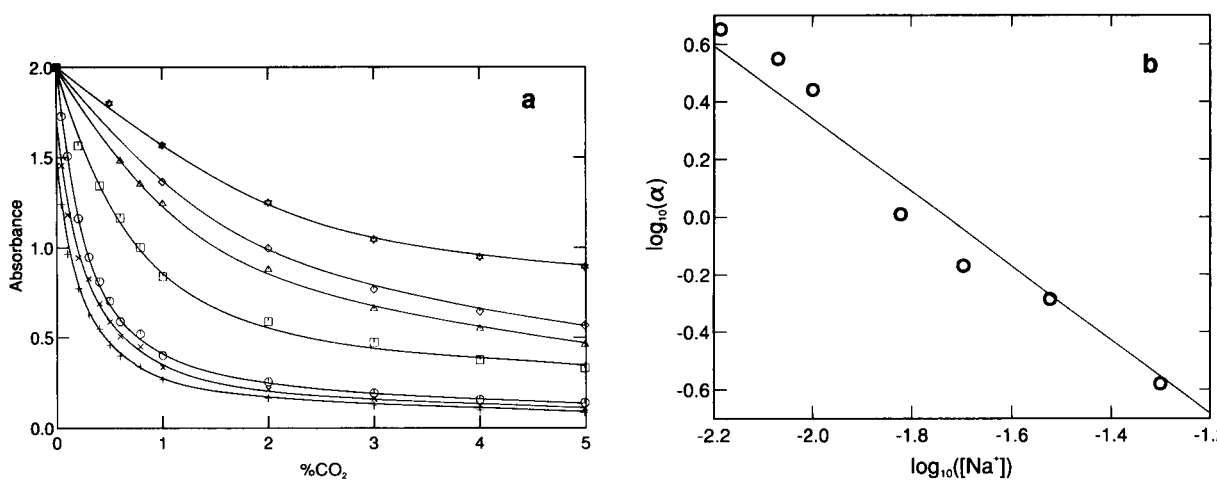

Fig. 5. (a) Plot of Abs(D^-) versus %CO_2 for an aqueous solution containing 5×10^{-5} mol dm^{-3} MCP and the following initial base concentrations (from top to bottom): 5×10^{-2}, 3×10^{-2}, 2×10^{-2}, 1.5×10^{-2}, 10^{-2}, 8.5×10^{-3} and 6.5×10^{-3} mol dm^{-3}. (b) Plot of log α, the gradient of the R versus %CO_2 plot for each the different curves in (a), versus log[Na^+]. The results of a least squares analysis of this data are as follows: number of points = 7, gradient = -1.46 ± 0.11, intercept = -2.54 ± 0.99.

From Eqn. 5, the gradient, α, of the R versus $\%CO_2$ plot illustrated in Fig. 4 should be equal to $1/\%CO_2(S = 1/2) = K_{a1}K_H/K_D[Na^+]$. Thus, if the initial base concentration was varied but the dye type and concentration kept the same, a plot of log α versus log[Na^+] should be a good straight line with a gradient $= -1$. In a second set of experiments, the observed variation in Abs(D^-) as a function of $\%CO_2$ for different initial NaOH concentrations, spanning the range 5×10^{-2} mol dm^{-3} to 6.5×10^{-3} mol dm^{-3}, was studied using MCP (5×10^{-5} mol dm^{-3}) and the results of this work are illustrated in Fig. 5a. From the plot of this data in the form of R versus $\%CO_2$ a different value for α was obtained for each of the initial base concentrations tried used. The subsequent plot of log α versus log [Na^+] is illustrated in Fig. 5b and is a good straight line as predicted from theory, although the gradient, -1.46 ± 0.11, is more negative than predicted, for reasons which remain unclear at the moment.

The theoretical curves illustrated in Fig. 3b provide a good starting place for the choice of dye and initial base concentration for a CO_2 optical sensor with an optimal response at certain defined level of CO_2. When considering the construction of such a CO_2 optode, we can identify the choice of the dye with its associated pK_D and the initial base concentration, through the use of the theoretical curves illustrated in Fig. 3, as a form of coarse theoretical tuning of the sensor. Once the sensor is constructed, from the data in Fig. 5 it appears that some fine adjustment in its sensitivity can achieved through a slight variation in the initially chosen base concentration.

COLOURIMETRIC AND FLUORIMETRIC PLASTIC FILM CO_2 SENSORS

Although in aqueous solution the values of the equilibrium constants associated with the key reactions listed in Table 1 are well established, this is not the case where the medium is largely non-aqueous, as for some of the colourimetric and fluorimetric sensors listed in Table 3. As an example of the latter type of sensor, we have recently developed a range of water-insoluble plastic film colourimetric and fluorimetric sensors with the basic composition dye/phase transfer agent/polymer/plasticiser/support in which the overall medium is hydrophobic and water, a prerequisite of any CO_2 optical sensor which utilises the reaction equations in Table 1, is incorporated into the film through the phase transfer agent.

It is generally accepted that when a phase transfer agent is used to extract an an ion from a polar medium, such as water, into one which is less polar, such as ethyl cellulose, a small number of molecules of water of solvation accompany the ion pair. Thus, in our work, the quaternary ammonium cation, Q^+, of the phased transfer agent, Q^+OH^-, has the dual function of solubilising the hydrophilic anion of the dye, i.e., D^-, in the plastic film, by forming an ion pair, and providing the water for CO_2 to interact with; the tetraoctylammonium cation–dye ion-pair in the film is best formulated as: $\{Q^+D^- \cdot xH_2O\}$. The lipophilic base, $\{Q + OH^- \cdot xH_2O\}$, is in vast excess compare with the dye and this excess maintains the dye in its deprotonated form, as Q^+ slowly degrades with time [7].

If, under these largely non-aqueous conditions, the key equilibrium reactions are still effectively similar to those listed in Table 1, then, given the apparent high concentration of initial base used in the films, i.e., $[Q^+OH^- \cdot xH_2O] \simeq 0.3$ mol dm^{-3}, it appears reasonable to suppose that there might exit for the optical films the same hyperbolic relationship between $\%CO_2$ and Abs(D^-), or $I_f(D^-)$, as predicted by Eqn. 5, or Eqn. 6, respectively, for aqueous solution. And, indeed, previous work on these plastic film sensors has established the existence of a hyperbolic relationship between $\%CO_2$ and Abs(D^-), or $I_f(D^-)$, as predicted by Eqn. 5, or Eqn. 6.

In order to test further the extent of the parallel behaviour of the CO_2 film sensors, compared to the aqueous solution CO_2 sensors, a number of mainly colourimetric, plastic CO_2 optical film sensors, containing different dyes (with different pK_D values), were prepared and their individual response curves as a function of different $\%CO_2$ levels determined. From the results of this work it was possible to determine the value of $\%CO_2(S$

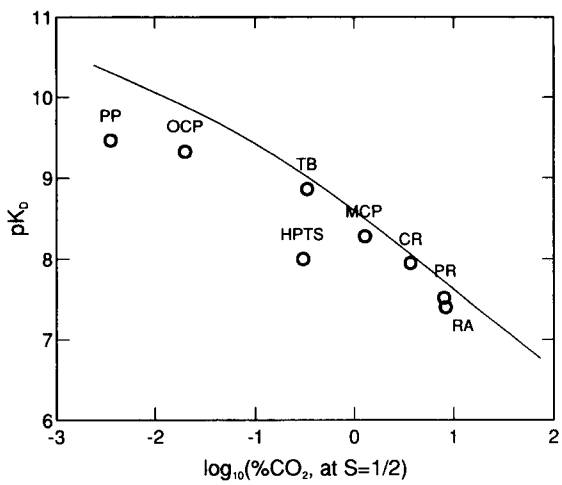

Fig. 6. Plot of pK_D (in aqueous solution) versus $\log\{\%CO_2(S = 1/2)\}$ for an aqueous solution containing $< 10^{-4}$ mol dm^{-3} of dye and an initial base concentration = 0.1 mol dm^{-3}; the data used to construct the solid line were calculated using Eqn. 2 of the model; the data points, however, refer to results determined in actual experiments on plastic films CO_2 sensors which differed only in that they utilised different dyes (abbreviations used to identify the different dyes are as in Table 2).

$= 1/2)$ for each film and the subsequent plot of this data in the form of pK_D (in aqueous solution) versus $\log\{\%CO_2(S = 1/2)\}$ for the plastic colourimetric films is illustrated in Fig. 6 and is very similar in shape to the profile illustrated in Fig. 3 for the aqueous solution-based optical CO_2 sensors, although shifted to some extent. This shift is very likely to be associated with the different concentrations of base resent, i.e., 0.01 mol dm^{-3} NaOH for the aqueous solutions and nominally 0.3 mol dm^{-3} $Q^+OH^- \cdot xH_2O$ for the plastic film sensors.

In the absence of values of the appropriate equilibrium constants for the reactions in Table 1 in the film, the theoretical plot of pK_D versus $\log\{\%CO_2(S = 1/2)\}$ illustrated in Fig. 6 (solid line), which gives a quite reasonable fit to the data, was constructed using Eqn. 2 and values of K_H, K_{a1} and K_{a2} for an aqueous solution with an initial ionic strength and base concentration equal to 0.1 and 0.1, respectively. (It should be noted that the concentration of the lipophilic base in the films is nearer 0.3 mol dm^{-3} however, its effective concentration is likely to be much smaller and the value of 0.1 mol dm^{-3} represents a best fit value derived from the model.) Further work showed that the sensitivity of any individual plastic film CO_2 sensors prepared, decreased with increasing initial base concentration (tetraoctylammonium hydroxide is the base in all the films), as predicted for an aqueous solution CO_2 optode, by Eqns. 5 and 6, and observed for the aqueous colourimetric sensor in Fig. 5a. From the results of our work on plastic film sensors for CO_2 it appears that the response of the sensors depends strongly upon the pK_D of the dye and the initial base concentration, as has been found with the aqueous solution based CO_2 sensors. The solid line in Fig. 6, provides a valuable rough guide to choosing a dye for a film sensor with a desired $\%CO_2$ sensitivity.

Conclusion

The basic theory behind conventional colourimetric and fluorimetric optical sensors for CO_2 has been examined and the key effect on sensor response of initial base concentration and dye acid dissociation constant, quantified. The results of our work obtained in aqueous solution using a variety of different dyes and initial base concentrations are consistent with the predictions made by the theoretical model. Workers interested in constructing an optical CO_2 sensor will be able to readily identify the optimum dye/initial base combination for their sensor by using the collection of model-generated pK_D versus $\%CO_2$ curves for different initial base concentrations, illustrated in Fig. 3; the response of the sensor can be subsequently fine-tuned through a minor variation in the initial base concentration. The model and all its predictions appears also to apply to the new range of plastic film CO_2 sensors developed by our group.

We gratefully acknowledge support of this research by Johnson and Johnson Professional Products Ltd.

REFERENCES

1 O.S. Wolfbeis (Ed.), Fiber Optic Chemical Sensors and Biosensors, Vols. I and II, CRC Press, Boca Raton, FL, 1991.
2 G.G. Vurek, P.J. Feustel and J.W. Severinghaus, Ann. Biomed. Eng., 11 (1983) 499.
3 J.A. Berman, J.J. Furgiuele and G.F. Marx, Anesthesiology, 60 (1984) 613.
4 M.D. DeGrandpre, Anal. Chem., 65 (1993) 331.
5 E.C. Stanford, U.S. Pat., 3,068,073 (1962).
6 M. Koch and R.C. Murray, U.S. Pat., 4,943,364 (1990).
7 A. Mills, Q. Chang and N. McMurray, Anal. Chem., 64 (1992) 1383.
8 O.S. Wolfbeis. L.J. Weis, M.J.P. Leiner and W.E. Ziegler, Anal. Chem., 60 (1988) 2028.
9 C. Munkholm, D.R. Walt and F.P. Milanovich, Talanta, 35 (1988) 109.
10 Y. Kawabata, T. Kamichika, T. Imasaka and N. Ishibashi, Anal. Chim. Acta, 219 (1989) 223.
11 G. Orellana, M.C. Moreno-Bondi, E. Segovia and M.D. Marazuela, Anal. Chem., 64 (1992) 2210.
12 A. Mills and Q. Chang, Analyst (London), 118 (1993) 838.
13 J.N. Butler, Carbon Dioxide Equilibria and their Applications, Addison-Wesley, Reading, 1982, Chap. 2.
14 J.W. Severinghaus and A.F. Bradley, J. Appl. Phys., 13 (1958) 515.
15 I.M. Kolthoff, Acid-Base Indicators, MacMillan, New York, 1937.
16 F.J. Green, The Sigma-Aldrich Handbook of Stains, Dyes and Indicators, Aldrich, Milwaukee, WI, 1990.
17 L. Meites, Handbook of Analytical Chemistry, McGraw-Hill, New York, 1963.
18 E.E. Sager, A.A. Maryott and M.R. Schooley, J. Am. Chem. Soc., 70 (1948) 732.
19 O.S. Wolfbeis, E. Fürlinger, H. Kronis and H. Marsoner, Fresenius Z. Anal. Chem., 314 (1983) 119.

Analytica Chimica Acta, 285 (1994) 125–133
Elsevier Science B.V., Amsterdam

Electrocatalytic oxidation of reduced nicotinamide coenzymes at Methylene Green-modified electrodes and fabrication of amperometric alcohol biosensors

Qijin Chi and Shaojun Dong

Laboratory of Electroanalytical Chemistry, Changchun Institute of Applied Chemistry, Chinese Academy of Sciences, Changchun, Jilin 130022 (China)

(Received 25th April 1993; revised manuscript received 2nd September 1993)

Abstract

Chemically modified electrodes with Methylene Green adsorbed on the graphite surface and incorporated into carbon paste exhibit excellent electrocatalytic ability for oxidation of NADH. Alcohol dehydrogenase, nicotinamide adenine dinucleotide (NAD^+) and mediator were incorporated into a carbon paste matrix to yield an alcohol sensor. The enzyme and cofactor retain their bioactivity within the matrix. The surface of the sensor is protected by coverage with a poly(ester sulphonic acid) cation exchanger to form a membrane, which effectively prevents the aqueous soluble species from dissolving out from the enzyme electrode and reduces or eliminates the interference from electroactive anions. The oxidation current of the NADH formed by enzymatic reaction serves as the response for target analytes. The reagentless sensor shows steady-state signals within 50 s, owing to the intimate contact between the biocatalytic and sensing sites. The influence of various experimental conditions was explored for optimum analytical performance. The sensor remained relatively stable for about 15 days.

Keywords: Amperometry; Biosensors; Alcohols; Enzyme electrodes

Amperometric biosensors have continued to receive active attention in recent years [1–5], partly because they have high sensitivity and a rapid response to substrates. These advantages are very important for clinical, industrial and commercial applications. Besides various oxidases used as biocatalytic components, which have been studied extensively [6–10], a few dehydrogenases, such as glucose dehydrogenase [11–13], glutamate dehydrogenase [14], L-lactic dehydrogenase [15] and alcohol dehydrogenase (ADH) [16], have been used in the fabrication of amperometric biosensors. However, this kind of enzyme depends on aqueous soluble nicotinamide adenine dinucleotide (NAD^+) for their activity. Hence in classical dehydrogenase sensors, NAD^+ is often added to the analytical system. This not only wastes the reagent but is also inconvenient in practical applications. Several recent reports have shown that biocatalysts can be incorporated into carbon paste matrices while retaining their catalytic activity [17–19]. Few reports have pointed out that enzymes can be stabilized by incorporation into carbon paste [20,21], which is possibly ascribable to the hydrophobic environment of the

Correspondence to: S. Dong, Laboratory of Electroanalytical Chemistry, Changchun Institute of Applied Chemistry, Chinese Academy of Sciences, Changchun, Jilin 130022 (China).

SSDI 0003-2670(93)E0510-E

carbon paste. These studies provide an effective way for overcoming the drawback of dehydrogenase-based sensors as described above. Glucose dehydrogenase [22], alcohol dehydrogenase [23] and glutamate dehydrogenase [24] have already been successfully investigated by incorporation the enzymes and coenzymes together into carbon paste.

Another problem concerning dehydrogenase-based amperometric sensors is the difficulty of oxidation of reduced nicotinamide coenzymes (including NADH and NADPH). The formal potential of the NAD^+–NADH redox couple is −0.56 V vs. SCE at pH 7.0 [25], but the overpotential required to oxidize NADH is ca. 1.1 V at pH 7.0 for carbon material electrodes [26] and 1.3 V at the Pt electrode [27]. The high overpotential limits the use of direct electrochemical detection approaches for monitoring NADH formation in enzymatic reactions. Therefore, there have been numerous attempts to enhance the electron-transfer kinetics using various kinds of mediators [28]. Meldola Blue has been found to be a very effective catalyst for this purpose and it has been used in the construction of an amperometric glucose sensor [22,23]. Persson and Gorton [29,30] have studied the relationship between mediator structure and electrocatalytic properties for oxidation of NADH. Hajizadeh et al. [31] have shown that a thionine-modified graphite electrode exhibits electrocatalytic activity and it was used in the flow-injection analysis of NADH. We have investigated the electrocatalytic properties of three organic dyes (Toluidine Blue, Methylene Blue and Methylene Green) for oxidation of NADH. They all exhibit excellent catalytic activity, Methylene Green (MG) being the best [32,33].

This paper describes an amperometric alcohol sensor that was fabricated by the incorporation of ADH, NAD^+ and MG into the carbon paste matrix. The resulting sensor is protected by coverage with a poly(ester sulphonic acid) cation exchanger to form a membrane. This membrane prevents the aqueous soluble species from dissolving out into the contacting solution and also blocks relevant negatively charged interfering compounds from reaching the carbon paste surface.

EXPERIMENTAL

Materials and apparatus

Alcohol dehydrogenase (from yeast, 350 U/mg, EC 1.1.1.1) and nicotinamide adenine dinucleotide were purchased from Sigma. 1,4-Dihydronicotinamide adenine dinucleotide was obtained from the Shanghai Institute of Biochemistry, Chinese Academy of Sciences. Methylene Green was obtained from the Second Factory of Shanghai Reagents and was of analytical-reagent grade. Graphite powder (spectroscopically pure) was obtained from Beijing Chemicals and further ground into fine power in a mortar before use. Silicone grease (Type 275) was received as a gift from Beijing Institute of Chemical Engineering. The poly(ester sulphonic acid) cation exchanger (Eastman AQ-29D; 30%, w/w) was obtained from Eastman Chemicals. Methanol, ethanol, propan-1-ol, propan-2-ol, butan-1-ol, butan-2-ol and 1-amyl alcohol were of analytical-reagent grade (> 99.5%) from Beijing Chemicals. Other reagents used were of analytical-reagent grade. All solutions were prepared with doubly distilled water.

Electrochemical experiments were conducted on an FDH 3204 potentiostat (Shanghai) with a Gould Series 60000 X–Y recorder (Shenyang, China). A three-electrode system was employed with Ag/AgCl (saturated KCl) as reference electrode and a platinum wire as auxiliary electrode. All buffer solutions were deoxygenated for > 30 min before electrochemical experiments. The experimental temperature was kept constant (26 ± 0.5°C) by a thermostatted water-bath.

Preparation of graphite and chemically modified graphite electrodes

A spectroscopic graphite rod (diameter 6 mm) was cut to a length of 0.8 cm, extracted with anhydrous methanol for 24 h to remove organic contaminants, dried and placed in melted paraffin for 30 min for impregnation. The resulting rod was tightly sealed in a shrinkable PTFE tube (ca. 4 cm in length), leaving the end of the rod uncovered, forming a disc electrode. The graphite electrode was polished with fine emery paper and rinsed thoroughly with doubly distilled water be-

fore use. The treated graphite electrode was immersed in 1 mM MG solution for 10 min and then rinsed with doubly distilled water, forming an MG-modified electrode.

Preparation of carbon paste and chemically carbon paste electrodes

The MG-modified carbon paste was prepared by thoroughly mixing 56% (w/w) graphite powder, 40% silicone grease and 4% MG in a mortar. Similarly, mixtures containing various amounts of ADH and NAD^+ were thoroughly combined in a mortar to form a uniform paste.

A portion of the modified carbon paste was packed into the end of a PTFE tube (5 mm i.d.) and a copper wire was inserted through the opposite end to establish electrical contact. The outer end part of the electrode was polished with fine emery paper to improve adherence of the Eastman AQ-29D film. This film was obtained by dipping the electrode into a 1% (w/w) solution of AQ-29D for 30 s, each dipping forming a layer membrane. Between dippings, the electrode was allowed to dry for > 15 min at room temperature, with the electrode surface hanging down. After the last dipping, the electrode was allowed to dry for 2 h before use. The method described here is similar to that reported by Bremle et al. [22].

Between measurements, the enzyme electrode were stored in a dry state at 4°C.

RESULTS AND DISCUSSION

Electrochemical behaviour of mediator-modified carbon paste

The electrochemical behaviour of the MG-modified carbon paste was studied by using cyclic voltammetry. Figure 1 shows cyclic voltammograms obtained with the modified electrode at different scan rates. Well defined peaks are observed between +0.1 and −0.1 V vs. Ag/AgCl. The potential difference of the peaks is ca. 100 mV at 30 mV s^{-1}, which is much larger than that (ca. 20 mV) of MG adsorbed on a graphite electrode. This means that electron transfer rate of MG incorporated into carbon paste is slower

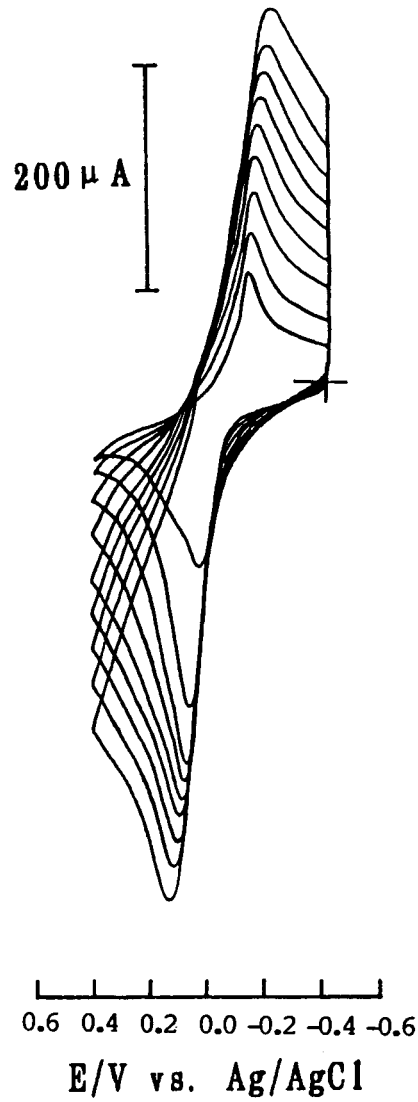

Fig. 1. Cyclic voltammograms of MG (4%, w/w)-modified carbon paste in 0.1 M phosphate buffer (pH 8.1) at scan rates of 30, 40, 50, 60, 70, 80, 90 and 100 mV s^{-1}.

than that of MG adsorbed on the graphite electrode. The slower electron transfer rate possibly results from matrix blocking, because the mediator is tightly entrapped in carbon paste.

The dependence of the peak current on scan rate is shown in Fig. 2. The peak current (i_p) is a linear function of the scan rate up to 50 mV s^{-1} (Fig. 2A), which demonstrates that the electrode reaction is characteristic of a surface wave. How-

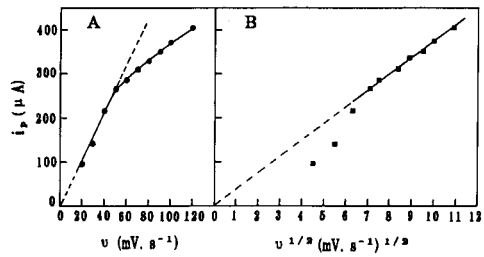

Fig. 2. Dependence of peak current on scan rate for MG-modified carbon paste. Experimental conditions as in Fig. 1.

ever, above 50 mV s^{-1} i_p depends linearly on the square root of the scan rate (Fig. 2B). As is known, a diffusion-limiting reaction is expected to give a linear relationship between i_p and the square root of the scan rate. As both oxidized and reduced mediator already are present at the electrode surface, there should be no indication of a diffusional rate-limiting effect due to redox reactant transport. However, it is noted that the electrode reaction is accompanied by protonation. As the protons have to be exchanged with the solution, their transport can give rise to a diffusional scan-rate dependence at higher scan rates [34]. The formal potential ($E^{\circ\prime}$), estimated from the mid-point of the anodic and the cathodic peaks, changes with pH and intersects at pH 6.5. Between pH 1.0 and 6.5, $E^{\circ\prime}$ decreases with increasing pH with a slope of ca. 60 mV pH^{-1}. The slope for the second linear region (pH 6.5–11) is ca. 30 mV pH^{-1}. The result suggests that the reaction scheme can be proposed as follows:

$$\text{pH 1.0–6.5: } MG^+ + 2H^+ + 2e \rightleftharpoons MGH^+ \quad (1)$$

$$\text{pH 6.5–11: } MG^+ + H^+ + 2e \rightleftharpoons MGH \quad (2)$$

Electrocatalytic oxidation of NADH

Preliminary experiments were carried out using a glassy carbon electrode (GCE) (0.28 cm^2) as a working electrode. Cyclic voltammetry was employed to examine whether MG dissolved in the aqueous solution possesses electrocatalytic activity toward the oxidation of NADH. Cyclic voltammograms obtained under various experimental conditions are shown in Fig. 3. MG itself in buffer solution gave a quasi-reversible redox pair with a cathodic peak potential of −0.09 V and an anodic peak potential of 0.02 V (Fig. 3a). The adsorption of MG on the mirrored GCE surface is difficult, unlike that on the graphite electrode. After the experiment shown in Fig. 3a, the GCE was rinsed and immersed in the blank solution, and cyclic voltammetry demonstrated that no electroactive species exist on the electrode surface. At a bare GCE, an anodic peak of NADH appears at 0.7 V in the absence of the mediator (Fig. 3b). After adding the mediator, oxidation of NADH starts at −0.2 V and reaches a maximum

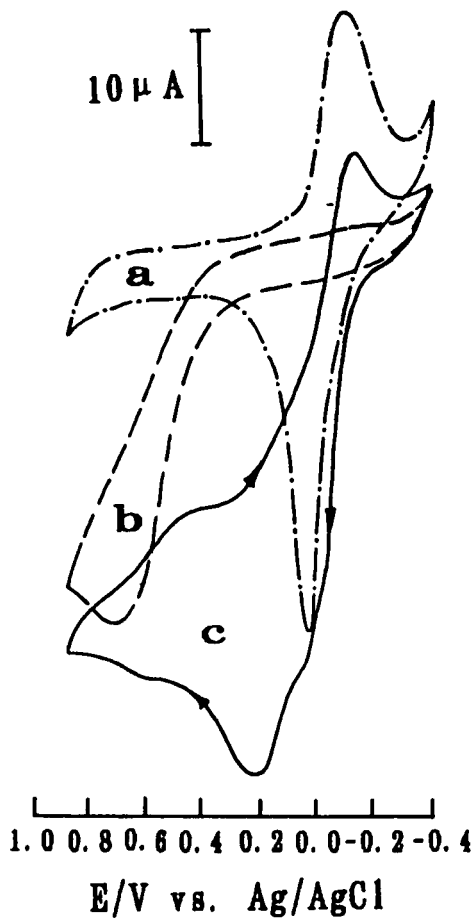

Fig. 3. Cyclic voltammograms obtained with a bare glassy carbon electrode in 0.1 M phosphate buffer containing (a) 0.4 mM MG, (b) 2.5 mM NADH and (c) 0.4 mM MG+2.5 mM NADH. Scan rate, 50 mV s^{-1}.

value at +0.2 V (Fig. 3c). A substantial (ca. 500 mV) decrease in the overvoltage and an obvious increase in the anodic current are obtained. This demonstrates that MG is an effective mediator for the oxidation of NADH.

Figure 4 shows cyclic voltammograms obtained with an MG-adsorbed graphite electrode in blank buffer (Fig. 4b) and with 2.5 mM NADH added to the buffer (Fig. 4c). The anodic wave of NADH is observed at +0.14 V. Similarly, electrocatalytic activity of the MG-modified carbon paste towards the oxidation of NADH is demonstrated, as shown in Fig. 5; the anodic potential of NADH appears at +0.1 V in neutral solution. A reaction scheme similar to the Michaelis–Menten expression [35] has been demonstrated by Gorton and co-workers

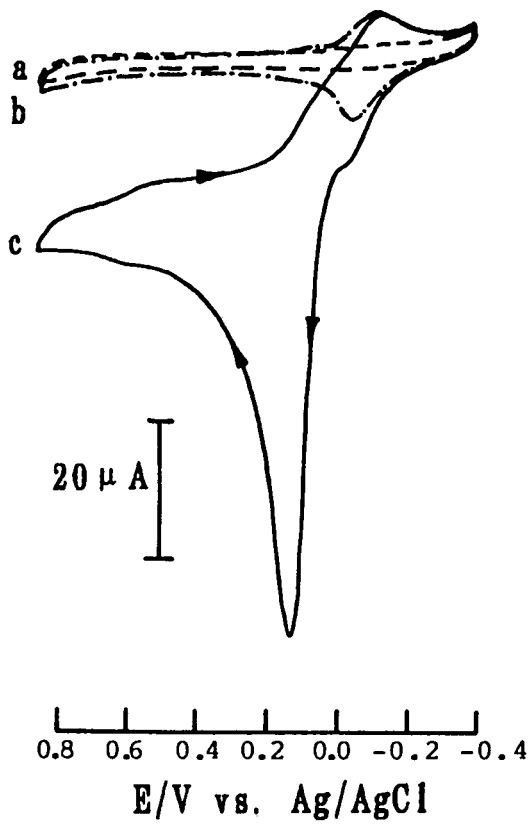

Fig. 4. Cyclic voltammograms obtained (a) at an unmodified graphite electrode in 0.1 M phosphate buffer (pH 6.5), and at an MG-modified graphite electrode (b) without and (c) with 2.5 mM NADH. Scan rate, 20 mV s^{-1}.

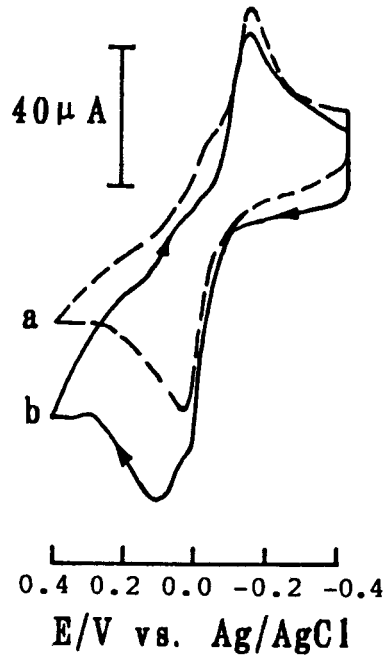

Fig. 5. Cyclic voltammograms obtained with an MG-modified carbon paste electrode in 0.1 M phosphate buffer, (a) without and (b) with 2.5 mM NADH. Scan rate, 50 mV s^{-1}.

[28–30,36,37]. We have also investigated the reaction mechanism between NADH and MG using a rotating disc electrode [33], with results similar to those reported by Gorton et al. [36]. When NADH from the contacting buffer reaches the electrode surface, it will react with the oxidized form of the mediator, MG^+. First a complex will be formed, which will then decomposes into NAD^+ and the reduced form of the mediator, MGH [36,37]. The reduced form of the mediator will be electrochemically reoxidized when the applied potential is more positive than the formal potential of the MG^+/MGH redox couple.

$$NADH + MG^+ \rightleftharpoons [MG^+ \cdot NADH] \longrightarrow NAD^+ + MGH \quad (3)$$

$$MGH \rightleftharpoons MG^+ + H^+ + 2e \quad (4)$$

$$NADH \longrightarrow NAD^+ + H^+ + 2e \quad (5)$$

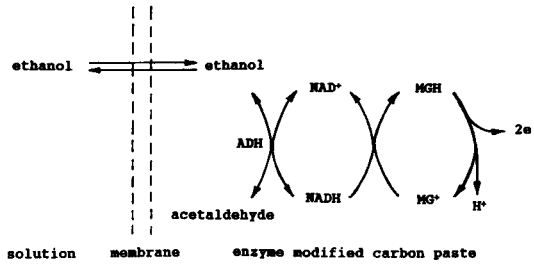

Fig. 6. Scheme of response ADH-based amperometric sensor to ethanol.

Response of ADH-based amperometric sensor to alcohol

When the biocatalysts (ADH and NAD^+) and the mediator have been incorporated into carbon paste to form a sensor, all necessary chemicals are present within the carbon paste to obtain a response to alcohol. For this sensor the response scheme, with ethanol as an example, is illustrated in Fig. 6. Ethanol will pass through the membrane from the contacting solution and reach the electrode surface, where it will be enzymatically oxidized to form acetaldehyde and NADH. The NADH generated will be reoxidized by MG^+ to form NAD^+ and MGH, which in turn is electrochemically reoxidized at the applied potential. A similar response scheme was first described by Gorton et al. [23]. They found that the stability of chemically modified carbon paste (CMCP) was very limited, only about 10% of the response remaining after 1 day. This is possibly due to the lack of a protective membrane. When a polymer (e.g., Eastman AQ-29D) was applied to the surface of the CMCP, the stability was obviously improved [22].

When the sensor coated with two layers of the polymer was immersed in stirred blank buffer solution at 0.25 V, a stable baseline was obtained with a small background current after about 10 min. The substrate solution was then injected into the cell. Figure 7 shows the amperometric responses of such a sensor to successive concentration increments of various alcohols. Except for methanol, the sensor rapidly responds to millimolar concentration changes of six alcohols and reaches a steady state within 50 s. After having responded to 3 mM ethanol, the sensor was removed and re-immersed in the stirred blank buffer solution. The response returned to the baseline within 2 min.

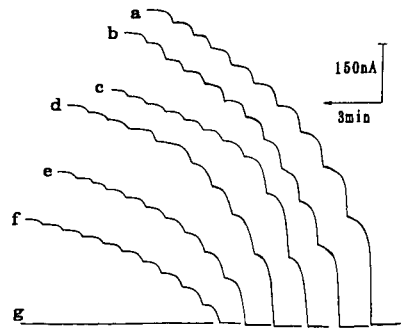

Fig. 7. Current–time curves obtained at the MG (4%), ADH (10%) and NAD^+ (15%) modified carbon paste electrode covered with two layers of the polymer with increasing concentration of alcohol in 3.0 mM steps. (a) Ethanol; (b) propan-1-ol; (c) propan-2-ol; (d) butan-1-ol; (e) 1-amyl alcohol; (f) butan-2-ol; (g) methanol. Operating potential, +0.3 V; electrolyte, 0.1 M phosphate buffer (pH 8.8).

Figure 8 shows the dependence of the response to ethanol on the applied potential and the solution pH. The response starts at −0.2 V and reaches a maximum value at potentials between +0.3 and +0.4 V. The maximum response is obtained in the solution of pH 8.8 at +0.3 V. Therefore, an operating potential of +0.3 V and a buffer solution of pH 8.8 were used in subsequent experiments.

The enzyme-modified carbon paste allows one to control the loading of the biological modifier. The effect of the ADH content was evaluated

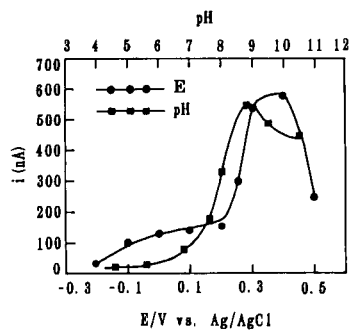

Fig. 8. Dependence of 10 mM ethanol response at the same electrode as in Fig. 7 on the operating potential and solution pH.

from calibration graphs for ethanol (not shown). In the present experiment, a mixture of ca. 50 mg was applied for each electrode, so ADH loadings of 2.5, 5.0, 10 and 15% are equivalent to 438, 875, 1750 and 2625 U, respectively. At lower ADH loadings (e.g., 2.5 or 5.0%, w/w), a wider linear range was obtained, but the response sensitivity was very low (e.g., only 4.5 nA l $mmol^{-1}$ for the 2.5% ADH loading). The linear response was only up to 2.5 mM ethanol when a 15% ADH loading was used, and moreover the responses were smaller than those for the 10% ADH content when the ethanol concentrations were above 10 mM. Therefore, in the present experiment a 10% ADH loading is suitable for obtaining high sensitivity and a relatively wide linear range.

Figure 9 shows the calibration graphs for the same prepared sensor (10% ADH, 15% NAD^+ and 4% MG) for ethanol while covered with different layers of the polymer. As expected, with increasing thickness of the membrane the response decreased gradually. When the electrode was covered with more than eight layers of the polymer, it hardly responded to ethanol. The result possibly arises from the increase in the resistance to mass transport by the membrane. In addition, the layer number of the membrane also affects the linear range and the stability of the sensor. As can be seen from Fig. 9, the higher

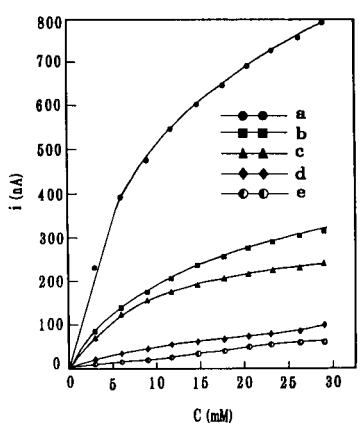

Fig. 9. Calibration graphs for ethanol with five identically prepared electrodes (10% ADH, 15% NAD^+ and 4% MG loadings), covered with (a) two, (b) three, (c) four, (d) six and (e) eight layers of the polymer. Other conditions as in Fig. 7.

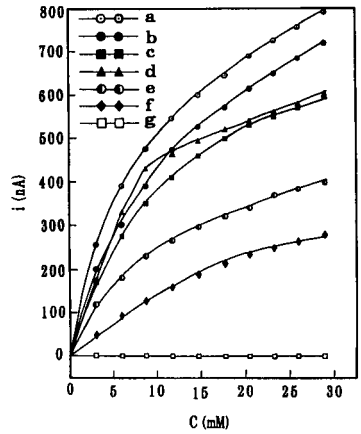

Fig. 10. Dependence of the steady-state current on the concentration of (a) ethanol, (b) propan-1-ol, (c) butan-1-ol, (d) propan-2-ol, (e) 1-amyl alcohol, (f) butan-2-ol and (g) methanol. Data from Fig. 7.

response from a twice-dipped electrode (Fig. 9a) results in a calibration graph that starts to deviate from linearity at a lower ethanol concentration than that of an electrode covered with six dippings (Fig. 9d). This result may be due to the difference in the concentration gradient of ethanol between the solution and the electrode surface (see Fig. 6). When the membrane is thin, the concentration gradient must be smaller. This means that the concentration of ethanol reaching the electrode surface is large in the given solution, hence the response of the enzyme to ethanol will be saturated at lower concentrations of ethanol solution. Therefore, the calibration graph starts to deviate from linearity at a lower ethanol concentration. A similar explanation can be given to the situation with a thick membrane. Similar results have been reported and used to extend the linear range of glucose sensors by means of covering with polymers [38,39].

Figure 10 shows the dependence of the steady-state amperometric response of the sensor on the concentration of seven different alcohols. With the exception of ethanol, the sensor can respond to six other alcohols. This is in agreement with the known fact that the yeast ADH can readily oxidize primary alcohols (with the exception of methanol) and slowly oxidize secondary alcohols [40]. However, the trend in response

TABLE 1

Parameters of the sensor response to various alcohols

Alcohol	Linear range (mM)	Sensitivity [a] (nA l mmol^{-1})	Relative response [b]	K_M^{app} (mM)
Ethanol	0.04–6.0	68	100	11.6
Propan-1-ol	0.09–7.5	54	90	14.1
Propan-2-ol	0.10–8.0	47	78	15.1
Butan-1-ol	0.40–8.5	39	76	15.6
1-Amyl alcohol	0.40–6.5	28	49	16.8
Butan-2-ol	1.0–16.5	13	35	32.2
Methanol	0	0	–	–

[a] Slope of linear portion. [b] At 20 mM.

sensitivity (ethanol > propan-1-ol > propan-2-ol > butan-1-ol > 1-amyl alcohol > butan-2-ol > methanol in the present experiments) differs partly from the known biospecificity of the solution-phase enzyme [41]. This change is possibly caused by slight differences in the conformation between the immobilized enzyme and the solution-phase enzyme, but the exact reason for this change is not understood completely. The apparent Michaelis–Menten constants (K_M^{app}) were calculated from the slopes of the linear portion of the corresponding electrochemical Eadie–Hofstee plots [42]. The sensor characteristics of the response to seven alcohols are summarized in Table 1.

The response current of the enzyme electrode covered with two dippings for 3 mM ethanol is 255 nA, whereas for the same concentration of uric acid and ascorbic acid they are 3 and 10 nA, respectively. The relative responses of the latter two are 1.2 and 3.9%, respectively. If the enzyme electrode is covered with three or more dippings, however, no responses for these two electroactive anions are observed.

A series of eight successive measurements of 10 mM ethanol yielded a relative standard deviation of 3.1%. The enzyme electrode covered with two layers of the polymer remained stable for about 15 days when it was stored in a dry state at 4°C.

Conclusion

Methylene Green has been demonstrated to be an effective mediator toward oxidation of NADH. The electrode chemically modified by incorporating MG into carbon paste remains stable with respect to electrocatalytic activity in solutions of pH 4–9. It has been shown that an alcohol dehydrogenase and its cofactor can be immobilized and retain their activity within carbon paste. When a poly(ester sulphonic acid) cation exchanger is covered on the outer of the chemically modified carbon paste to form a membrane, which effectively prevents the aqueous soluble species from dissolving out into the test solution and also prevents relevant negatively charged interfering compounds from reaching the electrode surface, the resulting sensor responds rapidly to six alcohols. The present experiments show that the 10% ADH and 15% NAD^+ contents are suitable for a high sensitivity and relatively wide linear range. A sensor covered with two layers of the AQ polymer remained stable for ca. 15 days when it was stored in a dry state at 4°C.

The support of the National Natural Foundation of China is gratefully appreciated.

REFERENCES

1 K. Yokoyama, E. Tamiya and I. Karube, Electroanalysis, 3 (1991) 469.
2 F. Pariente, L. Hernandez and E. Lorenzo, Bioelectrochem. Bioenerg., 27 (1992) 73.
3 M.H. Smit and G.A. Rechnitz, Anal. Chem., 64 (1992) 245.
4 S. Kakura and R.P. Buck, Bioelectrochem. Bioenerg., 28 (1992) 387.
5 S.M. Zakeeruddin, D.M. Fraser, M.-K. Nazeeruddin and M. Gratzel, J. Electroanal. Chem., 337 (1992) 253.
6 S.J. Updike and G.P. Hicks, Nature, 214 (1967) 986.
7 T. Ikeda, Y. Hashimoto, M. Senda and Y. Isono, Electroanalysis, 3 (1991) 891.
8 T. Tatsuma and T. Watanabe, Anal. Chim. Acta, 242 (1991) 85.
9 Z. Sun and H. Tachikawa, Anal. Chem., 64 (1992) 1112.
10 J.C. Cooper and E.A.H. Hall, Biosensors Bioelectron., 7 (1992) 473.
11 F. Schubert, D. Kirstein, K.L. Schroeder and F.W. Scheller, Anal. Chim. Acta, 169 (1985) 391.
12 G. Marko-Varga, R. Appelqvist and L. Gorton, Anal. Chim. Acta, 179 (1986) 371.
13 G. Palleschi, G.G. Guilbault, G.J. Lubrano and M.A. Nabi Rahni, Anal. Chim. Acta, 192 (1987) 339.

14 S. Yabuki, F. Mizutani, T. Katssura and M. Asai, Bioelectrochem. Bioenerg., 28 (1991) 489.
15 J.C. Hoogvliet, P.J.H. Van Os, E.J. van der Mark and W.P. van Bennekom, Biosensors Bioelectron., 6 (1991) 413.
16 J. Wang, E. Gonzalez-Romero and M. Ozsoz, Electroanalysis, 4 (1992) 539.
17 J. Wang, L.H. Wu, Z.Z. Lu, R. Li and J. Sanchez, Anal. Chim. Acta, 228 (1990) 251.
18 A. Amine, J.-M. Kauffmann, G.J. Patriarche and A.E. Kaifer, Anal. Lett., 24 (1991) 1293.
19 A. Amine, J.-M. Kauffmann and G.J. Patriarche, Talanta, 38 (1991) 107.
20 M. Bonakdar, J.L. Vilchez and H.A. Mottola, J. Electroanal. Chem., 226 (1989) 47.
21 P.A. Nader, S.S. Vivis and H.A. Mottola, J. Electroanal. Chem., 284 (1990) 323.
22 G. Bremle, B. Persson and L. Gorton, Electroanalysis, 3 (1991) 77.
23 L. Gorton, G. Bremle, E. Csoregi, G. Jonsson-Petterson and B. Persson, Anal. Chim. Acta, 249 (1991) 43.
24 A. Amine and J.-M. Kauffmann, Bioelectrochem. Bioenerg., 28 (1992) 117.
25 H.K. Chenault and G.M. Whitesides, Appl. Biochem. Biotechnol., 14 (1987) 147.
26 J. Moirous and P.J. Elving, Anal. Chem., 50 (1978) 1056.
27 H. Jaegfeldt, J. Electroanal. Chem., 110 (1980) 295.
28 L. Gorton, J. Chem. Soc., Faraday Trans. 1, 82 (1986) 1245.
29 B. Persson and L. Gorton, J. Electroanal. Chem., 292 (1990) 115.
30 B. Persson, J. Electroanal. Chem., 287 (1990) 61.
31 K. Hajizadeh, H.T. Tang, H.B. Halsall and W.R. Heineman, Anal. Lett., 24 (1991) 1453.
32 Q. Chi and S. Dong, Electroanalysis, in press.
33 Q. Chi and S. Dong, J. Electroanal. Chem., in press.
34 A.P. Brown and F.C. Anson, J. Electroanal. Chem., 92 (1978) 133.
35 L. Michaelis and M. Menten, Biochem. Z., 49 (1913) 333.
36 L. Gorton, A. Torstensson, H. Jaefeldt and G. Johansson, J. Electroanal. Chem., 161 (1984) 103.
37 F. Ni, H. Feng, L. Gorton and T.M. Cotton, Langmuir, 6 (1990) 66.
38 N. Cleland and S. Enfors, Anal. Chem., 56 (1984) 1880.
39 L.X. Tan, Z.B. Koochaki and P.M. Vadgama, Anal. Chim. Acta, 232 (1990) 357.
40 T.E. Barman, Enzyme Handbook, Vol. 1, Springer, Berlin, 1969, p. 23.
41 T. Bicsak, L. Kann, A. Reiter and T. Chase, Arch. Biochem. Biophys., 216 (1982) 1982.
42 R.A. Kamin and G.S. Wilson, Anal. Chem., 52 (1980) 1198.

Analytica Chimica Acta, 285 (1994) 135–141
Elsevier Science B.V., Amsterdam

Electrochemically pretreated glassy carbon as a chromatographic sensor for cationic and redox species

Tsutomu Nagaoka, Michihito Katayama, Michio Fujimoto, Hidenobu Nakao and Kotaro Ogura

Department of Applied Chemistry and Chemical Engineering, Faculty of Engineering, Yamaguchi University, 2557 Tokiwadai, Ube 755 (Japan)

Tetsuo Okada

Faculty of Liberal Arts, Shizuoka University, Shizuoka 422 (Japan)

(Received 21st June 1993; revised manuscript received 10th September 1993)

Abstract

On oxidative electrochemical pretreatment, the surface of glassy carbon electrodes becomes porous and it adsorbs ions by electrochemical charging. In potentiometric experiments, the potential at a treated carbon electrode increased with increase in the concentration of ionic species, and the electrode was evaluated as an ion detector for ion chromatography. The carbon electrode could detect cations down to 1×10^{-11} mol (5×10^{-7} M in 20 μl) when used with an ion-exchange column without a suppressor system and had better sensitivity than conductivity detectors. Further, the redox reactions of the surface sites that were created by pretreatment were reversible, and the electrode potential remained constant after injections of redox analyte.

Keywords: Ion chromatography; Potentiometry; Cationic species; Glassy carbon electrodes; Redox species

Various forms of carbon respond to pH and have been used in pH measurements and acid–base potentiometric titrations [1–6]. Although many workers have studied carbonaceous materials as pH sensors, the response of such sensors for other ionic species has not been reported. In this work, the potentiometric response of electrochemically treated glassy carbon for ionic species was studied.

Oxidative treatment of glassy carbon creates a surface covered with porous oxide that can take up ions by electrochemical charging. The average radii of the surface pores are 10–20 Å, depending on the method used in oxidation [7–11]. Negatively charged pore surfaces take up cations and positively charged pore surfaces take up anions [7,8,11]. Although untreated carbon fibre is fairly porous, only the surface pores that are created by oxidative treatment can take up ions [8]. This paper discusses the application of the electrode as a cation sensor and as a redox sensor.

Correspondence to: T. Nagaoka, Department of Applied Chemistry and Chemical Engineering, Faculty of Engineering, Yamaguchi University, 2557 Tokiwadai, Ube 755 (Japan)

EXPERIMENTAL

Electrode preparation

The anodization of carbon electrodes (Tokai, Grade GC-20, 3 or 6 mm in diameter) at +1.8 V vs. Ag/AgCl/sat. KCl in pH 7 phosphate buffer for 1–60 min was followed by cathodization at −1.5 V for about 1 min [7,8,11–13]. When the responses for hydroxide and sulphate ions were studied, the surface of the treated electrode was coated with a droplet of Nafion 117 solution

SSDI 0003-2670(93)E0503-Y

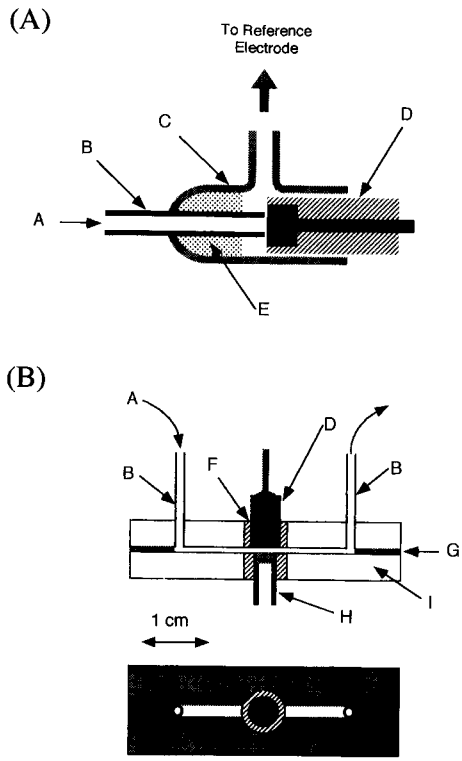

Fig. 1. Cross-sections of the cells used in (A) flow-injection and (B) LC measurements. A = mobile phase flow; B = stainless-steel tube (i.d. 1 mm); C = Pyrex glass tube (o.d. 1 cm); D = carbon electrode; E = ceramic bond; F = silicone-rubber tube seal; G = silicone-rubber spacer; H = reference electrode, I = PTFE body.

(Aldrich) and then allowed to air dry. The electrode thus prepared was soaked in 1×10^{-5} M aqueous tetraethylammonium perchlorate (TEAP) solution for 12 h before use.

Apparatus

Flow-injection experiments were carried out with an EYELA Model MP-3 pump, a laboratory-made injector (15 μl) and a measurement cell. The response of the treated electrode was virtually independent of the flow-rate in the range 0.42–1.2 ml min^{-1} (conditions used in this study). Liquid chromatographic (LC) experiments were carried out with a TOSOH IC-cation column, a Shimadzu LC-6A pump, a Rheodyne Model 7125 injector with a 20-μl sample loop and a measurement cell. Measurements were made at 25°C unless stated otherwise. Figure 1 shows the measurement cells used here: cell A was used in flow-injection experiments and cell B in LC experiments. Glassy carbon rods of 3 and 6 mm diameter were used in cells A and B, respectively. The potential was measured with a Hewlett-Packard HP34401A multimeter (input impedance 10 MΩ, resolution ± 0.1 μV) interfaced with an Apple Macintosh SE computer. The reference electrodes used here were Ag/AgCl/saturated KCl. A resistor of 1 MΩ was installed in parallel with the carbon and reference electrodes to increase the baseline stability and the signal-to-noise ratio in LC experiments. An average noise amplitude of ca. 2 μV was achieved without using a Faraday cage. Conductivity was measured with a TOSOH IC-8010 five-electrode conductivity detector.

Chemicals

All the metal salts used were of analytical-reagent grade and were used without further purification.

RESULTS AND DISCUSSION

Potentiometric responses of the carbon electrode

Figure 2 shows the voltammograms of treated and untreated glassy carbon electrodes, and the

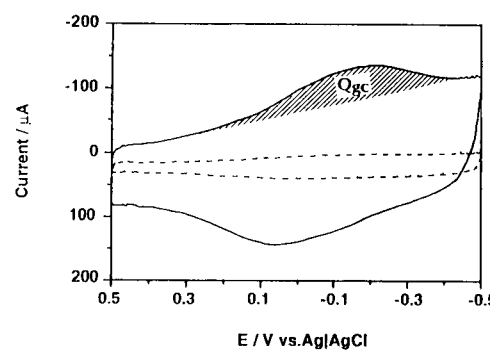

Fig. 2. Cyclic voltammograms of (solid line) treated glassy carbon and (dashed line) freshly polished carbon in phosphate buffer (pH 7.0). The areas of the cathodic peaks (Q_{gc}) were 3.5×10^{-4} C for treated carbon and 2.4×10^{-5} C for untreated (polished) carbon; the diameters of the electrodes were 3 mm.

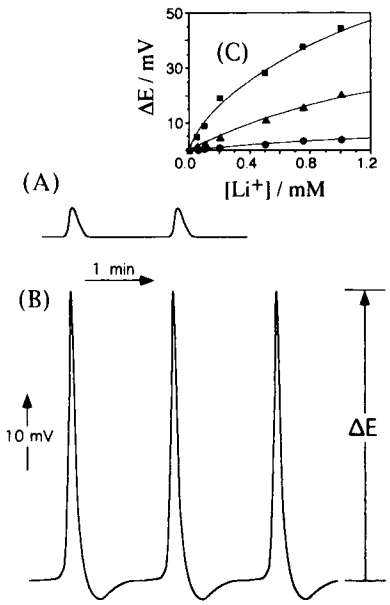

Fig. 3. Flow-injection responses obtained at (A) a freshly polished glassy carbon electrode ($Q_{gc} = 2.4\times10^{-5}$ C) and (B) a treated electrode ($Q_{gc} = 3.5\times10^{-4}$ C), and (C) responses of the carbon electrodes treated for different oxidation times. Q_{gc}: (●) $= 6.4\times10^{-5}$; (▲) $= 2.0\times10^{-4}$; (■) $= 7.4\times10^{-4}$ C. Mobile phase, 10 μM aqueous TEAP; flow-rate, 0.6 ml min^{-1}; analyte volume injected, 15 μl; ΔE is defined by the difference in potential between the peak maximum and baseline.

increase in charging current after oxidative treatment can be assigned to greater surface roughness. The amount of oxide is dependent on the anodization time and is characterized well by the cathodic peak area (Q_{gc} in Fig. 2).

The responses of the glassy carbon electrodes in flow-injection experiments are shown in Fig. 3; the untreated electrode has much smaller responses than the treated electrode. Table 1 summarizes the responses of the treated electrode to various ions; $\Delta E/\Delta C$ means the electrode sensitivity for low ion concentrations and $\Delta E/\Delta$ log C the sensitivity for high ion concentrations, where C is the concentration of an ionic species. The $\Delta E/\Delta C$ value for protons was the largest of all the $\Delta E/\Delta C$ values for the monovalent cations, probably owing to specific adsorption of protons. The $\Delta E/\Delta C$ values for the divalent metal perchlorates were higher than those for the monovalent ions. Table 1 also shows that all the $\Delta E/\Delta$ log C values except for tetraethylammonium hydroxide (TEAOH) are positive, indicating that the cations listed have higher absolute sensitivities than the anions. The positive responses result probably because cations are adsorbed on the electrode surface and/or because cations dominate over anions in the diffuse double layer arising from negative surface potential caused by the polar oxygen sites.

Divalent metal sulphates showed substantially smaller sensitivities than corresponding perchlorates (see Table 2). As correction of free ion

TABLE 1

Responses of treated glassy carbon electrodes in flow-injection experiments [a]

Compound	$\Delta E/\Delta$ log C [b] (mV)	$\Delta E/\Delta C$ [c] (V l mol^{-1})
$HClO_4$	37	113
$LiClO_4$	42	60
NaF	44	54
NaCl	42	68
$NaNO_3$	41	61
$NaClO_4$	42	69
KCl	44	72
NH_4Cl	38	81
$(C_2H_5)_4NOH$	−47	−38
$(C_2H_5)_4NClO_4$	44	52
$Ba(ClO_4)_2$	59	114
$Mg(ClO_4)_2$	63	140
$NiCl_2$	58	139

[a] Carrier solution, 10 μM aqueous TEAP; injection volume, 15 μl; $Q_{gc} = 7.4\times10^{-4}$ C. [b] Metal ion concentration, $2\times10^{-4}-1\times10^{-3}$ M; estimated accuracy, ±3 mV. [c] Metal ion concentration, $5\times10^{-5}-2\times10^{-4}$ M; estimated accuracy, ±5 V l mol^{-1}.

TABLE 2

Effects of anions on responses of the treated electrode [a]

Compound	$\Delta E/\Delta$ log C (mV)	
	Without Nafion	With Nafion
$Ba(ClO_4)_2$	59	
$Mg(ClO_4)_2$	63	64
$MgSO_4$	37	56
$CaSO_4$	39	
$CuSO_4$	40	
$FeSO_4$	30	

[a] Metal ion concentration, $2\times10^{-4}-1\times10^{-3}$ M; other conditions as in Table 1.

concentration for ion pairing ($M^{2+} + SO_4^{2-} \rightleftharpoons MSO_4$) did not give substantial increases in the sensitivities, the smaller values for the sulphates can be attributed to the greater negative responses for divalent anions. The anion effect was removed effectively by modifying the treated surface with Nafion (see Table 2). As the sensitivities for the divalent cations were also higher than those for the monovalent ions, it is concluded that the electrode has higher absolute sensitivities for divalent than for monovalent ions.

The remarkably strong negative response for OH^- (Table 1) arises from specific adsorption on acidic surface sites. However, the interaction was reversible as the potential returned to the original value after injected sample plugs had passed the electrode. The negative response for TEAOH in Table 1 cannot be attributed to a decrease in proton concentration for the following reasons: as seen in Fig. 4, the slope for the electrode coated with Nafion (the transference numbers of cations in Nafion are very close to unity in the dilute ionic solutions used here, so it is unlikely that a substantial amount of OH^- permeates through the membrane [14]) at high pH is smaller than that without Nafion, and there are two linear

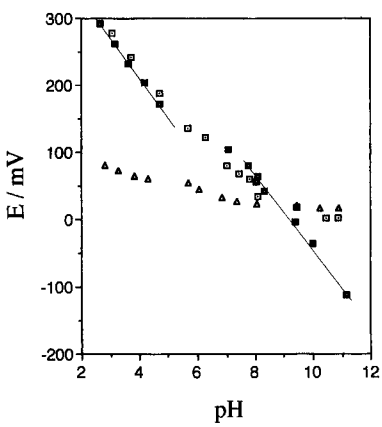

Fig. 4. Electrode responses for H^+ and OH^- in batchwise experiments at 26°C. The pH was adjusted by adding HCl to a pH 11 aqueous solution containing 1 mM TEAOH + 5 mM TEAP. The electrodes used were (□) coated and (■) not coated with Nafion after pretreatment, and (△) coated with Nafion without pretreatment. The Q_{gc} values were 7.4×10^{-4} C for the treated electrodes and 2.4×10^{-5} C for the untreated electrode.

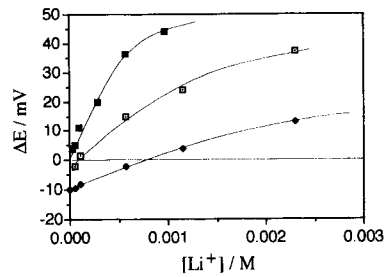

Fig. 5. Effect of ionic strength of mobile phase on sensitivity. A 15-μl volume of Li^+ solution was injected; mobile phase, (■) = 0.01, (□) = 0.1 and (♦) = 1.0 mM aqueous TEAP; flow-rate, 0.54 ml min^{-1}; $Q_{gc} = 3.9 \times 10^{-4}$ C.

regions for the uncoated electrode. Consequently, the electrode should respond to protons in the acidic region (pH < 5) and to hydroxide ions in the basic region (pH > 8). The electrode coated with Nafion on an untreated surface gave much smaller responses than the electrode coated on a treated surface, indicating that the membrane potential produced by the Nafion layer is not important.

Figure 5 shows the dependence of the responses for Li^+ on the concentration of base electrolyte. The sensitivity increased with decrease in TEAP concentration, probably because the diffuse double layer mainly consists of cations at low TEAP concentrations owing to the negative oxygen sites and/or because hydrophobic TEA^+ adsorbs more strongly than Li^+. The negative responses arising when $[Li^+] < [TEA^+]$ are due to a decrease in total ionic concentration, as the injected solution did not contain TEAP.

The sensitivity decreased with increase in TEAP concentration but became almost constant for [TEAP] > 5 mM. In analytical applications this is an important advantage of the carbon electrode over conductimetry especially at high salt concentrations because the detection limit in conductimetry will decrease almost linearly with increase in ionic strength.

Application in ion chromatography

The electrode was applied to LC using a cation-exchange column without a suppressor system (see Fig. 6). As nitric acid solutions were used as the mobile phase, the negative responses

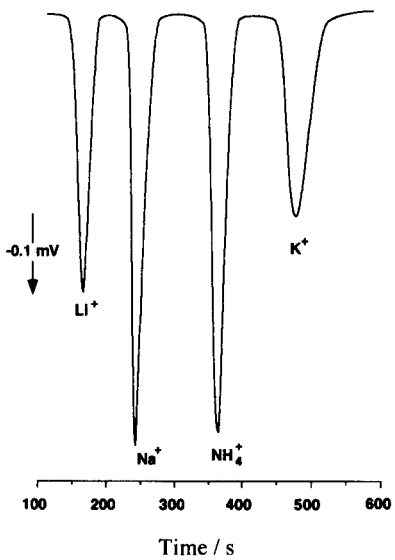

Fig. 6. Ion chromatogram for the 20-μl injection of 4.6 nmol $LiClO_4$, 7.1 nmol Na^+, 8.7 nmol NH_4^+ and 8.2 nmol K^+. Mobile phase, 2.0 mM nitric acid; flow-rate, 1.2 ml min^{-1}; column temperature, 35°C; $Q_{gc} = 7.4 \times 10^{-4}$ C.

observed for the injection of alkali metal cations are based on the higher $\Delta E/\Delta C$ for protons. In Fig. 7 the sensitivity of the carbon electrode is compared with that of conductimetry. To achieve high sensitivity and stability, the conductivity detectors used in LC adopt elaborate designs such as a five-electrode configuration [15,16]. The detection limit of a TOSOH IC-8010 conductivity detector for Li^+ was ca. 10^{-6} M in 20 μl, which is comparable to the values reported for other LC detectors [17,18].

As seen in Fig. 7, the signal-to-noise ratio and baseline stability of the carbon sensor are better than those for conductimetry. The noise amplitude of the carbon sensor system is ca. 2 μV, so that the detection limit (signal-to-noise ratio = 2) is about 1×10^{-11} mol (5×10^{-7} M in 20 μl). A linear working range of four decades is comparable to that for conductivity detectors, and the sensitivity of the carbon electrodes was fairly stable (variation < 5% per month). The present detector therefore has a great advantage over conductivity detectors in that its design is much simpler.

To evaluate ion-exchange membranes as chromatographic ion detectors, several workers have studied the potentiometric responses of such membranes, but poor sensitivities (detection limit ca. 10^{-8} mol) limit the application of these sensors to an LC system [19–21].

Responses to redox compounds

Redox species in solution also influenced the electrode potential. Interestingly, the potential remained constant after each injection of redox analyte, and the potential changes were proportional to the amount of the analyte injected (see Fig. 8). This memory effect was not observed for metallic electrodes such as Pt microdisc, at which peak-shaped signals were obtained. Therefore,

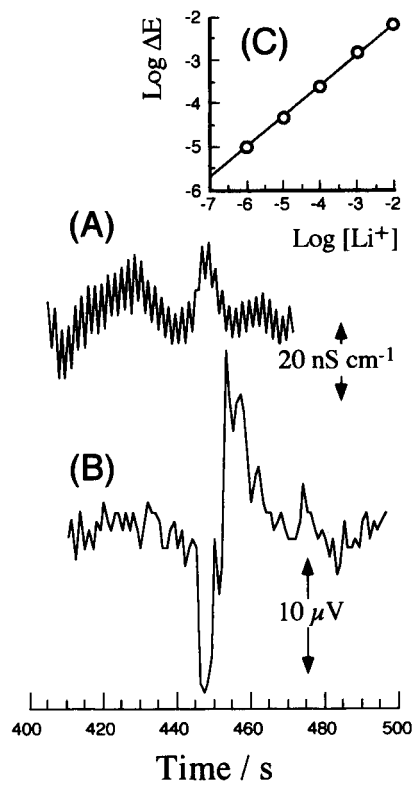

Fig. 7. Comparison of (A) conductimetric response with (B) potentiometric response. The LC responses were for 20-μl injections of 1.0 μM Li^+ at a flow-rate of 1.0 ml min^{-1}; mobile phase, 0.6 mM nitric acid; column temperature, 25°C. (C) Calibration graph for the carbon electrode; ΔE and $[Li^+]$ are in V and M, respectively.

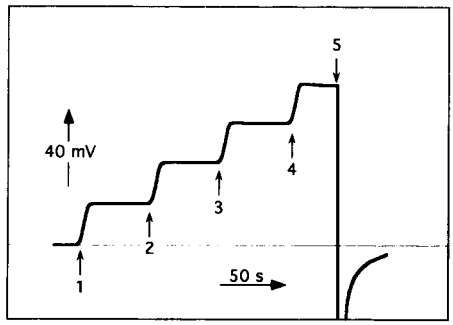

Fig. 8. Stepwise increases in output potential for injections of 0.5 mM KIO_3 + 0.1 M H_2SO_4 (20 μl). Responses 1–4 indicate injections of KIO_3 and response 5 shows the discharge of the electrode; carrier solution, 0.1 M H_2SO_4.

the effect suggests that the surface sites (or oxide layer) on the carbon are involved in the response and that the concentrations of the reduced and oxidized sites remain constant even after redox plugs have passed through the cell. As shown in Fig. 9, the electrode responds to both the reducing and oxidizing agents, so that the sites should involve both oxidizable and reducible functional groups. Further, alternate injections of reducing and oxidizing agents resulted in a series of negative and positive responses. Various forms of oxygen surface sites such as carbonyl, carboxyl and phenol have been suggested from the results of x-ray photoelectron spectroscopy and other experiments [22–28], but there is still much controversy about the identification. The functional groups were thus reversible in redox reactions, suggesting that the electrode potential can be expressed in terms of the Nernst equation. To see if this is the case, the output (ΔE) was plotted against log $\Gamma(Ox)/\Gamma(Red)$ for KIO_3, where $\Gamma(Ox)$ and $\Gamma(Red)$ are the surface concentrations of oxidized and reduced sites, respectively, assuming that the reaction of the surface sites consists of simple electron transfer ($Ox + ne \rightleftharpoons Red$) and that injected KIO_3 reacts quantitatively with the surface sites, Red. The resulting plot gave a linear relationship with a slope of 60 mV per decade ($r^2 = 0.99$) when $n = 1$, $\Gamma(Ox)_0 = 9$ and $\Gamma(Red)_0 = 88$ nmol, where $\Gamma(Ox)_0$ and $\Gamma(Red)_0$ are the initial surface concentrations of Ox and Red, respectively. Values of n greater than unity led to calculated slopes much larger than the theoretical values, i.e., $59/n$ mV per decade. Reduction with naphthalene-1,4-diol also gave a linear relationship (62 mV per decade, $r^2 = 0.98$) when $n = 1$.

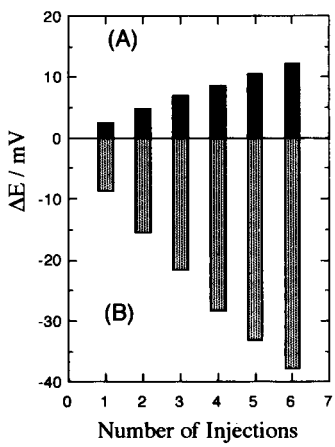

Fig. 9. Changes in the output potential for the injections of (A) 0.01 mM KIO_3 + 0.1 M H_2SO_4 and (B) 0.1 mM naphthalene-1,4-diol + phosphate buffer (pH 7) (20 μl). Carrier solution: (A) 0.1 M H_2SO_4, (B) deaerated phosphate buffer (pH 7).

The electrode potential decreased gradually after injections because of the self-discharge of the electrode. This decrease was relatively clear when the output voltage was high (see the potential decrease after the fourth injection in Fig. 8). The rate of the decrease was unchanged even when the multimeter was replaced with a pH meter, which had an input impedance higher than the multimeter, suggesting that the surface sites react with water and/or trace amounts of redox impurities in the carrier solution. The output of the carbon electrode is reset by making momentarily an electrical contact with the reference electrode (see response after 5 in Fig. 8).

A resistor that is connected to the carbon and reference electrodes in parallel discharges the carbon electrode, altering the stepwise responses to normal peaks. Therefore, the carbon sensor with the discharge resistor can be a cheap substitute for the electrochemical detector in LC, and, further, integration of peaks is possible if the resistor is disconnected.

The memory effect brings about some baseline instability when the electrode is used as a detec-

tor in ion chromatography, because a trace amount of redox impurities in the mobile phase can alter the output potential continuously during measurements. However, this effect can be eliminated safely by the installation of a discharge resistor, and good baseline stability with a negligible decrease in signal intensity was obtained with a 1-MΩ resistor.

The authors acknowledge helpful discussions with Professor T. Sata.

REFERENCES

1 F.J. Miller, Anal. Chem., 35 (1963) 929.
2 J. Dolezal and K. Stulík, J. Electroanal. Chem., 17 (1968) 87.
3 V.J. Jennings and P. Pearson, Nature, 256 (1975) 31.
4 V.J. Jennings, Analyst, 106 (1981) 1344.
5 J.E. Morgan, V.J. Jennings and J. Lindley, Analyst, 110 (1985) 639.
6 T.E. Edmonds, Anal. Chim. Acta., 175 (1985) 1.
7 I. Watanabe, T. Nagaoka, T. Fukunaga, T. Yoshino, T. Nakayama and S. Okazaki, Anal. Chem., 60 (1988) 2766.
8 T. Nagaoka and Y. Uchida and K. Ogura, J. Chem. Soc., Faraday Trans. 1, 85 (1989) 3757.
9 L.J. Kepley and A.J. Bard, Anal. Chem., 60 (1988) 1459.
10 G. Picq, R. Reeves, P. Ribourg and P. Vennereau, J. Electroanal. Chem., 162 (1984) 225.
11 Y. Uchida, T. Nagaoka and K. Ogura, Bunseki Kagaku, 40 (1991) 13.
12 T. Nagaoka, T. Sakai, K. Ogura and T. Yoshino, Anal. Chem., 58 (1986) 1953.
13 T. Nagaoka and T. Yoshino, Anal. Chem., 58 (1986) 1037.
14 T. Sata, In Ion Exchange Membranes (R&D Report No. 18), CMC Press, Tokyo, 1981, pp. 223–257.
15 N. Baba, K. Hosako, S. Matsusita and Y. Tada, Res. Rep. TOSOH, 27 (1983) 21.
16 J.M. Keller, Anal. Chem., 53 (1981) 345.
17 H. Sato, Bunseki Kagaku, 31 (1982) 97.
18 J.S. Fritz, D.T. Gjerde and R.M. Becker, Anal. Chem., 52 (1980) 1519.
19 U.G. Spencer and F. Lindstrom, Anal. Chim. Acta, 27 (1962) 573.
20 P.C. Mangelsdorf and T.R.S. Wilson, J. Phys. Chem., 152 (1978) 349.
21 R.S. Deelder, H.A.J. Linssen, J.G. Koen and A.J.B. Beeren, J. Chromatogr., 203 (1981) 153.
22 W.G. Collier and T.P. Tougas, Anal. Chem., 59 (1987) 396.
23 T.P. Tougas and W.G. Collier, Anal. Chem., 59 (1987) 2269.
24 G.E. Cabaniss, A.A. Diamantis, W.R. Murphy, Jr., R.W. Linton and T.J. Meyer, J. Am. Chem. Soc., 107 (1985) 1845.
25 J. Schreurs, J. Van den Berg, A. Wonders and E. Barendrecht, Recl. Trav. Chim. Pays-Bas, 103 (1984) 251.
26 R.C. Engstrom and V.A. Strasser, Anal. Chem., 56 (1984) 136.
27 I.-F. Hu, D.H. Karweik and T. Kuwana, J. Electroanal. Chem., 188 (1985) 59.
28 N. Cenas, J. Rozgaite, A. Pocius and J. Kulys, J. Electroanal. Chem., 154 (1983) 121.

Analytica Chimica Acta, 285 (1994) 143–159
Elsevier Science B.V., Amsterdam

Chemiluminescence detection in liquid chromatography based on photo-oxygenation involving reactive oxygen intermediates

H.A.G. Niederländer, C. Gooijer and N.H. Velthorst

Department of General and Analytical Chemistry, Free University, De Boelelaan 1083, 1081 HV Amsterdam (Netherlands)

(Received 23rd April 1993; revised manuscript received 11th September 1993)

Abstract

A luminol chemiluminescence (CL) detection system for reversed-phase liquid chromatography (RPLC), based on on-line photochemical production of organic hydroperoxides is presented. Tetramethylethylene (TME) was used as a reagent for generation of hydroperoxides in a post-column photochemical reactor, which is based on photo-oxygenation induced by the analytes eluting from the column. In the detector cell CL is generated by the microperoxidase (MP-11) catalyzed reaction of the photochemically produced hydroperoxides and luminol. The experimental parameters were optimized considering the photochemical reactor and the chemiluminescence detector independently. Optimization of the parameters was directed towards detection of analytes in a gradient reversed-phase chromatographic system and thus restricted by the eluent composition used for separation. The solvent composition was not varied freely; in order to achieve compatibility of the (new) detection system and (gradient) RPLC, it is largely determinated by the eluent required to perform the chromatographic separations. The applicability of the optimized system was evaluated for some model analytes and comparisons were made to the CL detection system based on photochemical generation of dioxetanes and to UV–visible absorption detection. Mechanistic implications with respect to the photo-induced production of hydroperoxides in the photochemical reactor were considered and the influences of some known singlet oxygen quenchers and radical chain inhibitors on the signal were measured. The detection system was applied to the detection of polar pollutants in a gradient reversed-phase chromatographic system, analyzing spiked academic solutions and tap-water samples, in the latter case combined with on-line trace enrichment techniques.

Keywords: Chemiluminescence; Liquid chromatography; Luminol; Photo-oxygenation; Reactive oxygen intermediates

Chemiluminescence (CL) detection in column liquid chromatography (CLC) is known for its extraordinary sensitivity for certain analytes [1,2]. Unfortunately its applicability seems to be rather limited. A basic, but not always sufficient, condition is that the analytes are fluorescent [1,2] (either exhibiting native fluorescence, or provided by a fluorescent tag via chemical derivatisation), or that they play an important role in the mechanism of the CL reaction [1,2]. A well-known example of the latter class is hydrogenperoxide, a crucial compound in for instance the peroxyoxalate CL reaction and the luminol reaction [3–5]. Hydrogen peroxide can be the analyte itself, but also interesting combinations with immobilized enzyme reactors (IMERS) [6–9] and photochemical reactors producing hydrogenperoxide [10–12] have been reported.

Our attention is directed on the CL detection of non-fluorescent analytes (without invoking

Correspondence to: C. Gooijer, Department of General and Analytical Chemistry, Free University, De Boelelaan 1083, 1081 HV Amsterdam (Netherlands).

SSDI 0003-2670(93)E0515-9

chemical derivatisation), as an alternative for UV–visible absorption detection in CLC. Upon irradiation, for this type of analyte, various non-luminescent routes are involved in the deactivation of excited states. In the presence of oxygen one of the most important routes for deactivation is through (direct or indirect) transfer of energy or charge to oxygen. In preceding papers we made use of energy transfer resulting in the formation of singlet molecular oxygen, O_2 ($^1\Delta_g$), a reactive form of oxygen [13,14]. Singlet oxygen was utilized to generate, on-line, 1,2-dioxetanes, which were subsequently detected via thermally induced CL. In the present paper it is the goal to generate noncyclic organic peroxides instead of dioxetanes, which can be eventually detected by standard luminol CL [15–17].

Whether dioxetanes or noncyclic organic peroxides are formed depends on the reagent, provided with an activated carbon–carbon double bond, to capture singlet oxygen. For the formation of dioxetanes, 1,2-diethoxyethene (DEE) has shown to be appropriate [13,14]. 2,3-Dimethyl-2-butene (tetramethylethylene, TME) is expected to be suitable for the generation of noncyclic peroxides. TME is known to react with singlet oxygen by an ene-type mechanism [18]. However TME might also act in an alternative way, for instance as a donor in photoinduced electron transfer [19–22], which may lead to photoinduced electron transfer oxygenation, in situations where the singlet oxygenation is slow [23–26].

In the present paper, first some mechanistic aspects involving TME as reagent are discussed, in order to facilitate an interpretation of the chromatographic results obtained. Subsequently the optimization of the chromatographic system is outlined, considering the post-column photochemical reactor and CL detector performances. The applicability of the system is shown for analyses of polar pollutants in tap water samples, with emphasis on intrinsic selectivity.

MECHANISTIC ASPECTS

As indicated above, upon irradiation of analytes (eluting from the chromatographic column) in the presence of TME, not only have photochemical reactions involving singlet oxygen (Scheme 1) to be considered but also photoinduced electron transfer might play a role. Within this context it is appropriate to distinguish pathways in which the radical ion pair formed dissociates rapidly (Scheme 2) and slowly (Scheme 3).

$$\text{Sensitizer} + h\nu \xrightarrow{k_{abs.}} {}^1\text{Sensitizer}^* \quad (1)$$

$${}^1\text{Sensitizer}^* \xrightarrow{k_{IC}} \text{Sensitizer} \quad (2)$$

$${}^1\text{Sensitizer}^* + O_2\left({}^3\Sigma_g\right) \xrightarrow{k_q(1)} {}^3\text{Sensitizer}^* + O_2\left({}^1\Delta_g\right) \quad (3)$$

$${}^1\text{Sensitizer}^* \xrightarrow{k_{ISC}} {}^3\text{Sensitizer}^* \quad (4)$$

$${}^3\text{Sensitizer}^* + O_2\left({}^3\Sigma_g\right) \xrightarrow{k_q(2)} \text{Sensitizer} + O_2\left({}^1\Delta_g\right) \quad (5)$$

$$O_2\left({}^1\Delta_g\right) \xrightarrow{\tau^{-1}({}^1O_2)} O_2\left({}^3\Sigma_g\right) \quad (6)$$

$$\text{RH} + O_2\left({}^1\Delta_g\right) \xrightarrow{k_{add.}} \text{RO}_2\text{H} \quad (7)$$

Scheme 1.

Singlet oxygen, Scheme 1

Singlet (excited molecular) oxygen is photochemically generated by energy transfer from an excited sensitizer (the analyte eluting from the column) to triplet ground state molecular oxygen [27]. Singlet as well as triplet excited sensitizers can transfer their energy to oxygen (Eqns. 3 and 5) [27–29], but since the lifetime of a triplet excited state is much longer than the lifetime of a

$$\text{Sensitizer} + h\nu \xrightarrow{k_{abs.}} \text{Sensitizer}^* \quad (8)$$

$$\text{Sensitizer}^* + \text{RH} \xrightarrow{k_{ET}(1)} (\text{Sensitizer}^{\cdot-}\,\text{RH}^{\cdot+}) \quad (9)$$

$$(\text{Sensitizer}^{\cdot-}\,\text{RH}^{\cdot+}) \xrightarrow{k_q(3)} \text{Sensitizer} + \text{RH} \quad (10)$$

$$(\text{Sensitizer}^{\cdot-}\,\text{RH}^{\cdot+}) \rightarrow \text{Sensitizer}^{\cdot-} + \text{RH}^{\cdot+} \quad (11)$$

$$\text{Sensitizer}^{\cdot-} + O_2\left({}^3\Sigma_g\right) \xrightarrow{k_{ET}(2)} \text{Sensitizer} + O_2^{\cdot-} \quad (12)$$

$$\text{RH}^{\cdot+} + O_2^{\cdot-} \xrightarrow{k_{add.}(1)} \text{oxygenation products} \quad (13)$$

$$\text{RH}^{\cdot+} + O_2\left({}^3\Sigma_g\right) \xrightarrow{k_{add.}(2)} \text{RHO}_2^{\cdot+} \quad (14)$$

$$\text{RHO}_2^{\cdot+} + \text{RH} \xrightarrow{k_{ET}(3)} \text{RH}^{\cdot+} + \text{oxygenation products} \quad (15)$$

$$(\text{Sensitizer}^{\cdot-}\,\text{RH}^{\cdot+}) + \text{R'OH} \rightarrow \text{Sensitizer}^{\cdot-} + \text{H}^+ + \text{R'ORH}^{\cdot} \quad (16)$$

$$\text{R'ORH}^{\cdot} + O_2\left({}^3\Sigma_g\right) \xrightarrow{k_{add.}(3)} \text{R'ORHO}_2^{\cdot} \quad (17)$$

$$\text{R'ORHO}_2^{\cdot} \xrightarrow{(1)e^-,(2)H^+} \text{R'ORHO}_2\text{H} \quad (18)$$

Scheme 2.

$$\text{Sensitizer} + h\nu \xrightarrow{k_{abs.}} \text{Sensitizer}^* \quad (8)$$

$$\text{Sensitizer}^* + \text{RH} \xrightarrow{k_{ET}(1)} (\text{Sensitizer}^{\cdot-}\ \text{RH}^{\cdot+}) \quad (9)$$

$$(\text{Sensitizer}^{\cdot-}\ \text{RH}^{\cdot+}) \xrightarrow{k_{prot.trans.}} \text{Sensitizer H}^{\cdot} + \text{R}^{\cdot} \quad (19)$$

$$\text{R}^{\cdot} + \text{O}_2\left(^3\Sigma_g\right) \xrightarrow{k_{add.}(4)} \text{RO}_2^{\cdot} \quad (20)$$

$$\text{RO}_2^{\cdot} + \text{RH} \xrightarrow{k_{HAD}} \text{RO}_2\text{H} + \text{R}^{\cdot} \quad (21)$$

Scheme 3.

singlet excited state, the quantum yield for energy transfer from a triplet excited state is strongly dominating [27,28].

Once singlet oxygen is generated, its fate is determined by its lifetime in solution (Eqn. 6), the amount of capture reagent (RH) added (Eqn. 7) and of course the presence of other singlet oxygen quenchers.

The lifetime of singlet oxygen in most solvents used for CLC is very short (only 2–30 μs) [30]. Therefore the rate constant, k_{add}, for reaction of RH with singlet oxygen has to be large. TME reacts with singlet oxygen by an ene-type mechanism, with a reaction rate constant of about 4×10^7 l mol^{-1} s^{-1} [18], so that, depending on the solvent concerned, a TME concentration of 10^{-3} to 10^{-2} M will be required to achieve a quantum yield for production of the noncyclic organic peroxide of about 50%. It should be noted that the sensitizer is not consumed during these processes; thus in principle a large amount of peroxide can be produced for every sensitizer molecule entering the photochemical reactor.

Photoinduced electron transfer, Scheme 2

If oxygenation is initiated by photoinduced electron transfer, the excited sensitizer, with either singlet or triplet spin multiplicity, interacts directly with the reagent RH (Eqn. 9). An obvious requirement for electron transfer is that the electron affinity of the excited sensitizer exceeds the ionization potential of the reagent [23]. The resulting radical ion pair may collapse again within the solvent cage (Eqn. 10), or dissociate to give free ions (Eqn. 11). Subsequently, the radical anion of the sensitizer can act as a donor towards molecular oxygen and restore the sensitizer in the ground state, thus generating superoxide anion (Eqn. 12) [23]. The final step is an addition of superoxide anion to the donor radical cation, $RH^{\cdot+}$, giving rise to oxygenation products (Eqn. 13) [23,24,31,32].

Alternatively the donor radical cation may add to molecular ground state oxygen leading to a chain electron transfer radical cation mechanism (Eqns. 14 and 15) [23,24,31,32].

The choice of the solvent is very important, since the ion pair, formed upon electron transfer (Eqn. 9), will generally only dissociate rapidly in polar solvents [20,33]. Furthermore in hydroxylic solvents, the solvent, denoted as R'OH, may act as a nucleophile towards the donor radical cation (Eqn. 16), facilitating oxygen (Eqns. 17 and 18) [31,34,35] and leading to organic hydroperoxides.

It is known from the literature that TME can act as a donor in photoinduced electron transfer depending on the sensitizer concerned [19–22]. According to Scheme 2 (Eqns. 16 and 17), in hydroxylic solvents enhanced oxygenation of the TME donor radical cation may become important, leading to noncyclic hydroperoxides, so that luminol CL will be applicable for detection. Ethylenes carrying aromatic substituents are generally more susceptible to photoinduced electron transfer oxygenation than TME [24,31,32], but the photo-oxygenation products obtained are generally no hydroperoxides.

Photoinduced electron transfer, Scheme 3

The photoinduced electron transfer reaction may result in a complex between the sensitizer radical anion and the donor radical cation that does not dissociate. In that case electron transfer (Eqn. 9) may be followed by proton donation from $RH^{\cdot+}$ to the radical anion, resulting in a net hydrogen abstraction from the donor by the sensitizer (Eqn. 19) [24,36]. This will lead to a photo-oxygenation of RH, resulting in organic peroxide products (Eqns. 20 and 21). For TME, proton transfer after electron transfer leads to an allyl radical carrying methyl substituents which give extra stabilization [37–39]. If the solvent can act as a hydrogen atom donor [10,36,38,39], it will take part in the radical chain process resulting in long radical chain oxidations.

To summarize this section it should be emphasized that the three mechanistic schemes discussed all lead to the production of (various) organic hydroperoxides. Although detailed structural information about the photochemically generated products is lacking, nevertheless luminol CL can be invoked to detect them [15–17].

EXPERIMENTAL

Equipment

For convenience, three aspects of the experimental set-up are described separately, viz., the chromatographic part, the photochemical reactor part and the CL detector part (see Fig. 1).

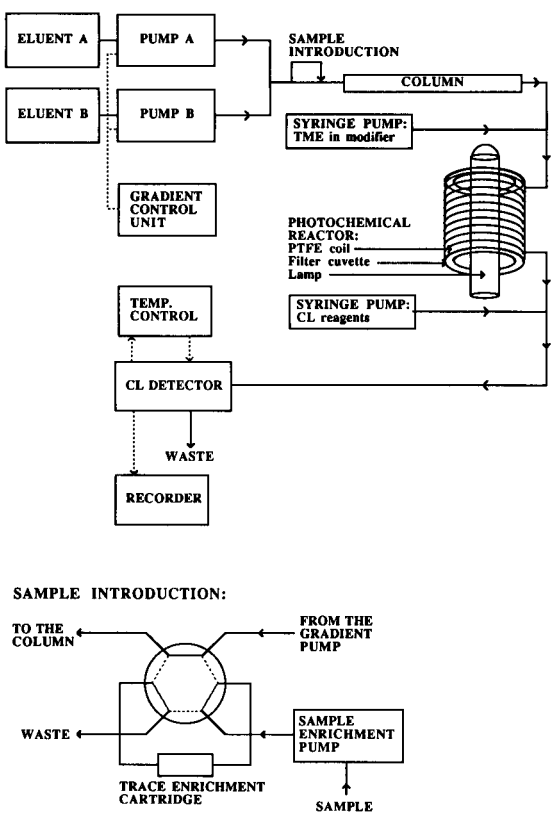

Fig. 1. Experimental set-up for photoinduced oxygenation of TME with CL detection in an LC system. Samples are introduced in a 20-μl injection loop, or by means of a trace enrichment set-up.

The chromatographic part is composed of two Model 400 solvent delivery systems, controlled by the computer of a 1000 S diode array detector (Applied Biosystems, Ramsey, NJ), an analytical column (25 cm × 4.6 mm i.d.), packed with 5-μm Hypersil C_{18} particles (Shandon, Runcorn) and a laboratory-made six-port injection valve (Free University, Amsterdam), equipped with a 20-μl injection loop. For trace enrichment of the analytes the injection loop is exchanged with a laboratory-made cartridge holder (Free University), containing a 10 mm × 4 mm trace enrichment cartridge, packed with 40-μm Bondesil C_{18} particles (Analytichem, Harbor City, CA). Both conditioning of the cartridges and sampling is done with a Model 410 solvent delivery system (Kontron, Zürich). Chromatograms are recorded on a Model BD12 recorder (Kipp & Zonen, Delft).

The photochemical reactor part consists of a Model 93110 (90-W, 25 mm arc length) medium-pressure mercury lamp (Philips, Eindhoven), mounted with a laboratory-made cylindrical quartz filter cuvette (9 mm path length) (Free University). Filter solutions are pumped round, through the filter cuvette and a water cooler, with a Model 1022 centrifugal pump (Eheim, Berlin). The polytetrafluoroethylene (PTFE) reactor tubing (Eriks, Alkmaar), 0.33 mm i.d., 0.73 mm o.d., is knitted around the filter cuvette (diameter 5.7 cm), to decrease band broadening. The tubing is 2.0–10.0 m in length, providing reaction times ranging from 30 s to 2 min 33 s at flow-rates of 0.34 to 0.59 ml min^{-1}.

TME is added with a laboratory-made syringe pump (Free University) at a flow-rate of 0.09 ml min^{-1}. The CL reagents (luminol and microperoxidase) are added with a laboratory-made syringe pump (Free University) at a flow-rate of 0.2 ml min^{-1}.

The CL detector part consists of a Model 970 fluorescence detector (Applied Biosystems) with the lamp turned off and with a 25-μl detector cell installed. The stainless-steel bar containing the cell compartment is adapted with a thermocouple and a thermocoaxial electrical heater. The temperature is controlled with a laboratory-made electronic temperature programmer (Free University) at 45.0 ± 0.1°C. Boiling and creation of

bubbles inside the detector cell are avoided by operating the detector at about 4.5 bar back-pressure.

For comparison with UV absorption detection the CL detector is exchanged for a Model 20 UV–visible variable-wavelength detector (Carlo Erba, Milan).

Batch experiments were performed in a laboratory-made batch CL detector, consisting of a brass cuvette holder for an 1-cm pathlength cuvette, a filter box and a photomultiplier housing. The cuvette holder is provided with channels for circulating water from a thermostat bath, Lauda-Thermostat type B1 (MGW-Lauda). The filter box contains a lens, with a focal point coinciding with the centre of the cuvette, and a 2-cm pathlength filter cuvette, containing a 1.14 M copper sulfate solution. A Hamamatsu R-212 photomultiplier tube (Hamamatsu, Middlesex, NJ) is mounted in the photomultiplier housing, connected to a Thorn EMI PM28B high-voltage power supply (delivered by Intechmij, Diemen), operated at 750 V. Signals are processed by an Ortec Brookdeal 5C1 photon counting device and recorded on a Model BD12 recorder.

Chemicals and reagents

2,3-Dimethyl-2-butene (tetramethylethylene, TME) was delivered by Aldrich (Brussels) and purified by distillation prior to use. A fresh solution in the gradient modifier solvent was made every two or three days. Luminol was supplied by Janssen Chimica (Tilburg) and microperoxidase (MP-11) by the Sigma (St. Louis, MO). Both CL reagents were used as obtained. From a stock of luminol in methanol and a stock of microperoxidase in buffer solution, a fresh solution in methanol–water (70 + 30, v/v), at a pH of 9.9 (4×10^{-3} M $Na_2B_4O_7$ buffer), was made every day.

Acetonitrile was purchased from Westburg (Leusden) and methanol from Baker (Deventer), both LC grade. Milli-Q water was prepared by ultrafiltration using a Milli-Q system (Millipore, Bedford, MA). Disodium terborate, disodium hydrogenphosphate, sodium dihydrogenphosphate, potassium dichromate, potassium hydrogenphthalate, potassium iodide and acetic acid were supplied by Baker.

The various analytes and quenchers were supplied by Fluka (Bornem), Aldrich (Brussels), Kodak (Rochester, NJ), Riedel-de Haen (Seelze) and Jansen Chimica (Tilburg). They all were at least 95% pure. Stock standard solutions of the analytes and quenchers (10^{-3} to 10^{-4} M) were prepared (every 1 or 2 months) in acetonitrile, methanol, or eluent and stored at 4°C in the dark.

Filter solutions were made in deionized water. They will be referred to in the text as follows: $\lambda \geqslant 240$ nm is 40% (w/v) acetic acid, $\lambda \geqslant 260$ nm is 1.2% (w/v) potassium iodide in 0.5 M sodium hydroxide, $\lambda \geqslant 300$ nm is 0.6% (w/v) potassium hydrogenphthalate and $\lambda \geqslant 495$ nm is 0.5% (w/v) potassium dichromate.

Procedures

The model analytes and the quenchers were analysed in an isocratic CLC system and a flow-injection analysis (FIA) system, respectively. The mobile phase composition was acetonitrile–water (80 + 20, v/v) for the model analytes and acetonitrile–5×10^{-3} M buffer (pH 6.6) (70 + 30, v/v) for the quenchers.

The gradient conditions for analysis of polar pollutants in academic solutions and tap-water samples were as follows: solvent A, modifier–5×10^{-3} M phosphate buffer (pH 6.6) (90 + 10, v/v) and solvent B, modifier–5×10^{-3} M phosphate buffer (pH 6.6) (10 + 90, v/v), where the modifier is either acetonitrile, or methanol. The gradient profile started at 95% B (0 min), changed linearly to 95% A (36 min) and was kept constant at 95% A (46 min); finally it was changed linearly back to 95% B (48 min). The flow-rate was 0.5 ml min^{-1}.

The trace enrichment cartridges were cleaned prior to use by a gradient run and conditioned before each run with 50 ml of Milli-Q water (5 ml min^{-1}). Subsequently 100 ml of sample was enriched on the cartridges at a flow-rate of about 5 ml min^{-1}. The adsorbed material in the cartridges was desorbed by coupling the cartridges on line with the analytical column and starting the gradient run.

In the batch experiments a quartz cuvette, containing 1 ml of a solution [methanol water (70 + 30, v/v)] buffered with 4×10^{-3} M $Na_2B_4O_7$ at pH 9.9, containing luminol and microperoxidase at the desired concentrations, is placed in the batch detector and stirred until the desired temperature is reached. 0.5 ml of 7.3×10^{-6} M rose bengal and 1.0×10^{-2} M of TME in methanol, oxygenated for 30 min in front of a 150-W xenon arc lamp, is added with a syringe within 1 s (through a septum in the cuvette holder housing) and the CL is monitored.

RESULTS AND DISCUSSION

In order to optimize the detection system concerned, i.e., photochemical generation of reactive oxygen intermediates leading to a product that can be detected by luminol chemiluminescence, it is appropriate to make a distinction between the photochemical reactor conditions and the chemiluminescence detector conditions. Subsequently in this section an evaluation of the results will be presented, with emphasis on the reaction mechanism that plays a role in reversed-phase eluents and on the potential applicability of the detection method described in comparison to the possibilities provided by the dioxetane chemiluminescence method reported earlier [13,14].

In the final part of this section the present method is applied to the gradient LC of polar pollutants in tap-water, utilizing trace enrichment techniques, recently improved in our laboratory [40,41].

It should be emphasized that for the optimization of the photochemical processes and of the chemical luminescence detection processes there is no freedom of solvent choice; the choice is determined by the eluent composition utilized to achieve optimum separation. In order to realise a broad applicability of the detection method under concern, the choice of the eluent should not be limited at all (in the ideal situation). Our attention is focused on reversed-phase eluents, covering about 80% of the LC analyses.

Photochemical reactor

As outlined in the introductory part, the reagent chosen to react with the reactive oxygen intermediates is TME.

The remaining reactor parameters that have to be considered are: (i) the spectral window that can be applied in the photochemical reactor (evidently auto-oxidation of TME, giving rise to a high background signal, has to be prevented), (ii)

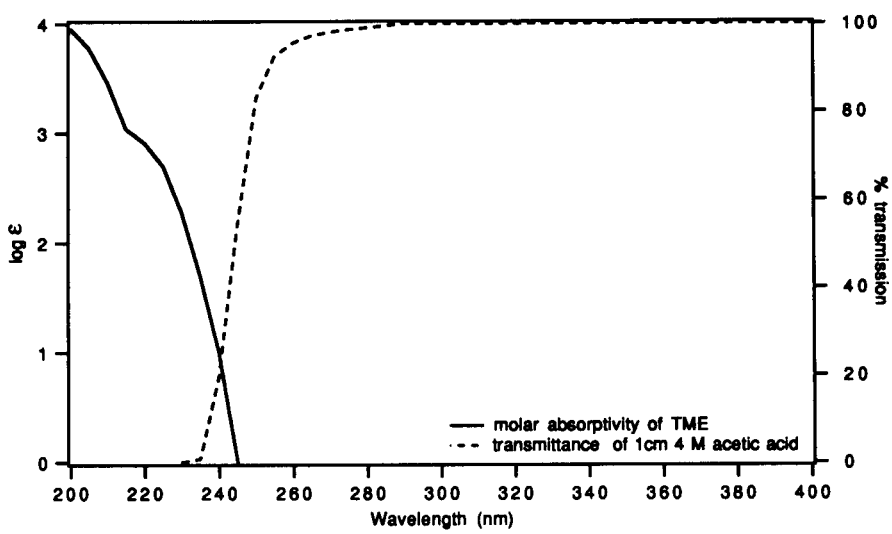

Fig. 2. Absorption spectrum of TME and transmittance of the filter solution (4 M acetic acid) in the 9-mm cuvette.

the concentration of TME, (iii) the influence of the solvent composition and (iv) the irradiation time. Of course these parameters will not be fully independent. However, since the specific nature of the eluting analytes will also play a role, it is not our objective to define the optimum strictly, but only to achieve amenable conditions.

Spectral window. The choice of TME as the reagent (RH) for oxidation is based on its absorption spectrum on the one hand and its reactivity (both towards singlet oxygen and in photoinduced electron transfer) on the other. If RH would absorb radiation at the wavelengths where the photochemical reactor is operated, this will normally result in autoxidation, thus giving a high background signal. For this reason only a reagent with a limited absorption spectrum will allow a large spectral window for irradiation of the sensitizers. TME absorbs light in the region between 200 and 240 nm, thus leaving the complete lamp spectrum longer than 240 nm open for irradiation (Fig. 2). Irradiation of TME can be avoided with a 4 M (1 cm pathlength) acetic acid filter, absorbing the short wavelength irradiation of the lamp with a cut-off at 240 nm (Fig. 2).

Concentration of TME. The first point to be noted here is that TME is needed to generate a CL signal. In absence of TME not any (background) signal is detected, whereas in the presence of TME, but in absence of analytes, a background is observed.

The reactor concentration of TME has to be high, since its quenching reaction with excited sensitizer (Eqn. 9) and/or its reaction with singlet oxygen (Eqn. 7) has to compete with the rapid decay of these species. It was observed that increasing the TME concentration with a factor of 12 from 2.5×10^{-3} to 3.0×10^{-2} M only results in a 4-fold increase in sensitized organic peroxide yield. Since background oxidation also increases with TME concentration, higher concentrations than 5×10^{-3} M will not significantly improve sensitivity. In practice, if chromatographic gradient profiles starting at high water percentages are used, TME concentrations should not exceed 5×10^{-3} M, for solubility reasons.

Solvent composition. Depending on the irradiation wavelengths applied, the solvent composition proved to have a large effect on the background yield of organic peroxide. For methanol as modi-

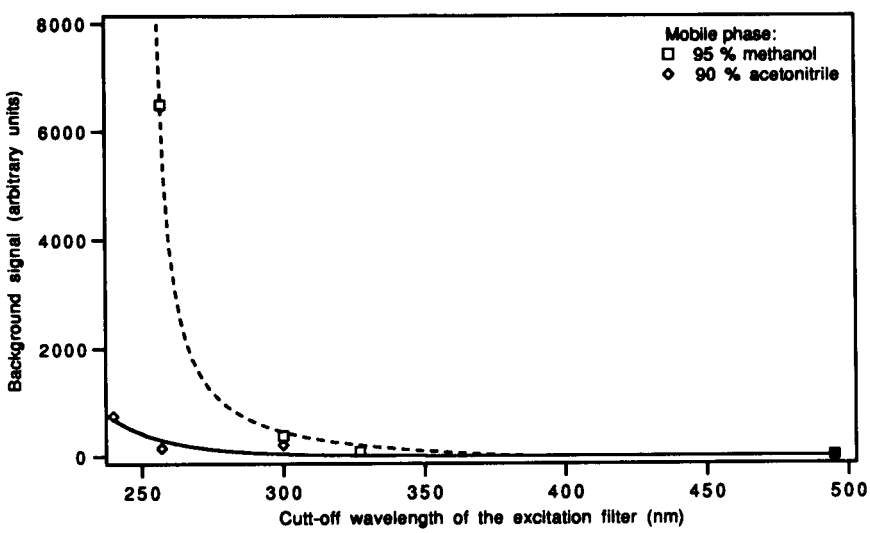

Fig. 3. Influence of the excitation window on the background CL intensity in a flow system for two mobile phase modifiers (acetonitrile and methanol). Relative standard deviation ranges from 10% for the low background signals to 20% for the highest background signal.

$$R_aOOR_b + h\nu \rightarrow R_aO^{\cdot} + R_bO^{\cdot} \quad (22)$$

$$R_aO^{\cdot} + R_cH \rightarrow R_aOH + R_c^{\cdot} \quad (23)$$

$$R_c^{\cdot} + O_2\left({}^3\Sigma_g\right) \rightarrow R_cO_2^{\cdot} \quad (24)$$

$$R_cO_2^{\cdot} + R_cH \rightarrow R_cO_2H + R_c^{\cdot} \quad (25)$$

Scheme 4.

fier, background oxidation is very high if irradiation includes wavelengths shorter than 300 nm (Fig. 3). On the contrary the use of acetonitrile as modifier does not result in high background oxidation at short irradiation wavelengths (Fig. 3).

The strong wavelength dependence of the background oxidation may be explained by the photoinduced homolytic dissociation that is well known for peroxides [42]. Organic peroxides absorb light at short wavelengths up to about 300 nm. Absorption may cause rupture of the O–O bond resulting in two organic oxy-radicals, thus initiating radical chain processes (Scheme 4).

The strong background observed in methanol compared to the background in acetonitrile can be ascribed to the hydrogen donor ability of the solvent, which is absent in acetonitrile, but might be important for methanol [10,38,39]. Presumably methanol acts as a hydrogen atom donor in the radical chain process (Scheme 4) and/or as a nucleophile in a photoinduced electron transfer oxygenation (Scheme 2) as described by Mattes and Farid [34,35].

From a chromatographic points of view these findings imply that separations can only be performed in methanol–water provided that the photochemical reactor is operated at wavelengths longer than 300 nm. For acetonitrile such a serious limitation is not encountered. Therefore most analyses described below were performed in acetonitrile–water mixtures which generally offer similar chromatographic separation power as methanol–water eluents.

Irradiation time. The optimal irradiation time was determined in a LC system utilizing acetonitrile–water (80 + 20, v/v) as the mobile phase, by recording the CL signal-to-noise ratio as a function of irradiation time. As expected, the optimum is dependent on the analyte (sensitizer) under consideration. For rose bengal there is no more improvement in signal-to-noise ratio for irradiation times longer than about 90 s (Fig. 4). For 4,4′-dichlorobiphenyl and 4,4′-dibromobiphenyl, however, the signal-to-noise ratio does not reach a maximum in a relevant time range; it increases linearly with the irradiation time up to 150 s (Fig. 4). For 1,4-dinitronaphthalene and

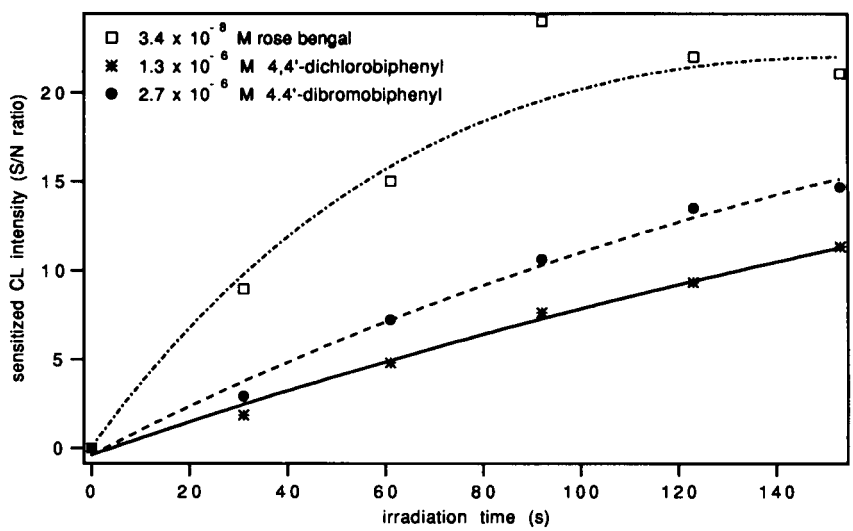

Fig. 4. Influence of irradiation time on signal-to-noise ratio for three model analytes (rose bengal, 4,4′-dichlorobiphenyl and 4,4′-dibromobiphenyl) in a flow system. Mobile phase, acetonitrile–water (80 + 20, v/v). Relative standard deviation is about 40% for rose bengal and 15% for both other compounds.

2,2′-dibromobiphenyl a quenching effect is found for irradiation times shorter than about 40 s; for irradiation times longer than 60 s the signal-to-noise ratio increases (more or less) linearly for 1,4-dinitronaphthalene and exponentially for 2,2′-dibromobiphenyl (Fig. 5). The background signal is relatively insensitive to irradiation time and only rises by a factor of about 1.5 from a background-to-noise ratio of 40 at 30 s to 60 at 150 s irradiation time. Taking into account that, for practical reasons, the irradiation time should be as short as possible, the obtained results indicate that an amenable irradiation time of 90 s should be sufficient. Besides it is noted that the standard deviation in the signal-to-noise ratio of rose bengal is relatively large (40%), since it elutes at t_0 (zero retention).

Chemiluminescence detector

Although in many luminol chemiluminescence applications hydrogen peroxide is the peroxide applied, luminol CL is also applicable to organic peroxides, provided that microperoxidase (at a high pH) is utilized as the catalyst [15–17]. Hence in order to achieve optimum detection conditions the parameters to be considered are the concentration of luminol and of the catalyst and the role of the temperature and solvent composition. As regards the last parameter it should be realized that in the chromatographic system luminol and microperoxidase are added as a solution in methanol–water (70 + 30, v/v), irrespective of the eluent composition utilized. Besides it is noted that using isoluminol as an alternative to luminol does hardly influence the signal-to-background ratio obtained; in the present paper the attention is confined to luminol.

Ideally the organic peroxides are exclusively generated through photo-oxygenation induced by the analytes eluting from the chromatographic column. In reality there is a background caused by organic peroxides present in the eluent and reagent flows and/or generated during the irradiation.

Batch experiments. Chemiluminescence intensity was recorded as a function of time, for various luminol concentrations, microperoxidase concentrations and temperatures. The chemiluminescence profile shows a maximum, within 60 s after starting depending on temperature and reagent concentration, followed by a slow decay back to zero intensity. The effects of the variables are well characterised by the values of maximum intensity and integrated intensity. No background CL was measured if luminol, the catalyst, or the peroxide were absent.

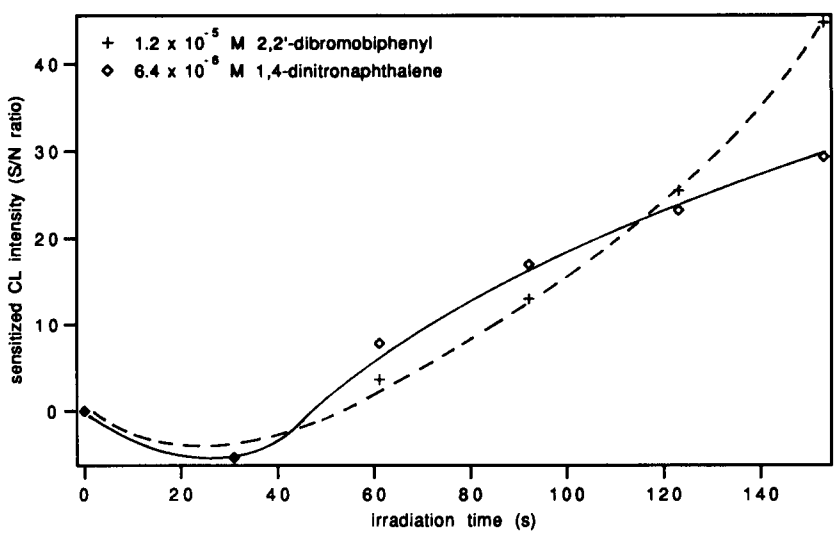

Fig. 5. Influence of irradiation time on signal-to-noise ratio for two model analytes (2,2′-dibromobiphenyl and 1,4-dinitronaphthalene) in a flow system. Mobile phase, acetonitrile–water (80 + 20, v/v). Relative standard deviation is 15%.

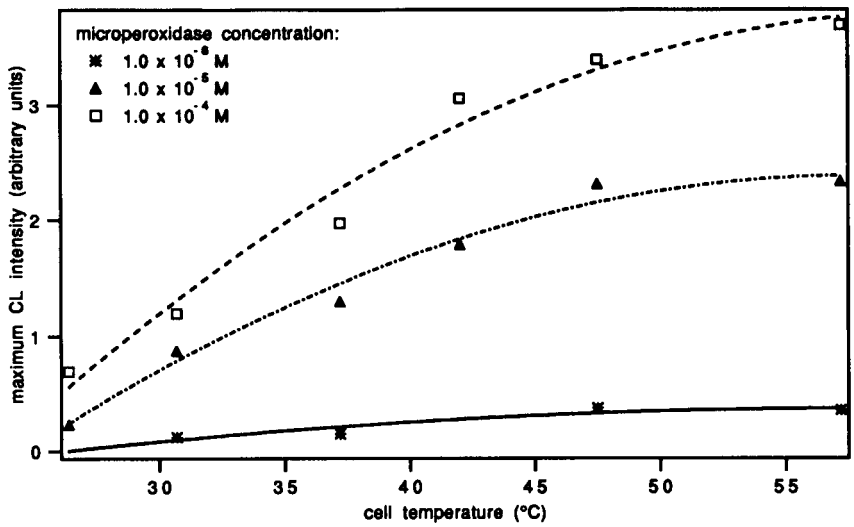

Fig. 6. Influence of cell temperature on maximum CL intensity in a batch system, for three microperoxidase concentrations. Relative standard deviation is estimated to be about 10%.

The experiments (performed at pH 9.9) revealed that the maximum value of the CL signal increases almost in proportion on raising the luminol concentration up to about 2.3×10^{-3} M. Higher luminol concentrations are not amenable for solubility reasons; in practice the luminol concentration was kept as high as possible.

Furthermore it was observed that maximum chemiluminescence intensity increases about one decade upon increasing the MP-11 concentration from 1.0×10^{-6} to 1.0×10^{-5} M; subsequently it rises by only a factor of about 1.5 upon going to 1.0×10^{-4} M (see Fig. 6). Moreover a microperoxidase concentration as high as 1.0×10^{-4} M also causes very fast chemiluminescence kinetics giving rise to short chemiluminescence pulses, with little integrated intensity, that are difficult to handle. From Fig. 7 it can be seen that, even

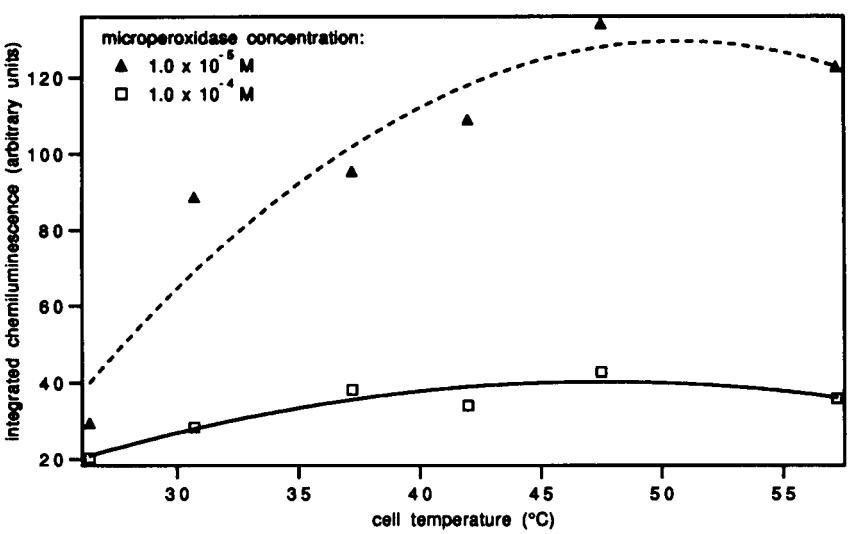

Fig. 7. Influence of cell temperature on integrated CL intensity in a batch system, for two microperoxidase concentrations. Relative standard deviation is estimated to be about 10%.

though the maximum chemiluminescence intensity is somewhat higher for 1.0×10^{-4} M MP-11 than for 1.0×10^{-5} M, the integrated chemiluminescence intensity is much more favourable for 1.0×10^{-5} M MP-11.

Raising the temperature does result in higher maximum chemiluminescence intensities and faster kinetics at the catalyst concentrations examined, but only a little extra intensity is gained at temperatures higher than 45°C. Figure 6 shows maximum chemiluminescence intensity as a function of temperature for three microperoxidase concentrations and Fig. 7 shows the integrated chemiluminescence intensity as a function of temperature for the two highest microperoxidase concentrations.

The above results indicate that a microperoxidase concentration of 1.0×10^{-5} M at a temperature of about 45°C gives optimum results. Higher MP-11 concentrations are not needed, an interesting result from an economic point of view.

Flow experiments. It should be realized that in a flow system only a part of the total (integrated) CL intensity is monitored, i.e., the part corresponding with the residence time of the sample in the detector flow cell. Without considering details such as analyte eluting band profile, consumption of peroxides and luminol during the CL reaction and possible temperature gradient in the detector cell, under the flow conditions in our system the maximum CL intensity in the batch experiments is a good indication for the CL signal recorded in the flow system. Since higher temperatures and higher MP-11 concentrations have only a little effect on the maximum chemiluminescence intensities observed in the batch experiments (see Fig. 6), in LC a microperoxidase concentration of 1.0×10^{-5} M and a detector cell temperature of 45°C were applied. Under these circumstances, it was observed that a set-up without a mixing-coil in between the addition point of the chemiluminescence reagents, and the detector gives the best results. The relatively high temperature in the detector flow cell, as compared to the temperature in the mixing coil and the connections to the detector (ambient temperature), does probably imply that the CL kinetics are determined mainly by the residence time in the detector flow cell.

Evaluation

Model studies. The investigations outline above indicate that optimization of the experimental parameters for reactor and detector results in a detection system that can be used in a reversed-phase chromatographic system with a wide variety of mobile phase compositions. At irradiation wavelengths longer than 240 nm, acetonitrile–water mixtures are appropriate, while at wavelengths longer than 300 nm both acetonitrile–

TABLE 1

Comparison of detection limits for some model analytes obtained by (1) photoinduced oxygenation of TME with luminol CL detection for two irradiation windows, transmitting at wavelengths longer than 240 and 260 nm respectively; (2) dioxetane CL detection for an irradiation window transmitting at wavelengths longer than 260 nm; (3) UV–visible absorption detection at optimum wavelengths longer than 260 nm

Analyte	Detection limits (signal-to-noise ratio = 3) (mol l^{-1})			
	Method B [b]		Method A [b]	UV absorption
	$\lambda \geqslant 240$ nm	$\lambda \geqslant 260$ nm	$\lambda \geqslant 260$ nm	$\lambda \geqslant 260$ nm
1,4-Dinitronaphthalene	5×10^{-7}	7×10^{-7}	5×10^{-7}	3×10^{-7}
1,4-Dibromonaphthalene	3×10^{-7}	4×10^{-7}	2×10^{-7}	2×10^{-7}
2,2′-Dibromobiphenyl	– [a]	1×10^{-6}	2×10^{-7}	2×10^{-7}
4,4′-Dichlorobiphenyl	– [a]	4×10^{-7}	5×10^{-8}	1×10^{-7}
Rose bengal	3×10^{-9}	3×10^{-9}	5×10^{-9}	2×10^{-8}
Anthracene	3×10^{-8}	– [a]	2×10^{-8}	2×10^{-7}

[a] Not measured, [b] Method B is photo-oxygenation of TME with luminol CL detection, method A is photo-oxygenation of DEE with dioxetane CL detection.

water and methanol–water mixtures are applicable. In the experiments described below TME was added as a solution in the mobile phase modifier and the CL reagents as a solution in methanol–water (70 + 30, v/v), buffered at pH 9.9, irrespective of the eluent applied.

Reversed-phase liquid chromatograms for some model analytes in an isocratic system [acetonitrile–water (80 + 20, v/v)], applying two irradiance conditions, were recorded and the associated molar concentration detection limits (signal-to-noise ratio = 3) were calculated. Linear calibration graphs were obtained over at least two decades of concentration starting from the detection limit ($r \geqslant 0.998$, $n = 5$).

In Table 1 the present results, denoted as method B, are compared to those obtained by the photochemically induced dioxetane chemiluminescence detection system described in a previous paper [14], denoted as method A, and to data obtained by UV–visible absorption detection.

The collected data (Table 1) show that for most compounds the limits of detection obtained by UV absorption and the two CL detection methods are similar, i.e., of the order of 10^{-7} M. However, some exceptions should be noted, i.e., 4,4′-dibromobiphenyl, rose bengal and anthracene; especially the latter two are clearly better detected by methods A and B.

Another point to be noted is that the present CL method and method A show some difference in selectivity. Upon irradiation in the region $\geqslant$ 260 nm there is only a minor difference in the detection by method A or B for 1,4-dinitronaphthalene, 1,4-dibromonaphthalene and rose bengal; on the contrary, for 2,2′-dibromobiphenyl and 4,4′-dichlorobiphenyl detection by method B is about one order of magnitude less sensitive than detection by method A. Such a difference should not be expected if in both methods A and B exclusively the singlet oxygen pathway would be operative. Presumably, the mechanisms responsible for the photochemical production of a reactive oxygen intermediate are fundamentally different.

Mechanistic implications. It is known that method A is exclusively based on singlet oxygen formation eventually leading to dioxetanes. On

TABLE 2

Effects of some known singlet oxygen quenchers and radical chain inhibitors on the luminol chemiluminescence signal based on rose bengal photoinduced oxygenation of TME. (A) The effect on the photoinduced oxygenation of TME and the luminol chemiluminescence detection together (total process). (B) The separate effect on the luminol chemiluminescence detection (detector process)

quencher	Concentration range [b] (mol l^{-1})	Stern-Volmer constants for quenching (l mol^{-1})	
		Total process	Detector process
For singlet oxygen			
DABCO [a]	1×10^{-5}–1×10^{-3}	no quenching	no quenching
Triethylamine	4×10^{-4}–4×10^{-3}	no quenching	not measured
Pentamethylpiperidine [a]	2×10^{-5}–2×10^{-3}	non-linear quenching [c]	non-linear quenching [c]
For radical chains			
Trolox [a]	1×10^{-7}–1×10^{-5}	1.5×10^{6} [d]	1.4×10^{6} [d]
BHT [a]	1×10^{-6}–1×10^{-4}	8×10^{4} [d]	7×10^{4} [d]
2,6-Di-*tert*-butylphenol	1×10^{-6}–6×10^{-4}	9×10^{3} [d]	9×10^{3} [d]
Benzoquinone	1×10^{-8}–1×10^{-6}	4×10^{7} [d]	3×10^{7} [d]

[a] DABCO-1,4-Diazabicyclo[2,2,2]octane, pentamethylpiperidine = 1,2,2,6,6-pentamethylpiperidine, Trolox = 6-hydroxy-2,5,7,8-tetramethylchroman-2-carboxylic acid; BHT = 2,6-di-tert-butyl-4-methylphenol. [b] Injected concentrations, dilution in the reactor is a factor 1.33. [c] All concentrations gave a similar amount of quenching, in the detector as well as in the total process (about 17% decrease in signal intensity). [d] Relative standard deviations are about 10% for Trolox and benzoquinone and about 3% for BHT and 2,6-di-*tert*-butylphenol.

the contrary, as outlined above, in method B in addition to the mechanism in Scheme 1 the pathways in Scheme 2 or Scheme 3 might play a role.

As far as its reactivity is concerned TME is a known reagent for singlet oxygen, with a high reaction rate constant [18]. TME is also a well-studied donor in photoinduced electron transfer processes, with good (sufficient) electron donating ability [19–22]. Oxygenation of TME usually commences through addition of singlet oxygen [20], but if the oxygen concentration is relatively low, or if hydroxylic solvents are used [34,35], some sensitizers may give rise to photoinduced electron transfer oxygenation.

In order to get some insight in the "TME mechanism", operative in reversed-phase solvents, a FIA system was utilized to monitor the influence of some potential quenchers. Rose bengal was spiked into the TME flow and irradiation was at $\geqslant 495$ nm, to generate a continuous signal at a signal-to-noise ratio of about 80. Then 1,4-diazabicyclo[2,2,2]octane (DABCO), a well-known singlet oxygen quencher [30], was injected in the main flow. No quenching of the chemiluminescence signal was observed (Table 2), which clearly indicates that the singlet oxygen mechanism does not play a significant role under the experimental conditions concerned; obviously another reaction pathway is followed. This might be unexpected since rose bengal is a known singlet oxygen sensitizer [27]. However, as shown in the literature, rose bengal can also act as an acceptor in photoinduced electron transfer [43,44]. Therefore, even for rose bengal, in the presence of TME oxygenation may be caused by a photoinduced electron transfer mechanism. This assumption is supported by results obtained for some other potential quenchers in the same FIA system. Indeed injecting some known radical chain inhibitors [23,42,45] and superoxide scavengers [23,46] leads to a strong quenching of the recorded signal (Table 2). Unfortunately also the luminol CL reaction is negatively influenced; in fact the corrections for quenching effects on the detector processes are so large, that possible effects in the photochemical reactor are largely obscured (Table 2).

Application to polar pollutants

Academic solutions. Polar pollutants represent a class of analytes with an increasing importance in analytical chemistry [47,48]. In a reversed-phase gradient chromatographic system some polar pollutants were determined by UV absorption detec-

TABLE 3

Comparison of detection limits for some polar pollutants in a gradient LC system obtained by (1) photoinduced oxygenation of TME with luminol CL detection for two irradiation windows, transmitting at wavelengths longer than 240 and 300 nm, and two gradient modifiers; (2) dioxetane CL detection for an irradiation window, transmitting at wavelengths longer than 240 nm, and acetonitrile as the gradient modifier; (3) UV–visible absorption detection at 300 nm and acetonitrile as the gradient modifier

Analyte	Detection limits (signal to noise ratio = 3) (mol l^{-1})				
	Method B [a]			Method A [a]	UV
	Methanol, $\lambda \geqslant 300$ nm	Acetonitrile		Acetonitrile, $\lambda \geqslant 240$ nm	Acetonitrile, $\lambda = 300$ nm
		$\lambda \geqslant 300$ nm	$\lambda \geqslant 240$ nm		
Warfarin	3×10^{-6}	5×10^{-7}	4×10^{-7}	2×10^{-5}	4×10^{-7}
Metamitron	2×10^{-8}	3×10^{-8}	2×10^{-8}	3×10^{-6}	4×10^{-7}
Dinoterb	$> 10^{-4}$	$> 10^{-4}$	$> 10^{-4}$	$> 10^{-4}$	1×10^{-6}
2-Aminoanthraquinone	8×10^{-7}	5×10^{-6}	1×10^{-6}	1×10^{-5}	2×10^{-7}
3,3'-Dichlorobenzidine	4×10^{-7}	3×10^{-6}	4×10^{-6}	1×10^{-5}	8×10^{-7}
1-Aminoanthraquinone	6×10^{-7}	4×10^{-6}	1×10^{-6}	2×10^{-6}	4×10^{-7}

[a] Method B is photo-oxygenation of TME with luminol CL detection, method A is photo-oxygenation of DEE with dioxetane CL detection.

tion and the two photochemically initiated chemiluminescence detection methods denoted as A and B. The associated detection limits, calculated from the chromatograms, are presented in Table 3; no corrections were made for differences in retention times.

Table 3 reveals some interesting features. First of all, comparing luminol CL detection (method B) and dioxetane CL detection (method A) in acetonitrile, both after irradiation at wavelengths $\geqslant 240$ nm, the detection limits observed follow the same trend, but the values obtained in method B are clearly more favorable (at least one order of magnitude, except for 1-aminoanthraquinone). Secondly, the data measured in methods A and B depend strongly on the analyte concerned, whereas for UV absorption detection the detection limits obtained are very similar (ranging from 10^{-7} to 10^{-6} M).

The most striking results are obtained for dinoterb, metamitron and 3,3′-dichlorobenzidine. Dinoterb, having a concentration detection limit of 1×10^{-6} M in UV absorption detection, cannot be detected by CL up to concentrations as high as 1×10^{-4} M. For metamitron the luminol CL detection limit is 2×10^{-8} M (20-fold more favorable than in UV absorption), whereas the dioxetane CL detection limit (3×10^{-6} M) is 8-fold worse compared to UV absorption. Rather unexpected, 3,3′-dichlorobenzidine produces a negative (inverted) chromatographic peak in luminol CL, whereas in dioxetane CL and of course in absorption detection a normal, positive peak is observed. Thus, the detection limit in method B (4×10^{-6} M), presented in Table 3, is associated with a negative peak. Apparently 3,3′-dichlorobenzidine operates as a sensitizer in method A, as anticipated, but as a quencher (of the background signal) in method B.

It is not easy to give a full explanation for these observations. Of course, in general terms the different behaviors should be ascribed to the fact that in method A the formation of singlet oxygen is the crucial step, whereas in method B photoinduced electron transfer might be of utmost importance. Thus, method A will be most sensitive for analytes with a high intersystem crossing efficiency to produce triplet excited states upon irradiation. Method B will be especially sensitive for analytes with a high electron affinity. In the specific case of 3,3′-dichlorobenzidine, the analyte behaves similar to the radical chain inhibitors and/or superoxide scavengers assembled in Table 2: it probably quenches both the photochemical processes and the luminol CL detection processes.

At any rate, from an analytical point of view, the results indicate an interesting feature of selectivity for the detection methods concerned, especially for method B, the luminol CL detection method.

As anticipated on the basis of the mechanistic aspects discussed above, for method B there is a strong influence of the modifier on the detection limits observed. In view of the hydrogen donating potential of methanol, higher CL signals would be expected for methanol than for acetonitrile. Such a trend is indeed observed, especially for the analytes eluting at long retention times (high modifier concentrations); i.e., 2-aminoanthraquinone, 3,3′-dichlorobenzidine and 1-aminoanthraquinone. It should be noted that part of this modifier effect may also be due to the better nucleophilicity of methanol over acetonitrile, possibly resulting in enhanced oxygenation as described in Eqns. 16, 17 and 18 in Scheme 2.

As was stated previously, in order to avoid a high background level, an irradiation window with a cut-off at shorter wavelengths than 300 nm can only be applied if acetonitrile is used as a modifier. At wavelengths longer than 300 nm the difference in background signal-to-noise ratio for both modifiers is only a factor of two; i.e., 70 and 150 for acetonitrile and methanol respectively. From Table 3 it can be seen that, for acetonitrile as a modifier, using $\geqslant 240$ nm excitation does not seriously improve the detection limits obtained. The background signal-to-noise ratio also changes marginally as compared to $\geqslant 300$ nm excitation, i.e., from 70 to 100. Thus applying an excitation filter at a shorter cut-off wavelength than 300 nm will only be useful for analytes that do not absorb radiation at longer wavelengths.

Tap water samples. The applicability of CL detection initiated by photo-oxygenation of TME (method B) in standard reversed-phase LC sys-

tems is illustrated by the analyses of polar pollutants in tap water, using preconcentration and gradient elution separation techniques.

Analysis systems for polar pollutants have been developed, in order to monitor them in various types of water [40,41]. These systems generally make use of gradient column liquid chromatography. On-line trace enrichment techniques and diode array detection are used to enhance sensitivity and selectivity respectively [40,41].

The detection method (method B) discussed in the present paper offers an interesting different selectivity compared to absorption detection, as can be seen from the example described below.

A tap water sample was spiked with polar pollutants at concentrations of 4 to 80 ng ml^{-1} and acidified to pH 3. A portion of 100 ml of the sample was preconcentrated on a RP-18 trace enrichment cartridge and subsequently separated by acetonitrile–water gradient elution over a RP-18 analytical column, as described in the experimental section. Detection was performed on-line by luminol chemiluminescence detection based on photoinduced oxygenation of TME (method B). The resulting chromatogram is presented in Fig. 8.

It is obvious that the pollutants shown give good chromatographic peaks in the low ng ml^{-1} range; signal-to-noise ratios are between 40 and 600 on a CL background signal-to-noise ratio of about 50. For warfarin, chloridazon, bromacil and 1-aminoanthraquinone sub-ng ml^{-1} detection limits are found (0.2–0.7 ng ml^{-1}, $0.7–3.1 \times 10^{-9}$ mol l^{-1}). For atrazine a relatively high detection limit is obtained (6 ng ml^{-1}, 3.0×10^{-8} mol l^{-1}), which will be mainly due to its unfavorable ab-

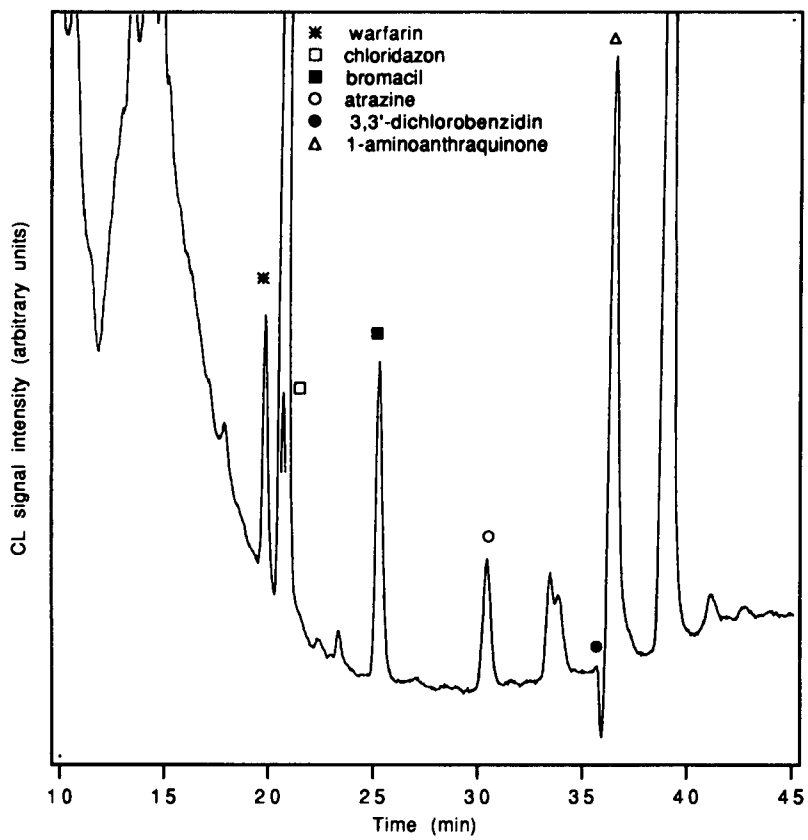

Fig. 8. Chromatogram of 100 ml of enriched tap water spiked with 6 polar pollutants. Concentrations in tap water are: warfarin, 4 ng ml^{-1}; chloridazon, 49 ng ml^{-1}; bromacil, 19 ng ml^{-1}; atrazine, 82 ng ml^{-1}; 3,3′-dichlorobenzidine, 26 ng ml^{-1}; 1-aminoanthraquinone, 45 ng ml^{-1}. The signal for chloridazon is at half scale.

sorption spectrum (the absorption of atrazine is mainly situated at wavelengths < 240 nm). For 3,3′-dichlorobenzidine, as was stated previously, an inverted (negative) chromatographic peak is obtained. Although this leads to a relatively high detection limit (2 ng ml^{-1}, 0.9×10^{-8} mol l^{-1}), selectivity is greatly enhanced. Whereas in UV absorption detection, where of course only positive chromatographic peaks are obtained, it would be impossible to distinguish the almost coeluting 1-aminoanthraquinone and 3,3′-dichlorobenzidine, for the luminol chemiluminescence detection system described both compounds are clearly observable.

Conclusions

The new detection method in column liquid chromatography described above, i.e., post-column photo-oxygenation of TME (induced by the eluting analytes) and subsequent luminol chemiluminescence detection, can be successfully applied as an alternative for UV–visible absorption detection. For various analytes it offers comparable sensitivity but quite a different selectivity, in comparison to absorption detection. The method can be applied in (gradient) reversed-phase separations using acetonitrile–water; in methanol–water its applicability is limited to analytes with an absorption spectrum extending to wavelengths longer than 300 nm.

The same experimental set-up can be utilized to monitor dioxetane CL; in that case 1,2-diethoxyethene (DEE) is used instead of TME. It should be emphasized that (most probably) the photo-oxygenation mechanisms for DEE and TME are essentially different: the present results indicate that, contrary to DEE, for TME photoinduced electron transfer initiates the reaction, whereas singlet oxygen hardly plays any role. This is in line with the observations that typical singlet oxygen quenchers like DABCO do not influence the detection process at all. The above considerations imply that the flow system developed here might be utilized to characterize quenching agents, frequently used in farmacological studies on oxidative stress [49]. These investigations are currently underway [50].

REFERENCES

1 C. Gooijer, N.H. Velthorst and R.W. Frei, in K. Zech and R.W. Frei (Eds.), Selective Sample Handling and Detection in High Performance Liquid Chromatography, Part B (Journal of Chromatography Library, Vol. 39B), Elsevier, Amsterdam, 1989, p. 260.
2 T.A. Nieman, in J.W. Birks (Ed.), Chemiluminescence and Photochemical Reaction Detection in Chromatography, VCH, New York, 1989, p. 99.
3 P. van Zoonen, D.A. Kamminga, C. Gooijer, N.H. Velthorst and R.W. Frei, Anal. Chim. Acta, 167 (1985) 249.
4 P. van Zoonen, D.A. Kamminga, C. Gooijer, N.H. Velthorst, R.W. Frei and G. Gübitz, Anal. Chim. Acta, 1974 (1985) 151.
5 K. Hool and T.A. Nieman, Anal. Chem., 60 (1988) 834.
6 D.T. Bostick and C.M. Hercules, Anal. Chem., 47 (1975) 447.
7 G. Scott, W.R. Seitz and J. Ambrose, Anal. Chim. Acta, 115 (1980) 221.
8 D. Pilosof and T.A. Nieman, Anal. Chem., 54 (1982) 1698.
9 P. van Zoonen, I. de Herder, C. Gooijer, N.H. Velthorst, R.W. Frei, E. Küntzberg and G. Gübitz, Anal. Lett., 19 (1986) 1949.
10 M.S. Gandelman and J.W. Birks, J. Chromatogr. 242 (1982) 21.
11 J.R. Poulson, J.W. Birks, G. Gübitz, P. van Zoonen, C. Gooijer, N.H. Velthorst and R.W. Frei, J. Chromatogr., 360 (1986) 371.
12 J.R. Poulson, J.W. Birks, P. van Zoonen, C. Gooijer, N.H. Velthorst and R.W. Frei, Chromatographia, 21 (1986) 587.
13 H.A.G. Niederländer, F.W. Engelaer, C. Gooijer and N.H. Velthorst, in P.E. Stanley and L.J. Kricka (Eds.), Bioluminescence and Chemiluminescence Current Status, Wiley, Chichester, 1991, p. 227.
14 H.A.G. Niederländer, W. van Assema, F.W. Engelaer, C. Gooijer and N.H. Velthorst, Anal. Chim. Acta, 255 (1991) 395.
15 Y. Yamamoto, M.H. Brodsky, J.C. Baker and B.N. Ames, Anal. Biochem., 160 (1987) 7.
16 B. Frei, Y. Yamamoto, D. Niclas and B.N. Ames, Anal. Biochem., 160 (1988) 120.
17 T. Miyazawa, K. Yasuda, K. Fujimoto and T. Kaneda, Anal. Lett., 21 (1988) 1033.
18 K. Gollnick and H.J. Kuhn, in H.H. Wasserman and R.W. Murray (Eds.), Singlet Oxygen (Organic Chemistry, Vol. 40), Academic Press, New York, 1979, p. 287.
19 D.R. Arnold, P.C. Wong, A.J. Maroulis and T.S. Cameron, Pure Appl. Chem., 52 (1980) 2609.
20 A. Albini and S. Spreti, Gazz. Chim. Ital., 115 (1985) 227.
21 J. Gersdorf, J. Mattay and H. Görner, J. Am. Chem. Soc., 109 (1987) 1203.
22 J. Mattay, J. Gersdorf and K. Buchkremer, Chem. Ber., 120 (1987) 307.
23 L. Lopez, in J. Mattay (Ed.), Photoinduced Electron Transfer, Part I (Topics in Current Chemistry, Vol. 156), Springer Verlag, Berlin, 1990, p. 117.

24 K. Gollnick and A. Schnatterer, Photochem. Photobiol., 43 (1986) 365.
25 C.S. Foote, Tetrahedron, 41 (1985) 2221.
26 Y. Araki, D.C. Dobrowolski, T.E. Goyne, D.C. Hanson, Z.Q. Jiang, K.J. Lee and C.S. Foote, J. Am. Chem. Soc., 106 (1984) 4570.
27 I. Rosenthal, in A.A. Frimer (Ed.), Singlet Oxygen, Vol. I (physical-chemical aspects), CRC Press, Boca Raton, FL, 1985, p. 13.
28 B. Stevens, K.L. March and J.A. Barltrop, J. Phys. Chem., 85 (1981) 3079.
29 D.C. Dobrowolski, P.R. Ogilby and C.S. Foote, J. Phys. Chem., 87 (1983) 2261.
30 B.M. Monroe, in A.A. Frimer (Ed.), Singlet Oxygen, Vol. I (physical-chemical aspects), CRC Press, Boca Raton, FL, 1985, p. 177.
31 J. Eriksen and C.S. Foote, J. Am. Chem. Soc., 102 (1980) 6083.
32 A.P. Schaap, K.A. Zaklika, B. Kaskar and L.W.-M. Fung, J. Am. Chem. Soc., 102 (1980) 389.
33 G.J. Kavarnos, in J. Mattay (Ed.), Photoinduced Electron Transfer, Part I (Topics in Current Chemistry, Vol. 156), Springer Verlag, Berlin, 1990, p. 21.
34 S.L. Mattes and S. Farid, J. Chem. Soc. Chem. Commun., (1980) 457.
35 S.L. Mattes and S. Farid, J. Am. Chem. Soc., 104 (1982) 1454.
36 N.J. Turro, in Modern Molecular Photochemistry, Benjamin/Cummings, Menlo Park, CA, 1978, p. 362.
37 N.J. Turro, K. Shima, C.-J. Chung, C. Tanielian and S. Kanfer, Tetrahedron Lett., 21 (1980) 2775.
38 H.G. Viehe, R. Merényi, L. Stella and Z. Janousek, Angew. Chem., Int. Ed. Eng., 18 (1979) 917.
39 G.A. Russel, in J.K. Kochi (Ed.), Free Radicals, Part I, Wiley, Chichester, 1973, p. 275.
40 E.R. Brouwer, T.M. Tol, H. Lingeman and U.A.Th. Brinkman, Chromatographia, submitted for publication.
41 J. Slobodnik, E.R. Brouwer, R.B. Geerdink, W.H. Mulder, H. Lingeman and U.A.Th. Brinkman, Anal. Chim. Acta., 268 (1992) 55.
42 Y. Ogata, K. Tomizawa and K. Futura, in S. Patai (Ed.), Peroxides (The Chemistry of Functional Groups), Wiley, Chichester, 1983, p. 711.
43 M. Kojima, Y. Kurijama, H. Sakuragi and K. Tokumaru, Bull. Chem. Soc. Jpn., 64 (1991) 2724.
44 T. Sarna, J. Zajac, M.K. Bowman and T.G. Truscott, J. Photochem. Photobiol (A: Chem.), 60 (1991) 295.
45 G. Scott, Pure Appl. Chem., 52 (1980) 365.
46 A.A. Frimer, in S. Patai (Ed.), Peroxides (The Chemistry of Functional Groups), Wiley, Chichester, 1983, p. 429.
47 E.R. Brouwer, I. Liska, R.B. Geerdink, P.C.M. Frintrop, W.H. Mulder, H. Lingeman and U.A.Th. Brinkman, Chromatographia, 32 (1991) 445.
48 I. Liska, E.R. Brouwer, A.G.L. Ostheimer, H. Lingeman, U.A.Th. Brinkman, R.B. Geerdink and W.H. Mulder, Int. J. Environ. Anal. Chem., 47 (1992) 267.
49 P. Di Mascio, M.E. Murphy and H. Sies, Am. J. Clin. Nutr., 53 (1991) 194S.
50 H.A.G. Niederländer, M.M. de Jong, C. Gooijer and N.H. Velthorst, in preparation.

Analytica Chimica Acta, 285 (1994) 161–168
Elsevier Science B.V., Amsterdam

Separation of metal ions by reversed-phase liquid chromatography using on-column complexation with 2-pyridinecarboxylic acid

Pavel N. Nesterenko, Gul'banu Zh. Amirova and Taisia A. Bol'shova

Department of Analytical Chemistry, Lomonosov State University, 117899, Moscow (Russian Federation)

(Received 28th April 1993; revised manuscript received 26th July 1993)

Abstract

Picolinic acid was used as an on-column chelating agent for the reversed-phase liquid chromatographic separation of manganese(II), copper(II), nickel(II), cobalt(II), cadmium(II) and zinc(II). The effects of picolinic acid concentration, pH and type and content of organic solvent on the retention of transition metal ions have been studied. The possibility of sensitive UV detection of complexes at 235 nm is demonstrated. Data on the use of studied system for the determination of some metal ions in a galvanic bath waste water are presented.

Keywords: Liquid chromatography; Complexation; Metal ions; Picolinic acid; Pyridinecarboxylic acid; Waters

In recent years, on-column complexation has become one of the most promising techniques in the separation of metal ions by reversed-phase liquid chromatography (RPLC) or complexation ion chromatography (IC) [1,2]. The on-column formation of complexes allows the direct introduction of metal ions into the chromatographic system, which eliminates the extraction step in sample preparation. The presence of a complexing agent in mobile phase also provides stabilization of the separated form of the complexes and a higher reproducibility of analysis.

However, this technique requires good kinetics of complexation and no ligand interference in the detection of metal ions. The application of many reagents such as quinolin-8-ol, 4-(2-pyridylazo)resorcinol, dithiocarbamates, *o*-phenanthroline and complexones as chelating additives to the mobile phase in RPLC were reviewed by Marina et al. [1]. The application of *N*-propionyl-*N*-methylhydroxylamine [3], nitrosonaphthol sulphonates [4] and trisodium 2-(*p*-sulphophenylazo)-1,8-dihydroxynaphthalene-3,6-disulphonate [5] for this purpose has also been reported.

Pyridinecarboxylic acids are a promising group of reagents for on-column complexation. These compounds are water-soluble and rapidly form stable water-soluble complexes with transition metals. 2,6-Pyridinedicarboxylic acid (dipicolinic acid) is a commonly used eluent in IC for the separation of lanthanides and transition metals [6,7]. However, little attention has been paid to the use as an eluent additive of another good chelating agent with a similar structure, 2-pyridinecarboxylic (picolinic acid). There are only a few reports on the application of picolinic acid for the separation of alkali metals by cation-exchange chromatography [8] and for the separation of transition metals by complexation chromatography [9,10].

Correspondence to: P.N. Nesterenko, Department of Analytical Chemistry, Lomonosov State University, 117899, Moscow (Russian Federation).

SSDI 0003-2670(93)E0474-L

These applications of mobile phases containing picolinic acid involved indirect spectrophotometric detection at 320 nm for alkali metal ions [8] and postcolumn reaction with quinolin-8-ol and spectrophotometric detection at 405 nm for transition metals [9,10]. There have been no attempts to use the absorption of metal complexes with picolinic acid in the UV region for direct spectrophotometric detection.

The purpose of this work was to develop an RPLC method based on metal complexation with picolinic acid for the separation and determination of transition metals.

EXPERIMENTAL

Apparatus

Liquid chromatography was carried out using a Beckman (Berkeley, CA) Model 114M pump fitted with a Rheodyne (Cotati, CA) Model 7125 injection valve equipped with a 20-μl loop. Spherisorb ODS (250 × 4.6 mm i.d., 5-μm) and Ultrasphere ODS (250 × 4.6 mm i.d., 5-μm) columns were employed for optimization of separation and for the determination of transition metals in waste waters. The chromatograms were detected using a Linear (Reno, NV) UVIS 204 variable-wavelength spectrophotometric detector equipped with a micro flow cell (volume 9 μl, path length 3 mm). All separations were performed at a flow-rate of 1.0 ml min^{-1}.

Absorption spectra of complexes and the mobile phase were obtained in the stop-flow mode with a Linear UVIS 204 UV–visible scanning detector and with a Hitachi Model 124 spectrophotometer.

Reagents

Mobile phases with pH between 3.5 and 7.5 were prepared by adjusting the pH of 10^{-2}–10^{-3} M picolinic acid with 1 M sodium hydroxide solution followed by mixing with an organic solvent in the required proportions. Before use the mobile phase was filtered using a Millipore system with 0.47-μm filters.

Pure picolinic acid was purchased from Reakhim (Moscow) and recrystallized from water before use. Analytical-reagent grade metal nitrate salts were used. LC-grade acetonitrile, methanol and tetrahydrofuran were purchased from J.T. Baker (Phillipsburg, NJ). Water was purified by distillation of demineralized water. Metal ion stock solutions were prepared by dissolving the corresponding analytical-reagent grade nitrates in distilled water. Iron(II) was used in the form of ammonium iron(II) sulphate.

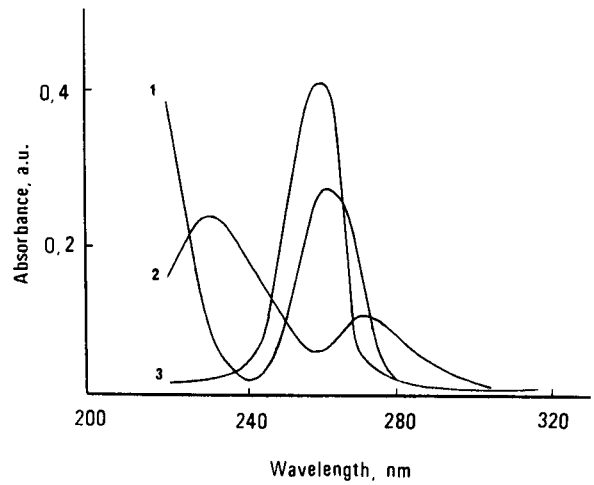

Fig. 1. Absorption spectra of (1) the mobile phase, consisting of acetonitrile–water (6+94, v/v), containing 5×10^{-3} M picolinic acid (pH 6.0) and of on-column formed complexes of (2) nickel and (3) cobalt.

RESULTS AND DISCUSSION

Detection of metal–picolinic acid complexes

The absorption spectra (Fig. 1) indicate two absorption maxima in the UV region both for picolinic acid at wavelengths of $\lambda^1_{pic} = 210$ nm ($\varepsilon^1_{pic} = 7300$ l mol^{-1} cm^{-1}) and $\lambda^2_{pic} = 265$ nm ($\varepsilon^2_{pic} = 4000$ l mol^{-1} cm^{-1} [11]) and for metal complexes ($\lambda^1 = 230$ nm; $\lambda^2 = 265$ nm). There is a significant difference between the wavelength of the first absorption maximum for the complexes and for the reagent. This provides the possibility of detection of metals as complexes. It is convenient that almost all of the investigated metal complexes have similar absorption spectra. The only exception is the picolinate of cobalt(II), which has a single absorption band with a maximum at

TABLE 1

Molar absorptivities (l mol^{-1} cm^{-1}) of metal complexes with picolinic acid at pH 7.0

Metal	Ni(II)	Co(II)	Cu(II)	Pb(II)	Fe(III)	HPic
ε(235 nm)	2.2×10^3	3.1×10^3	6.7×10^3	4.0×10^3	5.0×10^3	50
ε(280 nm)	1.0×10^3	1.1×10^3	8.0×10^2	8.0×10^2	1.0×10^3	3
ε(310 nm)	2.0×10^2	1.5×10^3	1.5×10^2	–	3.3×10^3	0

265 nm (Fig. 1). The molar absorptivities of the metal chelates at different wavelengths are presented in Table 1. Based on these results, a wavelength of 235 nm was chosen as optimum for the direct detection of separated metal ions.

Separation of metal–picolinic acid complexes

To establish the optimum chromatographic conditions, the effect of the mobile phase composition on the retention of on-column formed complexes was investigated. Picolinic acid can be considered as a multifunctional component of the mobile phase which provides simultaneously complexing, buffering and colour-forming actions. The degree of complexation of metal ions depends mainly on the pH of the mobile phase and the concentration of ligand in mobile phase.

Influence of mobile phase pH

Picolinic acid is a strong chelating agent which produces stable complexes with a large number of transition metals in weak acid and neutral media. It has been shown [12,13] that full complexation for all the studied metals in solution can be achieved with a ten-fold excess of picolinic acid at pH 6.

The influence of pH on the retention of some metal complexes with a constant concentration of picolinic acid in the eluent is shown in Fig. 2. The curves obtained consist of three different parts. First, an increase in retention time with increase in pH of the mobile phase from 4.5 to 5.5–6.0 was observed for Fe(II), Mn(II) and Co(II), that is, for the metals producing the least stable complexes among those examined. Apparently, this effect can be simply explained by an increase in the degree of complex formation. Second, the retention of all the metals studied hardly changed in the pH range 6.0–7.0, indicating relatively rapid and complete formation of stable $MPic_3$ complexes for Ni(II), Co(II), Mn(II), Fe(II, III) and an $MPic_2$ complex for Cu(II). Third, a further increase in pH up to 8.0 decreases the retention of iron(III). It is evident that this effect is connected with the partial formation of a more stable $Fe(OH)Pic_2$ hydroxy complex (log $\beta_3 = 23.8$ [13]) in neutral and slightly basic media. This complex, of course, is weakly retained in comparison with $FePic_3$. It leads to better selectivity of the separation of Fe(III) and Mn(II). However, the efficiency of separation decreases with increase in pH.

Summarizing the data obtained, the pH range 6.0–7.0 provides the optimum conditions for the formation and selective separation of metal complexes with picolinic acid. It is also in good agreement with the demand of restricted pH for the stable operation of chromatographic columns packed with silica-based sorbents.

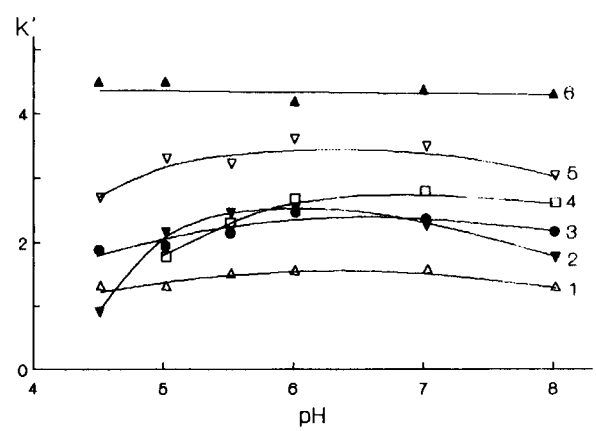

Fig. 2. Influence of pH on the retention of metal–picolinic acid complexes. Column, Ultrasphere ODS (250 × 4.6 mm i.d.; 5 μm). Mobile phase, acetronitrile–water (1 + 9, v/v) containing 5×10^{-3} M picolinic acid. 1 = Ni(II); 2 = Fe(III); 3 = Co(II); 4 = Mn(II); 5 = Fe(II); 6 = Cu(II).

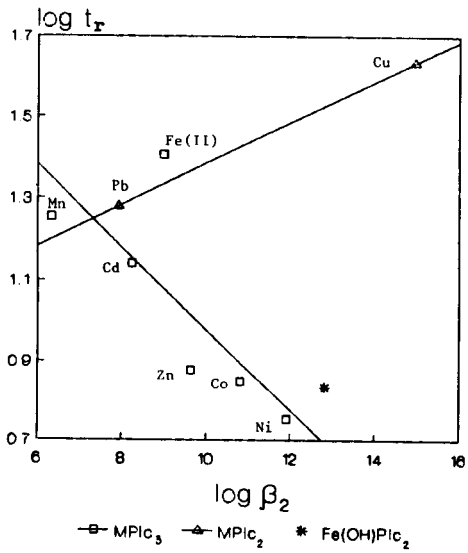

Fig. 3. Relationship between log t_r and log β_2 [12] of the neutral $MPic_2$ and negatively charged $MPic_3$ complexes of transition metals with picolinic acid. □ = $MPic_3$; △ = $MPic_2$; * = $Fe(OH)Pic_2$.

The retention order of the metals obtained at the optimum pH value is well correlated with the charge and the composition of the complexes formed. As shown in Fig. 3, the more stable the neutral complex $MPic_2$, the stronger is its retention in the column. In contrast, the retention of negatively charged $MPic_3$ complexes decreases with increasing stability of the complexes. Overall, for the neutral complexes with a metal-to-ligand ratio of 1:2 the retention time is greater than for negatively charged complexes with a ratio of 1:3.

Influence of concentration of chelating agent

Another factor of great significance for the retention of transition metal complexes is the concentration of picolinic acid in the mobile phase. The retention of metals with on-column complexation is due to the effects of different separated forms of the metals, such as Me, MeL and MeL_2. A higher concentration of ligand in the mobile phase leads to more complete and rapid complexation. It provides a longer section of column through which the injected metals pass in a more hydrophobic and more strongly retained form. Figure 4 shows the effect of picolinic acid concentration in the mobile phase on the retention times of five metal ions and complexes. For Co(II), Ni(II), Mn(II) and Fe(II) the capacity factors increase as the concentration of picolinic acid in the mobile phase increases. At the same time, the peak areas of all the complexes were approximately constant in the picolinic acid concentration range 2.0×10^{-3}–1×10^{-2} M (Table 2). This corresponds to the completness of the complexation in the output from the chromatographic column and to the identity of the eluted forms.

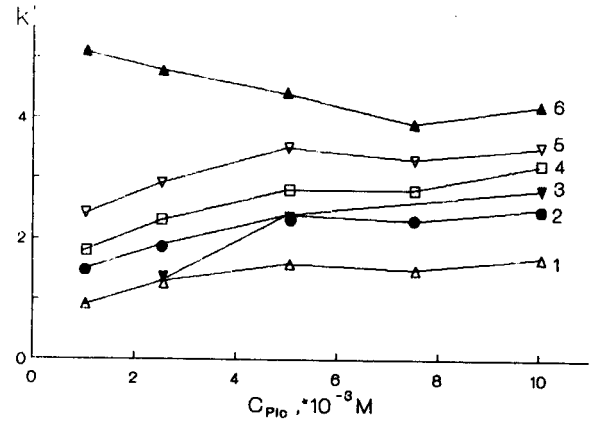

Fig. 4. Effect of concentration of picolinic acid on the retention of metal complexes. Column, Ultrasphere ODS (250×4.6 mm i.d.; 5 μm). Mobile phase, acetonitrile–water (1+9, v/v) containing picolinic acid (pH 7.0). 1 = Ni(II); 2 = Co(II); 3 = Fe(III); 4 = Mn(II); 5 = Fe(II); 6 = Cu(II).

TABLE 2

Variation of peak area (S, integr. units$\times 10^{-5}$) of various metals with concentration of picolinic acid in the mobile phase [Spherisorb ODS column, 250×4.6 mm i.d., with acetonitrile–water (1+9) containing picolinic acid (pH 7.0) as eluent]

Metals	Concentration of picolinic acid (10^{-3} M)				
	1.0	2.5	5.0	7.5	10.0
Copper	27	30	33	32	31
Cobalt	131	133	130	126	128
Iron(II)	72	69	73	65	70
Iron(III)	122	117	132	–	–
Manganese	18	30	34	31	32

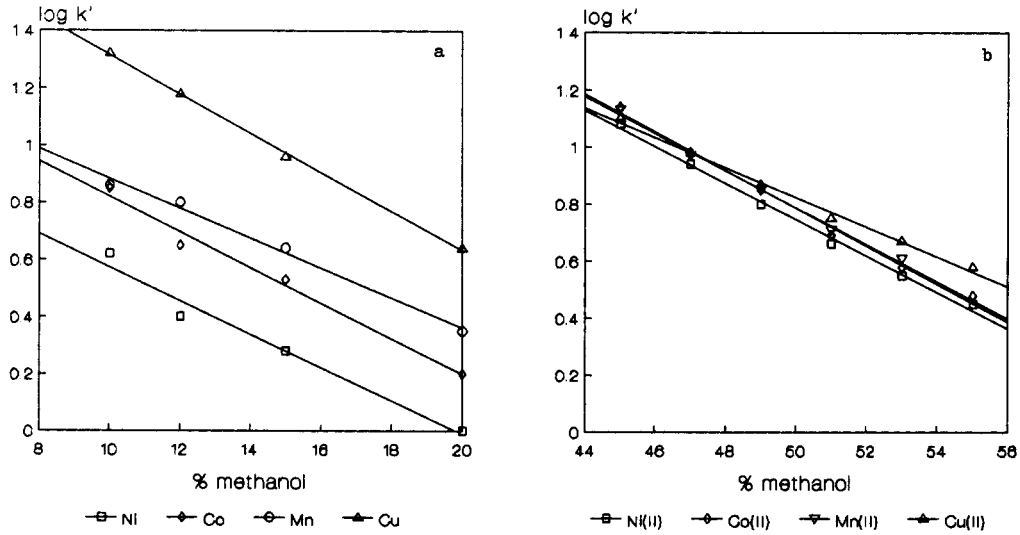

Fig. 5. Effect of the methanol concentration in the mobile phase on the retention of on-column formed complexes of metals with (a) picolinic acid and (b) quinol-8-ol (calculated from [18]). Column: (a) Spherisorb ODS (250 × 4.6 mm i.d.; 5 μm); (b) LiChrosorb RP-8 (150 × 4.6 mm i.d.; 5 μm). Concentration of reagent in mobile phase, 5×10^{-3} M. pH = (a) 7.0 and (b) 8.5. (a) □ = Ni(II); ◇ = Co(II); ○ = Mn(II); △ = Cu(II). (b) □ = Ni(II); ◇ = Co(II); ▽ = Mn(II); △ = Cu(II).

Also, it was found that the chromatographic peaks of all the complexes were broadened with concentrations of picolinic acid in the mobile phase lower than 2×10^{-3} M. This fact corresponds to the data obtained by RPLC with another complexing agent, EDTA [14]. Such broadening of peaks may be caused by the deficiency of picolinic acid in the mobile phase necessary to suppress the adsorption of complexes on active sites of reversed-phase silica [15]. On the other hand, the baseline noise with spectrophotometric detection at 235 nm is high when the picolinic acid concentration in the mobile phase is above 2×10^{-3} M. Hence a 2×10^{-3} M concentration of reagent was adopted as the optimum for further experiments.

Influence of nature and percentage of organic solvent

Figure 5 shows that the logarithm of the capacity factor (log k') for the on-column formed complexes of manganese, copper, nickel and cobalt decreases linearly with the increasing methanol content in the mobile phase. It is important that the variation of organic solvent content does not produce changes in the retention order of the complexes. However, the peaks were broadened and tailed when a low content of organic solvent was present.

Acetonitrile, methanol and tetrahydrofuran were examined as organic modifiers. A comparison of the influence of these solvents on the retention of the copper complex with picolinic acid is presented in Fig. 6. In all instances log k'

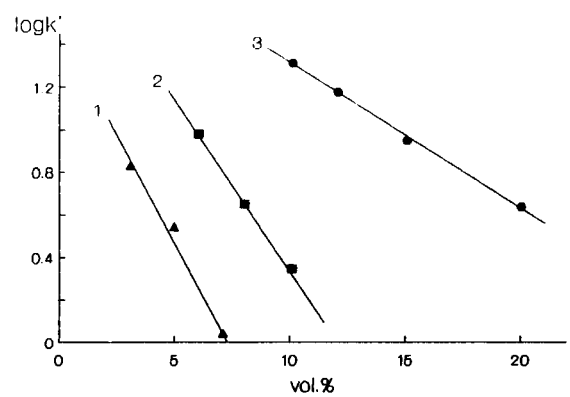

Fig. 6. Influence of the nature of the organic solvent in the mobile phase on the retention of copper picolinate. Mobile phase, 5×10^{-3} M picolinic acid (pH 7.0) with various concentrations of (1) tetrahydrofuran, (2) acetonitrile and (3) methanol.

TABLE 3

Variation of efficiency (N, theoretical plates), peak area (S, integr. units) and selectivity of separation ($\alpha = k'_i/k'_{i+1}$) with temperature of column [a]

Temperature (°C)	Parameter	Ni(II)		Co(II)		Zn(II)		Cd(II)		Mn(II)		Fe(II)
20	$N \times 10^{-3}$	0.7		1.8		2.0		2.3		3.9		2.2
	$S \times 10^{-6}$	3.5		8.1		3.9		4.6		3.0		0.3
	α		1.40		1.10		2.18		1.36		1.75	
32	$N \times 10^{-3}$	1.9		1.5		1.9		2.6		4.3		3.7
	$S \times 10^{-6}$	3.5		8.0		3.8		3.1		2.4		1.0
	α		1.61		1.27		2.42		1.92		2.83	
45	$N \times 10^{-3}$	1.0		1.4		–		3.9		5.5		No peak
	$S \times 10^{-6}$	3.1		7.5		–		2.3		1.7		obtained
	α		1.84		1.36		2.41		2.09			
65	$N \times 10^{-3}$	– [b]		2.8		2.8		7.4		4.8		No peak
	$S \times 10^{-6}$			7.8		5.0		5.3		4.1		obtained
	α		2.26		1.70		2.26		2.46			

[a] Chromatographic conditions: column, Spherisorb ODS (250 × 4.6 mm i.d.); mobile phase, acetonitrile–water (6 + 94) containing 2×10^{-3} M picolinic acid (pH 7.0); flow-rate, 1 ml min^{-1}.

of the copper complex decreased linearly with increase in organic solvent content. This is in good agreement with the theory of RPLC. The selectivity of separation of complexes with picolinic acid was similar for the different organic solvents. Overall, the eluent based on acetonitrile–water provides better chromatographic separation than the methanol–water and tetrahydrofuran–water eluents from the point of view of broadening and symmetry of the peaks. The optimum resolution of peaks was obtained with 6–8% acetonitrile.

It is interesting to compare the selectivity of the RPLC separation of on-column formed complexes with picolinic acid and with the commonly used quinolin-8-ol. The results obtained (Fig. 5) demonstrate the advantage of the former reagent.

Influence of column temperature

The possible usefulness of increasing the temperature of the chromatographic column is based on two main factors. First, it leads to higher efficiency of separation owing to a decrease in the viscosity of the mobile phase. Second, it facilitates the rapid and complete complexation of the separated metals. The effect of increasing the column temperature was evaluated by comparison of the retention times, column efficiency, selectivity and peak areas obtained for various metals at 20, 32, 45 and 65°C (Table 3). As shown in Fig. 7, the retention of the complexes with picolinic acid decreases with increase in column temperature. It is interesting that the relationships between log k' and $1/T$ are not linear, which contradicts the theory of chromatography, but it can be explained by non-equilibrium complexation of the metals with picolinic acid at the top of chromatographic column. However, in each instance the values of peak areas obtained for

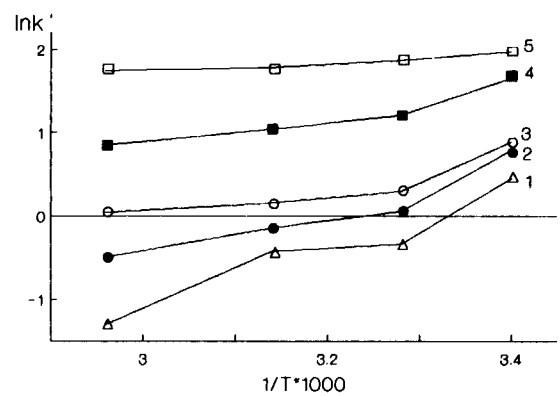

Fig. 7. Dependence of log k' of picolinates of (1) nickel, (2) cobalt, (3) zinc, (4) cadmium and (5) manganese on $1/T$. Column, Spherisorb ODS (250×4.6 mm i.d.; 5 μm). Mobile phase, acetonitrile–water (6+94) containing 2×10^{-3} M picolinic acid (pH 7.0); flow-rate, 1.0 ml min^{-1}.

TABLE 4

Calibration data and detection limits for trace metal analysis [a]

Metal	Range (ng)	Slope (integr. units ng^{-1})	Intercept on peak area axis	r	R.S.D. (%) [b]	Detection limit at 235 nm (ng)
Zn(II)	5 – 800	2.00×10^7	-0.11×10^6	0.999	0.29	2.5
Cd(II)	20 –1000	1.0×10^7	-5.5×10^6	0.999	2.72	10
Mn(II)	2.5–1000	1.6×10^7	-0.03×10^6	0.999	0.12	1
Cu(II)	20 – 200	4.6×10^7	-0.25×10^6	0.988	1.49	10
Ni(II)	20 –5000	3.5×10^7	-1.8×10^6	0.998	0.86	15
Fe(II)	10 –5000	2.6×10^7	-8.9×10^6	0.999	3.39	5
Co(II)	10 –5000	4.1×10^7	-1.4×10^6	0.998	1.21	1

[a] Mobile phase and column as in Fig. 8, [b] $n = 3$.

equal amounts of injected metal ions at different temperatures were similar (Table 3).

An increase in column efficiency up to 1.5–3.0 times with increase in column temperature was observed for all the metals. At the same time the selectivity of separation (α) remained virtually unchanged over the temperature range studied and the level of noises of the spectrophotometric detector increased significantly. Hence it was concluded that room temperature provides the optimum conditions for the determination of metals.

Loadability of column

A practically important aspect of the application of the proposed method is the loadability of the column with on-column formation of complexes. The maximum amount of ions that can be injected into the column is proportional to the concentration of complexing agent in the eluent, column length, retention times of metal ions and metal-to-ligand ratio for the complexes produced [16]. A 5% decrease in column efficiency due to complex formation should be also taken into consideration [17]. From the above, one can calculate that the loadability of the column under the optimum conditions should be equal to 5 μg. A similar value was obtained from the data for the maximum amounts of metal ions that produce a linear response of detector (Table 4).

A typical chromatogram for the separation of the seven complexes under the optimum conditions is shown in Fig. 8. All peaks are well resolved.

Determination of transition metals

The proposed RPLC method can be applied to the determination of transition metal ions in in-

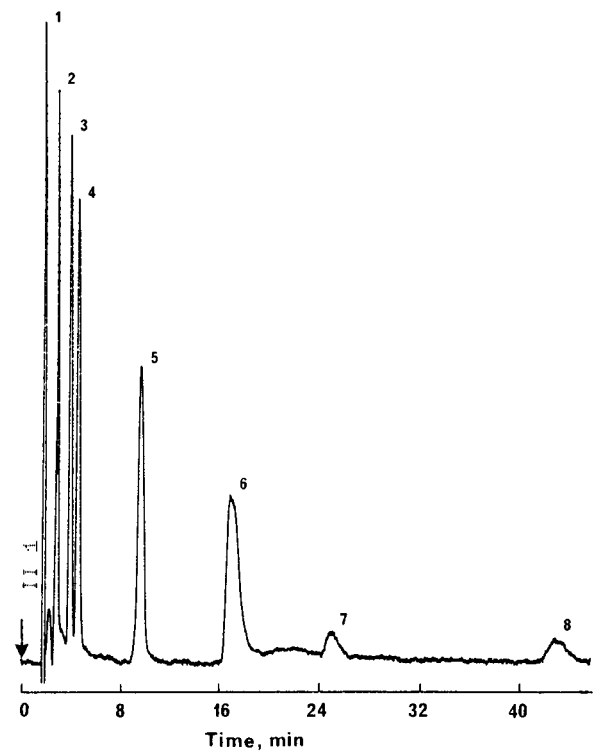

Fig. 8. Chromatogram of standard mixture of metals. Column, Spherisorb ODS (250×4.6 mm i.d.; 5 μm). Mobile phase, acetonitrile–water (6+94, v/v) containing 2×10^{-3} M picolinic acid (pH 7.0); flow-rate, 1.0 ml min^{-1}; detection at 235 nm; injection volume, 50 μl. Peaks: 1 = system peak; 2 = 68 ng Ni(II); 3 = 339 ng Co(II); 4 = 678 μg Zn(II); 5 = 1.7 μg Cd(II); 6 = 1.27 μg Mn(II); 7 = 200 ng Fe(II) 8 = 1.86 μg Cu(II).

TABLE 5

Determination of metals in industrial waste water from a galvanic bath (for passivation of Zn and Cd) ($n = 5$, $P = 0.95$)

Metal	Concentration (mg ml^{-1})[a]	
	RPLC	ICP-AES [b]
Zn	0.70 ± 0.06	0.77 ± 0.02
Cd	14.4 ± 0.4	19.1 ± 0.6
Mn	0.03 ± 0.004	0.03 ± 0.006
Cu	0.03 ± 0.004	0.06 ± 0.002

[a] Mean ± S.D. ($n = 5$), [b] Inductively coupled plasma atomic emission spectrometry performed on an ICAP-9000 instrument (Thermo-Jarrell Ash).

dustrial waters, e.g., in waste waters from galvanic baths. The calibration graphs for transition metals were obtained by plotting peak area against concentration of metal ions injected. The calibration data are presented in the Table 4. The detection limits were calculated by using a signal-to-noise ratio of 2:1. The relative standard deviation obtained for 3–4 injections of the same sample ranged from 3 to 6%.

The results of the application of the method to the analysis of industrial waters are summarized in Table 5. The concentrations of zinc, manganese, copper and cadmium in waste water from a galvanic bath were determined from the calibration graphs. No special pretreatment of the samples was applied before analysis except dilution with distilled water in a ratio of 1:50.

Conclusions

The proposed method using on-column complexation with a picolinic acid-containing eluent appears to have considerable potential for the separation and determination of transition metal ions in the ng range by RPLC with direct injection of the sample and spectrophotometric detection of metal complexes in the UV region at 235 nm. The applicability of the method to the analysis of industrial waters has been demonstrated.

REFERENCES

1 M.L. Marina, J.C. Diez-Masa and M.V. Dabrio, J. Liq. Chromatogr., 12 (1989) 1973.
2 J. Vialle, M.C. Bertrand, M. Kolosky, O. Paisse and G. Raffin, Analusis, 17 (1989) 376.
3 S. Srijaranai, N. Ryan, N. Mitchell and J.D. Glennon, in P.A. Williams and M.J. Hudson (Eds.), Recent Developments in Ion Exchange, Elsevier Applied Science, Barking, 1990, p. 311.
4 H. Siren and M.L. Riekkola, J. Chromatogr., 590 (1992) 263.
5 F. Fernandez, M.L. Marina and A.R. Rodriguez, Microchem. J., 44 (1991) 335.
6 G. Bonn, S. Reiffenstuhl and P. Jandik, J. Chromatogr., 499 (1990) 669.
7 R.A. Cochrane, Trace Metal Removal from Aqueous Solutions, Proceedings of Annual Chemical Congress, Warwick, 1986, London, 1986, p. 197.
8 R.C.L. Foley and P.R. Haddad, J. Chromatogr., 366 (1986) 13.
9 P.N. Nesterenko and T.A. Bolshova, Vestn. Mosk. Univ., Khim., 31 (1990) 167.
10 P.N. Nesterenko, I.B. Yuferova and G.V. Kudryavtsev, Zh. Vses. Khim. Ova., 34 (1989) 426.
11 R.W. Green, J. Am. Chem. Soc., 79 (1957) 5608.
12 E. Casassas and G. Fonrodona, Polyhedron, 7 (1988) 684.
13 G. Anderegg, Helv. Chim. Acta, 43 (1960) 414.
14 M.L. Marina, J.C. Diez-Masa and M.V. Dabrio, J. High Resolut. Chromatogr. Chromatogr. Commun., 9 (1986) 300.
15 D.W. Roberts, R.J. Ruane and I.D. Wilson, J. Chromatogr., 471 (1989) 437.
16 R. Vespalec, M. Vrchlabsky and M. Cigankova, Folia, 26 (1985) 5.
17 R.P.W. Scott, J. Chromatogr. Sci., 18 (1971) 449.
18 A. Berthod, M. Kolosky, J.L. Rocca and O. Vittori, Analusis, 7 (1979) 395.

Analytica Chimica Acta, 285 (1994) 169–176
Elsevier Science B.V., Amsterdam

Ion chromatography for monitoring biotechnological processes

Part I. System development for analysis of industrial cultivation media of microorganisms

Ute Scheller, Detlef Siedenberg and Karl Schügerl

Institut für Technische Chemie, Universität Hannover, Callinstr. 3, D-30167 Hannover (FRG)

(Received 6th August 1993; revised manuscript received 10th September 1993)

Abstract

An ion-exchange chromatographic method was developed for measuring chloride, phosphate, nitrate, and sulfate anions in model media, and chloride, phosphate and sulfate anions in industrial cultivation media of microorganisms. By optimisation, an analysis time of 14 min was obtained. An ion-exclusion chromatographic method was developed for the measurement of glucose, lactic, acetic and citric acid concentrations in model and industrial cultivation media of microorganisms. By optimisation, an analysis time of 10 min was reached. The prerequisite of these analyses is proper sample preparation, the removal of proteins from the sample in particular, which is discussed in detail in this publication.

Keywords: Ion-exchange; Chromatography; Sample preparation; Inorganic anions; Ion exclusion; Glucose; Organic acid anions

Ion chromatography (IC) became a very popular method for chemical analysis in environmental control [1]. However, only few reports are known about its application in process control [2,3]. Its application in the analysis of components in biological media is limited because of the high protein content and ion strength in these media. The aim of the present investigations was the adaptation of ion chromatography for the determination of components in biological media with high protein content.

Correspondence to: K. Schugerl, Institut für Technische Chemie, Universität Hannover, Callinstr. 3, D-30167 Hannover (FRG).

EXPERIMENTAL

Applied system and its operation

A high pressure titanium pump (Gynkotek, Model 300 C), applicable up to 500 bar, was combined with pulsation damper (PD-1 Gynkotek), injection valve (C6W Valco Instruments), different columns (Table 1), UV detector (UVD-160, Gynkotek) for the analysis of inorganic ions, and refractive index (RI) detector (ERC-7515 A, Erma Cr., Inc.) for organic acids and sugars. The evaluation of the measurements was performed by means of an integrator (SP 4270, Spectra Physics) and a chromatography data station (APEX, Autochrom) (Fig. 1).

SSDI 0003-2670(93)E0502-X

TABLE 1

Separation columns applied in the investigations

Columns for ion-exchange chromatography
PRP-X 100 Hamilton 250×4.6 mm with precolumn; basic anion exchanger: styrene–divinylbenzene modified with trimethyl ammonium groups (10 μm particle size)
Polyspher IC AN-2, Merck 120×4.6 mm, styrene–divinylbenzene (9 μm particle size)
GAT-Wescan 269-029, GAT 250×4.6 mm with precolumn, styrene–divinylbenzene (10 μm particle size)
Columns for ion-exclusion chromatography
Nucleosil 5NH_2, Macherey-Nagel 200×4 mm, silicagel modified with amino (NH_2) groups for sugar analysis
Polyspher OA HY, Merck, 300×6.5 mm with precolumn, styrene–divinylbenzene cation exchanger for separation of organic acids with low pK_S
KC 811, Shodex, Showa Denko, 300×8 mm with precolumn
KC 810P, 50×6 mm surface sulfonated styrene–divinylbenzene cation exchanger for low molecular weight organic acids, sugars, alcohols, aldehydes and nitriles

On account of possible capillary plugging, the eluents were prepared with bidistilled water, filtered with a 0.2-μm membrane (cellulose acetate, Sartorius) and degassed for 10 min in an ultrasonic bath.

The potassium hydrogenphthalate (KHP) eluent (KHP dissolved in bidistilled water with the pH set with NaOH solution) for ion-exchange chromatography was permanently gassed with helium during the measurements. Such treatment was not necessary for the eluents (0.005 M H_2SO_4 and 0.03 mol l^{-1} H_3PO_4) in ion-exclusion chromatography. The pH value and the concentrations of the eluents were varied to find the optimal conditions.

The pump was regularly rinsed with distilled water, the capillary system with dilute NaOH solution and bidistilled water, the injection valve was cleaned in an ultrasonic bath and the UV detector with methanol. With regular service, the system could operate for a long time without breakdown. (For more details, see [4]).

Cleanliness of the columns (particularly free of protein) is especially important, since they could not be regenerated.

RESULTS AND DISCUSSION

Optimization of sample preparation

Because of the complex composition of industrial cultivation media, especially their high protein (up to 20 g l^{-1}) and salt contents, it was important to pretreat the samples and remove the medium components which damage the columns or impair their performance. The use of a precolumn was not sufficient.

For the precipitation of proteins, the following methods were tested:

(a) Sample: a 1:1 mixture with methanol was treated at 4°C for 10 min, and the precipitate was separated by centrifugation.

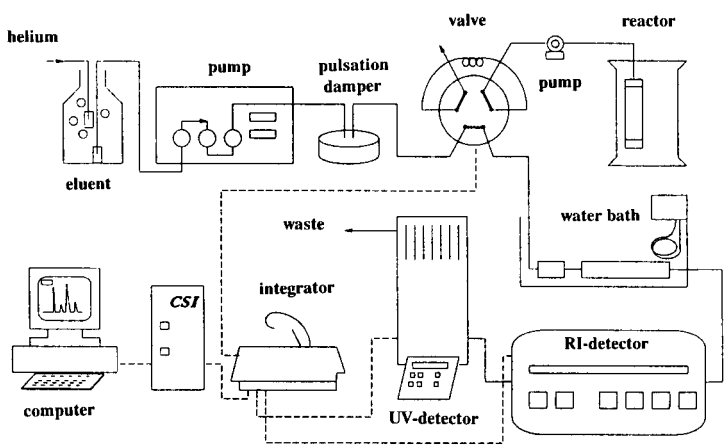

Fig. 1. On-line ion chromatographic analyser system.

(b) Sample: a 20% solution in trichloroacetic acid (TCA) was treated at 4°C for 10 min, and the precipitate was separated by centrifugation.

(c) Sample: a 5:1 mixture in 100 g l^{-1} 5-sulfosalicylic acid solution was diluted to 1:100, and the precipitate was removed [4].

The dissolved protein content was determined by the method described by Bradford [6] and Sedmak and Grossberg [7]. The methanol and TCA methods were not suitable for protein separation, since the solution changed colour after the treatment. The 5-sulfosalicylic acid treatment rendered satisfactory results, but was disadvantageous due to its strongly diluted sample.

This method was used for off-line IC analysis of the medium components.

Solid-phase extraction. The proteins were adsorbed on the solid phase (silica surface modified by C_8 and C_{18} chains, Chromabond, Macherey-Nagel). After a short time, however, the precolumn was loaded and no additional protein was adsorbed. The method was unsuitable for protein removal.

Micro- and ultrafiltration. At high protein concentrations (e.g., 20 g l^{-1} during the cultivation of *Bacillus licheniformis*), 90–95% of the proteins were retained by the microfiltration method (0.2 μm pores). Yet 1–2 g l^{-1} protein was still too high for the ion chromatograph.

By using a 100 kD-UF membrane (polysulfon, Sartorius), the residual protein concentration amounted to 0.3–0.5 g l^{-1}, and with the 20 kD-UF membrane (polysulfon and/or fluorpolymer, DDS, DK Naskov), a residual protein of 0.03 g l^{-1} was obtained. The latter sample is suitable for IC analysis. Due to the low transmembrane permeation rate, however, sample filtration with 20 kD-UF membrane is not suited for on-line analysis.

Dialysis. A dialyser cell (Skalar Analytics) with a regenerated cellulose membrane (thickness 12 μm, 10–14 kDa, Serva), distilled water, and bubble separator for the dialysate side were applied for the investigations (Fig. 2). The sample and dialysate flow-rates were maintained with microcassette pumps 304-MC (Watson-Marlow).

Cocurrent and countercurrent sample/dialysate flows with different flow-rates were tested, and the following optimal conditions were ascertained: countercurrent flow with a sample flow-rate of 0.3 ml min^{-1} and a dialysate flow-rate of 0.09 ml min^{-1}. The response time of this system was 12 min. By sampling with a microfiltration cross-flow module (Biopem, B. Braun Melsungen) [8], separation cell (Amafilter) [9], cross-flow module (Waters-Millipore [9]), or with a tubular filter (ABC Bioverfahrenstechnik [10]), the dialysate did not contain any protein.

This system was employed for on-line IC monitoring of the components during cultivation processes.

To gain more information about the influence of the membrane on the chromatogram, two membranes of different thickness were applied:

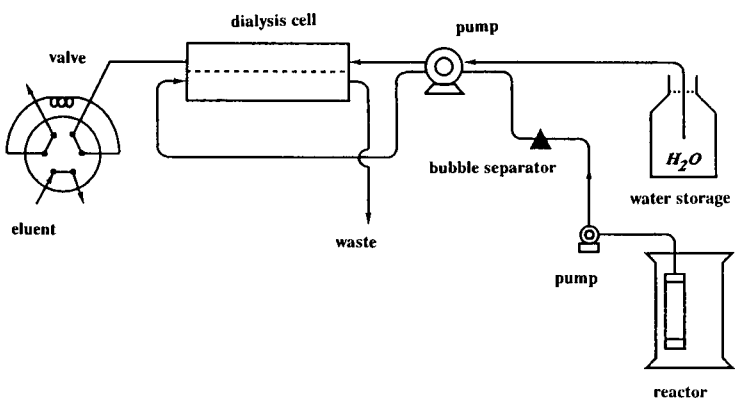

Fig. 2. Integration of the dialyser cell into the IC system.

membranes with 10–12 kD and a thickness of 75 μm (Reichelt) and 10–14 kD and a thickness of 12 μm (Serva). The peak heights of the anorganic anions were much higher by using the thin membrane.

With increasing operation time, the transmembrane permeation rate diminished due to membrane fouling, but it could be kept constant by rinsing it with an NaOH solution.

A comparison of the chromatograms having the same membranes used in both the ultrafiltration and the dialysis mode indicated that by applying the ultrafiltration method low-molecular proteins remained in the sample, but dialysates were free of proteins.

Electrodialysis. Dialysis is a rather slow process. To reduce the response time of the analyser system, an acceleration of the dialysis would be necessary. An electrodialyser cell was constructed and tested with model medium and cultivation medium. The peak height of the phosphate standard was increased by a factor of 1.83 by applying a charge of 2 V on the electrodes. If an electrolyte was used as dialyser liquid, the factor was 3.53. However, if the anion mixture was employed, the increase of the peak height was rather small due to the presence of an electrolyte in the dialyser liquid: 12% for acetate, 5% for chloride, 13% for phosphate and 42% for sulfate. No electrodialyser was used for process monitoring, however, it would be worthwhile to carry out further investigations with an improved electrodialyser.

Optimization of the chromatographic analysis

Ion-exchange chromatography. For the analysis of the inorganic ions (chloride, phosphate, sulfate, nitrate) three columns were tested. The shortest column, IC AN-2 (Merck) (120 mm long), showed the longest analysis times (60 min at eluent pH value of 4.25 and 1 ml min^{-1} eluent flow-rate and 35 min at 2 ml min^{-1} eluent flow-rate).

The 250 mm long GAT-Wescan column (Gamma Analysen Technik) showed the shortest analysis times (12 min at pH 7.0 and 32 min at pH 4.24), but the resolution of the peaks was unsatisfactory.

The PRP-X 100 column (Hamilton) gave the best results. It was operated at pH 7.0 with an eluent flow-rate of 1 ml min^{-1} and had an analysis time of 15.5 min. The excellent performance of this column has already been described by Lee [11]. In spite of its high performance it was the less expensive column.

For the evaluation of the sensitivity measurements, two different detection methods were employed: UV and RI. The sensitivity with indirect

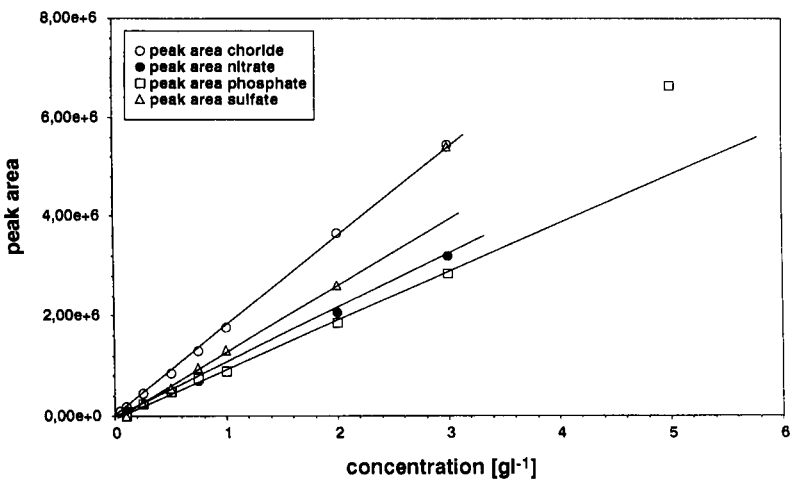

Fig. 3. Calibration diagrams of chloride, nitrate, phosphate and sulfate anions measured with the PRP-X 100 column at pH 7 and an eluent flow-rate of 1 ml min^{-1}.

UV detection is higher than that with RI detection. The detection was performed at the maximum of the absorbance of KHP (280 nm at pH 4 and 275 nm at pH 7). The proteins also have a high absorbance at these wavelengths. This is one of the reasons why proteins must be removed from the sample, another one is the fast deterioration of the column performance in presence of proteins in the sample.

In Fig. 3, the calibration diagrams of chloride, phosphate, sulfate, and nitrate are shown. In the cultivation medium, the anions were present in the following concentrations: 1–2 g l^{-1} phosphate, 0.5 g l^{-1} chloride and sulfate. They are in the linear calibration range. Nitrate was not present in the medium.

The relative standard deviations of the measurements were evaluated for the linear range from 10 measurements: 1.3% for chloride, 1.2% for phosphate, 1.7% for nitrate and 1.5% for sulfate.

To optimize the peak resolution, pH, temperature, ion strength and elution flow-rate were varied.

In Fig. 4, the retention time is plotted as a function of the eluent concentration. With increasing concentration, the retention time decreased and at high concentrations, the peak resolutions deteriorated. Sufficient resolution and a short analysis time were obtained with an eluent concentration of 2 mmol l^{-1}.

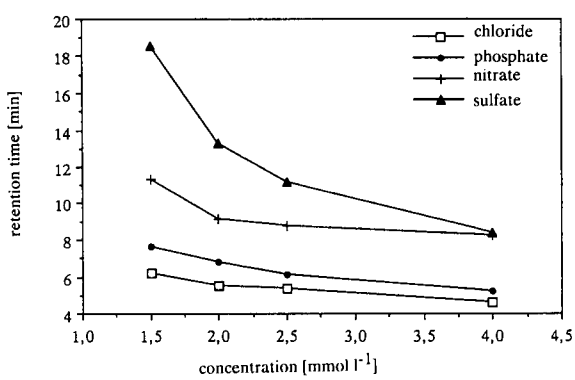

Fig. 4. Retention times of chloride, phosphate, nitrate and sulfate as a function of the eluent concentration with the PRP-X 100 column at pH 7 and a flow-rate of 1 ml min^{-1}.

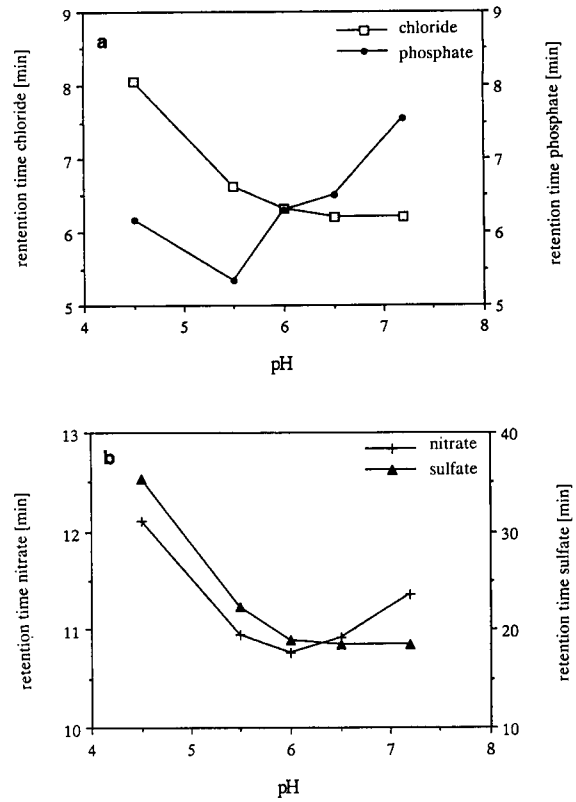

Fig. 5. Retention times as a function of pH using the with PRP-X 100 column. (A) Chloride and phosphate. (B) Nitrate and sulfate.

In Fig. 5, the influence of the pH value on the retention times of chloride, phosphate, sulfate, and nitrate are shown. At pH 4.4 and 7, the resolutions are sufficient. However, because of the long retention time at pH 4.5, pH 7 was chosen for the IC analysis.

In Fig. 6, the retention times are depicted as a function of the elution flow-rate. With increasing flow-rate, the retention time as well as the resolution diminished. At 1 ml min^{-1}, the resolution was sufficiently high and the retention time was below 15 min.

The temperature did not influence the retention times considerably in the range from 30–45°C.

In Fig. 7, the chromatogram of a chloride, phosphate, nitrate, and sulfate mixture is shown evaluated under optimized operation conditions

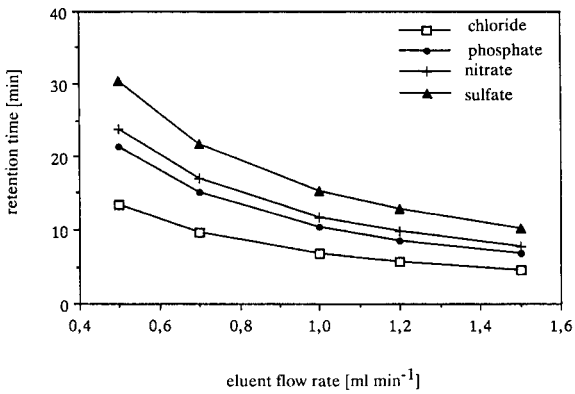

Fig. 6. Retention times of chloride, phosphate, nitrate and sulfate as a function of the eluent flow-rate with PRP-X 100 at pH 7.

with a PRP-X 100 column at 2 mmol l^{-1} KHP eluent concentration, pH 7, 1 ml min^{-1} eluent flow-rate, 30°C with an UV detector at 275 nm.

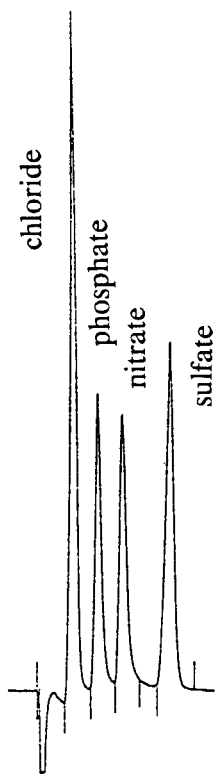

Fig. 7. Chromatogram of a standard solution of inorganic anions.

TABLE 2

Retention times (min) of the investigated components using two different columns at 0.7 ml min^{-1} 0.03 M H_3PO_4 eluent

Column	Polyspher	Ionpak
Citric acid	5.04	9.7
Glucose	5.53	10.36
Lactic acid	8.01	13.60
Acetic acid	9.47	15.60

The analysis time was 14 min and the detection limit for phosphate 0.005 g l^{-1}.

Ion-exclusion chromatography. Different organic acids and sugars were separated and analysed on the ion-exclusion columns. In the present paper, the analyses of acetic, citric and lactic acid and glucose with the Nucleosil $5NH_2$ (Machery-Nagel), Polyspher OA HY (Merck) and Ionpak KC-811 (Showa Denko) columns are considered, with UV detection at 205 nm. With 0.03 M H_3PO_4 eluent at 0.7 ml min^{-1}, satisfactory separation was obtained with model medium in 15.5 min with the Nucleosil $5NH_2$ column. However, no separation of lactic and acetic acid peaks was possible, when cultivation medium was used. Therefore, this column is not taken into consideration any further.

The separation of these components – also with cultivation medium – was possible under the above given conditions with the Polyspher OA HY and Ionpak KC-811 columns. The retention times of the components for these two columns are shown in Table 2. The resolution was the same in both columns, but the analysis with the Polyspher column took only 10 min, while the Ionpak column needed 16 min.

The 0.005 mol l^{-1} H_2SO_4 eluent showed similar results. This eluent was used for process monitoring, as recommended by the column manufacturer.

With increasing temperature, the retention times of the analytes did not change, only the pressure drop decreased from 85 to 70 bar.

With increasing eluent flow-rate the retention times decreased (Fig. 8). At 0.7 ml min^{-1}, still, sufficient resolution was obtained. Therefore, this elution rate was chosen for analysis.

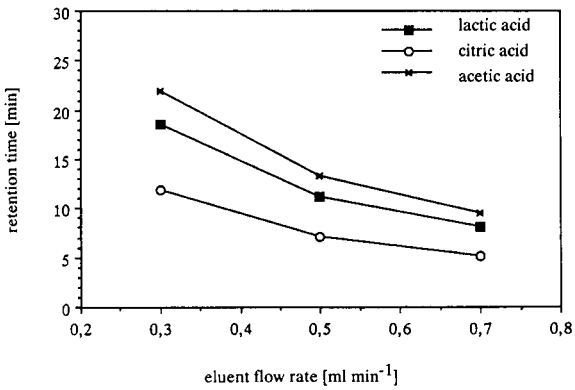

Fig. 8. Retention times of organic acid anions as a function of the eluent flow-rate with a Polyspher column at pH 2.13.

The UV detector as well as the RI detector were used. The UV detector showed higher sensitivity than the RI detector in the analysis of the organic acids. Yet, glucose could only be detected by the RI detector. The IC chromatograms of the two detectors deviated a great deal from each other. Due to several UV-active components in the cultivation media, many more peaks appeared by using the UV detector than with the RI detector, which impeded the evaluation of the chromatograms.

In Table 3, the advantages and disadvantages of the two detectors for the analysis of the cultivation media are shown. The long analysis times with the UV detector are due to several UV-active medium components which have high retention times. On account of the possibility of glucose detection, the RI detector was used for monitoring of the medium components.

In Fig. 9 the calibration diagrams for glucose, lactic, citric and acetic acid with the RI detector

TABLE 3

Advantages and disadvantages of the UV and RI detectors for analysis of cultivation media

RI detector	UV detector
Low sensitivity	High sensitivity
Sensitive for temperature variatons	Stable against temperature variations
Analysis time, 15 min	Analysis time, 45 min
Glucose is detected	Glucose is not detected

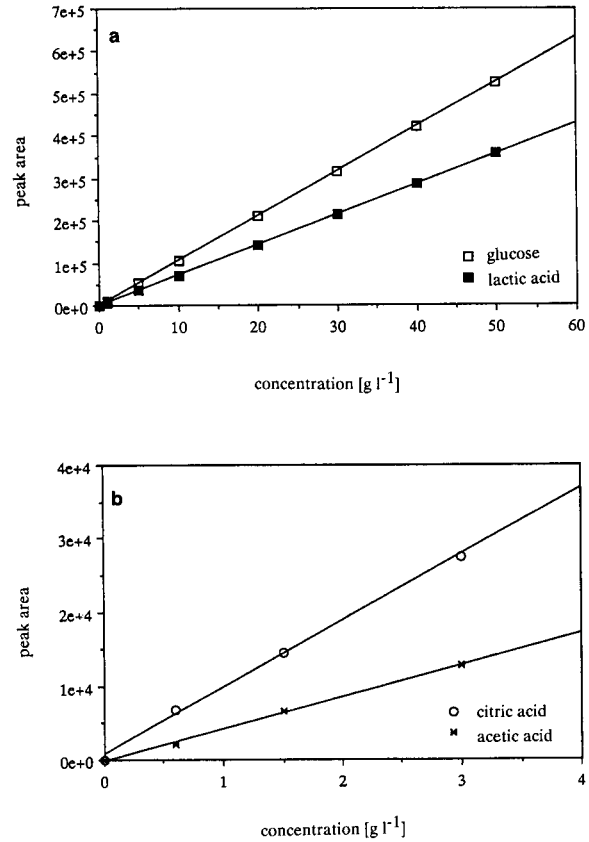

Fig. 9. Calibration diagrams with the Polyspher column and RI detector at 35°C. (A) Glucose and lactic acid. (B) Citric and acetic acid.

are depicted. Because of the high glucose and lactic acid concentrations in the culture medium, their calibration diagrams were evaluated up to 50 g l^{-1}. Only low amounts of acetic and citric acids were present in the culture medium, therefore, the calibrations only covered concentrations up to 3 g l^{-1}. In the investigated ranges, linear relationships between peak areas and concentrations prevailed.

Conclusions

We succeeded in analysing inorganic anions (chloride, phosphate, nitrate and sulfate) in industrial cultivation media within 14 min by means of ion-exchange chromatography and glucose, acetic, citric and lactic acid within 10 min with ion-exclusion chromatography.

The prerequisite for the analyses was careful sample preparation, i.e., the removal of proteins from the sample in particular. These short analysing times allow monitoring of these medium components during cell growth and product formation and this information is used for process control, which will be considered in the second part of this paper [12].

REFERENCES

1 D.T. Gjerde and J.S. Fritz, Ion chromatography, Hüthig Verlag, Heidelberg, 2nd edn., 1987.
2 J. Weiss, Handbuch der Ionenchromatographie, VCH, Weiterstadt, 2. Aufl., 1991.
3 P.R. Haddad and P.E. Jackson, Ion Chromatography, Elsevier, Amsterdam, 1990.
4 Ute Scheller, Ionenchromatographie zur Überwachung biotechnologischer Prozesse, Dissertation, University of Hannover, 1991.
5 J. Möller, Penicillin-Produktion mit einem Hochleistungsstamm von *Penicilliun chrysogenum* - Chromatographische Methoden zur Prozesskontrolle, Dissertation, University of Hannover, 1987.
6 M.M. Bradford, Anal. Biochem., 72 (1976) 248
7 J.J. Sedmak and S.E. Grossberg, Anal. Biochem., 79 (1977) 544
8 B. Braun Melsungen, Operation Manual, 1986.
9 U. Hübner, Entwicklung neuer On-line-Analysenmethoden zur Steuerung und Regelung von Proteasefermentationen, Dissertation, University of Hannover, 1991.
10 H. Graf, D. Wentz and K. Schügerl, Biotechnol. Techniques, 5 (1991) 183
11 D.P. Lee, J. Chromatogr. Sci., 22 (1984) 327.
12 U. Scheller, D. Siedenberg, U. Hübner, M. Siebold, G. Kretzmer and K. Schügerl, Anal. Chim. Acta, in press.

Determination of ^{99}Tc in sea water at ultra low levels

Qingjiang Chen, H. Dahlgaard and S.P. Nielsen

Risø National Laboratory, P.O. Box 49, DK-4000 Roskilde (Denmark)

(Received 7th June 1993; revised manuscript received 23rd August 1993)

Abstract

A method based on the collection of ^{99}Tc from 500 l sea water samples by anion exchange and further extraction of TcO_4^- into 5% triisooctylamine–xylene has been improved to include a decontamination factor 6.5×10^5 for uranium. The detection limit for ^{99}Tc is thereby reduced to 3 mBq/m^3.

Keywords: Ion exchange; Sea water; Technetium; Waters; Uranium

Technetium-99 has a long half-life ($t_{1/2} = 2.1 \times 10^5$ year) and a relatively high fission yield (6%). Technetium-99 is released to the environment from nuclear power plants, nuclear fuel production, nuclear weapons testing and nuclear medicine. Although the present environmental levels of ^{99}Tc are very low and difficult to assay, ^{99}Tc is nevertheless of potential radiological relevance to the collective long-term dose to man. Technetium-99 can further be utilized as a special tracer in the marine environment [1], since it behaves conservatively in relation to sedimentation.

The radiochemical assay of environmental ^{99}Tc requires the separation of very small amounts of a low-energy β-emitter ($E_{max} = 0.293$ MeV). Ruthenium-103 and -106 are the major contaminants. We have previously presented [2] a method for collecting ^{99}Tc from 200–400 l of sea water by anion exchange. Decontamination of $^{103,106}Ru$ was achieved by repeated evaporation of RuO_4 from 0.05 M sulphuric acid at 100°C, followed by extraction of TcO_4^- into 5% triisooctylamine–xylene at controlled valency. Decontamination factors for Ru were between 3×10^5 and 2×10^7, with an average overall radiochemical yield of 70% for Tc.

More recently, Matsuoka et al. [3] have presented a radioanalytical procedure using Rhenium as a nonisotopic carrier of ^{99}Tc. The procedure includes precipitation as Tc_2S_7, transfer to TcO_4^- and extraction with methyl ethyl ketone, followed by anion exchange. The detection limit (3σ) for sea water (300 l sample) was 5×10^{-5} Bq/l. An equivalent procedure described recently by Harvey et al. [4] is based on anion exchange, precipitation of technetium first as Tc_2S_7 and then as tetraphenyl arsonium salt, followed by radiometric assay. It claims a detection limit for sea water of 4×10^{-4} Bq/l, based on a sample of only 40 l.

Morita et al. [5] have used inductively coupled plasma mass spectrometry (ICP-MS) instead of β-counting as the final step in their ^{99}Tc assay. They decontaminate for Ru by extracting with several organic reagents such as triisooctylamine, tributylphosphate and cyclohexanone, achieving a decontamination factor of 7×10^4. The detection limit is given as equivalent to 1.1 mBq/ml, in this case referring to a final volume of about 10 ml

Correspondence to: H. Dahlgaard, Risø National Laboratory, P.O. Box 49, DK-4000 Roskilde (Denmark).

SSDI 0003-2670(93)E0507-4

after treatment of soil samples with a Tc recovery of 80%. A final detection limit of electrodeposited ^{99}Tc as low as equivalent to 1 μBq has been claimed by Sattelberger et al. [6], using laser resonance ionisation mass spectrometry, which apparently also guarantees an almost unambiguous element and isotope assignment. Even more sensitive results – down to 0.1 μBq – have been achieved by Rokop et al. [7] based on negative thermal ionisation mass spectrometry.

As the extra $^{103,106}Ru$ contamination of the European waters after the Chernobyl accident in 1986 loses its significance, it becomes relatively more important to avoid interference from a natural contamination of sea water with ^{238}U, ^{228}Th, ^{226}Ra and ^{210}Po. In the present communication we have improved our previous method [2] with regard to the extraction with triisooctylamine prior to the final electrodeposition. This has added an extra decontamination factor of 5×10^3 to an interference by ^{238}U.

EXPERIMENTAL

According to the procedure previously reported [2], ^{99}Tc is extracted as TcO_4^- with 5% triisooctylamine in xylene following a repeated evaporation of RuO_4, after acidification (0.5 M H_2SO_4) and oxidation with 30% H_2O_2. To see what happens to U and Th under these and similar conditions, ^{238}U and ^{228}Th were added in duplicate as test samples to 0.5 M H_2SO_4 and oxidised either as usual with H_2O_2, or with $K_2S_2O_8$ to avoid the possible formation of peroxy uranium and thorium complexes. The solutions were then extracted with TIOA–xylene and electrodeposited in the usual manner.

Having proven the advantage of an oxidation with $K_2S_2O_8$, the next step was to test the whole procedure. To 1 l sea water samples were added in duplicate either ^{210}Po or a mixture of ^{238}U, ^{228}Th, ^{236}Ra and ^{210}Po. The assays were performed as previously described [2], apart from an oxidation with $K_2S_2O_8$ instead of H_2O_2.

Finally, a series of 200 and 500 l natural sea water samples were assayed as in the above. A flow sheet of the total procedure is presented in

1. Filter 500 ℓ seawater through paper filter and add ^{99m}Tc.
2. Stir to allow isotope exchange. Let stay for 30 min.

⇓

3. The 500 ℓ seawater is passed through 2 parallel columns (17 x 4 cm AG1 - X_4, 100 - 200 mesh). Flowrate ~ 145 ml/min per column, i.e. ~ 28 hours.
4. Wash the columns each with 1500 ml 0.5 N NaOH and 1500 ml 0.5 N HNO_3.
5. Strip each column with 550 ml 14.4 N (65%) HNO_3. Total stripping time ~ 50 min.
6. Combine the two eluates, and determine yield by γ-counting ^{99m}Tc (normally close to 100%) if procedure is halted.

⇓

7. If procedure has been halted, add new ^{99m}Tc spike.
8. Add 1 ml 3 M $NaNO_3$ and reduce eluate to 0.5 ml by heating.
9. Add 0.5 ml 10 N H_2SO_4. Dilute to 20 ml. Add 1 ml 5% NaClO. Heat for 10 min.
10. Dilute to 100 ml. Add 0.5 ml 20 mg/ml $AgNO_3$ and 0.5 ml 10 mg/ml $FeCl_3$. Add NaOH to pH = 9. Heat for 5 min. Filter the solution. Wash the precipitate 3 times with water (pH = 9). Discard precipitate.

⇓

11. Add 0.5 ml 5 mg/ml $RuCl_3$ and 1 ml 5% NaClO. Keep pH = 9. Heat for 5 min to allow the isotope exchange to be completed and to get RuO_4. The solution should be bright yellow: if not, add more 5% NaClO. Add 1 ml 5% NaClO in excess.
12. Acidify the solution to pH = 2-3 with 10 N H_2SO_4.
13. Heat for 15 min in order to evaporate the RuO_4. The bright yellow disappears and the solution is colourless.
14. Repeat 11-13 two times. Third run without $RuCl_3$ carrier.

⇓

15. Acidify the solution to 1 N H_2SO_4. Add 2g $K_2S_2O_8$ and dilute to 100 ml. Transfer the solution to a 250 ml separator.
16. Extract with 80 ml 5% TIOA (tri-isooctylamine)/xylene. Shake for 5 min.
17. Wash the organic phase 2 times, each time with 80 ml H_2O. Shake for 5 min (for U, Th decontamination).
18. Backextract with 20 ml 2 N NaOH. Shake for 2 min. Backextract once more with 5 ml 0.5 N NaOH, shake for 2 min.

⇓

19. Evaporate the solution to 20 ml for electrodeposition.
20. The current is 300 mA. It takes at least 5 h or over night.
21. Clean the disc for NaOH by dipping it (hold with a pincers) in H_2O. Heavy flushing will cause loss of activity. The Chemical yield is determined by γ-counting of ^{99m}Tc. It is normally 70-80%.

Fig. 1. Determination of ^{99}Tc in sea water. Flow sheet for 500 l water sample.

Fig. 1. Compared to the original procedure [2], we have made further changes at these points:

(1) The samples are not treated with 100 ml 30% H_2O_2 and acidified to pH 1 with H_2SO_4 to begin with, in order to avoid uranium anion formation. The natural oxygen content of sea water is anyway sufficient to ensure TcO_4^-.

(2) The columns are first washed with 1500 ml 0.5 M NaOH, rather than with deionized water, to stabilise the absorption of $^{99}TcO_4^-$ and avoid other anions. The columns are finally stripped with 14 M HNO_3 rather than with 10 M HNO_3 to enhance stripping efficiency.

(3) The final TIOA–xylene extract is washed only with H_2O (2x80 ml) and not first with 80 ml 0.5 M H_2SO_4 containing $K_2S_2O_8$. Uranium and

Th are more efficiently back-extracted at low acidity than at high.

The efficiency of TcO_4^- extraction with 5% TIOA–xylene by varying the shaking of the extraction funnels was also investigated. In one series, shaking by hand for 2 min gave a chemical yield of $87.7 \pm 0.6\%$, while shaking by machine for 5 min gave $59.8 \pm 4.6\%$; i.e., shaking by hand was both more efficient and more reproducible.

The chemical yield is determined by γ-counting (NaI detector) of ^{99m}Tc ($t_{1/2} = 6$ h) eluted from a ^{99}Mo source adsorbed on Al_2O_3. To avoid buildup of ^{99}Tc in the ^{99m}Tc source, that could contaminate the ultra low samples, the "cow" is eluted at least daily.

After any trace of ^{99m}Tc has decayed, the electroplated samples are β-counted on a Risø produced low background gas flow GM counter with a window density < 1 mg/cm^2 [2].

RESULTS AND DISCUSSION

Decontamination factors are shown in Table 1.

It appears that an oxidation with H_2O_2 and subsequent extraction with TIOA–xylene does not in any way discriminate against U, and only to a minor degree against Th. We would attribute this lack of an effect to the formation of peroxy complexes such as $[UO_2(O_2H)_4]^{-2}$, which could be dissolved in the organic phase. An alternative oxidation with $K_2S_2O_8$ leads to a discrimination against U by a factor 5.0×10^3 and against Th by a factor 130.

Much larger decontamination factors are obtained (Table 1) when we include the whole procedure. Uranium is now decontaminated by a factor 6.5×10^5, and not just 5.0×10^3, and Th by a factor 6.0×10^6; due above all to the initial ion exchange step. Woodhead [8] presents an overview of natural radionuclides in surface sea water with the salinity of 35‰. Apart from the obvious cations ^{40}K and ^{87}Rb, the following natural radionuclides are the most abundant, measured in Bq/m^3: ^{238}U, 44; ^{228}Ra, 0.4–37; ^{226}Ra, 1.3–3.1; ^{210}Pb, 0.4–5.0; ^{210}Po, 0.2–3.7. This means in the present case that ^{210}Po presents the relatively greatest problem among the α-emitters, with a decontamination factor that has been determined as 6.4×10^3 and 1.8×10^3, i.e., about a hundred times lower than that for U and Ra.

Measurements (Table 1) on natural sea water show decontamination factors for ^{210}Po that are the same as those found after direct addition of

TABLE 1

Decontamination factors after various procedures, based on α-spectroscopy

Process investigated	Nuclide	Sea water sample (l)	Test sample (ml 0.5 M H_2SO_4)	Oxidation		5% TIOA xylene (ml)	Radioactivity (Bq)			Decontamination factor
				30% H_2O_2 (ml)	$K_2S_2O_8$ (g)		Added		Recovered	
							Sea water	test		
Extraction with triiso-octylamine	^{238}U		10	0.5	–	10		0.14	0.13	1.1
			20	–	0.6	20		0.19	3.8×10^{-5}	5.0×10^3
	^{228}Th		10	0.5	–	10		0.21	7.7×10^{-3}	27
			20	–	0.6	20		0.24	1.8×10^{-3}	1.3×10^2
Total procedure	^{210}Po	1.0		–	2.0	40	5000		0.78	6.4×10^3
	^{238}U	1.0		–	2.0	40	200		3.1×10^{-4}	6.5×10^5
	^{228}Th						1200		2.0×10^{-4}	6.0×10^6
	^{226}Ra						100		3.7×10^{-4}	2.7×10^5
	^{210}Po						100		5.7×10^{-2}	1.8×10^3
	^{210}Po	200		–	2.0	80	0.2 [a]		1×10^{-4}	2×10^3
		500		–	2.0	80	0.5 [a]		6×10^{-5}	8×10^3

[a] Estimated natural level.

^{210}Po to sea water samples. This strengthens the significance of the other decontamination factors presented in Table 1.

Finally, the samples where known amounts of ^{210}Po had been added to 1 l of sea water were also counted in the same manner as in the measurement of ^{99}Tc β-activity. This was done to evaluate the contamination by ^{210}Pb, which is a β-emitter in natural equilibrium with ^{210}Po. Results showed 0.58 and 0.049 Bq recovered, relative to 0.78 and 0.057 found by α-spectroscopy (Table 1), which agrees with a known efficiency of 0.8 by the β-counter towards α-activity in the samples. There was thus no indication of any extra ^{210}Pb β-activity that could have affected the measurement of ^{99}Tc.

Equivalent to the 500 l sea water samples presented in Table 1, which were taken on the continental shelf west of Scotland (56°N, 8°W), further 7 × 500 l sea water samples were taken in the mid-Atlantic near the Azores islands (41°N, 18°W). While ^{210}Po could be detected (Table 1) off the coast of Scotland, no ^{210}Po or any other natural radionuclides were found by α-spectroscopy in the mid-Atlantic samples, in agreement with the physical distance to sources on land. The counting of β-activity in the 7 mid-Atlantic samples gave an average value of ^{99}Tc = 5.3 mBq/m^3 with a S.D. = 0.9 mBq/m^3. Assuming identity of the 7 samples and a detection limit of 3 × S.D. we get an overall empirical detection limit of 3 mBq ^{99}Tc/m^3. This value would clearly be very little affected by the 6×10^{-5}–10^{-4} Bq ^{210}Po/sample recovered in two other sets of samples (Table 1).

A final determination of ^{99}Tc by sophisticated methods such as laser resonance mass spectrometry [6] and negative thermal ionisation mass spectrometry [7] can measure levels as low as 0.1–1 μBq. Nevertheless, the present method, which is based on traditional β-counting, has been shown in practice to be well-suited for the assay of ^{99}Tc in sea water at ultra low levels.

The present work was supported by the EEC Marine Science and Technology Programme, Contract No. MAST-052-C.

REFERENCES

1 A. Aarkrog, L. Carlsson, Q.J. Chen, H. Dahlgaard, E. Holm, L. Huynh-Ngoc, L.H. Jensen, S.P. Nielsen and H. Nies, Nature, 335 (1988) 338.
2 Q. Chen, H. Dahlgaard, H.J.M. Hansen and A. Aarkrog, Anal. Chim. Acta, 228 (1990) 163.
3 N. Matsuoka, T. Umata, M. Okamura, N. Shiraishi, N. Momoshima and Y. Takashima, J. Radioanal. Nucl. Chem., Articles, 140 (1990) 57.
4 B.R. Harvey, R.D. Ibbett, K.J. Williams and M.B. Lovett, The Determination of Technetium-99 in Environmental Materials, Aquat. Environ. Prot.: Analyt. Meth., MAFF Direct. Fish. Res., Lowestoft, Vol. 8, 1991, 22 pp.
5 S. Morita, C.K. Kim, Y. Takaku, R. Seki and N. Ikeda, Appl. Radiat. Isot., 42 (1991) 531.
6 P. Sattelberger, M. Mang, G. Herrmann, J. Riegel, H. Rimke, N. Trautmann, F. Ames and H.-J. Kluge, Radiochim. Acta, 48 (1989) 165.
7 D.J. Rokop, N.C. Schroeder and K. Wolfsberg, Anal. Chem., 62 (1990) 1271.
8 D.S. Woodhead, in Q. Kinne (Ed.), Contamination due to Radioactive Materials, Marine Ecology, Vol. V, Part 3, Wiley, Chichester, 1984, p. 1618.

Analytica Chimica Acta, 285 (1994) 181–192
Elsevier Science B.V., Amsterdam

Algorithm for the assessment of peak purity in liquid chromatography with photodiode-array detection

F. Cuesta Sánchez [1], M.S. Khots and D.L. Massart

Pharmaceutical Institute, Vrije Universiteit Brussel, Laarbeeklaan 103, B-1090 Brussels (Belgium)

J.O. De Beer

Institute for Hygiene and Epidemiology, J. Wytsmastraat 14, B-1050 Brussels (Belgium)

(Received 23rd April 1993; revised manuscript received 17th September 1993)

Abstract

An algorithm for peak purity analysis based on the Gram-Schmidt orthogonalization method is described. The data are pretreated by using two different normalization techniques. The performance of this approach is investigated for liquid chromatography with photodiode-array detection (LC-DAD) data. The results are compared with the ones obtained by means of fixed size window evolving factor analysis (FSW EFA). The effects of heteroscedasticity and non linearities are discussed.

Keywords: Liquid chromatography; Principal component analysis; Detection limits; Orthogonalization; Peak purity control

Analysis of the data obtained from liquid chromatography with photodiode-array detection (LC-DAD) is a common way to determine the number of chemical species present in a sample, as well as the concentration profile and the spectrum of each compound. No assumption concerning the number of components, shape of the signal or separation between the components is needed. LC-DAD yields a data table $\mathbf{X}$ $(I \times J)$, where the I rows are absorption spectra measured at regular time intervals (objects) and the J columns are chromatograms measured at different wavelengths (variables).

Most of the techniques are based on the concept of principal component analysis (PCA) and factor analysis (FA). Some examples are iterative target transformation factor analysis (ITTFA) [1–3], evolving factor analysis (EFA) [4,5], heuristic evolving latent projections method (HELP) [6–8]. Fixed-size window EFA (FSW), a new modification of EFA was developed by Keller and Massart [9] and others [10,11]. PCA is performed on a fixed sized moving window of spectra, instead of an increasing number. Tauler [12] applies SPectra FACtor analysis (SPFAC) to LC-DAD data for the determination of the number of components, estimation of the concentrations profiles of every component and determination of the individual spectra of the components in the mixture. SPFAC procedure is a combination of known techniques based on PCA. A review is given by Castledine and Fell [13].

Similar problems were already treated in 1979 for mass spectral data by Rasmussen et al. [14]. They applied three methods to determine the

Correspondence to: D.L. Massart, Pharmaceutical Institute, Vrije Universiteit Brussel, Laarbeeklaan 103, B-1090 Brussels (Belgium).

[1] On leave from: The Department of Physical Chemistry, Faculty of Chemistry, Salamanca University, Spain.

SSDI 0003-2670(93)E0531-B

number of components in a mixture and, in a second step, the spectra of the components were obtained and compared to reference spectra. The latter step is not relevant to us since we have no such references available. One of the methods used the Gram-Schmidt vector orthogonalization technique that consists in sequentially computing a set of base vectors, obtaining at the end a matrix of orthogonal base vectors. Reference spectra are compared with the base vectors by computing the orthogonal distance.

The goal is to detect very small amounts of impurities (down to 0.1%) present under a chromatographic peak, even if resolution is low and the spectra of the analytes are highly similar.

For reasons explained in the discussion, we wondered whether the use of principal components has a real advantage.

In this paper, a simple algorithm for the detection of impurities under a chromatographic peak is proposed. It is not based on PCA but on the Gram-Schmidt orthogonalization technique. Although its applicability is not restricted to LC-DAD data, this experimental model was chosen because it is a widespread technique and experimental data were available.

This orthogonalization technique was also previously applied to mass spectrometric analysis by Khots et al. [15] for the assessment of chromatographic peak purity in multicomponent mixtures of organic substances, and for the determination of the basic constituents of the products resulting from the catalytic conversion of individual hydrocarbons [16].

THEORY

After pretreatment of the data matrix by putting negative values equal to zero, a row vector $\mathbf{x}_m = \{x_{m1}, \ldots, x_{mJ}\}$, called "base" vector, is selected, on which will be projected each other row vector $\mathbf{x}_i = \{x_{i1}, \ldots, x_{iJ}\}$ of the data matrix. The "base" vector is the row in the data table that has the highest sum of squares of all the elements in the row, i.e., the spectrum with the highest overall absorbance.

Prior to the orthogonalization, the data matrix is normalized to give the same statistical weight to each row of the data table, e.g., to each spectrum recorded at a specific time. Normalization is carried out in two different ways. Depending on the normalization technique applied, the algorithm will be called Method 1 and Method 2 to make easier the comparison between the two procedures.

Method 1

Normalization is carried out by dividing each element in a given data row by the square root of the sum of the squares of all the elements in the row.

$$\mathbf{z}_i = \left\{ \frac{x_{ij}}{\|\mathbf{x}_i\|} \right\} = \left\{ \frac{x_{ij}}{\sqrt{\sum_{j=1}^{J} x_{ij}^2}} \right\} \tag{1}$$

Starting from the first spectrum measured, each spectrum is projected onto the "base" vector, which was previously normalized, and the vector $\mathbf{y}_i$ $(i = 1 \ldots I)$, orthogonal to the "base" vector, is determined. This is equivalent to applying the Gram-Schmidt orthogonalization technique to a set of two vectors.

$$\mathbf{y}_i = \mathbf{z}_i - (\mathbf{z}_i, \mathbf{z}_m)\mathbf{z}_m \tag{2}$$

Afterwards, the length of the vectors $\mathbf{y}_i$ is calculated

$$\|\mathbf{y}_i\| = \sqrt{\sum_{j=1}^{J} y_{ij}^2} \tag{3}$$

and plotted against analysis time. The procedure is illustrated in Fig. 1. To explain the procedure the spectrum is reduced to two wavelengths (244 and 280 nm) of which we know that they differentiate relatively well between the two substances. In practice, we would not know this and therefore these figures are only given to demonstrate what is done. In Fig. 1a, we observe points such as A, the point representing the "base" vector, and B situated on a line with other points representing measurements of the pure main component. Points C and D are on another line, and due to

the pure "impurity". Point E is a mixture point. There are many points, such as F, close to zero due to noise. The result after application of Eqn. 1 is to put all the points at the same distance from the origin while respecting the angle between the vectors going from the origin to each point (Fig. 1b). The points A and B are close together and so are C and D, but C and D are in another location than A and B. Point E is found in between and the noise points such as F are scattered in all directions. One then measures the distances of each point to the base vector by measuring the length of the vector orthogonal to the base vector (Fig. 1c). As a result, the largest lengths will correspond to the projections of the noise spectra, while the ones that represent the main component will yield orthogonal vectors **y** with lengths close to zero (Fig. 1d). C and D, representing the second component, have more or less the same length, more distant from zero and E falls in between.

In fact, one measures the sinus of the angle determined by the "base" vector and each row vector, what is called dissimilarity by Excoffier et al. [17]. In this sense, the measurement obtained can also be related to the correlation coefficients between the two spectra (reference and "base" spectra), since these coefficients represent the cosine of the angle between two vectors.

Method 2

The fact that the orthogonal vectors obtained from the projection of the noise spectra onto the "base" vector have the highest length, makes difficult the detection of small concentrations of impurity, when the resolution is low. An improvement was made by changing the normalization process. It is carried out by dividing all the elements in the data matrix by the Euclidean norm of the "base" vector

$$\mathbf{z}_i = \left\{ \frac{x_{ij}}{\|\mathbf{x}_m\|} \right\} = \left\{ \frac{x_{ij}}{\sqrt{\sum_{j=1}^{J} x_{mj}^2}} \right\} \tag{4}$$

As before, to illustrate this method the spectrum is reduced to two wavelengths (244 and 280

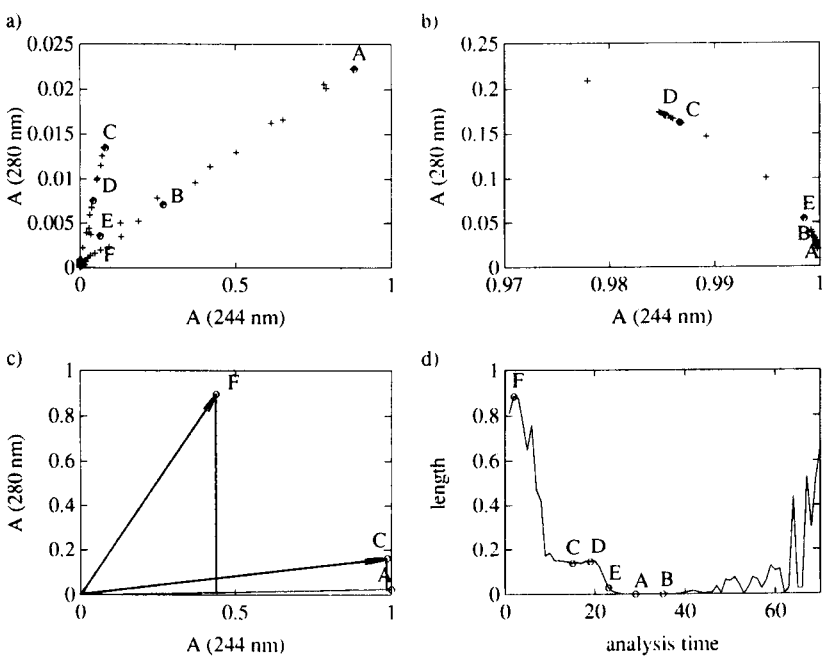

Fig. 1. Method 1: (a) absorbance data at 280 nm vs. absorbance data at 244 nm for $R_s = 1$ and 10% impurity; (b) previous data normalized; (c) orthogonal vectors obtained from a noise spectrum (F), impurity spectrum (C) and main component spectrum (A); (d) length of the orthogonal vectors vs. analysis time.

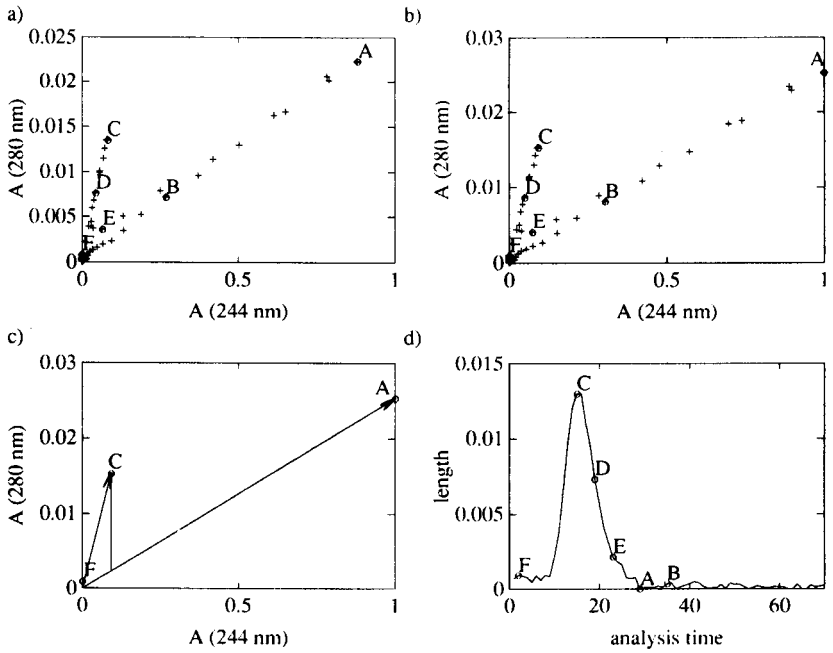

Fig. 2. Method 2: (a) absorbance data at 280 nm vs. absorbance data at 244 nm for $R_s = 1$ and 10% impurity; (b) previous data normalized; (c) orthogonal vectors obtained from a noise spectrum (F), impurity spectrum (C) and main component spectrum (A); (d) length of the orthogonal vectors vs. analysis time.

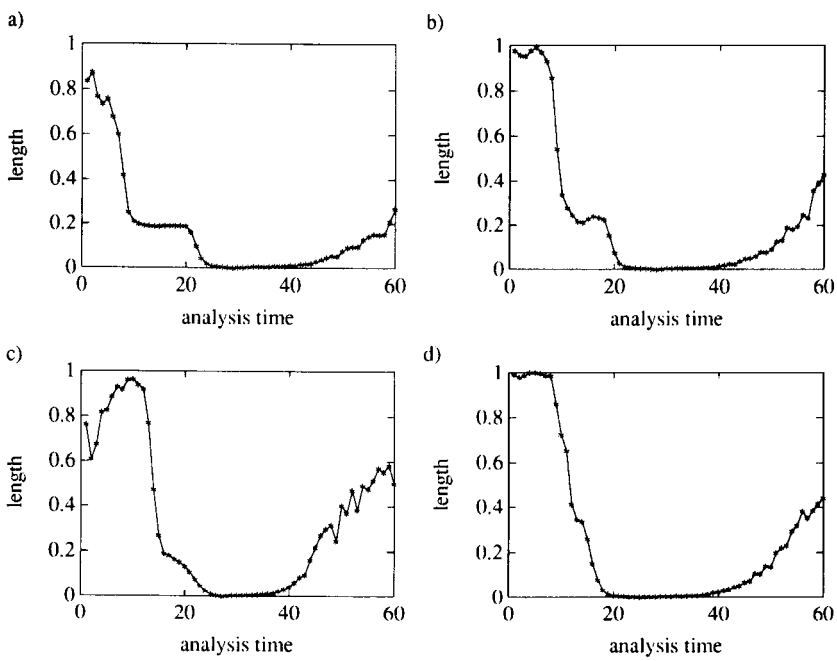

Fig. 3. Length of the orthogonal vectors obtained from Method 1 vs. analysis time for: (a) 10% impurity ($R_s = 1$), (b) 0.5% impurity ($R_s = 1$), (c) 10% impurity ($R_s = 0.4$), (d) pure hydrocortisone.

nm). In Fig. 2a, which is equal to Fig. 1a, points A and B represent the main component, C and D the impurity, E a mixture of both and F noise. After normalization, applying Eqn. 4, the normalized vectors have the same distribution as the original vectors, although their length is a little bit increased since the normalization is carried out using as normalization constant the Euclidean norm of the "base" vector, and this is a little bit lower than one (Fig. 2b). Therefore, points such as F, representing noise, remain very close to zero. Points corresponding to the main compound, such as A and B, are lying on a line, while the points due to the noise, C and D, are situated on a different line. The points related to mixtures are located between these two lines. Afterwards, the distance between each point and the "base" vector is calculated, by measuring the length of the vector orthogonal to the "base" vector (Fig. 2c). As a result, the largest orthogonal vectors are the ones obtained from the projection of the row vectors of the impurity (C and D), while the orthogonal vectors that come from the row vectors of the main component (A and B) and the noise (F) have a length close to zero (Fig. 2d).

DATA

The application of these algorithms was studied on a LC-DAD data set published by Keller et al. [18]. The samples consisted of hydrocortisone and different concentrations of prednisone. The latter was considered as impurity and its relative concentration ranged from 0.1 to 100%. Chromatographic separation quality between the two analytes was varied from $R_s = 0.1–1$.

RESULTS AND DISCUSSION

Method 1

Examples of results obtained are given in Fig. 3.

In Fig. 3a it can be seen that up to time 10 there is no compound present. From time 10 till time 20, the length of the orthogonal vectors obtained is constant, indicating the elution of a species. The elution of the main compound takes place between time 22 and 40, approximately, since the value of the length is practically zero. For $R_s = 1$ the presence of an impurity is very clear, even if its concentration is only 0.5% (Fig.

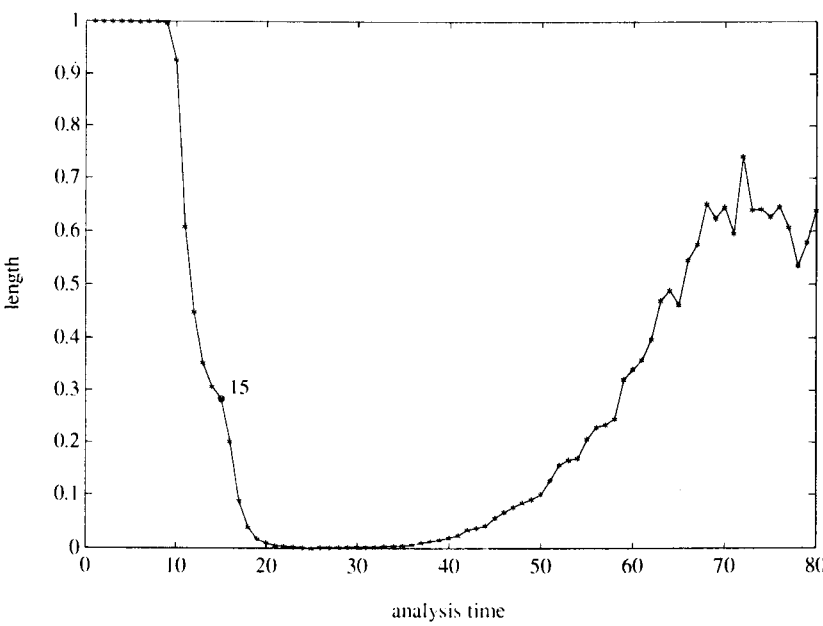

Fig. 4. Method 1: length of the orthogonal vectors vs. analysis time for the case of $R_s = 1$ and 0.1% impurity.

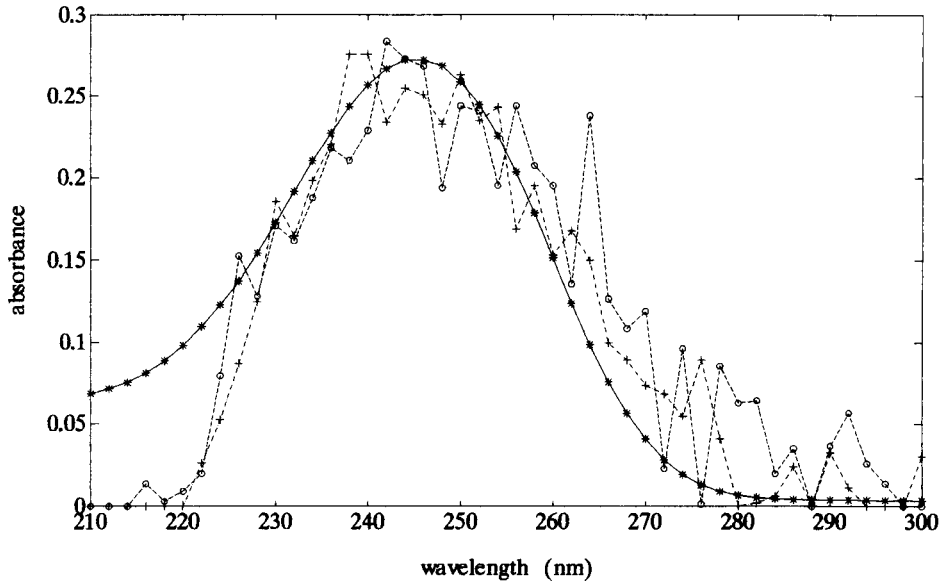

Fig. 5. Spectra of pure hydrocortisone at time 25 (*) and 14 (○), and 0.1% impurity, $R_s = 1$ at time 15 (+).

3b). The result obtained for $R_s = 0.4$ and 10% of impurity is given in Fig. 3c.

In Fig. 3d the result for "pure" hydrocortisone is shown. An inflection at times 13 and 14 was noted. Such an inflection can be seen also for the case of $R_s = 1$ and 0.1% of impurity around the times 14 and 15 (Fig. 4). Therefore it was considered possible that an impurity was present in the

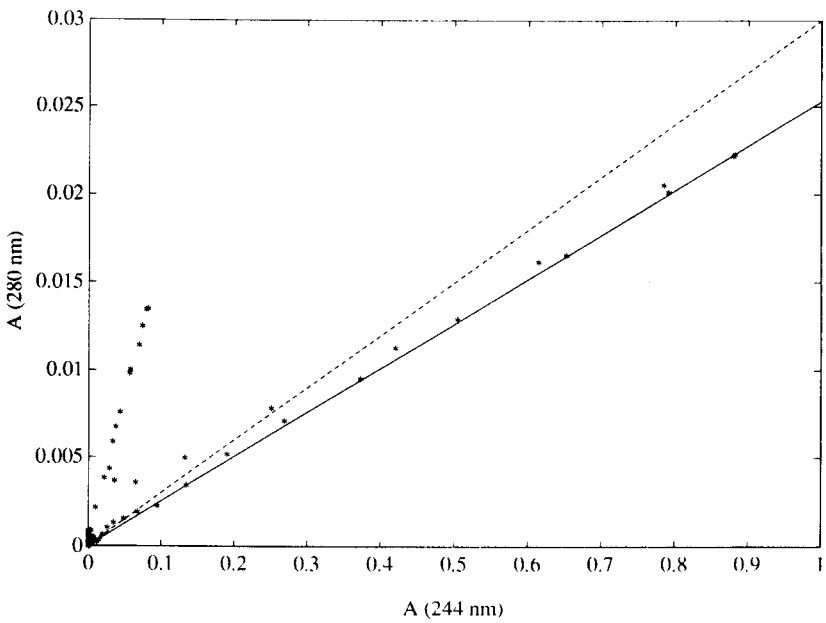

Fig. 6. Comparison between the "base" vector (solid line) and the first principal component (dashed line), for the case of $R_s = 1$ and 10% impurity.

"pure" hydrocortisone. To check such a possibility, the normalized spectra of the "pure" hydrocortisone for time 25 (main peak) and for time 14 (inflection) together with the spectra for the case of $R_s = 1$ and 0.1% of impurity at time 15 were plotted (Fig. 5). These spectra are now compared and found to be similar. Probably the hydrocortisone standard was accidentally contaminated with prednisone. This is a good test of the method since it shows that it is possible to detect 0.1% of impurity for the case of $R_s = 1$, even when such an impurity was not expected.

As resolution and concentration of the impurity become lower, the method fails. This can due to the fact that in the case of resolution 1, the "base" vector contains information only about the main component, but when the resolution is smaller, the "base" vector contains also information about the impurity.

This was also our motivation to study techniques that are not based on PCA, namely that the first principal component contains information about the main component but also about the impurity (Fig. 6). Furthermore, sloping or non-zero baselines, correlated noise, and heteroscedasticity can result in more significant PCs than chemical species present and the failure of the method.

Method 2

With method 1, the length of the orthogonal vector depends only on the angle between the "base" vector and each row vector, since the vectors are normalized to length one; while with method 2 it depends on the angle and on the length of each normalized row vector. A detailed explanation will be given for the case of $R_s = 1$ and 10% of impurity (Fig. 7a). The vectors due to the noise, from time 0 till 10 and from 40 till 60, approximately, will yield orthogonal vectors with length close to zero, since their length is around 10^{-3}. The vectors representing the main compound (from time 24 till 40) have the largest length but, as the angle determined by each vector and the "base" vector is close to zero, the length of the orthogonal vector is also close to zero (ca. 2×10^{-3}). The vectors of the impurity, from time 10 till 20, have intermediate length,

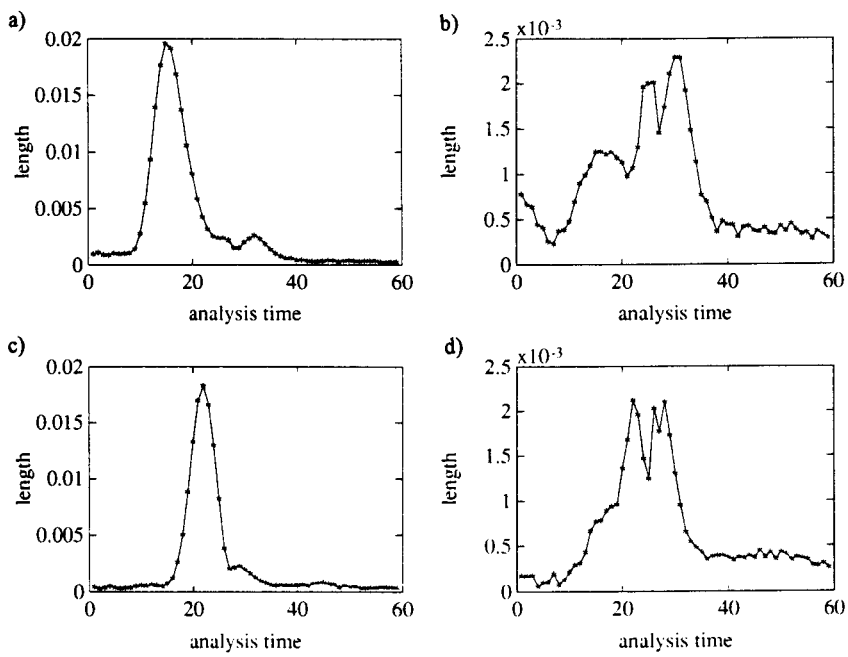

Fig. 7. Length of the orthogonal vectors obtained from Method 2 vs. analysis time for: (a) 10% impurity ($R_s = 1$), (b) 0.5% impurity ($R_s = 1$), (c) 10% impurity ($R_s = 0.4$), (d) pure hydrocortisone.

and in our example the angle with respect to the "base" vector is around 11°, so their orthogonal vectors have the largest length, being the maximum value at time 15.

The result obtained for $R_s = 1$ and 0.5% of impurity is given in Fig. 7b.

The improvement introduced by this second method is evident for the case of 10% of impurity and $R_s = 0.4$ (Fig. 7c).

In Fig. 7d the result for "pure" hydrocortisone is shown. A small shoulder from time 14 to 19, indicates the presence of an impurity.

Method 2 performs somewhat better than Method 1 for the detection of impurities (Fig. 8), although it fails when the resolution is very low, since the "base" vector subtracts information about all the compounds eluting. However, it is possible to reach slightly better detection limits than Keller et al. [18] obtained by means of fixed size window evolving factor analysis FSW EFA.

To confirm the result it is useful to look at the spectra corresponding to several times in the different regions shown in Figs. 3 and 7. In Fig. 9 one can see that the spectrum corresponding to time 30 is different to the one corresponding to time 15.

Limits of the methods

Heteroscedasticity, i.e., noise that depends on the magnitude of the signal, is one of the main problems for the application of techniques based on PCA [19]. To check the performance of Method 1 and 2 in presence of heteroscedastic noise, a noise function was added to the experimental data of the absorbance values. Method 1 behaves in the same way as with homoscedastic data, reaching the same detection limits (Fig. 10). The absorbance data due to the main compound suffer greater variation since they are the highest in magnitude while the ones corresponding to noise or to the impurity are less affected. Therefore, the orthogonal distances of the noise or impurity vectors to the "base" vector will be the same or almost the same, but the ones of the main compound vectors will be somewhat higher than zero, since the points are less aligned so the angles between each vector and the "base" vector are greater.

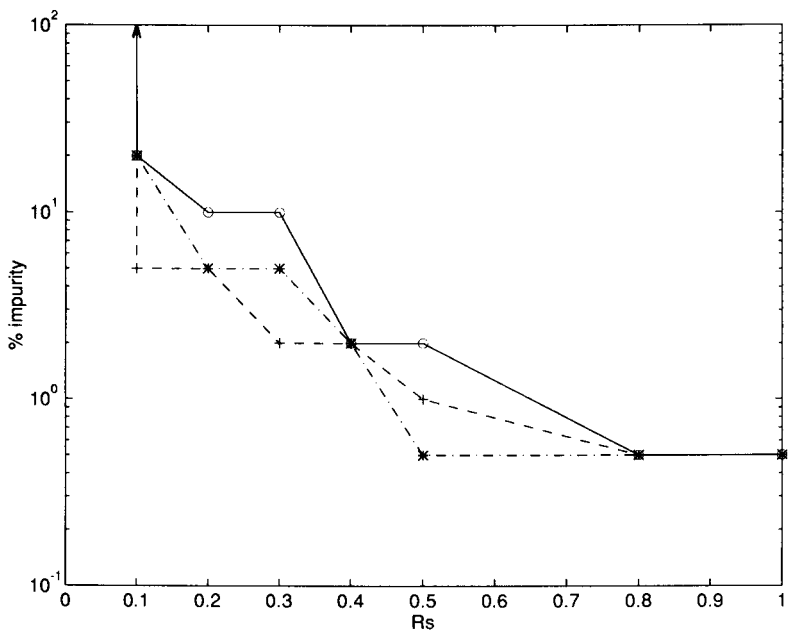

Fig. 8. Detection limits for an impurity obtained with Method 1 (solid line), Method 2 (dashed line) and FSW EFA method (dash-dotted line).

As was explained before, with Method 2 the length of the orthogonal vectors depends on the length of the normalized row vectors, and on the angles between each row vector and the "base" vector. The length and the direction of the vectors representing noise and impurity are only slightly affected, so their orthogonal distance to the "base" vector is almost the same. However, because of the heteroscedasticity, the angle between the vectors representing the main compound and the "base" vector is higher than zero (ca. 4° in our case). This, together with the fact that they have the largest length, makes that their orthogonal vectors have the highest length. Therefore, although the orthogonal vectors due to the impurity have the same length as before, now the detection of the impurity is more difficult (Fig. 11).

One limitation common to both methods is that the data should follow Beer's law as well as to have an intrinsic order.

In general, these methods perform more or

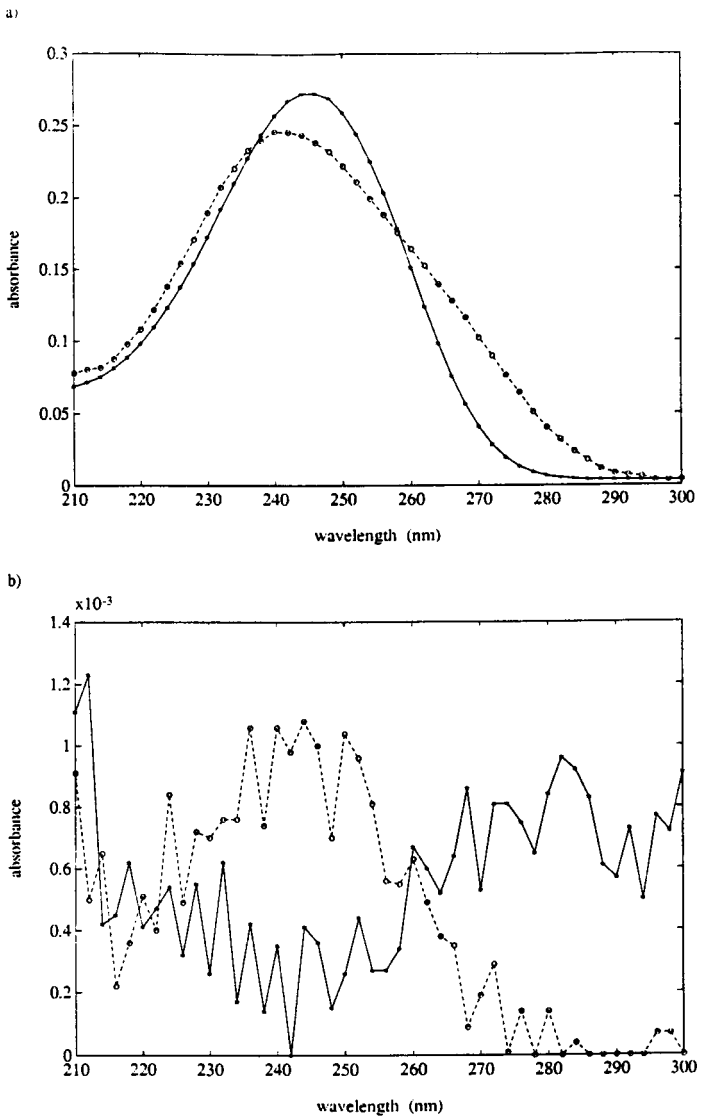

Fig. 9. Absorbance vs. wavelength for $R_s = 1$ and 10% impurity for (a) time 30 (solid line) and time 15 (dashed line) and (b) time 2 (solid line) and time 60 (dashed line).

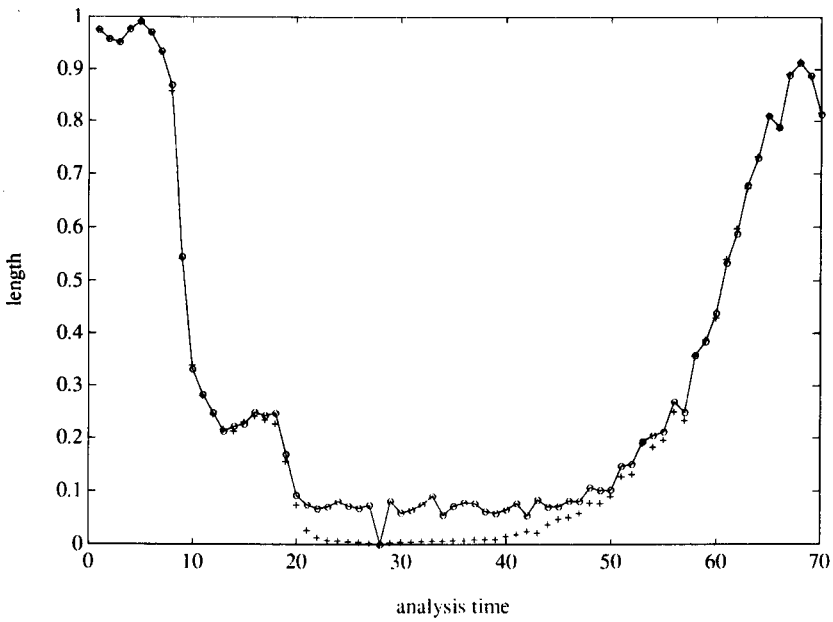

Fig. 10. Performance of Method 1 in presence of heteroscedastic noise (○) and homoscedastic noise (+) for $R_s = 1$ and 0.5% of impurity.

less similarly to the FSW EFA method [9]. Keller et al. [20] showed that also HELP [6–8] and MCA [17] give rather similar results for the data set studied. We showed ourselves (unpublished results) that a method based on biplots of the log double-centered or the double closed data also

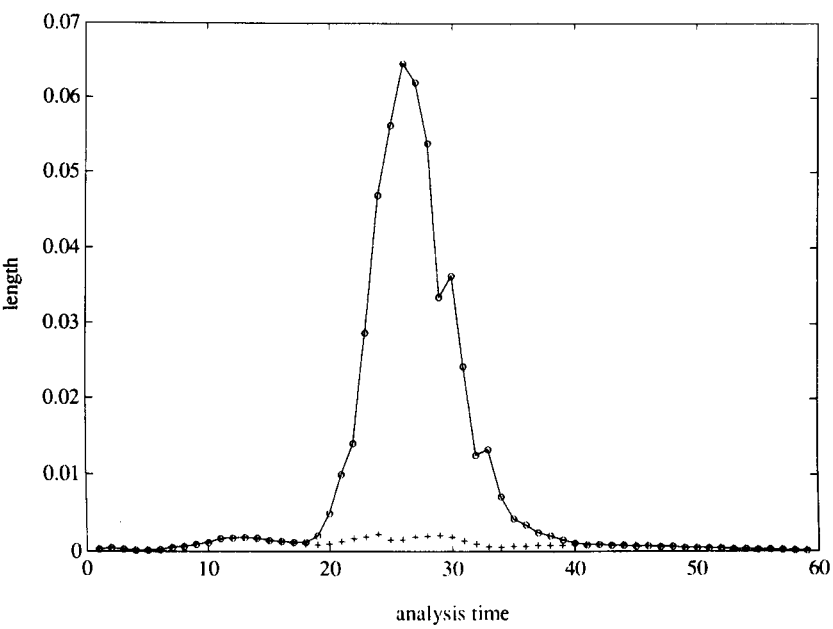

Fig. 11. Performance of Method 2 in presence of heteroscedastic noise (○) and homoscedastic noise (+) for $R_s = 1$ and 1% of impurity.

have the same detection limit. This remarkable similarity between many different methods seems to show that a more fundamental limit has been reached. This can be understood better from Fig. 12. These figures show the impurity chromatographed at a level of concentration equivalent to 0.1% compared to hydrocortisone. The first figure (Fig. 12a) gives the peak observed at

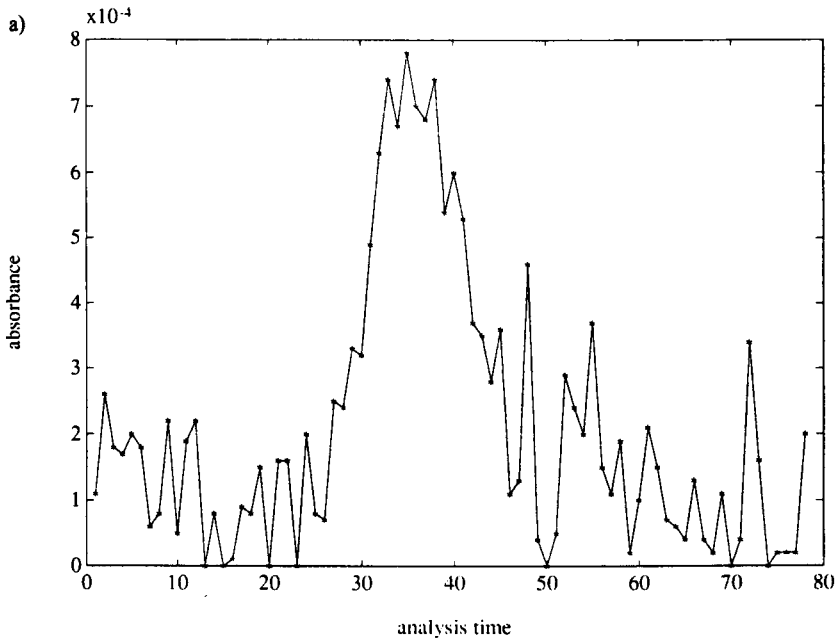

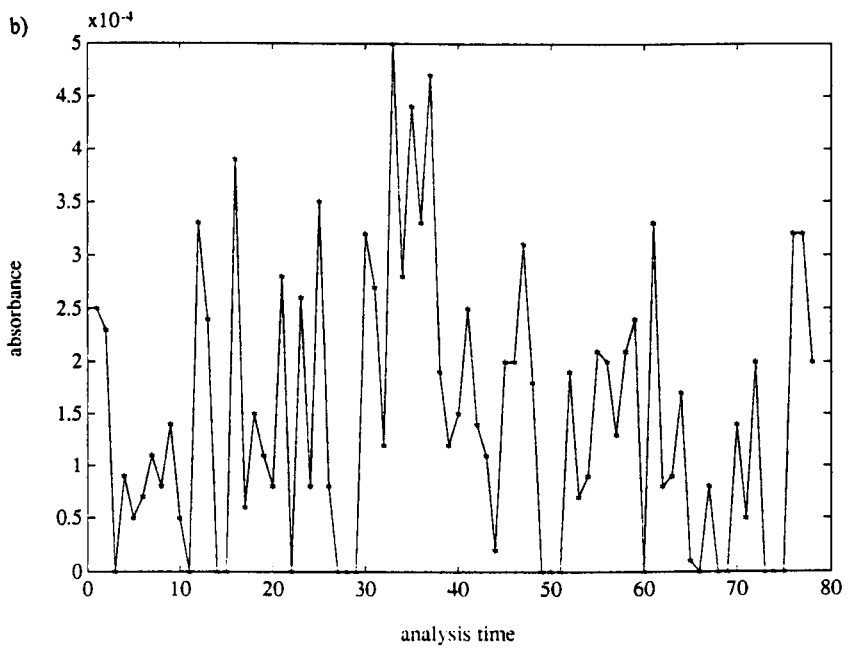

Fig. 12. Chromatogram of 0.1 mg ml^{-1} of prednisone at (a) 240 nm (b) 274 nm.

240 nm, the wavelength with maximum absorbance. However, the discrimination is due to the wavelength range around 274 nm. Figure 12b shows the chromatogram at that wavelength. Clearly, the problem is not only to detect the impurity under a 1000 × larger peak with a similar spectrum, but also to detect the peak as such. To achieve better results, there are therefore two possibilities. One is to reduce noise, so that the signal of the impurity can be observed better and the other is to increase the amount of substance injected. Since diode arrays have a rather limited linearity range, this will introduce non-linearities and it should be noted that all the methods described higher implicitly require linearity. From a chemometric point of view, this means that an advance in this field requires that one should concentrate on methods that eliminate better the effect of noise, probably by signal treatment, or methods than can cope with non-linearity or both together.

D.L. Massart and M.S. Khots thank the NFWO, FGWO and ChemoAC for financial assistance.

REFERENCES

1 B.G.M. Vandeginste, W. Derks and G. Kateman, Anal. Chim. Acta, 173 (1985) 253.
2 B.G.M. Vandeginste, G. Kateman, J.K. Strasters, H.A.H. Billiet and L. de Galan, Chromatographia, 24 (1987) 127.
3 G.G.R. Seaton and A.F. Fell, Chromatographia, 24 (1987) 208.
4 H. Gampp, M. Maeder, C.J. Meyer and A.D. Zuberbühler, Talanta, 32 (1985) 1133; 33 (1986) 943.
5 M. Maeder and A. Zilian, Chemom. Intell. Lab. Syst., 3 (1988) 205.
6 O.M. Kvalheim and Y.Z. Liang, Anal. Chem., 64 (1992) 936.
7 Y.Z. Liang, O.M. Kvalheim, H.R. Keller, D.L. Massart, P. Kiechle and F. Erni, Anal. Chem., 64 (1992) 946.
8 H.R. Keller, D.L. Massart, Y.Z. Liang and O.M. Kvalheim, Anal. Chim. Acta, 267 (1992) 63.
9 H.R. Keller and D.L. Massart, Anal. Chim. Acta, 246 (1991) 379.
10 J. Kankare, J. Lukkari, T. Pajunen, J. Ahonen and C.J. Visby, Electroanal. Chem., 295 (1990) 59.
11 E.R. Malinowski, J. Chemom., 6 (1992) 29.
12 R. Tauler, G. Durand and D. Barcelo, Chromatographia, 33 (1992) 244.
13 J.B. Castledine and A.F. Fell, J. Pharm. Biomed. Anal., 11 (1993) 1.
14 G.T. Rasmussen, B.A. Hohne, R.C. Wieboldt and T.L. Isenhour, Anal. Chim. Acta, 112 (1979) 151.
15 M.S. Khots and N.M. Bogel'fer, J. Anal. Chem., 35 (1980) 1432.
16 M.S. Khots, I.S. Shapiro and G.B. Belan, J. Anal. Chem., 40 (1985) 1630.
17 J.L. Excoffier, M. Joseph, J.J. Robinson and T.L. Sheehan, J. Chromatogr., 631 (1993) 15.
18 H.R. Keller, D.L. Massart and J.O. De Beer, Anal. Chem., 65 (1993) 471.
19 H.R. Keller, D.L. Massart, Y.Z. Liang and O.M. Kvalheim, Anal. Chim. Acta, 263 (1992) 29.
20 H.R. Keller, P. Kiechle, F. Erni, D.L. Massart and J.L. Excoffier, J. Chromatogr., 641 (1993) 1.

Analytica Chimica Acta, 285 (1994) 193–208
Elsevier Science B.V., Amsterdam

Expert system for the voltammetric determination of trace metals

Part IV. Methods for speciation of chromium and arsenic

M. Esteban and C. Ariño

Departament de Química Analítica, Universitat de Barcelona, Av. Diagonal 647, 08028 Barcelona (Spain)

I. Ruisánchez, M.S. Larrechi and F.X. Rius

Departament de Química, Universitat Rovira i Virgili (Tarragona), Pl. Imperial Tàrraco 1, 43005 Tarragona (Spain)

(Received 8th February 1993; revised manuscript received 20th April 1993)

Abstract

A previously described expert system for the voltammetric determination of Cu, Zn, Cd, Pb, In, Ni, Co, Tl, Hg, V and Se (optionally also Te) is enlarged and improved by including methods for speciation of chromium and arsenic. Voltammetric procedures for the quantification of Cr(III), Cr(VI), As(III) and As(V) are considered, Cr(III) and As(V) being determined by the difference between total chromium and Cr(VI), and total arsenic and As(III) respectively. The techniques implemented are differential pulse polarography, differential pulse anodic stripping voltammetry, differential pulse cathodic stripping voltammetry and differential pulse adsorptive stripping voltammetry, using mercury drop electrodes and a rotating gold electrode. The expert system is developed using KES (knowledge engineering system).

Keywords: Voltammetry; Arsenic; Chromium; Expert system; Metal speciation; Chemometrics; Trace metals

In previous papers [1,2], a knowledge-based expert system for the voltammetric determination of several trace metals was described. Elements considered were Cu, Zn, Cd, Pb, In, Ni, Co, Tl, Hg, V and Se (optionally also Te). The techniques implemented were differential pulse polarography (DPP), differential pulse anodic stripping voltammetry (DPASV), differential pulse cathodic stripping voltammetry (DPCSV) and differential pulse adsorptive stripping voltammetry (DPAdSV), using mainly mercury drop electrodes (SMDE and HMDE).

Correspondence to: M. Esteban, Departament de Química Analítica, Facultat de Química, Universitat de Barcelona, Av. Diagonal 647, 08028 Barcelona (Spain).

The expert system is designed for those users who have some knowledge in electrochemical analysis but cannot be considered as specialists. Furthermore, it can be a valuable tool for teaching electroanalytical methods and for showing applicability of expert systems.

In this paper, an enhancement of the previously described expert system is reported, which is devoted to the speciation of chromium and arsenic.

Chromium is an important ecotoxic trace metal which can be present, in natural waters, in two oxidation states: the reactive and toxic Cr(VI) and the relatively inert Cr(III). Cr(VI) is present at various concentration levels, 0.1–0.5 $\mu g\ l^{-1}$, in ocean waters [3], to 200 $\mu g\ l^{-1}$ in some poluted ground waters [4].

SSDI 0003-2670(93)E0459-K

Atomic absorption spectrometry (AAS), with flame or graphite furnace, and voltammetry have been used for the determination of chromium. The disadvantages of the spectroscopic methods are that they usually need a preconcentration step or multiple injection in the graphite furnace. The preconcentration methods most frequently described are ionic exchange and dithiocarbamate chelate extraction in different organic solvents [5]. Furthermore, only the total chromium can be determined, and no distinction can be made between different oxidation states. The main advantage of voltammetric methods is the possibility to distinguish between total chromium and Cr(VI). Furthermore, these methods allow the determination of concentrations levels similar to those found in ocean waters.

Arsenic is also an important ecotoxic metal present in natural waters (polluted or not). It can be found as As(III) or As(V), as well as methanearsonic acid [$MeAsO(OH)_2$], dimethylarsinic acid [$Me_2AsO(OH)$] and other organoarsenic compounds. The concentration of total arsenic in water is up to 2 $\mu g\ l^{-1}$, in non-polluted waters, and about 75 $\mu g\ l^{-1}$ in many polluted waters, the limit of toxicity being 50 $\mu g\ l^{-1}$ of total arsenic [6].

In recent years, a number of papers have been published on the determination of arsenic species at the trace level. Voltammetric methods allow us to distinguish between As(III) and As(V) since As(V) is electroinactive, and it has to be reduced by chemical means prior to its determination.

The knowledge base used in the improvement of the expert system allows the determination in waters, by voltammetric means, of Cr(III), Cr(VI) and total chromium, as well as the determination of As(III), As(V) and total arsenic. Application of the methods proposed to other types of samples is described.

KNOWLEDGE BASE

Speciation of chromium

In the scheme proposed for the speciation of chromium, it is necessary to distinguish between two main options: Option 1, which allows the determination of total chromium [without the distinction between Cr(III) and Cr(VI)], and Option 2, which allows the determination of Cr(VI) and Cr(III), the concentration of Cr(III) being obtained from the difference between total chromium and Cr(VI).

Option 1 is based on the use of DPAdSV onto an HMDE [7,8]. Before applying the electroanalytical technique recommended, all the chromium must be in the form of Cr(VI) (Fig. 1). Thus, Cr(III) is converted to Cr(VI) by UV irradiation of the sample, in the presence of a small amount of H_2O_2 at neutral pH [8]. Within Option 1, two sub-options are included, which differ only in the concentration range recommended for each: below and above 2 $\mu g\ l^{-1}$ for sub-options 1 [7] and 2 [8] respectively. However, the electroanalytical methods of sub-options 1 and 2 are practically equal: after the reduction of Cr(VI) to Cr(III), complexes of Cr(III) with diethylenetriaminepentacetic acid (DTPA) are collected by adsorption onto an HMDE at -1.0 V. This method has a limit of detection of 5.2 $ng\ l^{-1}$ (in sea water) [7].

After the determination of total chromium (Fig. 1), the expert system asks the user for his/her interest in the concentration of Cr(III). In the afirmative case, the user can receive information about the determination of Cr(III) if the proper choice is made at the end of process shown in Fig. 1. This further option is not shown in Fig. 1.

However, for the determination of Cr(III) and Cr(VI), or only Cr(VI), Option 2 should be chosen at the beginning of the process (for determining chromium species).

In Option 2, the expert system guides the user to determine Cr(VI) and, indirectly, Cr(III) (Fig. 2). Option 2 includes four possibilities (sub-options) of choice, which depend on their respective useful concentration range. Sub-option 1 also recommends DPAdSV onto an HMDE, as for the determination of total chromium (Option 1; Fig. 1). In natural waters, for the analysis of Cr(VI) in the presence of Cr(III), no previous treatment of the sample is required (neither UV irradiation nor H_2O_2 treatment), in order to avoid the oxidation of Cr(III) to Cr(VI). A waiting time of at least 15 min, after the addition of DTPA, is

required before the accumulation step [7] (see Fig. 2).

The method proposed in sub-option 2, which is shown in Fig. 3, allows the determination of Cr(VI) in the concentration range between 35 $\mu g\ l^{-1}$ and 2 $mg\ l^{-1}$, and it is based on the reduction of Cr(VI) in an acetate buffer medium containing ethylenediamine, by DPP [9]. Determination must be performed without previous UV irradiation of the sample, in order to avoid the interference of Cr(III). A reduction peak at −0.05 V vs. SCE is observed for Cr(VI). Sub-options 3 and 4 recommend the dilution of the sample to reach the concentration ranges of the methods described in sub-options 1 and 2 respectively.

Speciation of arsenic

The knowledge base for the speciation of arsenic is divided into three main options. Option 1 is only devoted to the determination of As(III), Option 2 to the total arsenic, while Option 3 to the determination of As(III) and As(V). The aim of the third option is the speciation of arsenic in environmental samples.

For the particular case of determining only As(III) (Option 1), two methods are recommended. They are similar and appropriate for the $ng\ ml^{-1}$ level. The method referred to under sub-option 1 is based on CSV onto an HMDE [10]. For the preconcentration of As(III) onto the electrode, the presence of Se(IV) is necessary (Fig. 4). In view of observations by Holak [10], a probable explanation of the role of Se(IV) is that at potentials between −0.25 and −0.5 V, As(III) reacts with the mercuric selenide deposited, forming arsenic selenide and mercury:

$$2As^{3+} + 3HgSe + 6e^- \rightarrow As_2Se_3 + 3Hg$$

This would explain the apparent shift toward the positive potential of the first wave of arsenic. At a potential of about −0.72 V, arsenic selenide is reduced, resulting in arsine and hydrogen selenide:

$$As_2Se_3 + 12e^- + 12H^+ \rightarrow 2AsH_3 + 3H_2Se$$

Since in the present procedure, mercuric selenide strips just before arsenide, some overlapping of the two peaks occurs. To overcome this difficulty, the voltage during the equilibration period was set at the point at which mercuric selenide would be stripped, thus eliminating the undesired current during the subsequent voltage scan.

An alternative method, referred to under sub-option 2, can be used [11]. Such a method is also based on DPCSV onto an HMDE, but in this case in the presence of Cu(II) (Fig. 5). In the pre-electrolysis of As(III) in a Cu(II)-containing solution, an intermetallic compound of the composition Cu_3As is probably formed on the mercury surface [11]. Its redissolution by cathodic stripping on the basis of a further reduction of arsenic to As^{3-} leads to a current signal linearly related to the concentration of arsenic, in the range of 0.2 to 20 $\mu g\ l^{-1}$.

If the approximate concentration of As(III) is unknown, method under sub-option 1 is recommended.

When the determination of total arsenic is desired (Option 2), which is very common in the study of natural waters and drinking waters, two methods (sub-options 1 and 2, Fig. 6) are recommended. Both methods are based on the determination of As(III). Obviously, in order to apply these methods for the determination of total arsenic, a previous reduction of the electroinactive As(V) to As(III) is required. Systematic investigations were performed in order to propose methods for the quantitative reduction of As(V) to As(III). In the two methods proposed, different chemical procedures for the reduction of As(V) are recommended.

The first method (sub-option 1, Fig. 6) is based on the determination of As(III) in the presence of Cu(II) by DPCSV onto an HMDE [12]. This method presents high coincidences with method referred to under sub-option 2, in option 1 [11]. However, by comparison of the electrochemical basis of the process mentioned by Henze et al. [11] and Sadana [12], a disagreement in the nature of the intermediate process assumed can be noted. Thus, Sadama summarizes the role of copper through the formation of a copper amalgam. Further, arsenic may react to form copper arsenide during the deposition step as shown in the equation

$$2As^{3+} + 3Hg(Cu) + 6e^- \rightarrow Cu_3As_2 + 3Hg$$

Figure 1, Determination of total Cr by using Differential Pulse Adsorptive Stripping Voltammetry (DPAdSV) onto the Hanging Mercury Drop Electrode (HMDE).

Which of the following cations are to be determined?

1. Cu Zn Cd Pb
2. Ni Co
3. Tl
4. Se
5. Hg
6. V
7. Cr
8. As
9. others

=? **7**

The methods recommended here are developed to analyse natural waters whether polluted or otherwise. These methods have been selected because of the relevance of their performance characteristics published in the literature.

Which chromium species do you want to determine?

1. Total Cr
2. Cr(VI) and/or Cr(III)

Note: If you are interested in determining Cr(III) is necessary to determine first the total chromium according to the methodology described in option 1.
(Enter a number)

=? **1**

Do you know the approximate metal-ion concentration?

1. yes
2. no

=? **1**

What is the concentration range of Cr in the sample?

1. if [Cr] < 2 μg/l
2. if [Cr] > 2 μg/l

Note: The method indicated in option 2 is the same as the method in option 1. Due to the sensitivity of the method, concentration levels below 2 μl/l are recommended. It should be noted that the relatively inert Cr(III) species and the more toxic reactive Cr(VI) species are present in natural waters at various concentrations ranging from 0.1-0.5 μg/l in ocean waters up to 200 μg/l in polluted ground waters.

(Enter a number)
=? **1**

You should use Differential Pulse Adsorptive Stripping Voltammetry (DPAdSV) using the Hanging Mercury Drop Electrode (HMDE).

Note: The stripping voltammetric scan produces a peak at -1.22 V, at the bottom of the hydrogen wave. The peak is due to the reduction of Cr(III) to Cr(II). The scan is preceded by the adsorptive accumulation of Cr(III) complexes of diethylenetriaminepentacetic acid (DTPA). The Cr(III) is produced freshly during the adsorption step due to the reduction of the dissolved Cr(VI) at the electrode surface during the deposition at -1.0 V. This Cr(III) subsequently forms a complex with DTPA, which is adsorbed onto the mercury drop.

The medium conditions are:

The application of the methods recommended requires that all the chromium should always be in the form of Cr(VI) at the moment of the accumulation step. The Cr(III) is converted into Cr(VI) by UV-irradiation of the sample for 3 or 4 hours, if possible, in the presence of a small amount of H_2O_2 at neutral pH (pH = 7 - 8.5, as for instance the natural pH of the sea waters). The conditions of the cell-medium are: 0.5 mol/l of KNO_3, 0.02 mol/l of acetate buffer (pH = 5.2) and 2.5 E-3 M of DTPA (diethylenetriaminepentacetic acid).

The instrumental parameters are:

Er = Ag/AgCl or Standard Calomel Electrode. Ew = HMDE.
Eaux = Pt or glassy carbon, Eads = -1.0 V vs. Ag/AgCl
tads = 60 - 120 s, tr = 10 s
scan mode DP
pulse = 25 mV (in general, between 10 and 100 mV), v = 20 mV/s.
t(pulse) = 100 ms (in general, between 30 and 100 ms).
Ei = -1.0 V, Ef = -1.4 V. (both vs. Ag/AgCl)

Do you observe different peaks in the voltammograms?
1. yes
2. no
=? **1**

If the potential value is: Ep = -1.22 V vs. Ag/AgCl, the peak will be due to the total Cr(VI) in the solution after the oxidation step by chemical means.

Could you measure the peak height precisely?
1. yes
2. no
=? **1**

The quantitative procedure is based on the multiple standard addition method and the standard solution used is a Cr(VI) solution.

Parameters of the calibration curve:

slope = ... (value according to input experimental data)
intercept (at y = 0) = ... (value according to input experimental data)

The concentration of the cation Cr <1.00> given in mol/l, is the absolute value of .... (value according to experimental data)

In the stripping mode, a cathodic scan is applied, where copper arsenide is reduced to arsine at a potential of about -0.72 V, and hydrogen is evolved, as shown in the following equation

$$Cu_3As_2 + 12H^+ + 3Hg + 12e^- \rightarrow 2AsH_3 + 3H_2 + 3Hg(Cu)$$

Figure 2, Determination of Cr (VI) by using Differential Pulse Adsorptive Stripping Voltammetry (DPAdSV) onto the Hanging Mercury Drop Electrode (HMDE).

Which of the following cations are to be determined?

1. Cu Zn Cd Pb
2. Ni Co
3. Tl
4. Se
5. Hg
6. V
7. Cr
8. As
9. others

=? **7**

The methods recommended here are developed to analyse natural waters whether polluted or otherwise. These methods have been selected because of the relevance of their performance characteristics published in the literature.

What chromium species do you want to determine?

1. Total Cr
2. Cr(VI) and/or Cr(III)

Note: If you are interested in determining Cr(III) is necessary to determine first the total chromium according to the methodology described in option 1.

(Enter a number)
=? **2**

Do you know the approximate metal-ion concentration?

1. yes
2. no

=? **1**

What is the concentration range of Cr(VI) in the sample?

1. if [Cr(VI)] < 2 μg/l
2. if 35 μg/l < [Cr(VI)] < 2 mg/l
3. if 2 μg/l < [Cr(VI)] < 35 μg/l
4. if 2 mg/l < [Cr(VI)]

(Enter a number)

=? **1**

You should use Differential Pulse Adsorptive Stripping Voltammetry (DPAdSV) using a Hanging Mercury Drop Electrode (HMDE).

Note: The stripping voltammetric scan produces a peak at -1.22 V, at the bottom of the hydrogen wave. The peak is due to the reduction of Cr(III) to Cr(II). The scan is preceded by the adsorptive accumulation of Cr(III) complexes of diethylenetriaminepentacetic acid (DTPA).The Cr(III) is produced freshly during the adsorption step due to the reduction of the dissolved Cr(VI) at the electrode surface during the deposition at -1.0 V. This Cr(III) subsequently forms a complex with DTPA, which is adsorbed onto the mercury drop.

The medium conditions are:

The determination of Cr(VI) in natural waters, in presence of Cr(III), requires that you do not apply any sample treatment (neither UV-irradiation nor H_2O_2-oxidation) which could involve the oxidation of Cr(III) to Cr(VI). Furthermore, you must wait for at least 15 minutes after the addition of diethylenetriaminepentacetic acid (DTPA), before the accumulation step.

The conditions of the cell-medium are: 2.5 E-3 M of DTPA, 0.02 mol/l of acetate buffer and NH_3 up to pH = 6.8. After 15 minutes of purging with a N_2 stream, so as to eliminate the interference of Cr(III), the pH must be adjusted to 5.2 by addition of HCl.

The instrumental parameters are:

Er = Ag/AgCl or Standard Calomel Electrode. Ew = HMDE.
Eaux = Pt or glassy carbon, Eads = -1.0 V vs. Ag/AgCl
tads = 60 - 120 s, tr = 10 s
scan mode DP
pulse = 25 mV (in general, between 10 and 100 mV), v = 20 mV/s.
t(pulse) = 100 ms (in general, between 30 and 100 ms).
Ei = -1.0 V, Ef = -1.4 V. (both vs. Ag/AgCl)

Did you observe different peaks in the voltammograms?
1. yes
2. no

=? 1

If the potential value is: Ep = -1.22 V vs. Ag/AgCl, the peak will be due to the presence of Cr(VI) in the original solution.

Arsenic (V) did not give a reduction peak with 5 μg ml^{-1} of Cu(II). It is known to be electroinactive; therefore chemical pre-reduction of As(V) to As(III) is essential for the determination of total arsenic.

An alternative method is proposed (sub-option 2, Fig. 7), which is based on the deposition of As from an acid solution onto a rotating gold electrode, followed by anodic stripping of the As by DP mode [13]. This method has been widely used for the determination of As(III) and As(V) in natural waters and drinking waters. In order to determine total arsenic, As(V) must be first reduced to As(III) by chemical means (Fig. 7).

The main disadvantage of this method is the use of a solid electrode, the rotating Au electrode. The expert system includes the recommendations for the preparation of the electrode, which have a key role in the use of solid electrodes.

When both As(III) and As(V) are to be determined (Option 3), the two methods mentioned in Option 2 are recommended. Thus, As(III) can be determined without previous reduction of the sample. Further, if a previous reduction of the sample is carried out, the total arsenic can be determined, and then As(V) can be estimated by substraction (Figs. 8 and 9).

Conclusions

The enhancement here described of the expert system for the voltammetric determination of trace metals may be very useful for solving prob-

Figure 3, Determination of Cr (VI) by using Differential Pulse Polarography (DPP) onto the Dropping Mercury Electrode (DME) or the Static Mercury Drop Electrode (SMDE).

What is the concentration range of Cr(VI) in the sample?
1. if [Cr(VI)] < 2 μg/l
2. if 35 μg/l < [Cr(VI)] < 2 mg/l
3. if 2 μg/l < [Cr(VI)] < 35 μg/l
4. if 2 mg/l < [Cr(VI)]

(Enter a number)
=? **2**

You should use Differential Pulse Polarography (DPP), using the Dropping Mercury Electrode (DME) or the Static Mercury Drop Electrode (SMDE).

Note: The differential pulse polarographic scan of a sample containing Cr(VI) produces a peak at -0.05 V (vs. SCE) in an acetate buffer medium containing ethylenediamine. The determination must be carried out without UV-irradiation treatment. Cr(III) does not interfere.

The medium conditions are:
The application of the method to water samples only requires the filtration of the sample. The conditions of the cell-medium must be: 0.1 M of acetate buffer and 5.0 E-3 M of ethylenediamine.

The instrumental parameters are:
Er = Ag/AgCl or Standard Calomel Electrode (SCE). Ew = DME or SMDE
Eaux = Pt or glassy carbon,
scan mode DP
pulse = 25 mV (in general, between 10 and 100 mV), v = 20 mV/s.
t(pulse) = 50 ms (in general, between 30 and 100 ms). t(drop) = 0.5 -1 s.
Ei = 0.1 V, Ef = -0.3 V. (both vs. SCE)

Did you observe different peaks in the voltammograms?
1. yes
2. no

=? **1**

If Ep = -0.05 V vs. SCE, the peak will be due to the presence of Cr(VI) in the original solution.

From the shape of the peaks, does it appear that these peaks are generated by only one chemical species?
1. yes
2. no

=? **1**

Can you measure the peak height precisely?
1. yes
2. no

=? **1**

Connection with external program COOK'S2

The concentration of total chromium is ... (value according to input experimental data)
The concentration of Cr(VI) is .... (value according to input experimental data)

Figure 4, Determination of As (III) by using Cathodic Stripping Voltammetry (CSV) onto the Hanging Mercury Drop Electrode (HMDE).

Which of the following cations are to be determined?
1. Cu Zn Cd Pb
2. Ni Co
3. Tl
4. Se
5. Hg
6. V
7. Cr
8. As
9. others

=? **8**

What As species do you want to determine?
1. As (III)
2. Total arsenic
3. Both As(III) and As (V) individually

(Enter a number)
=? **1**

Do you know the approximate metal-ion concentration?

1. yes
2. no

=? **1**

What is the concentration range of As(III) in the sample?
1. if [As(III)] > 2 ppb
2. if 0.2 ppb < [As(III)] < 20 ppb

Note: In order to apply the method described under option 1 for the analysis of samples such as foods, several factors have to be considered. According to Holak (Anal.Chem. 52 (1980) 2189) digestion of the sample in a closed system ensures that no arsenic is lost through evaporation. Heating with magnesium nitrate ensures the destruction of all traces of organic matter. Reduction with sodium bromide in the presence of hydrazine sulphate is effective and does not introduce interfering ions into the solution.

Interference due to copper and other cations is easily eliminated by removing them from solution by extraction with dithizone in carbon tetrachloride.

According to Henze (Mikrochim. Acta II, (1981) 343), reduction of As(V) (which is the usual state in natural samples) to As(III) is readily achieved using sodium sulphite.

(Enter a number)
=? **1**

You should use Cathodic Stripping Voltammetry (CSV), using the Hanging Mercury Drop Electrode (HMDE).

The medium conditions are: 0.72 M H_2SO_4 containing 50 ppm of Se(IV).

The instrumental parameters are:

Er = Ag/AgCl or Standard Calomel Electrode. Ew = HMDE.
Eaux = Pt or glassy carbon.
Epe = -0.5 V during tp = 1.5 min.
Potential scan from Er = -0.6 V to Ef = -1. V at v = 50 mV/s.
Er = -0.6 V during tr = 15 s. (see note)
(Note: After preelectrolysis at Epe = -0.5 V, the potential is switched to -0.6 V (during the rest period), and afterwards, the negative scan is started.)

Interferences:

Cu(II) at tenfold excess respect to As(III) can interfere. Therefore, a previous extraction with dithizone is recommended. If you are interested in examining bibliographical references, enter:
display attach Arsenium of kb.

Set up the polarograph according to the conditions mentioned; connection is established with external program which plots the voltammogram. The voltammogram is:

..... (the voltammogram corresponding to the experimental conditions is shown here)

Did you observe different peaks in the voltammograms?
1. yes
2. no

=? 1

If you observe a peak at Ep = -0.75 V vs. Ag/AgCl, the peak will be due to the presence of As(III).

Figure 5, Determination of As (III) by using Differential Pulse Cathodic Stripping Voltammetry (DPCSV) onto the Hanging Mercury Drop Electrode (HMDE).

What As species do you want to determine?
1. As (III)
2. Total arsenic
3. Both As(III) and As (V) individually

(Enter a number)
=? 1

lems which need of the speciation of As and Cr. For this goal, well-tested methods and very common voltammetric techniques are recommended. In the unique case of recommending a solid electrode (rotating Au electrode), instructions for the preparation of the electrode are given.

Economic support from the Spanish Ministry of Education and Science is acknowledged (DGICYT projects No. BP90-0453 and BP90-0821).

Do you know the approximate metal-ion concentration?
1. yes
2. no

=? 1

Which is the concentration range of As in the sample?
1. if [As(III)] > 2 ppb
2. if 0.2 ppb < [As(III)] < 20 ppb

(Enter a number)
=? 2

You should use Differential Pulse Cathodic Stripping Voltammetry (DPCSV), using the Hanging Mercury Drop Electrode (HMDE).

The medium conditions are: 1 M HCl containing 2.0 E-3 M $CuCl_2$.

The instrumental parameters are:
Er = Ag/AgCl or Standard Calomel Electrode. Ew = HMDE.
Eaux = Pt or glassy carbon,
Epe = -0.55 V vs. Ag/AgCl during tp = 1 - 2 min. tr = 10 - 20 s.
Ef = -1. V, pulse = 50 mV, v = 10 mV/s.

Set up the polarograph according to the conditions mentioned; connection is established with external program which plots the voltammogram. The voltammogram is:

..... (the voltammogram corresponding to the experimental conditions is shown here)

Do you observe different peaks in the voltammograms?
1. yes
2. no

=? 1

If you observe a peak at Ep = -0.78 V vs. Ag/AgCl, the peak will be due to the presence of As(III).

Figure 6, Determination of total arsenic by using Differential Pulse Cathodic Stripping Voltammetry (DPCSV) onto the Hanging Mercury Drop Electrode (HMDE).

What As species do you want to determine?
1. As (III)
2. Total arsenic
3. Both As(III) and As (V) individually

(Enter a number)
=? 2

For the determination of both As(V) and total As in natural waters, two methods are recommended, the main difference being the type of electrode used. For users without experience in solid electrodes, the method described in option 1 is recommended. Both methods have similar performance characteristics.

Which method have you selected?

1. DPCSV onto an HMDE
2. DPASV onto an Au electrode.

(Enter a number)
=? **1**

Electroinactive As(V) must be reduced first to As (III); for this purpose, an aliquot of 10 ml of sample is transferred to a 50 ml beaker containing 1.46 g of sodium chloride and 0.25 g of hydrazinium chloride. Arsenic(V) is reduced to As(III) by adding 3.15 ml of concentrated hydrochloric acid and 1 ml of 48% hydrobromic acid, covering the beaker with a watch glass, and heating the mixture for 45 min on a steam bath set at 95-100°C. The solution is allowed to cool to room temperature and the contents are transferred quantitatively to a 50 ml volumetric flask and diluted to volume with a 0.25 % (w/v) hydrazinium chloride solution.

You should use Differential Pulse Cathodic Stripping Voltammetry (DPCSV) onto the Hanging Mercury Drop Electrode (HMDE).

The medium conditions are:

A 10 ml aliquot of the sample is transferred to the cell and acidified to 0.75 M with HCl. The sample is then spiked with 50 μl of stock Cu(II) solution (1000 ppm).

The instrumental parameters are:

Er = Ag/AgCl or Standard Calomel Electrode. Ew = HMDE.
Eaux = Pt or glassy carbon,
Epe = -0.6 V, tpe = 2 min, tr = 30 s
Ef = -0.9 V, pulse = 75 mV, v = 10 mV/s.

Did you observe different peaks in the voltammograms?
1. yes
2. no

=? **1**

If you observe a peak at Ep = -0.72 V vs. Ag/AgCl, the peak will be due to the presence of As(III).

Figure 7, Determination of total arsenic by using Differential Pulse Anodic Stripping Voltammetry (DPASV) onto the Rotating Gold Electrode.

What As species do you want to determine?
1. As (III)
2. Total arsenic
3. Both As(III) and As (V) individually

(Enter a number)
=? **2**

Which method have you selected?
1. DPCSV onto an HMDE.
2. DPASV onto an Au electrode.

(Enter a number)
=? **2**

Electroinactive As(V) must be reduced first to As (III); for this purpose, an aliquot of the sample is transferred to the cell which is then closed off with a Teflon stoppered having inlet and outlet holes for nitrogen. The solution is heated in a water bath to about 80°C. Sulphur dioxide is passed through the solution for 2 min leaving the cell closed off for 5 min. After this period, SO_2 is again bubbled through the solution for about 30 s to ensure complete saturation of the solution with SO_2. After 5 min N_2 is passed through the solution for 10 min. The sample is then cooled somewhat and 1 ml of conc H_2SO_4 is added. The solution is heated to 95°C and N_2 is bubbled through for 15 min and the solution is cooled to room temperature and ascorbic acid and, if necessary, HCl is added for the As(III) determination. Evaporation losses are made up with H_2O. The final volume of the solution was 20 ml. The determination of As(III) is then carried out as follows.

You should use Differential Pulse Anodic Stripping Voltammetry (DPASV), using the rotating gold Electrode.

Preparation of the gold Electrode:

The gold electrode which is stored in air when not used, should be cleaned once a day prior to a set of determinations by polishing it lightly with 0.25 μm Al_2O_3 and immersing it in chromic-sulphuric acid for 10 min. After rinsing the electrode with H_2O the conditioning is carried out in a 1 M H_2SO_4 solution (deaerated with N_2) by applying a potential of 2.5 V vs. SCE for 20 s, followed by a potential of 0 V for 7 s. The electrode is rotated and N_2 is passed through the solution during this step. When not in use the cell with sulphuric acid solution should simply be left stoppered. Contamination of the 1 M H_2SO_4 solution with chloride ions should be kept to a minimum. Therefore, the electrodes should be rinsed throughly with H_2O after they have been used in solutions with high chloride contents (e.g. sea water). After conditioning, the cell with the H_2SO_4 solution is exchanged for the one containing the sample solution without rinsing the electrodes.

The medium conditions are:

An aliquot of the sample solution is transferred to the cell which is then closed off with a Teflon stopper with inlet and outlet holes for nitrogen. After deaerating the solution with N_2 for 10 min about 20 mg of ascorbic acid, 1 ml of conc. H_2SO_4 and 0.1 ml of conc. HCl are added. If the sample already has a high chloride content (e.g. sea waters) addition of HCl can be omitted. The final volume was 20 ml. The solution is cooled to room temperature under N_2 purging. After the gold electrode has been conditioned as described above, the sample cell is put into place for the determination.

The optimal instrumental conditions are:

Er = Ag/AgCl or standard calomel electrode (SCE). Ew = rotating Au.
Eaux = Pt or glassy carbon.
pulse = 50 mV (in general, between 10 and 100 mV.)
v = 10 mV/s, tpulse = 30 - 100 ms.
Epe = -0.25 V, Ef = +0.1 V. tpe = 2 - 4 min, tr = 30 s.
rotating speed = 3000 rpm.

Did you observe different peaks in the voltammograms?
1. yes
2. no
=? **1**

If you observe a peak at E_p = -0.05 V vs. Ag/AgCl, the peak will be due to the presence of As(III). The peak will correspond to the total arsenic in solution due to the previous reduction of As(V) to As(III).

Figure 8, Determination of As (III) and As (V) by using Differential Pulse Anodic Stripping Voltammetry (DPASV) onto the Rotating Gold Electrode.

What As species do you want to determine?
1. As (III)
2. Total arsenic
3. Both As(III) and As (V) individually
(Enter a number)
=? **3**

For the determination of As(V) and/or total As in natural waters, two methods are recommended, the main difference being in the type of electrode used. For users without experience in solid electrodes, the method described in option 1 is recommended. Both methods have similar performance characteristics.

Which method have you selected?
1. DPCSV onto an HMDE.
2. DPASV onto an Au electrode.
(Enter a number)
=? **2**

The concentration of As(V) is determined by calculating the difference between the total Arsenic and the As(III) concentrations; you should begin with the determination of As(III); for this purpose. The conditions are as described in Figure 7 but avoiding the previous reduction of As(V) to As(III).

In order to carry out the quantification, the calibration curve should be obtained. The quantitative procedure is based on the multiple standard addition method, and the response signal considered is the peak height in the voltammogram. The most appropriate concentration range for the calibration plot is:

- lowest value: 50% lower than the minimum value found in references and
- highest value: 150% higher than the maximum value found in references.

After the calibration curve has been plotted, it can be validate by several statistical tests; for this purpose, the system calls the external program COOK'S2.

Parameters of the calibration curve:

slope = ... (value according to experimental data)

intercept (at y = 0) = ... (value according to experimental data)

The concentration of the cation As(III) <1.00> given in mol/l, is the absolute value of .... (value according to experimental data)

Now, you should carry out the determination of total As in order to determine As(V) by finding the difference between total As and As(III).

The conditions are as described in Figure 7 (full procedure)

The concentration of total As is: .... (value according to experimental data)

The concentration of As(V) is (Difference between total As and As(III): .... (value according to experimental data)

Figure 9, Determination of As (III) and As (V) by using Differential Pulse Cathodic Stripping Voltammetry (DPCSV) onto the Hanging Mercury Drop Electrode (HMDE).

What As species do you want to determine?
1. As (III)
2. Total arsenic
3. Both As(III) and As (V) individually

(Enter a number)
=? **3**

Which method have you selected?
1. DPCSV onto an HMDE
2. DPASV onto an Au electrode.

(Enter a number)
=? **1**

The concentration of As(V) is determined by calculating the difference between the total Arsenic and the As(III) concentrations; you should begin with the determination of As(III); for this purpose the conditions are as described in Figure 6 (but avoiding the previous reduction of As(V) to As(III)).

Set up the polarograph according to the conditions mentioned; Connection is established with external program which plots the voltammogram. The voltammogram is:

Did you observe different peaks in the voltammograms?
1. yes
2. no

=? **1**

If you observe a peak at Ep = -0.72 V vs. Ag/AgCl, the peak will be due to the presence of As(III).

From the shape of the peaks, does it appear that these peaks are generated by only one chemical species?
1. yes
2. no

=? **1**

Can you measure the peak height precisely?
1. yes
2. no

=? **1**

In order to carry out the quantification, the calibration curve should be obtained. The quantitative procedure is based on the multiple standard addition method, and the response signal considered is the peak height in the voltammogram. The most appropriate concentration range for the calibration plot is:

- lowest value: 50% lower than the minimum value found in references and
- highest value: 150% higher than the maximum value found in references.

After the calibration curve has been plotted, it can be validate by means of several statistical tests; for this purpose, the system calls the external program COOK'S2.

Parameters of the calibration curve:
slope = ... (value according to experimental data)

intercept (at y = 0) = ... (value according to experimental data)

The concentration of the cation As <1.00> given in mol/l, is the absolute value of .... (value according to experimental data)

Now, you should carry out the determination of total As in order to determine As(V) by finding the difference between the total Arsenic and the As(III) concentrations. The conditions are as described in Figure 6 (full procedure including the previous reduction of As(V) to As(III)).

REFERENCES

1 M. Esteban I. Ruisánchez, M.S. Larrechi and F.X. Rius, Anal. Chim. Acta, 268 (1992) 95, 107; Trends Anal. Chem., 11 (1992) 135.
2 M. Esteban, C. Ariño, I. Ruisánchez, M.S. Larrechi and F.X. Rius, Anal. Chim. Acta, 284 (1993) 435.
3 K.W. Bruland, in J.P. Riley and R. Chester (Eds.), Chemical Oceanography, Academic Press, London, 2nd edn., 1983, pp. 157–220.
4 E.E. Carry, in S. Langard (Ed.), Biological and Environmental Aspects of Chromium, Elsevier, Amsterdam, 1982, Chap. 3.
5 Y.A. Zolotov, G.I. Malofeeva, O.M. Putrukhin and A. Timerbaev, Pure Appl. Chem., 59 (1987) 497.
6 W.R. Cullen and K.J. Reiner, Chem. Rev., 89 (1989) 713.
7 M. Boussemant, C.M.G. van den Berg and M. Ghaddaf, Anal. Chim. Acta, 262 (1992) 103.
8 J. Golimowski, P. Valenta and H.W. Nürnberg, Fresenius' Z. Anal. Chem., 322 (1985) 315.
9 S.T. Crosmun and T.R. Mueller, Anal. Chim. Acta, 75 (1975) 199.
10 W. Holak, Anal. Chem., 52 (1980) 2189.
11 G. Henze, A.P. Joshi and R. Neeb, Fresenius' Z. Anal. Chem., 300 (1980) 267.
12 R.S. Sadana, Anal. Chem., 55 (1983) 304.
13 F.G. Bodewig, P. Valenta and H.W. Nürnberg, Fresenius' Z. Anal. Chem., 311 (1982) 187.

Analytica Chimica Acta, 285 (1994) 209–222
Elsevier Science B.V., Amsterdam

Empirical pattern recognition/expert system for molecular weight estimation of low resolution mass spectra

Donald R. Scott

Atmospheric Research and Exposure Assessment Laboratory, U.S. Environmental Protection Agency, Research Triangle Park, NC 27711 (USA)

(Received 4th June 1993)

Abstract

A fast, personal-computer based method of estimating molecular weights of organic compounds from low resolution mass spectra has been redesigned and implemented with a rule-based expert system. It has a sequential design with a pattern recognition classifier followed by filter and molecular weight estimator modules for each of six classes. The classes are nonhalobenzenes, chlorobenzenes, bromo- and bromochloroalkanes/alkenes, mono- and di-chloroalkanes/alkenes, tri-, tetra- and pentachloroalkanes/alkenes and unknowns. The classifier was derived from 106 NIST/EPA/MSDC reference spectra. The filters employ computed series of allowed molecular weights and selected base peaks for each class, except unknown, to reduce misclassification. Empirical linear corrections from the training spectra are applied to two mass spectral features, MAXMASS and HIMAX1, to yield estimates and lower limits to the molecular weights. Extensive testing of the system was conducted with 32 test, 99 randomly chosen and 37 field gas chromatographic–mass spectrometric (GC–MS) spectra and results were compared to those from STIRS. The median absolute deviations from the true molecular weights of the test, random and field GC–MS spectra with the expert system were all 1 dalton (average 5.6, 7.3, 5.9 daltons, respectively). This approach also was evaluated with 400 spectra of volatile and nonvolatile compounds of pharmaceutical interest. The median and average absolute deviations from the true molecular weights of the 400 spectra were 2 and 10 daltons. Classification of the evaluation spectra, including many incomplete spectra, was very good with accuracies of 97 (test, random and pharmaceutical) and 95% (field GC–MS).

Keywords: Mass spectrometry; Pattern recognition; Expert system; Molecular weight estimation

The availability of a simple and rapid method of estimating molecular weights of unknown compounds from their low resolution mass spectra could be very useful in interpreting these spectra. The approximate molecular weight could be used in library searches to limit possible candidates and to accelerate the search process. In the case of complex spectra, e.g., GC–MS data of environmental and other complex samples, where many spectra are never identified, the approximate molecular weight and a class assignment could give partial identification information. The self training interpretive retrieval system (STIRS) [1,2] is the most widely known computer-aided technique for molecular weight estimation. However, since it requires a full library search, it is relatively slow and requires relatively large amounts of storage memory. In conjunction with the development of a pattern recognition/expert system for classification and identification of toxic and other volatile organic compounds from GC–MS

Correspondence to: D.R. Scott, U.S. Environmental Protection Agency, Research Triangle Park, NC 27711 (USA)

SSDI 0003-2670(93)E0527-E

data [3,4], a rapid and simple method for estimating molecular weights has been developed and extensively evaluated [5–8]. A pattern recognition based classifier is followed by molecular weight estimators for each class. This method uses a set of empirical rules which were developed by, and implemented with, an inductive rule-based expert system. It is based on the direct linear relationship of two easily determined mass spectral features, MAXMASS and HIMAX1, with the true average molecular weight.

Recent evaluations of the classifier in both the identification expert system [4] and in version 3 of the molecular weight prediction system [8] have shown that misclassification of spectra, particularly those apparently containing halogens, was a problem. These misclassifications were the source of errors in some molecular weight predictions. The system has been completely redesigned to eliminate these problems, even with incomplete spectra. The molecular weight estimation modules also have been redesigned and rederived. The latest version of the NIST/EPA/MSDC mass spectral database has been used for the training and evaluation spectra involved in these modifications. Thorough evaluation of the redesigned system with a wide variety of reference spectra and field GC–MS data has shown that misclassifications have been drastically reduced and that the estimates of molecular weights have improved.

METHODS

The shell system used for development and testing of the expert system was 1ST-CLASS FUSION, version 2.0, which is an inductive rule-building program using the ID3 algorithm. During development the shell system was used with the ID3 mode or in "customize" mode, where the developer can edit previously derived rules or develop his own rules. The derived rules are presented in the form of a graphically displayed binary decision tree. Details concerning the shell program are given elsewhere [9,10]. Development and evaluation of the system were performed on MS-DOS-based personal computers.

The STIRS programs were contained on a compact disk, the 1988 Wiley Registry of Mass Spectral Data, which was used with a personal computer. STIRS predictions of molecular weights were determined without initial guesses by the operator and the most probable one was used.

The 400 pharmaceutical spectra were obtained from J.T. Clerc and S. Heuerding of the Institute of Pharmacy, University of Bern, Switzerland and came from a database at ETH Zürich [11]. All other reference spectra used to derive or test the algorithms were from the NIST/EPA/MSDC Database, Personal Computer Version 4, hereafter called the NIST Database. All spectral intensities were ternary encoded. Intensities (relative to the base peak intensity of 100%) of 0 to 4.99% were assigned values of 0, those of 5 to 49.9%, values of 0.5 and those of 50 to 100%, values of 1.0. No masses below 39 daltons were used in the rules, except for MAXMASS or HIMAX1 variables. Values of the masses for MAXMASS, HIMAX1 or the base peak were input in response to the queries from the expert system. All evaluation spectra were manually input into the molecular weight prediction system.

SYSTEM DESIGN AND OPERATION

The design of the expert system was sequential and employed a "divide and conquer" strategy. A pattern recognition-based classifier was followed by molecular weight estimators and then by filters to reduce misclassifications. These filters were then followed by molecular weight estimators. Each of the six classes, except the very large unknown class, had its own set of filters and molecular weight estimator. The actual path through the system starts with the classifier where a spectrum is assigned a class. The spectrum then passes to the molecular weight estimator for that class where a tentative molecular weight is assigned. If the tentative molecular weight is acceptable for a member of that class, then the spectrum passes the first filter and proceeds to the next filter for the assigned class. If the spectrum contains no base peaks which are excluded in the second class filter, then the tentative

molecular weight is assumed to be correct and is displayed along with the lower limit to the molecular weight and the class. A spectrum can be assigned to the unknown class directly from the classifier or by being rejected from the two filters. The unknown class is a very large one consisting of all spectra which do not fit into the other five groups. An important design specification was the very narrow definition of the allowed members of the five major classes so that only chemi-

TABLE 1

Training set classification and molecular weight results

Class	Structure	Number in set
Nonhalobenzenes	Benzene	1
	Alkylbenzenes	10
	Alkenylbenzenes	1
	Phenylketones	1
	Phenylaldehydes	1
	Benzonitriles	1
Chlorobenzenes	Chlorobenzene	4
	Alkylchlorobenzenes	3
	Alkenylchlorobenzenes	1
Mono- and dichloro-alkanes/alkenes	Monochloroalkanes	4
	Monochloroalkenes	1
	Dichloroalkanes	8
	Dichloroalkenes	3
	Monochloroepoxyalkane	1
	Monochlorooxyalkene	1
Tri-, Tetra- and penta-chloroalkanes/alkenes	Trichloroalkanes	5
	Trichloroalkenes	1
	Tetrachloroalkanes	6
	Tetrachloroalkenes	1
	Pentachloroalkanes	1
Bromo- and bromochloro-alkanes/alkenes	Monobromoalkanes	4
	Dibromoalkanes	7
	Tribromoalkanes	1
	Monobromoalkenes	2
	Monobromomonochloroalkanes	3
	Monobromodichloroalkanes	1
	Monobromotrichloroalkanes	1
	Dibromomonochloroalkanes	1
Unknown	Cyclic ethers	3
	Acyclic hydrocarbons	13
	Cyclic hydrocarbons	3
	Unsaturated hydrocarbons	3
	Aldehydes	3
	Ketones	3
	Alcohols	2
	Acids	1
Classification accuracy:		100%
Molecular weight absolute deviations:	median	0.0 daltons
	average	0.17 daltons

cal structures present in the training spectra were represented. Details of the various modules are described below.

Communications between the system and the user occur via screen messages and requested information is input from the computer keyboard. The user is asked for the intensities of key masses and for the values of MAXMASS (the largest mass with an intensity of at least 5%), HIMAX1 (the largest mass with an intensity of at least 1%) and the base peak. A typical session for acetaminophen [*p*-(acetylamino)phenol], which has a molecular weight of 151 and is a member of the unknown class, is shown below. Note that intensity data is ternary encoded. This entire session, including looking for peak intensities and manual input of responses, took about 45 s.

Query	Response
What is the intensity of mass peak 42? (Enter 0, 0.5 or 1.)	0
What is the intensity of mass peak 49?	0
What is the intensity of mass peak 77?	0
What is the intensity of mass peak 63?	0
What is the intensity of mass peak 75?	0
What is the intensity of mass peak 96?	0
What is the intensity of mass peak 76?	0
What is the intensity of mass peak 107?	0
What is the intensity of mass peak 41?	0
What is the intensity of mass peak 93?	0
What is the intensity of mass peak 108?	0.5
What is the mass for MAXMASS?	151
What is the mass for HIMAX1?	152
What is the mass of the base peak above mass 30?	109
What is the intensity of mass peak 43?	0.5

The first eleven responses are necessary to classify the spectrum. The next two are used to calculate the molecular weight and its lower limit. The last two are used to determine if this spectrum should be passed or rejected by the base peak filter for the nonhalobenzene class. In this case the spectrum was rejected as a member of the nonhalobenzene class, to which it belongs in a broad sense, and passed to the unknown class for molecular weight estimation.

The system produced the following response to the data input: THE CLASS OF THIS COMPOUND IS UNKNOWN, BUT ITS ESTIMATED MOLECULAR WEIGHT IS 152±5 DALTONS. A LOWER LIMIT TO ITS MOLECULAR WEIGHT IS 146.5 DALTONS.

The error listed is a probable error determined with a robust statistic from evaluation tests. The average of (MAXMASS and HIMAX1) less 5 daltons was used as the lower limit. Similar results would be obtained with spectra of the other five classes with the appropriate class and molecular weight displayed.

SYSTEM DEVELOPMENT

Classifier

The classifier is the initial and most important module in the system. It provides partial identification information and directs the spectrum to one of six different class routes including the unknown class. The classifier rules were derived from a training set of 106 NIST reference spectra of compounds whose structures are listed in Table 1. These training spectra consisted of the spectra of a 75 member target set and an additional 31 spectra for the unknown class. The names of the specific training compounds are given elsewhere [6]. The classes determined by the classifier were nonhalobenzenes, chlorobenzenes, bromo- and bromochloroalkanes/alkenes, mono- and dichloroalkanes/alkenes, tri-, tetra- and pentachloroalkanes/alkenes and unknowns (all others). These particular classes had been previously determined from the training set data using unsupervised SIMCA pattern recognition techniques and shown with cross validation to be statistically valid [9,12]. All peak intensities were ternary encoded to introduce some fuzziness into the rules and to reduce the use of low intensity masses in the resulting rules.

In deriving the new classifier rules with the ID3 algorithm, the 14 masses (39, 42, 49, 55, 63, 76, 77, 93, 96, 107, 108, 122, 129, 165) from the previous classifier [4] were initially used with the NIST training spectra. However, these masses were not sufficient to completely separate the six classes and masses 41 and 75 were added. It was found that complete separation could then be accomplished via the ID3 algorithm with only 15 of these masses, i.e., by omitting mass 165. The largest number of branches in the resulting decision tree involved the bromo- and bromochloroal-

kane/alkene and mono- and dichloroalkane/alkene classes. The fewest number of branches were concerned with the nonhalobenzene, unknown and chlorobenzene classes.

Misclassification filters

The filters are a very important part of the total system. They serve to refine the assignments from the classifier module and to prevent the application of incorrect estimator rules. They effectively define the specific members of the five major classes. In recent evaluations of the classifier [4,8] it was found that some of the more unusual chemical structures present in test spectra were being misclassified as chlorine or bromine containing compounds. Examples are 4-diethylaminobenzaldehyde, classified as a chlorobenzene, or 5-ethyl-5-isopentylbarbituric acid, as a bromo alkane/alkene, both of which should have been classified as unknown. Misclassification also occurred because of incomplete spectra. As a result, molecular weight estimation rules for the wrong class were used resulting in erroneous predictions.

In the original classifier [4] rather broad definitions of the five major classes were allowed. Filters were not designed to strictly limit the classified spectra to only those specific chemical structures in the training set. This caused some of the misclassification problems. In designing the present filters a very strict definition of the chemical structures represented by the training set was employed. For example, in the mono- and dichloroalkane/alkene class no hydroxychloro- or aminochloroalkanes/alkenes were included. The advantage of the new filters is that the classes are narrowly defined and resulting classification is accurate. The only penalty for rejection by the filters was classification as an unknown and molecular weight estimation using unknown class rules, which are fairly accurate even for other classes.

The first filter following the classifier and molecular weight estimator is a computed one with a different filter for each class except unknown. This filter only passed those molecular weights which could possibly arise from the series of chemical structures, including higher molecular weight members, represented in the training set compounds. Error bands of ± 1 dalton about these computed values were allowed for all filters. An example for the mono- and dichloroalkane/alkene class would consist of the series of molecular weights of all compounds from chloromethane through chlorooctane and dichlorohexane, including all corresponding chloroalkenes with up to three double bonds. This type of filter, which is essentially a limited structure generator, was effective at lower molecular weights; but at higher molecular weights the series of allowed molecular weights was essentially continuous. Upper limits for passing these filters were established at 218 (nonhalobenzenes), 198 (chlorobenzenes), 154 (mono- and dichloroalkanes/alkenes), 252 (tri-, tetra- and pentachloroalkanes/alkenes) and 200 daltons (bromo- and bromochloroalkanes/alkenes). Spectra with higher estimated molecular weights were routed to the unknown class estimator.

These computed filters were followed by base peak filters, one for each class, except for the unknown class. Base peaks of compounds which were originally misclassified in either the 99 randomly selected NIST spectra or the 400 pharmaceutical spectra described later were used. Frequently the base peak of the misclassified spectrum was unusual enough to be used alone as an exclusion criterion. However, in some cases the base peaks of the misclassified spectra were identical to some in the training set spectra. In these latter cases other masses were used with the base peaks in the filters. An example is shown above under *System Design and Operation* where the intensity of mass 43 is requested after the base peak mass.

In every case where a base peak alone or with other peaks was used in these filters, a complete sequential search of the 62235 spectra in the NIST mass spectral database was performed to insure that no legitimate members of the particular class were being excluded. Compounds of all molecular weights were included in these searches and the elemental composition and intensity of mass peaks were used as search constraints. Every individual branch in every class filter was checked for selectivity.

Molecular weight estimators

The estimator modules, one for each of the six classes, provide the molecular weights and the calculated lower limits. Recently [5] it was found that MAXMASS, the highest observed mass with an intensity of at least 5% of the base peak, has a linear correlation with the molecular weight of 400 randomly selected volatile organic compounds from the NIST mass spectral database. For these spectra MAXMASS predicted the molecular weights within a few mass units for 72% of the spectra. In later studies [7] it was found that the use of another spectral feature, HIMAX1, together with MAXMASS was more effective in predicting molecular weights. HIMAX1 is the highest observed peak with an intensity of at least 1%. These two spectral features are very efficient indicators of the molecular ion mass. For example in the set of 400 pharmaceutical spectra, MAXMASS, without corrections, is equal to the mass of the molecular ion 27.5% of the time and within one dalton of the molecular ion mass another 27.5% of the time. HIMAX1 is directly equal to the molecular ion mass 16.2% of the time and within one dalton another 39.3%. MAXMASS and HIMAX1 are equal 24% of the time. An illustration of the relationship between the molecular weight and MAXMASS and HIMAX1 for the set of 400 pharmaceutical spectra is shown in Fig. 1.

The basis of the estimator modules is the application of linear corrections to HIMAX1 to estimate the molecular weight. The linear corrections for each class module were empirically determined by the ID3 algorithm from the appropriate sets of training spectra. A single conflict in the derived rules for the unknown class was resolved by using the average of the conflicting corrections. Both MAXMASS and HIMAX1 occurred in all class rules. MAXMASS appeared as a preliminary sorting variable, but the corrections were only applied to HIMAX1. The resulting modules consisted of 7 lines for the nonhalobenzene and chlorobenzene classes to 41 lines for the very diverse unknown class. Applied corrections ranged from −4.6 daltons for the tri-, tetra- and pentachloroalkane/alkene class to +34.4 daltons for the same class. The smallest corrections appeared in the nonhalobenzene and chlorobenzene classes.

The lower limits to the molecular weights were determined from the average of MAXMASS and HIMAX1 less 5 daltons. The correction to the average was required to adjust for the occurrence of halogen isotopic peaks. This method was tested with the training set of compounds and with 400

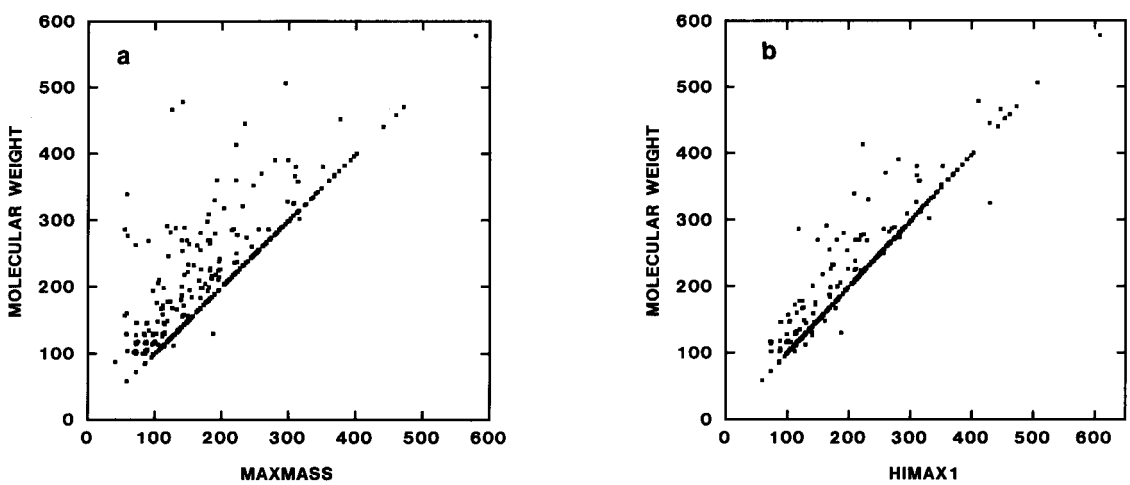

Fig. 1. Linear relationship between (a) MAXMASS and (b) HIMAX1 and molecular weight (58–578 daltons) for 400 pharmaceutical mass spectra. Note the three spectra below the 1:1 diagonal line in (a) which are probably incorrect.

randomly selected spectra. Of these 506 spectra only four from the random compounds had molecular weights lower than the estimated lower limits. These four spectra all appeared to be contaminated with high mass ions, which would cause the lower limits to be too high.

Probable errors associated with the molecular weight estimates were calculated with a robust statistic, the median absolute deviation, and the Shapiro-Wilk equation. The median absolute deviation of molecular weight estimates for each evaluation set was first determined. Then the absolute deviations of each estimate in the set from this median deviation were calculated. The median of these latter absolute deviations was then multiplied by five to yield the probable error for the set. This probable error corresponds to error limits of about 3.5 times the standard deviation for a normal distribution. The probable error for the unknown class, determined from the 99 random spectra, was ± 5 daltons and for all other classes, determined from the training spectra, was ca. ± 1 dalton.

SYSTEM EVALUATION

Training and test spectra

The optimum performance for the system should be obtained by testing with the 106 training spectra from which the classification and molecular weight estimation rules were derived. The evaluation results for this set are listed at the end of Table 1. The median and average absolute deviations from the true molecular weights were 0.0 and 0.17 daltons for the expert system vs. 1.0 and 11 daltons for STIRS. The classification accuracy with the expert system was 100%. These excellent results obtained with the training spectra show that the mathematical basis for the classification scheme and molecular weight estimation procedure is fundamentally correct.

The system also was tested with a variety of spectra of other compounds, none of which had been used in deriving the rules. These included a test set of 32 spectra of volatile compounds consisting of 15 alkanes and alkenes, 9 aldehydes, ketones and alcohols, 2 chloro alkanes/alkenes and 6 substituted benzenes. The benzenes included nitro-, chloro-, fluoro-, bromo- and bromochloro-substituents. The molecular weights of these compounds ranged from 30 daltons for formaldehyde to 236 daltons for 1,4-dibromobenzene. A list of the compounds and the test results are given in Table 2. The median and average absolute deviations for this set were 1.0 and 5.6 daltons vs. 0.0 and 7.1 daltons for STIRS.

TABLE 2

Molecular weight and classification results with test compounds

Compound	Molecular weight estimates		
	True	STIRS (daltons)	Expert 5.1
Trichlorofluoromethane	137	136	124
2,3-Dimethyloctane	142	98	114
Pentane	72	72	71
2,3,3-Trimethylbutene-1	98	98	98
2-Butanone	72	72	72
2-Butene-1-ol	72	114	72
Hexane	86	114	85
Decane	142	142	142
2-Methylhexane	100	100	100
2-Ethylhexanal	128	128	128
2,2,4-Trimethylpentane	114	99	99
2-Methylnonane	142	142	142
2-Heptene	98	98	98
2-Propanone	58	58	58
1-Heptanol	116	98	114
2-Propenal	56	56	57
2-Methylheptane	114	114	129
Chloroethene [a]	62.5	62	63
4,5-Dimethyl-1-hexene	112	112	96
Formaldehyde	30	30	30
2,2-Dimethylheptane	128	113	113
Acetaldehyde	44	44	45
2,5-Dimethylheptane	128	128	128
Nitrobenzene	123	123	129
2,3-Dimethylheptane	128	112	86
1,4-Dibromobenzene	236	234	239
5-Methyl-3-hexanone	114	114	114
2,4-Dimethylhexane	114	142	114
2,2,4-Trimethylheptane	142	127	127
1,3,5-Trichlorobenzene	181	180	183
Fluorobenzene	96	96	96
1-Bromo-4-chlorobenzene	191.5	190	195
Average absolute deviation		7.1	5.6
Median absolute deviation		0	1.0
Classification accuracy			97%

[a] Compound in italics was incorrectly classified as unknown.

TABLE 3

Classification and molecular weight results for random NIST reference spectra

Compound	True mol. wt.	Predicted molecular weight	
		STIRS (daltons)	Expert system 5.1
Acetylene	26	26	27
cis-1-Methyl-9-oxabicyclo[6.1.0]nonane	140	140	140
Butyne-2-1,4-diol	86	86	86
Benzenecarbothioic acid, *O*-ethyl ester	166	166	168
4-Pentanal	84	84	84
5-(Hydroxymethyl)-2-furancarboxylic acid	142	142	143
o-Menthene-8	138	138	139
2-Methoxy-2-propenylbenzene	148	148	149
Methylsulfonylbenzene	156	156	156
Diethylcarbothioic acid, *S*-ethyl ester	161	161	162
1-(7-Oxabicyclo[4.1.0]hept-1-yl)ethanone	140	140	140
2-Methyl-2-(1-methylethoxy)propane	116	101	101
5-Amino-2-hydroxybenzoic acid	153	153	154
1-(2-Methylcyclopropyl)ethanone	98	98	116
1-Butylpiperidine	141	182	141
Dimethoxyacetic acid, methyl ester	134	103	103
1-Bromo-2,2-dimethylpropane [a]	151	150	152
2-(1*H*-Tetrazol-5-yl)pyridine	147	150	147
3-Methoxy-2-methylpropene-1	86	116	87
(1,1-Dimethylethoxy) (1-methylethylidene)-cyclopropane	154	97	97
2-Mercaptoethanol	78	106	96
Methylpyrazine, 1-oxide	110	110	110
2-Methylthietane	88	88	89
2-Butanethiol	90	90	91
4-Fluoro-3-nitrobenzenamine	156	156	157
1-Bromo-2-propanol	139	123	128
Cyanoacetic acid	85	56	85
(*E*)-3-Methyl-3-pentenoic acid, methyl ester	128	128	128
5-Methylisothiazole	99	99	114
2-phenylhydrazinecarboxamide	151	151	152
4-(Methoxydimethylsilyl)1-butanamine	161	162	146
1-Propanesulfonic acid, methyl ester	138	138	138
1,4-Dichlorocyclohexane	153	152	154
Bicyclo[3.3.1]nonan-9-one	138	138	139
4-Oxo-2-pentynoic acid, ethyl ester	140	125	126
1-Amino-2-methylpyridinium chloride	145	108	108
1,1-(1,2-Phenylenedicarbonyl)bispiperidine	300	300	300
3-Cyclohexyl-5-phenyl-1,2,3-oxathiazol-idine-2-oxide	265	200	201
3-Ethyl-3-methoxy-1-pentyne	126	112	96
2-Methyl-2-propenoic acid, ethyl ester	114	114	129
1,1,1,3,3,3-Hexafluoropropane	152	152	134
(*Z*)-3-Hexenoic acid, methyl ester	128	128	129
1,1-Methylenebis-1*H*-pyrrole	146	146	147
7-Thiabicyclo[4.1.0]heptane	114	114	115
2-Chloro-1,1,1-trifluoroethane	118	118	118
(*Z*)-2-Hexen-1-ol acetate	142	142	142
2-[[(1-Methylethyl)thio]methyl]furan	156	156	157
4-Methyl-2-pentenoic acid, ethyl ester	142	142	142

TABLE 3 (continued)

Compound	True mol. wt.	Predicted molecular weight	
		STIRS (daltons)	Expert system 5.1
Carbonocyanidic acid, ethyl ester	99	98	97
1,1,1-Trifluoromethanamine	85	85	85
1,1′-Oxybispentane	158	158	158
2-Nitroethenylbenzene	149	149	150
(*R**,*S**)-3-chloro-4-methyl-2-pentanol	137	100	100
5-Methyl-3-methylene-2-hexanone	126	126	127
1*H*-pyrazole-3-ethanamine	111	82	82
2,6-Dimethylbenzenamine	121	121	127
3-Hydroxybutanoic acid, ethyl ester	132	117	116
trans-1,4-Dimethyl-3-piperidinol	129	129	126
2-ethyl-4,5-dihydro-1*H*-imidazole	98	98	115
trans-2-Ethenyl-2,4-dimethyl-1,3-dioxolane	128	128	114
(*E*,*E*)-1,5-Cyclooctadiene	108	108	108
cis-Octahydropentalene	110	110	110
Chloromethoxyethane	95	110	98
N-(Phenylmethylene)-1-propanamine	147	146	148
1-Methyl-3-nitrobenzene	137	137	138
4-Methoxy-2-methylpyrimidine	124	124	130
2-Propenoic acid, trimethylsilyl ester	144	144	144
3-Ethoxypropanenitrile	99	129	97
Carbonic acid, diethyl ester	118	150	90
6-Methyl-5-methylene-2-heptanone	140	140	140
(*E*)-3-(3,4-Dihydro-2*H*-pyrrol-5-yl)-2-propenamide	138	138	140
2-Ethylhexanoic acid, methyl ester	158	158	143
cis-1-Ethyl-4-methylcyclohexane	126	126	127
Isobutylisopropylsulfide	132	132	134
1-Butynyltrimethylsilane	126	126	126
3-Oxepanemethanol	130	126	109
2-Pentene	70	98	70
d,l-Isovaline, ethyl ester	145	116	115
3-Ethoxy-2-butenoic acid, ethyl ester	158	158	159
1-(3-Methyloxiranyl)ethanone	100	85	85
5-Nonen-2-one	140	140	140
2-Butenylhydrazine	86	102	86
Tetrazolo [1,5-*b*]pyridazine	121	121	126
4-Morpholineethanolthiol	147	167	147
3-Methyl-2(5*H*)-furanone	98	98	98
(*Z*)-2-Heptenal	112	113	111
2-(1-Methylethyl)-1,3-oxathiane	146	146	148
2-Ethyl-2-methylbutanoic acid	130	131	131
1-(Dimethylamino)-2-propanol	103	103	102
5-(1,3-Dimethylbutylidene)-1,3-cyclopentadiene	148	148	149
α,α′,4,4-tetramethyl-1,2-oxazetidine-2-acetonitrile	154	184	154
3-Heptyne	96	96	113
Ethylcyclopropane	70	70	70
trans-4*a*,5,6,7,8,8*a*-Hexahydro-2-methyl-1,4-benzodioxin	154	154	155
Formic acid, propyl ester	88	101	73
2,3,3-Trimethylbicyclo[2.2.1]heptan-2-ol	154	154	154

(Continued on p. 28)

TABLE 3 (continued)

Compound	True mol. wt.	Predicted molecular weight	
		STIRS (daltons)	Expert system 5.1
3-Hepten-2-one	112	112	112
Methylpropanedinitrile	80	80	97
Methyl-2,6-di-*O*-acetyl-3,4-di-*O*-methyl-α′-D-mannopyranoside	306	306	275
Average absolute deviation		7.0	7.3
Median absolute deviation		0.0	1.0
Classification accuracy			97%

[a] Compounds in italics were incorrectly classified.

The classification accuracy was 97%, with only chloroethene misclassified as unknown instead as monochloroalkane/alkene. Even with this misclassification the molecular weight estimate for chloroethene was within 0.5 dalton of the true value. These results show that the system works well with spectra from a range of volatile compounds.

Random spectra

Rule-based expert systems are usually assumed to be valid only within the specific domain which is defined by the training set. Therefore, the present system should perform well within the narrowly defined five main classes and to a lessor extent within the much larger unknown class. Expert systems are hardly ever evaluated outside of their training domain. However, our previous tests [4–8] with similar systems have shown that they have a much greater domain of competence than usually assumed. In order to test the limits of the system, an extreme test of robustness was performed. A set of 99 NIST reference spectra of compounds with molecular weights less than 350 was selected at random and used to evaluate the system. The types of compounds included were various hydrocarbons; oxygenated hydrocarbons; nitrogen and sulfur containing compounds; chloro-, bromo- and other halogen-substituted hydrocarbons; pyridines and pyrazines; and various substituted benzenes. This evaluation set, with its wide variety of chemical structures, had caused many misclassification problems in the past [4,7]. The list of compounds included and the test results are given in Table 3. The median and average absolute deviations were 1.0 and 7.3 daltons vs. 0.0 and 7.0 daltons for STIRS. The classification accuracy was 97% with only three compounds, 1-bromo-2,2-dimethylpropane, 1,4-dichlorocyclohexane and *trans*-1,4-dimethyl-3-piperidinol, misclassified, the first two as unknown and the last as mono- or dichloroalkane/alkene. This classification accuracy was a great improvement over the previous poor result of 76%. Performance with this set of randomly selected spectra should approximate the worst system performance.

Pharmaceutical spectra

The results of the evaluations given above indicate that median absolute deviations of 1.0 dalton for molecular weight estimates and very high classification accuracies can be attained with the present system, even outside the original domain. As part of a comparison with another method for estimating molecular weights [11], 400 mass spectra of compounds of primarily pharmaceutical interest were used to evaluate the present system. These organic compounds were comprised only of carbon, hydrogen, nitrogen and oxygen and their molecular weights ranged from 58 to 578 daltons with an average of 207 daltons. A wide variety of structures of volatile and nonvolatile compounds was included in this set with formulas ranging from $C_3H_4O_2$ (acrylic acid) to $C_{32}H_{38}N_2O_8$ (11-demethoxyreserpine). The general types of chemical composition and empirical formulas are summarized in Table 4. Most of the struc-

TABLE 4

Composition of 400 pharmaceutical spectra

Type	Range of formula	Number of spectra
Hydrocarbons	C_7H_{14} to $C_{36}H_{26}$	58
Hydrocarbons with oxygen	$C_3H_4O_2$ to $C_{35}H_{70}O_1$	182
Hydrocarbons with nitrogen	$C_5H_{14}N_2$ to $C_{27}H_{21}N_1$	45
Hydrocarbons with oxygen and nitrogen	$C_4H_9N_1O_2$ to $C_{32}H_{38}N_2O_8$	115

tures were in the unknown class with only eleven nonhalobenzenes included, within the present narrow class definitions. Forty percent of these spectra were incomplete at masses below 55. The incomplete spectra and variety of chemical structures produced many misclassification problems in previous evaluations [8].

The results of the evaluation of this set are listed in Table 5. The median and average absolute deviations of the predicted molecular weights from the true values were 2.0 and 10 daltons vs. 1.5 and 13 daltons for the best previous results [8]. These molecular weight results are similar to, but larger than, those for the random spectra. The classification accuracy was 97% with mostly nonhalobenzenes misclassified, within the strict class definitions. This is a great improvement over the previous classification accuracy of 63%. These results show that the present system works very well with a variety of volatile and nonvolatile compounds even though many have incomplete spectra.

Field GC–MS spectra

All of the previous evaluation sets consist of either NIST reference spectra or reference spectra from a Swiss database. A final test was made with GC–MS data obtained from field samples of volatile ambient air contaminants collected on Tenax. These data contain many unresolved mixtures and spectra with missing low intensity peaks due to the very low concentrations of pollutants. Thirty-seven scans were selected to represent typical results. A major problem with the use of these data for evaluation tests is that the identity, and therefore the class and molecular weight, of many of the compounds can not be firmly established. Each of the spectra was subjected to a library search using a new and effective algorithm developed at the National Institute of Standards and Technology by Stein [13]. These search results along with previous SIMCA pattern recognition class assignments [4] and knowledge of the two internal standards (perfluorotoluene and 1-fluoro-4-iodobenzene) and usual ambient air components were used to establish identities. In some cases compounds with different molecular weights were equally likely. For these cases an average molecular weight was used to calculate the deviations. The assumed identities and test results including lower limits to the molecular weights are listed in Table 6. For the 37 GC–MS scans the median and average absolute deviations for the molecular weight estimates were 1.0 and 5.9 daltons. For the 25 scans where STIRS results were available, the median and average deviations were 7.0 and 10.9 daltons. The lower limits deviated from the assumed molecular weights by only 5, median, and 11, average, daltons. The classification accuracy was 95% with 1,1,1-trichloroethane and toluene misclassified as unknown. Considering the complexity of the samples, these results are excellent.

Conclusions

The empirical approach for estimating molecular weights described here is simple, fast and accurate. The sequential design, based on a pat-

TABLE 5

Classification and molecular weight predictions with 400 pharmaceutical spectra

Class	Number	Classification accuracy (%)	Mol. wt. absolute deviation	
			Median	Average
All classes	400	97.5	2.0	10

TABLE 6

Classification and molecular weight results on GC–MS field data

No.	Identification	Molecular weight			
		Expected	STIRS	Expert mol. wt.	Lower limit
287	Pentane	72	114	72	59.5
294	1,1,2-Trichloro-1,2,2-trifluoroethane	187	151	155	150
303	2-Methyl-1-propen-1-one/ 2-methyl-2-propenal	70	70	69	65
338	Perfluorotoluene	236	255	237	231.5
344	*1,1,1-Trichloroethane* [a]	133	132	126	115
355	Benzene	78	78	78	74
390	2,2,3- or 2,2,4-Trimethyl-pentane/2,2-dimethylhexane	114	–	99	73.5
401	Heptane	100	100	100	95
415	2- or 3-heptene	98	116	97	93
425	Methylcyclohexane/ 4,4-dimethyl-2-pentene	98	98	100	95
471	*Toluene*	92	118	109	87.5
490	2-Methylheptane	114	114	129	101.5
494	2,4-Dimethylpentanal/ 2-methylpentanal	114 100	–	100	87.5
508	Hexanal	100	112	111	99.5
524	3-Methyleneheptane/ 3-ethyl-4-methyl-1-pentene	112	140	130	92.5
527	1-Octene/pentylcyclopropane	112	130	111	93
538	1,2-, 1,3- or 1,4-dimethyl-cyclohexane	112	–	111	107
555	2-, 3- or 4-octene	112	–	111	107
570	2-, 3- or 4-octene	112	130	111	107
617	1,1,3-Trimethylcyclohexane/ 1- or 2-ethyl-2,4-dimethyl-cyclohexane	126 140	111	111	106.5
643	Ethylbenzene	106	106	106	101.5
663	*o*-, *m*- or *p*-xylene	106	106	106	101.5
687	2,4-Dimethylhexane/ 2,6-dimethylheptane	114 128	114	114	94.5
712	*o*- or *p*-xylene	106	–	106	101.5
728	2-Methyl-1-octene/ 2,6-dimethyl-1-heptene	126	–	126	106.5
740	1-Nonene/ 1-octene	126 112	126	126	106.5
776	2-, 3- or 4-nonene	126	126	126	121
790	Isopropylbenzene	120	120	120	115.5
795	2-, 3- or 4-nonene	126	–	126	121
830	propylcyclohexane/ isopropylcyclohexane	126	–	126	121
883	1-Ethyl-2- or -4-methyl benzene/1,2,4-trimethylbenzene	120	120	120	115.5
888	1-Ethyl-2-, -3- or -4-methylbenzene	120	–	120	115.5
904	1-Ethyl-2-, -3- or -4-methylbenzene	120	–	120	115.5

TABLE 6 (continued)

No.	Identification	Molecular weight			
		Expected	STIRS	Expert mol. wt.	Lower limit
966	1,2,4-Trimethylbenzene/ 1-ethyl-2- or -4-methyl-benzene	120	–	120	115.5
974	Octanal	128	146	148	129
1026	2,4-Dimethylheptane/ nonane	128	–	99	87
1082	1-Fluoro-2-, -3- or -4-iodobenzene	222	222	223	217.5
Average absolute deviation			10.9	5.9	11.0
Median absolute deviation			7	1	5
Classification accuracy				95%	

[a] Compounds in italics were incorrectly classified as unknown.

tern recognition classifier followed by effective filters and estimators, was easy to develop and implement with the rule-building expert shell. The "divide and conquer" strategy used allowed detailed and accurate rules to be developed for each class. The use of the two spectral features, MAXMASS and HIMAX1, as a basis for molecular weight prediction and the underlying classification structure have been shown to be correct in extensive testing. The strict definitions of class members used in the redesigned filters were very effective in eliminating misclassification problems and subsequent inaccurate molecular weight predictions. The only penalty for being rejected by a filter and classified as an unknown class member is that the molecular weight estimate will be calculated from the unknown class rules, which are usually fairly accurate even for other class members.

This system has been subjected to very severe and extensive testing with reference and field GC–MS spectra from different sources and a wide variety of chemical structures. The evaluation results show that the system performs extremely well in its original training domain of volatile compounds. For these 106 compounds the median and average absolute deviations from the true molecular weights were only 0.0 and 0.2 daltons with a classification accuracy of 100%. Furthermore, it performed very well in a greatly extended domain of higher molecular weight compounds with chemical structures completely different from those in the training set. Results from the 99 random and 400 pharmaceutical spectra yielded median and average absolute deviations of 1–2 and 7–10 daltons with classification accuracies of 97%. Much of the success of the prediction technique is due to the approximate identity of HIMAX1 and the molecular weight in most spectra. Another factor in its success is the ability of the training set to successfully represent other members of the defined classes. This is particularly striking in the unknown class where only 31 spectra represent an extremely large class of compounds.

The methods used in this system have a number of advantages besides speed and ease of use. The entire spectrum is not required and therefore, the method will work even with incomplete spectra. Only key masses for classification, the base and associated masses for filters and MAXMASS and HIMAX1 are needed. Partial identification information is provided in the form of a class assignment and a reliable lower limit to the molecular weight also is given. Since only MAXMASS and HIMAX1 are used with the appropriate rules, some molecular weight information is available for mixtures. The estimate for mixtures will be that for the component with the highest HIMAX1 value, which is usually the one with the highest molecular weight.

This expert system also has some weaknesses. Low molecular weight compounds with few and/or low mass peaks will almost always be

classified as unknown due to the rule structure. An example is shown with chloroethene in the 32 member test set where it was designated as unknown. Spectra contaminated by ions of much higher mass than the molecular ion will yield erroneously high molecular weight predictions. Compounds that fragment and leave essentially no detectable masses near the original molecular ion mass will yield erroneously low molecular weight estimates. Some of these latter compounds occur in the target set and are actually correctable with the present rules. Other examples are some phthalates, nitro compounds and alkanes which occur in the random and pharmaceutical evaluation spectra.

This expert system, even with its weaknesses, should be a very useful aid in the interpretation of complex GC–MS or other mass spectra. It is much faster and easier to use than STIRS yielding comparable or better accuracy. The probable error of the estimated molecular weights with spectra of compounds similar to those in the training set should be ± 1 dalton with a classification accuracy approaching 100%. For other spectra, particularly those in the unknown class, the probable error should be ± 5–10 daltons with a classification accuracy of ca. 95%. The lower limits to the predicted molecular weights, which are very accurate, also can be used to limit the range of possible molecular weights, unless spectra are contaminated with high mass ions.

The information in this document has been subjected to Agency review and approved for publication. The mention of trade names or commercial products does not constitute endorsement or recommendation for use. A copy of the expert system may be obtained from the author by sending a floppy disk to the address above.

REFERENCES

1 K. Mun, R. Venkataraghavan and F.W. McLafferty, Anal. Chem., 53 (1981) 179.
2 F.W. McLafferty and D.B. Stauffer, J. Chem. Inf. Comput. Sci., 25 (1985) 245.
3 D.R. Scott, Anal. Chim. Acta, 223 (1989) 105.
4 D.R. Scott, Anal. Chim. Acta, 265 (1992) 43.
5 D.R. Scott, Anal. Chim. Acta, 246 (1991) 391.
6 D.R. Scott, Chemom. Intell. Lab. Syst., 12 (1991) 189.
7 D.R. Scott, Chemom. Intell. Lab. Syst., 16 (1992) 193.
8 D.R. Scott, A. Levitsky and S.E. Stein, Anal. Chim. Acta, 278 (1993) 137.
9 D.R. Scott, Anal. Chim. Acta, 211 (1988) 11.
10 D.R. Scott, Chemom. Intell. Lab. Syst., 8 (1990) 245.
11 S. Heuerdling and J.T. Clerc, Chemom. Intell. Lab. Syst., 20 (1993) 57.
12 D.R. Scott, Anal. Chem., 58 (1986) 881.
13 S.E. Stein and D.R. Scott, J. Am. Soc. Mass Spec., (1993) submitted for publication.

Analytica Chimica Acta, 285 (1994) 223–235
Elsevier Science B.V., Amsterdam

Integrated approach for ^{13}C nuclear magnetic resonance shift prediction, spectral simulation and library search

H.N. Cheng and Leo J. Kasehagen [a]

Hercules Incorporated, Research Center, Wilmington, DE 19808 (USA)

(Received 16th June 1993)

Abstract

A computer approach is developed that permits fast estimation of the ^{13}C chemical shifts of common organic compounds, spectral simulation of these compounds, and shift/structure search in a user-maintained spectral library. In the first part of this PC-based program (called CSPEC2), the ^{13}C shifts are predicted on the basis of empirical additive shift rules, and are applicable to carbons contained in commonly occurring organic functional groups, including olefins, acetylenes, aromatics and carbonyls. Structure input and modification are facilitated and shift accuracy improved through the availability of library compounds and the use of a "parent structure" option. The predicted shifts for any compound can be displayed as a printed output, as a file, or as a simulated spectrum. In the second part of the program, partial ^{13}C shifts, molecular formula, or chemical names can be searched sequentially in the spectral library. The use of this computer program is illustrated by suitable examples. Major advantages of this approach include the ease of use and the ability to modify the additivity shift parameters or to add additional functional groups to the program.

Keywords: Nuclear magnetic resonance spectroscopy; Library search; Shift prediction; Spectral simulation

^{13}C NMR is a well-established analytical technique for structure determination of organic compounds [1–5]. The advantage of ^{13}C NMR are the large ^{13}C shift dispersion (220 ppm), and the fact that neighboring atoms (as far as ϵ position away) affects the shift position. As a result, in most cases a one-to-one correspondence can be made between an organic structure and the ^{13}C NMR spectrum.

In the use of ^{13}C NMR spectroscopy for organic structure determination, two general approaches have been adopted: predictive and interpretive approaches. In the *interpretive* approach, the user focuses on the observed spectrum and asks what substructure or functionality corresponds to the shift and intensity features of the spectrum. An early effort in this direction was provided by Dalrymple et al. [6], and subsequently incorporated in the NIH/EPA database [7]. Many sophisticated programs have been developed using elements of artificial intelligence. Among the more well known efforts are the DENDRAL project developed by the Stanford group [8–10], the CASE system developed by Munk and Christie [11], CHEMICS from the Japanese workers [12,13], DARC/EPIOS from the French group [14,15], and the ACCESS program [16] subsequently incorporated in the commercially available INKA system [17]. This is an area of rather intense research activity [18–21], and has been reviewed [22].

In the *predictive* approach, one starts with an organic structure known or suspected to be pres-

Correspondence to: H.N. Cheng, Hercules Incorporated, Research Center, Wilmington, DE 19808 (USA).

[a] Present address: Department of Chemical Engineering and Material Science, University of Minnesota, Minneapolis, MN 55455 (USA).

SSDI 0003-2670(93)E0528-F

ent in the sample and estimates the expected ^{13}C shifts. The observed and the expected ^{13}C NMR shifts are compared, and the suspected structure is either confirmed to be present or rejected. The key to this approach is to estimate the ^{13}C shifts of organic compounds. In the literature, ^{13}C shift prediction has been carried out using three different methods. A commonly used method is to examine families of related compounds and to devise shift rules that govern these compounds. This method was pioneered by Paul and Grant [23], initially for hydrocarbons. In subsequent years, linear additive empirical shift rules have been devised for most organic functional groups [1–5,24–28]. Clerc et al. [29] and Pretsch et al. [30] have generalized the additive rules. A number of computer programs utilizing the Clerc–Pretsch rules have been published [31–35]. Updates and expansions of the rules have been reported [32,35,36].

The second method in shift prediction is to search a spectral library [37–40] or database [17,41] for the ^{13}C shifts of the compound in question. Several search methods have been published [42–46]. An advantage is that no estimation is needed and the actual shift values are obtained. For compounds not in the library, estimates can be made from the shifts of compounds in similar chemical environments. This method has been used in shift prediction in several commercial software routines [17,41,47].

The third method involves structural descriptors [48–51] based on electronic and geometrical structural features in a series of related compounds. The descriptors can then be used to formulate empirical rules for the prediction of ^{13}C shifts.

In this work, we have combined features of both the predictive and the interpretive approaches in one computer program. Earlier, a user-friendly PC-based computer program had been written (called CSPEC) that permits shift prediction and spectral simulation of aliphatic carbons [35]. We have now extended the predictive approach to include the ^{13}C shifts of all common sp^2 and sp carbon types. In addition, a user-maintained spectral library has been set up, and feature-oriented searches can be made. The resulting computer program (called CSPEC2) is capable of shift prediction, spectral simulation, and structure search and has many convenient add-on features.

RESULTS AND DISCUSSION

Overall scheme

The overall logic used in program CSPEC2 is given in Fig. 1. The Command Center is where the program starts and where it returns after a command is executed. At the Command Center, the user can enter or modify a structure at any time. After the structure is entered on the screen, one of the ten following commands can be given. The use of the Esc (escape) key returns the program to the previous command or directly back to the Command Center.

F1 (Optn): Accesses help screen or parameter modification routine.

F2 (Calc): Calculates chemical shifts of structure entered.

F3 (Fix): Prompts user to manually enter the shift of each carbon in the structure. Saves structure to user-specified file. (This command can be used to save parent and reference structures in the library.)

F4 (Pcalc): Calculates shifts using parent structure loaded in by the user as the starting point; vide infra.

F5 (Reassn): Reassigns shifts loaded from a file after the structure has been altered. It allows a reference structure to be expanded or contracted on the screen, for editing purposes.

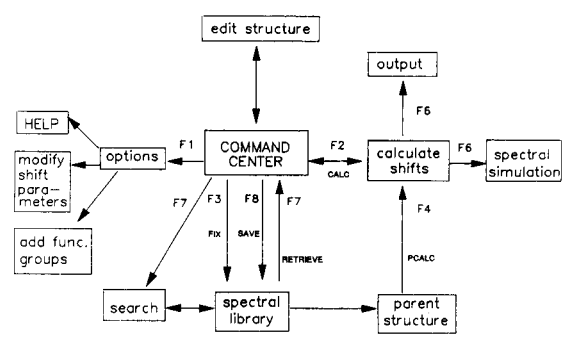

Fig. 1. Schematic diagram of program CSPEC2.

F6 (Out): Produces ^{13}C NMR data from structure. There are four output options: (1) data file containing the plot, (2) rough bar graph plot on the printer, (3) screen plot for CGA/VGA monitors, and (4) printout of the structure and shifts.

F7 (LD/SR): Prompts user for structure to be loaded from the library. The subcommand L displays a list of structures in the library. The subcommand S can be used to search the spectral library.

F8 (Save): Saves current structure. If ^{13}C NMR shifts have been calculated or entered, they will be saved also.

F9 (Clr): Clears structure and all calculations.

F10 (Quit): Exits CSPEC2 program.

There are several ways whereby the program can be used. In the predictive approach, the user usually uses the following sequence of steps: (1) enter the structure on the screen; (2) edit the structure, as needed; (3) calculate the shifts {F2}; (4) produce a printout of the shifts or the simulated spectrum {F6}.

If the structure of interest is in the spectral library, the user can retrieve the structure from the library and obtain the shifts directly {F7}. If the library does not contain the structure but contains a related structure, the user can retrieve that structure on the screen {F7}, modify it, and calculate the shifts {F2 or F4}.

In the interpretive approach, the user provides the available information one step at a time (shifts, molecular formula, or name), and queries the spectral library at every step {F7}. The library responds by giving the number of "hits" at every query. With successive steps, the number of hits is narrowed until the right answer (or a small number of possibilities) is reached.

Structure input

A structure can be entered on the screen in a similar fashion as on paper. The atoms or functional groups are connected by the suitable bond symbols: single bond ★; double bond =; triple bond #; aromatic @.

Most functional groups commonly encountered in organic structures are directly recognizable by this program. A list of acceptable functional groups is given in Table 1. (Functional groups not in Table 1 can be read as components, vide infra. Additional functional groups not in Table 1 can be added by the user through the option {F1} feature.) A functional group may be written as a character string or written out atom-by-atom. Groups that should be written out atom-by-atom are: alkanes, alkenes, alkynes, esters and amides. Groups that can be written in either way

TABLE 1

Functional groups that are built-in [a,b] in program CSPEC2 and recognizable by code

Code	Description	Code	Description
(A) Functional groups represented by character strings			
C	paraffin	SCN	thiocyanate
OH	alcohol	SO	sulfoxide
O	ether	SO2	sulfone
SH	thiol	SO3H	sulfonate
S	thioether	CNOS	oxime, *syn*
NH_2	prim. amine	CNOA	oxime, *anti*
NH_3^+	prim. ammonium	CHO	aldehyde
NH	sec. amine	CO	ketone
NH_2^+	sec. ammonium	COOH	acid
N	tert. amine	COO-	carboxylate
NH^+	tert. ammonium	COCL	acyl chloride
N^+	quat. ammonium	OOH	hydroperoxy
F	fluoro	OO	peroxy
CL	chloro	PH	phenyl
BR	bromo	NCO	isocyanate
I	iodo	NCS	isothiocyanate
CN	nitrile	NO2	nitrate
NC	isonitrile	EPOX	epoxy
(B) Functional groups that must be written explicitly (atom-by-atom [c]			
		O =	
C★C	alkane	C★O	ester
C=C	alkene (cis and/or trans)	O =	
C#C	alkyne	C★N	amide
(C) Functional groups that can be written either way			
	phenyl		aldehyde
	ketone		acid
	nitrile		isonitrile

[a] Functional groups not in the list can be entered atom-by-atom. The component shift calculation [35] will be invoked if the component functional groups can be recognized. [b] This list can be expanded by using the Option {F1} command. [c] When written atom-by-atom, the shifts of carbons within the functional group are also computed.

include phenyl, ketones, aldehydes and acids. If a functional group contains a carbon and the user is interested in the ^{13}C shift of that carbon, the user must write out explicitly atom-by-atom the functional group in question.

The following examples should help clarify this point:

isopropanol

```
C★C★★C
  ★
  OH
```

cyclopentane

```
 C★C★C
 ★   ★
 C★★★C
```

cis-2-pentene

```
C   C★★C
★   ★
C═══C
```

toluene

```
C@@C@@C
@      @
@      @
C@@C@@C★★★C
```

or

```
C★★★PH
```

acetone

```
    O
    ═
C★★★C★★★C
```

or

```
C★★★CO★★★C
```

acetic acid

```
    O
    ═
C★★★C★★★OH
```

or

```
C★★★COOH
```

Note that there are two ways to depict toluene, acetone and acetic acid. When written explicitly atom-by-atom, the shifts of the aromatic carbons, the ketone carbon, and the acid carbon are also estimated. When written as strings, only the aliphatic carbons are calculated for their shifts.

In the above example, consecutive multiple bond symbols (e.g., ★★★, or any number of asterisks) have been used equivalently as a single bond (★). The multiple bond symbols enable a crowded structure to be spread out. Editing of the structure can be accomplished by using the arrow keys, home key, end key, backspace key, delete key and space bar as in word processing.

Shift prediction

Shift rules. The basis of shift prediction is the empirical additive shift rules. The first comprehensive set of rules for aliphatic carbons of different functional groups were devised by Clerc and Pretsch [29,30]. The use of empirical additive rules can be regarded as an a priori method. In an earlier work [35], these rules have been refined by taking account of the degree of substitution of the carbon in question. The rules take on the following form:

$$\delta_{calc} = \pm A_0 + \sum n_i A_i + \sum S_i + \sum D_i \qquad (1)$$

where $A_0 = -2.3$, n_i and A_i are the number of and the empirical shift parameter for the functional group(s) that are ith position away, and S_i and D_i are the steric and the disubstitution correction parameters, respectively. These parameters are used without modification in this work.

For the olefins, shift additivity rules were proposed by Dorman et al. [52]. Much effort has been made over the years to extend the rules for various substituents as reviewed in several standard texts [1–5]. We shall use the parameters given by Wehrli et al. [5] and the latest results of Fürst et al. [36]. The following equation and olefin structure are used:

$$\overset{\gamma'}{C}-\overset{\beta'}{C}-\overset{\alpha'}{C}-\overset{k'}{C}=\overset{k}{C}-\overset{\alpha}{C}-\overset{\beta}{C}-\overset{\gamma}{C}$$

$$\delta_{calc} = 123.3 + \sum A_i + \sum A_{i'} + \text{correction terms} \qquad (2)$$

where the shift of the carbon k is calculated, A_i corresponds to shift parameters for functional groups α, β, γ to the carbon k, and $A_{i'}$ corresponds to shift parameters for functional groups α', β', γ' across the double bond. For future reference, the shift parameters are given in Table 2.

A similar equation can be used for the shifts of the alkyne carbons [30,53]. The numbering and the equation are given below:

$$-\overset{\gamma'}{C}-\overset{\beta'}{C}-\overset{\alpha'}{C}-\overset{k'}{C}\equiv\overset{k}{C}-\overset{\alpha}{C}-\overset{\beta}{C}-\overset{\gamma}{C}-$$

$$\delta_{calc} = 72.8 + \sum A_i + \sum A_{i'} \qquad (3)$$

The parameters are given in Table 3. Only selected functional groups are represented in Table 3.

The ^{13}C shifts of benzene derivatives can also be estimated using empirical shift additive rules.

Several compilations have been made [54]. We chose the parameters given by Levy et al. [3].

$$\delta_{calc} = 128.5 + \sum T_q \quad (4)$$

where T_q is the substituent at position q (q = *ipso*, *ortho*, *meta* or *para*). For convenience, the shift values are summarized in Table 4.

The ^{13}C shifts for the carbonyls are calculated using separate base values for different functional groups and empirical additive shift rules. Previously, Brown [53] has compiled a list of such rules. These rules have been amplified by Fürst et al. [36]. For carboxylic acids and esters, the rules are straightforward:

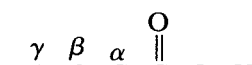

$$\delta_{calc} = 166 + \sum A_i \quad (5)$$

where the parameters A_i are given in Table 5. For ketones and aldehydes a similar rule holds:

$$\delta_{calc} = 193.0 + \sum A_i \quad (6)$$

and the shift parameters A_i are given in Table 6.

TABLE 2

Alkene shift parameters used in program CSPEC2

Substituent	Parameters A_i					
	α	α'	β	β'	γ	γ'
C (sp^3)	+10.6	−7.9	+4.9	−1.8	−1.5	+1.5
-OH (alcohol)	–	–	+6	−1		
-OR (ether)	+23.9	+37.1	+2	−1		
-CO- (ketone)	+8.9	+6.5				
-CHO (aldehyde)	+15.3	+14.5				
-COOH (acid)	+5	+9.81				
-COOR (ester)	+7.8	+5.5				
-CN (nitrile)	−15.1	+14.2				
-Cl (chloro)	+2.8	−6.1	−1	+2		
-Br (bromo)	−8.6	−0.9	0	+2		
-I (iodo)	−38.1	+7				
$-C_6H_5$ (phenyl)	+12.5	−11				
-N < (amine)	18.20	−28.4				
> N + < (ammonium)	5.1	−5.2				
-F (fluoro)	24.9	−34.3				
$-NO_2$ (nitrate)	22.3	−0.9				
-NCO- (urethane)	8.0	−25.8				
-CNOS/CNOA (oxime)	8.3	4.3				
-COCl (acyl Cl)	8.1	14.0				
-OC(O)- (ester)	19.9	−28.2				
-C(O)N- (amide)	7.5	5.8				
-NC(O)- (amide)	8.0	−25.8				
-C≡C- (alkyne)	−6.0	5.9				
-C=C- (alkene)	13.6	−7.0				
-NC (isonitrile)	−3.9	−2.7				
Correction terms						
α, α' (*trans*)	0					
α, α' (*cis*)	−1.1					
α, α	−4.8					
α', α'		+2.5				
β, β			+2.3			
All others	0					

For ketones and aldehydes a similar rule holds:

$$\delta_{calc} = 193.0 + \sum A_i \quad (6)$$

and the shift parameters A_i are given in Table 6.

For amides, however, consideration needs to be made for substituents on either side of the amide:

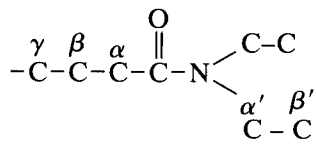

$$\delta_{calc} = 165.0 + \Sigma A_i$$

The additive rules are given in Table 7. Shift parameters for functional groups not given are arbitrarily set to zero.

Similar rules as Eqn. 6 hold for nitriles and isonitriles. The base values are 110.9 and 150.0 ppm, respectively. The shift parameters are summarized in Table 8.

As an example of how these rules work, the ^{13}C shifts of tyrosine are calculated.

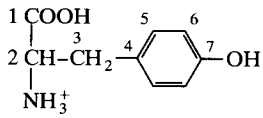

C_1: δ_{calc} = base + α(C) + β(C) + $\gamma(\phi)$ + $\beta(NH_3^+)$ = 166 + 11 + 3 + 0 + 0 = 180

C_2: δ_{calc} = base + α(COOH) + $\alpha(NH_3^+)$ + α(C) + $\beta(\phi)$ − S(t, 2) = −2.3 + 22.1 + 29.8 + 9.1 + 9.0 − 3.7 = 64.0

C_3: δ_{calc} = base + α(C) + β(COOH) + $\beta(NH_3^+)$ + $\alpha(\phi)$ − S(s, 3) = −2.3 + 9.1 + 1.9 + 6.3 + 22.5 − 2.5 = 35.0

C_4: δ_{calc} = base + *ipso*(C) + *para*(OH) = 128.5 + 9.2 − 7.4 = 130.3

C_5: δ_{calc} = base + *ortho*(C) + *meta*(OH) = 128.5 + 0.7 + 1.4 = 130.6

C_6: δ_{calc} = base + *ortho*(OH) + *meta*(C) = 128.5 − 12.8 − 0.1 = 115.6

C_7: δ_{calc} = base + *ipso*(OH) + *para*(C) = 128.5 + 26.9 − 3.0–152.4

The printout from program CSPEC2 for tyrosine is given in Fig. 2.

In the printout, the carbon positions are represented by the vertical and the horizontal grid positions. Alternatively, the cursor can be placed over individual carbons, and the shift of that carbon is displayed on the lower right corner of the screen. In the example in Fig. 2, the cursor (not visible in the figure) is situated at position 12,24, and the shift is 152.4 for that carbon.

Shift computation. From the input structure, the program uses a tree logic to calculate the ^{13}C shifts. The logic is slightly modified from that in the previous efforts (CSHIFT and CSPEC) [32,35]. In this case, special provisions have been made such that configurational isomers (e.g., *trans/cis*) are differentiated. For example, the *cis* and the *trans* shift rules apply to the following depiction of a disubstituted olefin.

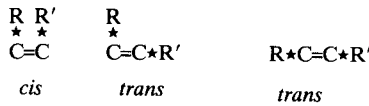

Parent structure. Sometimes in shift estimation, instead of starting from scratch (the a priori

TABLE 3

Alkyne shift parameters used in program CSPEC2

Substituent	Parameters A_i					
	α	α'	β	β'	γ	γ'
C	6.9	−5.7	4.8	2.3	−0.13	−1.30
$-C_6H_5$	11.8	5.0			–	–
−C≡C−	−4.0	−8.1				
−C=C−	10.0	7.2	–	–	−0.13	−1.30
−OH	–	–	3.3	6.7	–	–
−O−	10.7	−51.8	4.8	2.3	−0.13	−1.30
−S−	−4.9	7.6	4.8	2.3	−0.13	−1.30
−CHO	9.0	10.3	–	–	–	–
−CO−	4.3	3.0	4.8	2.3	−0.13	−1.30
−COOH	1.2	5.8	–	–	–	–
−COOR	2.1	4.1	–	–	–	–

TABLE 4

Shift parameters for substituted benzenes used in program CSPEC2

Substituent	Parameter T_q			
	ipso	*ortho*	*meta*	*para*
C (sp^3)	9.2	0.7	−0.1	−3.0
-OH (alcohol)	26.9	−12.8	1.4	−7.4
-O- (ether)	31.4	−14.4	1.0	−7.7
-SH (thiol)	2.1	7.0	0.3	−3.2
-S- (thioether)	10	−1.9	0.2	−3.6
$-NH_2$ (prim. amine)	18.2	−13.4	0.8	−10
$-NH_3^+$ (prim. ammonium)	0.1	−5.8	2.2	2.2
-NH- (sec. amine)	21.4	−16.2	0.8	−11.6
$-NH_2^+$ (sec. ammonium)	0 [a]			
-N< (tert. amine)	22.5	−15.4	0.9	−11.5
-NH+ (tert. ammonium)	0 [a]			
>N+< (quat. ammonium)	19.5	−7.3	2.5	2.4
-F (fluoro)	34.8	−13	1.6	−4.4
-Cl (chloro)	6.3	0.4	1.4	−1.9
-Br (bromo)	−5.8	3.2	1.6	−1.6
-I (iodo)	−34.1	8.9	1.6	−1.1
-CN (nitrile)	−15.7	3.6	0.7	4.3
$-NO_2$ (nitrate)	19.9	−4.9	0.9	6.1
-NCO (isocyanate)	5.1	−3.7	1.1	−2.8
-NCS (isothiocyanate)	3.0	−2.7	1.3	−1.0
-SCN (thiocyanate)	−3.7	2.5	2.2	2.2
-SO- (sulfoxide)	17.6	−5.0	1.1	2.4
-SO2 (sulfone)	12.3	−1.4	0.8	5.1
$-SO_3H$ (sulfonate)	15.0	−2.2	1.3	3.8
-CNOS (oxime, syn)	0 [a]			
-CNOA (oxime, anti)	0 [a]			
-CHO (aldehyde)	8.2	1.2	0.5	5.8
-CO- (ketone)	8.9	0.1	−0.1	4.4
-COOH (acid)	2.1	1.6	−0.1	5.2
$-COO^-$ (carboxylate)	9.7	4.6	2.2	4.6
-COCl (acyl chloride)	4.7	2.7	0.3	6.6
$-C_6H_5$ (phenyl)	13.1	−1.1	0.5	−1.1
-OOH (hydroperoxy)	0 [a]			
-OO- (peroxy)	0 [a]			
-COO- (ester)	2.0	1.2	−0.1	4.3
-OCO- (ester)	22.4	−7.1	0.4	−3.2
-CONH- (amide)	5.0	−1.2	0.1	3.4
-NHCO- (amide)	9.7	−8.1	0.2	−4.4
-C≡C- (alkyne)	−6.2	3.6	−0.4	−0.3
-C=C- (alkene)	8.9	−2.3	−0.1	−0.8
EPOX (epoxy)	9.2	−3.1	−0.1	−0.5
-NC (isonitrile)	−1.8	−2.2	1.4	0.9

[a] Parameters left at 0 because no data are available.

method), it is easier to start with a compound where all the ^{13}C shifts have been experimentally determined. This compound has been called a "parent structure" [35]. The parent structure can be any compound in the spectral library. It can be

TABLE 5

Shift parameters used in program CSPEC2 for carboxylic acids and esters

Substituent	Parameters, A_i			
	α	β	γ	X
C	11	3	−1	−5
$-C_6H_5$	6	1	0	−8
-C=C-	4	0	0	−9
-CHO	−0.7	–	–	−1.0
-CO-	−0.7	–	–	−1.0
-COOH	−5.9	−7.8	−8.0	
-C≡C-	−6.0			
-COOR	−2.6	−4.4	−0.5	
-O-	−9.5			

TABLE 6

Shift parameters used in program CSPEC2 for ketones and aldehydes

Substituent	Parameters, A_i		
	α	β	γ
C	6.5	2.6	0
$-C_6H_5$	−3.0	0	0
-C=C-	−3.0	0	1.0
-S-	−3.0	–	–
-Cl	−27	−5.4	–
-Br	−35	−7.5	–
-I	−42	–	–
-O-	−20		
-N<	−23		
-OCO-	−37		
-NHCO-	−30		
-COOH	−7.7		
-C≡C-	−18.0		
-CO-	−3.0		
-CHO	−3.0		

TABLE 7

Shift parameters used in program CSPEC2 for amides

Substituent	Parameters, A_i				
	α	β	γ	α'	β'
C	7.7	4.5	−0.7	−1.5	−0.3
$-C_6H_5$	4.7	–	–	−4.5	–
-C=C-	3.3	–	–	−5.4	–
-O-	−5.7	–	–	−6.7	–
-S-	4.1	–	–	–	–
-N-	–	–	–	−2.4	–
-Cl	–	5.0	–	–	–
-CHO	−3.0	–	–	−2.0	–
-CO-	−3.0	–	–	−2.0	–

TABLE 8

Shift parameters used in program CSPEC2 for nitriles and isonitriles

Substituent	Parameters, A_i			
	α	β	γ	δ
(A) Nitriles (base = 110.9)				
C	7.2	2.5	−0.8	−0.5
–COOH	–	−3.6	–	–
–CN	–	−7.6	−2.6	
–C=C–	6.4			
–S–	0.8			
(B) Isonitriles (base = 150.0)				
C	8.1	−1.2	−0.6	0
–C=C–	14.8	0.2		

retrieved, modified to a slightly different structure, and the ^{13}C shifts of the modified structure estimated from either the shifts of the parent structure (using the F4 command) or from a priori principles (using the F2 command). In the case of parent structure computation (F4 command), two columns of shifts are produced. The first column is calculated as if the F2 command is selected. The second column gives the modified shifts using the parent structure feature. An example is shown in Fig. 3 for the shift calculation of alanine based on glycine as the parent structure.

The parent structure feature provides some time savings in inputting of structures and also an

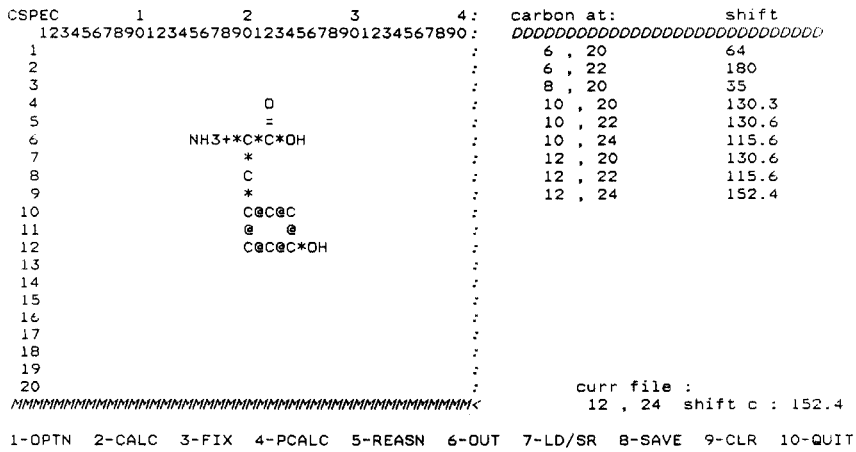

Fig. 2. Printout format for a sample calculation on the program CSPEC2. The ^{13}C shifts of tyrosine are being computed on the a priori basis.

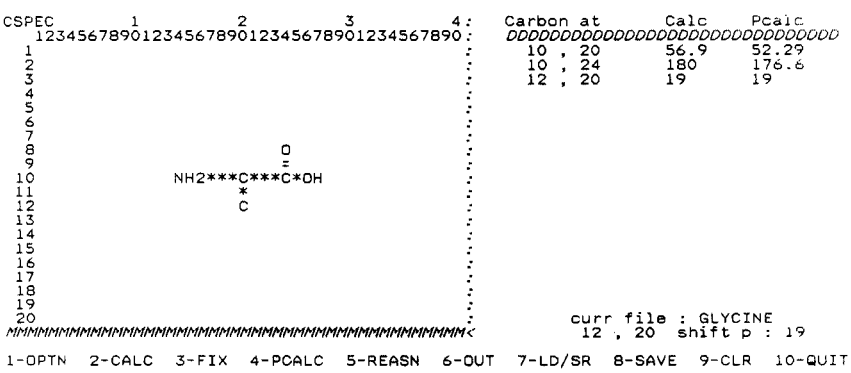

Fig. 3. Calculation of the ^{13}C shifts of alanine, using parent structure option; the parent structure is glycine.

alternative estimate of the shifts. It allows the user to start from a compound with known ^{13}C shifts and then add empirical additive parameter values as needed to reach the modified structure. The feature is especially useful for ring or multiple ring compounds. Another use is to estimate the shifts of compounds containing functional groups not in the functional group table (Table 1). For example, the sulfite functional group is not in Table 1, but the ^{13}C shifts of diethylsulfite are known. If the shifts of dibutylsulfite is needed, the user can start with diethylsulfite (in the library), modify the structure to dibutyl, and use the parent structure calculation.

Output

The output can be made in any one of the four formats: printout of predicted shifts, data file, bar graph, or plot. The printout option is self-explanatory (e.g., Figs. 2 and 3). The data file option is provided in order to allow the spectral data to be used in conjunction with graphics software packages such as SLIDEWRITE [55]. The bar graph option provides a low-resolution spectrum on the printer.

The plot option is very useful for spectral matching. It produces a simulated NMR spectrum (with spectral noise, if chosen) for the compound in question. Program CSPEC2 chooses the first available shift data with the following priority: (1) parent calculation values, (2) known shift values, and (3) a priori calculated values. An additional option is available to insert a comment along the top of the graph. Together with the choice of spectral noise, a fake NMR spectrum that bears remarkable similarity to a real spectrum can be produced with little effort. An example is shown for the simulated spectrum of tyrosine (Fig. 4).

Spectral library

Command F7 (load/search) provides for both retrieval of compounds and access to the spectral library.

Library acquisition. The program currently has 200 compounds and their known shifts stored in the library. These contain many common organic compounds and are useful as potential parent structures. Most of the compounds have been taken from Johnson and Jankowski [37]. The prospective user is encouraged to enter additional compounds into the library. The spectral library can be built in two ways. First, a structure can be entered as usual, and the F3 command used for the manual entry of known ^{13}C shifts. Alternatively, the entered structure and the calculated shifts can be saved through the F8 command. In either case, a library of compounds and (known or calculated) shifts can be built up.

Compound list. Each file in the library is given a mnemonic name of no more than eight al-

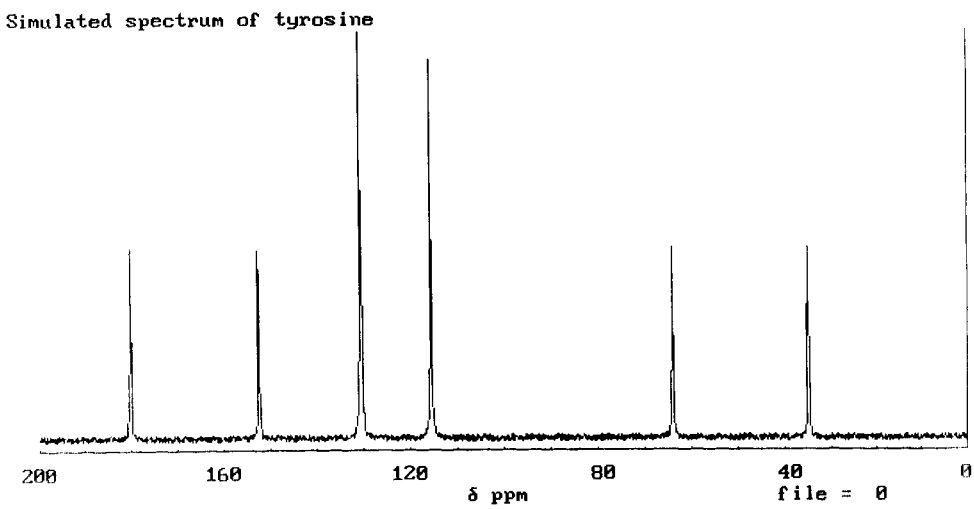

Fig. 4. Simulated spectrum of tyrosine; spectral noise has been added for realistic effect.

phanumeric characters. If the mnemonics corresponding to a structure is entered, the structure (and associated shifts) are loaded directly and are visualized on the screen. The subcommand L gives a list of all the compounds in the library. In addition to the mnemonic name, the user can enter a full structure name, or a description of the compound in question. Any portion of this name or description can be searched via the search command.

Interpretive approach. The approach used is similar to that of Dalrymple et al. [6]. The search features in CSPEC are accessed by pressing F7 and choosing S for the search features. The user will be prompted for the search type: (1) name or description, (2) molecular formula, and (3) shift value

If the name or molecular formula options are chosen the user will be prompted for a search string. For example, if one wishes to display all the structures with ten carbons, simply enter C10. The search string for both the name and the molecular formula need not be complete and is not case sensitive. If the shift value option is chosen the user will be prompted for a shift value and a shift range. The shift range allows for lack of experimental precision and also differences in experimental and instrumental conditions for data reported in the literature.

After entering a search string or shift value, the program CSPEC2 will search the library for matches. The user can either choose to display one of the matched structures, narrow the list further by additional queries, or backup up to the previous step by using the escape key. Note that the names and molecular formulas of the structures are displayed exactly as supplied by the user when the structure is saved into the library. It is recommended that the order of elements in the molecular formula strings be consistent. The compounds supplied with program CSPEC2 use the following form: $C_uH_vN_wO_xS_yX_z$, where X is a halogen and u, v, w, x, y and z are the number of atoms of the elements.

Enhanced features

Help files. For the convenience of the user, a number of instructions are given in the help file. It can be accessed through the Options Command {F1}.

Functional groups. The program CSPEC2 presently has 42 functional groups with the empirical shift parameters built in the program (Table 1). The program recognizes these functionalities and will assign the correct shift parameters. If an unrecognized functionality or atom is encountered, the program will respond in two ways. If the functional group and its components are completely unrecognizable, the program will signal an error, ignores it, and calculates the expected shifts without the offending group. If a functional group (entered explicitly atom-by-atom) is not in the list in Table 1 but the components of the functional group are, the program will attempt to decipher the functional group by using the component shift concept [35]. In other words, the program will try to break up the functional group into smaller, recognizable components. For example, carbamate is not in the list in Table 1. If the user enters

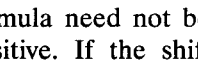

the program will estimate the carbon shift as well as the shifts of the carbons adjoining this functionality by using component shift additivity relationship. Thus, the shift of the carbon underlined below is estimated from ester oxygen (α to it) and amide (β to it):

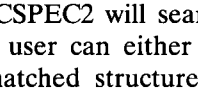

estimated shift $= -2.3 + 53.0 + 3.2 + 0.3 = 54.2$

Note that this use of component shifts is slightly different from the previous work [35].

Parameter modification. Program CSPEC2 allows the user to modify the empirical shift parameters used to calculate chemical shifts. In addition, the program also allows for eight user-defined atoms or functional groups. The user must supply the additive shift parameters for these user-defined groups. Both features are given in the Option Command {F1}. This option is particularly useful if a user is working with a specific atom or functional group for which the user has devised shift parameters and wants to use the

TABLE 9

Results of parent structure calculation for ethyl acrylate

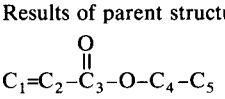

Carbon No.	Calc [a]	Pcalc [b]
1	130.3	129.80
2	131.9	129.19
3	165.0	165.89
4	57.4	57.40
5	15.2	12.59

[a] From a priori method. [b] From parent structure calculation (parent structure = butyl acrylate).

versatility of program CSPEC2 for shift prediction and spectral simulation.

Illustrations

As an example of how some of the features in program CSPEC2 can be used, we examine the shifts of ethyl acrylate and its polymer:

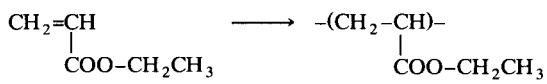

We first search the library for acrylate compounds. This can easily be done using F7 (load/search), subcommand S (search) and N (name), and entering "acryl." Three matches are found: acrylonitrile, methyl methacrylate and butyl acrylate. We choose butyl acrylate as the parent structure. Deletion of two carbons gives us ethyl acrylate. Use of parent structure calculation {F4} gives us the data given in Table 9.

Calculation of the shifts for poly(ethyl acrylate) can be carried out by entering the *pentamer* of ethyl acrylate and then take the shifts of the central monomer unit. The calculated result is shown below:

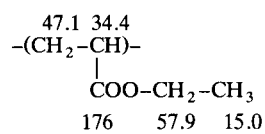

The interpretive approach can be illustrated using a test spectrum consisting of the following shifts: 54.8, 56.6, 68.3. If we input the shift 54.8 ± 1.0 and use the database of 200 compounds in program CSPEC2, we obtain ten candidates. The list of candidates is narrowed down to three by using the shift 56.6 ± 1.0. With the final shift (68.3 ± 1.0), only one compound is left: choline chloride. During the search, we can enter additional information (if available) to reject candidates (e.g., partial molecular formula or a name fragment). The shifts of all the candidates can also be individually examined, if needed.

EXPERIMENTAL

The program CSPEC2 requires an IBM or compatible personal computer. A printer is required for spectral simulation. A plotter and software package such as SLIDEWRITE [55] are recommended for more realistic spectral visualization. Currently the program is in a directory (CSPEC) and all saved structures are in a subdirectory, LIB.

The program was written using QuickBASIC and contains a number of commands particular to QuickBASIC. The program will not run, as currently written, in BASICA. All features of the earlier program CSPEC [35] have been retained in this program. Readers interested in this program may write to the authors for a working copy. Also available are the instructions and a brief tutorial.

Conclusion

In the use of ^{13}C NMR for organic structure determination, the most time-consuming part is spectral interpretation. The motivation for this program is to computerize the shift prediction and the library search operations in order to facilitate spectral interpretation. The major features of the program are:

(1) ease of use;

(2) little or no cost;

(3) provision for spectral visualization through simulation;

(4) combined predictive and interpretive approaches;

(5) flexibility in amending shift parameter values;

(6) flexibility to add additional functional groups;

(7) provision for enlarging the spectral library.

The authors wish to thank J. Reuben, E.A. Demgar, W.S. Duncan, and E. Laletas for using earlier versions of this program and for valuable suggestions for improvements. This is Hercules Research Center Contribution Number 2197.

REFERENCES

1 J.B. Stothers, Carbon-13 NMR Spectroscopy, Academic Press, New York, 1972.
2 E. Breitmaier and W. Voelter, ^{13}C NMR Spectroscopy, Verlag Chemie, Weinheim, 2nd edn., 1978.
3 G.C. Levy, R.L. Lichter and G.L. Nelson, Carbon-13 Nuclear Magnetic Resonance Spectroscopy, Wiley-Interscience, New York, 2nd edn., 1980.
4 H.-O. Kalinowski, S. Berger and S. Braun, Carbon-13 NMR Spectroscopy, Wiley, Chichester, 1988.
5 (a) F.W. Wehrli and T. Wirthlin, Interpretation of Carbon-13 NMR Spectra, Heyden, Philadelphia, 1978; (b) F.W. Wehrli, A.P. Marchand and S. Wehrli, Interpretation of Carbon-13 NMR Spectra, Wiley, Chichester, 2nd edn., 1988.
6 (a) B.A. Jezl and D.L. Dalrymple, Anal. Chem., 47 (1975) 203; (b) D.L. Dalrymple, C.L. Wilkins, G.W.A. Milne and S.R. Heller, Org. Magn. Reson., 11 (1978) 535.
7 S.R. Heller, J. Chem. Inf. Comput. Sci., 25 (1985) 224.
8 N.A.B. Gray, Prog. Nucl. Magn. Reson. Spec., 15 (1982) 201.
9 C. Djerassi, D.H. Smith, C.W. Crandell, N.A.B. Gray, J.G. Nourse and M.R. Lindley, Pure Appl. Chem., 54 (1982) 2425.
10 M.R. Lindley, N.A.B. Gray, D.H. Smith and C. Djerassi, J. Org. Chem., 47 (1982) 1027.
11 M.E. Munk and B.D. Christie, Anal. Chim. Acta, 216 (1989) 57; and references cited therein.
12 S. Sasaki and Y. Kondo, J. Chem. Inf. Computer Sci., 25 (1985) 252.
13 Y. Takahashi, S. Maeda and S. Sasaki, Anal. Chim. Acta, 200 (1987) 363; and references cited therein.
14 J.-E. Dubois, M. Carabedian and I. Dagane, Anal. Chim. Acta, 158 (1984) 217.
15 M. Carabedian, I. Dagane and J.-E. Dubois, Anal. Chem., 60 (1988) 2186; and references cited therein.
16 W. Bremser and W. Faschinger, Magn. Reson. Chem., 23 (1985) 1056; and references cited therein.
17 INKA Database, Scientific Information Service, Larchmont, NY.
18 J. Zhang and L. Xu, Anal. Chim. Acta, 210 (1988) 163.
19 S.-G. Yuan, Y.-W. Wang, D. Chen and C.-Z. Zheng, Anal. Chim. Acta, 221 (1989) 345.
20 J.P. Gastmans, J.C. Zurita, J. Sahao, Jr. and V.P. Emerenciano, Anal. Chim. Acta, 217 (1989) 85.
21 C. Jaime, Magn. Reson. Chem., 28 (1990) 42.
22 For reviews, see (a) Ref. 8; (b) J.T. Clerc (Ed.), Computer Techniques and Optimization, Vol. 5 (Anal. Chim. Acta, Vol. 133), Elsevier, Amsterdam, 1981; (c) L.A. Gribov and M.E. Elyashberg, CRC Crit. Rev. Anal. Chem., 8 (1979) 110; (d) Z. Hippe and R. Hippe, Appl. Spectrosc. Rev., 16 (1980) 135.
23 E.G. Paul and D.M. Grant, J. Am. Chem. Soc., 86 (1964) 2984.
24 H. Eggert and C. Djerassi, J. Am. Chem. Soc., 95 (1973) 3710.
25 J.E. Sarneski, H.L. Suprenant, F.K. Molen and C.N. Reilley, Anal. Chem., 47 (1975) 2116.
26 J.D. Roberts, F.J. Weigert, J.I. Kroschwitz and H.J. Reich, J. Am. Chem. Soc., 92 (1970) 1338.
27 A. Ejchart, Org. Magn. Reson., 9 (1977) 351.
28 R. Hagen and J.D. Roberts, J. Am. Chem. Soc., 91 (1969) 4504.
29 J.T. Clerc, E. Pretsch and S. Sternhell, ^{13}C-Kernresonanz-spectrokopie, Akademische Verlagsgesellschaft, Frankfurt-am-Main, 1973.
30 E. Pretsch, J.T. Clerc, J. Seibl and W. Simon, Tables of Spectral Data for Structure Elucidation of Organic Compounds, Springer, Berlin, 2nd edn., 1989.
31 J.T. Clerc and H. Sommerauer, Anal. Chim. Acta, 95 (1977) 33.
32 H.N. Cheng and S.J. Ellingsen, J. Chem. Inf. Comput. Sci., 23 (1983) 197.
33 R.A. Hearmon, Magn. Reson. Chem., 24 (1986) 995.
34 A. Fürst and E. Pretsch, Anal. Chim. Acta, 229 (1990) 17.
35 H.N. Cheng and M.A. Bennett, Anal. Chim. Acta, 242 (1991) 43.
36 (a) A. Fürst, E. Pretsch and W. Robien, Anal. Chim. Acta, 233 (1990) 213; (b) A. Fürst, E. Pretsch and W. Robien, Anal. Chim. Acta, 248 (1991) 415.
37 L.F. Johnson and W.C. Jankowski, Carbon-13 NMR Spectra, Krieger, Huntington, NY, 1978.
38 Sadtler standard Carbon-13 NMR Spectra, Bio-Rad Sadtler Division, Philadelphia, 1983.
39 W. Bremser, L. Ernst, B. Francke, R. Gerhards and A. Hardt, Carbon-13 NMR Spectral Data, VCH, Weinheim, 1986.
40 (a) E. Breitmaier, G. Haas and W. Voelter, Atlas of Carbon-13 NMR Data, Heyden, London, 1979. (b) C.J. Pouchert and J. Behnke, The Aldrich Library of ^{13}C and ^{1}H NMR Spectra, Aldrich, Milwaukee, WI.
41 SPECINFO Database, STN International, Columbus, OH.
42 W. Bremser, Anal. Chim. Acta, 103 (1978) 355.
43 C.W. v.d. Lieth, J. Seil, I. Köhler and H.J. Opferkuch, Magn. Reson. Chem., 23 (1985) 1048.
44 N.A.B. Gray, J.G. Nourse, C.W. Crandell, D.H. Smith and C. Djerassi, Org. Magn. Reson., 15 (1981) 375.
45 H. Kalchhauser and W. Robien, J. Chem. Inf. Comput. Sci., 25 (1985) 103.
46 (a) J. Zupan, M. Novic, S. Bohanec and M. Razinger, Anal. Chim. Acta, 200 (1987) 333. (b) L.S. Anker and P.C. Jurs, Anal. Chem., 64 (1992) 1157. (c) J.P. Doucet, A. Panaye, E. Feuilleaubois and P. Ladd, J. Chem. Inf. Comput. Sci., 33 (1993) 320.

47 Carbon-13 Database, Bio-Rad Sadtler Division, Philadelphia, PA.
48 G.W. Small and P.C. Jurs, Anal. Chem., 55 (1983) 1128.
49 M.L. Ranc and P.C. Jurs, Anal. Chim. Acta, 248 (1991) 183; and references cited therein.
50 J.M. Bernassau, M. Fetizon and E.R. Maia, J. Phys. Chem., 90 (1986) 6129.
51 J. Bastard, J.M. Bernassau, M. Fetizon and E.R. Maia, Magn. Reson. Chem., 26 (1988) 992.
52 D.E. Dorman, M. Jautelat and J.D. Roberts, J. Org. Chem., 36 (1971) 2757.
53 D.W. Brown, J. Chem. Educ., 62 (1985) 209; and references cited therein.
54 For example, (a) D.F. Ewing, Org. Magn. Reson., 12 (1979) 499; (b) R.A. Newmark, Comput. Chem., 10 (1988) 223; (c) R.A. Hearmon, H.-M. Liu, S. Laverick and P. Tayler, Magn. Reson. Chem., 30 (1992) 240.
55 Advanced Graphics Software, Carlsbad, CA.

Analytica Chimica Acta, 285 (1994) 237–246
Elsevier Science B.V., Amsterdam

Neural network approach to qualitative identification of fuels and oils from laser induced fluorescence spectra

John M. Andrews

Computer Sciences Corporation, 4045 Hancock Street, San Diego, CA 92110 (USA)

Stephen H. Lieberman

Naval Command, Control Ocean Surveillance Center; Research, Development, Test and Evaluation Division (NRaD), Code 521, San Diego, CA 92152-5000 (USA)

(Received 17th May 1993; revised manuscript received 27th July 1993)

Abstract

A series of software implemented, three-layer, backpropagation neural networks is trained to identify seven classes of petroleum hydrocarbon based fuels and oils from their fluorescence emission spectra. The classes include: 87 and 92 octane unleaded gasoline, diesel fuel No. 2, diesel fuel marine, JP5, and lube oils 2190 and 9250. The nitrogen laser induced fluorescence spectra of multiple samples of each class are collected through an optical fiber incorporated into a multichannel detection system. Thirty-six spectral examples of the seven fuel/oil classes are partitioned into seven separate paired combinations of training and test spectra. Each combination uses 29 spectra to independently train a network. The spectra from the remaining seven samples are used to test the trained network's ability to make generalized classifications. Networks trained with data sampled directly from the normalized fluorescence emission spectra accurately identify 96% of the test spectra. An additional series of networks is trained and tested using the same spectra but with principal component analysis (PCA) employed as a preprocessor. Networks trained using PCA processed spectral data achieve somewhat lower performance, successfully identifying only 90% of the test spectra.

Keywords: Fluorimetry; Principal component analysis; Fuels; Neural networks; Oils

Progress over the past decade in digital electronic technology has brought about many advances in the data acquisition and signal processing capabilities available to the analytical chemist. Concurrently, there have also been significant developments in instrumentation and sensor technology. Often however, the improved ability to rapidly collect raw data exceeds the ability to analytically process or efficiently extract the chemical information contained within that data. This can occur, for example, when trying to perform real-time discrimination of the subtle features contained within large multidimensional data arrays. There is a need therefore, for advanced data processing tools which will enable the researcher to more efficiently investigate, classify, analyze, or model complex sets of chemical data. Neural network based processing offers advantages which make it a good candidate for addressing this need.

One of the unique properties of artificial neural systems (ANSs) is their ability to learn by observation. An ANS can by adapting itself, au-

Correspondence to: J.M. Andrews, Computer Sciences Corporation, 4045 Hancock Street, San Diego, CA 92110 (USA).

SSDI 0003-2670(93)E0648-Q

tonomously learn to recognize key features in a data set by repetitiously examining examples of the same or similar data. This attribute provides an effective means of identifying patterns in new or intricate data. An ANS based analysis can be fully realized without the developer having any a priori assumptive knowledge of the problem's parameters. Hence ANSs are ideally suited for use in pattern recognition applications in which the pattern relationships have not previously been explained. They can also serve as a powerful tool to assist in knowledge acquisition, helping the researcher to gain insight into poorly understood systems [1].

Another attractive feature of ANSs is the speed at which a trained system, that is one which has learned to associate a set of patterns, can process information. Although training an artificial neural network can be tedious and may require many hours of dedicated computer time, a trained network processes information very quickly. A trained software implemented ANS modeled in a microcomputer environment is generally capable of supporting real-time applications. Furthermore, it is possible to develop hard wired solutions from software implemented ANS models, thereby taking true advantage of the parallel processing power inherent in neural network architecture.

There are numerous ANS paradigms, some of which are more effective than others at addressing certain specific processing needs. To date however, the multilayer backpropagation paradigm has been by far the most widely applied. A number of variants of the generic backpropagation algorithm have been developed and applied to problems in many areas. A detailed description of backpropagation is available from many sources [2–5].

The success and popularity of the backpropagation algorithm is based largely on its proven adeptness at solving pattern recognition problems. It has been demonstrated that any arbitrarily complex nonlinear associative mapping may be encoded into the weight space or memory of a backpropagation neural network [6]. In principle, a backpropagation ANS could be developed to solve any pattern recognition problem, providing of course that a solution exists. Also, like other ANS models, the backpropagation paradigm because of its parallel distributed architecture and intrinsic ability to generalize and form abstractions is to a relatively large extent immune to problems associated with incomplete and noisy data. These properties make backpropagation well suited to many signal analysis and processing problems which commonly arise in analytical chemistry, especially in situations where conventional techniques have in the past been found to be inadequate.

During the past several years there has been a growth of interest in use of ANSs in the field of analytical chemistry as researchers begin to explore potential applications. Many chemistry related implementations are concerned with spectral pattern interpretation and calibration issues. Nearly all rely on backpropagation. ANSs have been applied to the analysis of mass [7], infrared [8–12], NMR [13,14], atomic emission [15,16], gamma [17], and fluorescence [18,19] spectra. Overviews of chemistry related applications of ANSs have also been published [20,21].

This paper presents results of the use of a backpropagation neural network for qualitative identification of refined petroleum products from laser induced fluorescence spectra. The effort is motivated by the development in our laboratory of a fiber optic based fluorometer system for real-time, in situ field screening of petroleum hydrocarbon based fuels and oils in soil [22]. Because the system is capable of measuring fluorescence emission spectra of up to 1024 data points every second, a fast processing method is needed to enable rapid interpretation of the chemical information embedded in the raw spectral data.

Fluorescence spectroscopy is a sensitive, albeit non-selective, analytical technique. The UV–visible fluorescence spectrum produced by a fuel or oil product is a composite signal of the fluorogenic constituents of what is essentially a mixture. As many of the different petroleum products share common fluorogenic components, the resulting fluorescence spectra are sometimes very similar and difficult to discern.

Our interest therefore is to develop a data

processing method for real-time discrimination of fuels and oils in soil, utilizing small spectral differences to classify the fluorescence fingerprints of different petroleum hydrocarbon products. This would permit the field screening system to delineate and identify contamination from several possible sources.

The approach taken here in this preliminary investigation is to train a series of backpropagation neural networks using fluorescence spectral data obtained under controlled conditions in the laboratory. As there is no direct method for choosing an optimal network configuration, several network variations are trained and compared. One set of networks is trained using data sampled directly from the normalized spectra. A second series of networks is trained using principal component scores generated from the same spectra. It has been demonstrated [23,24] that for highly correlated data, such as is typical of many types of spectra, using principal component analysis (PCA) as a preprocessor for a neural network can reduce network complexity, decrease learning times, and improve generalization.

The net effect of PCA is to map each spectrum, or vector, into a data space of fewer dimensions while retaining the maximum variability in the data. Factor scores can then be calculated for each individual spectrum in the set and used as input to a neural network. A factor score is a scalar value representing the projection of a particular spectrum onto one of the axes of the new data space. It is the spectrum's component along that axis.

PCA is also used as a means of examining the data space in which the sample spectra reside. Reducing a data set down to three or fewer dimensions by eliminating the clutter of linearly dependent variables makes visualization much more natural.

EXPERIMENTAL

Oil / fuel sampling

A total of 36 samples representing seven general petroleum product types were collected at ten different locations in San Diego, including local military installations and commercial service stations. Products from at least five different refiners are represented in the set. The different oil/fuel types include: diesel No. 2, 87 and 92 octane unleaded gasolines, diesel fuel marine, JP5, and lube oils 9250 and 2190. Samples obtained from storage tanks, fuel pumps, and tanker trucks were collected and stored in commercially precleaned (I-Chem, Hayward, CA) glass bottles. Other samples were obtained from the collection of archived oil/fuel samples at the fuel laboratory, Naval Supply Center, San Diego, CA. Some samples taken from large capacity storage tanks probably represent brand mixtures, as product from several sources may be stored in the tanks together.

Spectroscopy

The laser induced fluorescence spectra were collected using a system built around an optical multichannel analyzer (EG&G PARC Model 1460). An essentially similar optical arrangement and detection scheme has previously been described [25].

The 337.1 nm emission of a pulsed nitrogen laser (PTI 2300) provided a means of sample excitation. The laser output was coupled into a 40 meter long, 500 μm diameter optical fiber through which it traveled to the sample. The oil/fuel samples were contained within a borosilicate glass vial placed at the distal end of the fiber. The induced fluorescence was collected by a second fiber which carried the emission signal from the sample to a grating spectrometer (Jarrell Ash MonoSpec 18). The dispersed light was detected by an intensified linear photodiode array (EG&G Model 1421) located at the exit slit of the spectrometer. The spectrometer/detector combination delivered a spectral resolution of 2.1 nm.

Time gating was used to reduce background noise. Following each laser shot a fast amplifier (EG&G Model 1304) was used to switch on the intensified photodiode array for a 20 ns duration. Sufficient delay was introduced between the laser pulse and the amplifier pulse to temporally separate the back scattered 337.1 nm excitation light from the longer lived fluorescence light arriving at the detector. This modulation scheme also

served to minimize the effects produced by stray light at the detector.

Principal component analysis

In order to reduce the number of input variables associated with each spectrum, principal component analysis (PCA) was performed on the set of sample spectra. The normalized spectra were sampled at 55 equally spaced wavelength units between 350 and 550 nm. Vectors made up of these 55 data points were use to generate the correlation matrix for the sample set. Normalized factor scores and factor loadings were determined after varimax rotation of the unrotated factor solution. The factor scores derived for each spectral case were then used to train and test neural networks. PCA was accomplished using a desktop computer and the commercially available statistical software package CSS:Statistica (StatSoft, Tulsa, OK).

Network design

Each of the networks that were trained had a similar architecture and identical learning rule parameters. Each consisted of three layers of neural nodes (or neurodes), designated the input, hidden, and output layers. The input layer incorporated one input neurode for each element of the spectral input vector. The output layer contained seven neurodes, one for each category of oil/fuel. All of the input neurodes were fully connected to every other neurode in both the hidden and output layers. The hidden layer neurodes were fully connected to the seven neurodes of the output layer. A single bias node was connected to every neural node in the network. The network is shown as part of Fig. 1.

The individual networks differed only in the number of hidden and input layer neurodes used. Networks trained on the directly sampled data utilized 20 input neurodes, this number corresponding to the size of the input vector. These networks employed either five, seven, nine, or eleven hidden layer neurodes. Networks trained on the PCA data had only three input elements and two, three, four, or five hidden layer neurodes.

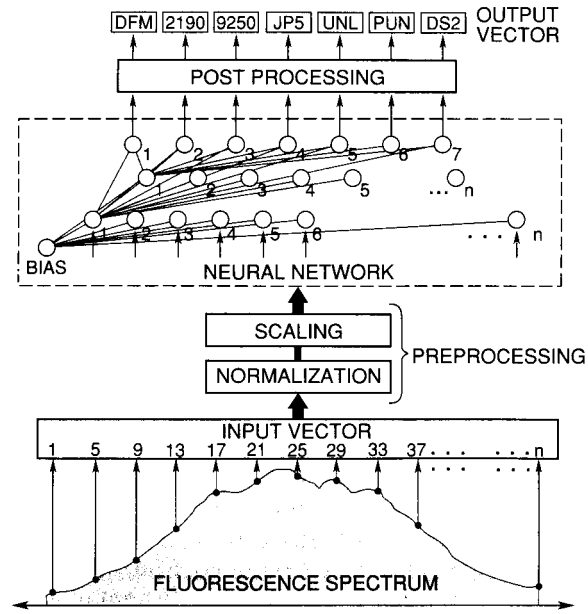

Fig. 1. Information flow from raw spectral data to final neural system output. The output values correspond to diesel fuel marine (DFM), lube oil 2190 (2190), lube oil 9250 (9250), JP5, 87 octane unleaded gasoline (UNL), 92 octane premium unleaded gasoline (PUN), and diesel fuel No. 2 (DS2). Only the interconnections for the first neurode in each layer are shown.

The neural system was modeled in software on a desktop computer (IBM compatible Intel i486/33 MHz) using NeuralWorks Professional II/PLUS (Neuralware, Pittsburgh, PA) neural network development tool. Data traveled through the networks in a feedforward fashion from input to hidden to output layers. After a network was trained, lateral inhibitory connections were included between the neurodes of the output layer. This served to insure that only the output neurode with the highest activation level would have a nonzero output. Training utilized a standard backpropagation control strategy. The cumulative generalized delta rule was employed with momentum for learning. Connection weights were updated during training according to the learning rule as follows:

at each iteration:

$$M_{(n)} = M_{(n-1)} + C_1 \cdot E \cdot x$$

at each epoch:

$$W_{(n)} = W_{(n-1)} + M + C_2 \cdot M_{(\text{previous})}$$

$$(M = 0)$$

where n = iteration index; C_1, C_2 = learning coefficients; E = local error at each node; and x = input through the connection. The learning coefficient C_1 was initially set to 0.125 for the hidden layer neurons and 0.10 for the output layer neurons. The momentum coefficient C_2 started at a value of 0.2. C_1 and C_2 were programmed to decrease exponentially in a series of steps as learning progressed. The epoch size was set to four iterations.

A hyperbolic transfer function was applied to the weighted input sum (Σ) at every neuron as:

$$\text{Neurode output} = \frac{(e^{+\Sigma} - e^{-\Sigma})}{(e^{+\Sigma} + e^{-\Sigma})}$$

Training with spectral data sets

The 36 sample spectra were used to form seven different combinations of paired training/test sets. Each of the training sets consisted of 29 spectra paired with the desired network output vector for each spectrum. The corresponding test set consisted of the seven remaining spectra, one representative of each oil/fuel class. The test set was used to test the networks post training performance. Each of the 36 spectral cases were included as part of at least one test set. The spectra included in the seven training/test data sets were identical for both the networks trained using direct spectral data and for those trained on the PCA reduced data. For training/testing with direct spectral data, 20 points were sampled from the normalized spectrum of each case. These points corresponded to the fluorescence intensity at approximately equally spaced wavelengths between 350 and 500 nm.

The data processing flow from raw spectra to final class identification is shown in Fig. 1. Initial preprocessing of the data included normalization of all of the spectra to unit area so as to eliminate the possibility of network discrimination due to quantitative variances in the data. For the networks trained using factor scores, PCA is considered to be included as part of the preprocessing. Prior to network processing, values used as input to the networks were scaled to values ranging from -1.0 and $+1.0$. This involved a linear mapping of the lowest raw value in a set of input fields to -1.0, mapping the highest raw value to $+1.0$ and scaling the in between values accordingly. This is to avoid saturation of the transfer function during initial training. The desired output vectors included in the training sets were scaled to values between -0.8 to $+0.8$ for same reason. Values higher than these are likely to hinder training.

The normalized scaled spectral data points or PCA scores were then fed into the input layer of the network. The network processed the data in the usual feedforward manner. The value at each output neurode was expected to lie between -1.0 and $+1.0$ corresponding to the limits of the transfer function. The actual values were linearly rescaled to a value between 0.0 and 1.0. It is this final output which was interpreted in terms of class type.

Prior to training, every network was initialized by assigning a random value to each of its connection weights. The final equilibrium state of a network is partially dependent upon these starting values. To increase the likelihood of finding an optimal solution, each network was trained six times for a given training/test set. Each time a different random combination of initial weight values was used.

Training consisted of running each of the input/output pairs of the training set successively through the network in random order. After each iteration the weights were adjusted according to the learning rule. Each network was trained for 24 000 iterations. RMS output error was evaluated against the test set every 2000 iterations. After each testing period, the network was saved only if the RMS output error for the test set was lower than for any previous period. This was done to avoid overtraining, a situation in which a network learns to identify the unique features of a specific spectrum or set of spectra, thereby limiting its ability to generalize.

An additional step was taken with the five and seven hidden neurode networks trained on the

direct data. After training was complete, the number of interneurode connections within each of the two networks was reduced through pruning. Connections with associated weight values falling within the lowest 20% in terms of absolute magnitude were removed and the networks retrained. It is often suggested that simpler networks, that is those with fewer interconnections, tend to generalize better. Hence the number of connections within the two smallest networks in this series was reduced even further to investigate whether this would lead to improved generalization.

Performance was evaluated on the network's ability to generalize. That is the network's ability to use its stored knowledge of the spectral characteristics of the samples in the training set and apply these to make generalized identifications of similar but different spectra of the same class types. Relative network classification error was measured as the root-mean-square (RMS) error at the output layer as follows:

$$\sqrt{\frac{\sum_{i=0}^{7}(A_i - D_i)^2}{7}}$$

when A = actual output at node i; and D = desired output at node i. The RMS measurements were made using the actual neurode activation levels, before the addition of any inhibitory output connections which constrain the output of each neurode to a value of exactly zero or one.

RESULTS AND DISCUSSION

Fluorescence spectra

The normalized fluorescence spectra of each of the samples used to train and test the networks are displayed in Figs. 2–8. Note that whereas the spectral data sets for diesel fuel marine (DFM) in Fig. 8, diesel No. 2 in Fig. 2, and the unleaded fuels in Figs. 3 and 4 are relatively self similar in terms of their spectral characteristics, the spectra of lube oil 2190 (Fig. 7) and JP5 (Fig. 5) appear to fall into two distinctly recognizable subclasses. One of the JP5 subclasses has among its distin-

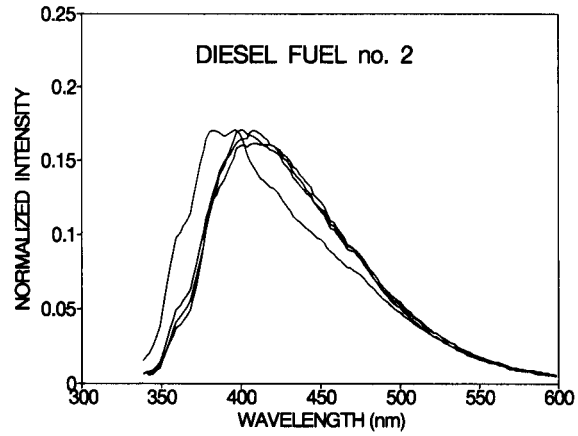

Fig. 2. Fluorescence spectra of diesel fuel No. 2.

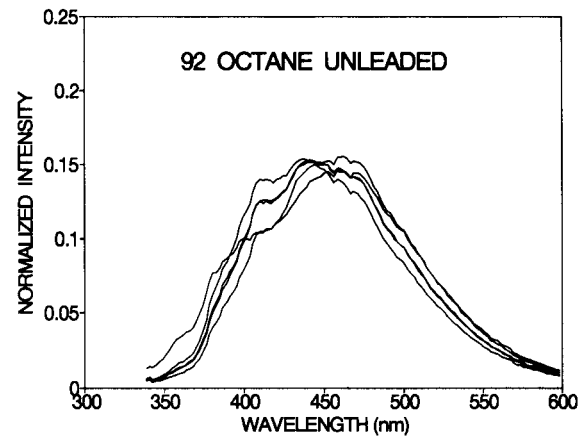

Fig. 3. Fluorescence spectra of 92 octane unleaded gasoline.

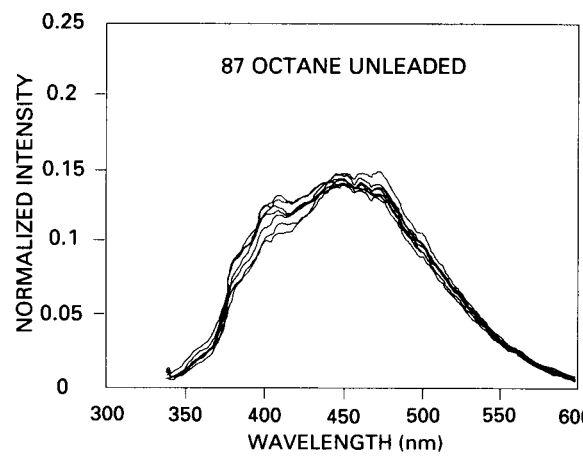

Fig. 4. Fluorescence spectra of 87 octane unleaded gasoline.

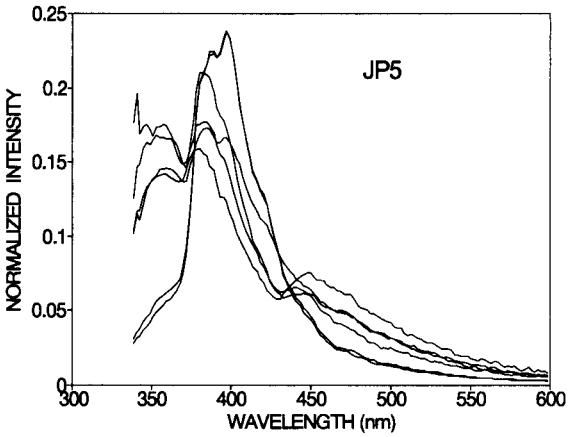

Fig. 5. Fluorescence spectra of JP5.

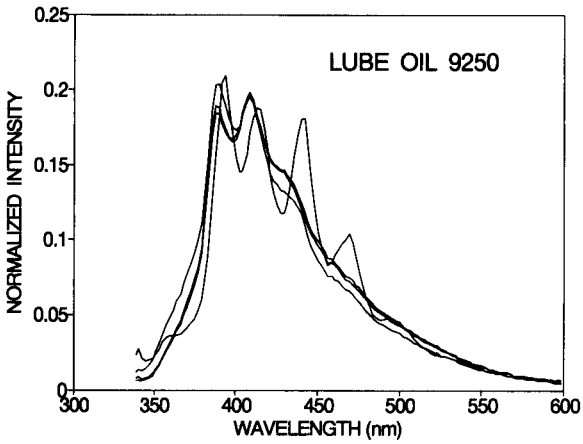

Fig. 6. Fluorescence spectra of lube oil 9250.

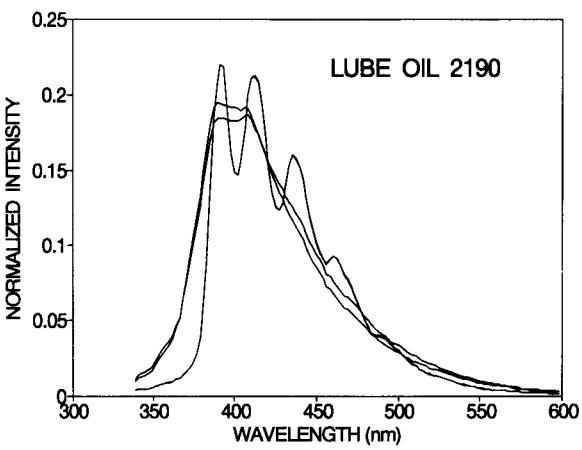

Fig. 7. Fluorescence spectra of lube oil 2190.

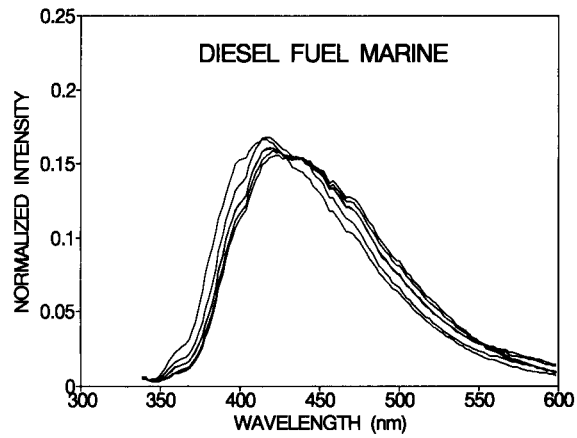

Fig. 8. Fluorescence spectra of diesel fuel marine.

guishing features a relative fluorescence intensity greater than 0.1 at 350 nm, the second has a relative fluorescence intensity of less than 0.05 at 350 nm. Likewise, the spectra of lube oil 2190 appear as two basic varieties, one of which has more spectroscopic structure than the other.

Lack of consistency in the fluorescence signature of a single oil/fuel type can arise due to differences either in the refining process or in the starting crude material. The networks were not trained to separately categorize each subtype of lube oil 2190 or JP5 though this would have been possible. Rather they were trained to recognize each subtype as belonging to the appropriate overall class.

PCA results

PCA resulted in the extraction of three factors which together account for 97.3% of the variance in the data. The eigenvalues, expressed as the relative proportion of the total variance extracted by each factor are 72.7%, 22.1%, and 2.4% respectively. Additional factors had absolute eigenvalues significantly less than 1.0 and did not meet the Kaiser criterion [26] for retention.

To better visualize the input data space, factor scores for the 36 sample spectra are plotted in Fig. 9. It can be seen that the individual oil/fuel spectra generally form clusters by which the various classes may be identified. Two exceptions are noted however. One is a premium (92 octane)

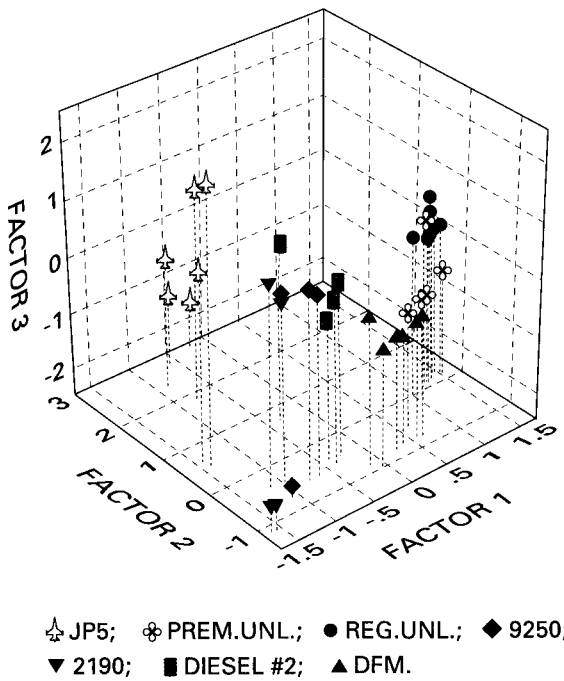

Fig. 9. PCA scores for 36 sample spectra.

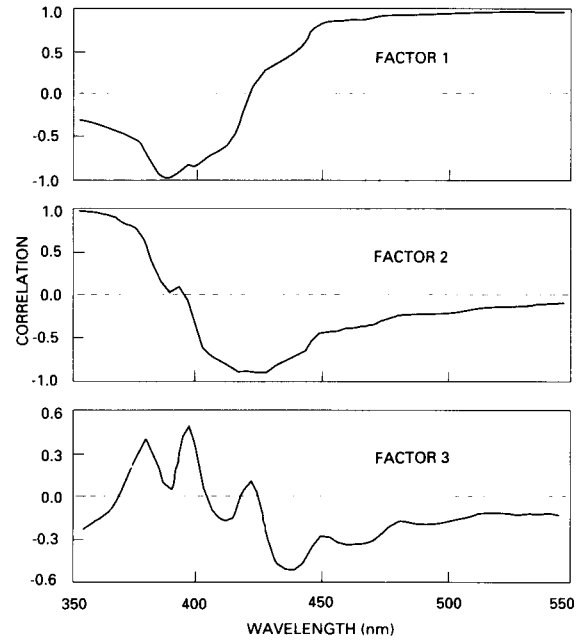

Fig. 10. Loadings for each of the three PCA extracted factors.

unleaded fuel sample which lies closely grouped with the cluster of regular (87 octane) unleaded samples. The other is a 9250 lube oil sample which lies apart from the other 9250 samples and is more closely associated with two 2190 samples in the lower corner of the figure.

The normalized loadings for each factor are plotted in Fig. 10. Factor loadings represent the correlations between each original spectral data point and the new PCA derived factors. The uppermost graph shows that there is a high degree of correlation between the first factor and data points sampled beyond 475 nm. That these points are highly intercorrelated was verified by inspection of the correlation matrix. For that reason, we chose not to utilize data points farther out than 500 nm in preparing the direct data, non-PCA, input vectors. Including additional data sampled from beyond this point would only have provided redundant information already available in the 450–500 nm part of the spectrum.

Network results using direct input

A total of six networks were trained and tested using directly sampled input data. This includes networks with five, seven, nine, and eleven hidden layer neurodes along with pruned versions of the five and seven hidden neurode networks. Figure 11 shows the RMS output error for the networks plotted against each of the seven data test sets. It can be seen that the resulting RMS values are more dependent upon which data set was used rather than upon the specific network configuration. Across the series, the RMS num-

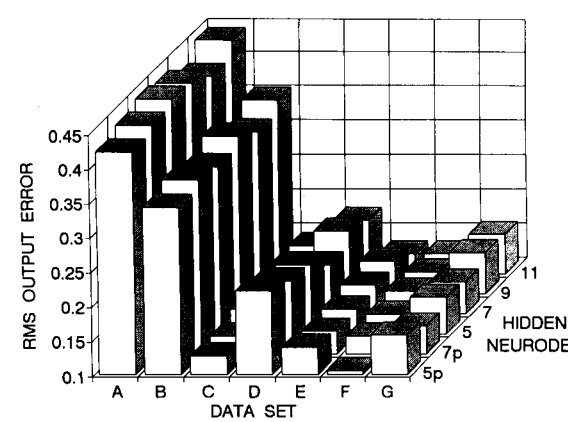

Fig. 11. RMS output error for each of the networks trained using direct spectral input data sets.

TABLE 1

Mean training and test set RMS values and number of correctly identified spectra for each network

Hidden Neurodes	Direct data input						PCA score input			
	11	9	7	5	7p	5p	5	4	3	2
Avg. Test set RMS	0.219	0.218	0.217	0.218	0.215	0.216	0.330	0.352	0.354	0.36
Avg. Training set RMS	0.159	0.145	0.129	0.149	0.128	0.138	0.207	0.223	0.229	0.26
Number correct of 49	47	47	46	47	47	47	44	44	42	40
Percent correct of 49	96	96	94	96	96	96	90	90	86	82

bers are significantly higher for test sets A and B. Each of these two test sets contain as one of its members, one of the two spectra mentioned above as clustering with another class. No network was able to correctly identify either of these spectra. Both were consistently categorized as belonging to the class to which they most closely cluster. That is, the premium unleaded sample in test set A was mistaken for regular unleaded, and the 9250 sample in test set B was classified as 2190. As the test sets were small, consisting of only seven cases each, even one erroneous classification leads to a large RMS error value.

With one exception, each of the networks correctly identified all of the other 34 spectral cases. The mean training and test set RMS values, averaged over the seven data sets, are tabulated in the first part of Table 1. The table also includes the number of correctly identified spectra for each network. Overall, network performance was consistent at around 96% (47/49 correct). A more conservative estimate of network performance can be made by not counting the test spectra which were used in more than one test set, and allowing that two of the thirty six total samples were misidentified. This would put the accuracy at 94% (34/36).

Network results using PCA scores

Network performance resulting from the use of PCA as a preprocessor was not as good as with the directly sampled data. This is an indication that some information was lost in the PCA analysis. RMS output error values for the PCA trained networks are shown in the second part of Table 1. The networks' ability to classify spectra improved as the number of hidden layer neurodes were increased. The best networks, the four and five hidden neurode networks, were able to properly identify 44 of 49 or 90% of the test spectra. Again, as some spectra were used with more than one test set, one could say that 32 of the 36 total samples, or 89%, were correctly classified. Two of the spectra that the PCA trained networks misclassified were the same two spectra that the direct data networks missed.

Conclusion

The work presented here has demonstrated that a backpropagation neural network can be trained to effectively make generalized classifications of fluorescence spectra. With this particular set of spectra, PCA preprocessing does not seem to offer any advantages over using direct spectral data. However, it is possible that an alternate network configuration or different training parameters could yield improved results with regard to classification of the PCA derived sample data.

Future performance enhancements are likely to be realized by the use of a broader based training set. The two spectra which were misclassified, belonging to the premium unleaded and the 9250 samples which individually cluster more closely to another class, stand out because neither was adequately represented in the training set of the networks on which they were tested.

Had examples of similar spectra been included in the training sets, it is probable that both would have been correctly identified.

REFERENCES

1 K.G. Coleman and S. Watenpool, AI Expert, 7 (1992) 36.
2 P.K. Simpson, Artificial Neural Systems, Pergamon, New York, 1990, pp. 112–120.
3 P.D. Wasserman, Neural Computing Theory and Practice, Van Nostrand Reinhold, New York, 1989, Chap. 3.
4 R. Hecht-Nielson, Neurocomputing, Addison-Wesley, New York, 1990, pp. 124–137.
5 R.C Eberhart and R.W. Dobbins, Neural Network PC Tools, Academic Press, San Diego, CA, 1990, Chap. 2.
6 R. Hecht-Nielson, Proc. Int. Joint Conf. on Neural Networks, I (1989) 593–611.
7 B. Curry and D.E. Rumelhart, Tetrahedron Comput. Methodol., 3 (1990) 213.
8 E.W. Robb and M.E. Munk, Mikrochim. Acta, I (1990) 131.
9 M.E. Munk, M.S. Madison and E.W. Robb, Mikrochim. Acta, II (1991) 505.
10 J.R. Long, V.G. Gregoriou and P.J. Gemperline, Anal. Chem., 62 (1990) 1791.
11 B.J. Wythoff, S.P. Levine and S.A. Tomellini, Anal. Chem., 62 (1990) 2702.
12 K. Tanabi, T. Tamura and H. Uesaka, Appl. Spectrosc., 46 (1992) 807.
13 J.U. Thompson and B.J. Meyer, Magn. Reson., 84 (1989) 212.
14 M. Kjaer and F.M. Poulson, J. Magn. Reson., 94 (1991) 659.
15 M. Glick and G.M. Hieftje, Appl. Spectrosc., 45 (1991) 1706.
16 C. Schierle, M. Otto and W. Wegscheider, Fresenius' J. Anal. Chem., 343 (1992) 561.
17 P. Olmos, J.C. Diaz, J.M. Perez, G. Garcia-Belmonte, P. Gomez and V. Rodellar, Nucl. Instr. Meth. Sec. A., (1992) 167.
18 J.M. Andrews and S.H. Lieberman, Proc. SPIE-Int. Soc. Opt. Eng. 1992, 1587, Chem., Biochem., Environ. Fiber Sens. 3, pp. 30–38.
19 T.J. McAvoy, H.T. Su, N.S. Wang, M. He, J. Horvath and H. Semerjian, Biotech. Bioeng., 40 (1992) 52.
20 P.A. Jansson, Anal. Chem., 63 (1991) 357A.
21 J. Zupan and J. Gasteiger, Anal. Chim. Acta, 248 (1991) 1.
22 S.E. Apitz, L.M. Borbridge, G.A. Theriault and S.H. Lieberman, Analusis, 20 (1992) 461.
23 P.J. Gemperline, J.R. Long and V.G. Gregoriou, Anal. Chem., 63 (1991) 2313.
24 C. Borggaard and T. Henrik, Anal. Chem., 64, (1992) 545.
25 S.H. Lieberman, G.A. Theriault, S.S. Cooper, R.S. Olsen and P.W. Lurk, Second International Symposium: Field Screening Methods for Hazardous Wastes and Toxic Chemicals, 1991, pp. 57–65.
26 H.F. Kaiser, Educ. Psych. Meas., 20 (1960) 141.

PUBLICATION SCHEDULE FOR 1994

	S'93	O'93	N'93	D'93	J	F	M	A	M			
Analytica Chimica Acta	281/1 281/2 281/3	282/1 282/2 282/3	283/1 283/2	283/3 284/1 284/2	284/3 285/1–2 285/3	286/1 286/2 286/3	287/1–2 287/3 288/1	288/2 288/3 289/1	289/2–3 290/1 290/2			
Vibrational Spectroscopy		6/1			6/2		6/3		7/1			

INFORMATION FOR AUTHORS

Detailed "Instructions to Authors" for *Analytica Chimica Acta* was published in Volume 256, No. 2, pp. 373–376. Free reprints of the "Instructions to Authors" of *Analytica Chimica Acta* and *Vibrational Spectroscopy* are available from the Editors or from: Elsevier Science B.V., P.O. Box 330, 1000 AH Amsterdam, The Netherlands. Telefax: (+31-20) 5862459.

Manuscripts. The language of the journal is English. English linguistic improvement is provided as part of the normal editorial processing. Authors should submit three copies of the manuscript in clear double-spaced typing on one side of the paper only. *Vibrational Spectroscopy* also accepts papers in English only.

Rapid publication letters. *Letters* are short papers that describe innovative research. Criteria for letters are novelty, quality, significance, urgency and brevity. Submission data: max. of 2 printed pages (incl. Figs., Tables, Abstr., Refs.); short abstract (e.g., 3 lines); *no* proofs will be sent to the authors; submission on floppy disc; *no* revision will be possible.

Abstract. All papers and reviews begin with an Abstract (50–250 words) which should comprise a factual account of the contents of the paper, with emphasis on new information.

Figures. Figures should be prepared in black waterproof drawing ink on drawing or tracing paper of the same size as that on which the manuscript is typed. One original (or sharp glossy print) and two photostat (or other) copies are required. Attention should be given to line thickness, lettering (which should be kept to a minimum) and spacing on axes of graphs, to ensure suitability for reduction in size on printing. Axes of a graph should be clearly labelled, along the axes, outside the graph itself. All figures should be numbered with Arabic numerals, and require descriptive legends which should be typed on a separate sheet of paper. Simple straight-line graphs are not acceptable, because they can readily be described in the text by means of an equation or a sentence. Claims of linearity should be supported by regression data that include slope, intercept, standard deviations of the slope and intercept, standard error and the number of data points; correlation coefficients are optional.

Photographs should be glossy prints and be as rich in contrast as possible; colour photographs cannot be accepted. Line diagrams are generally preferred to photographs of equipment. Computer outputs for reproduction as figures must be good quality on blank paper, and should preferably be submitted as glossy prints.

Nomenclature, abbreviations and symbols. In general, the recommendations of IUPAC should be followed, and attention should be given to the recommendations of the Analytical Chemistry Division in the journal *Pure and Applied Chemistry* (see also *IUPAC Compendium of Analytical Nomenclature, Definitive Rules*, 1987).

References. The references should be collected at the end of the paper, numbered in the order of their appearance in the text (*not* alphabetically) and typed on a separate sheet.

Reprints. Fifty reprints will be supplied free of charge. Additional reprints (minimum 100) can be ordered. An order form containing price quotations will be sent to the authors together with the proofs of their article.

Papers dealing with vibrational spectroscopy should be sent to: Dr J.G. Grasselli, 150 Greentree Road, Chagrin Falls, OH 44022, U.S.A. Telefax: (+1-216) 2473360 (Americas, Canada, Australia and New Zealand) or Dr J.H. van der Maas, Department of Analytical Molecular Spectrometry, Faculty of Chemistry, University of Utrecht, P.O. Box 80083, 3508 TB Utrecht, The Netherlands. Telefax: (+31-30) 518219 (all other countries).

0003-2670/94/$07.00

This issue is printed on acid-free paper.

PRINTED IN THE NETHERLANDS

Vibrational Spectra and Structure

A Series of Advances

Volume 20

edited by **J.R. Durig**, College of Science and Mathematics,
University of South Carolina, Columbia, SC, USA

The current volume comprises five chapters, three of which address recent advances in experimental techniques for providing information on biomolecular reaction paths, for determining linewidth and small frequency shifts, and for applying the microwave Fourier transform technique to experiments of static gases in waveguide cells. Chapters 4 and 5 consider *ab initio* calculations for both inorganic and organic systems.

Contents:

"Each volume in this excellent series is eagerly awaited and the general reader is never disappointed."

Journal of Molecular Structure

1993 xx + 352 pages
Price: US $ 231.50 / Dfl. 370.00
ISBN 0-444-89865-4

ORDER INFORMATION

For USA and Canada
ELSEVIER SCIENCE PUBLISHERS
Judy Weislogel
P.O. Box 945
Madison Square Station,
New York, NY 10160-0757
Tel: (212) 989 5800
Fax: (212) 633 3880

In all other countries
ELSEVIER SCIENCE PUBLISHERS
P.O. Box 211
1000 AE Amsterdam
The Netherlands
Tel: (+31-20) 5803 753
Fax: (+31-20) 5803 705

US$ prices are valid only for the USA & Canada and are subject to exchange rate fluctuations; in all other countries the Dutch guilder price (Dfl.) is definitive. Books are sent postfree if prepaid.

ELSEVIER
SCIENCE PUBLISHERS

711/414\140\0001-00

0003-2670(19940120)285:1/2;1-F